NASA TECHNICAL NOTE

NASA TN D-5819

c. 1

NASA TN D-5819

THEORETICAL STUDY OF CONDITIONS LIMITING V/STOL TESTING IN WIND TUNNELS WITH SOLID FLOOR

by Harry H. Heyson

Langley Research Center
Hampton, Va. 23365

NATIONAL AERONAUTICS AND SPACE ADMINISTRATION • WASHINGTON, D. C. • JUNE 1970

1. Report No. NASA TN D-5819	2. Government Accession No.	3. Recipient's Catalog No.
4. Title and Subtitle THEORETICAL STUDY OF CONDITIONS LIMITING V/STOL TESTING IN WIND TUNNELS WITH SOLID FLOOR		5. Report Date June 1970
		6. Performing Organization Code
7. Author(s) Harry H. Heyson		8. Performing Organization Report No. L-7042
9. Performing Organization Name and Address NASA Langley Research Center Hampton, Va. 23365		10. Work Unit No. 721-01-12-01-23
		11. Contract or Grant No.
12. Sponsoring Agency Name and Address National Aeronautics and Space Administration Washington, D.C. 20546		13. Type of Report and Period Covered Technical Note
		14. Sponsoring Agency Code
15. Supplementary Notes		

16. Abstract

Under sufficiently large wake deflections, the forward portion of the wake is found to flow forward along the floor leading to a vortex pattern which results in Rae's limits (Journal of Aircraft, May-June 1967). Although wind-tunnel data cannot normally be corrected successfully beyond these limits, it may be possible to obtain ground-effect data for conditions more severe than those implied by Rae.

17. Key Words (Suggested by Author(s)) Wind tunnels V/STOL		18. Distribution Statement Unclassified – Unlimited	
19. Security Classif. (of this report) Unclassified	20. Security Classif. (of this page) Unclassified	21. No. of Pages 328	22. Price* $3.00

*For sale by the Clearinghouse for Federal Scientific and Technical Information Springfield, Virginia 22151

THEORETICAL STUDY OF CONDITIONS LIMITING V/STOL TESTING IN WIND TUNNELS WITH SOLID FLOOR

By Harry H. Heyson
Langley Research Center

SUMMARY

Theoretical study indicates that, under sufficiently severe conditions, the forward portion of the wake will flow forward along the floor. The location of the consequent rolled-up vorticity results in the testing limits found previously by Rae (Journal of Aircraft, May-June 1967). The predominant factor determining the initial flow reversal of the wake is wake deflection. Separation of the flow on the ceiling of a closed tunnel is also indicated, but at substantially more severe conditions. While it is doubtful that wind-tunnel data corresponding to free-air conditions can be corrected successfully beyond Rae's limits, it may be possible to obtain wind-tunnel data for ground-effect conditions well beyond these limits.

INTRODUCTION

Many of the theoretical assumptions which result in comparatively simple corrections for wind-tunnel tests of conventional aircraft are inadequate for tests of V/STOL models. The principal assumptions of classical theory that are violated in V/STOL testing are that the wake is undeflected from the free-stream direction and that the wall-induced velocities are only small perturbations on the free-stream velocity.

To a certain extent, the aforementioned assumptions have been removed from more recent theoretical treatments (refs. 1 to 4) intended specifically for use with V/STOL models. On the other hand, recent experimental evidence (particularly ref. 5) indicates that there are definite limits beyond which the theory of references 1 to 4 cannot be applied.

In an effort to explore the reason for these limits, the present investigation examines the entire flow in the wind tunnel rather than only that portion induced by the tunnel boundaries. The analysis assumes a simple lifting rotor as representative of a very high-lift, large-downwash lifting system. For computational simplicity, the rotor wake is presumed to pass downward and rearward in a straight line until it meets the floor, after which the wake is assumed to flow off along the floor. Even though such an idealized wake could not exist in its own induced field, it is shown that the assumed wake does indicate, at least qualitatively, the correct experimentally known wake deformations.

Thus, examination of the predicted deformations in the tunnel yields qualitative information regarding the effects of the walls on the general flow within the tunnel boundaries.

It will be shown that the limits proposed by reference 5 appear to be associated with a region of reversed flow on the floor of the tunnel. The effects of a number of parameters (wake skew angle, wind-tunnel width-height ratio, height of the model above the floor, ratio of model size to tunnel size, and angle of attack (representing changes in drag-lift ratio)) on the region of reversed flow are studied in some detail.

Certain preliminary results of this investigation, for one rotor and one wind-tunnel configuration, have been published previously as reference 6.

SYMBOLS

The symbols used in this paper largely conform to those of references 1 to 4 with only minor exceptions. Extensive use is made of direct output from digital computers and digitally controlled plotters. The available symbols and lack of lower case letters in the output of these devices necessitate deviations from the symbols used in the text. The alternate versions, indicated in parentheses, show the forms used in machine-prepared tables and figures. The appendixes of this paper use symbols which may differ from those of the main text. Separate symbol lists are provided, where required, in the appendixes.

A_m momentum area of lifting system

A_T cross-sectional area of test section

B semiwidth of test section

b complete span of model

C_D (CD) generally, induced drag coefficient, D/qS

C_L (CL) lift coefficient, L/qS

C_{Lhb} lift coefficient based on wind-tunnel area below model and within span, L/qhb

C-O-B abbreviation for closed-on-bottom-only

D generally, induced drag

H	semiheight of wind tunnel
h	height of model above floor
L	lift
q (Q)	dynamic pressure, $\frac{1}{2}\rho V^2$
q_c (QC)	dynamic pressure corrected for boundary interference
R	rotor radius
S	area of lifting system
u,v,w	induced velocity components, parallel to X-, Y-, and Z-axes
V	forward velocity or uncorrected wind-tunnel velocity
V_c	wind-tunnel velocity corrected for boundary interference
w_0	mean, or momentum theory, value of induced velocity parallel to Z-axis, positive when directed upward
X,Y,Z	in wind tunnel: Cartesian coordinate system centered in wind tunnel at model; X positive rearward; Y positive to right; Z positive upward for rotor: Cartesian coordinate system centered in, and oriented with respect to, rotor tip-path plane; directions as above
x,y,z (X,Y,Z)	distances from origin along X-, Y-, and Z-axes
x_f	distance behind model of the intersection of the wake and the floor
α (ALPHA)	rotor tip-path-plane angle of attack, positive when upward in front
α_c	corrected angle of attack
γ (GAMMA)	width-height ratio of wind tunnel, B/H
Δu	boundary-induced interference velocity parallel to X-axis, positive rearward

Δw boundary-induced interference velocity parallel to Z-axis, positive upward

$\Delta\alpha$ (D ALPHA) boundary-induced additive correction to angle of attack

ζ (ZETA) ratio of tunnel semiheight to the height of the model above floor, H/h

η (ETA) in references 2 to 4, distance from model to right-hand tunnel boundary divided by tunnel semiwidth (Throughout the present paper, $\eta = 1$.)

ρ mass density of test medium

σ (SIGMA) ratio of rotor radius to tunnel semiwidth, R/B

χ (CHI) wake skew angle, angle measured from negative Z-axis to center of wake, positive rearward

RESULTS AND DISCUSSION

DISTRIBUTION OF WALL-INDUCED INTERFERENCE

In general, wind-tunnel-interference calculations omit the direct effect of the model and are concerned only with the additional effects created by the near proximity of the wind-tunnel boundaries. At the outset it will be instructive to examine the manner in which the boundary-induced interference velocities vary throughout the wind tunnel.

In the present study, which assumes that the model is a simple lifting rotor, the interference velocities are easily obtained using the computer program given as appendix K of reference 4. This program provides the interference at a tail behind a rotor; simple modifications (to set the tail span equal to zero and to enclose the tail length and height within DO-loops scanning the X-Z plane of the tunnel) produce the results shown in figure 1 for a series of decreasing wake skew angles. In figure 1, the rotor has uniform load distribution, is mounted 30 percent of a semiheight above the center of a square, closed test section, with $\sigma = 0.6$ and $\alpha = 0^{\circ}$. For each wake angle, contours of equal values of the ratios $\Delta w/w_0$ and $\Delta u/w_0$ have been obtained by noting that, in references 1 to 3, $A_m/A_T = \frac{\pi}{4}\sigma^2\gamma$.

Interference at $\chi = 90^{\circ}$

Figure 1(a) shows the interferences at $\chi = 90^{\circ}$, that is, when the wake passes directly rearward as in classical wind-tunnel-interference theory. Observe that w_0 is always negative for positive lift. Thus, except for a few regions far forward of the rotor (where the rotor produces upwash in free air) the vertical interference is always in the nature of an upwash which increases with distance downstream. Since the rotor is mounted above the centerline, the interference is greater above the rotor than below the rotor. (A centered rotor would produce a field symmetric about the X-Y plane.) The longitudinal interference is significant only near the model and results from the effective bound vortex represented by the rotor. An increase in velocity above the rotor and a decrease below the rotor are evident, with the values above the rotor being somewhat greater than those below the rotor. (This pattern would be antisymmetric about the X-Y plane if the rotor were centrally located.)

Now the effect of these interference velocities is to alter the effective angle of attack and forward velocity of the rotor; thus, from reference 2

where

$$\left.\begin{aligned} \alpha_c &= \alpha + \Delta\alpha \\ \Delta\alpha &= \frac{\frac{\Delta w}{V}}{1 + \frac{\Delta u}{V}} \end{aligned}\right\} \tag{1}$$

and

so that

$$\left.\begin{aligned} \frac{q_c}{q} &= \left(1 + \frac{\Delta u}{V}\right)^2 + \left(\frac{\Delta w}{V}\right)^2 \\ \frac{V_c}{V} &= \sqrt{\left(1 + \frac{\Delta u}{V}\right)^2 + \left(\frac{\Delta w}{V}\right)^2} \end{aligned}\right\} \tag{2}$$

Examination of equations (1) and (2) indicates that it is the ratios with respect to V rather than the ratios with respect to w_0 which are of primary concern. The ratios with respect to V are obtained by observing that

$$\left.\begin{aligned} \frac{\Delta w}{V} &= \left(\frac{\Delta w}{w_0}\right)\left(\frac{w_0}{V}\right) \\ \frac{\Delta u}{V} &= \left(\frac{\Delta u}{w_0}\right)\left(\frac{w_0}{V}\right) \end{aligned}\right\} \tag{3}$$

where, for the conditions of figure 1 ($\alpha = 0^o$), equation (A8) of appendix A shows that

$$\frac{w_0}{V} = -\cot \chi \tag{4}$$

Strict application of equations (1) to (4) indicates that the effect of the interference at $\chi = 90^o$ is identically zero. This result is expected since, with $w_0 = 0$ (eq. (4)), there is no lift on the rotor.

The result at $\chi = 90^o$ is not, however, trivial. Provided that w_0 is small and that the wake does not depart by more than a few degrees from the horizontal, the actual value of w_0/V, rather than the theoretical value (eq. (4)), must be used in equations (1) to (3) to obtain usable results. It will be observed that this treatment of wall effects for the limiting case of $\chi = 90^o$ is the procedure used in most wind-tunnel-interference theory.

Interference at $\chi = 70^o$

Similar interference-velocity contours for a more heavily loaded operating condition ($\chi = 70^o$) are shown in figure 1(b). It may be noted that the wall-induced interference grows rapidly as the distance along the wake increases. At the intersection of the wake and the floor, it is obvious that the vertical interference must be exactly equal, but opposite to, the vertical velocity produced by the rotor in free air, otherwise there would be flow through the floor. The longitudinal interference at the rotor remains small, but this interference also increases rapidly with distance along the wake. At the floor, the longitudinal interference opposes the tunnel velocity ahead of the wake and augments it behind the wake. Following equations (3) and (4), the magnitude of the longitudinal interference is found to be about 11 percent of the tunnel velocity for the largest contour $\left(\Delta u/w_0 = \pm 0.3\right)$ shown in figure 1(b).

Interference at $\chi = 50^o$

As the rotor lift is increased to produce a wake skew angle of 50^o (fig. 1(c)) the primary effect on $\Delta w/w_0$ is merely an increased gradient along the wake. This is the expected result since the effect of the floor is still to just cancel the free-air field, but the length of the wake within the tunnel is reduced. A similar increased gradient is noticed for the longitudinal interference; however, in this case the levels of interference at the floor also increase to approximately twice those obtained at $\chi = 70^o$. Together with the increase in w_0/V, the net result is longitudinal interferences at the floor which are about 50 percent as great as the tunnel velocity.

Interference at $\chi = 30^{\circ}$ and 10°

Figures 1(d) and 1(e) show continuations of the same trends as the wake steepens. The maximum indicated longitudinal interference velocities on the floor become about 1.4 and 5.0 times the tunnel velocity for $\chi = 30^{\circ}$ and 10°, respectively.

In the face of such extreme wall-induced interferences, it is obvious that the local flow (and the wake, which follows the local flow) near the floor must undergo drastic deformations. The magnitude of the anticipated deformations is so great that quantitatively accurate theoretical results can not be obtained by the present methods; however, qualitatively, it appears that the theory does indicate the correct trends to be observed in the flow patterns. The remainder of this paper will be concerned with an examination of the nature and effects of these deformations.

INDUCED FIELD OF A LIFTING ROTOR

The complete flow within the wind tunnel consists not only of the boundary-induced interference velocities, but also the general tunnel velocity and the velocities induced directly by the model. The tunnel velocity presents no difficulty since, in the theory, it merely requires the addition of a constant term to the calculated flow. The induced field of the rotor is more involved, and its calculation will be examined in this section of the paper.

Method of Calculation

For many purposes, it is adequate to represent a rotor wake as a skewed elliptically cylindrical surface of uniformly distributed vorticity. This wake model has been used extensively in the past (refs. 7 to 10) and has been shown experimentally (refs. 9, 11, and 12) to yield usable results for the time-averaged induced field of the rotor. Even in ground effect, where the real wake may be extremely distorted when compared to the simple cylinder, usable qualitative results are obtained (ref. 13). Since the present study is qualitative in nature, the simple cylindrical wake is used herein, thus avoiding the computational complexity inherent in a more detailed representation.

The component of induced velocity normal to the rotor disk (w) is available in the form of nondimensional charts in several papers (for example, refs. 8, 9, and 14). No similar charts are available for the u and v components of the field. In any event, for the present purpose, where the field at large distances from the rotor is required, it is necessary to obtain the values by the direct numerical integration of equations (9), (11), and (13) of reference 10 (with $f(\psi)$ in that paper set equal to 1.0 so as to obtain the field for a uniformly loaded disk).

Typical Calculated Field

A sample of the field calculated in this manner is presented for the X-Z plane of a rotor ($\chi = 50^{\circ}$) in figure 2. Along the X-axis, the normal component (w) of induced velocity changes from an upwash ahead of the rotor to an increasingly large downwash at the trailing edge of the rotor, after which the downwash decreases asymptotically to zero at an infinite distance downstream. Passing downward along the wake, it is observed that the downwash increases and essentially achieves its ultimate uniform value of $w/w_0 = 2$ within a diameter of the rotor. The longitudinal component (u) is of the nature of a sink in the region above the rotor and draws the flow into the wake. Within the wake, the flow is directed rearward, essentially achieving its ultimate value of $u/w_0 = 2 \tan(\chi/2)$ (refs. 6 and 7) within a diameter of the rotor; however, outside the wake and below the rotor, the flow is generally retarded. In particular, in the lower left quadrant of figure 2, the longitudinal component of rotor-induced velocity is such as to augment the previously discussed tendency of the wall-induced velocities to oppose the tunnel velocity.

Effect of Disk-Load Distribution

In general, the actual rotor disk-load distribution is far from uniform (ref. 9) and the nonuniformity of loading has strong local effects on the distribution of induced velocities in the rotor field. This effect will be examined briefly in a later section of this paper, but the computed results presented herein are largely for uniform loading. Justification for this usage is obtained from reference 11 which indicates that the field of a uniformly loaded rotor is a close approximation to the experimentally determined average field over a span equal to that of the rotor.

COMPLETE FLOW IN WIND TUNNEL

Calculated Flow Based on Vortex-Cylinder Wakes

Calculation procedures.- The complete flow in the wind tunnel is the sum of the wall-induced interference, the rotor-induced field, and the free-stream velocity. The accuracy of the calculation, at least for the assumed wake model, is dependent upon the consistency with which the image wakes used to represent the boundaries represent the wake within the tunnel. It is desirable to use the same representation for all of the wakes, both interior and exterior to the test section.

Appendix B presents the derivation of an extended version of reference 1, which maintains the desired consistency of representation but which, in its original form, suffers from several defects. In common with reference 1, the theory presented in appendix B is restricted to zero angle of attack since this restriction is inherent to the methods of superposition used in the derivation. The longitudinal and lateral interference velocities are incorporated in the revised theory by an application of the equations of reference 10. Appendix B also revises the image system of reference 1 so that the rotor may assume any arbitrary vertical position in the tunnel. Appendix C presents the FORTRAN program used to obtain the results presented herein.

Calculated results.- The theoretical results obtained herein are presented in the form of vectorial flow charts prepared on a digitally controlled plotter (CALCOMP). Appendix D presents the most general of the FORTRAN programs used to prepare control tapes for the automatic plotter. This program is illustrative of the general technique.

Vectorial flow charts of the complete flow are presented in figures 3 to 30 for the same conditions as in figure 1. In addition, similar charts are presented in figures 3 to 30 for the equivalent conditions in free air, in ground effect, and in a wind tunnel closed only on the bottom. Included in figures 3 to 30 are the flows in the X-Z plane, in the plane of the floor, and in a transverse plane through the center of the intersection of the wake and the floor. Isometric projections of the flow are also provided. Table I summarizes the conditions considered and provides, in addition, the calculated corrections, both to free air and to ground effect, as obtained from references 2 to 4.

Before examining the computed flows it should be noted that reference 15 (see also refs. 6 and 9) has shown that the effect of wake rollup is to effectively modify the wake skew angle to some greater mean value. This feature has not been included in the present analysis since it leads to certain inconsistencies in depicting the entire flow. The present study is intended to be qualitative only and the effect of wake rollup will be minimized herein by comparing flows corresponding generally to the same wake angles.

The general growth of the rotor free-air flow field with decreasing skew angle (increasing C_L) is evident in figures 3 to 30. Except at the lowest wake angle (10°) there is an upwash at the leading edge of the rotor disk. This implies that the initial path of the front part of the wake will be upward, returning back downward through the disk shortly thereafter. The flow at the trailing edge of the disk is sharply downward, and for high lift coefficients ($\chi < 40^{\circ}$) is actually directed forward to some extent as well. In the longitudinal (X-Z) plane the net result is contraction of the actual wake. These features are actually observed in flow visualization studies. (See, for example, ref. 16 and fig. 19 of ref. 2.)

The effect of imposing additional restraints on the flow depends, of course, on the nature and location of the restraint. Thus, the rotor-induced vertical velocities are cancelled at the ceiling of the closed tunnel and augmented at the upper boundary of the closed-on-bottom-only tunnel. At an equivalent height above the rotor, ground effect is hardly noticeable. It is noteworthy that the flow at the ceiling can actually be reversed for sufficiently severe conditions. (See fig. 9(c) in which $\chi = 10^{\circ}$.) In practice, such a flow reversal would lead to large-scale separation of the flow from the ceiling, with consequent extreme effects on the entire flow (ref. 17). The large downwashes for similar conditions at the upper boundary of the closed-on-bottom-only tunnel should lead to similar concern about the actual behavior of the main wind-tunnel stream (parts (d) of figs. 14 to 16).

The floor is solid for all three constraint configurations considered herein, and the effects are strikingly similar as a result. Within the primary rotor wake the flow generally turns sharply rearward at the floor; however, as the wake steepens below angles of 30^{o} an increasing portion of the forward wake turns forward. This behavior is required in order to approach the symmetrical conditions which must exist in hovering ($\chi = 0^{o}$). Large lateral velocities are observed at the sides of the wake near the floor (figs. 10 to 30) indicating that the wake will spread laterally at the floor.

Behind the wake near the floor, there are a general acceleration of the flow and an upwash that are in sharp contrast to the general deceleration and downwash that are present in free air. The calculated results indicate that the actual rear portion of the wake probably will, in reality, turn rearward well above the floor and be carried off in such a manner as to approach the floor only asymptotically, if at all.

The flow near the floor in front of the wake is the most complex and the most interesting. At very mild conditions, such as $\chi = 70^{o}$ (figs. 3, 17, and 24), the flow in this region, although slightly slower than in free air, is still predominantly rearward. Thus, the forward portion of the wake will turn rearward at the floor, and the entire wake will travel off above the floor. Under such conditions, the wake will, in all probability, never actually reach the floor. Instead, it will sink until the self-induced vertical velocities of the wake are in equilibrium with the boundary-induced upwash and thereafter will continue in distorted form but with no further downward progress. This behavior is verified by experiment (ref. 16).

When the wake skew angle is depressed to 60^{o} (figs. 4, 18, and 25), the calculated flow ahead of the wake at the floor is observed to be essentially stagnant. The forward edge of the wake, which is carried off with the average of the velocities just inside and just outside the vortex sheet, will still travel rearward; however, the turn rearward would be expected to be sharper and closer to the floor. With more sharply inclined wakes (figs. 6 to 9, 19 to 23, and 26 to 30), the calculated flow in this location is actually directed forward,counter to the prevailing tunnel velocity. The strength and extent of the reversed flow region grows as the wake angle steepens. In addition, the rearward flow just within the wake edge weakens. Finally, at some wake angle in the vicinity of $\chi = 40^{o}$ (figs. 6, 20, and 27) the average longitudinal velocity across the forward edge of the wake passes through zero. For sharper wake angles, below 30^{o} (figs. 7 to 9, 21 to 23, and 28 to 30), the presence of a large standing vortex on the floor is indicated.

On the floor, except near the side boundaries, the flow is essentially identical (figs. 17 to 23) for all constraint configurations considered herein. This result occurs because, at such close proximity, the image directly below the floor, which represents ground effect, is responsible for such large interference velocities that the sum of the effects of all the other images (provided to represent the top and sides of the tunnels) is insignificant by comparison. Near the side constraints, however, there are significant differences (figs. 10 to 30). Compared to ground effect, the flow in the closed tunnel is squeezed inward, and the flow in the closed-on-bottom-only tunnel is drawn outward.

Effect of wake distortions.- The foregoing analysis, which is predicated upon the assumption of a rigid wake, has indicated the presence of a large degree of wake distortion. These distortions must now be examined to determine whether or not the changes in the field caused by the distortions augment or diminish the trends indicated by the simplified theory.

Figure 31 presents a sketch of the deformed and undeformed wakes near the floor. The direction of vorticity in the real wakes and their images in the floor is indicated. In the rear (and also near the sides of the wake for which a similar sketch could be drawn) it is evident that the velocities will be generally increased at the floor and that the increased velocities will cover a larger region of the floor than for the undisturbed case.

In the forward region the flow reversal is augmented. The extent to which the distortion adds to the computed velocities as the wake changes from a rearward deformation at low lift to a forward deformation (as indicated in fig. 31) should be particularly large. As a result, the actual reversal in direction of the wake as C_L increases should occur with a "snap" action. Considerable hysteresis might be expected; that is, if the reversal resulted from a small increase in C_L, a substantially larger decrease in C_L might be required to remove the reversal.

In the presence of a thick boundary layer, considerable local unsteadiness might be expected at the change in direction of the wake. This unsteadiness may be only local and not be of any consequence at the model. Both before and after the wake reverses there will be a steady flow. Thus, there may be no unsteadiness noted at the model at all, and the presence or absence of unsteadiness is no criterion as to the presence or absence of the phenomenon.

Most of the features of the flow that have just been discussed have been observed experimentally. (See, for example, refs. 18 to 20.)

Final form of wake.- The forward-going portion of the wake is overrun by the free-stream velocity and is immediately below a region of upwash. Consequently, a large standing vortex will form on the floor in front of the wake. Even the present rigid-wake calculations indicate this behavior (figs. 7 to 9 and 28 to 30), and the effect of wake distortion is to magnify the result.

The general nature of the flow on the floor (figs. 17 to 30) is such as to transport this rolled-up vorticity sidewards and rearward along a more-or-less parabolic path. This path will be somewhat narrower in the closed tunnel, and somewhat wider in the closed-on-bottom-only tunnel, than in ground effect. In ground effect, the path of the vorticity will continue smoothly beyond the region for which results are presented in figures 3 to 30. In the tunnel with open sides (parts (d) of figs. 3 to 30), the consequent path of the vorticity after reaching the sides of the tunnel is somewhat problematical and this path can probably be determined only by experiment. In the closed tunnel the vorticity, upon nearing the walls, will be predominantly influenced by its own image in the walls (not present in the theoretical treatment) which will drive the rolled-up vorticity up the walls as it passes rearward. A sketch of the resulting wake pattern is presented in figure 32.

Many experimental studies indicate that the indicated wake shape is correct. The flow studies of reference 16 clearly show the rolled-up vorticity flowing upward along the sides of the tunnel; unfortunately however, the windows of the tunnel used for the studies reported in reference 16 were too small to show the behavior on the floor. Reference 19 presents sketches of the observed flow, which, in the fully developed state, are essentially identical to figure 32. (See, in particular, fig. 10 of ref. 19.)

Reference 21 presents tuft-grid flow studies of a helicopter rotor in a 30 by 60 foot (9 by 18 meter) closed-on-bottom-only wind tunnel. Figure 33 presents a comparison of the calculated flow and the observed flow. The general nature of the field is represented reasonably well by the theory, with the experimental rollup, as expected, being somewhat more severe than indicated by the theory. At the location of the tuft-grid, about 2 feet (0.6 meter) to the side of the center of the tunnel, the flow should be essentially similar to that in either ground effect or in a closed tunnel.

Although the treatment herein is specifically for rotors, it is noted that the same general results should be obtained for any high-lift system. This observation is verified by wind-tunnel studies of fan-in-wing models (ref. 19), rotors and lifting propellers (refs. 5 and 20), and jet-flap models (refs. 15 and 18), as well as ground-effect studies of tilt-wing (ref. 22) and deflected-slipstream (ref. 23) aircraft. In addition, similar results have been observed in unpublished studies by Eldridge (see ref. 24) utilizing jet-lift models.

Effect on wind-tunnel data.- A wind-tunnel flow pattern, similar to that of figure 32, is obviously greatly different than the flow in free air. Consequently, the forces measured on the model will not be representative of those which would be obtained in free air, and it is not possible to directly relate the measured data in any simple manner to an equivalent free-air flight condition.

Since data taken under conditions of this nature are neither valid nor truly useful, it is obvious that there is some limit beyond which tests of a particular model in a particular tunnel cannot be obtained. This limit does not necessarily correspond to the initial behavior of the leading edge of the wake; for example, the large lateral velocities at the edge of the wake near the floor could,for narrow tunnels and wide models, conceivably start the rolled-up vortices of figure 32 even before the leading edge of the wake snaps forward.

The effect at the model of the rolled-up vortices will depend upon their strength (determined by some combination of model size, model forces, and tunnel velocity) and their location with respect to the model (determined by some combination of model size, tunnel size, tunnel velocity, and tunnel proportions). One parameter which indirectly incorporates many of these test conditions has been shown in reference 24 to correlate the "limit" data of reference 5. This is the ratio of the impingement distance of the wake on the floor behind the model to the model span, or

$$\frac{x_f}{b} = \frac{h}{b} \tan \chi \tag{5}$$

The actual correlation is shown in figure 34 where it may be seen that x_f/b, for the data of reference 5, falls into two bands (dependent upon the presence or absence of large fillets in the tunnel corners) which are a function of the wind-tunnel proportions only. Two additional points indicated on the figure show that essentially the same limiting values are obtained for a jet-flap model (ref. 15) and a tilt-wing model (ref. 25).

The data of reference 5 were all obtained near zero drag-lift ratios ($\alpha = 3^{\circ}$, so that $D/L \approx 0.05$), and little experimental evidence is available at other drag-lift ratios. The point shown for the jet-flap model was obtained at $D/L \approx 0.3$ and provides an indication that, at least, in this range D/L has little effect other than its influence on χ. (See eq. (A5) of appendix A.) A certain amount of caution should be used in extrapolating to extremely different conditions in using equation (5).

Equation (5) indicates that testing may be extended to higher lifts or lower speeds if the height of the model above the floor is increased. Experimental confirmation of this result has been obtained recently (ref. 20).

Corrections for extreme conditions.- Conceptually at least, it is possible to include the actual self-induced wake distortions in the wall-interference theory and to obtain the wall-induced interference as the difference between the free-air and wind-tunnel fields. Initial efforts in this direction for moderately heavily loaded wings have already been published (refs. 26 and 27). Under conditions as severe as those considered herein, the analysis would be considerably more involved than in recent so-called free-wake analyses (such as ref. 28). Even presuming that convergent numerical results were obtained, there is considerable doubt that the large field distortions obtained could be converted into satisfactory data corrections (refs. 5 and 24). In any event, such an effort would appear uneconomic in relation to the storage and speed available in current digital computers.

Calculations Based on Doublet-String Wakes

At this point it would be desirable to survey a number of conditions other than the one treated so far. Unfortunately, such a survey is not economically feasible with the program of appendix C which, on the CDC 6600 computer, requires approximately 0.3 minute per point (or 5 hours for fig. 24). A faster, although also somewhat limited method, is developed and used in the succeeding portions of this paper.

Calculation procedures.- Fundamentally, reference 2 develops wall effects by considering the limiting case of a vanishingly small model as represented by a wake that is an inclined line density distribution of doublets. Finite-size models can be treated in this method by superposing the computer interference fields of a suitable assemblage of such doublet-string wakes (refs. 2 to 4).

Figure 35 shows the pattern of doublet-string wakes used in references 3 and 4 to represent a rotor of finite size and compares this assemblage to the uniform skewed vortex cylinder employed in appendix B. In the limit, if an infinite number of doublet strings distributed uniformly through the cylinder were employed, the field would be identically that of the cylinder. Indeed, a more elaborate version of this technique has been used to calculate rotor blade loads (ref. 29). However, when only 20 strings are employed, as in references 3 and 4, the field within and very near the wake will be somewhat "lumpy" compared to that of the vortex cylinder. Normally, however, distances this close to the wake are not involved in wall-effect calculations.

The treatment of references 3 and 4 is not limited to zero angle of attack as is the theory presented in appendix B. Although identical superposition techniques are used (see ref. 2), the individual semi-infinite doublet strings, each representing only a small part of the wake, are independently truncated at the floor. Nonuniformity of load distribution requires no significant increase in computer time since the effect of a nonuniform load distribution is represented by a simple rearrangement of the assemblage of doublet strings (ref. 3).

Because of the lumpiness of the field of the doublet-string model, the velocities produced by the rotor itself must be obtained from the vortex-cylinder model. For angles of attack other than zero, the wake skew angle, distances, and velocities, all of which are determined from an axis system embedded in the tip-path plane, must be properly adjusted to correspond with the wind-tunnel axes.

Since the representation of the real rotor wake is different from that of its images, erroneous results will be obtained at the immediate intersection of the real wake and the image wake below the floor. Since none of the doublet strings in the arrangement used in references 3 and 4 lie on the longitudinal axis of the wake, the computed velocities on this axis are relatively lower than they should be. Thus the combination of the two representations on the floor should indicate a flow through the floor. This effect will cover the greatest region when the wake and its image graze along the floor at high wake skew angles and, the affected region will diminish with decreasing skew angles. In the flow charts presented herein the most obviously incorrect of the flow vectors affected by this mismatch have been deleted, although vestiges of the aforementioned behavior remain.

Because of the deleted vectors near the floor there is a substantial loss of precision in the most interesting region of the flow. Certain conclusions can be drawn, however, from the nearby flow.

The theoretical treatment of references 2 to 4 does not include the lateral component of wall-induced interference. While this component could be obtained by differentiating equations (1) and (7) of reference 2 with respect to y and then proceeding as in appendix B, the effort does not appear to be productive because of the aforementioned imprecision in the most interesting region of the flow. Instead, the present results will be confined to the X-Z plane of the tunnel where symmetry requires that the lateral interference velocities are zero.

The required modifications to the program of appendix K of reference 4 are straightforward with the real wake being incorporated from reference 10 by means of subroutines RTRLØAD and ROTVEL which are given as part of appendix C in this paper. Consequently, a complete listing of the program is not included herein. The complete program, running on the CDC 6600 computer requires about 1/2 second per point (compared to 0.3 minute for the program of appendix B). Results for a triangular disk-load distribution require about 10 percent more time, solely spent in evaluating the field of the real wake.

Figures 36 to 125 present flow charts, based on a doublet-string representation of the wake, for a wide variety of operating conditions and rotor and wind-tunnel configurations. Table II, which serves as an index to these figures, also presents the calculated average boundary-induced interference as obtained from appendix H of reference 4.

Comparison of results from two methods.- Figures 37, 40, 43, and 45, prepared using the doublet-string wake, are otherwise identical to figures 3, 5, 7, and 9, respectively, which were prepared using vortex-cylinder wakes. Comparison of the corresponding figures of these sets indicates that the results are practically identical.

Effect of constraint configuration.- Although there are significant differences throughout the remainder of the flow, the flow near the floor is essentially identical for the three constraint configurations. (Compare parts (b), (c), and (d) of each figure.) The reason for this behavior is the consistently closed lower boundary in all three configurations.

Effect of wake skew angle.- Comparisons at equal angles of attack, between figures 36 to 125 indicate that the dominant parameter affecting the flow reversal on the floor ahead of the wake is the wake skew angle. Irrespective of the values used for any of the other parameters in the calculation, this flow is never reversed for a skew angle of 70° and is always reversed for a skew angle of 30°. With some allowance for the different location of the constant grid of vector locations with respect to the wake under varying conditions, it would appear that the flow is also always reversed at a wake skew angle of 50°.

The actual rollup of the rotor wake is ignored in the calculated flow. Since the actual wake follows a rearward curving path as it rolls up and since this path should, for an otherwise constant model, be a function of only the model dimensions, it would be anticipated that the actual local wake skew angle near the floor will be larger for small models than for large models. Further, since the predominant influence on the flow is the image in the floor, and even more specifically, those portions of this image nearest the floor, a certain interrelationship between size and wake angle should be observed in the real wind tunnel. Although the wake angle will still be the predominant influence, the required wake skew angle, as computed at the rotor, may be somewhat smaller for smaller models.

Effect of angle of attack (D/L).- The effects of large excursions in angle of attack (corresponding to large changes in D/L) are shown in figures 36 to 125 to be relatively small for a constant wake angle. This observation is particularly true when the large requisite changes in force coefficients are considered (table II). At constant wake angle, the strength and extent of the region of reversed velocity ahead of the wake are slightly decreased for negative angle of attack and slightly increased for positive angle of attack.

On the other hand, the rearward velocities within the wake are increased substantially at negative angles and correspondingly decreased at positive angles. Since the point at which the wake flips forward rather than rearward depends upon the average longitudinal velocity on each side of the vortex sheet, a somewhat steeper wake angle will be required for wake reversal at large negative α. Consequently, at wake reversal, the reversed region ahead of the wake may, by virtue of the steepened wake angle, be larger and stronger than the corresponding flow at $\alpha = 0^{\circ}$.

The behavior to be expected of the real curved wake is unclear. The vastly increased force coefficients at negative angle of attack will result in a more rigid wake with a larger angle of inclination with respect to the floor. This effect would tend to counter the effect of rollup. The actual behavior probably can only be determined from well-planned experiments.

Effect of model vertical location.- Figures 36 to 65 illustrate the flow for three different vertical locations of the model above the wind-tunnel floor. There is no effect evident on the initial appearance of reversed flow on the floor. The vertical extent of the reversed flow region diminishes somewhat with decreasing model height; however, the decrease in model height is more than adequate to maintain the rotor within the region of maximum disturbance at the lower wake angles.

Considerations of rollup, however, lead to the conclusion that the local wake angle at the floor will be smaller at the higher model locations. Thus, when real wakes are considered, some delay in flow reversal may be expected for high model mountings. This result is indicated from the experiments of reference 20; however, the results presented therein probably are influenced to a greater degree by the subsequent path of the rolled-up vorticity than they are by the initiation of wake reversal.

The flow at the ceiling of the closed tunnel is affected greatly by model height. The tendency of the flow to reverse, and consequently to separate, from the ceiling is increased substantially by raising the model. Thus, there are limits to which the effects of flow reversal can be modified by changes in model height. Too high a model height may produce more severe effects in the tunnel than those which the experimenter is attempting to avoid.

For the range of model heights considered herein, ceiling separation always requires more severe testing conditions than those required to initiate flow reversals. Thus, within these limits, tests conducted with larger values of x_f/b than those presented in figure 34 will most likely be safe from the occurrence of ceiling separation.

Effect of rotor load distribution.- The flows shown in figures 66 to 75 for a triangular load distribution may be compared directly with figures 46 to 55 to determine the effect of load distribution. Although major differences due to loading are evident within the wake, any differences in the region of the floor in front of the wake are insignificant.

Effect of relative rotor size.- Figures 76 to 85, 46 to 55, and 86 to 95 present sequences of flow charts which differ only by uniform increments in the ratio of rotor diameter to tunnel width. The overall interference level in the tunnel increases almost, but not quite (see ref. 3), as rapidly as the ratio of rotor area to tunnel area ($\pi\sigma^2\gamma/4$). The reversed flow region at the floor is noticeably stronger and more extensive for the larger rotors; however, there is no significant effect on the wake angle at which the calculated flow initially reverses. As noted earlier, there will be some interaction between rotor size and the local wake angle at the floor (due to rollup) which will result in a somewhat earlier appearance of reversal for larger rotors.

Effect of wind-tunnel proportions.- Figures 96 to 115 present flow charts for a width-height ratio (γ) of 2.0 with σ equal to 0.6 and 0.3. Figures 116 to 125 present similar charts for $\gamma = 0.5$ and $\sigma = 0.6$. Comparisons between these charts and figures 36 to 95 indicate that the net effect of width-height ratio on the flow at the floor is negligible. The effects shown in figures 96 to 126 are almost purely those which would have been expected on the basis of the interrelated effects of γ and σ in altering A_m/A_T $(=\pi\sigma^2\gamma/4)$ and R/h $(=\sigma\gamma\xi)$. As noted earlier, changes in tunnel proportions will alter the eventual path of the rolled-up vorticity and, in consequence, change the effect on the data.

COMPARISON WITH REFERENCE 18

Results of Reference 18

Using tufts and smoke streamers, reference 18 has studied the conditions under which "flow separation" initially occurs on the floor of a closed wind tunnel for jet-flap models. The correlation of such conditions is presented in terms of a lift coefficient C_{Lhb} based on the tunnel cross-sectional area below and within the wing span. The results are a function of the model drag-lift ratio, where, being the total balance force, the drag is the total drag. (Note that there will be some difference expected between this drag-lift ratio and the drag-lift ratio, defined in terms of induced drag, used in the remainder of the paper. This difference is ignored herein, since the profile portion of the experimental drag, including separation, cannot be estimated adequately.) The resulting critical values of C_{Lhb} are given in reference 18 as

$$C_{Lhb} = 3.0 \qquad \left(-1.0 \leqq \frac{D}{L} \leqq 0\right) \tag{6a}$$

$$C_{Lhb} = \frac{3.0}{\sqrt{1 + 4\left(\frac{D}{L}\right)^2}} \qquad \left(0 \leqq \frac{D}{L} \leqq 0.6\right) \tag{6b}$$

Techniques of Reference 18

Since reference 18 is concerned solely with the appearance of anomalous effects on the tunnel floor, it would appear at first glance to be ideal for correlation with the present theoretical study. Unfortunately, several features of the techniques used in reference 18 tend to cloud the comparison.

First, the results of reference 18 are based on tufts on the floor and smoke streamers introduced along the floor. Thus, at best, the point of "initial separation" most likely coincides with the initial appearance of a reversed flow region ahead of the wake rather than with the actual reversal of the wake itself. Information as to the behavior of the wake is absent, although it could have been obtained by introducing smoke into the wake at the model.

Secondly, there was a boundary layer of unknown thickness and condition present on the floor during the tests. As shown in reference 30, it is possible for the disturbance at the floor to propagate forward through the low-energy flow of the boundary layer with marked effects on the resultant flow. One solution to this problem is to eliminate the boundary layer on the flow by a technique such as that of references 31 and 32; however, such an approach would have been clearly beyond the scope of reference 18.

Finally, the models, which were all jet-flapped wings were somewhat limited in performance. Large negative drag-lift ratios can only be obtained at very low tunnel velocities and with large negative angles of attack. The low speeds present considerable difficulty in measuring the actual tunnel velocity, particularly in the presence of tunnel flows which may be reversed locally; the large negative angles of attack imply leading edge separation with a consequent "bluff-body" wake and large blockage.

Nevertheless, no alternate study is available which addresses itself so closely to the effects treated herein. The foregoing effects should be kept in mind throughout the subsequent discussion.

Comparison at $D/L = 0$

For zero drag, equation (A21) of appendix A shows that C_{Lhb} may be expressed as

$$C_{Lhb} = \frac{\pi(b/h)}{\tan\chi \sin\chi} \tag{7}$$

Equation (7) may be solved for b/h with $C_{Lhb} = 3.0$ to obtain the limiting span-height ratio at zero drag as

$$\frac{b}{h} = \frac{3}{\pi}\tan\chi \sin\chi \tag{8}$$

Equation (5), used earlier to correlate the data given by Rae in reference 5, similarly may be solved for the maximum allowable span-height ratio as

$$\frac{b}{h} = \frac{\tan\chi}{\left(x_f/b\right)} \tag{9}$$

If it is noted that x_f/b ranges between about 1.25 and 2.0 (fig. 34), and that the wake angles corresponding to Rae's limits (ref. 5) are on the order of 30^{o} to 60^{o}, equations (8) and (9) appear to lead to the same order of maximum allowable span. The comparison, however, is probably not legitimate since South in reference 18 was concerned solely with an initial disturbance at the floor, whereas Rae in reference 5 was concerned with determining the point at which wind-tunnel disturbances had grown so large that his force data was affected to a noticeable degree. The disparity of definition is obvious in equations (8) and (9). In agreement with the present theoretical study, equation (8) shows that there is no dependence whatever on the wind-tunnel proportions. As discussed previously, the effect on the data will be a function of the path of the entire rolled-up vortex system within the tunnel and this path in turn will be a function of the wind-tunnel proportions. This dependence is inherent in equation (9) since x_f/b is a function of the tunnel width-height ratio (fig. 34).

South's experiment (ref. 18) is more nearly comparable with the present study. Observe that for zero drag, equations (7) and (8) indicate that South's limit is primarily dependent on wake skew angle. A dependence on the span is also noted. As discussed previously (under the heading "Effect of Wake Skew Angle"), a similar dependence would be expected from the theory if wake rollup were considered.

Comparison at Positive D/L

Figure 126 compares South's limit (eq. (6b)) with the calculated values of C_{Lhb} (eq. (A21)) for a series of constant wake skew angles and three values of b/h. Irrespective of b/h, it may be seen that, for positive D/L, South's limit corresponds to a constant wake skew angle within the accuracy of the data of reference 18. (The data given in that paper scatter about the correlating curve by about ±0.5 in terms of C_{Lhb}.) There is, of course, a relationship between the wake angle and the span-height ratio in figure 126. At least in direction, this relationship is that which was anticipated earlier by considering the effect of rollup on the local wake angle near the floor.

Comparison at Negative D/L

The constant limiting value of $C_{Lhb} = 3.0$ for negative D/L is in glaring contrast to the behavior of the limiting values obtained under positive D/L conditions. There is no dependence of C_{Lhb} on the wake skew angle, whereas, even considering wake rollup, the theoretical study presented herein indicates that the flow reversal should still occur at a nearly constant wake angle.

The following analysis will indicate that the limits proposed in reference 18 can not be applied to conditions well beyond those examined in that paper; that is, to conditions representing, for example, a propeller in nearly axial flight.

Figure 127 shows the theoretical behavior of C_{Lhb} (for $b/h = 1.0$) at negative drag-lift ratios as great in magnitude as 100. Observe that for any wake angle other than 90^o, C_{Lhb} always becomes infinite at some value of D/L. Equation (A21) of appendix A yields this result since C_{Lhb} will approach infinity as the term $\tan \chi + D/L$ approaches zero. Since $\tan \chi = -\frac{V}{w_0} - \frac{D}{L}$ (eq. (A5) of appendix A), it is obvious that the infinite C_{Lhb} occurs when

$$0 = \tan \chi + \frac{D}{L} = -\frac{V}{w_0} - \frac{D}{L} + \frac{D}{L} = -\frac{V}{w_0}$$

or

$$V = 0 \quad \text{when} \quad \tan \chi = -\frac{D}{L} \tag{10}$$

This result would be anticipated since C_{Lhb}, being based on dynamic pressure, must become infinite under static thrust conditions. Equation (10) merely states the static thrust conditions in terms of χ and D/L. Since C_{Lhb} approaches infinity for $D/L = -\tan \chi$, it must certainly pass through any finite value first. The required value of D/L at constant χ and C_{Lhb} is obtained by solving equation (A21) for D/L to yield

$$D/L = -\tan \chi \pm \sqrt{\left(\pi/C_{Lhb}\right)(b/h)\sec \chi} \tag{11}$$

where the positive sign corresponds to forward flight and the negative sign corresponds to rearward flight which is not under consideration herein.

Figure 128 compares the values of D/L for zero velocity and for $C_{Lhb} = 3.0$. As anticipated, the constant value of C_{Lhb} (obtained for less negative D/L in ref. 18) would imply a flow reversal or "separation" on the floor of the tunnel for all static thrust conditions and for some speed range above $V = 0$, irrespective of model size, even if the model (a propeller, for example) were only slightly misalined with respect to the flow.

It should be observed that reference 18 notes that "The initial stages of separation did not necessarily produce a significant flow up the tunnel side walls in the vicinity of the model" (as in fig. 32). Subsequent discussion between the present author and the author of reference 18 has brought out that the quoted behavior was generally the case for negative D/L, but that, in general, abrupt and violent flow up the walls (as in fig. 32) followed the initial separation for positive D/L. Thus, there is a distinct possibility that two totally different phenomena were being observed in the tests of reference 18, with the results at negative drag-lift ratios being a merely local phenomenon resulting from the interaction of the model field with the poorly conditioned boundary layer that would be presumed to exist at such low tunnel speeds.

The disagreement at negative D/L between the present theoretical study and the results of reference 18 probably cannot be resolved until additional experimental evidence becomes available. On the other hand, it is certain that any disturbances resulting in gross deformations of the wake obtained at $C_{Lhb} = 3$ and large negative D/L must occur far downstream of the model; consequently, any effects on the measured model performance should be minor.

WIND-TUNNEL TESTS AT EXTREME CONDITIONS

Performance in Free Air

As is evident in figures 3 to 30 and 36 to 125, the flow near a model is decidedly distorted in the wind tunnel (compared to free air) when the wake deflection is sufficiently great. Even without flow reversal on the floor, small distortions (refs. 26 and 27) can have significant effects. The gross distortions of the wake shown by experiment (refs. 5, 19, and 20) and indicated by the present theoretical treatment when the direction of wake flow is reversed, can, and generally will, produce such large effects on the measured wind-tunnel data that even gross trends in the data must be viewed with skepticism. Tests under these conditions are pointless and should be avoided. If data are required in this regime, which generally encompasses only the very low-speed end of transition flight, several alternatives appear to be available. These include tests of a smaller model in a larger tunnel, the use of a tunnel with more favorable proportions (fig. 34), or outdoor testing with one of the free-flight or test-bed techniques.

The point at which wind-tunnel tests of a particular model should be abandoned can be determined at least roughly from the parameter x_f/b given in figure 34. Although reference 18 appears to yield more restrictive limits at large negative D/L than figure 34, it should be noted that reference 18 is not concerned with the effect on force measurements. The low wake deflections involved in the area of disagreement should result in placing the disturbances too far behind the model to have any significant effect on force measurements.

Wake distortion and its effect on the overall flow in the tunnel is not the only criterion affecting V/STOL wind-tunnel data. Wall corrections, such as those of references 2 to 4, can also become very large and very nonuniform over the model thus effectively distorting the aerodynamic shape of the model (ref. 24) until it no longer represents the geometric model for which data are desired. Indeed, since the flow both far forward of, and far behind, the model must be parallel to the walls, a large average correction always implies a large degree of nonuniformity (ref. 6). For large models, the errors associated with nonuniformity of wall interference may be more restrictive than the onset of extreme wake distortion.

The fact that the wall-interference theory (refs. 2 to 4) actually predicts the correct effects on the overall flow confirms its general applicability. Numerous experimental studies corroborate this result. Indications to the contrary, presented in reference 33, are disposed of in reference 6.

The applicability of the theory of references 2 to 4 is not limited, as suggested in reference 18, to the initial appearance of flow reversal, or separation, on the floor, since the linearly inclined wake of the theory represents a wake which stagnates on the floor at least as well as it represents a wake which curves rearward without touching the floor; indeed the theory even predicts the flow reversal. The initial rollup of the front of the wake on the floor may not have much effect at the model since the image of the rolled-up wake in the floor will tend to cancel the effect of the real wake distortion at the model location. Instead, the limit of applicability of the theory is the point at which the consequent strength and position of the rolled-up vorticity have become such as to affect the data significantly. This point is, of course, that found experimentally by Rae (refs. 5 and 20).

Performance in Ground Effect

The limiting conditions presented in figure 34 do not necessarily apply if the intent of the wind-tunnel tests is to obtain performance in ground effect. Examination of figures 10 to 30 leads to the observation that the flow in the tunnel will differ little from that in ground effect provided that the model span is modest in comparison with the tunnel width. The wake distortions and rollup will still occur, of course, but these distortions are present in ground effect also. Some other limiting condition will eventually be reached when the rolled-up vorticity is essentially at the model station when it starts up the wall; however, the requisite conditions will be substantially more severe than those of figure 34.

If the model is reasonably near the floor, interference at the model for the remaining three boundaries becomes small in comparison with the interference caused by the floor alone. (See ref. 2 and also table II for figs. 36 to 65.) Thus, neither the average wall effects nor their distribution will normally limit the extent of ground-effect tests. Neglect of the effect of the remaining walls is inherent in the data reduction for many tests and has been shown to yield good correlation with flight tests even for extraordinarily severe conditions (e.g., ref. 22).

At short distances from the floor it is necessary to provide some means of eliminating the boundary layer on the floor since this boundary layer and its effect on the flow field are not representative of true flight over a stationary surface. One successful means of treating the boundary layer is discussed in references 31 and 32.

Flow Surveys

Flow surveying, whether quantitatively or qualitatively (flow visualization), under severe conditions presents special problems since the desired information may be that at a point well removed from the model itself. Thus, figure 34, which applies only to force measurements at the model itself, is not applicable for determining limiting conditions for flow surveys. Even for mild conditions, such as in figure 3, the flow angles far down the wake are substantially different from those in free air. Under more severe conditions, such as in figures 7 to 9, there may be little resemblance between the flow in the tunnel and the flow in free air. Flow studies in this range of conditions (ref. 16) are useful only for examining wall effects per se.

On the other hand, the flow in ground effect can be surveyed successfully to a far greater degree in the tunnel. As before, it is necessary for the model to be relatively small in span with respect to the tunnel and for the model relatively near the floor. In addition, care must be taken with the boundary layer on the floor.

Under moderate conditions, flow surveys can be conducted quite successfully for V/STOL models. For example, calculations for the rotors of references 9 and 11 indicate that negligible wall interference was present. This result was obtained only because of the modest rotor size, the modest wake deflection, and the limited region surveyed.

CONCLUDING REMARKS

This study, based upon the theory of NASA TR R-124 and R-302 and an extended version of the theory of NASA TR R-71, indicates that the theory predicts the correct nature of the wake distortions which have been found to occur when testing V/STOL models under extreme conditions. The forward portion of the wake, which for moderate conditions flows rearward with the rest of the wake, will actually turn and flow forward if the overall wake deflection is sufficiently great. The forward-going portion of the wake will then roll up into a standing vortex on the floor, and its subsequent behavior appears to be that required to obtain the limiting conditions for V/STOL testing as found by Rae (Journal of Aircraft, May-June 1967).

Theoretically, the predominant factor determining the initial tendency of the wake to flow forward appears to be the wake skew angle. Considerations of wake rollup indicate that model size and height should also be involved. A theoretical dependence on angle of attack (or, more generally, drag-lift ratio) is indicated; however, the theoretical result might be somewhat altered if wake curvature were considered.

Flow conditions such as to induce ceiling separation in a closed tunnel, and extraordinary distortion of the free streamlines that are the real open boundaries in a closed-on-bottom-only tunnel, are also indicated by the theory. In all cases, however, flow reversal on the floor is indicated as occurring prior to these latter effects.

There is considerable doubt that wind-tunnel data obtained for conditions beyond Rae's limits are valid for free-air conditions. Valid ground-effect data can be obtained well beyond Rae's limits provided certain conditions of model size and height above the floor are met. Some treatment of the boundary layer on the floor will be necessary as well.

The effect of the calculated flow distortions is so great as to cast doubt on the effectiveness of wind-tunnel flow studies at the low-speed end of the transition range unless the results are intended to represent only the flow in ground effect.

Langley Research Center,
National Aeronautics and Space Administration,
Langley Station, Hampton, Va., February 18, 1970.

APPENDIX A

DERIVATION OF OPERATING PARAMETERS IN TERMS OF THE WAKE SKEW ANGLE

Symbols

A	aspect ratio, b^2/S
A_m	momentum area of lifting system
b	span of lifting system
C_D	induced-drag coefficient, D/qS
C_L	lift coefficient, L/qS
C_{Lhb}	lift coefficient based on tunnel cross-sectional area below and within model span, L/qhb
D	induced drag
h	height of model above floor
L	lift
n	ratio of induced velocities in final wake to induced velocities at lifting system
q	dynamic pressure, $\frac{1}{2}\rho V^2$
S	wing, or rotor disk, area
u_0	mean, or momentum theory, value of longitudinal induced velocity (in X-direction) at lifting system, positive rearward
V	forward velocity
V_R	absolute value of the resultant velocity at lifting system

w_0 mean, or momentum theory, value of vertical induced velocity (in Z-direction) at lifting system, positive upward

w_h reference velocity, that value of w_0 which would be obtained in hovering with $D = 0$

X,Y,Z Cartesian coordinate system fixed in model, X positive rearward, Z positive vertically, and Y to form a right-hand system

α angle of attack, positive nose-up

ρ mass density of fluid medium

χ wake skew angle, the angle from the negative Z-axis to the centerline of the wake at the model, positive rearward

Theory

Derivation of V/w_0.- From figure 129, it may be seen that

$$\tan \chi = \frac{V + u_0}{-w_0} = -\frac{V}{w_0} - \frac{u_0}{w_0} \tag{A1}$$

On the assumption that the total mass flow affected by the aerodynamic system is equivalent to that which would pass through area A_m with uniform velocity $V_R = \sqrt{(V + u_0)^2 + (-w_0)^2}$, the lift and induced drag (which may be negative to represent forward thrust) are

$$L = \rho A_m V_R\left(-nw_0\right) \tag{A2}$$

$$D = \rho A_m V_R\left(-nu_0\right) \tag{A3}$$

Dividing equation (A3) by equation (A2) yields

$$\frac{u_0}{w_0} = \frac{D}{L} \tag{A4}$$

so that equation (A1) becomes

$$\tan \chi = -\frac{V}{w_0} - \frac{D}{L} \tag{A5}$$

or

$$\frac{V}{w_0} = -\left(\tan \chi + \frac{D}{L}\right) \tag{A6}$$

In the case of a rotor, the resultant force vector will be, in general, essentially perpendicular to the tip-path plane; thus, for a rotor

$$\frac{D}{L} = \tan \alpha \tag{A7}$$

Substitution of equation (A7) in equation (A6) yields

$$\frac{V}{w_0} = -\left(\tan \chi + \tan \alpha\right) \tag{A8}$$

Derivation of C_L and C_D.- Define a reference velocity w_h as that vertical induced velocity which the system would require to hover with zero speed and induced drag and the same values of n and A_m that pertain in forward flight. From equation (A2) (since w_h is equal to w_0 under the aforementioned conditions)

$$L = \rho A_m |w_h| \left(-n w_h\right) \tag{A9}$$

Solving for w_h yields

$$w_h = -\sqrt{\frac{L}{n\rho A_m}} \tag{A10}$$

where the minus sign is required, since in the present coordinate system, a negative induced velocity (downward) is required to produce a positive lift (upward).

For wings and rotors, n takes the value 2 (that is, in the far wake, the induced velocities are twice those at the lifting system) and the momentum area A_m is essentially that of a circle circumscribing the lateral tips $\left(A_m = \pi b^2/4\right)$. Using these values and the definition of lift coefficient $\left(C_L = L/qS\right)$, equation (A10) may be rewritten as

$$\frac{w_h}{V} = -\sqrt{\frac{C_L\left(\rho/2\right)V^2 S}{2\rho \frac{\pi b^2}{4} V^2}} = -\sqrt{\frac{C_L S}{\pi b^2}} \tag{A11}$$

Now the aspect ratio A of the lifting system is

$$A = \frac{b^2}{S} \tag{A12}$$

so that equation (A11) becomes

$$\frac{w_h}{V} = -\sqrt{\frac{C_L}{\pi A}} \tag{A13}$$

From equation (14) of reference 34

$$|\chi| = \cos^{-1}\left(\frac{w_0}{w_h}\right)^2 \tag{A14}$$

or

$$\frac{w_0}{w_h} = \sqrt{\cos\chi} \tag{A15}$$

Thus, from equations (A13) and (A15)

$$\frac{V}{w_0} = \frac{V}{w_h}\frac{w_h}{w_0} = -\sqrt{\frac{\pi A}{C_L \cos\chi}} \tag{A16}$$

Now equate equations (A6) and (A16) to obtain

$$-\sqrt{\frac{\pi A}{C_L \cos\chi}} = -\left(\tan\chi + \frac{D}{L}\right) \tag{A17}$$

The solution of equation (A17) for C_L is

$$C_L = \frac{\pi A}{\left(\tan\chi + \frac{D}{L}\right)^2 \cos\chi} \tag{A18}$$

For a rotor, which has an aspect ratio of $4/\pi$, equation (A18) becomes

$$C_L = \frac{4}{(\tan\chi + \tan\alpha)^2 \cos\chi} \tag{A19}$$

And, again for a rotor, in consequence of equation (A4) and the definitions of the coefficients

$$C_D = C_L \tan \alpha = \frac{4 \tan \alpha}{(\tan \chi + \tan \alpha)^2 \cos \chi} \tag{A20}$$

Derivation of C_{Lhb}.- Reference 18 defines limiting minimum test speeds in terms of a lift coefficient C_{Lhb} based upon that portion of the cross-sectional area of the tunnel contained beneath the wing span, thus, from equation (A18)

$$C_{Lhb} = \frac{C_L}{A}\left(\frac{b}{h}\right) = \frac{\pi b/h}{\left(\tan \chi + \frac{D}{L}\right)^2 \cos \chi} \tag{A21}$$

APPENDIX B

DERIVATION OF ROTOR INDUCED VELOCITIES IN WIND TUNNELS AND GROUND EFFECT

Symbols

The analysis presented in the following pages is valid only for an angle of attack of zero. In consequence, the wind-tunnel axes are parallel to axes in the rotor tip-path plane. Extrapolation to other angles of attack must be attended with great caution, since the direct extrapolation results in inconsistencies in x, z, α, w_0, μ, λ, and χ.

B — wind-tunnel semiwidth

H — wind-tunnel semiheight

h — height of rotor above floor

m,N,n — integers

p — integer, $p = 1$ for u and $p = 0$ for v and w

q — integer, $q = 0$ for closed tunnel and $q = m + n$ for closed-on-bottom-only tunnel

R — rotor radius

R_c — distance from point at (x,y,z) to edge of rotor disk at ψ, $\sqrt{R^2 + x^2 + y^2 + z^2 - 2R(x \cos \psi + y \sin \psi)}$

r — radius of vortex cylinder

u,v,w — components of induced velocity along the X-, Y-, Z-axes, positive when directed along positive direction of axis

V — forward velocity

w_0 — induced velocity at center of uniformly loaded rotor (equal to mean, or momentum theory value of induced velocity normal to disk (ref. 35)), positive upward

X,Y,Z Cartesian axes centered in rotor, X positive rearward in plane of rotor, Z positive upward normal to plane of rotor, Y in plane of rotor to form a right-hand system

x,y,z distances along X-, Y-, and Z-axes

α angle of attack, positive nose-up ($\alpha = 0^{\circ}$ throughout present analysis)

γ wind-tunnel width-height ratio, B/H

ζ semiheight of wind tunnel divided by height of model above floor, H/h

λ rotor inflow ratio, $\left(V \sin \alpha + w_0\right)/\Omega R$

μ rotor tip-speed ratio, $V \cos \alpha/\Omega R$

$\bar{\nu}$ vectorial induced velocity, $u\bar{i} + v\bar{j}, + w\bar{k}$

σ ratio of rotor radius to tunnel semiwidth, R/B

χ wake skew angle, angle between negative Z-axis and centerline of wake at rotor, positive rearward, $\tan^{-1}(-\mu/\lambda)$ (for $\alpha = 0^{\circ}$)

ψ rotor azimuth angle, positive counterclockwise from downstream position

Ω rotor rotational speed

Subscripts:

G in ground effect

T in tunnel

t for triangular disk-load distribution

trunc for truncated wake

Theory

Uniform disk-load distribution.- As noted in an earlier section, the wake of a uniformly loaded rotor may be represented as a skewed cylindrical surface of uniformly distributed vorticity as in figure 130. Reference 10 obtains the induced velocities $\bar{\nu}(=u\bar{i} + v\bar{j} + w\bar{k})$ of this wake as (note $f(\psi) = 1$ in ref. 10)

$$\frac{u}{w_0} = \frac{1}{2\pi}\int_0^{2\pi} \frac{\left(\frac{z}{R} + \frac{R_c}{R}\cos\chi\right)\cos\chi\,d\chi}{\frac{R_c}{R}\left[\frac{R_c}{R} + \left(\cos\chi - \frac{x}{R}\right)\sin\chi + \frac{z}{R}\cos\chi\right]} \tag{B1}$$

$$\frac{v}{w_0} = \frac{1}{2\pi}\int_0^{2\pi} \frac{\left(\frac{z}{R} + \frac{R_c}{R}\cos\chi\right)\sin\chi\,d\chi}{\frac{R_c}{R}\left[\frac{R_c}{R} + \left(\cos\chi - \frac{x}{R}\right)\sin\chi + \frac{z}{R}\cos\chi\right]} \tag{B2}$$

$$\frac{w}{w_0} = \frac{1}{2\pi}\int_0^{2\pi} \frac{\left[1 - \left(\frac{x}{R}\cos\chi + \frac{y}{R}\sin\chi\right) + \frac{R_c}{R}\sin\chi\cos\chi\right]d\chi}{\frac{R_c}{R}\left[\frac{R_c}{R} + \left(\cos\chi - \frac{x}{R}\right)\sin\chi + \frac{z}{R}\cos\chi\right]} \tag{B3}$$

where equations (B1) and (B2) have been corrected for an error in sign in equations (11) and (13) of reference 10.*

Equations (B1) to (B3) serve to define the rotor field in free air. It is possible to superpose the results to obtain the field in ground effect as indicated in figure 131. The first step is to translate the velocity field downward and rearward to its point of intersection with the floor and then subtract the resulting field from the original free-air field to obtain the field of a truncated wake. Thus, if the free-air field is written symbolically as

$$\frac{\bar{\nu}}{w_0} = \frac{\bar{\nu}}{w_0}\left(\frac{x}{R}, \frac{y}{R}, \frac{z}{R}\right) \tag{B4}$$

the field of the truncated wake becomes

$$\left(\frac{\bar{\nu}}{w_0}\right)_{trunc} = \frac{\bar{\nu}}{w_0}\left(\frac{x}{R}, \frac{y}{R}, \frac{z}{R}\right) - \frac{\bar{\nu}}{w_0}\left(\frac{x}{R} - \frac{h}{R}\tan\chi, \frac{y}{R}, \frac{z}{R} + \frac{h}{R}\right) \tag{B5}$$

*Incorrectly ascribed to sign convention in reference 6.

It is important to note that this truncated wake will coincide with the portion of the wake above the floor only if $\alpha = 0^{\circ}$. For any other value of α, the technique is inappropriate and it would be necessary to return to reference 10 and perform the integrations along the wake to the floor, this distance being a function of azimuth angle and angle of attack. This effort does not seem warranted since the systems of references 2 to 4 will provide adequate results for most practical purposes.

The next step in obtaining the flow field in ground effect is to rotate the field of the truncated vortex cylinder about the longitudinal axis of its intersection with the ground (fig. 131) and add the original and truncated fields. Thus, since the v and w components of the field are reversed in sign during the rotation, the total induced field in ground effect is

$$\left(\frac{\bar{\nu}}{w_0}\right)_G = \frac{\bar{\nu}}{w_0}\left(\frac{x}{R}, \frac{y}{R}, \frac{z}{R}\right) - \frac{\bar{\nu}}{w_0}\left(\frac{x}{R} - \frac{h}{R}\tan\chi, \frac{y}{R}, \frac{z}{R} + \frac{h}{R}\right)$$
$$- (-1)^p \frac{\bar{\nu}}{w_0}\left(\frac{x}{R}, -\frac{y}{R}, -\frac{z}{R} - 2\frac{h}{R}\right)$$
$$+ (-1)^p \frac{\bar{\nu}}{w_0}\left(\frac{x}{R} - \frac{h}{R}\tan\chi, -\frac{y}{R}, -\frac{z}{R} - \frac{h}{R}\right) \tag{B6}$$

where p is an integer equal to 1 for the u component and is zero for the v and w components. For calculations with $\chi = 90^{\circ}$, the wake never reaches the floor so that the second and fourth terms of equation (B6) may be neglected.

Provided that the wind-tunnel floor is closed, the flow field in the wind tunnel is then obtained by reflecting the ground-effect field an infinite number of times in the horizontal and vertical boundaries, as in figure 132, to obtain

$$\left(\frac{\bar{\nu}}{w_0}\right)_T = \sum_{m=-\infty}^{\infty} \sum_{n=-\infty}^{\infty} \left\{(-1)^q \frac{\bar{\nu}}{w_0}\left[\frac{\frac{x}{H}}{\sigma\gamma}, \frac{\frac{y}{H} - 2m\gamma}{\sigma\gamma}, \frac{\frac{z}{H} - 4n}{\sigma\gamma}\right]\right.$$
$$- (-1)^q \frac{\bar{\nu}}{w_0}\left[\frac{\frac{x}{H} - \frac{1}{\zeta}\tan\chi}{\sigma\gamma}, \frac{\frac{y}{H} - 2m\gamma}{\sigma\gamma}, \frac{\frac{z}{H} - 4n + \frac{1}{\zeta}}{\sigma\gamma}\right]$$
$$- (-1)^q(-1)^p \frac{\bar{\nu}}{w_0}\left[\frac{\frac{x}{H}}{\sigma\gamma}, -\frac{\frac{y}{H} - 2m\gamma}{\sigma\gamma}, -\frac{\frac{z}{H} - 4n + \frac{2}{\zeta}}{\sigma\gamma}\right]$$
$$\left. + (-1)^q(-1)^p \frac{\bar{\nu}}{w_0}\left[\frac{\frac{x}{H} - \frac{1}{\zeta}\tan\chi}{\sigma\gamma}, -\frac{\frac{y}{H} - 2m\gamma}{\sigma\gamma}, -\frac{\frac{z}{H} - 4n + \frac{1}{\zeta}}{\sigma\gamma}\right]\right\} \tag{B7}$$

where q is an integer equal to $m + n$ if the tunnel is closed on the bottom only, and q is equal to zero in the case of a closed tunnel.

Notice that at $\chi = 90^{\circ}$, the truncation of the wake occurs infinitely far behind the model. Numerical calculations at $\chi = 90^{\circ}$ can therefore simply delete the second and fourth terms of equation (B7).

Equation (A6) (appendix A) yields a relationship between V and w_0 which may be used to convert equations (B6) and (B7) to yield the field in terms of the free-stream velocity rather than the mean rotor-induced velocity; that is, for $\alpha = 0^{\circ}$

$$\frac{V}{w_0} = -\tan \chi \tag{B8}$$

Thus equations (B6) and (B7) become

$$\left(\frac{\bar{\nu}}{V}\right)_G = -\left(\frac{\bar{\nu}}{w_0}\right)_G \cot \chi \tag{B9}$$

$$\left(\frac{\bar{\nu}}{V}\right)_T = -\left(\frac{\bar{\nu}}{w_0}\right)_T \cot \chi \tag{B10}$$

If the total flow throughout the field is desired, it is only necessary to add $\frac{V}{V} = 1$ to the u component of equations (B9) and (B10).

Triangular disk-load distribution.- In the case of a triangular disk loading, the rotor is represented by a series of concentric skewed cylinders precisely as in reference 9. (See fig. 133.) The outermost cylinder, which has a radius equal to that of the rotor, must have a vorticity strength equal to 1.5 times the vorticity strength of a uniformly loaded rotor if the overall lifts of the rotors are to be equal (ref. 9). The 10 inner cylinders are evenly spaced in radius (starting with $r/R = 0.05$) and each is assigned a vorticity strength of -0.15 in order to reduce the vorticity in a stepwise manner to zero at the hub. Since the dimensions of the fields of the various cylinders differ only by constant factors depending upon the individual cylinder radii, the induced velocities for the entire system of cylinders representing a rotor with a triangular disk-load distribution may be written immediately as

$$\left(\frac{\bar{\nu}}{w_0}\right)_t = 1.5 \frac{\bar{\nu}}{w_0}\left(\frac{x}{R}, \frac{y}{R}, \frac{z}{R}\right) - 0.15 \sum_{N=1}^{10} \frac{\bar{\nu}}{w_0}\left(\frac{\frac{x}{R}}{\frac{r}{R}}, \frac{\frac{y}{R}}{\frac{r}{R}}, \frac{\frac{z}{R}}{\frac{r}{R}}\right) \tag{B11}$$

where

$$\frac{r}{R} = \frac{N}{10} - 0.05$$

In order to obtain the fields of the triangularly loaded rotor in ground effect or in a wind tunnel, it is only necessary to use $\left(\frac{\bar{\nu}}{w_0}\right)_t$ rather than $\frac{\bar{\nu}}{w_0}$ in equations (B6) and (B7).

Conversion to tunnel centered coordinates.- The equations in this appendix are all developed in terms of an axis system centered in the rotor, whereas in the main text it is more convenient to treat an axis system centered in the tunnel. The only difference is in the X-axis which is translated through a distance $H\left(\frac{1}{\zeta} - 1\right)$. Thus, in terms of the tunnel coordinates the values for insertion in the equations of this appendix are

$$\left.\begin{aligned} x &= x_T \\ y &= y_T \\ z &= z_T - H\left(\frac{1}{\zeta} - 1\right) \end{aligned}\right\} \tag{B12}$$

APPENDIX C

FORTRAN PROGRAM FOR COMPUTING THE FLOW IN A WIND TUNNEL CONTAINING A LIFTING ROTOR

THIS PROGRAM WAS WRITTEN IN CDC FORTRAN, VERSION 2.1, TO RUN ON CDC 6000 SERIES COMPUTERS WITH THE SCOPE 3.0 OPERATING SYSTEM AND LIBRARY TAPE. MINOR MODIFICATIONS MAY BE REQUIRED PRIOR TO USE IN OTHER COMPUTERS. THIS PROGRAM HAS BEEN FOUND TO BE SATISFACTORY ON THE AFOREMENTIONED COMPUTERS WHICH CARRY THE EQUIVALENT OF APPROXIMATELY 15 DECIMAL DIGITS. COMPUTERS OF LESSER PRECISION MAY REQUIRE MODIFICATION TO DOUBLE PRECISION IN ORDER TO OBTAIN RESULTS OF EQUAL ACCURACY.

INPUT WILL BE FOUND AT ADDRESS 1 (LINE (C19)), IN FORMAT 100 (LINE (C 107)). THE REFERENCE ORIGIN IS THE CENTER OF THE ROTOR, WHICH IS REQUIRED TO BE AT AN ANGLE OF ATTACK OF ZERO. OUTPUT LOCATIONS (X, Y, AND ZT) ARE WITH RESPECT TO A REFERENCE ORIGIN SHIFTED VERTICALLY TO THE CENTER OF THE WIND TUNNEL. THE REQUIRED INPUT VARIABLES ARE:

LI — LOAD INDICATOR; LI=1 FOR UNIFORM DISK-LOAD DISTRIBUTION, LI=2 FOR TRIANGULAR DISK LOAD DISTRIBUTION. (THE USE OF LI=2 IS NOT RECOMMENDED BECAUSE OF EXCESSIVE RUNNING TIME.)

ZETA — SEMIHEIGHT OF TUNNEL DIVIDED BY HEIGHT OF ROTOR ABOVE FLOOR.

GAMMA — WIDTH-HEIGHT RATIO OF WIND TUNNEL.

SIGMA — RATIO OF ROTOR DIAMETER TO WIND-TUNNEL WIDTH.

CHI — WAKE SKEW ANGLE, DEG.

LOCATE — DISTANCE OF CALCULATION PLANE TO RIGHT OF ORIGIN, BEHIND ORIGIN, OR ABOVE FLOOR (DEPENDING ON MAPTYPE), NONDIMENSIONALIZED WITH RESPECT TO THE TUNNEL SEMIHEIGHT.

MAPTYPE — INSERT LONGITUDINAL, LATERAL, OR FLOOR (LEFT-JUSTIFIED) DEPENDING UPON DESIRED ORIENTATION OF CALCULATION PLANE.

THIS PROGRAM IS NOT SUITABLE FOR CASES WHERE SIGMA IS ZERO SINCE NUMEROUS DIVISIONS BY ZERO WOULD BE REQUIRED IN SUBROUTINE <ROTUN>. CASES WITH CHI EQUAL TO EITHER ZERO OR 90-DEGREES ARE REJECTED. THESE CASES WOULD REQUIRE A DIVISION BY EITHER ZERO OR INFINITY AT LINE (C 85).

```
      PROGRAM ROTWT (INPUT,OUTPUT,TAPE5=INPUT,TAPE6=OUTPUT,PUNCH)
C***********************************************************************
C*                                                                     *
C*        THIS MAIN PROGRAM SETS UP DO-LOOPS TO SCAN THE FLOW IN THE   *
C*    DESIRED REGION OF THE WIND TUNNEL.  IT OBTAINS THE INDUCED FIELD *
C*    IN TERMS OF THE MEAN INDUCED VELOCITY OF THE ROTOR AS WELL AS THE *
C*    COMPLETE FLOW IN TERMS OF THE FREE-STREAM VELOCITY.  A PUNCHED   *
C*    CARD OUTPUT OF THSE LATTER VELOCITIES IS PROVIDED FOR SUBSE-     *
C*    QUENT PROCESSING TO PRODUCE VECTOR PLOTS OF THE FLOW.  (SEE      *
C*    APPENDIX D.)  RESULTS ARE OBTAINED SIMULTANEOUSLY FOR FREE AIR,  *
C*    GROUND EFFECT, THE CLOSED WIND TUNNEL, AND A TUNNEL CLOSED ONLY  *
C*    ON THE BOTTOM.  ALL THREE COMPONENTS OF VELOCITY ARE OBTAINED.   *
C*                                                                     *
C***********************************************************************
      COMMON LI,ZETA,GAMMA,SIGMA,X,Y,Z,UOW,VOW,WOW,VELO(4,3)
      DIMENSION VEL(6),V(3)
      REAL LOCATE
      DATA (VEL(I),I=1,6)/4HU/WO,4HV/WO,4HW/WO,4HU/V ,4HV/V ,4HW/V /
    1 READ (5,100)  LI,ZETA,GAMMA,SIGMA,CHI,LOCATE,MAPTYPE
      IF (EOF,5)  999,2
    2 IF (LI.EQ.2)  GO TO 3
      ALOAD=10H UNIFORM
      GO TO 4
    3 ALOAD=10HTRIANGULAR
    4 WRITE (6,101)  SIGMA,GAMMA,ZETA,ALOAD,CHI
      PUNCH 100,  LI,ZETA,GAMMA,SIGMA,CHI,LOCATE,MAPTYPE
      IF (MAPTYPE.EQ.4HLATE)  WRITE (6,103)  LOCATE
      IF (MAPTYPE.EQ.4HLONG)  WRITE (6,104)  LOCATE
      IF (MAPTYPE.EQ.4HFLOO)  WRITE (6,108)  LOCATE
      WRITE (6,105)
      IQUIT=21
      IF (MAPTYPE.EQ.4HFLOO)  IQUIT=20
      DO 11 I1=1,IQUIT
      IF (MAPTYPE.EQ.4HFLOO)  GO TO 12
      ZT=-1.1+0.1*FLOAT(I1)
      Z=ZT+1.-1./ZETA
      IF (MAPTYPE.EQ.4HLATE)  GO TO 12
      Y=LOCATE
      IEND=25
      GO TO 13
   12 X=LOCATE
      IEND=10.*GAMMA+1.0
      IF (MAPTYPE.EQ.4HLATE)  GO TO 13
      ZT=-1.0+LOCATE
      Z=-1.0/ZETA+LOCATE
      XF=TAN(CHI*0.0174532925199)/ZETA
      IXF=XF
      ISTART=-2+IXF
      X=(FLOAT(ISTART)-0.2)+0.2*FLOAT(I1)
   13 DO 11  I2=1,IEND
      IF (MAPTYPE.NE.4HLONG)  GO TO 15
      X=-2.2+0.2*FLOAT(I2)
      GO TO 16
   15 Y=-0.1+0.1*FLOAT(I2)
      IF (I2.EQ.IEND)  Y=GAMMA
   16 CALL ROTUN  (CHI)
      WRITE (6,106)  X,Y,ZT
```

```
C*******************************************************************
C*                                                                 *
C*   THE FOLLOWING INDUCED VELOCITIES ARE IN TERMS OF WO:          *
C*                                                                 *
C*******************************************************************
      WRITE (6,102) (VEL(J),(VELO(I,J),I=1,4),J=1,3)
C*******************************************************************
C*                                                                 *
C*   NOTE THAT:                                                    *
C*                                                                 *
C*   I=1 IS IN FREE AIR          I=2 IS IN GROUND EFFECT           *
C*   I=3 IS IN CLOSED TUNNEL     I=4 IS IN TUNNEL CLOSED ONLY ON BOTTOM  *
C*                                                                 *
C*   J=1,2,3 ARE U,V, AND W COMPONENTS OF INDUCED VELOCITY         *
C*                                                                 *
C*******************************************************************
      IF (CHI.EQ.90.0)  GO TO 11
      IF (CHI.EQ. 0.0)  GO TO 11
      DO 5 I=1,3
    5 V(I)=VEL(I+3)
C*******************************************************************
C*                                                                 *
C*   CONVERT TO RATIO WITH RESPECT TO V, NOTE V/WO=TAN(CHI)        *
C*                                                                 *
C*******************************************************************
      DO 6  I=1,4
      DO 6 J=1,3
    6 VELO(I,J)=-VELO(I,J)/TAN(CHI*0.0174532925199)
C*******************************************************************
C*                                                                 *
C*   ADD FREE-STREAM VELOCITY TO U COMPONENT                       *
C*                                                                 *
C*******************************************************************
      DO 7  I=1,4
    7 VELO(I,1)=1.0+VELO(I,1)
      WRITE (6,102)   (V(J),(VELO(I,J),I=1,4),J=1,3)
C*******************************************************************
C*                                                                 *
C*   PUNCH OUTPUT FOR SUBSEQUENT PROCESSING                        *
C*                                                                 *
C*******************************************************************
      PUNCH 107,    (X,Y,ZT,((VELO(I,J),I=1,4),J=1,3))
   11 CONTINUE
      GO TO 1
C*******************************************************************
C*                                                                 *
C*   FORMATS                                                       *
C*                                                                 *
C*******************************************************************
  100 FORMAT (I1,F9.3,4F10.3,A4)
  101 FORMAT (1H1///50X*VELOCITIES NEAR A LIFTING ROTOR*///
     133X*SIGMA =*F8.3,10X*GAMMA =*F8.3,10X*ZETA =*F8.3//
     237X,A10,* DISK-LOAD DISTRIBUTION*10X*CHI =*F8.3//)
  102 FORMAT  (5X,A4,4F25.4)
  103 FORMAT (48X*TRANSVERSE SLICE AT X/H =*F9.3//)
  104 FORMAT (47X*LONGITUDINAL SLICE AT Y/H =*F9.3//)
  105 FORMAT (26X*IN FREE AIR*11X*IN GROUND EFFECT*8X*IN CLOSED TUNNEL*
     110X*IN C-O-B TUNNEL*/26X,11(1H-),11X,16(1H-),8X,16(1H-),10X,15(1H-
     2))
  106 FORMAT (//2X*X/H =*F7.3,5X*Y/H =*F7.3,5X*Z/H =*F7.3/)
  107 FORMAT (7F10.4/8F10.4)
  108 FORMAT (41X*HORIZONTAL PLANE AT Z/H =*F9.3* ABOVE FLOOR*//)
  999 STOP
      END
```

```
      SUBROUTINE ROTUN (ANGLE)
C***********************************************************************
C*                                                                     *
C*         THIS SUBROUTINE OBTAINS THE INDUCED VELOCITIES INCLUDING THE *
C*    REAL ROTOR FOR THE IMAGE SYSTEMS REPRESENTING THE VARIOUS BOUNDARY*
C*    CONDITIONS.                                                      *
C*                                                                     *
C***********************************************************************
      COMMON LI,ZETA,GAMMA,SIGMA,X,Y,Z,UOW,VOW,WOW,VELO(4,3)
      DO 4  I=1,4
      DO 4  J=1,3
    4 VELO(I,J)=0.0
      IF (ANGLE.EQ.90.0) GO TO 1
      TANC=TAN(ANGLE*0.0174532925199)
    1 AX=X $AY=Y $AZ=Z
      DO 2  M=1,7
      DO 2  N=1,7
      AM=FLOAT(M)-4.
      AN=FLOAT(N)-4.
      X=AX/(SIGMA*GAMMA)
      Y=(AY/(SIGMA*GAMMA))-2.*AM/SIGMA
      Z=(AZ-4.*AN)/(SIGMA*GAMMA)
      CALL RTRLOAD  (ANGLE)
      VELO(3,1)=VELO(3,1)+UOW
      VELO(3,2)=VELO(3,2)+VOW
      VELO(3,3)=VELO(3,3)+WOW
      VELO(4,1)=VELO(4,1)+((-1.)**(M+N))*UOW
      VELO(4,2)=VELO(4,2)+((-1.)**(M+N))*VOW
      VELO(4,3)=VELO(4,3)+((-1.)**(M+N))*WOW
      IF (M.NE.4.OR.N.NE.4) GO TO 3
      VELO(1,1)=VELO(2,1)=UOW
      VELO(1,2)=VELO(2,2)=VOW
      VELO(1,3)=VELO(2,3)=WOW
    3 IF (ANGLE.EQ.90.0) GO TO 5
      X=X-TANC/(SIGMA*GAMMA*ZETA)
      Z=Z+1./(SIGMA*GAMMA*ZETA)
      CALL RTRLOAD  (ANGLE)
      VELO(3,1)=VELO(3,1)-UOW
      VELO(3,2)=VELO(3,2)-VOW
      VELO(3,3)=VELO(3,3)-WOW
      VELO(4,1)=VELO(4,1)-((-1.)**(M+N))*UOW
      VELO(4,2)=VELO(4,2)-((-1.)**(M+N))*VOW
      VELO(4,3)=VELO(4,3)-((-1.)**(M+N))*WOW
      IF (M.NE.4.OR.N.NE.4)  GO TO 5
      VELO(2,1)=VELO(2,1)-UOW
      VELO(2,2)=VELO(2,2)-VOW
      VELO(2,3)=VELO(2,3)-WOW
    5 X=AX/(SIGMA*GAMMA)
      Y=-Y
      Z=(-AZ+4.*AN)/(SIGMA*GAMMA)-2./(SIGMA*GAMMA*ZETA)
      CALL RTRLOAD  (ANGLE)
      VELO(3,1)=VELO(3,1)+UOW
      VELO(3,2)=VELO(3,2)-VOW
      VELO(3,3)=VELO(3,3)-WOW
      VELO(4,1)=VELO(4,1)+((-1.)**(M+N))*UOW
      VELO(4,2)=VELO(4,2)-((-1.)**(M+N))*VOW
      VELO(4,3)=VELO(4,3)-((-1.)**(M+N))*WOW
      IF (M.NE.4.OR.N.NE.4) GO TO 6
      VELO(2,1)=VELO(2,1)+UOW
      VELO(2,2)=VELO(2,2)-VOW
```

```
      VELO(2,3)=VELO(2,3)-WOW                                          (C 182)
    6 IF (ANGLE.EQ.90.0)  GO TO 2                                      (C 183)
      X=X-TANC/(SIGMA*GAMMA*ZETA)                                      (C 184)
      Z=Z+1./(SIGMA*GAMMA*ZETA)                                        (C 185)
      CALL RTRLOAD  (ANGLE)                                            (C 186)
      VELO(3,1)=VELO(3,1)-UOW                                          (C 187)
      VELO(3,2)=VELO(3,2)+VOW                                          (C 188)
      VELO(3,3)=VELO(3,3)+WOW                                          (C 189)
      VELO(4,1)=VELO(4,1)-((-1.)**(M+N))*UOW                           (C 190)
      VELO(4,2)=VELO(4,2)+((-1.)**(M+N))*VOW                           (C 191)
      VELO(4,3)=VELO(4,3)+((-1.)**(M+N))*WOW                           (C 192)
      IF (M.NE.4.OR.N.NE.4) GO TO 2                                    (C 193)
      VELO(2,1)=VELO(2,1)-UOW                                          (C 194)
      VELO(2,2)=VELO(2,2)+VOW                                          (C 195)
      VELO(2,3)=VELO(2,3)+WOW                                          (C 196)
    2 CONTINUE                                                         (C 197)
      X=AX  $Y=AY  $Z=AZ                                               (C 198)
      RETURN                                                           (C 199)
      END                                                              (C 200)


      SUBROUTINE RTRLOAD (ANGL)                                        (C 201)
C*********************************************************************** (C 202)
C*                                                                   * (C 203)
C*       THIS SUBROUTINE PERFORMS A SUPERPOSITION ROUTINE TO OBTAIN  * (C 204)
C*   THE FIELD OF A TRIANGULARLY LOADED ROTOR IF REQUIRED.  THE      * (C 205)
C*   UNIFORMLY LOADED CASE FALLS DIRECTLY THROUGH TO SUBROUTINE      * (C 206)
C*   ROTVEL.                                                         * (C 207)
C*                                                                   * (C 208)
C*********************************************************************** (C 209)
      COMMON LI,ZETA,GAMMA,SIGMA,X,Y,Z,UOW,VOW,WOW,VELO(4,3)           (C 210)
      ACHI=ANGL  $UOWT=VOWT=WOWT=0.0  $AX=X  $AY=Y  $AZ=Z  $NRING=11   (C 211)
      STR=1.0  $IF (LI.EQ.1)  NRING=1  $DO 2  I=1,NRING                (C 212)
      IF (LI.EQ.1)  GO TO 1                                            (C 213)
      AI=FLOAT(I)  $R=0.1*AI-0.05  $X=AX/R  $Y=AY/R  $Z=AZ/R  $STR=-0.15 (C 214)
      IF (I.NE.11)  GO TO 1  $X=AX  $Y=AY  $Z=AZ  $STR=1.5             (C 215)
    1 CALL ROTVEL  (ANGL)                                              (C 216)
      UOWT=UOWT+UOW*STR  $VOWT=VOWT+VOW*STR  $WOWT=WOWT+WOW*STR        (C 217)
    2 CONTINUE  $UOW=UOWT  $VOW=VOWT  $WOW=WOWT                        (C 218)
      RETURN  $END                                                     (C 219)


      SUBROUTINE ROTVEL  (ACHI)                                        (C 220)
C*********************************************************************** (C 221)
C*                                                                   * (C 222)
C*       THIS SUBROUTINE OBTAINS THE INDUCED FIELD OF A UNIFORMLY    * (C 223)
C*   LOADED ROTOR USING THE EQUATIONS OF NASA TN D-394.  SEE NOTE    * (C 224)
C*   FOLLOWING LINE (C 276).                                         * (C 225)
C*                                                                   * (C 226)
C*********************************************************************** (C 227)
      COMMON LI,ZETA,GAMMA,SIGMA,X,Y,Z,UOW,VOW,WOW,VELO(4,3)           (C 228)
      REAL INCRE $TIGHT=0.00001 $RT=X*X+Z*Z $IF(RT.GT.2.0)TIGHT=TIGHT/RT (C 229)
      INCRE=1.0 $INT=4 $ITEST=2 $ITST=1 $RAD=0.0174532925199 $IT=1     (C 230)
```

```
      CHI=ACHI*RAD $IF (Y.LT.0.0.AND.ACHI.EQ.90.0) IT=2 $IF(IT.EQ.2)Y=-Y
      IF (ACHI.LE.90.0) GO TO 1 $ITEST=1 $CHI=(180.0-ACHI)*RAD $Z=-Z
    1 U=V=W=U1=V1=W1=UOW=VOW=WOW=0.0 $FAC=4.0 $PSI1=0.0 $IEND=360
      IF (ACHI.EQ.90.0) GO TO 2 $RW=Y*Y+(X+Z*TAN(CHI))**2-1.0
      IF (ABS(RW).LT.0.0001.AND.Z.LE.0.0) GO TO 3
    2 IF (ACHI.NE.90.0.OR.Y.GT.1.0) GO TO 7
      IF (ABS(Z).GT.0.00001.OR.Y.EQ.0.0) GO TO 7 $RR=X*X+Y*Y
      IF (RR.GT.1.0.AND.X.LT.0.0) GO TO 7
      IF (RR.GT.1.0.AND.X.GT.0.0) GO TO 4 $PSI1=180.0-ASIN(Y) $GO TO 7
    3 ZZ=X+Z*TAN(CHI) $PSI1=ATAN2(Y,ZZ) $GO TO 7
    4 DANGL=90.0-ASIN(Y)/RAD $IANGL=DANGL $INCRE=DANGL/FLOAT(IANGL)
      INT=1 $FAC=1.0 $IEND=2*IANGL+1 $GO TO 7
    5 INT=2 $GO TO 7
    6 INT=3 $IEND=363-4*IANGL $INCRE=(360.0-4.0*DANGL)/FLOAT(IEND-1)
    7 DO 19 I=1,IEND $PSI=FLOAT(I)*RAD+PSI1
      IF (INT.EQ.1) PSI=(90.0-INCRE*FLOAT(I-1))*RAD
      IF (INT.EQ.2) PSI=(90.0+INCRE*FLOAT(I-1))*RAD
      IF (INT.EQ.3) PSI=(90.0+2.0*DANGL+INCRE*FLOAT(I-1))*RAD
      SC=SIN(CHI) $CC=COS(CHI) $SP=SIN(PSI) $CP=COS(PSI)
      RC=SQRT(1.0+X*X+Y*Y+Z*Z-2.0*(X*CP+Y*SP))
      IF (RC.LT.0.00001) GO TO 9 $B=RC+(CP-X)*SC+Z*CC
      IF (ABS(B).LT.TIGHT) GO TO 10$A=1.0-(X*CP+Y*SP)+RC*SC*CP
      C=CP*(Z+RC*CC) $D=SP*(Z+RC*CC)
      U1=C/(B*RC) $V1=D/(B*RC) $W1=A/(B*RC) $GO TO 17
    9 U1=V1=W1=0.0 $IF (ACHI.NE.90.0) GO TO 15 $GO TO 17
   10 IF (ACHI.EQ.0.0) GO TO 14 $IF (ABS(Y).LT.0.00001) GO TO 13
   11 UB=VB=WB=0.0 $DO 12 J=1,2 $PSII=PSI-0.1*RAD
      IF (J.EQ.2) PSII=PSI+0.1*RAD
      RC=SQRT(1.0+X*X+Y*Y+Z*Z-2.0*(X*COS(PSII)+Y*SIN(PSII)))
      A=1.0-(X*COS(PSII)+Y*SIN(PSII))+RC*COS(PSII)*SC
      B=RC+(COS(PSII)-X)*SC+Z*CC $C=COS(PSII)*(Z+RC*CC)
      D=SIN(PSII)*(Z+RC*CC) $UA=C/(B*RC) $VA=D/(B*RC) $WA=A/(B*RC)
      UB=UB+UA $VB=VB+VA $WB=WB+WA
   12 CONTINUE $U1=UB/2.0 $V1=VB/2.0 $W1=WB/2.0
      IF (ITST.EQ.2) GO TO 16 $GO TO 17
   13 V1=0.0 $U1=X*SC*CC/(1.0-X*CP) $W1=1.0+X*SC*CP/(RC*(X-RC*SC))
      GO TO 17
   14 U1=-X/Z $V1=-Y/Z $W1=1.0 $GO TO 17
   15 AX=X $AZ=Z $Z=Z-100. $X=X-Z*SC/CC $ITST=2 $GO TO 11
   16 U1=U1/2.0 $V1=V1/2.0 $W1=W1/2.0 $X=AX $Z=AZ $ITST=1
   17 IF (INT.NE.4.AND.I.EQ.IEND) FAC=1.0 $UOW=UOW+U1*FAC*INCRE
      VOW=VOW+V1*FAC*INCRE $WOW=WOW+W1*FAC*INCRE
      IF (FAC.EQ.4.0) GO TO 18 $FAC=4.0 $GO TO 19
   18 FAC=2.0
   19 CONTINUE $IF (INT.EQ.1) GO TO 5 $IF (INT.EQ.2) GO TO 6
   20 UOW= UOW/1080.0 $VOW= VOW/1080.0 $WOW=WOW/1080.0
C***********************************************************************
C*                                                                     *
C*        NOTE THAT U/WO AND V/WO HAVE BEEN CORRECTED FOR AN ERROR     *
C*   IN SIGN IN EQUATIONS (11) AND (13) OF NASA TN D-394.              *
C*                                                                     *
C***********************************************************************
      IF (ITEST.EQ.1) Z=-Z $IF (IT.EQ.2) GO TO 21 $GO TO 22
   21 Y=-Y $VOW=-VOW
   22 RETURN $END
```

APPENDIX D

FORTRAN PROGRAM TO PREPARE CALCOMP TAPE FOR PLOTTING FLOW VECTORS

THE FOLLOWING PROGRAM IS THE MOST GENERAL OF THOSE USED TO PREPARE THE FLOW VECTOR FIGURES PRESENTED IN THIS PAPER. SINCE THE SOFTWARE ASSOCIATED WITH THE PLOTTERS IN OTHER COMPUTER INSTALLATIONS MAY VARY WIDELY, NO ATTEMPT IS MADE HEREIN TO PROVIDE THE LIBRARY SUBROUTINES FROM THE LANGLEY RESEARCH CENTER OF NASA. SINCE IT IS BELIEVED THAT MOST COMPUTING CENTERS WILL HAVE EQUIVALENT SUBROUTINES, THE FOLLOWING DESCRIPTIONS MERELY STATE THE FUNCTION OF THE SUB-ROUTINES AS USED HEREIN:

AXES	DRAW A TIC-MARKED AXIS, WITH VALUES AT THE TIC-MARKS, AND IDENTIFY THE AXIS.
CALPLT	MOVE PEN TO SPECIFIED X-Y COORDINATES.
CIRCLE	DRAW A SEMICIRCLE COUNTERCLOCKWISE FROM INITIAL X-Y COORD-INATES.
LINE	DRAW A CONTINUOUS LINE THROUGH AN ARRAY OF POINTS. (TWO ADDITIONAL FINAL POINTS SPECIFYING SCALES AND THE ORIGIN MUST ALSO BE GIVEN.)
NOTATE	DRAW ALPHANUMERIC INFORMATION FOR LABELLING.
NUMBER	CONVERT A FLOATING-POINT NUMBER TO ALPHANUMERIC INFORMA-TION, AND THEN DRAW FOR LABELLING.
PARROW	DRAW AN ARROW FROM ONE SET OF X-Y COORDINATES TO ANOTHER WITH AN ARROWHEAD OF SPECIFIED LENGTH.

INPUT TO THE PROGRAM WILL BE FOUND AT LINES (D 33), (D 35), AND (D 72). WITH THE EXCEPTION OF THE FIRST CARD, WHICH PROVIDES A FIGURE NUMBER, THE INPUT DATA IS PRECISELY THAT OBTAINED AS OUTPUT FROM THE PROGRAM OF APPENDIX C.

```
      PROGRAM CYLPLOT(INPUT,OUTPUT,TAPE5=INPUT,TAPE6=OUTPUT)              (D  1)
C******************************************************************      (D  2)
C*                                                                *      (D  3)
C*      THIS PROGRAM PREPARES A CALCOMP TAPE FOR PLOTTING THE FLOW *      (D  4)
C* VECTORS THROUGHOUT A PLANE NEAR A ROTOR IN AN ASSORTMENT OF WIND *    (D  5)
C* TUNNEL CONFIGURATIONS.  THE BASIC FLOW IS CALCULATED SEPARATELY *     (D  6)
C* IN THE MANNER OF NASA TR R-71, BUT WITH THE LONGITUDINAL AND    *     (D  7)
C* LATERAL VELOCITIES ADDED BY THE USE OF THE EQUATIONS OF NASA TN *     (D  8)
C* D-394.  PLANES MAY BE LONGITUDINAL, TRANSVERSE, OR THE FLOOR.   *     (D  9)
C*                                                                *      (D 10)
C******************************************************************      (D 11)
      DIMENSION VELO(4,3),XC(6),YC(6),XD(75),YD(75),SAV1(21,25),          (D 12)
     1    SAV2(21,25),SAV3(21,25),SAV4(21,25),SAV5(21,25),SAV6(21,25),    (D 13)
     2    SAV7(21,25),SAV8(21,25),SAV9(21,25),SAV10(21,25),SAV11(21,25),  (D 14)
```

```
     3    SAV12(21,25),SAV13(21,25),SAV14(21,25),SAV15(21,25)
      REAL  LOCATE
C**********************************************************************
C*                                                                   *
C*      INITIALIZE PLOTTER.                                          *
C*                                                                   *
C**********************************************************************
      CALL CALCOMP
      CALL LEROY
      CALL CALPLT (0.,0.,3)
      CALL CALPLT(0.,5.,3)
      PI=3.14159265358979
C**********************************************************************
C*                                                                   *
C*      READ IN FIGURE NUMBER AND THE VARIABLES FOR WHICH THE        *
C* VECTORS ARE COMPUTED.                                             *
C*                                                                   *
C**********************************************************************
    8 READ (5,107)  FIGURE
      IF (EOF,5)  999,1
    1 READ (5,100)  LI,ZETA,GAMMA,SIGMA,CHI,LOCATE,MAPTYPE
      IF (EOF,5)  999,2
    2 IF (LI.EQ.2)  GO TO 3
      ALOAD=10H UNIFORM
      GO TO 4
    3 ALOAD=10HTRIANGULAR
C**********************************************************************
C*                                                                   *
C*      WRITE OUT THE CASE BEING PLOTTED                             *
C*                                                                   *
C**********************************************************************
    4 WRITE (6,105)  SIGMA,GAMMA,ZETA,ALOAD,CHI
      IF (MAPTYPE.EQ.4HLATE)  WRITE (6,103)  LOCATE
      IF (MAPTYPE.EQ.4HLONG)  WRITE (6,104)  LOCATE
      IF (MAPTYPE.EQ.4HFLOO)  WRITE (6,106)
      WRITE (6,108)  FIGURE
C**********************************************************************
C*                                                                   *
C*      INITIALIZE DO-LOOPS AND POSITION AND VELOCITY DATA.          *
C*                                                                   *
C**********************************************************************
      IQUIT=21
      IF (MAPTYPE.EQ.4HFLOO)  IQUIT=20
      IEND=25
      IF (MAPTYPE.NE.4HLONG)  IEND=10.*GAMMA+1.
      DO 40  I=1,21
      DO 40  J=1,25
   40 SAV1(I,J)=SAV2(I,J)=SAV3(I,J)=SAV4(I,J)=SAV5(I,J)=SAV6(I,J)=
     1SAV7(I,J)=SAV8(I,J)=SAV9(I,J)=SAV10(I,J)=SAV11(I,J)=SAV12(I,J)=
     2SAV13(I,J)=SAV14(I,J)=SAV15(I,J)=0.0
C**********************************************************************
C*                                                                   *
C*      READ IN AND ORGANIZE POSITION AND VELOCITY DATA.             *
C*                                                                   *
C**********************************************************************
      DO 7  I1=1,IQUIT
      DO 7 I2=1,IEND
      READ (5,101)  (X,Y,ZT,((VELO(I,J),I=1,4),J=1,3))
      IF (EOF,5) 999,5
    5 SAV1(I1,I2)=X
      SAV2(I1,I2)=Y
```

```
      SAV3(I1,I2)=ZT
    6 SAV4(I1,I2)= VELO(1,1)
      SAV5(I1,I2)= VELO(1,2)
      SAV6(I1,I2)= VELO(1,3)
      SAV7(I1,I2)= VELO(2,1)
      SAV8(I1,I2)= VELO(2,2)
      SAV9(I1,I2)= VELO(2,3)
      SAV10(I1,I2)=VELO(3,1)
      SAV11(I1,I2)=VELO(3,2)
      SAV12(I1,I2)=VELO(3,3)
      SAV13(I1,I2)=VELO(4,1)
      SAV14(I1,I2)=VELO(4,2)
      SAV15(I1,I2)=VELO(4,3)
    7 CONTINUE
      IF (MAPTYPE.EQ.4HLONG) GO TO 80
      IF (MAPTYPE.EQ.4HFLOO) GO TO 150
C*********************************************************************
C*                                                                   *
C*     THIS SECTION PLOTS A TRANSVERSE PLANE.                        *
C*                                                                   *
C*********************************************************************
      SCALE=0.5
      DO 1000  IPLOT=1,4
      GO TO (31,32,33,34), IPLOT
   31 CALL NOTATE (1.0,-2.25,0.14,15H(A).- FREE AIR.,0.0,15)
      GO TO 35
   32 CALL NOTATE (1.0,-2.25,0.14,20H(B).- GROUND EFFECT.,0.0,20)
      GO TO 35
   33 CALL NOTATE (1.0,-2.25,0.14,20H(C).- CLOSED TUNNEL.,0.0,20)
      GO TO 35
   34 CALL NOTATE (0.5,-2.25,0.14,35H(D).- CLOSED-ON-BOTTOM-ONLY TUNNEL.
     1   ,0.0,35)
   35 GO TO (250,251,251,251), IPLOT
  250 CALL NOTATE (-1.5,-2.75,0.10,7HFIGURE ,0.0,7)
      CALL NUMBER (999.,999.,0.10,FIGURE,0.0,0)
      GO TO 252
  251 CALL NOTATE (1.0,-2.75,0.14,7HFIGURE ,0.0,7)
      CALL NUMBER (999.,999.,0.14,FIGURE,0.0,0)
  252 GO TO (36,37,37,38),IPLOT
   36 CALL NOTATE (999.,999.,0.10,46H- FLOW VECTORS IN A TRANSVERSE PLAN
     1E AT X/H = ,0.0,46)
      CALL NUMBER (999.,999.,0.10,LOCATE,0.0,3)
      CALL NOTATE (999.,999.,0.10,36H, CALCULATED USING VORTEX CYLINDERS
     1.,0.0,36)
      CALL NOTATE (-1.5,-3.0,0.10,63HLOCATION OF ROTOR AND INTERSECTION
     1OF WAKE AND PLANE ARE SHOWN.,0.0,63)
      GO TO 30
   37 CALL NOTATE (999.,999.,0.14,12H- CONTINUED.,0.0,12)
      GO TO 30
   38 CALL NOTATE (999.,999.,0.14,12H- CONCLUDED.,0.0,12)
   30 IF (IPLOT.NE.1)  GO TO 253
      CALL NOTATE (-1.5,-3.25,0.10,7HZETA = ,0.0,7)
C*********************************************************************
C*                                                                   *
C*     THIS NOTATION GROUP IS USED FOR ALL PLOTS.                    *
C*                                                                   *
C*********************************************************************
  129 CALL NUMBER (999.,999.,0.10,ZETA,0.0,3)
      CALL NOTATE (999.,999.,0.10,2H, ,0.0,2)
      CALL NOTATE (999.,999.,0.10,30,0.0,-1)
      CALL NOTATE (999.,999.,0.10,3H = ,0.0,3)
```

```
      CALL NUMBER (999.,999.,0.10,GAMMA,0.0,1)
      CALL NOTATE (999.,999.,0.10,2H, ,0.0,2)
      CALL NOTATE (999.,999.,0.10,40,0.0,-1)
      CALL NOTATE (999.,999.,0.10,3H = ,0.0,3)
      CALL NUMBER (999.,999.,0.10,SIGMA,0.0,2)
      CALL NOTATE (999.,999.,0.10,2H, ,0.0,2)
      CALL NOTATE (999.,999.,0.10,28,0.0,-1)
      CALL NOTATE (999.,999.,0.10,12H = 0.0 DEG, ,0.0,12)
      CALL NOTATE (999.,999.,0.10,43,0.0,-1)
      CALL NOTATE (999.,999.,0.10,3H = ,0.0,3)
      CALL NUMBER (999.,999.,0.10,CHI,0.0,1)
      CALL NOTATE (999.,999.,0.10,4H DEG,0.0,4)
      CALL NOTATE (999.,999.,0.10,18H, UNIFORM LOADING.,0.0,18)
      IF (MAPTYPE.EQ.4HLONG) GO TO 130
      IF (MAPTYPE.EQ.4HFLOO) GO TO 156
  253 XSTART=(GAMMA-1.0)/SCALE
      IF (GAMMA.GT.1.1) XSTART=(GAMMA-2.0)/SCALE
      XSTART1=XSTART-0.5
      AXIS=4.
      IF (GAMMA.GT.1.1) AXIS=8.
      CALL AXES(XSTART,4.5,0.0,AXIS,-1.,.5,2.0,2.5,3HY/H,.20, 3)
      CALL AXES(4.,-1.,0.,2.,0.,2.5,.4,2.5,15HVECTOR SCALE, V,.14,-15)
      CALL AXES(XSTART1,0.,90.,4.,-1.,.5,2.0,2.5,3HZ/H,.20,3)
C*********************************************************************
C*                                                                   *
C*       THIS SECTION PLOTS THE ROTOR AND THE INTERSECTION OF THE    *
C* WAKE AND THE PLOTTING PLANE.                                      *
C*                                                                   *
C*********************************************************************
      DO 64 JKLMN=1,4
      HH=(1.0-ZETA)/ZETA
      EDGE=-SIGMA*GAMMA
      IF (LOCATE.LE.EDGE) GO TO 62
      DO 61 JJ=1,73
      AJ=FLOAT(JJ)-1.0
      XD(JJ)=SIGMA*GAMMA*COS(AJ*PI/36.)
      YD(JJ)=(SIGMA*GAMMA*SIN(AJ*PI/36.)-LOCATE)/TAN(CHI*0.0174532925199
     1)+HH
      IF (YD(JJ).GT.HH) YD(JJ)=HH
      IF (YD(JJ).LT.(-1.0).AND.IPLOT.NE.1) YD(JJ)=-1.0
      IF (YD(JJ).LT.(-2.0)) YD(JJ)=-2.0
   61 CONTINUE
      XD(74)=-GAMMA
      YD(74)=-1.0
      XD(75)=YD(75)=SCALE
      CALL LINE(XD,YD,73,1,0,0,0)
   62 XD(1)=SIGMA*GAMMA
      XD(2)=-SIGMA*GAMMA
      YD(1)=YD(2)= HH
      XD(3)=-GAMMA
      YD(3)=-1.0
      XD(4)=YD(4)=SCALE
   64 CALL LINE (XD,YD,2,1,0,0,0)
C*********************************************************************
C*                                                                   *
C*       THIS SECTION PLOTS THE FLOW VECTORS.                        *
C*                                                                   *
C*********************************************************************
   63 DO 70 M=1,21
      DO 70 N=1,IEND
      GO TO (52,53,54,55),IPLOT
```

```
   52 V=SAV5(M,N)
      W=SAV6(M,N)
      GO TO 56
   53 V=SAV8(M,N)
      W=SAV9(M,N)
      GO TO 56
   54 V=SAV11(M,N)
      W=SAV12(M,N)
      GO TO 56
   55 V=SAV14(M,N)
      W=SAV15(M,N)
   56 Q=SQRT(V*V+W*W)
      ALNGTH=.07/SCALE
      IF(Q.LT.0.5) ALNGTH=(.7*Q*.2)/SCALE
      XA=(GAMMA+SAV2(M,N))/SCALE
      XB=(GAMMA+SAV2(M,N)+0.2*V)/SCALE
      YA=(1.0+SAV3(M,N))/SCALE
      YB=(1.0+SAV3(M,N)+0.2*W)/SCALE
      CALL PARROW(XA,YA,XB,YB,-1,ALNGTH)
      IF (N.EQ.1) GO TO 70
C***********************************************************************
C*                                                                     *
C*       NOTE THAT SYMMETRY IS USED TO OBTAIN THE LEFT-HAND HALF OF    *
C* THE PLANE.                                                          *
C*                                                                     *
C***********************************************************************
      XA=(GAMMA-SAV2(M,N))/SCALE
      XB=(GAMMA-SAV2(M,N)-0.2*V)/SCALE
      CALL PARROW(XA,YA,XB,YB,-1,ALNGTH)
   70 CONTINUE
      CALL CALPLT (30.,0.,-3)
 1000 CONTINUE
      GO TO 8
C***********************************************************************
C*                                                                     *
C*       THIS SECTION PRODUCES LONGITUDINAL PLANES.                    *
C*                                                                     *
C***********************************************************************
   80 DO 2000  IPLOT=1,4
      GO TO (21,22,23,24), IPLOT
   21 CALL NOTATE (4.0,-2.25,0.14,15H(A).- FREE AIR.,0.0,15)
      GO TO 25
   22 CALL NOTATE (4.0,-2.25,0.14,20H(B).- GROUND EFFECT.,0.0,20)
      GO TO 25
   23 CALL NOTATE (4.0,-2.25,0.14,20H(C).- CLOSED TUNNEL.,0.0,20)
      GO TO 25
   24 CALL NOTATE (3.5,-2.25,0.14,35H(D).- CLOSED-ON-BOTTOM-ONLY TUNNEL.
     1   ,0.0,35)
   25 GO TO (260,261,261,261), IPLOT
  260 CALL NOTATE (2.0,-2.75,0.10,7HFIGURE ,0.0,7)
      CALL NUMBER (999.,999.,0.10,FIGURE,0.0,0)
      GO TO 262
  261 CALL NOTATE (4.0,-2.75,0.14,7HFIGURE ,0.0,7)
      CALL NUMBER (999.,999.,0.14,FIGURE,0.0,0)
  262 GO TO (26,27,27,28), IPLOT
   26 CALL NOTATE (999.,999.,0.10,48H- FLOW VECTORS IN A LONGITUDINAL PL
     1ANE AT Y/H = ,0.0,48)
      CALL NUMBER (999.,999.,0.10,LOCATE,0.0,3)
      CALL NOTATE (999.,999.,0.10,36H, CALCULATED USING VORTEX CYLINDERS
     1.,0.0,36)
      CALL NOTATE (2.0,-3.00,0.10,49HROTOR AND FRONT AND REAR EDGES OF W
```

```
     1AKE ARE SHOWN.,0.0,49)
      GO TO 29
   27 CALL NOTATE (999.,999.,0.14,12H- CONTINUED.,0.0,12)
      GO TO 29
   28 CALL NOTATE (999.,999.,0.14,12H- CONCLUDED.,0.0,12)
   29 IF (IPLOT.NE.1)  GO TO 130
      CALL NOTATE (2.0,-3.25,0.10,7HZETA = ,0.0,7)
      GO TO 129
  130 CALL AXES(0.,4.5,0.0,10.,-2.,.5,2.0,2.5,3HX/H,.20, 3)
      CALL AXES(.5,-1.,0.,2.,0.,2.5,.4,2.5,15HVECTOR SCALE, V,.14,-15)
      CALL AXES(-.5,0.,90.,4.0,-1.,.5,2.0,2.5,3HZ/H,.20,3)
      SCALE=0.5
C***********************************************************************
C*                                                                     *
C*      THIS SECTION PLOTS THE ROTOR AND THE WAKE EDGES.               *
C*                                                                     *
C***********************************************************************
      XC(1)=(TAN(CHI*0.0174532925199)/ZETA)-SIGMA*GAMMA
      YC(1)=YC(4)=-1.0
      IF (XC(1).LE.3.0) GO TO 41
      YC(1)=(1./ZETA)-(3.0+SIGMA*GAMMA)/TAN(CHI*0.0174532925199)-1.0
      XC(1)=3.0
   41 XC(2)=-SIGMA*GAMMA
      YC(2)=YC(3)=(1./ZETA)-1.
      XC(3)=-XC(2)
      XC(4)=(TAN(CHI*0.0174532925199)/ZETA)+SIGMA*GAMMA
      XC(5)=-2.0
      YC(5)=-1.0
      XC(6)=YC(6)=SCALE
      IF (XC(4).LE.3.0)  GO TO 42
      YC(4)=(1./ZETA)-(3.0-SIGMA*GAMMA)/TAN(CHI*0.0174532925199)-1.0
      XC(4)=3.0
   42 CALL LINE(XC,YC,4,1,0,0,0)
C***********************************************************************
C*                                                                     *
C*      THIS SECTION PLOTS THE FLOW VECTORS.                           *
C*                                                                     *
C***********************************************************************
      DO 99 N=1,25
      DO 99 M=1,21
      GO TO (81,82,83,84) IPLOT
   81 U=SAV4(M,N)
      W=SAV6(M,N)
      GO TO 85
   82 U=SAV7(M,N)
      W=SAV9(M,N)
      GO TO 85
   83 U=SAV10(M,N)
      W=SAV12(M,N)
      GO TO 85
   84 U=SAV13(M,N)
      W=SAV15(M,N)
   85 Q=SQRT(U*U+W*W)
      ALNGTH=.07/SCALE
      IF(Q.LT.0.5) ALNGTH=(.7*Q*.2)/SCALE
      XA=(2.0+SAV1(M,N))/SCALE
      YA=(1.0+SAV3(M,N))/SCALE
      XB=(2.0+SAV1(M,N)+0.2*U)/SCALE
      YB=(1.0+SAV3(M,N)+0.2*W)/SCALE
      CALL PARROW (XA,YA,XB,YB,-1,ALNGTH)
   99 CONTINUE
```

```
      CALL CALPLT (35.,0.,-3)
 2000 CONTINUE
      GO TO 8
C**********************************************************************
C*                                                                    *
C*      THIS SECTION PRODUCES VECTOR PLOTS OF THE FLOW ON THE FLOOR.  *
C*                                                                    *
C**********************************************************************
  150 DO 3000  IPLOT=1,4
      GO TO (151,152,153,154)IPLOT
  151 CALL NOTATE (3.0,-1.75,0.14,15H(A).- FREE AIR.,0.0,15)
      GO TO 155
  152 CALL NOTATE (3.0,-1.75,0.14,20H(B).- GROUND EFFECT.,0.0,20)
      GO TO 155
  153 CALL NOTATE (3.0,-1.75,0.14,20H(C).- CLOSED TUNNEL.,0.0,20)
      GO TO 155
  154 CALL NOTATE (2.5,-1.75,0.14,35H(D).- CLOSED-ON-BOTTOM-ONLY TUNNEL.
     1   ,0.0,35)
  155 GO TO (270,271,271,271), IPLOT
  270 CALL NOTATE (1.0,-2.25,0.10,7HFIGURE ,0.0,7)
      CALL NUMBER (999.,999.,0.10,FIGURE,0.0,0)
      GO TO 272
  271 CALL NOTATE (3.0,-2.25,0.14,7HFIGURE ,0.0,7)
      CALL NUMBER (999.,999.,0.14,FIGURE,0.0,0)
  272 GO TO (171,172,172,173), IPLOT
  171 CALL NOTATE (999.,999.,0.10,33H- FLOW VECTORS IN PLANE OF FLOOR,,
     1     0.0,33)
      CALL NOTATE (999.,999.,0.10,36H  CALCULATED USING VORTEX CYLINDERS
     1.,0.0,36)
      CALL NOTATE (1.0,-2.50,0.10,50HINTERSECTION OF WAKE WITH PLANE OF
     1FLOOR IS SHOWN.,0.0,50)
      GO TO 174
  172 CALL NOTATE (999.,999.,0.14,12H- CONTINUED.,0.0,12)
      GO TO 174
  173 CALL NOTATE (999.,999.,0.14,12H- CONCLUDED.,0.0,12)
  174 IF (IPLOT.NE.1)  GO TO 156
      CALL NOTATE (1.0,-2.75,0.10,7HZETA = ,0.0,7)
      GO TO 129
  156 IFLOOR=TAN(CHI*0.0174532925199)/ZETA
      ISTART=-2+IFLOOR
      START=FLOAT(ISTART)
      CALL AXES(0.,-.5,0.0, 8.,START,.5,2.0,2.5,3HX/H,.20,-3)
      CALL AXES(7.,-1.,0.,2.,0.,2.5,.4,2.5,15HVECTOR SCALE, V,.14,-15)
      CALL AXES(-.5,0.,90.,2.0,0.,.5,2.0,2.5,3HY/H,.20,3)
  158 SCALE=.5
C**********************************************************************
C*                                                                    *
C*      PLOT THE INTERSECTION OF THE WAKE ON THE FLOOR.               *
C*                                                                    *
C**********************************************************************
      ROCIR=RFCIR=SIGMA*GAMMA/SCALE
      XCIR=((TAN(CHI*0.0174532925199)/ZETA)-START)/SCALE+ROCIR
      YCIR=0.
      CALL CIRCLE(XCIR,YCIR,0.0,180.0,ROCIR,RFCIR,3)
```

```
C***********************************************************************
C*                                                                     *
C*      THIS SECTION PLOTS THE FLOW VECTORS.                           *
C*                                                                     *
C***********************************************************************
      DO 199 M=1,20
      DO 199 N=1,IEND
      GO TO (160,161,162,163) IPLOT
  160 U=SAV4(M,N)
      V=SAV5(M,N)
      GO TO 164
  161 U=SAV7(M,N)
      V=SAV8(M,N)
      GO TO 164
  162 U=SAV10(M,N)
      V=SAV11(M,N)
      GO TO 164
  163 U=SAV13(M,N)
      V=SAV14(M,N)
  164 X=SAV1(M,N)
      Y=SAV2(M,N)
      Q=SQRT(U*U+V*V)
      ALNGTH=.07/SCALE
      IF (Q.LT.0.5) ALNGTH=(.7*Q*.2)/SCALE
      XA=(X-START)/SCALE
      XB=(X-START+.2*U)/SCALE
      YA=(      Y)/SCALE
      YB=(      Y+0.2*V)/SCALE
      CALL PARROW (XA,YA,XB,YB,-1,ALNGTH)
  199 CONTINUE
      CALL CALPLT (25.,0.,-3)
 3000 CONTINUE
      GO TO 8
C***********************************************************************
C*                                                                     *
C*      TERMINATE PLOTTING.                                            *
C*                                                                     *
C***********************************************************************
  999 CALL CALPLT(0.,0.,999)
C***********************************************************************
C*                                                                     *
C*      FORMATS.                                                       *
C*                                                                     *
C***********************************************************************
  100 FORMAT (I1,F9.3,4F10.3,A4)
  101 FORMAT (7F10.4/8F10.4)
  103 FORMAT (48X*TRANSVERSE SLICE AT X/H =*F9.3//)
  104 FORMAT (47X*LONGITUDINAL SLICE AT Y/H =*F9.3//)
  105 FORMAT (1H1////50X*VELOCITIES NEAR A LIFTING ROTOR*///
     133X*SIGMA =*F8.3,10X*GAMMA =*F8.3,10X*ZETA =*F8.3//
     237X,A10,* DISK-LOAD DISTRIBUTION*10X*CHI =*F8.3//)
  106 FORMAT (54X*VELOCITIES ON FLOOR*//)
  107 FORMAT  (F10.3)
      END
```

REFERENCES

1. Heyson, Harry H.: Jet-Boundary Corrections for Lifting Rotors Centered in Rectangular Wind Tunnels. NASA TR R-71, 1960.

2. Heyson, Harry H.: Linearized Theory of Wind-Tunnel Jet-Boundary Corrections and Ground Effect for VTOL-STOL Aircraft. NASA TR R-124, 1962.

3. Heyson, Harry H.: Use of Superposition in Digital Computers to Obtain Wind-Tunnel Interference Factors for Arbitrary Configurations, With Particular Reference to V/STOL Models. NASA TR R-302, 1969.

4. Heyson, Harry H.: Fortran Programs for Calculating Wind-Tunnel Boundary Interference. NASA TM X-1740, 1969.

5. Rae, William H., Jr.: Limits on Minimum-Speed V/STOL Wind-Tunnel Tests. J. Aircraft, vol. 4, no. 3, May-June 1967, pp. 249-254.

6. Heyson, Harry H.: The Flow Throughout a Wind Tunnel Containing a Rotor With a Sharply Deflected Wake. Aerodynamics of Rotary Wing and V/STOL Aircraft. Vol. II – Wind Tunnel Testing New Concepts in Rotor Control, Cornell Aeronaut. Lab., Inc., and U.S. Army Aviat. Mater. Lab., June 1969.

7. Coleman, Robert P.; Feingold, Arnold M.; and Stempin, Carl W.: Evaluation of the Induced-Velocity Field of an Idealized Helicopter Rotor. NACA WR L-126, 1945. (Formerly NACA ARR L5E10.)

8. Castles, Walter, Jr.; and De Leeuw, Jacob Henri: The Normal Component of the Induced Velocity in the Vicinity of a Lifting Rotor and Some Examples of Its Application. NACA Rep. 1184, 1954. (Supersedes NACA TN 2912.)

9. Heyson, Harry H.; and Katzoff, S.: Induced Velocities Near a Lifting Rotor With Nonuniform Disk Loading. NACA Rep. 1319, 1957. (Supersedes NACA TN 3690 by Heyson and Katzoff and TN 3691 by Heyson.)

10. Heyson, Harry H.: Equations for the Induced Velocities Near a Lifting Rotor With Nonuniform Azimuthwise Vorticity Distribution. NASA TN D-394, 1960.

11. Heyson, Harry H.: Preliminary Results From Flow-Field Measurements Around Single and Tandem Rotors in the Langley Full-Scale Tunnel. NACA TN 3242, 1954.

12. Heyson, Harry H.: Induced Velocity Near a Rotor and Its Application to Helicopter Problems. Proceedings of the Fourteenth Annual National Forum, Amer. Helicopter Soc., Inc., April 16-19, 1958, pp. 63-71. (Also available as: Induced Flow Near a Helicopter Rotor. Aircraft Engineering, vol. XXXI, no. 360, Feb. 1959, pp. 40-44.)

13. Heyson, Harry H.: An Evaluation of Linearized Vortex Theory as Applied to Single and Multiple Rotors Hovering In and Out of Ground Effect. NASA TN D-43, 1959.

14. Jewel, Joseph W., Jr.; and Heyson, Harry H.: Charts of the Induced Velocities Near a Lifting Rotor. NASA MEMO 4-15-59L, 1959.

15. Heyson, Harry H.; and Grunwald, Kalman J.: Wind-Tunnel Boundary Interference for V/STOL Testing. Conference on V/STOL and STOL Aircraft, NASA SP-116, 1966, pp. 409-434.

16. Lehman, August F.: Model Studies of Helicopter Rotor Flow Patterns in a Water Tunnel. No. 207, 24th Annual National Forum Proceedings, Amer. Helicopter Soc., May 1968. (See also Model Studies of Helicopter Rotor Flow Patterns, USAAVLABS-TR-68-17, U.S. Army, Apr. 1968.)

17. Kuhn, Richard E.; and Naeseth, Rodger L.: Tunnel-Wall Effects Associated With VTOL-STOL Model Testing. AGARD Rep. 303, Mar. 1959.

18. South, P.: Measurements of Flow Breakdown in Rectangular Wind Tunnel Working Sections. Aeronaut. Rep. LR-513 (NRC No. 10616), Nat. Res. Counc. Can. (Ottowa), Nov. 1968.

19. Lazzeroni, F. A.; and Carr, L. W.: Problems Associated With Wind Tunnel Tests of High Disk Loading Systems at Low Forward Speeds. Aerodynamics of Rotary and V/STOL Aircraft. Vol. II – Wind Tunnel Testing New Concepts in Rotor Control, Cornell Aeronaut. Lab., Inc., and U.S. Army Aviat. Mater. Lab., June 1969.

20. Rae, William H., Jr.; and Shindo, Shojiro: Comments on V/STOL Wind Tunnel Data at Low Forward Speeds. Aerodynamics of Rotary Wing and V/STOL Aircraft. Vol. II – Wind Tunnel Testing New Concepts in Rotor Control, Cornell Aeronaut. Lab., Inc., and U.S. Army Aviat. Mater. Lab., June 1969.

21. Jenkins, Julian L., Jr.: Trim Requirements and Static-Stability Derivatives From a Wind-Tunnel Investigation of a Lifting Rotor in Transition. NASA TN D-2655, 1965.

22. Goodson, Kenneth W.: Comparison of Wind-Tunnel and Flight Results on a Four-Propeller Tilt-Wing Configuration. Conference on V/STOL and STOL Aircraft, NASA SP-116, 1966, pp. 51-62.

23. Anderson, Seth B.; and Schroers, Laurel G.: A Review of Facilities and Test Techniques Used in Low-Speed Flight. Ann. N.Y. Acad. Sci., vol. 154, art. 2, Nov. 22, 1968, pp. 1094-1114.

24. Heyson, Harry H.: Wind-Tunnel Wall Effects at Extreme Force Coefficients. Ann. N.Y. Acad. Sci., vol. 154, art. 2, Nov. 22, 1968, pp. 1074-1093.

25. Grunwald, Kalman J.: Experimental Study of Wind-Tunnel Wall Effects and Wall Corrections for a General-Research V/STOL Tilt-Wing Model With Flap. NASA TN D-2887, 1965.

26. Joppa, Robert G.: Wall Interference Effects in Wind-Tunnel Testing of STOL Aircraft. J. Aircraft, vol. 6, no. 3, May-June 1969, pp. 209-214.

27. Hackett, J. E.; and Evans, M. R.: Vortex Wakes Behind High-Lift Wings. AIAA Pap. No. 69-740, July 1969.

28. Crimi, Peter: Prediction of Rotor Wake Flows. Aerodynamic Problems Associated With V/STOL Aircraft. Vol. I – Propeller and Rotor Aerodynamics, Cornell Aeronaut. Lab., Inc., and U.S. Army Aviat. Mater. Lab., June 1966.

29. Mil', M. L.; Nekrasov, A. V.; Braverman, A. S.; Grodko, L. N.; and Leykand, M. A.: Helicopters – Calculation and Design. Vol. I. Aerodynamics. NASA TT F-494, 1967, pp. 244-253.

30. Werlé, Henri: Simulation De L'Effet de Sol au Tunnel Hydrodynamique (Ground-Effect Simulation at the Water-Tunnel). La Rech. Aérospatiale, no. 95, July-Aug. 1963, pp. 7-15.

31. Turner, Thomas R.: Endless-Belt Technique for Ground Simulation. Conference on V/STOL and STOL Aircraft, NASA SP-116, 1966, pp. 435-446.

32. Turner, Thomas R.: A Moving-Belt Ground Plane for Wind-Tunnel Ground Simulation and Results for Two Jet-Flap Configurations. NASA TN D-4228, 1967.

33. Cook, Woodrow L.; and Hickey, David H.: Comparison of Wind-Tunnel and Flight-Test Aerodynamic Data in the Transition-Flight Speed Range for Five V/STOL Aircraft. Conference on V/STOL and STOL Aircraft. NASA SP-116, 1966, pp. 447-467. (Also available as Correlation of Wind-Tunnel and Flight-Test Aerodynamic Data for Five V/STOL Aircraft, AGARD Rep. 520, 1965.)

34. Heyson, Harry H.: Nomographic Solution of the Momentum Equation for VTOL-STOL Aircraft. NASA TN D-814, 1961. (Also available as V-STOL Momentum Equation. Space/Aeronaut., vol. 38, no. 2, July 1962, pp. B-18—B-20.)

35. Heyson, Harry H.: A Note on the Mean Value of Induced Velocity for a Helicopter Rotor. NASA TN D-240, 1960.

TABLE I

CALCULATED OPERATING CONDITIONS FOR FIGURES 3 - 30

SIGMA = .600 UNIFORM LOADING

ZETA = .769 ETA = 1.000

GAMMA = 1.000 ALPHA = 0.0

FIGURE NUMBERS	CHI, DEG.	FREE AIR CL	CORRECTIONS TO FREE AIR IN: GROUND EFFECT, D ALPHA, DEG.	GROUND EFFECT, QC/Q	CLOSED TUNNEL, D ALPHA, DEG.	CLOSED TUNNEL, QC/Q	C-O-B TUNNEL, D ALPHA, DEG.	C-O-B TUNNEL, QC/Q	CORRECTIONS TO GROUND EFFECT IN: CLOSED TUNNEL, D ALPHA, DEG.	CLOSED TUNNEL, QC/Q	C-O-B TUNNEL, D ALPHA, DEG.	C-O-B TUNNEL, QC/Q
3,10,17,24	70.0	1.5	.6	.97	3.5	1.02	-2.5	.96	2.9	1.04	-3.0	.99
4,11,18,25	60.0	2.7	1.2	.94	5.5	1.00	-3.0	.92	4.2	1.05	-4.1	.98
5,12,19,26	50.0	4.4	2.7	.90	8.3	.96	-2.8	.88	5.4	1.06	-5.2	.98
6,13,20,27	40.0	7.4	5.8	.85	13.0	.93	-1.3	.82	6.9	1.06	-6.6	.99
7,14,21,28	30.0	13.9	11.3	.83	20.6	.96	1.7	.78	9.2	1.07	-8.7	1.00
8,15,22,29	20.0	32.1	21.2	.88	33.2	1.14	7.5	.75	13.6	1.10	-12.8	1.03
9,16,23,30	10.0	130.6	41.9	1.34	55.1	2.38	21.0	.83	25.8	1.29	-24.4	1.18

TABLE II

CALCULATED CONDITIONS FOR FIGURES 36 - 125

ETA = 1.0

FIRST LINE GIVES CORRECTIONS TO FREE AIR
SECOND LINE GIVES CORRECTIONS TO GROUND EFFECT

FIG. NO.	GAMMA	ZETA	SIGMA	CHI, DEG.	ALPHA, DEG.	LOADING	FREE AIR CL	FREE AIR CD	GROUND EFFECT D ALPHA, DEG.	GROUND EFFECT QC/Q	CLOSED TUNNEL D ALPHA, DEG.	CLOSED TUNNEL QC/Q	C-O-B TUNNEL D ALPHA, DEG.	C-O-B TUNNEL QC/Q
36	1.0	.769	.60	70.0	20.0	UNIFORM	1.2	.4	.7	.97	3.2	1.02	-2.2	.96
									0.0	0.00	2.4	1.05	-2.9	.98
37	1.0	.769	.60	70.0	0.0	UNIFORM	1.5	0.0	.6	.97	3.5	1.02	-2.5	.96
									0.0	0.00	2.9	1.04	-3.0	.99
38	1.0	.769	.60	70.0	-20.0	UNIFORM	2.1	-.7	.3	.97	4.1	1.01	-2.9	.96
									0.0	0.00	3.7	1.04	-3.2	.99
39	1.0	.769	.60	50.0	20.0	UNIFORM	2.6	.9	2.9	.90	7.1	.99	-2.3	.87
									0.0	0.00	4.1	1.08	-4.9	.97
40	1.0	.769	.60	50.0	0.0	UNIFORM	4.4	0.0	2.7	.90	8.3	.96	-2.8	.88
									0.0	0.00	5.4	1.06	-5.2	.98
41	1.0	.769	.60	50.0	-20.0	UNIFORM	9.1	-3.3	2.3	.88	10.9	.92	-4.3	.88
									0.0	0.00	8.2	1.03	-6.2	1.00
42	1.0	.769	.60	30.0	20.0	UNIFORM	5.2	1.9	9.8	.86	15.2	1.01	2.4	.78
									0.0	0.00	5.7	1.13	-7.1	.96
43	1.0	.769	.60	30.0	0.0	UNIFORM	13.9	0.0	11.3	.83	20.6	.96	1.7	.78
									0.0	0.00	9.2	1.07	-8.7	1.00
44	1.0	.769	.60	30.0	-20.0	UNIFORM	101.4	-36.9	20.2	.71	48.5	1.00	-1.9	.69
									0.0	0.00	27.7	.97	-17.0	1.18
45	1.0	.769	.60	10.0	0.0	UNIFORM	130.6	0.0	41.9	1.34	55.1	2.38	21.0	.83
									0.0	0.00	25.8	1.29	-24.4	1.18
46	1.0	1.000	.60	70.0	20.0	UNIFORM	1.2	.4	1.2	.95	3.2	.97	-.9	.95
									0.0	0.00	2.0	1.02	-2.1	1.00
47	1.0	1.000	.60	70.0	0.0	UNIFORM	1.5	0.0	.9	.95	3.2	.97	-1.1	.95
									0.0	0.00	2.2	1.01	-2.0	1.00
48	1.0	1.000	.60	70.0	-20.0	UNIFORM	2.1	-.7	.6	.95	3.1	.96	-1.2	.95
									0.0	0.00	2.4	1.01	-1.8	1.00
49	1.0	1.000	.60	50.0	20.0	UNIFORM	2.6	.9	5.0	.85	8.2	.89	1.4	.83
									0.0	0.00	3.1	1.04	-3.4	.99
50	1.0	1.000	.60	50.0	0.0	UNIFORM	4.4	0.0	4.6	.84	8.5	.87	1.2	.84
									0.0	0.00	3.6	1.02	-3.2	1.00
51	1.0	1.000	.60	50.0	-20.0	UNIFORM	9.1	-3.3	3.9	.83	9.2	.82	.6	.83
									0.0	0.00	4.8	.98	-3.0	1.01
52	1.0	1.000	.60	30.0	20.0	UNIFORM	5.2	1.9	16.2	.82	19.9	.93	11.3	.76
									0.0	0.00	4.1	1.08	-4.8	.97
53	1.0	1.000	.60	30.0	0.0	UNIFORM	13.9	0.0	18.0	.79	24.1	.87	12.3	.75
									0.0	0.00	5.9	1.02	-5.2	1.00
54	1.0	1.000	.60	30.0	-20.0	UNIFORM	101.4	-36.9	32.3	.68	50.0	.80	21.9	.65
									0.0	0.00	15.7	.84	-7.5	1.12
55	1.0	1.000	.60	10.0	0.0	UNIFORM	130.6	0.0	54.6	1.95	60.6	2.76	47.1	1.41
									0.0	0.00	17.0	1.11	-15.0	1.07
56	1.0	1.429	.60	70.0	20.0	UNIFORM	1.2	.4	2.3	.92	3.8	.92	.8	.92
									0.0	0.00	1.4	1.00	-1.4	1.00
57	1.0	1.429	.60	70.0	0.0	UNIFORM	1.5	0.0	1.8	.92	3.2	.92	.5	.92
									0.0	0.00	1.4	1.00	-1.2	1.00
58	1.0	1.429	.60	70.0	-20.0	UNIFORM	2.1	-.7	1.1	.91	2.6	.91	.2	.92
									0.0	0.00	1.3	1.00	-.9	1.01
59	1.0	1.429	.60	50.0	20.0	UNIFORM	2.6	.9	10.6	.75	12.8	.77	8.1	.73
									0.0	0.00	2.0	1.02	-2.2	.99
60	1.0	1.429	.60	50.0	0.0	UNIFORM	4.4	0.0	9.5	.76	11.8	.77	7.3	.75
									0.0	0.00	2.1	1.00	-1.9	1.00
61	1.0	1.429	.60	50.0	-20.0	UNIFORM	9.1	-3.3	7.8	.73	10.6	.71	6.3	.74
									0.0	0.00	2.3	.97	-1.2	1.02
62	1.0	1.429	.60	30.0	20.0	UNIFORM	5.2	1.9	28.9	.86	30.6	.95	26.2	.80
									0.0	0.00	2.7	1.05	-3.2	.98
63	1.0	1.429	.60	30.0	0.0	UNIFORM	13.9	0.0	30.7	.81	33.8	.87	27.7	.77
									0.0	0.00	3.3	1.00	-3.0	1.00
64	1.0	1.429	.60	30.0	-20.0	UNIFORM	101.4	-36.9	52.7	.78	61.6	.85	48.4	.78
									0.0	0.00	6.9	.83	-2.4	1.10
65	1.0	1.429	.60	10.0	0.0	UNIFORM	130.6	0.0	67.5	3.69	69.3	4.32	65.6	3.17
									0.0	0.00	9.7	1.03	-8.6	1.02

TABLE II

CONTINUED.

FIG. NO.	GAMMA	ZETA	SIGMA	CHI, DEG.	ALPHA, DEG.	LOADING	FREE AIR CL	FREE AIR CD	CORRECTIONS IN GROUND EFFECT D ALPHA, DEG.	GROUND EFFECT QC/Q	CLOSED TUNNEL D ALPHA, DEG.	CLOSED TUNNEL QC/Q	C-O-B TUNNEL D ALPHA, DEG.	C-O-B TUNNEL QC/Q
66	1.0	1.000	.60	70.0	20.0	TRIANGULAR	1.2	.4	1.2	.96	3.3	.97	-1.0	.95
									0.0	0.00	2.1	1.02	-2.1	1.00
67	1.0	1.000	.60	70.0	0.0	TRIANGULAR	1.5	0.0	.9	.96	3.2	.97	-1.1	.95
									0.0	0.00	2.3	1.01	-2.0	1.00
68	1.0	1.000	.60	70.0	-20.0	TRIANGULAR	2.1	-.7	.6	.95	3.1	.97	-1.3	.95
									0.0	0.00	2.5	1.01	-1.8	1.00
69	1.0	1.000	.60	50.0	20.0	TRIANGULAR	2.6	.9	5.0	.85	8.3	.90	1.2	.83
									0.0	0.00	3.2	1.04	-3.5	.99
70	1.0	1.000	.60	50.0	0.0	TRIANGULAR	4.4	0.0	4.6	.85	8.5	.88	1.1	.84
									0.0	0.00	3.7	1.02	-3.3	1.00
71	1.0	1.000	.60	50.0	-20.0	TRIANGULAR	9.1	-3.3	3.9	.83	9.2	.83	.5	.84
									0.0	0.00	4.8	.98	-3.0	1.01
72	1.0	1.000	.60	30.0	20.0	TRIANGULAR	5.2	1.9	15.6	.84	19.4	.95	10.6	.77
									0.0	0.00	4.3	1.08	-4.9	.97
73	1.0	1.000	.60	30.0	0.0	TRIANGULAR	13.9	0.0	17.1	.81	23.2	.89	11.3	.76
									0.0	0.00	6.1	1.02	-5.3	1.00
74	1.0	1.000	.60	30.0	-20.0	TRIANGULAR	101.4	-36.9	30.1	.69	48.1	.80	19.7	.67
									0.0	0.00	15.8	.84	-7.6	1.13
75	1.0	1.000	.60	10.0	0.0	TRIANGULAR	130.6	0.0	52.2	1.82	58.9	2.60	43.9	1.31
									0.0	0.00	17.4	1.11	-15.3	1.07
76	1.0	1.000	.30	70.0	20.0	UNIFORM	1.2	.4	.3	.99	.8	.99	-.1	.99
									0.0	0.00	.4	1.00	-.5	1.00
77	1.0	1.000	.30	70.0	0.0	UNIFORM	1.5	0.0	.2	.99	.7	.99	-.2	.99
									0.0	0.00	.5	1.00	-.5	1.00
78	1.0	1.000	.30	70.0	-20.0	UNIFORM	2.1	-.7	.1	.99	.7	.99	-.3	.99
									0.0	0.00	.6	1.00	-.4	1.00
79	1.0	1.000	.30	50.0	20.0	UNIFORM	2.6	.9	1.2	.96	1.9	.96	.4	.95
									0.0	0.00	.7	1.01	-.8	1.00
80	1.0	1.000	.30	50.0	0.0	UNIFORM	4.4	0.0	1.1	.95	2.0	.96	.4	.95
									0.0	0.00	.8	1.00	-.7	1.00
81	1.0	1.000	.30	50.0	-20.0	UNIFORM	9.1	-3.3	.9	.95	2.1	.94	.2	.95
									0.0	0.00	1.2	.99	-.7	1.00
82	1.0	1.000	.30	30.0	20.0	UNIFORM	5.2	1.9	4.2	.92	5.1	.94	3.0	.91
									0.0	0.00	.9	1.02	-1.1	.99
83	1.0	1.000	.30	30.0	0.0	UNIFORM	13.9	0.0	4.9	.90	6.3	.91	3.6	.90
									0.0	0.00	1.4	1.00	-1.2	1.00
84	1.0	1.000	.30	30.0	-20.0	UNIFORM	101.4	-36.9	8.6	.82	12.8	.79	6.3	.84
									0.0	0.00	3.6	.94	-2.0	1.03
85	1.0	1.000	.30	10.0	0.0	UNIFORM	130.6	0.0	22.1	1.00	25.7	1.06	18.6	.95
									0.0	0.00	4.1	1.01	-3.6	1.00
86	1.0	1.000	.90	70.0	20.0	UNIFORM	1.2	.4	2.5	.91	8.7	.98	-3.9	.90
									0.0	0.00	6.0	1.06	-6.1	.99
87	1.0	1.000	.90	70.0	0.0	UNIFORM	1.5	0.0	2.0	.91	8.3	.96	-3.7	.90
									0.0	0.00	6.1	1.05	-5.4	1.00
88	1.0	1.000	.90	70.0	-20.0	UNIFORM	2.1	-.7	1.3	.91	7.6	.94	-3.4	.91
									0.0	0.00	6.0	1.03	-4.4	1.01
89	1.0	1.000	.90	50.0	20.0	UNIFORM	2.6	.9	11.8	.73	20.8	.91	.6	.65
									0.0	0.00	8.9	1.14	-9.8	.97
90	1.0	1.000	.90	50.0	0.0	UNIFORM	4.4	0.0	10.4	.75	20.5	.86	.7	.70
									0.0	0.00	9.5	1.07	-8.4	1.00
91	1.0	1.000	.90	50.0	-20.0	UNIFORM	9.1	-3.3	8.5	.71	21.9	.77	-.1	.71
									0.0	0.00	11.6	1.00	-7.2	1.04
92	1.0	1.000	.90	30.0	20.0	UNIFORM	5.2	1.9	30.8	.88	37.5	1.30	18.9	.63
									0.0	0.00	11.0	1.25	-13.3	.94
93	1.0	1.000	.90	30.0	0.0	UNIFORM	13.9	0.0	32.6	.83	44.1	1.20	18.8	.63
									0.0	0.00	15.0	1.11	-13.3	1.03
94	1.0	1.000	.90	30.0	-20.0	UNIFORM	101.4	-36.9	55.4	.82	79.3	1.85	33.3	.56
									0.0	0.00	38.8	.90	-16.6	1.35
95	1.0	1.000	.90	10.0	0.0	UNIFORM	130.6	0.0	68.8	4.03	74.4	7.65	59.2	1.93
									0.0	0.00	37.9	1.67	-34.4	1.43

TABLE II

CONCLUDED.

FIG. NO.	GAMMA	ZETA	SIGMA	CHI, DEG.	ALPHA, DEG.	LOADING	FREE AIR CL	FREE AIR CD	GROUND EFFECT D ALPHA, DEG.	GROUND EFFECT QC/Q	CLOSED TUNNEL D ALPHA, DEG.	CLOSED TUNNEL QC/Q	C-O-B TUNNEL D ALPHA, DEG.	C-O-B TUNNEL QC/Q
96	2.0	1.000	.60	70.0	20.0	UNIFORM	1.2	.4	4.1	.86	5.1	.89	2.2	.84
									0.0	0.00	1.0	1.03	-1.8	.98
97	2.0	1.000	.60	70.0	0.0	UNIFORM	1.5	0.0	3.2	.86	4.9	.89	1.0	.84
									0.0	0.00	1.6	1.03	-2.1	.99
98	2.0	1.000	.60	70.0	-20.0	UNIFORM	2.1	-.7	2.2	.86	5.0	.89	-.7	.84
									0.0	0.00	2.6	1.03	-2.7	.98
99	2.0	1.000	.60	50.0	20.0	UNIFORM	2.6	.9	21.1	.68	21.9	.73	18.6	.64
									0.0	0.00	1.2	1.05	-2.4	.98
100	2.0	1.000	.60	50.0	0.0	UNIFORM	4.4	0.0	16.7	.69	19.4	.73	13.3	.66
									0.0	0.00	2.5	1.02	-3.1	.99
101	2.0	1.000	.60	50.0	-20.0	UNIFORM	9.1	-3.3	13.3	.63	20.6	.67	6.8	.61
									0.0	0.00	6.0	.99	-5.3	1.00
102	2.0	1.000	.60	30.0	20.0	UNIFORM	5.2	1.9	41.8	1.08	41.1	1.18	40.2	.98
									0.0	0.00	1.2	1.09	-3.1	.97
103	2.0	1.000	.60	30.0	0.0	UNIFORM	13.9	0.0	43.4	.96	46.0	1.07	39.7	.85
									0.0	0.00	4.1	1.02	-4.9	1.00
104	2.0	1.000	.60	30.0	-20.0	UNIFORM	101.4	-36.9	69.5	1.11	80.3	1.83	59.5	.66
									0.0	0.00	22.1	.86	-15.4	1.17
105	2.0	1.000	.60	10.0	0.0	UNIFORM	130.6	0.0	74.8	6.53	75.8	7.61	73.3	5.36
									0.0	0.00	11.8	1.06	-14.0	1.05
106	2.0	1.000	.30	70.0	20.0	UNIFORM	1.2	.4	1.2	.95	1.5	.97	.8	.95
									0.0	0.00	.3	1.01	-.5	.99
107	2.0	1.000	.30	70.0	0.0	UNIFORM	1.5	0.0	.9	.95	1.5	.96	.3	.95
									0.0	0.00	.5	1.01	-.6	.99
108	2.0	1.000	.30	70.0	-20.0	UNIFORM	2.1	-.7	.6	.95	1.5	.96	-.3	.95
									0.0	0.00	.9	1.01	-.9	.99
109	2.0	1.000	.30	50.0	20.0	UNIFORM	2.6	.9	5.0	.85	5.3	.86	4.3	.84
									0.0	0.00	.3	1.02	-.6	.99
110	2.0	1.000	.30	50.0	0.0	UNIFORM	4.4	0.0	4.6	.84	5.6	.85	3.6	.84
									0.0	0.00	.9	1.01	-1.0	.99
111	2.0	1.000	.30	50.0	-20.0	UNIFORM	9.1	-3.3	3.9	.83	6.1	.83	2.0	.82
									0.0	0.00	2.0	1.00	-1.8	1.00
112	2.0	1.000	.30	30.0	20.0	UNIFORM	5.2	1.9	16.2	.82	16.4	.85	15.5	.80
									0.0	0.00	.4	1.03	-.8	.99
113	2.0	1.000	.30	30.0	0.0	UNIFORM	13.9	0.0	18.0	.79	19.5	.81	16.3	.77
									0.0	0.00	1.4	1.01	-1.6	1.00
114	2.0	1.000	.30	30.0	-20.0	UNIFORM	101.4	-36.9	32.3	.68	40.1	.74	25.6	.62
									0.0	0.00	6.7	.94	-5.6	1.03
115	2.0	1.000	.30	10.0	0.0	UNIFORM	130.6	0.0	54.6	1.95	56.2	2.13	52.6	1.76
									0.0	0.00	4.2	1.01	-4.8	1.00
116	.5	1.000	.60	70.0	20.0	UNIFORM	1.2	.4	.3	.99	3.0	1.01	-1.6	.98
									0.0	0.00	2.7	1.02	-2.0	.99
117	.5	1.000	.60	70.0	0.0	UNIFORM	1.5	0.0	.2	.99	3.0	1.01	-1.6	.98
									0.0	0.00	2.7	1.02	-1.8	.99
118	.5	1.000	.60	70.0	-20.0	UNIFORM	2.1	-.7	.1	.99	2.9	1.00	-1.5	.98
									0.0	0.00	2.7	1.01	-1.6	.99
119	.5	1.000	.60	50.0	20.0	UNIFORM	2.6	.9	1.2	.96	5.7	1.01	-2.3	.92
									0.0	0.00	4.4	1.06	-3.4	.97
120	.5	1.000	.60	50.0	0.0	UNIFORM	4.4	0.0	1.1	.95	5.8	1.00	-2.1	.93
									0.0	0.00	4.6	1.04	-3.2	.98
121	.5	1.000	.60	50.0	-20.0	UNIFORM	9.1	-3.3	.9	.95	6.0	.97	-1.9	.93
									0.0	0.00	5.0	1.02	-2.8	.98
122	.5	1.000	.60	30.0	20.0	UNIFORM	5.2	1.9	4.2	.92	10.2	1.04	-.7	.86
									0.0	0.00	6.0	1.10	-4.8	.95
123	.5	1.000	.60	30.0	0.0	UNIFORM	13.9	0.0	4.9	.90	12.4	.98	-.3	.86
									0.0	0.00	7.3	1.06	-5.0	.97
124	.5	1.000	.60	30.0	-20.0	UNIFORM	101.4	-36.9	8.6	.82	24.1	.82	1.2	.84
									0.0	0.00	14.2	.92	-6.5	1.06
125	.5	1.000	.60	10.0	0.0	UNIFORM	130.6	0.0	22.1	1.00	38.5	1.47	8.1	.84
									0.0	0.00	20.3	1.19	-14.1	1.02

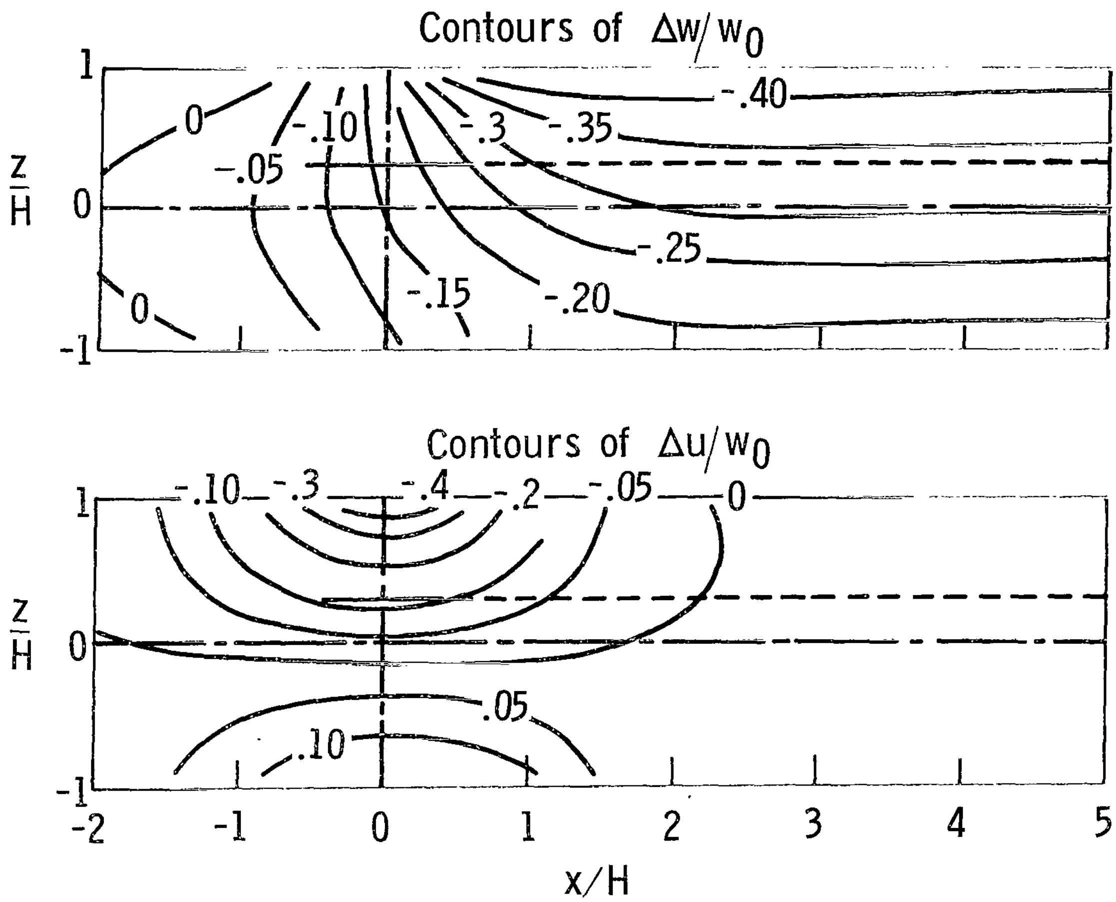

(a) $\chi = 90^{\circ}$; $w_0/V = 0$.

Figure 1.- Wall-induced interference velocities for a uniformly loaded rotor mounted 30 percent of a semiheight above the centerline of a square, closed wind tunnel. $\sigma = 0.6$.

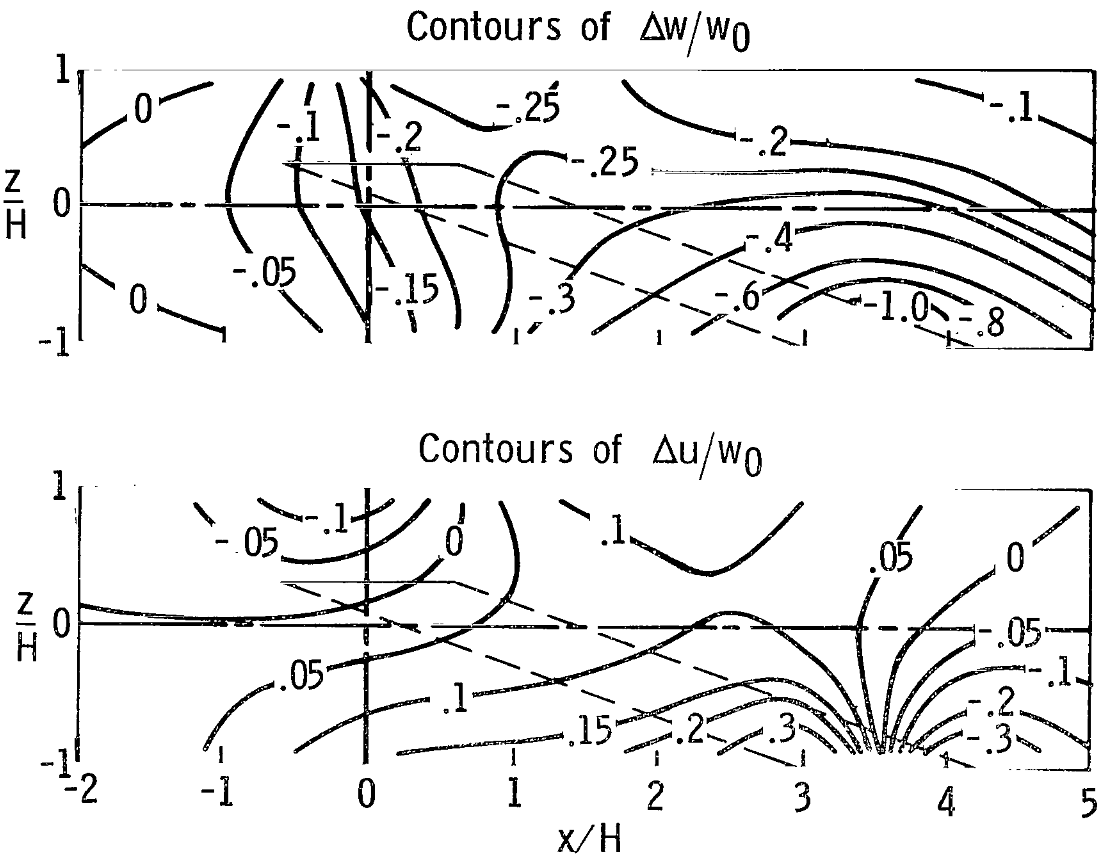

(b) $\chi = 70^{\circ}$; $w_0/V = -0.36$.

Figure 1.- Continued.

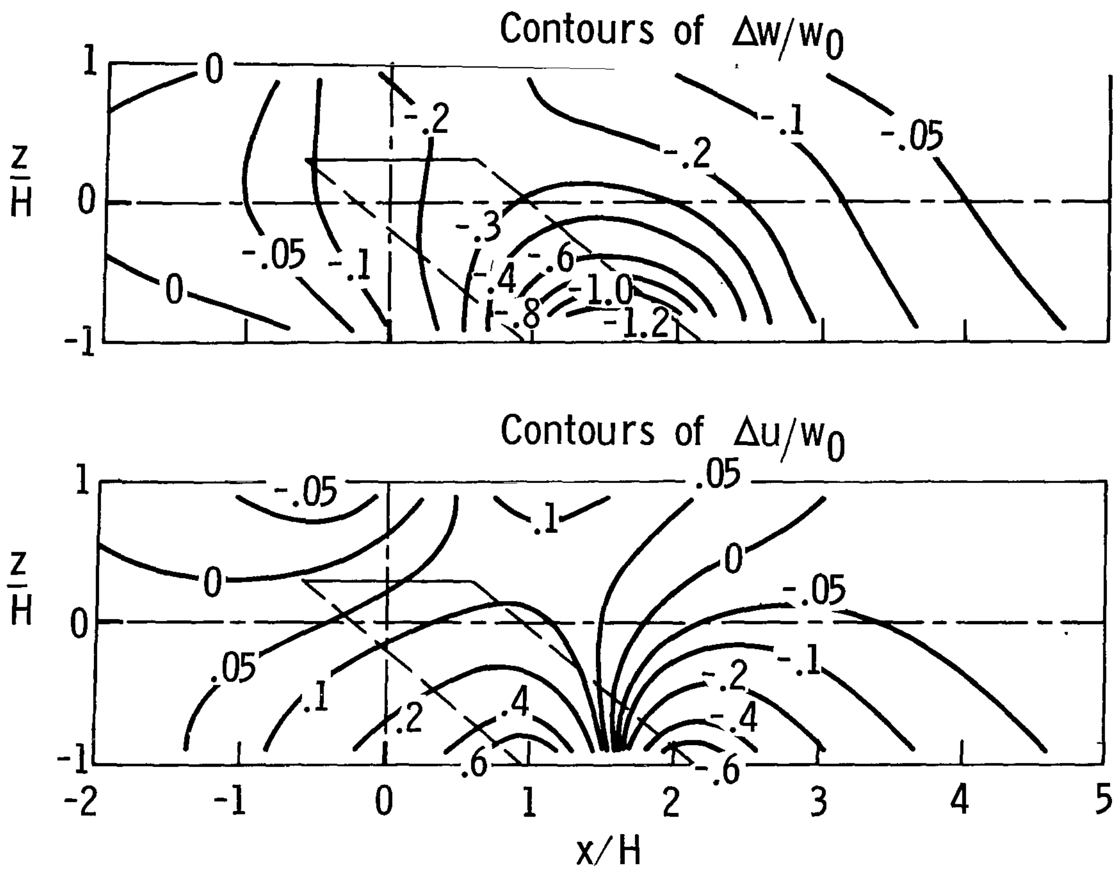

(c) $\chi = 50^o$; $w_0/V = -0.84$.

Figure 1.- Continued.

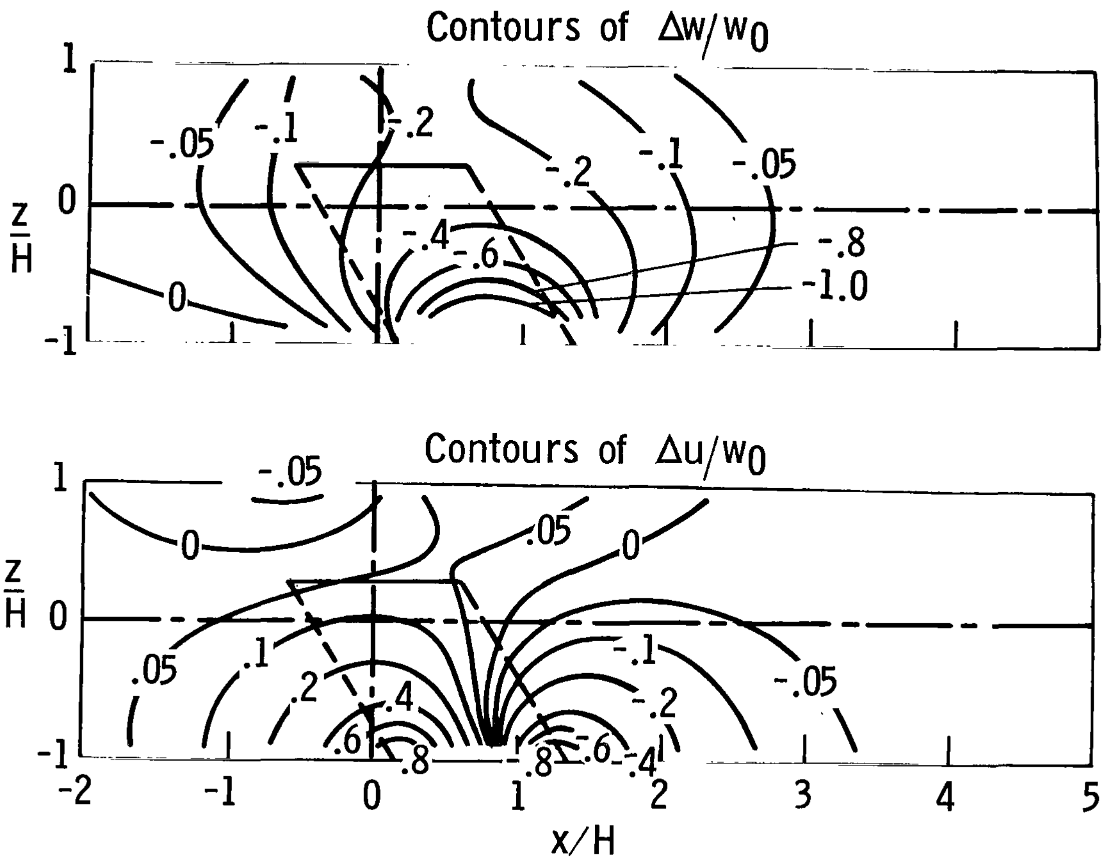

(d) $\chi = 30^o$; $w_0/V = -1.73$.

Figure 1.- Continued.

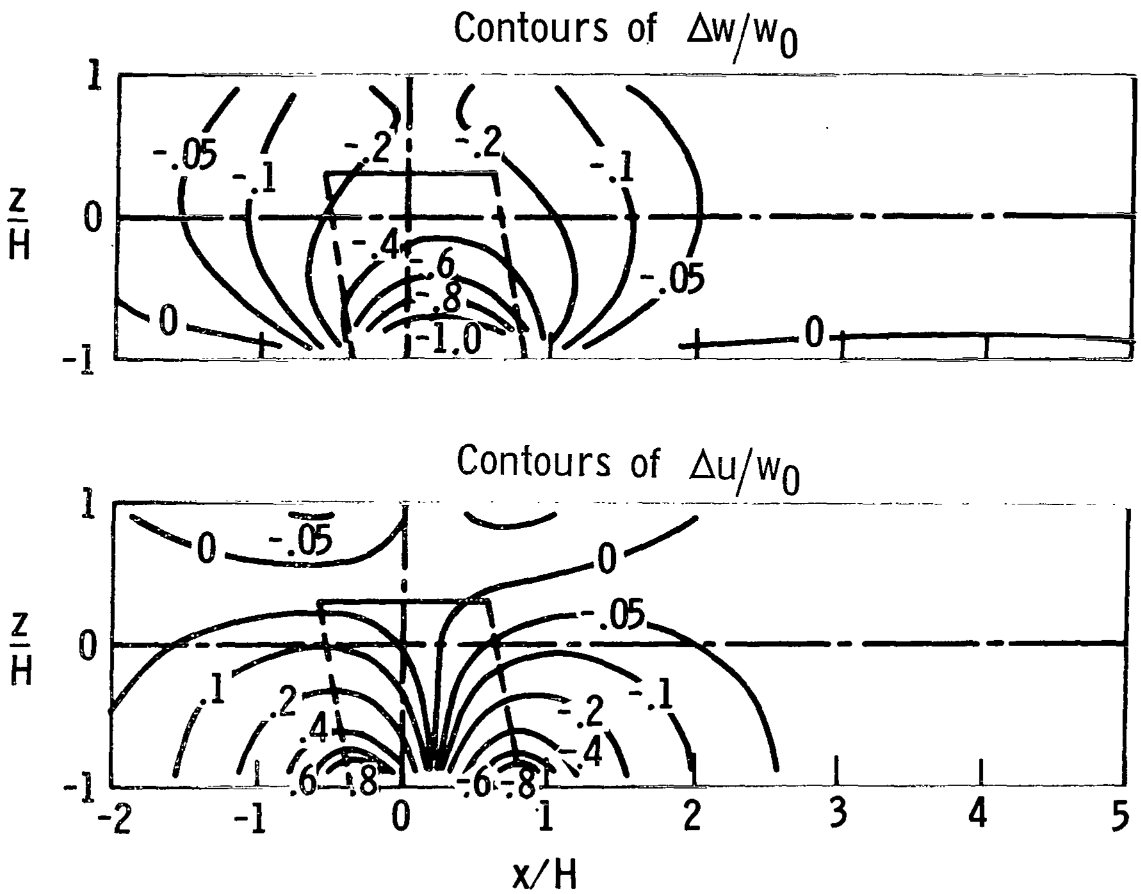

(e) $\chi = 10^{\circ}$; $w_0/V = -5.67$.

Figure 1.- Concluded.

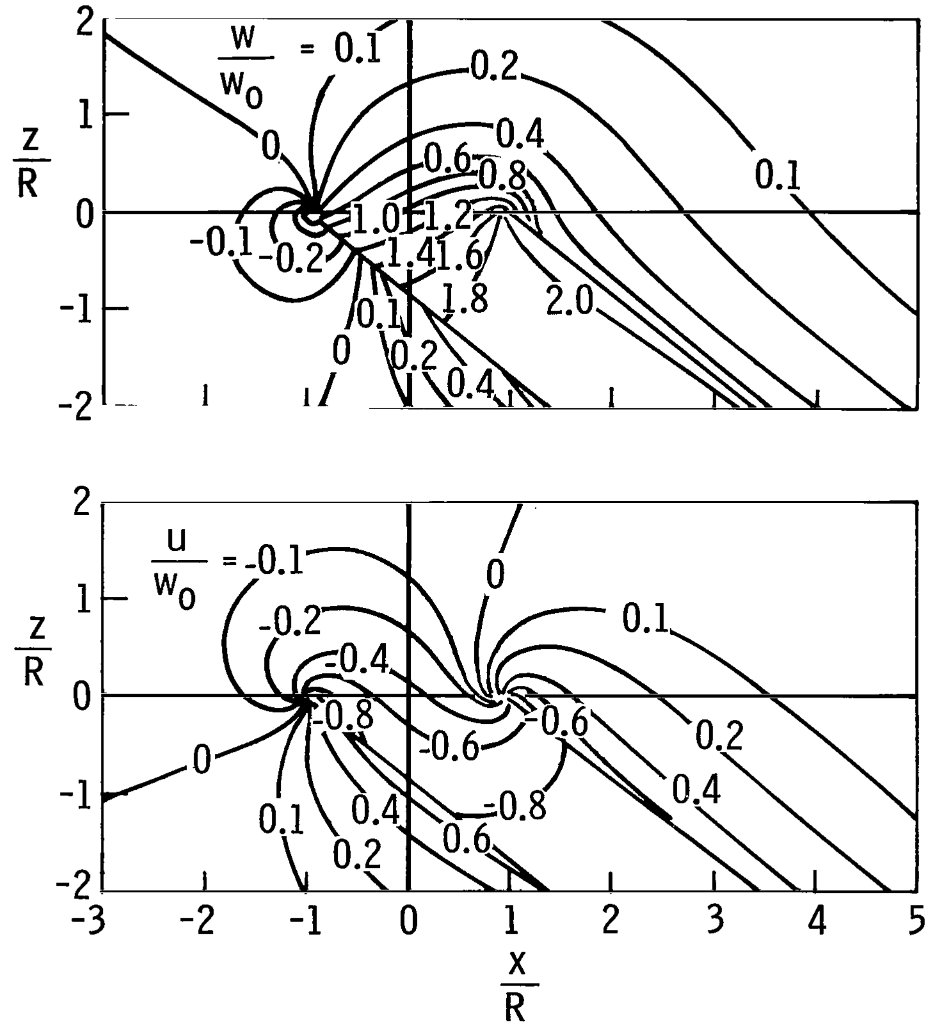

Figure 2.- Induced field of a uniformly loaded rotor at $\chi = 50^0$.

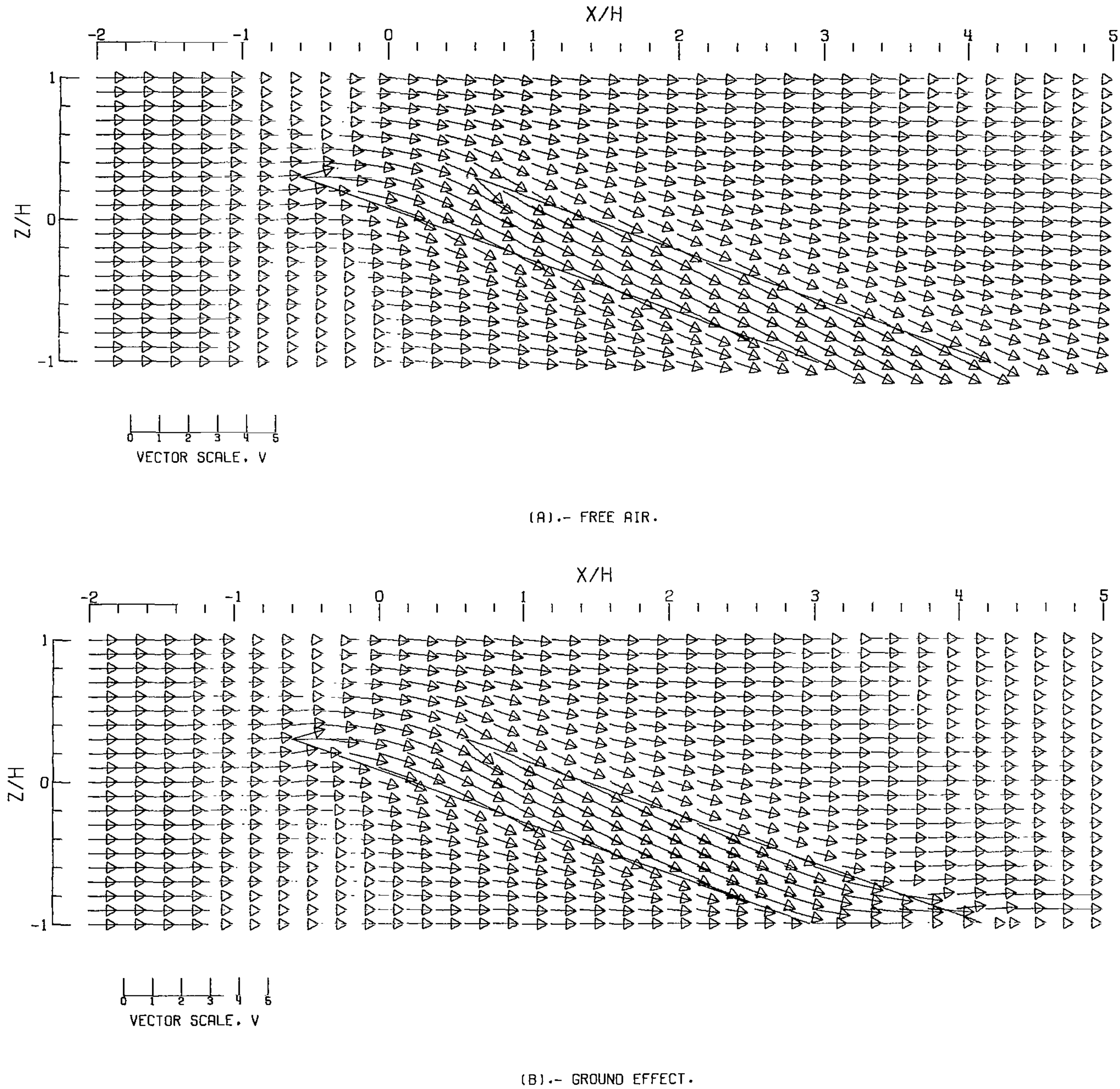

Figure 3.- Flow vectors in the X–Z plane, calculated using vortex cylinders. The rotor and the edges of the wake are shown. $\zeta = 0.769$; $\gamma = 1.0$; $\sigma = 0.60$; $\alpha = 0.0^0$; $\chi = 70.0^0$; uniform loading.

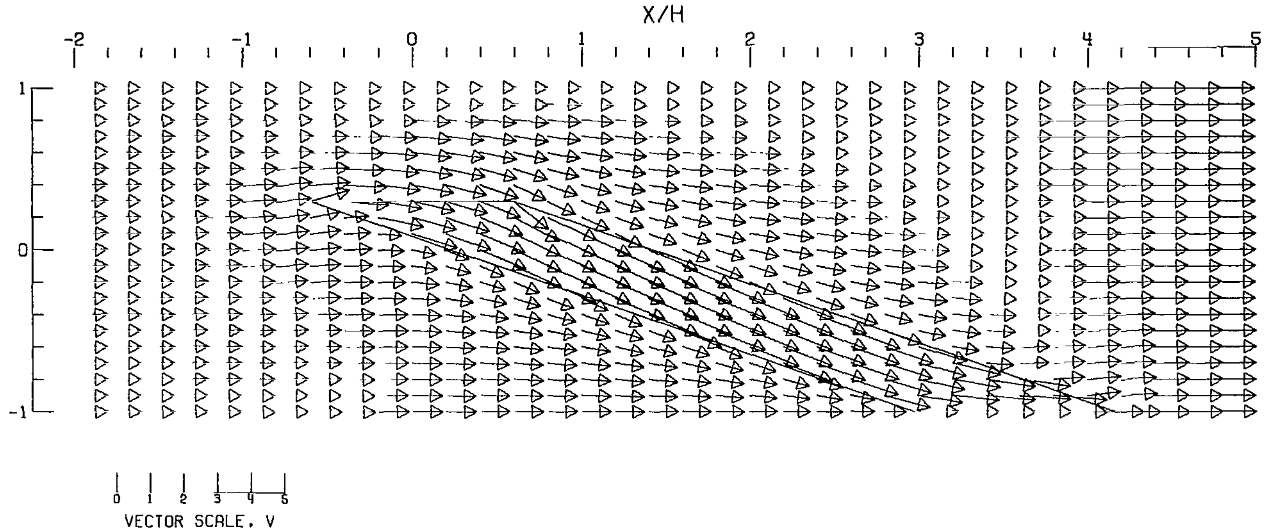

(C).- CLOSED TUNNEL.

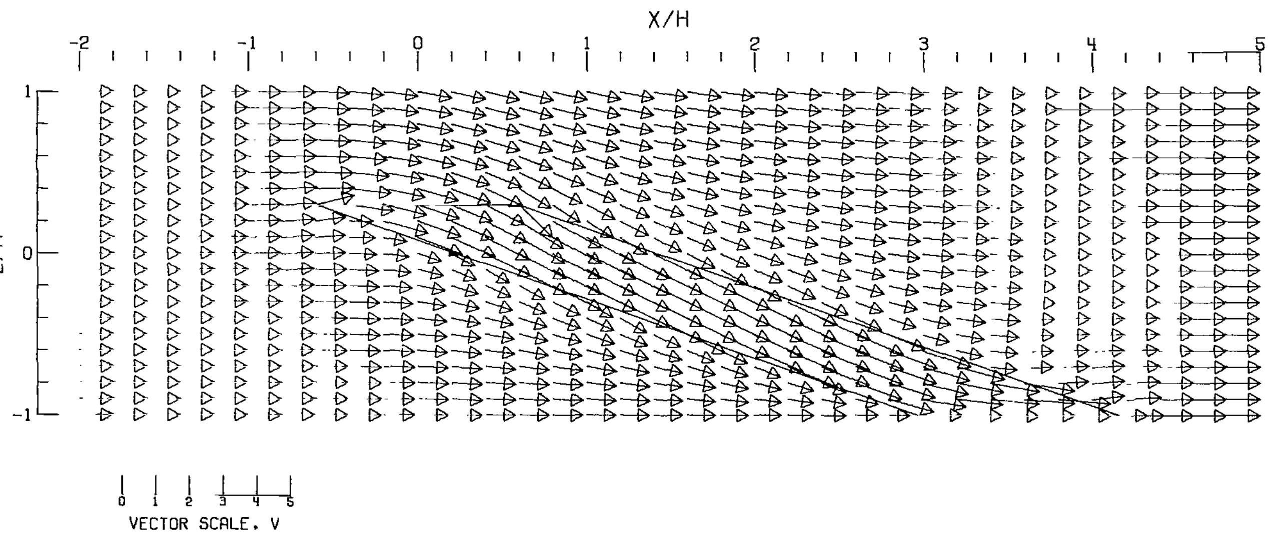

(D).- CLOSED-ON-BOTTOM-ONLY TUNNEL.

Figure 3.- Concluded.

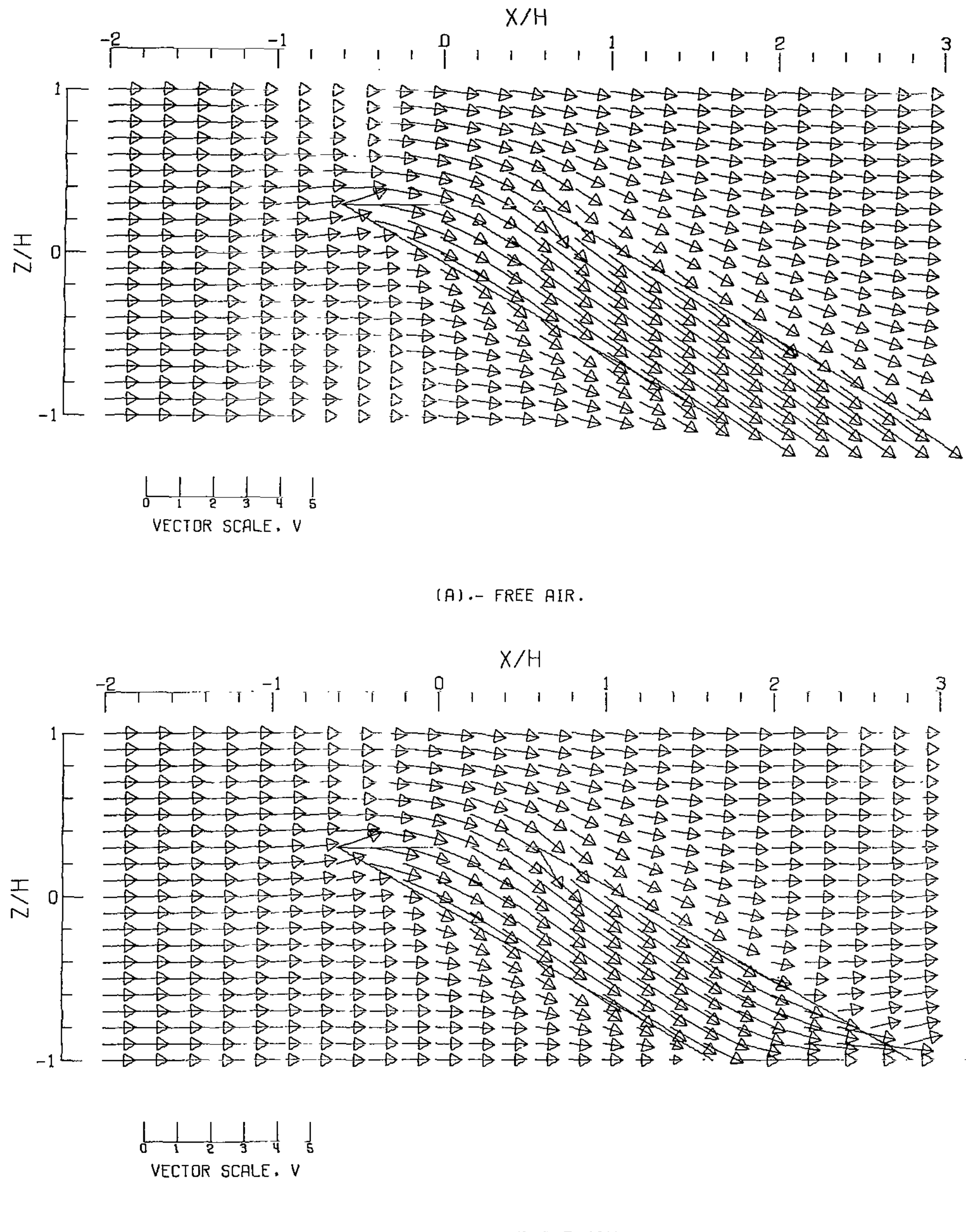

Figure 4.- Flow vectors in the X-Z plane, calculated using vortex cylinders. The rotor and the edges of the wake are shown. $\zeta = 0.769$; $\eta = 1.00$; $\gamma = 1.000$; $\sigma = 0.600$; $\alpha = 0.0^{0}$; $\chi = 60.000^{0}$; uniform loading.

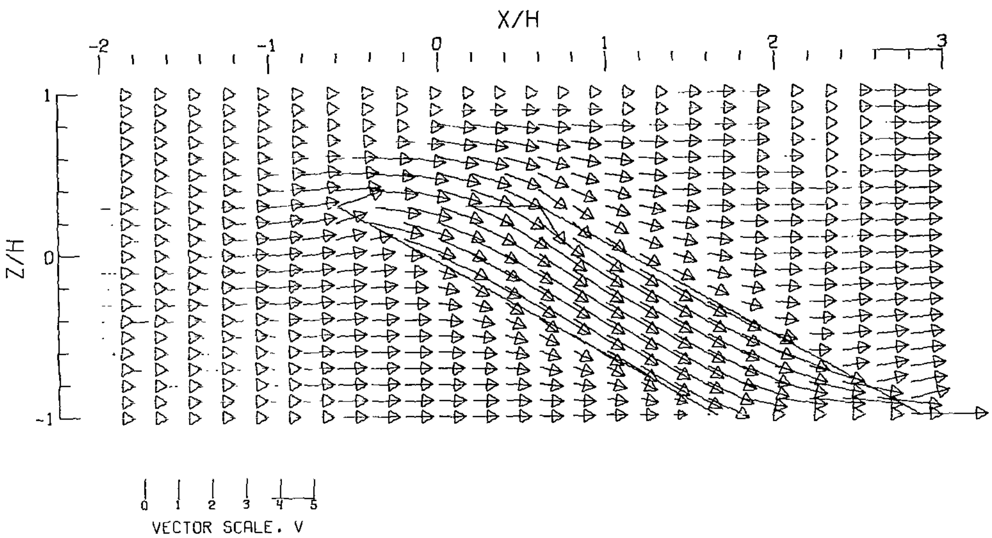

(C).- CLOSED TUNNEL.

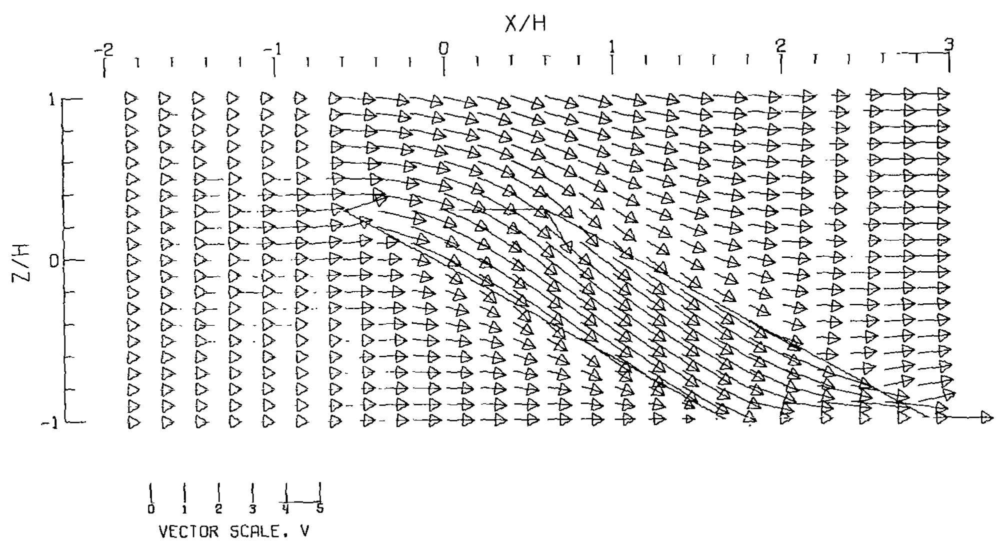

(D).- CLOSED-ON-BOTTOM-ONLY TUNNEL.

Figure 4.- Concluded.

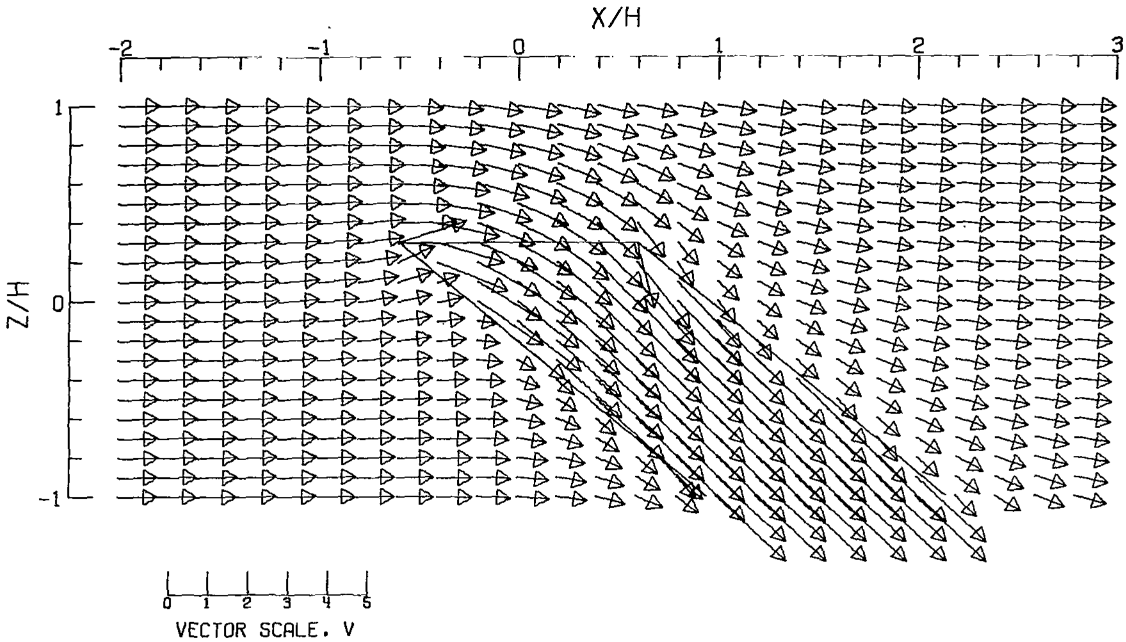

(A).- FREE AIR.

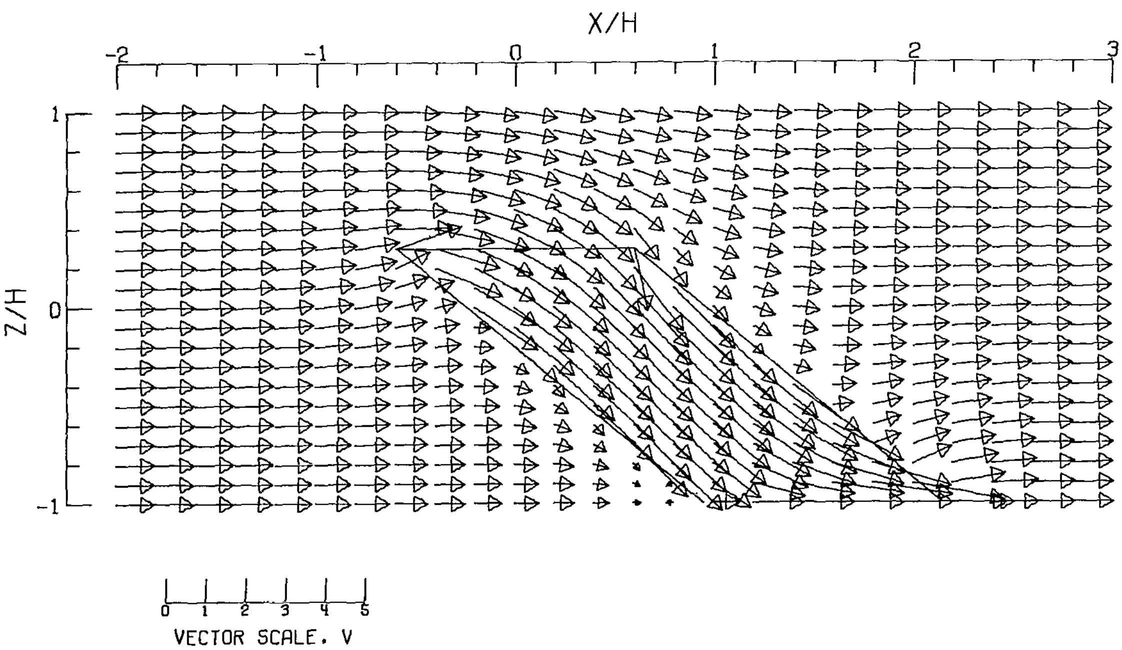

(B).- GROUND EFFECT.

Figure 5.- Flow vectors in the X-Z plane, calculated using vortex cylinders. The rotor and the edges of the wake are shown. ζ = 0.769; η = 1.00; γ = 1.000; σ = 0.600; α = 0.0°; χ = 50.000°; uniform loading.

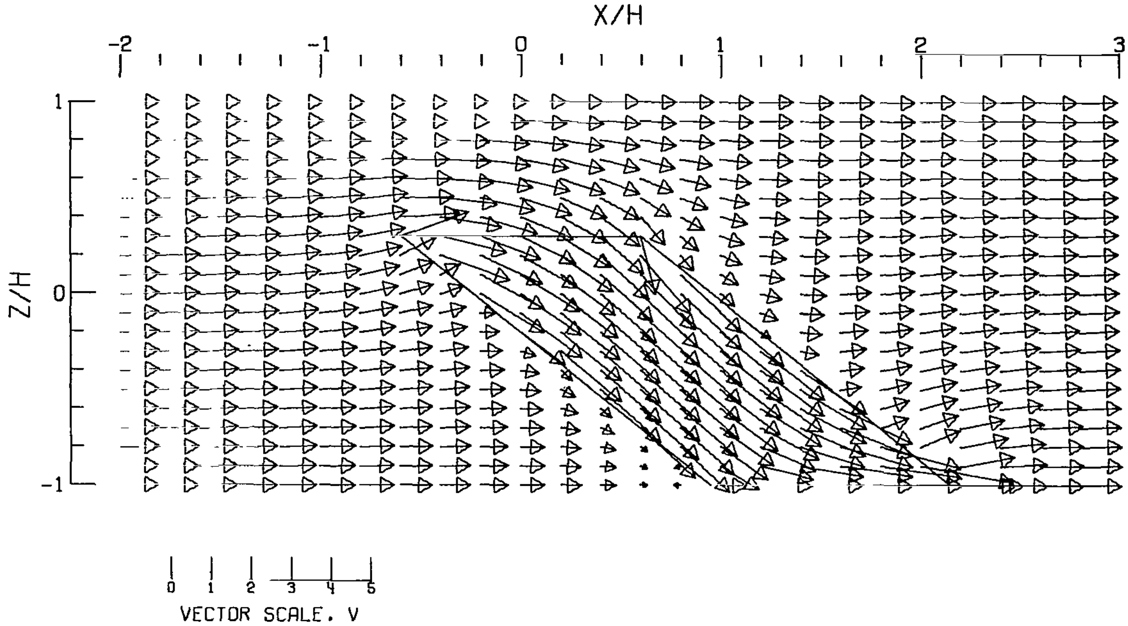

(C).- CLOSED TUNNEL.

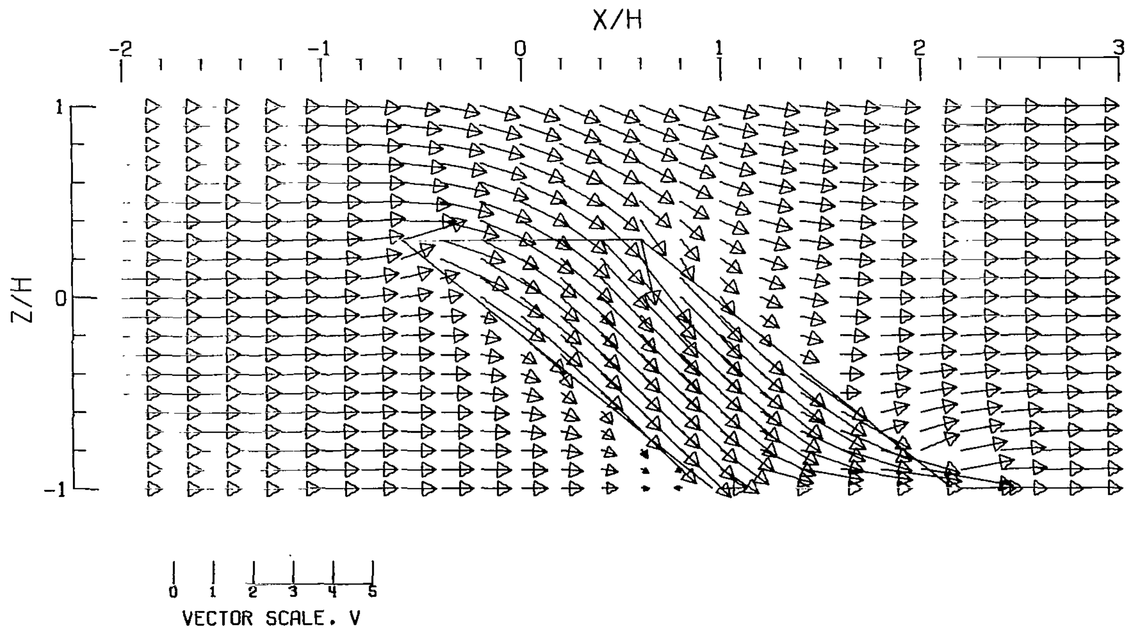

(D).- CLOSED-ON-BOTTOM-ONLY TUNNEL.

Figure 5.- Concluded.

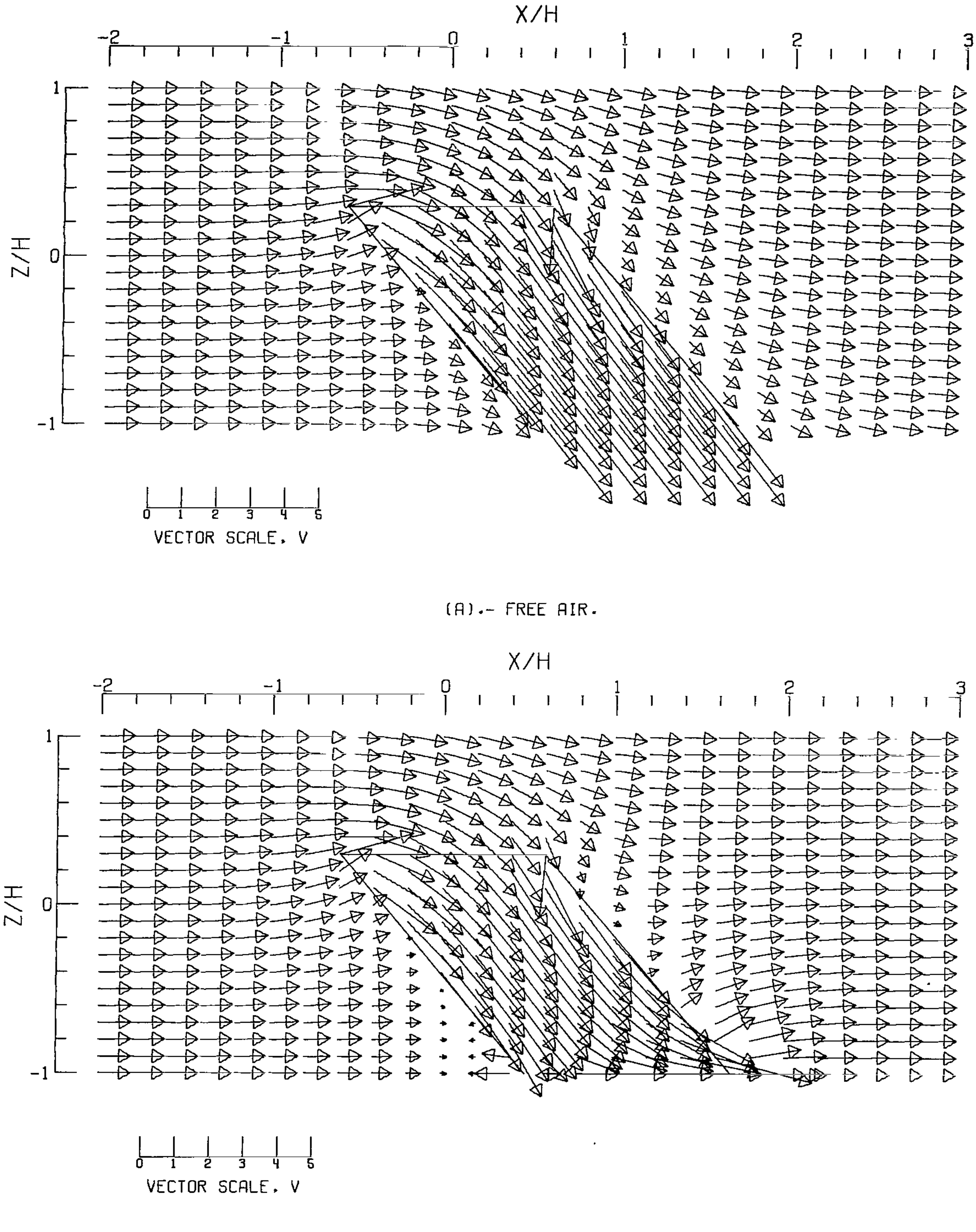

Figure 6.- Flow vectors in the X-Z plane, calculated using vortex cylinders. The rotor and the edges of the wake are shown. ζ = 0.769; η = 1.00; γ = 1.000; σ = 0.600; α = 0.0°; χ = 40.000°; uniform loading.

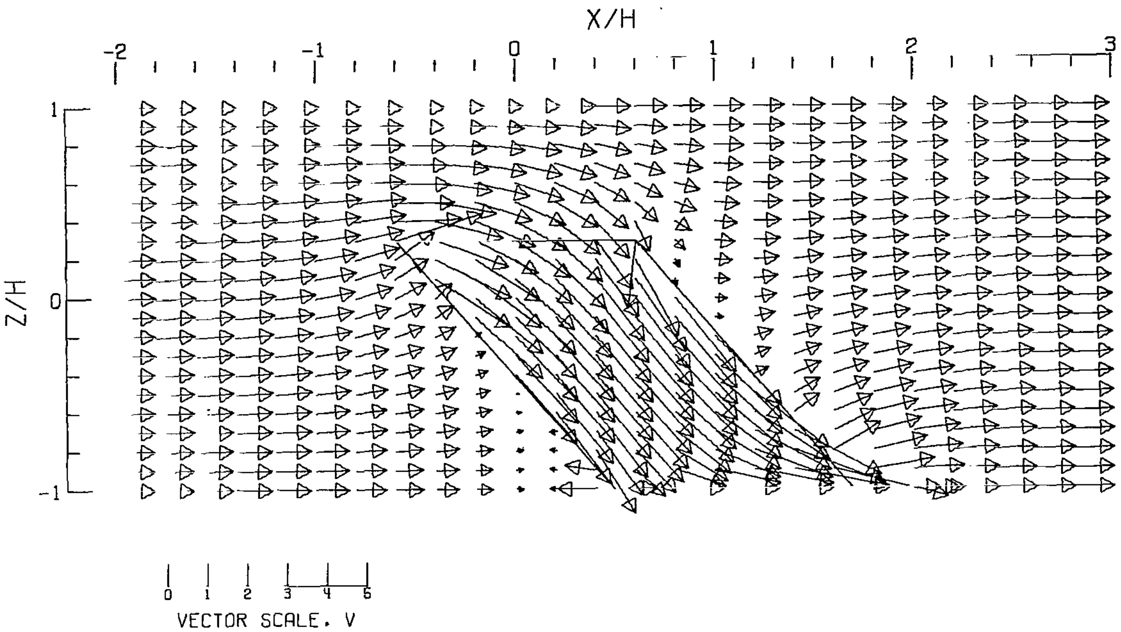

(C).- CLOSED TUNNEL.

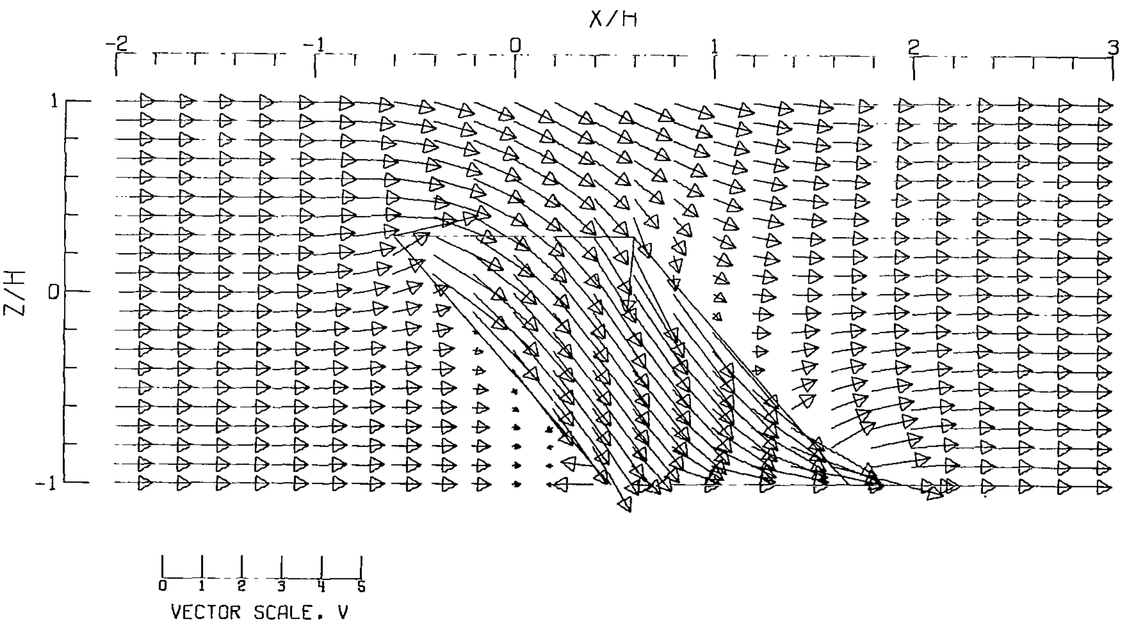

(D).- CLOSED-ON-BOTTOM-ONLY TUNNEL.

Figure 6.- Concluded.

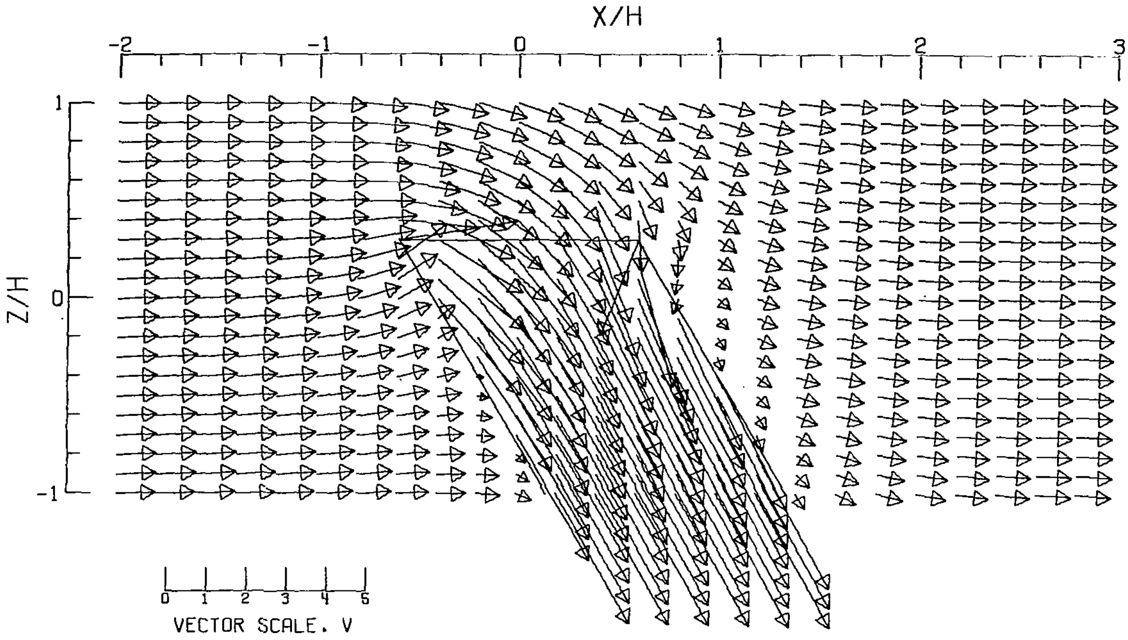

(A).- FREE AIR.

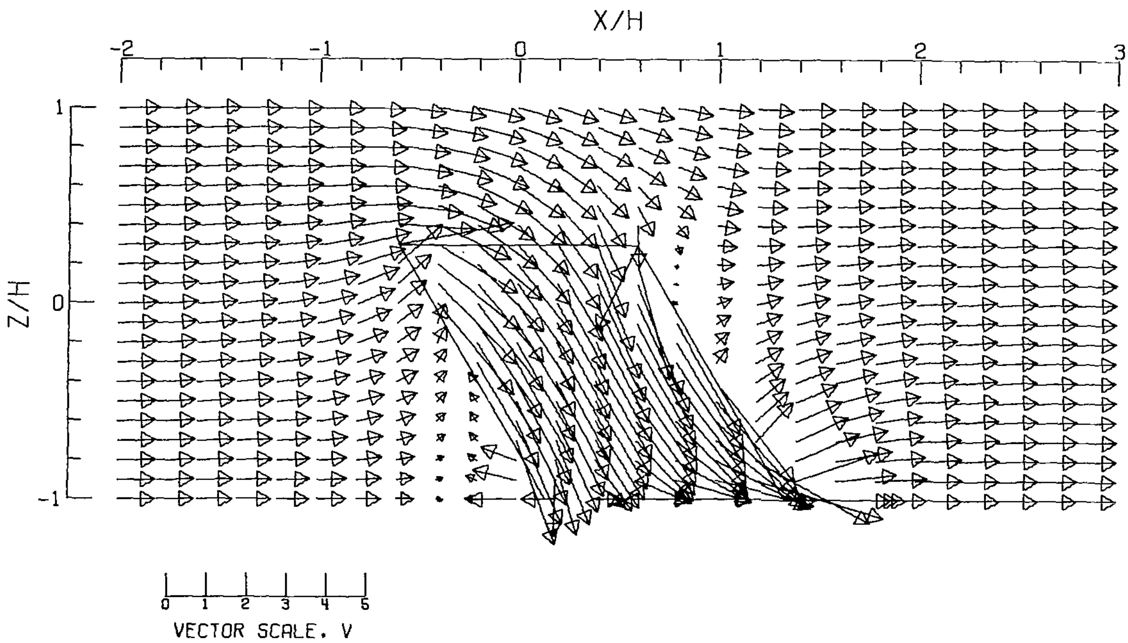

(B).- GROUND EFFECT.

Figure 7.- Flow vectors in the X-Z plane, calculated using vortex cylinders. The rotor and the edges of the wake are shown. $\zeta = 0.769$; $\eta = 1.00$; $\gamma = 1.000$; $\sigma = 0.600$; $\alpha = 0.0^{\circ}$; $\chi = 30.000^{\circ}$; uniform loading.

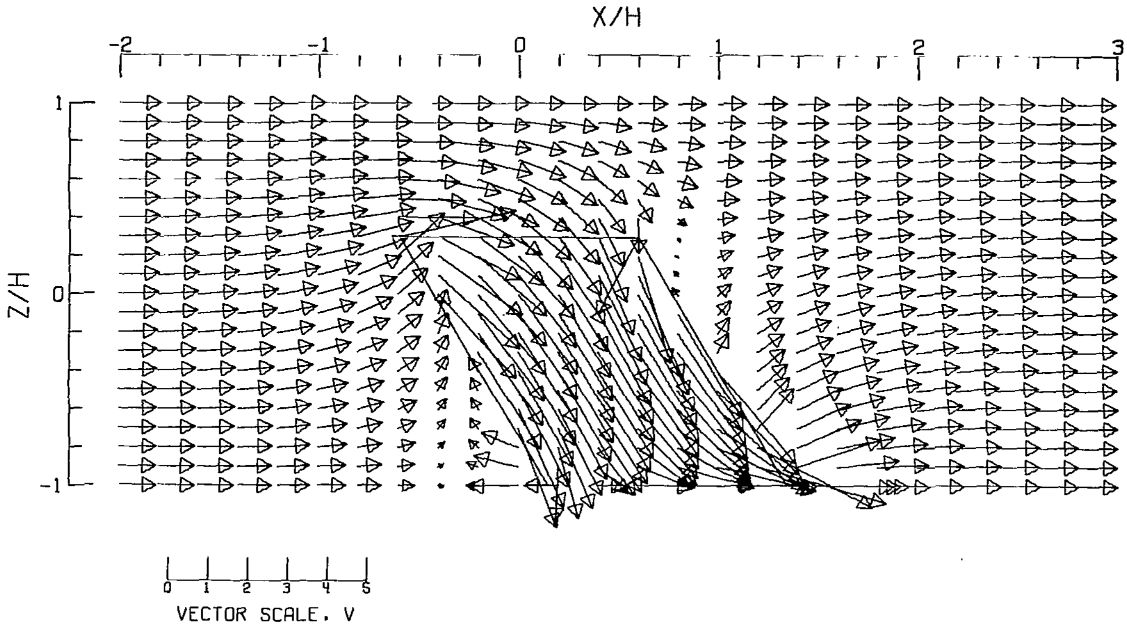

(C).- CLOSED TUNNEL.

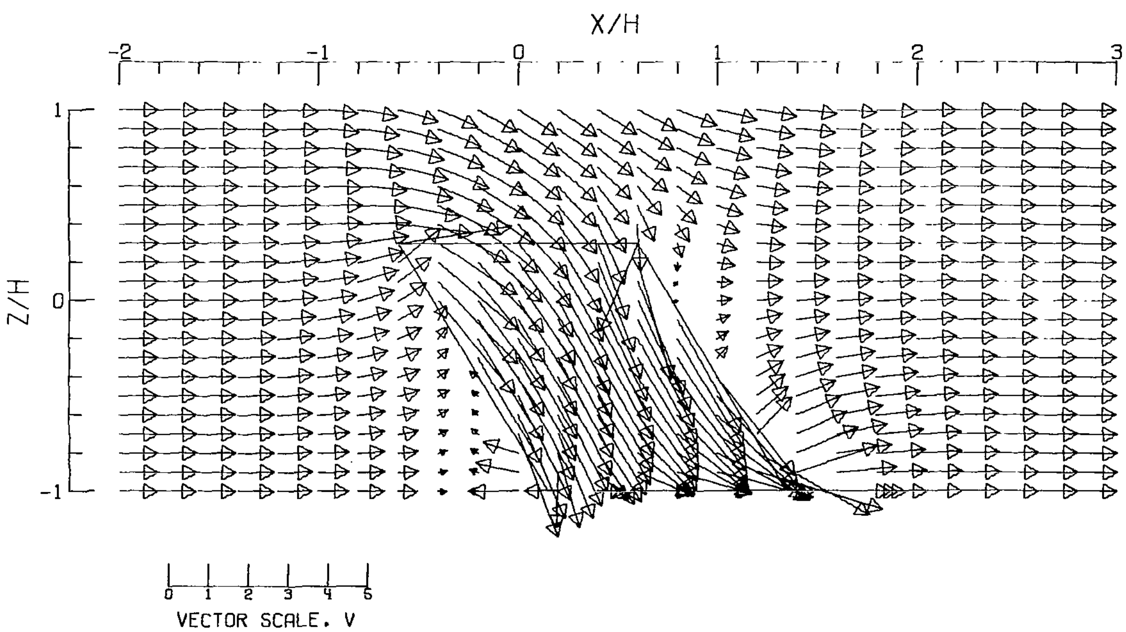

(D).- CLOSED-ON-BOTTOM-ONLY TUNNEL.

Figure 7.- Concluded.

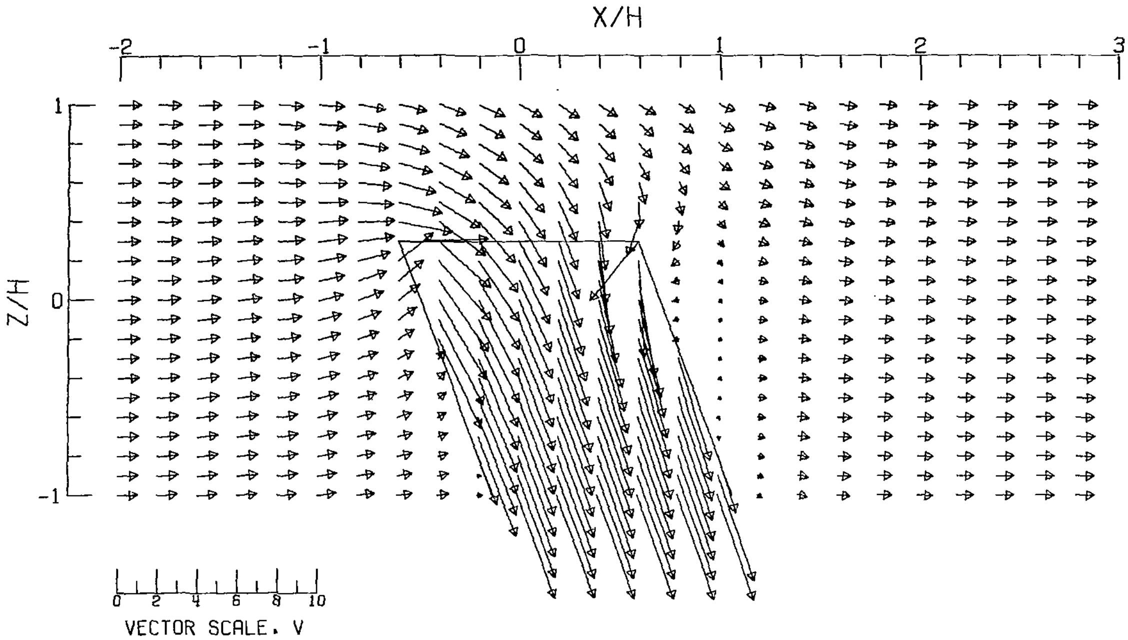

(A).- FREE AIR.

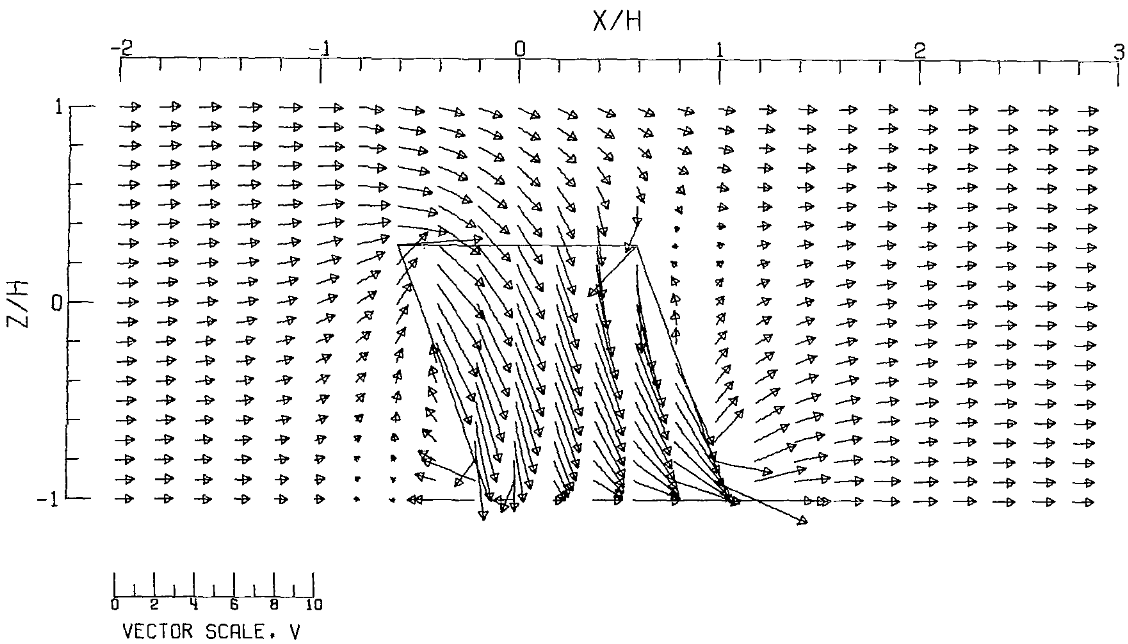

(B).- GROUND EFFECT.

Figure 8.- Flow vectors in the X-Z plane, calculated using vortex cylinders. The rotor and the edges of the wake are shown. ζ = 0.769; η = 1.00; γ = 1.000; σ = 0.600; α = 0.0°; χ = 20.000°; uniform loading.

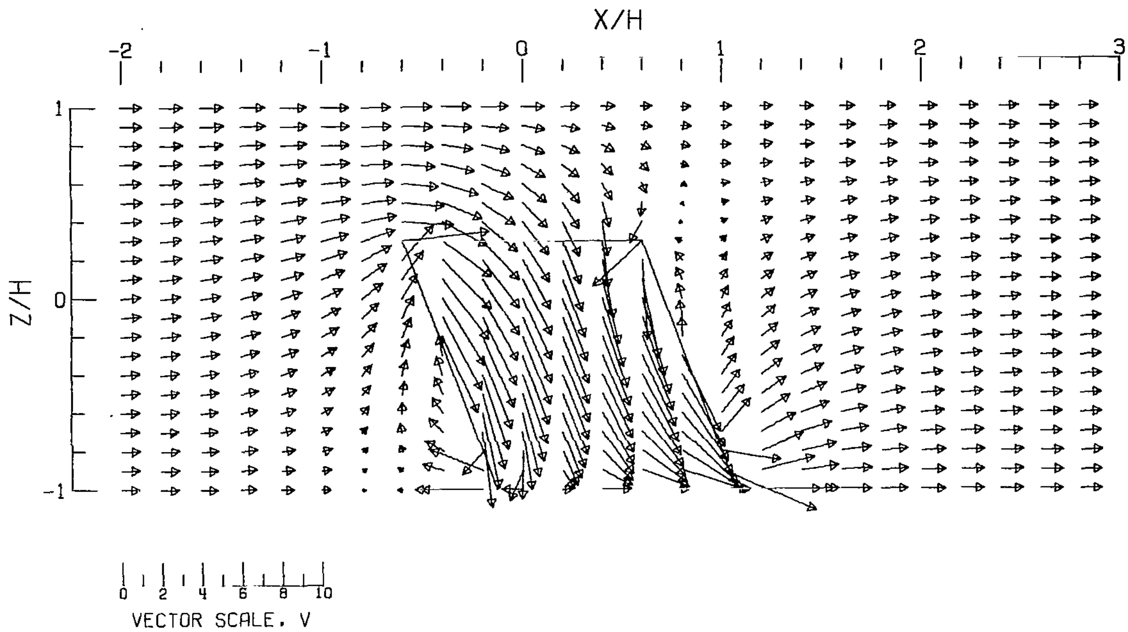

(C).- CLOSED TUNNEL.

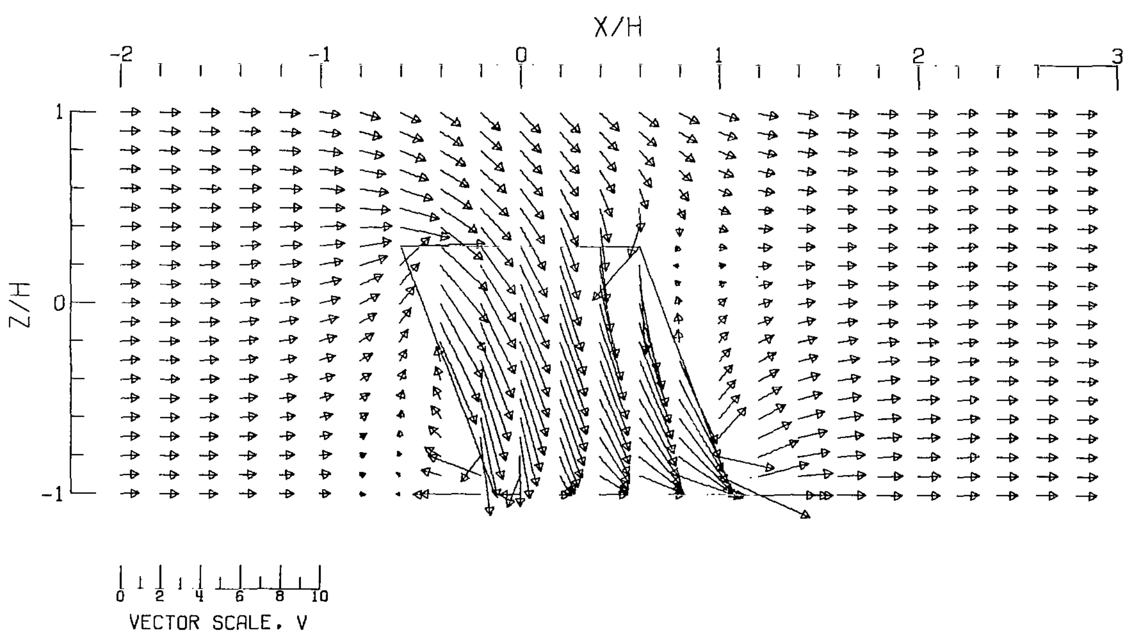

(D).- CLOSED-ON-BOTTOM-ONLY TUNNEL.

Figure 8.- Concluded.

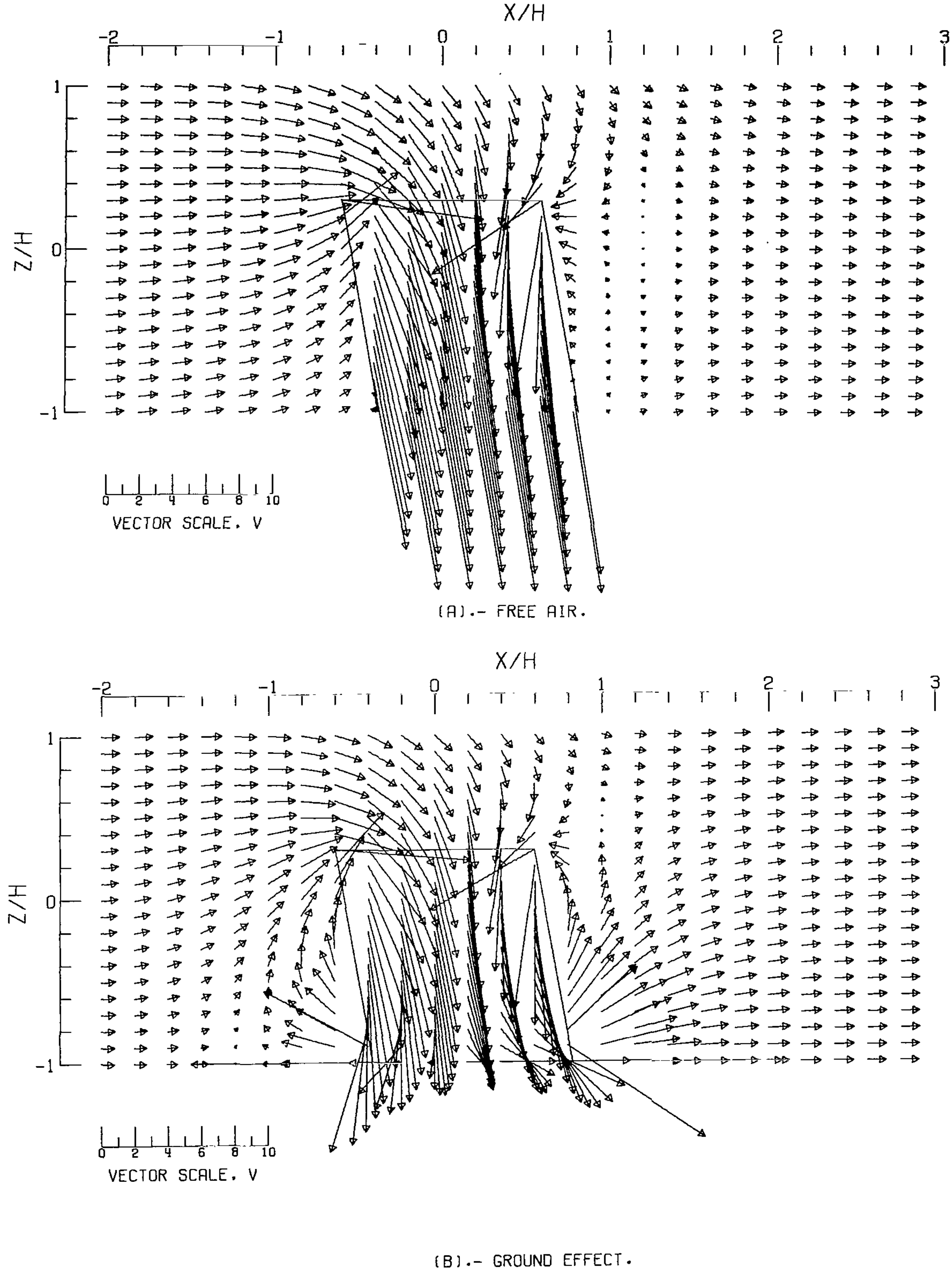

Figure 9.- Flow vectors in the X-Z plane, calculated using vortex cylinders. The rotor and the edges of the wake are shown. $\zeta = 0.769$; $\eta = 1.00$; $\gamma = 1.000$; $\sigma = 0.600$; $\alpha = 0.0^{0}$; $\chi = 10.000^{0}$; uniform loading.

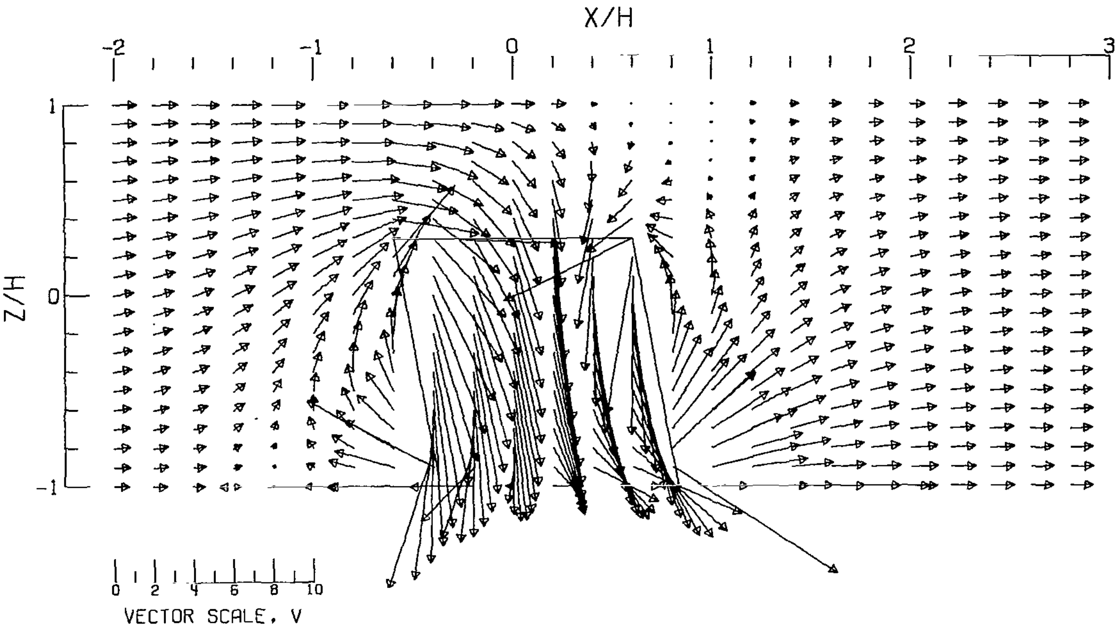

(C).- CLOSED TUNNEL.

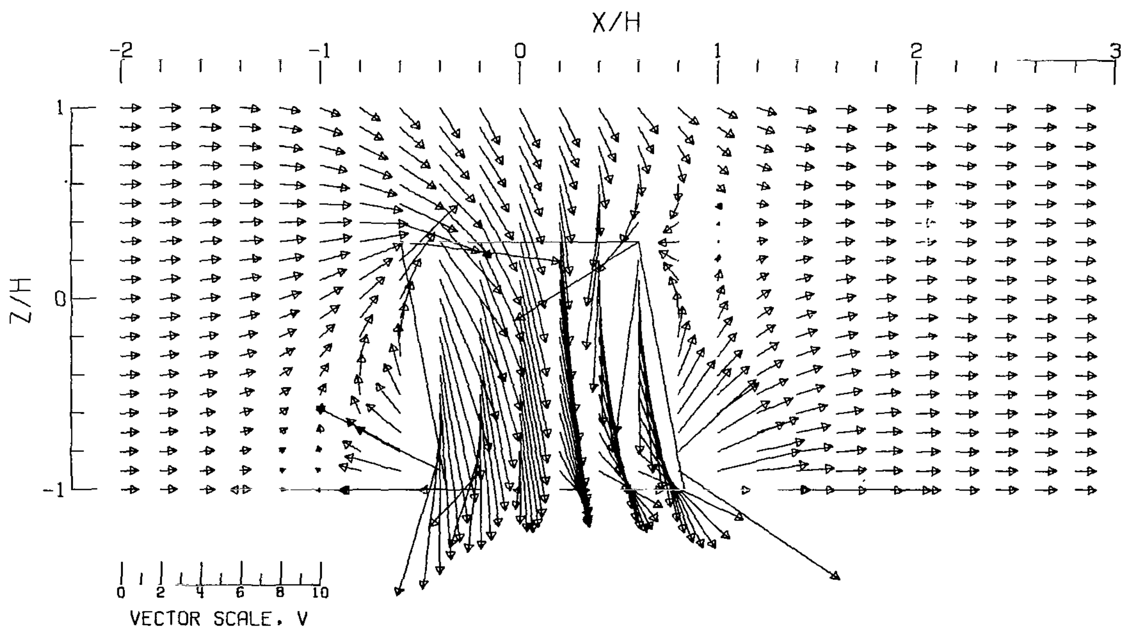

(D).- CLOSED-ON-BOTTOM-ONLY TUNNEL.

Figure 9.- Concluded.

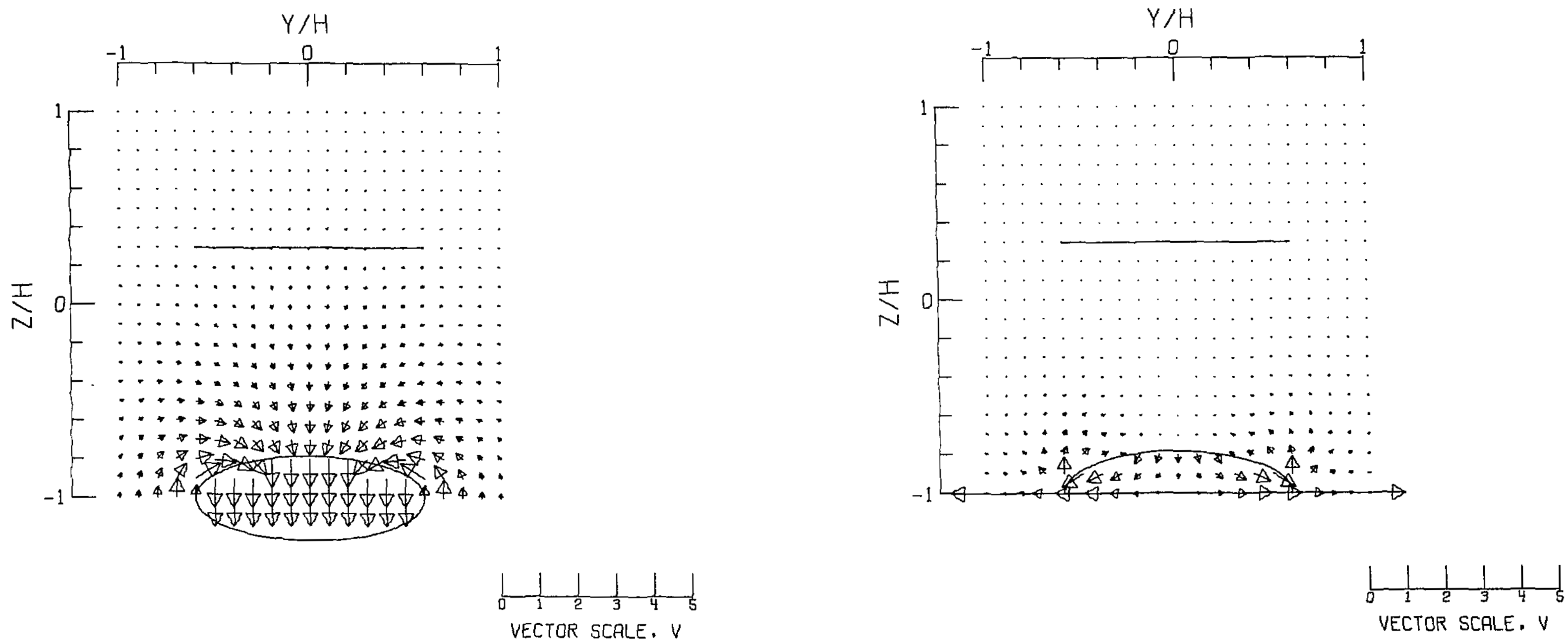

(A).- FREE AIR.

(B).- GROUND EFFECT.

Figure 10.- Flow vectors in a transverse vertical plane at $x/H = 3.571$, calculated using vortex cylinders. The location of the rotor and the intersection of the wake on the vertical plane are shown. $\zeta = 0.769$; $\eta = 1.00$; $\gamma = 1.000$; $\sigma = 0.600$; $\alpha = 0.0^{\circ}$; $\chi = 70.000^{\circ}$; uniform loading.

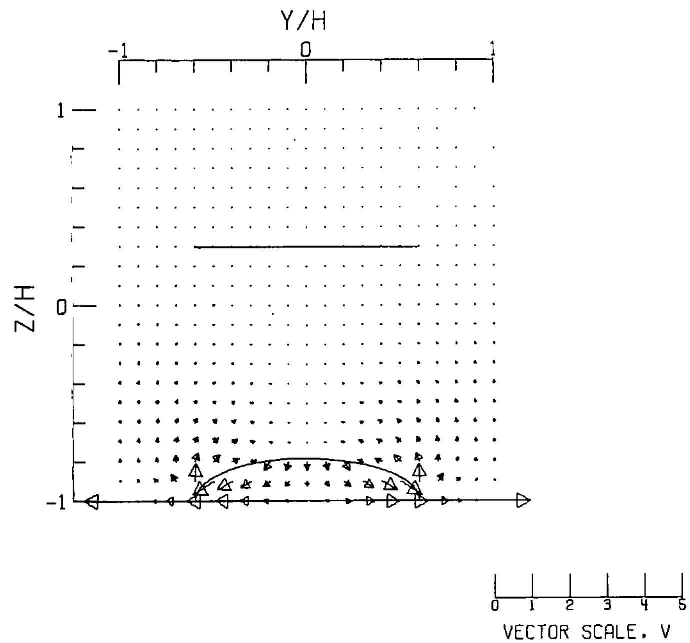

(C).- CLOSED TUNNEL.

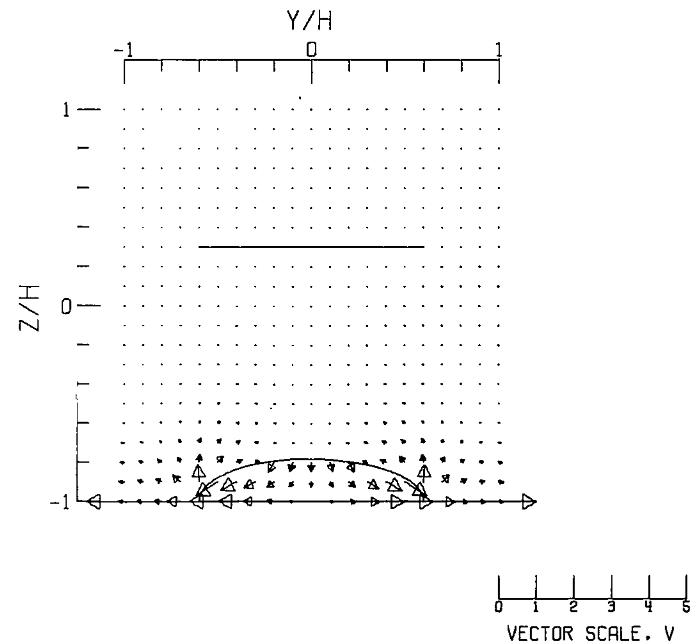

(D).- CLOSED-ON-BOTTOM-ONLY TUNNEL.

Figure 10.- Concluded.

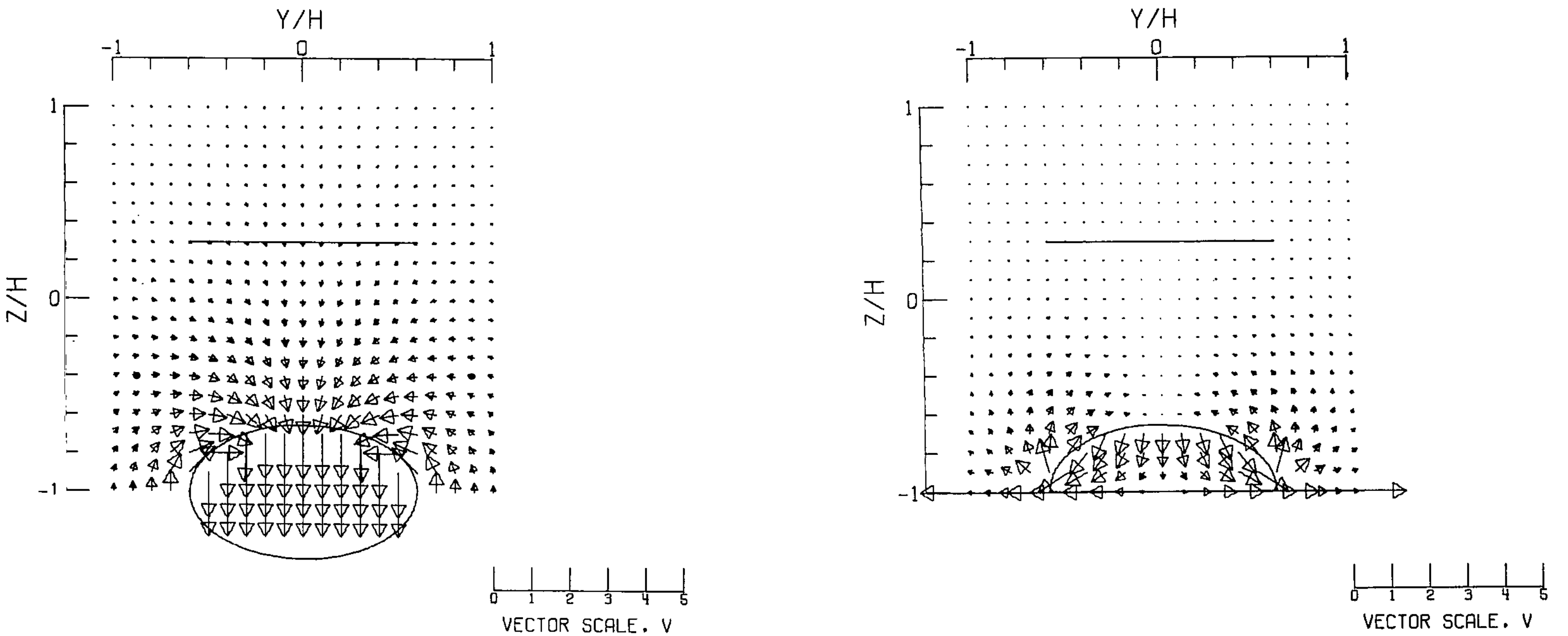

(A).- FREE AIR.

(B).- GROUND EFFECT.

Figure 11.- Flow vectors in a transverse vertical plane at $x/H = 2.250$, calculated using vortex cylinders. The location of the rotor and the intersection of the wake on the vertical plane are shown. $\zeta = 0.769$; $\eta = 1.00$; $\gamma = 1.000$; $\sigma = 0.600$; $\alpha = 0.0^{\circ}$; $\chi = 60.000^{\circ}$; uniform loading.

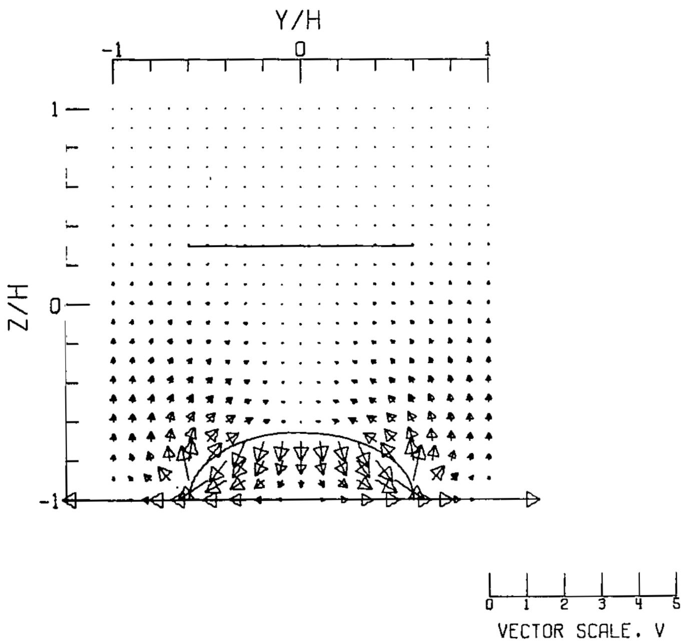

(C).– CLOSED TUNNEL.

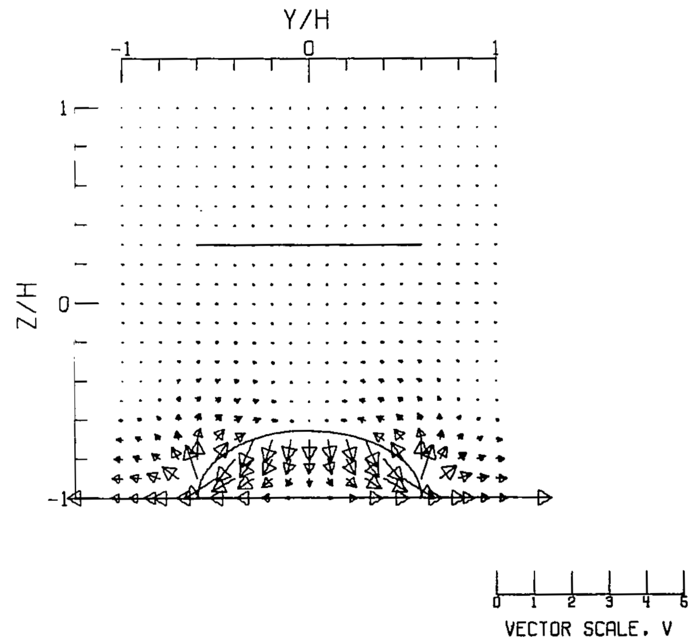

(D).– CLOSED-ON-BOTTOM-ONLY TUNNEL.

Figure 11.- Concluded.

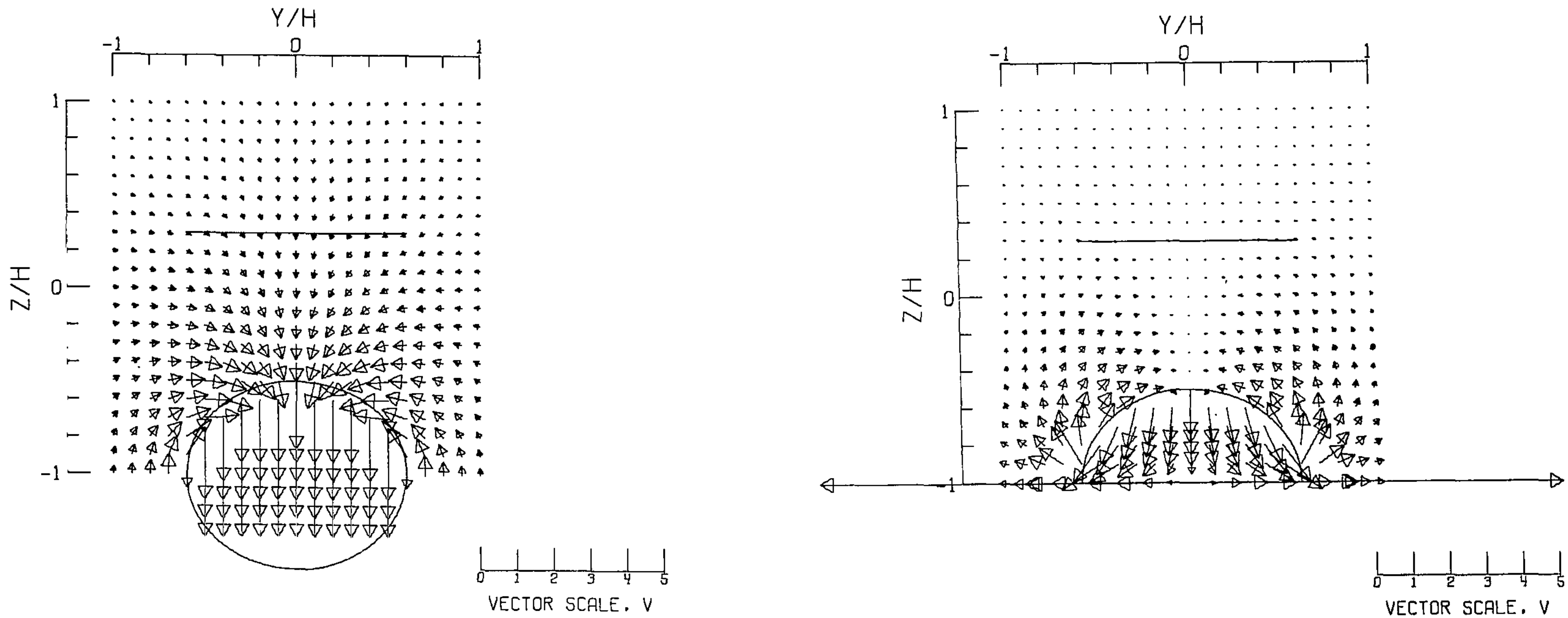

(A).- FREE AIR.

(B).- GROUND EFFECT.

Figure 12.- Flow vectors in a transverse vertical plane at x/H = 1.550, calculated using vortex cylinders. The location of the rotor and the intersection of the wake on the vertical plane are shown. ζ = 0.769; γ = 1.0; σ = 0.60; α = 0.0°; χ = 50.0°; uniform loading.

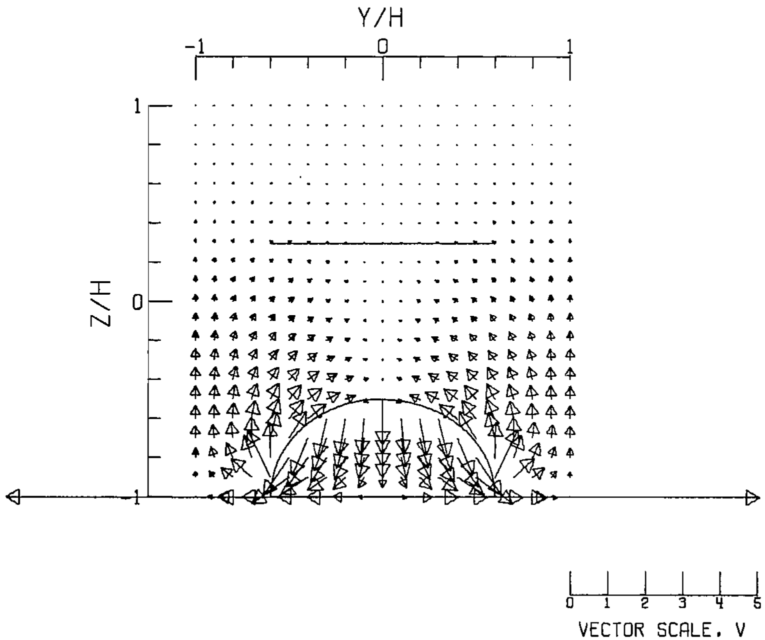

(C).- CLOSED TUNNEL.

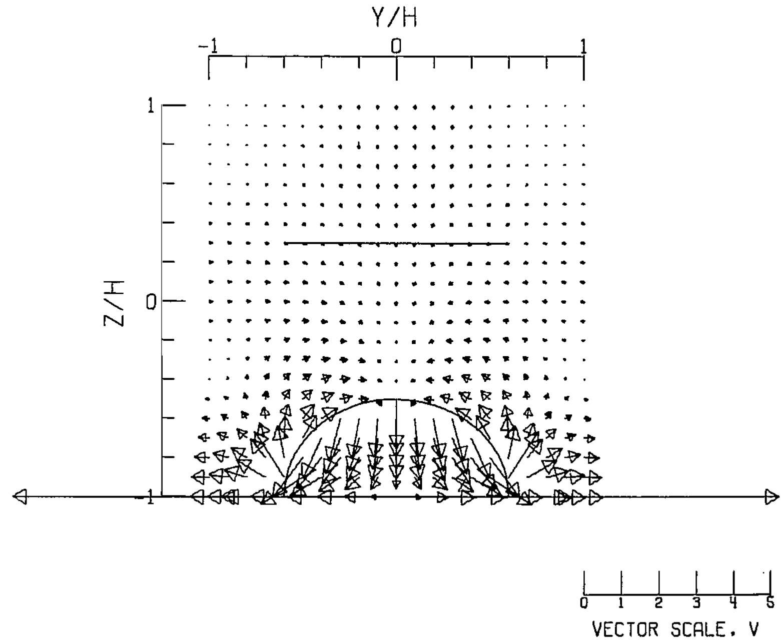

(D).- CLOSED-ON-BOTTOM-ONLY TUNNEL.

Figure 12.- Concluded.

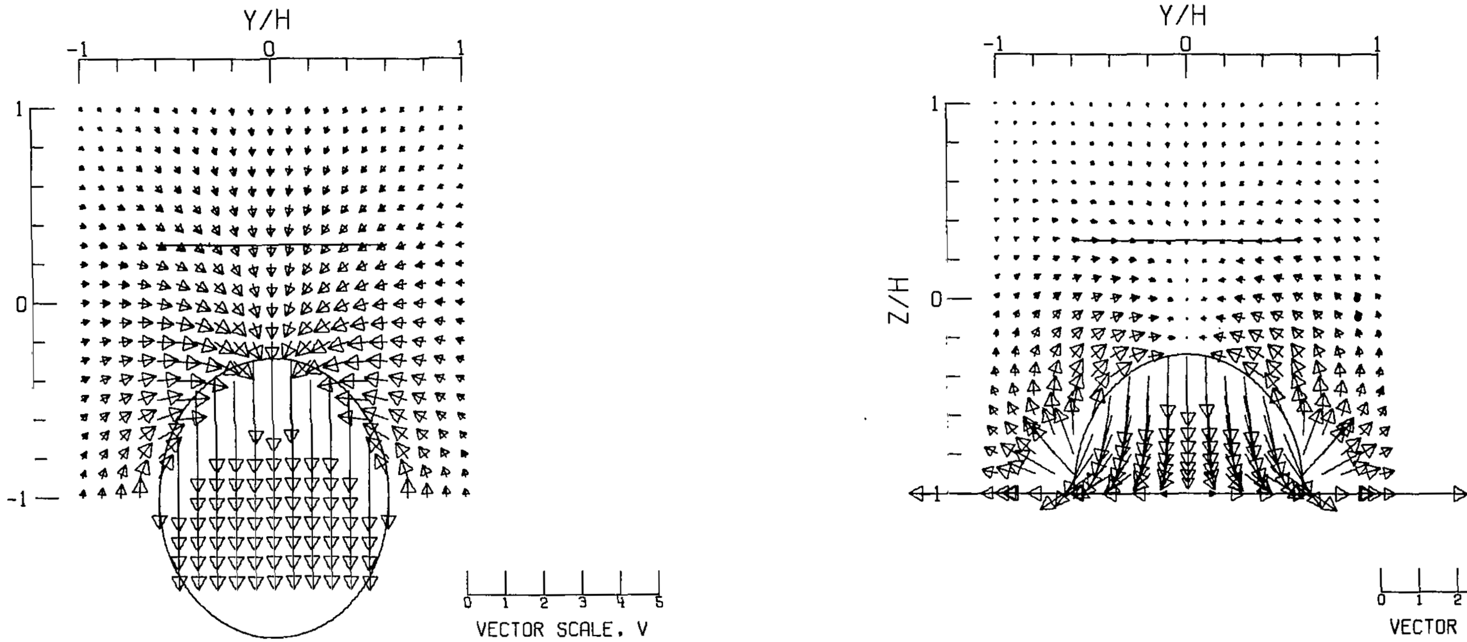

(A).- FREE AIR.

(B).- GROUND EFFECT.

Figure 13.- Flow vectors in a transverse vertical plane at $x/H = 1.091$, calculated using vortex cylinders. The location of the rotor and the intersection of the wake on the vertical plane are shown. $\zeta = 0.769$; $\eta = 1.00$; $\gamma = 1.000$; $\sigma = 0.600$; $\alpha = 0.0^{\circ}$; $\chi = 40.000^{\circ}$; uniform loading.

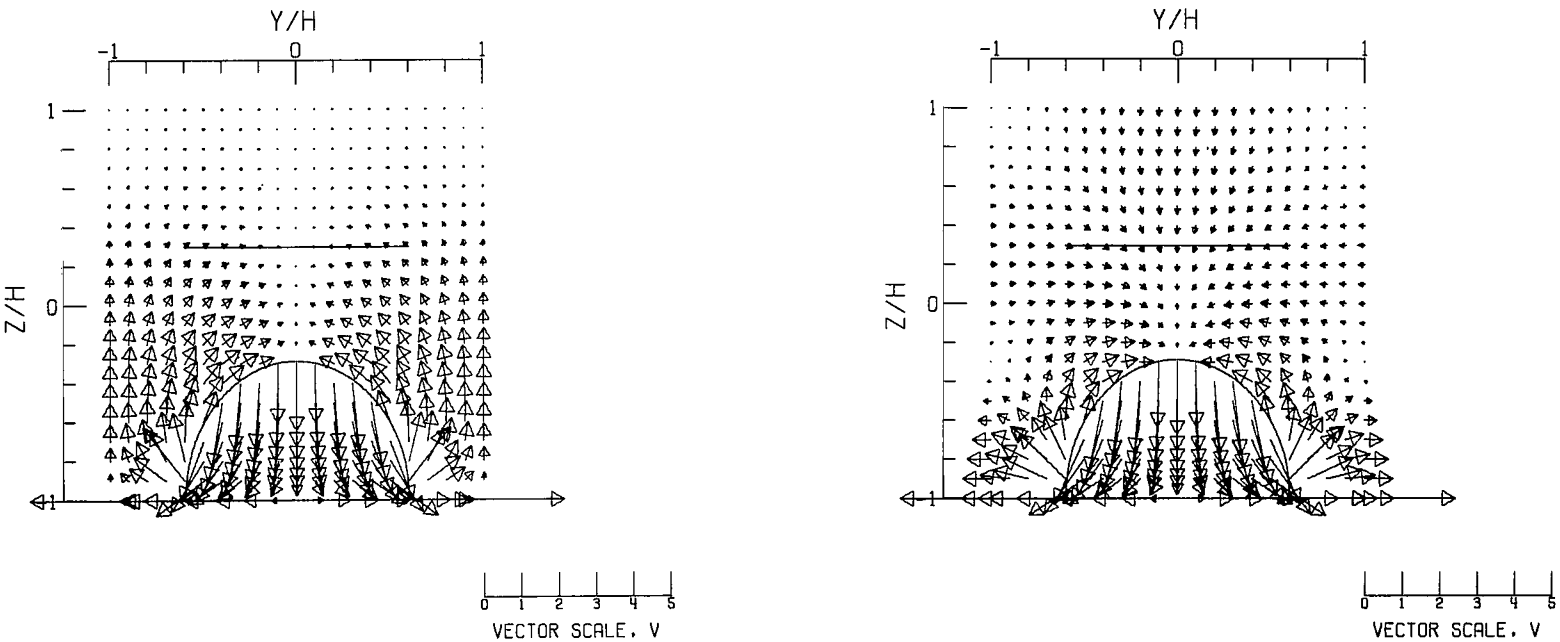

(C).- CLOSED TUNNEL.

(D).- CLOSED-ON-BOTTOM-ONLY TUNNEL.

Figure 13.- Concluded.

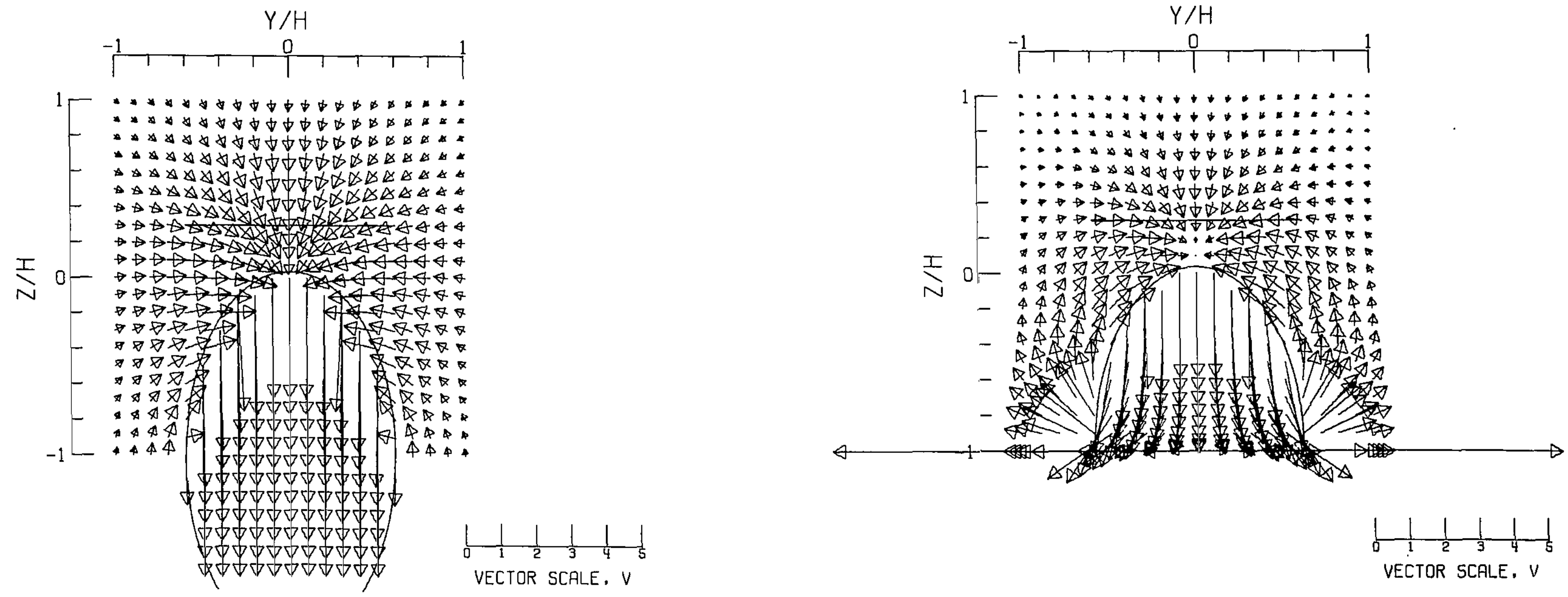

(A).- FREE AIR.

(B).- GROUND EFFECT.

Figure 14.- Flow vectors in a transverse vertical plane at $x/H = 0.750$, calculated using vortex cylinders. The location of the rotor and the intersection of the wake on the vertical plane are shown. $\zeta = 0.769$; $\eta = 1.00$; $\gamma = 1.000$; $\sigma = 0.600$; $\alpha = 0.0^{\circ}$; $\chi = 30.000^{\circ}$; uniform loading.

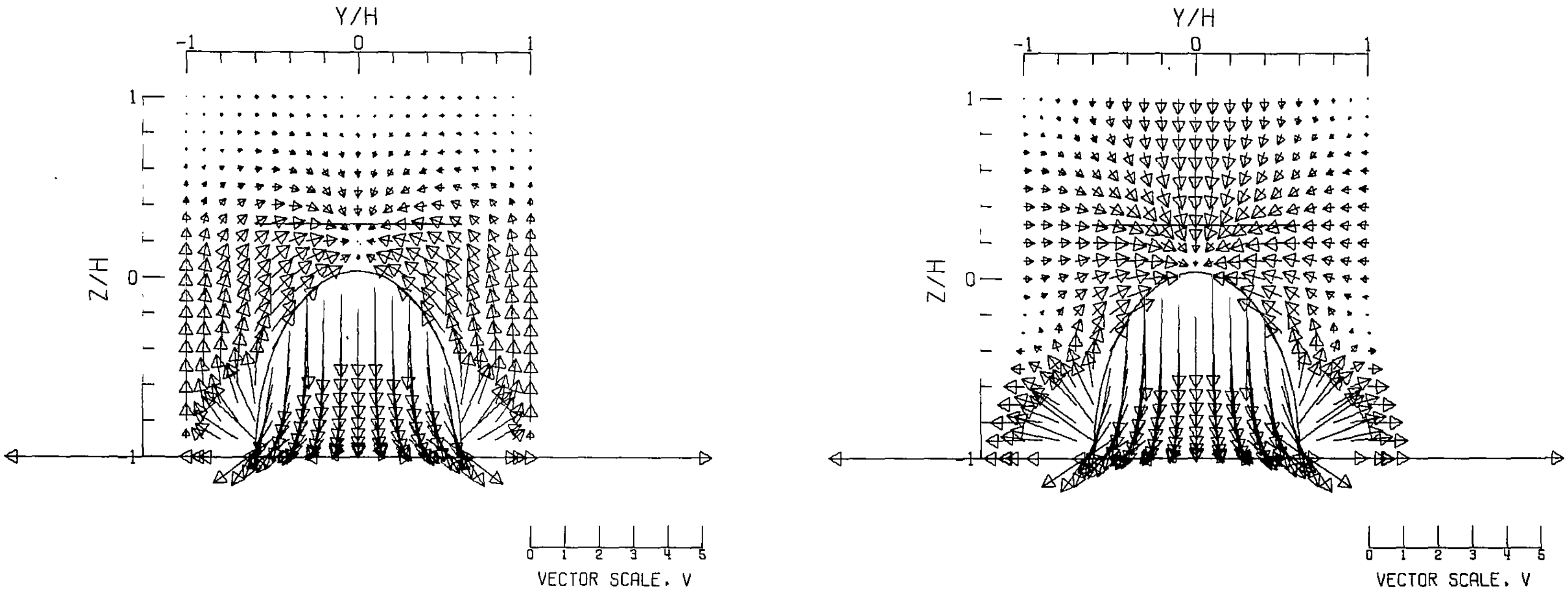

(C).- CLOSED TUNNEL.

(D).- CLOSED-ON-BOTTOM-ONLY TUNNEL.

Figure 14.- Concluded.

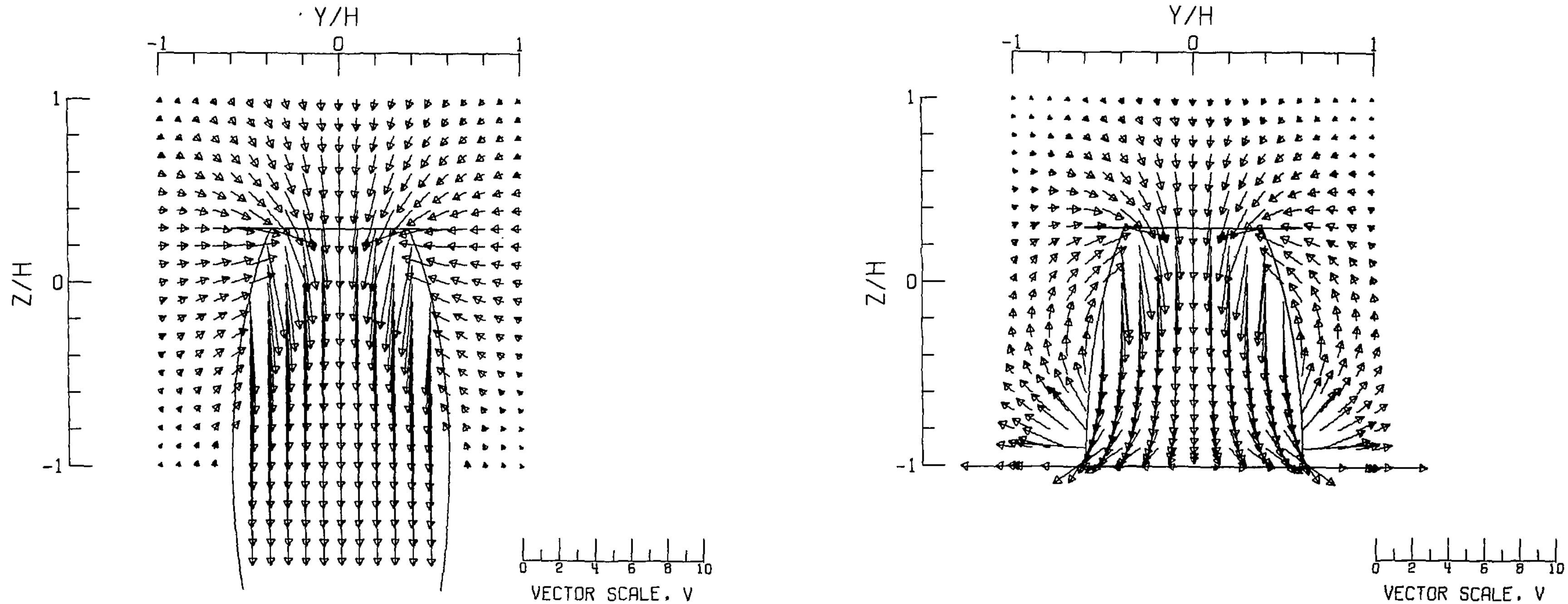

(B).- GROUND EFFECT.

(A).- FREE AIR.

Figure 15.- Flow vectors in a transverse vertical plane at x/H = 0.464, calculated using vortex cylinders. The location of the rotor and the intersection of the wake on the vertical plane are shown. ζ = 0.769; η = 1.00; γ = 1.000; σ = 0.600; α = 0.0°; χ = 20.000°; uniform loading.

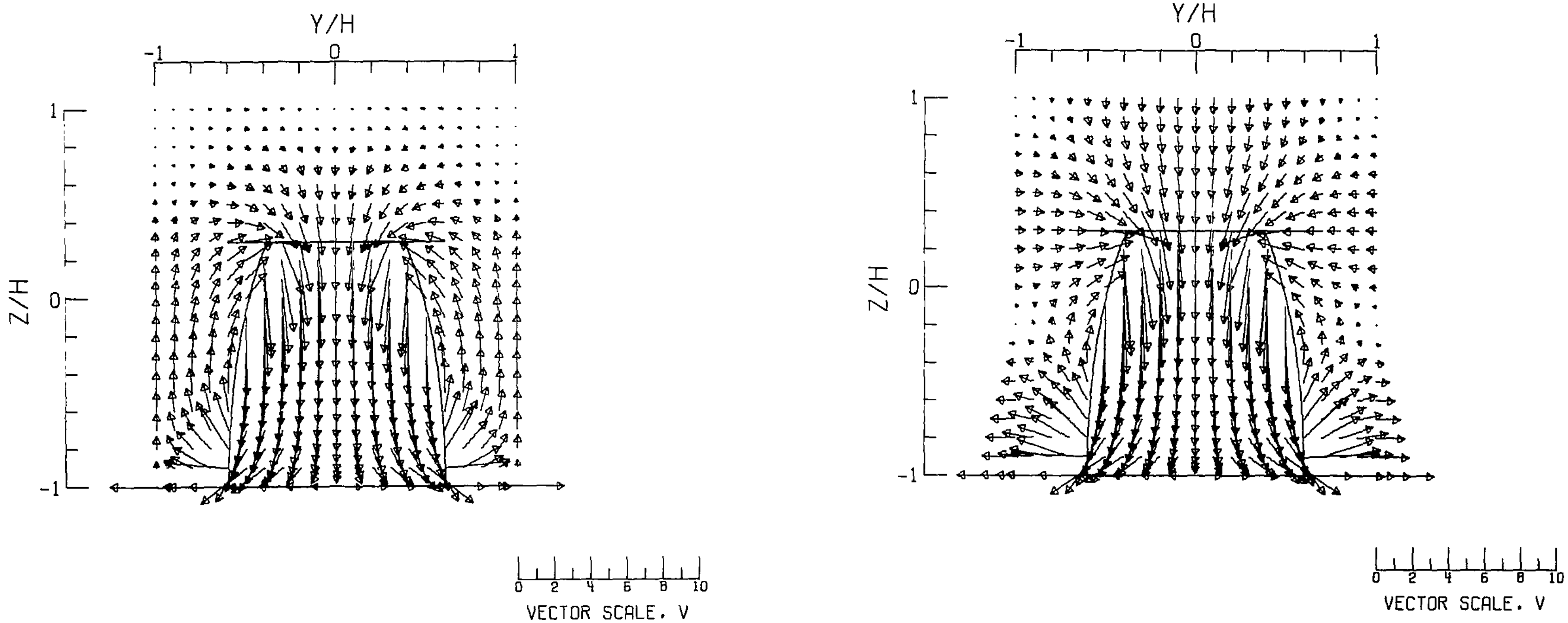

(C).- CLOSED TUNNEL.

(D).- CLOSED-ON-BOTTOM-ONLY TUNNEL.

Figure 15.- Concluded.

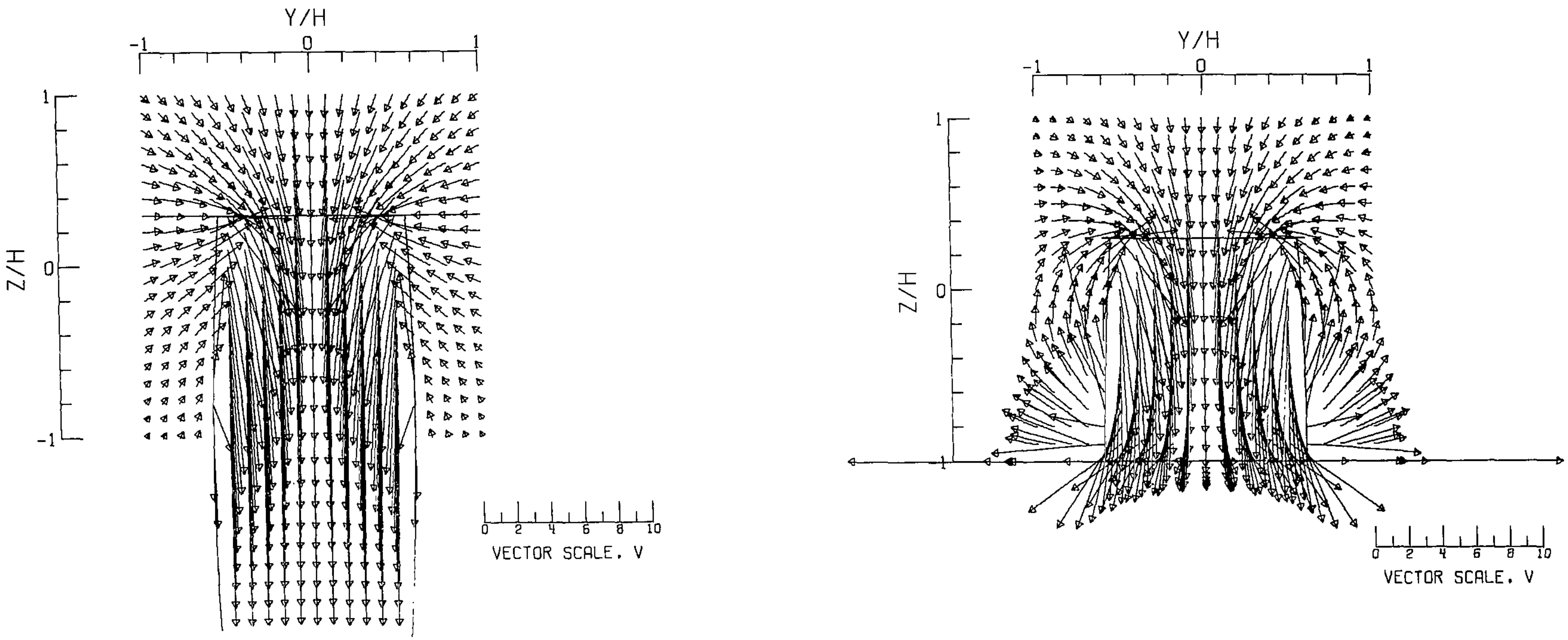

(A).- FREE AIR.

(B).- GROUND EFFECT.

Figure 16.- Flow vectors in a transverse vertical plane at $x/H = 0.229$, calculated using vortex cylinders. The location of the rotor and the intersection of the wake on the vertical plane are shown. $\zeta = 0.769$; $\eta = 1.00$; $\gamma = 1.000$; $\sigma = 0.600$; $\alpha = 0.0^{\circ}$; $\chi = 10.000^{\circ}$; uniform loading.

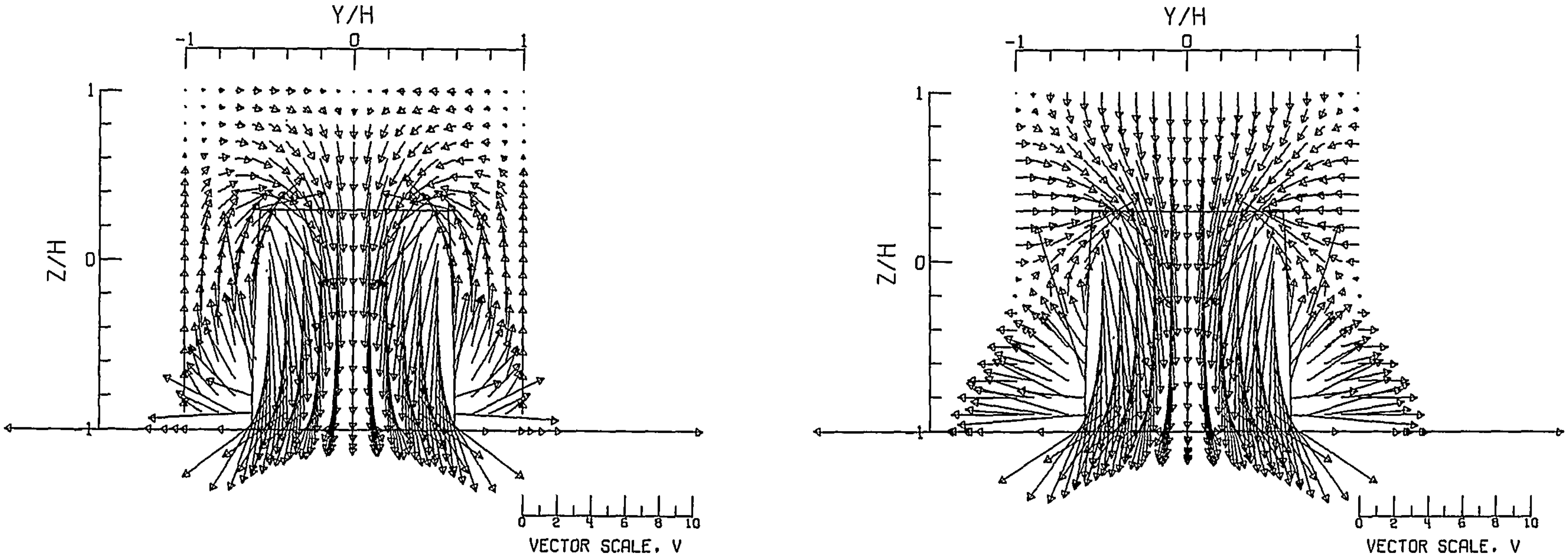

(C).- CLOSED TUNNEL.

(D).- CLOSED-ON-BOTTOM-ONLY TUNNEL.

Figure 16.- Concluded.

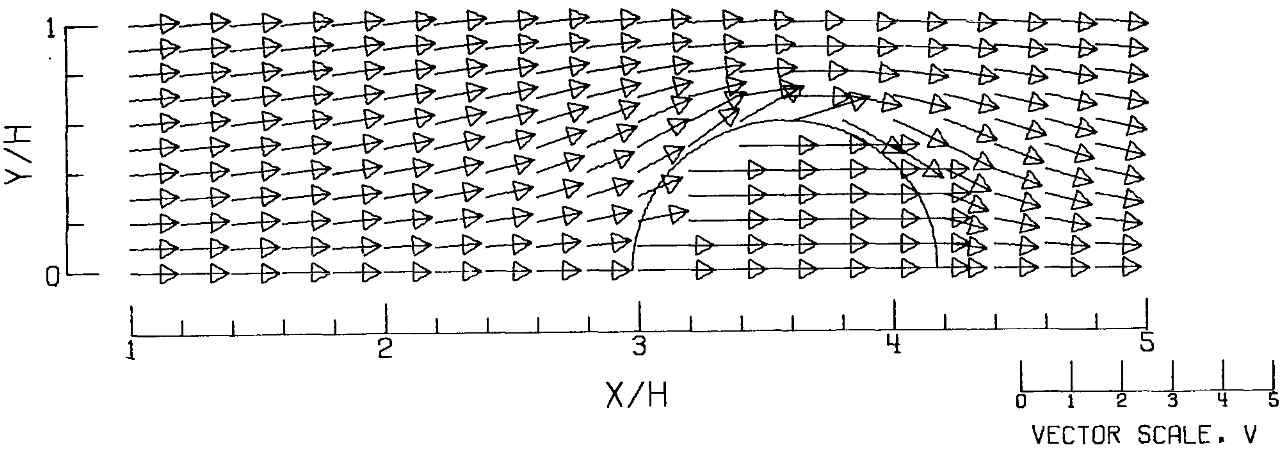

(A).- FREE AIR.

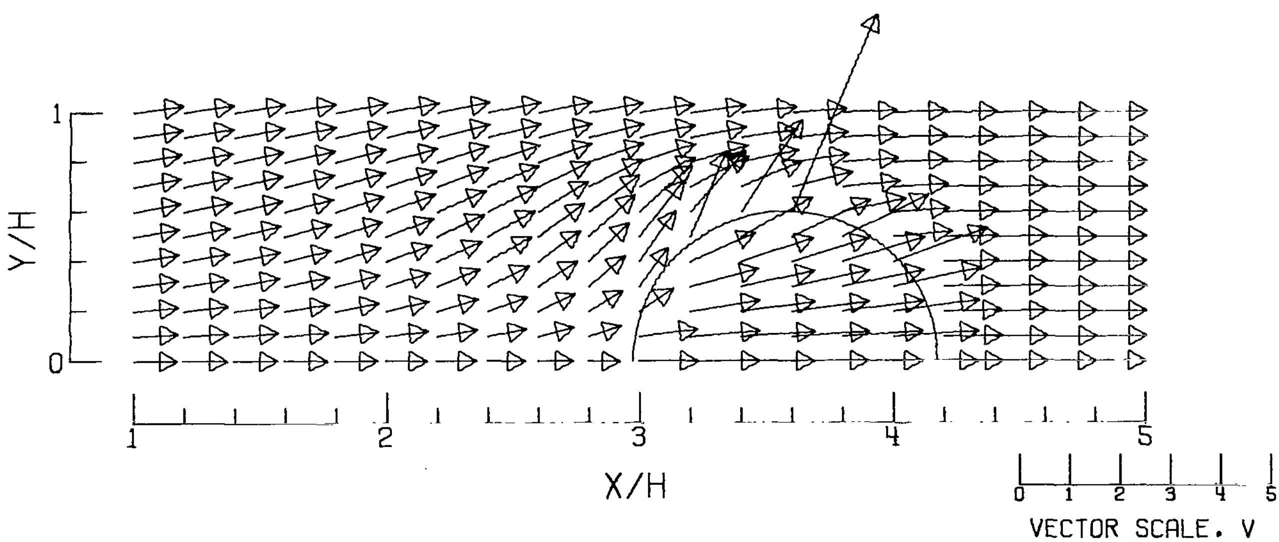

(B).- GROUND EFFECT.

Figure 17.- Flow vectors in the plane of the floor, calculated using vortex cylinders. The intersection of the wake and the plane is shown. ζ = 0.769; η = 1.00; γ = 1.000; σ = 0.600; α = 0.0°; χ = 70.000°; uniform loading.

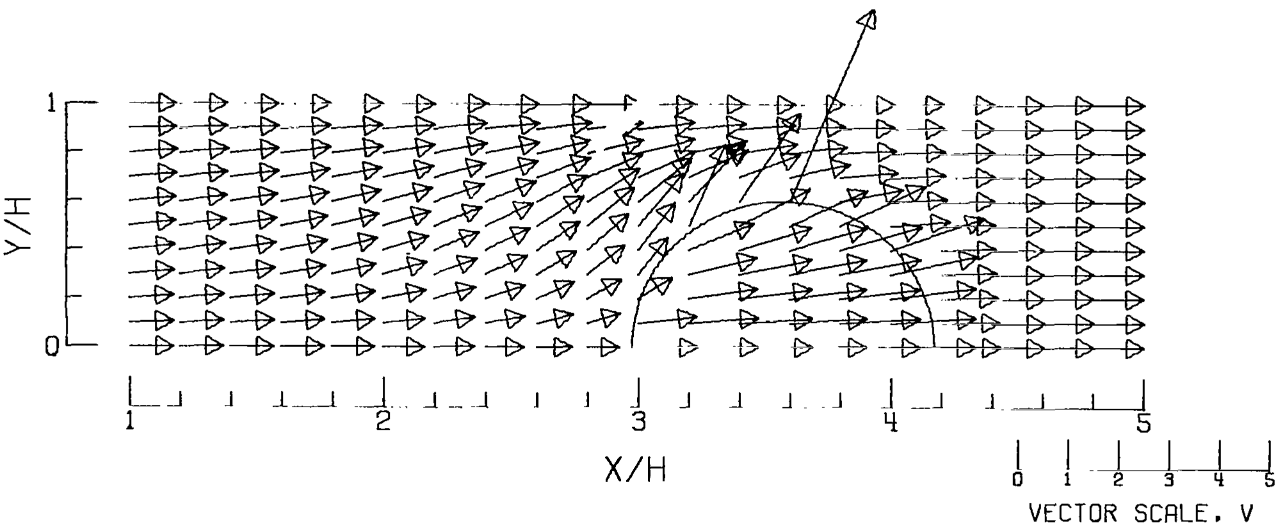

(C).- CLOSED TUNNEL.

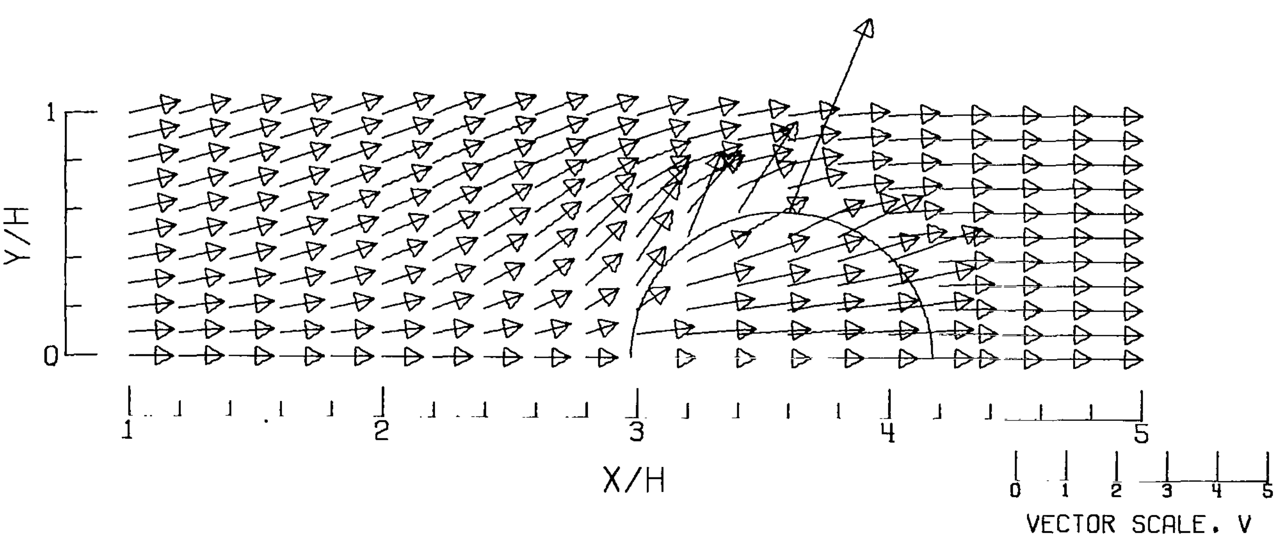

(D).- CLOSED-ON-BOTTOM-ONLY TUNNEL.

Figure 17.- Concluded.

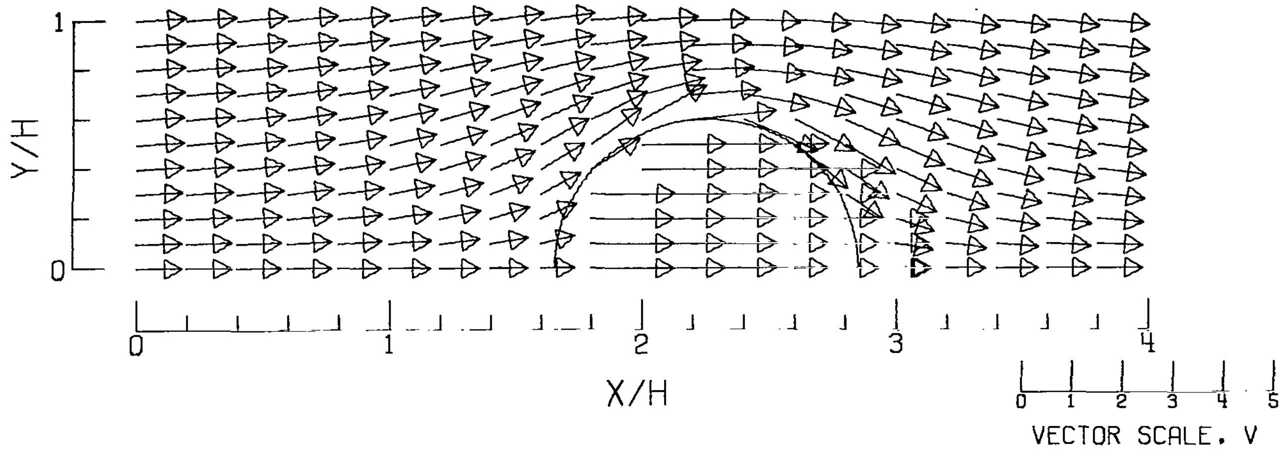

(A).- FREE AIR.

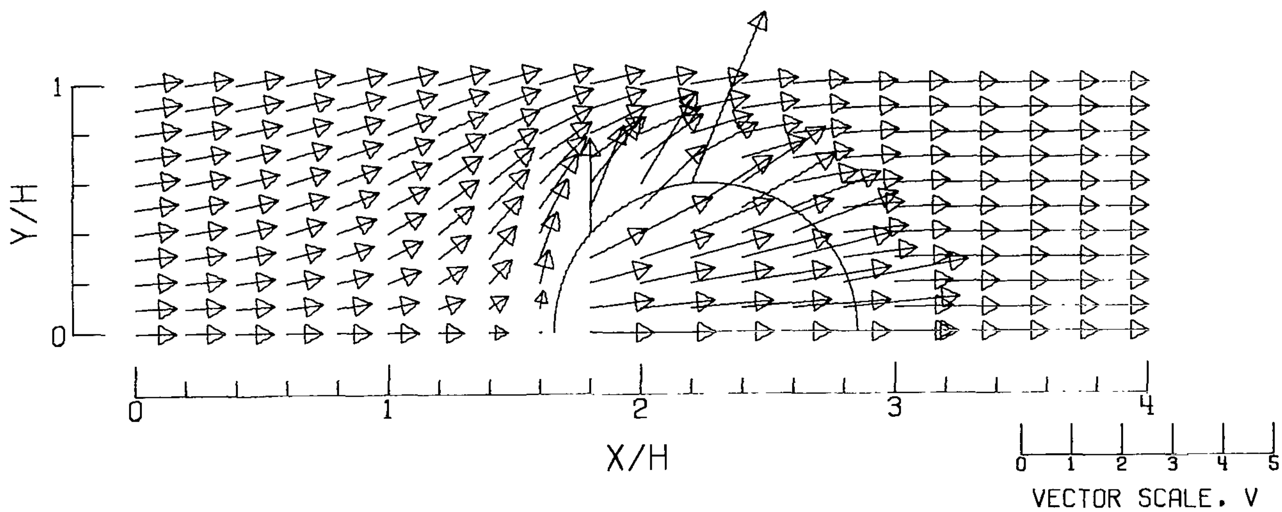

(B).- GROUND EFFECT.

Figure 18.- Flow vectors in the plane of the floor, calculated using vortex cylinders. The intersection of the wake and the plane is shown. ζ = 0.769; η = 1.00; γ = 1.000; σ = 0.600; α = 0.0°; χ = 60.000°; uniform loading.

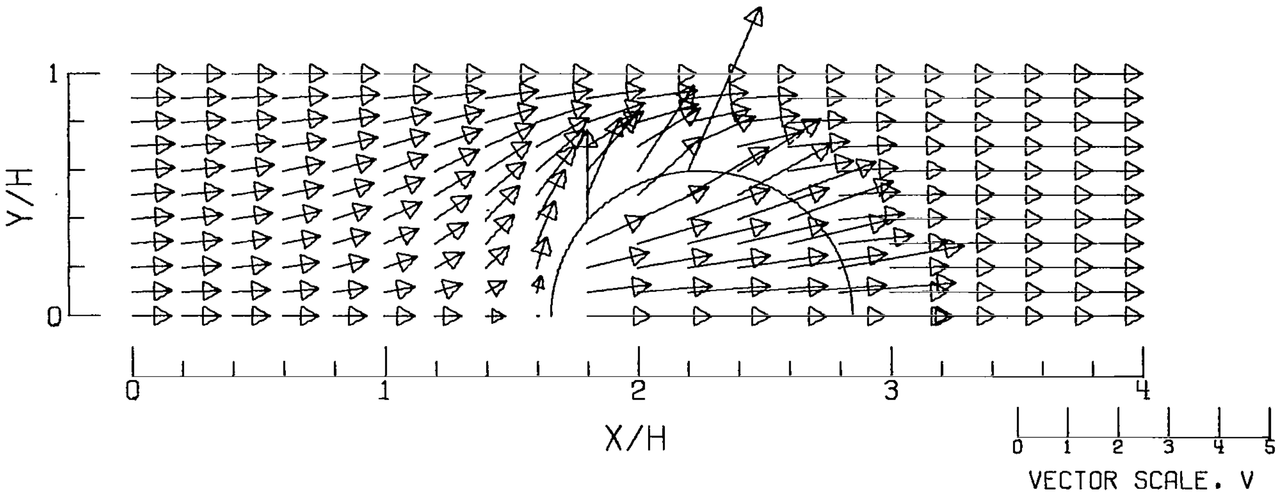

(C).- CLOSED TUNNEL.

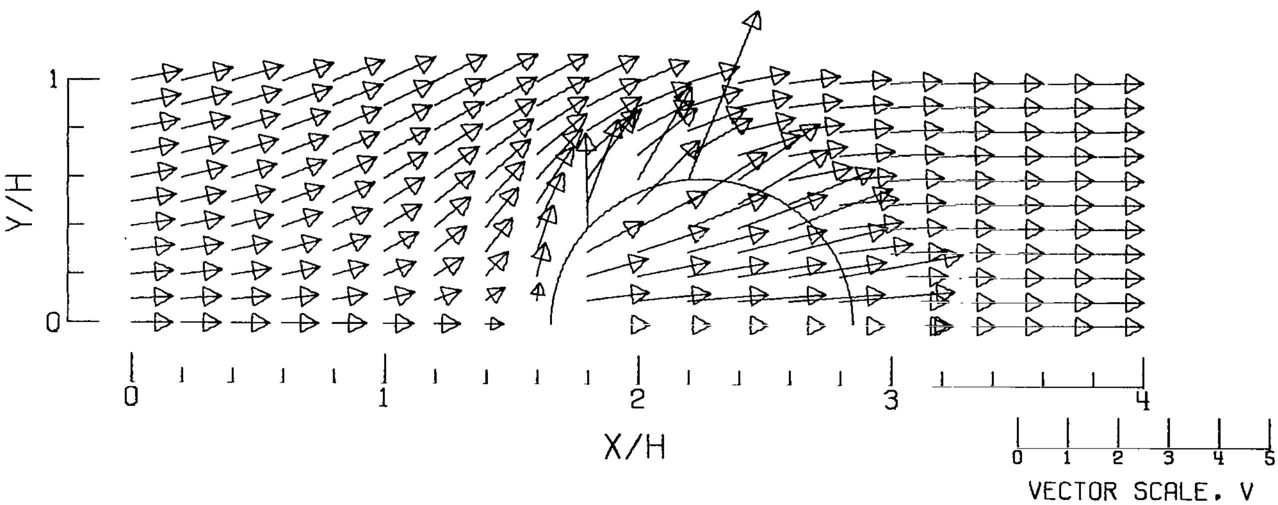

(D).- CLOSED-ON-BOTTOM-ONLY TUNNEL.

Figure 18.- Concluded.

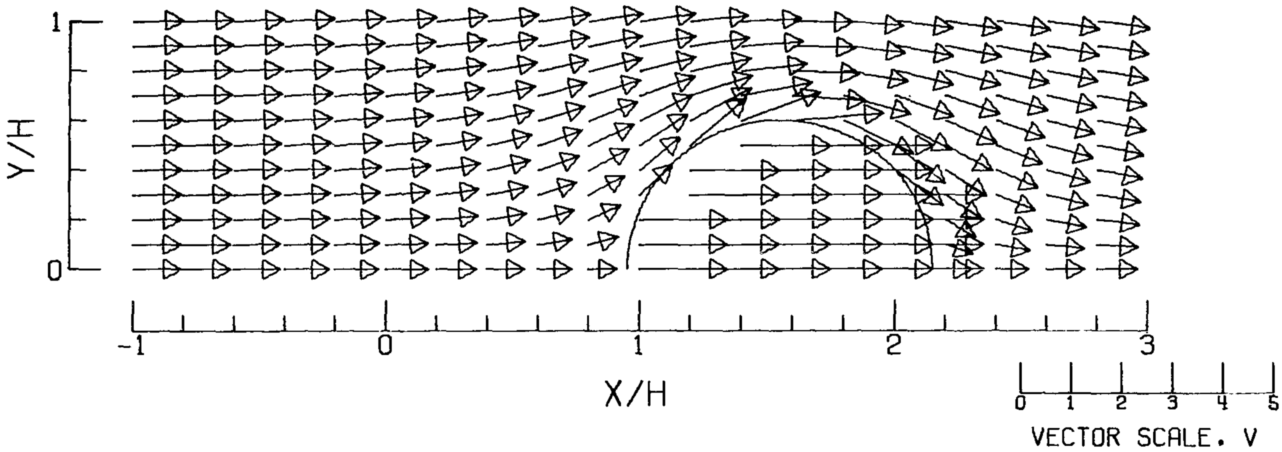

(A).- FREE AIR.

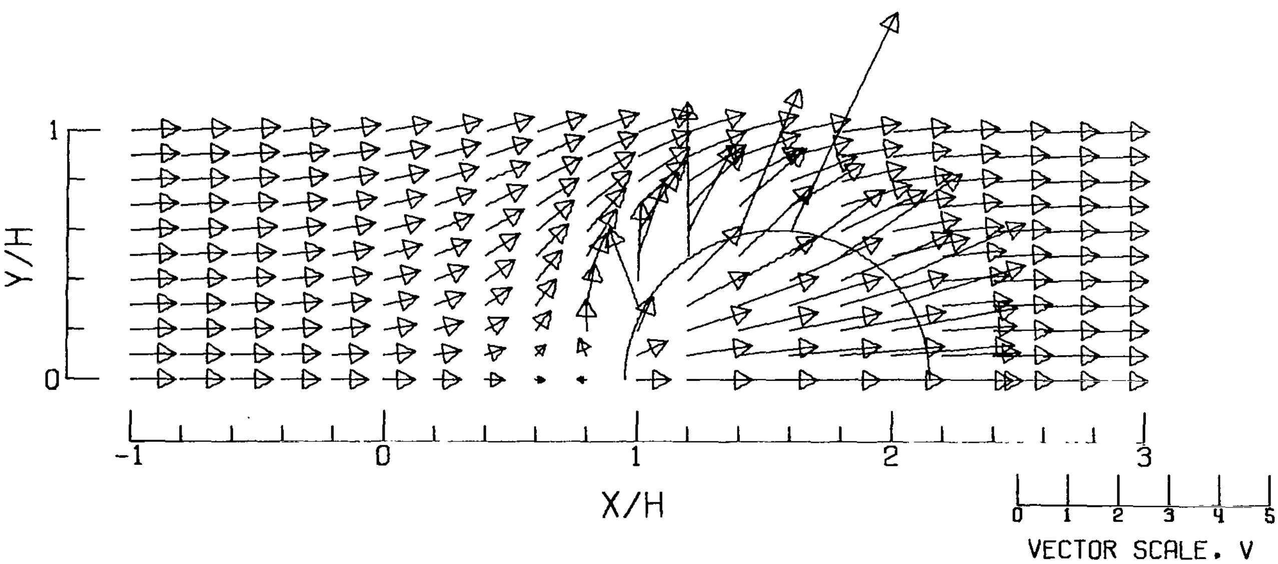

(B).- GROUND EFFECT.

Figure 19.- Flow vectors in the plane of the floor, calculated using vortex cylinders. The intersection of the wake and the plane is shown. $\zeta = 0.769$; $\eta = 1.00$; $\gamma = 1.000$; $\sigma = 0.600$; $\alpha = 0.0^{0}$; $\chi = 50.000^{0}$; uniform loading.

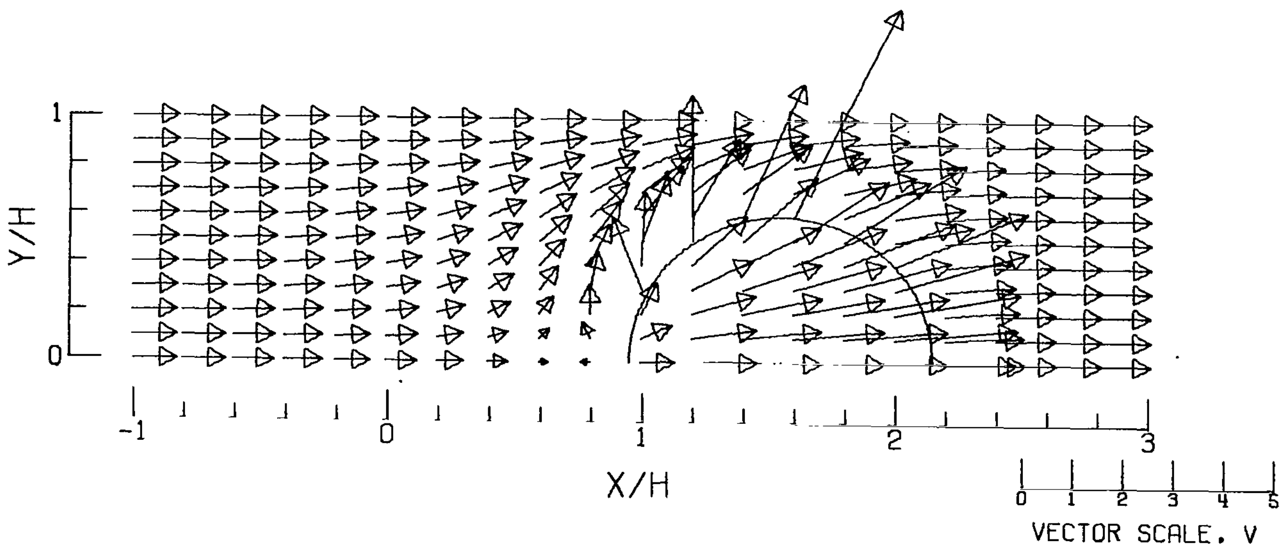

(C).- CLOSED TUNNEL.

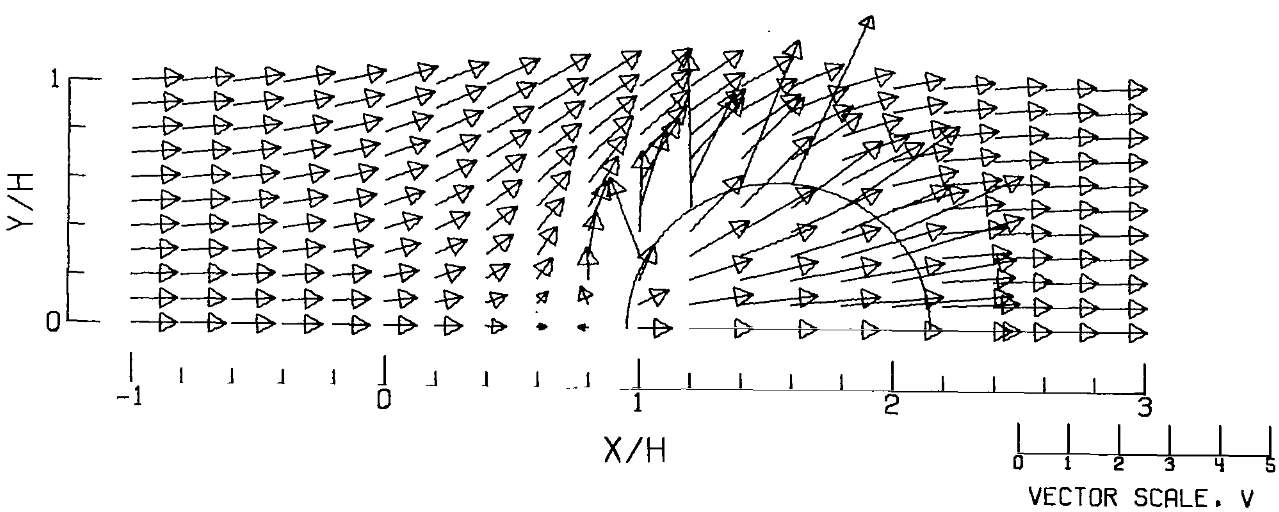

(D).- CLOSED-ON-BOTTOM-ONLY TUNNEL.

Figure 19.- Concluded.

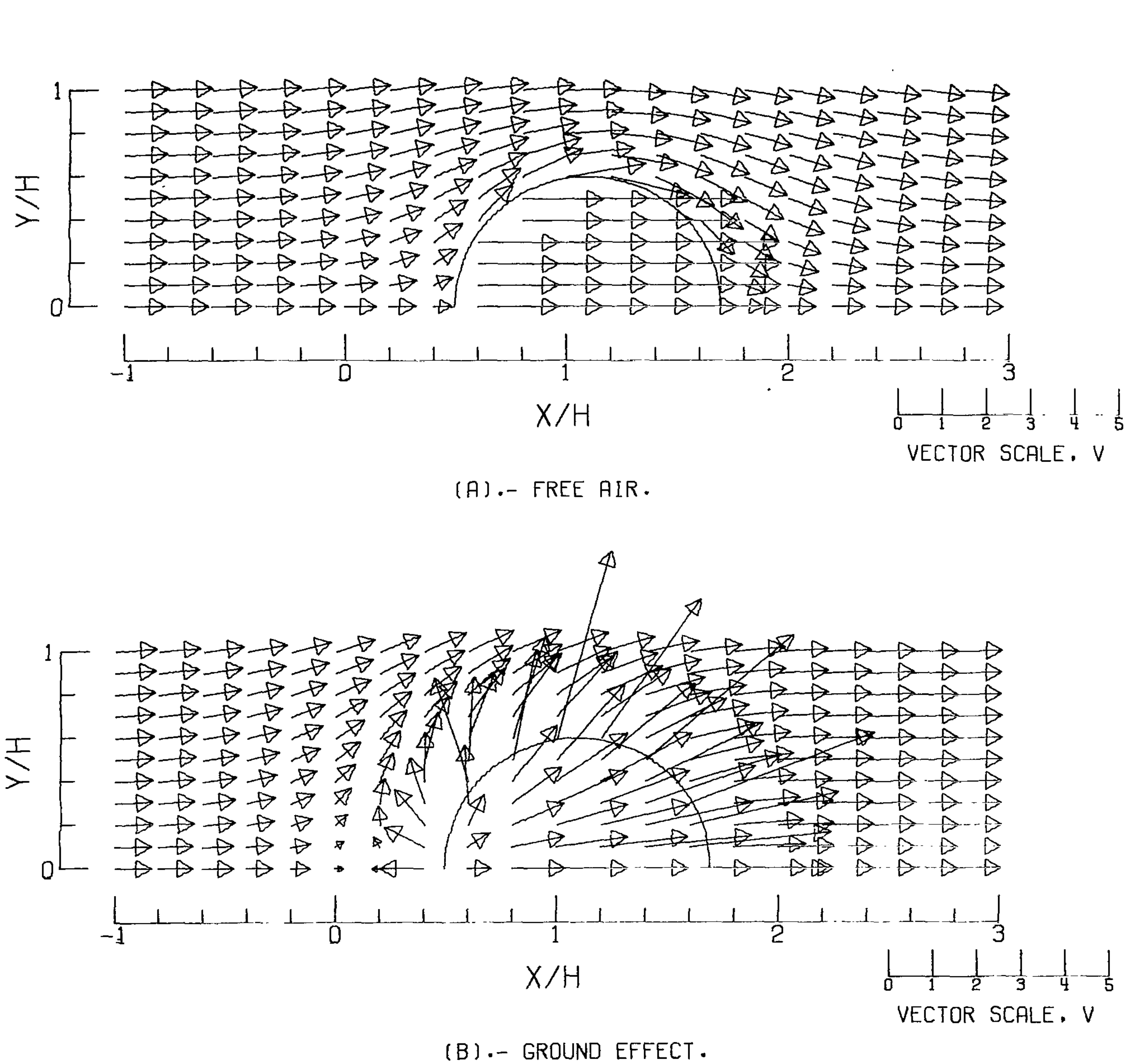

Figure 20.- Flow vectors in the plane of the floor, calculated using vortex cylinders. The intersection of the wake and the plane is shown. ζ = 0.769; η = 1.00; γ = 1.000; σ = 0.600; α = 0.0°; χ = 40.000°; uniform loading.

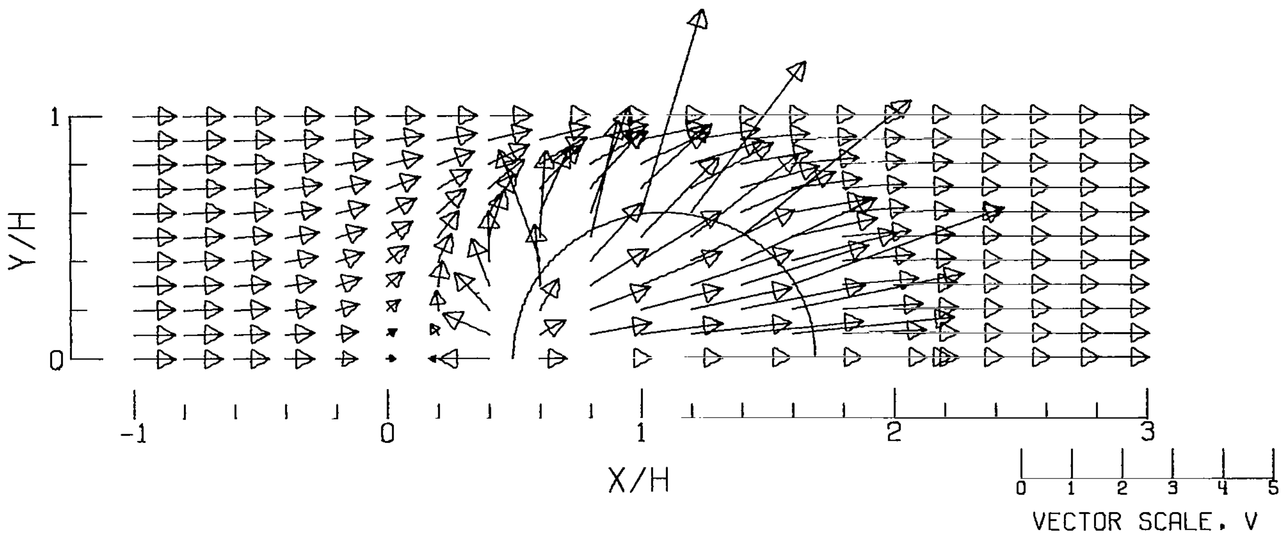

(C).- CLOSED TUNNEL.

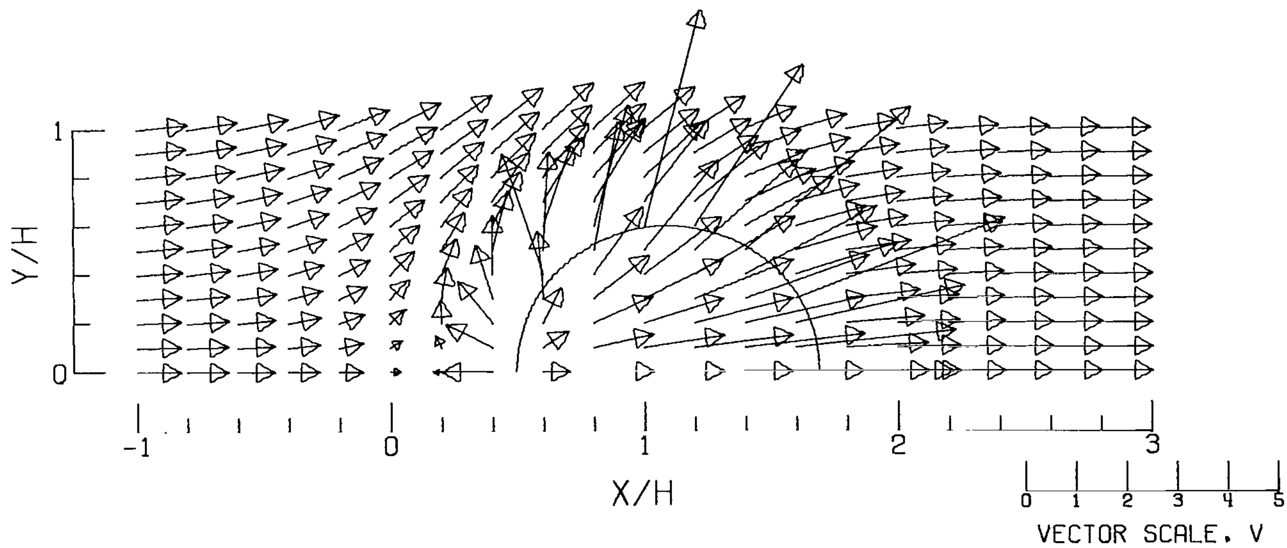

(D).- CLOSED-ON-BOTTOM-ONLY TUNNEL.

Figure 20.- Concluded.

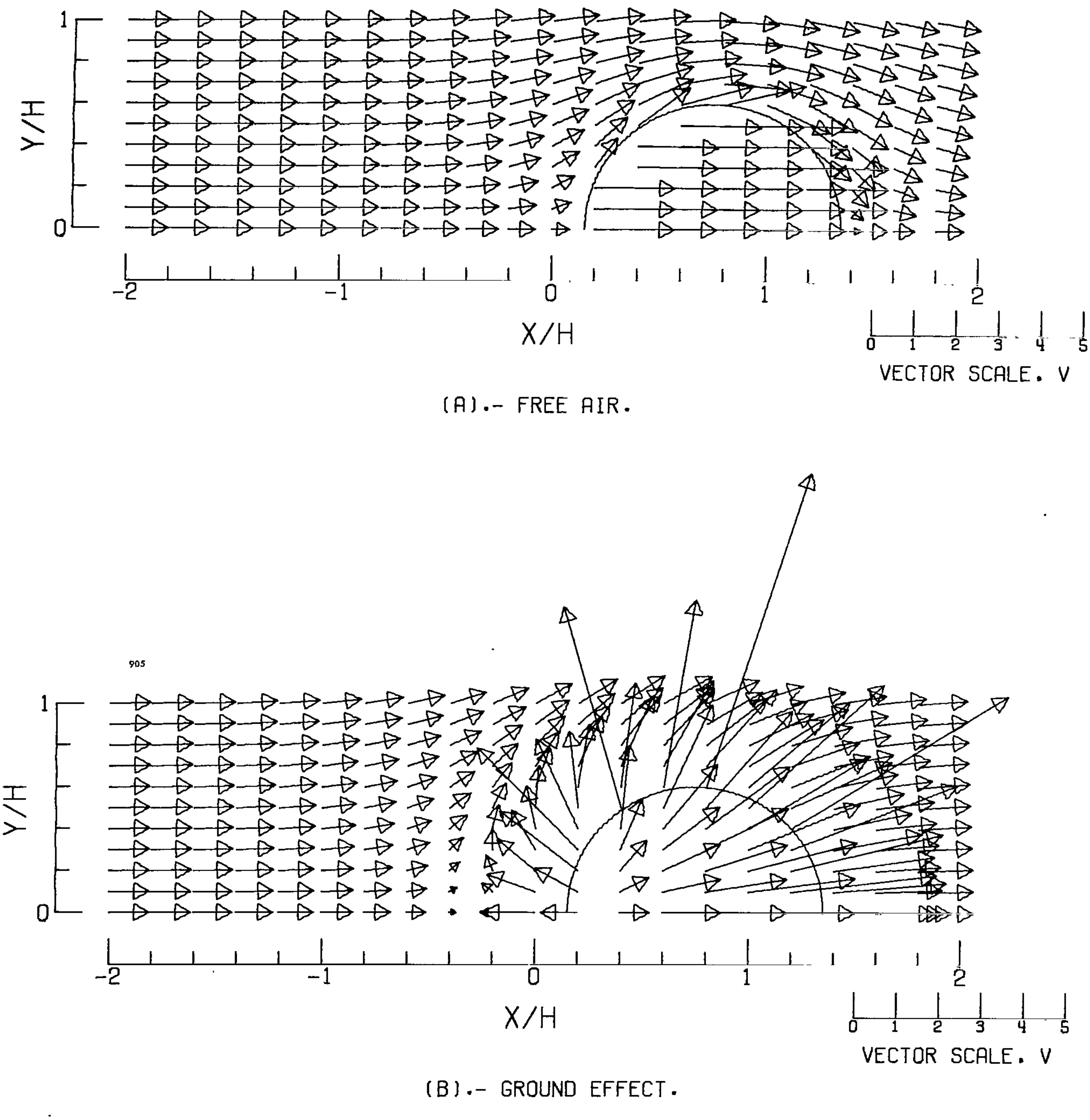

Figure 21.- Flow vectors in the plane of the floor, calculated using vortex cylinders. The intersection of the wake and the plane is shown. ζ = 0.769; η = 1.00; γ = 1.000; σ = 0.600; α = 0.0°; χ = 30.000°; uniform loading.

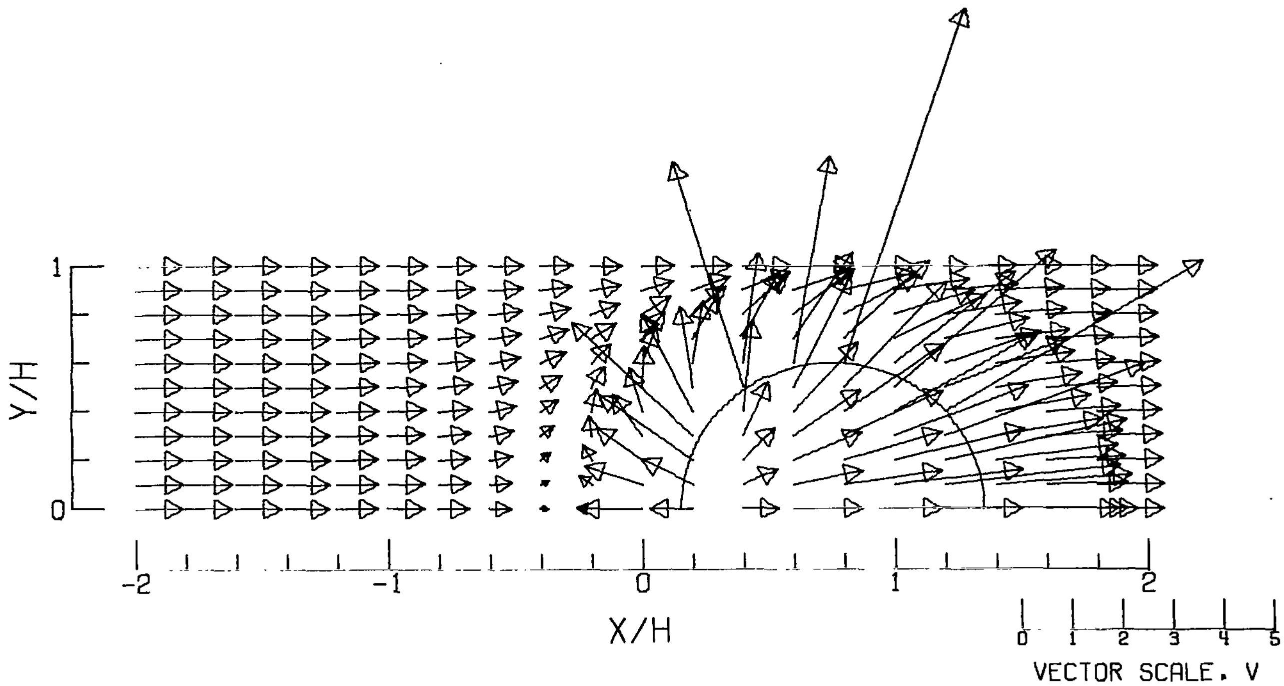

(C).- CLOSED TUNNEL.

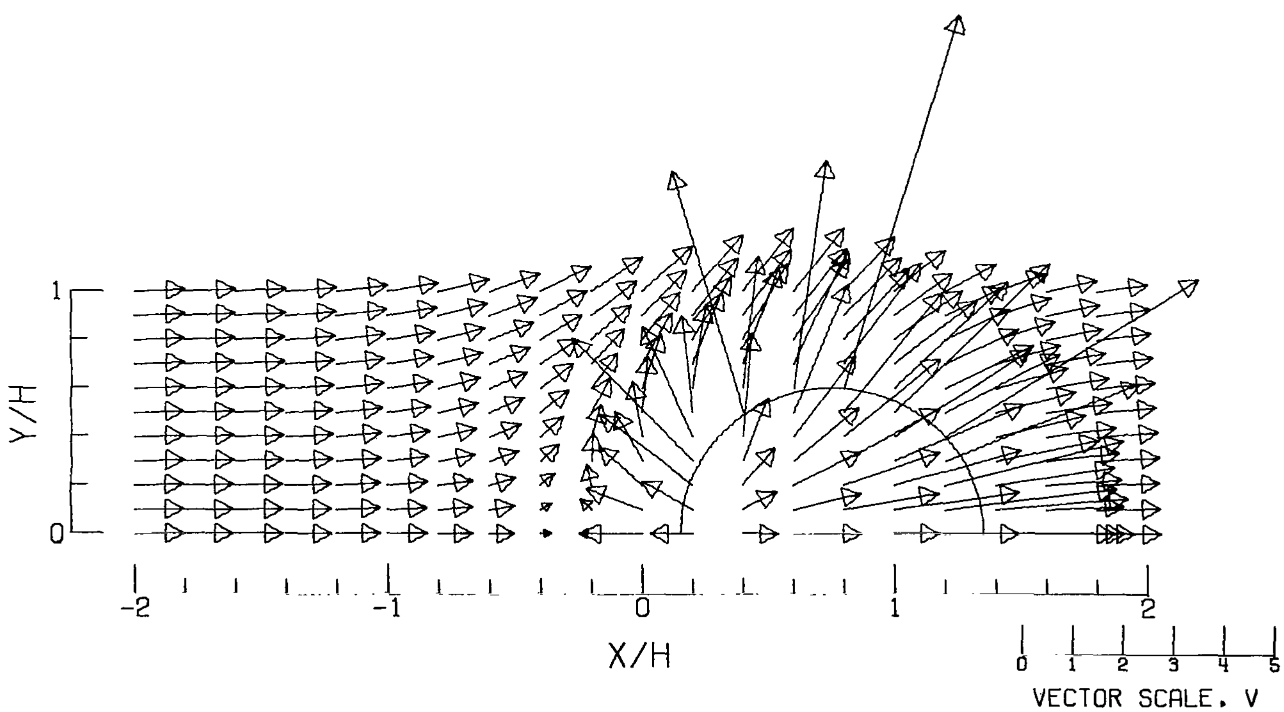

(D).- CLOSED-ON-BOTTOM-ONLY TUNNEL.

Figure 21.- Concluded.

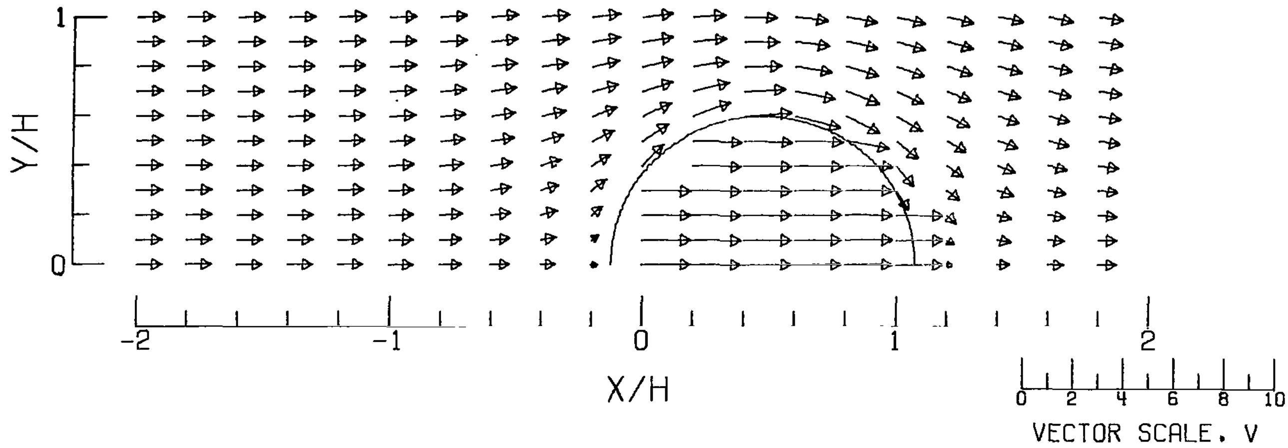

(A).- FREE AIR.

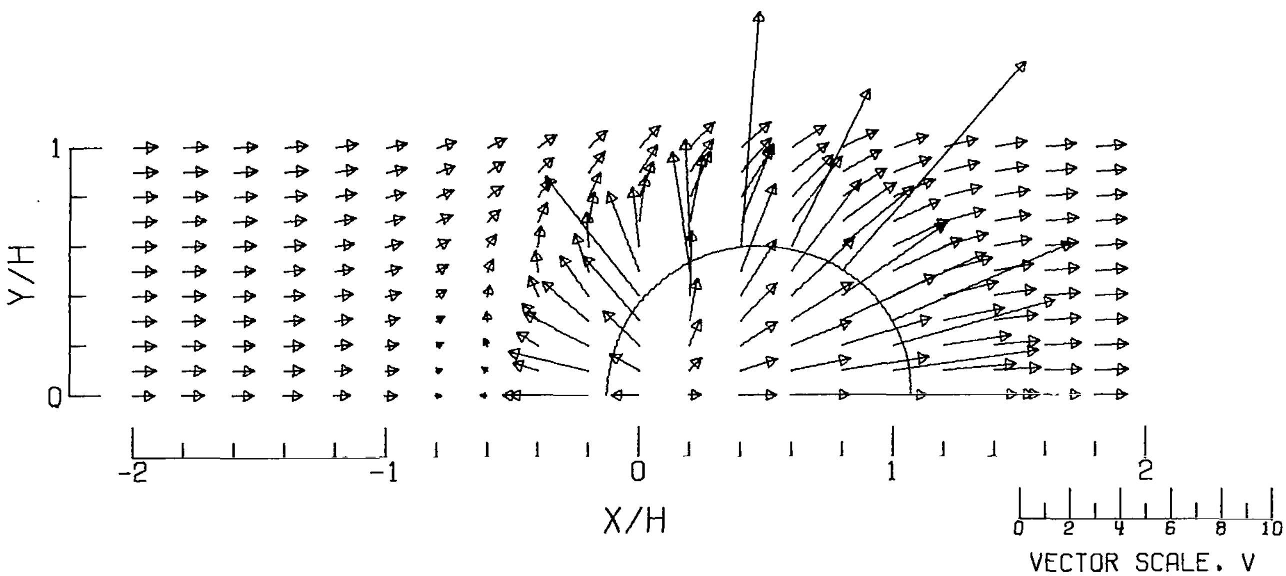

(B).- GROUND EFFECT.

Figure 22.- Flow vectors in the plane of the floor, calculated using vortex cylinders. The intersection of the wake and the plane is shown. ζ = 0.769; γ = 1.0; σ = 0.60; α = 0.0°; χ = 20.0°; uniform loading.

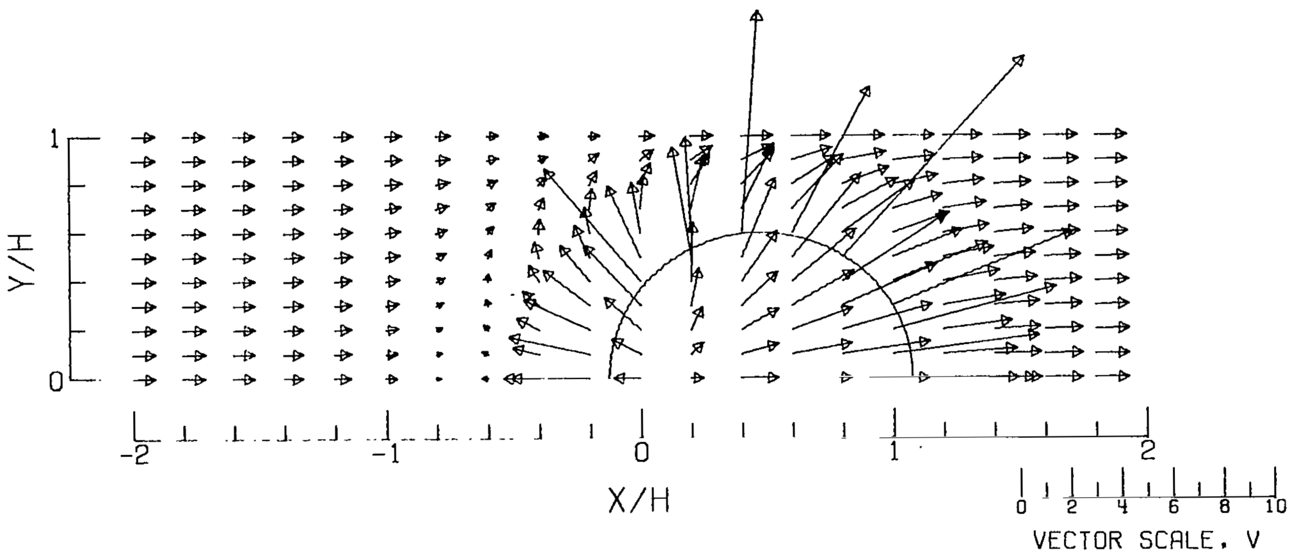

(C).- CLOSED TUNNEL.

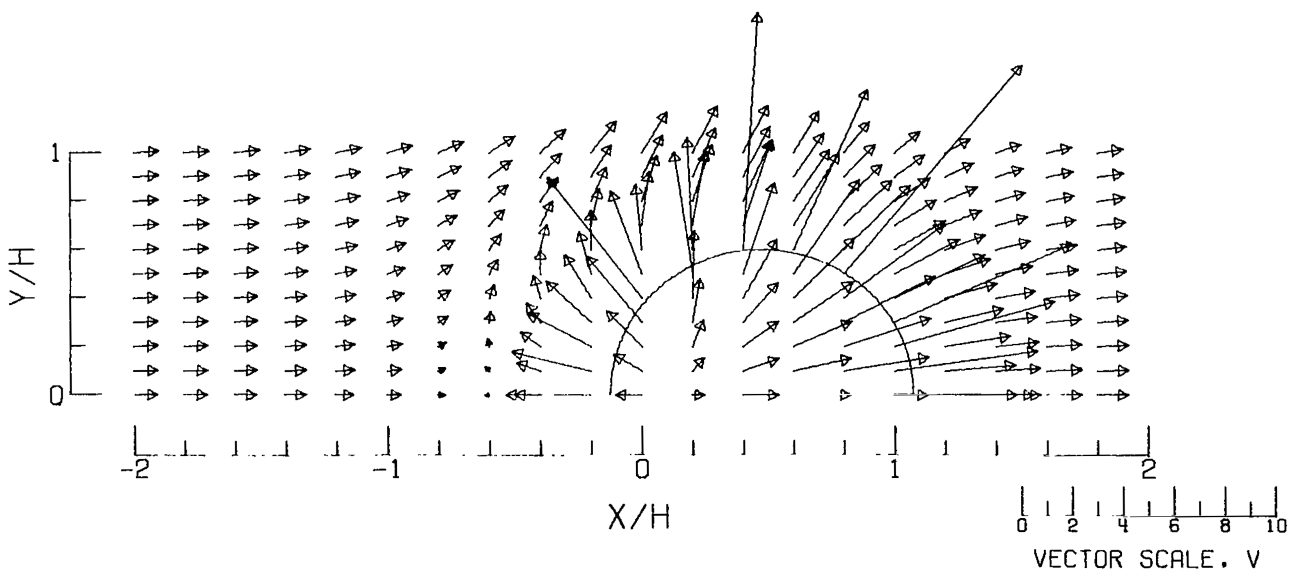

(D).- CLOSED-ON-BOTTOM-ONLY TUNNEL.

Figure 22.- Concluded.

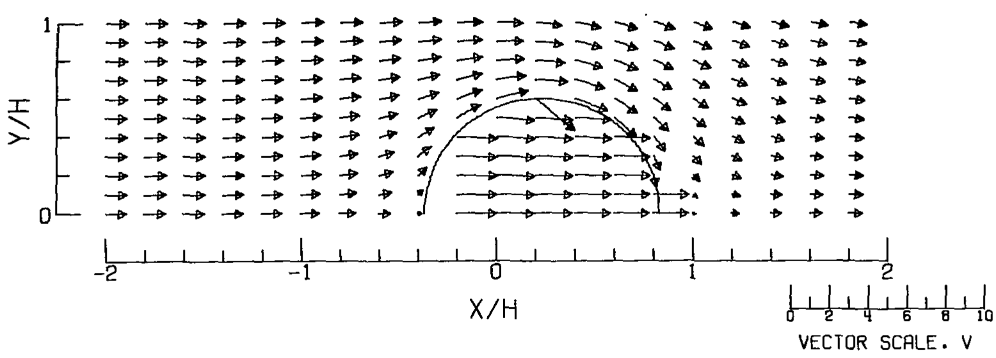

(A).- FREE AIR.

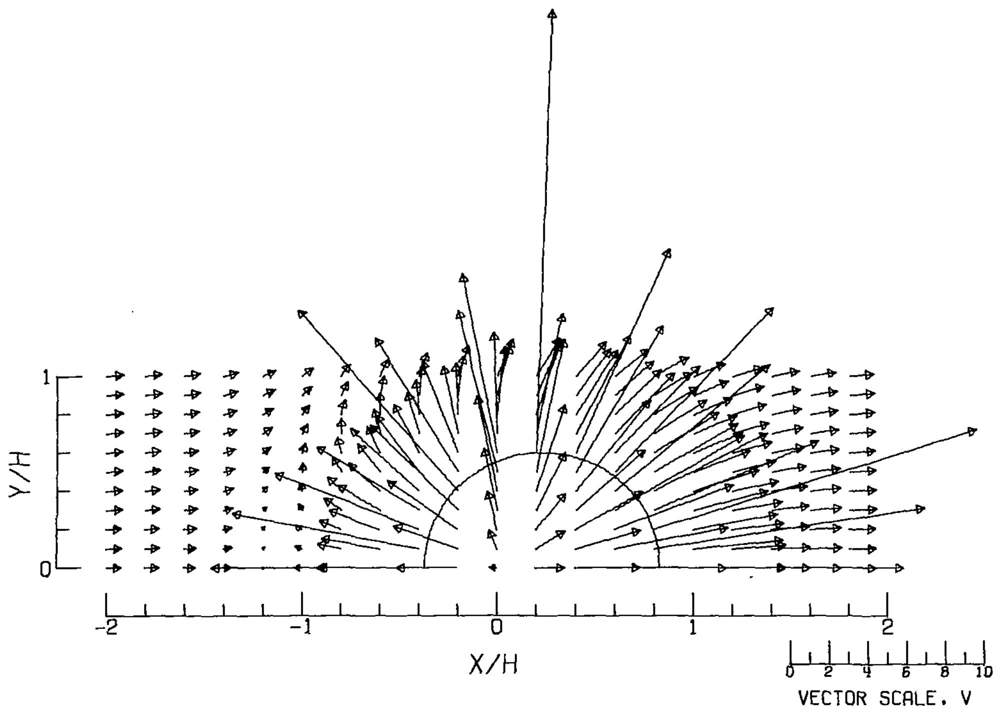

(B).- GROUND EFFECT.

Figure 23.- Flow vectors in the plane of the floor, calculated using vortex cylinders. The intersection of the wake and the plane is shown. ζ = 0.769; γ = 1.0; σ = 0.60; α = 0.0°; χ = 10.0°; uniform loading.

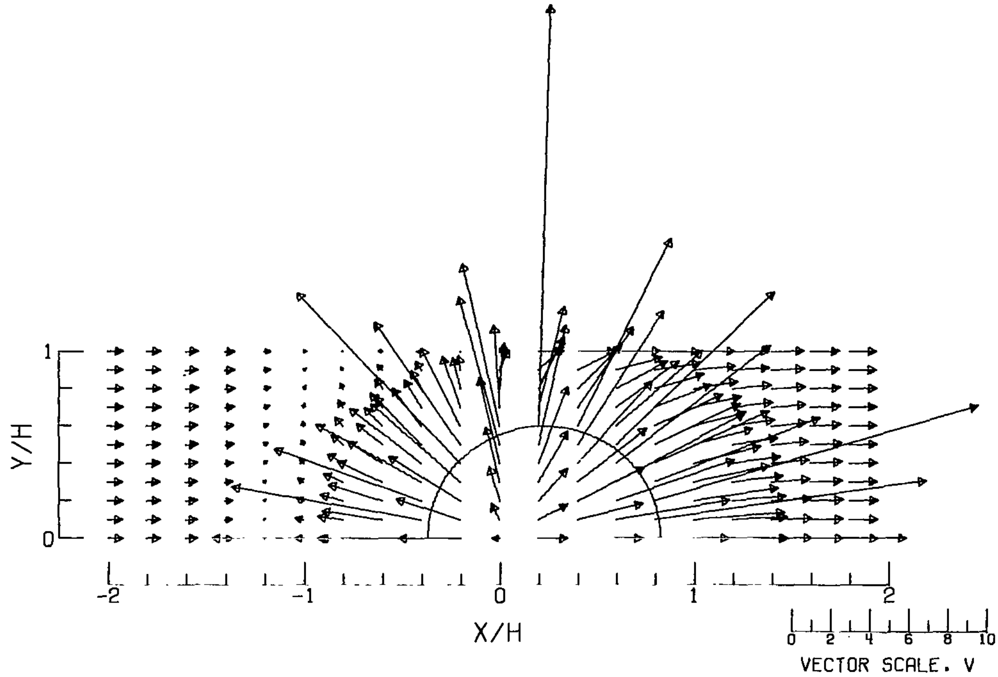

(C).- CLOSED TUNNEL.

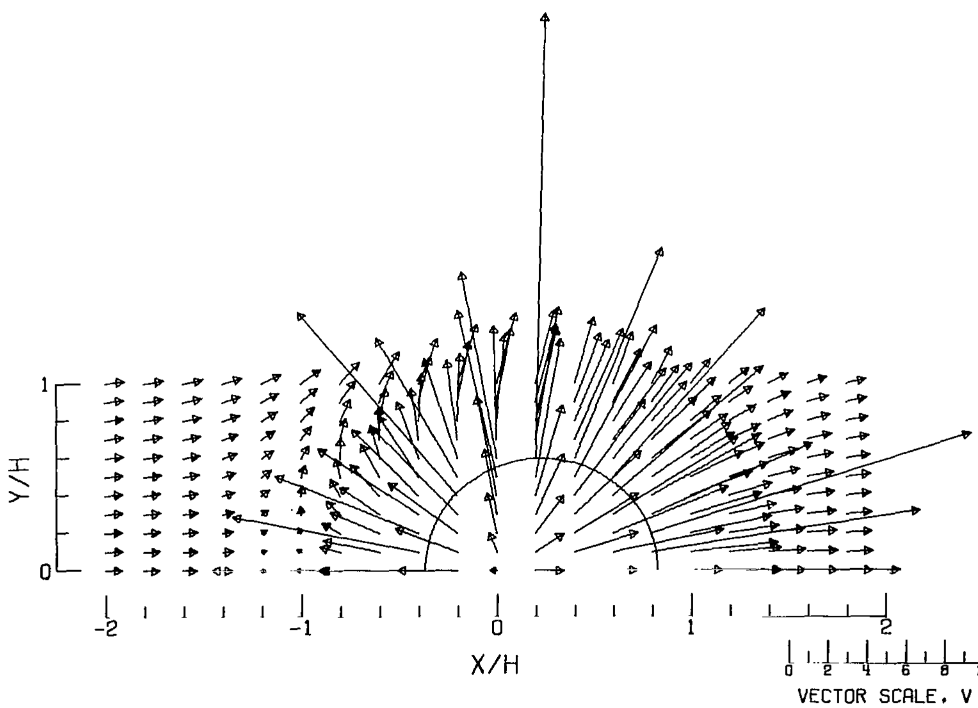

(D).- CLOSED-ON-BOTTOM-ONLY TUNNEL.

Figure 23.- Concluded.

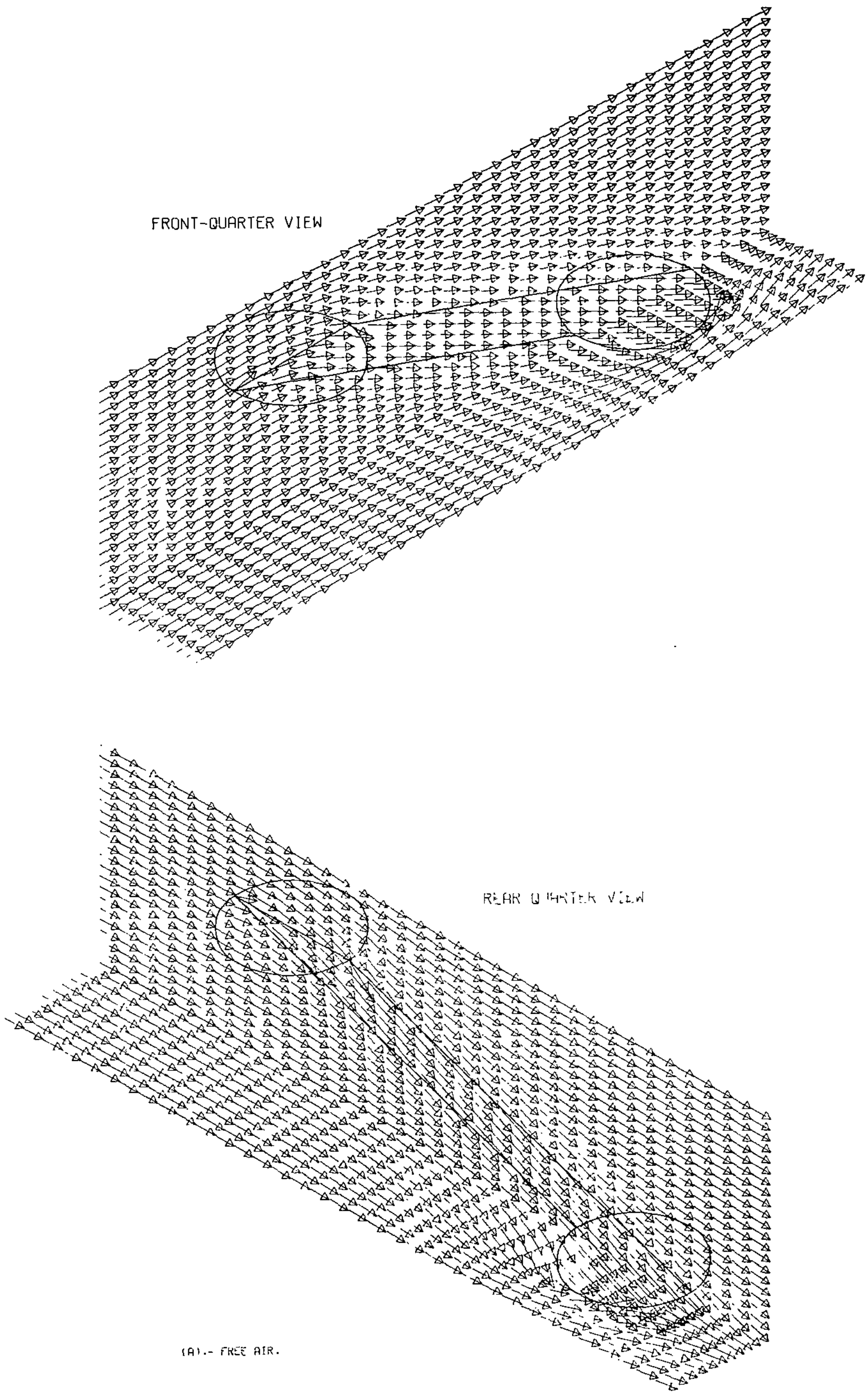

Figure 24.- Isometric views of the flow vectors near a rotor, calculated using vortex cylinders. The rotor and the intersections of the wake with the X-Z plane and the plane of the floor are shown. Because of symmetry, only the vectors in the right-hand half of the plane of the floor are given. $\zeta = 0.769$; $\eta = 1.0$; $\gamma = 1.0$; $\sigma = 0.60$; $\alpha = 0.0^{\circ}$; $\chi = 70.0^{\circ}$; uniform loading.

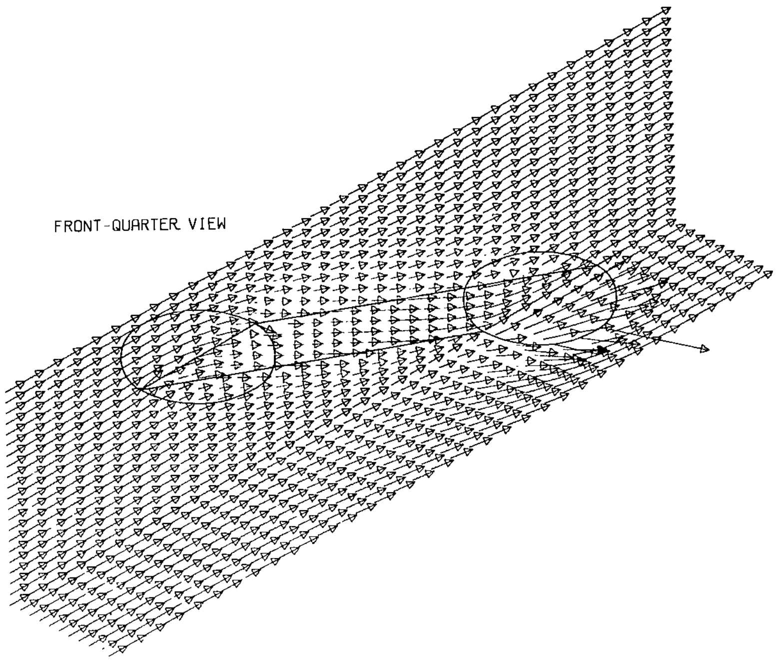

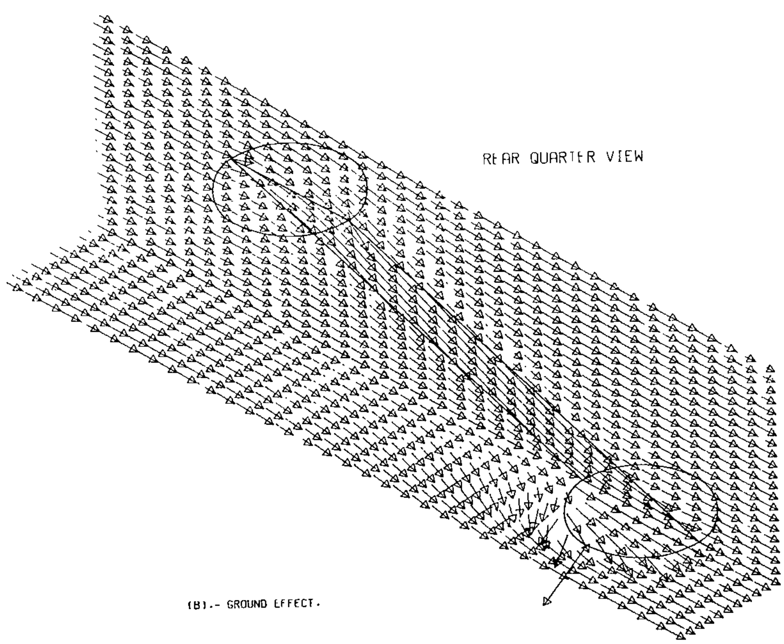

(B).- GROUND EFFECT.

Figure 24.- Continued.

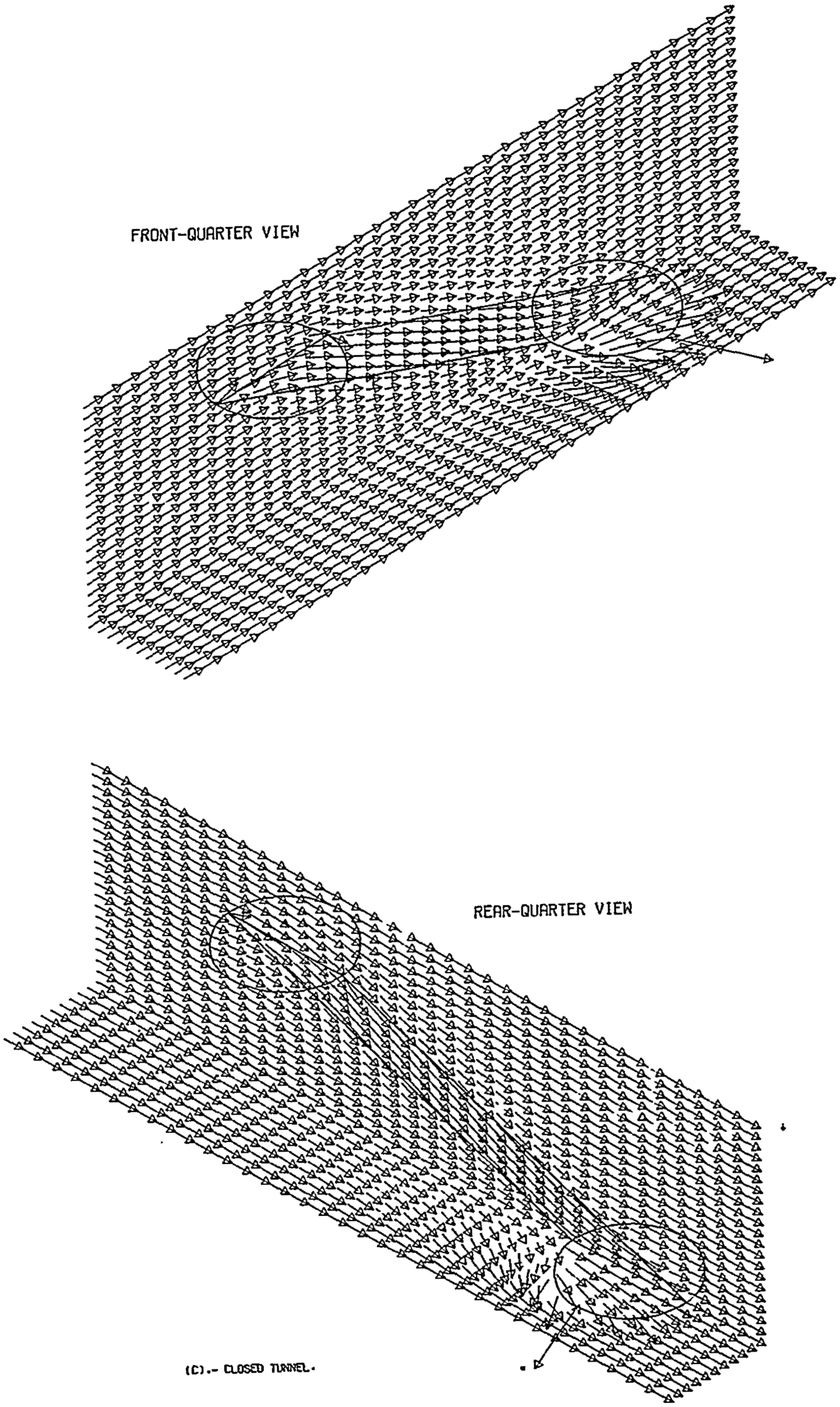

Figure 24.- Continued.

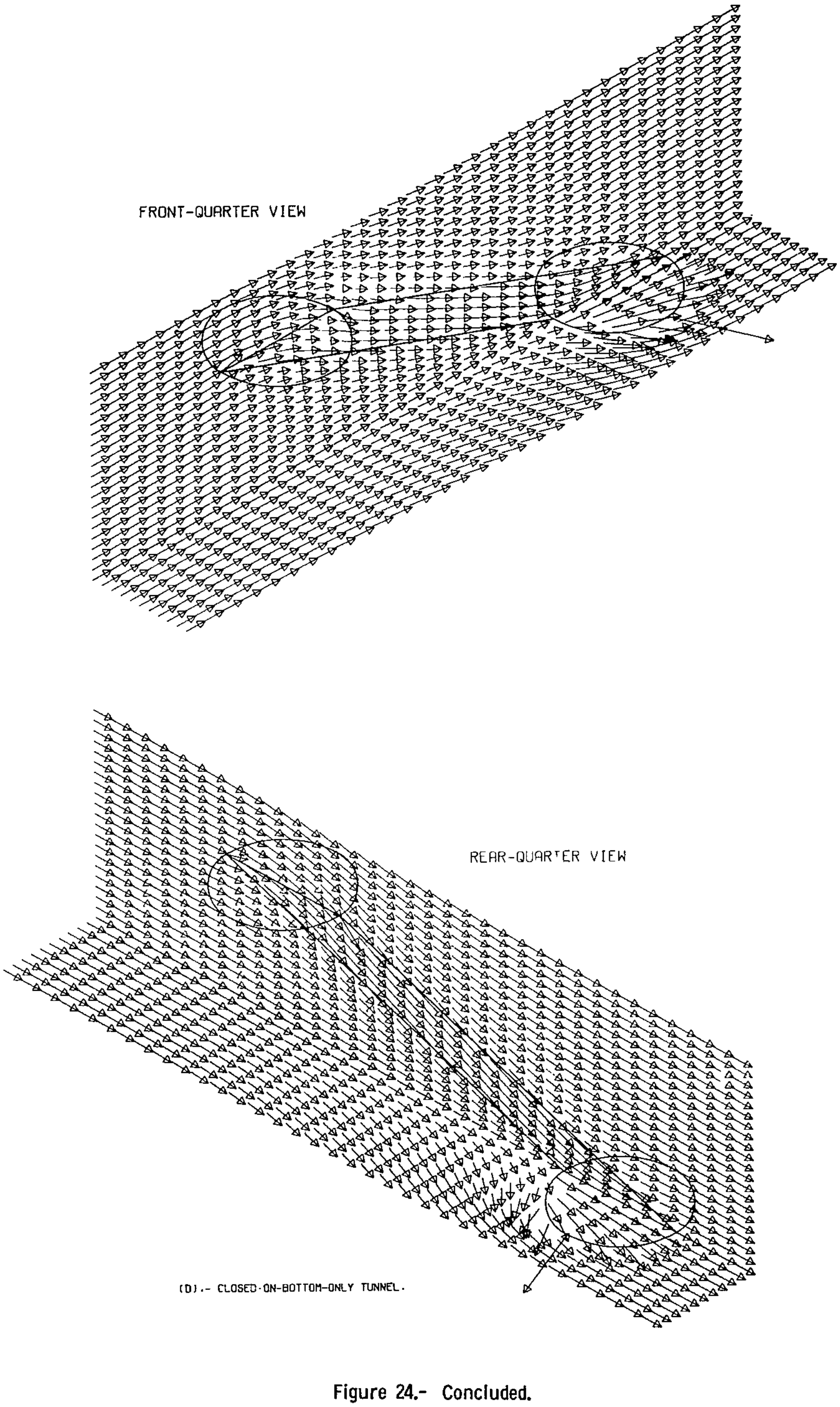

Figure 24.- Concluded.

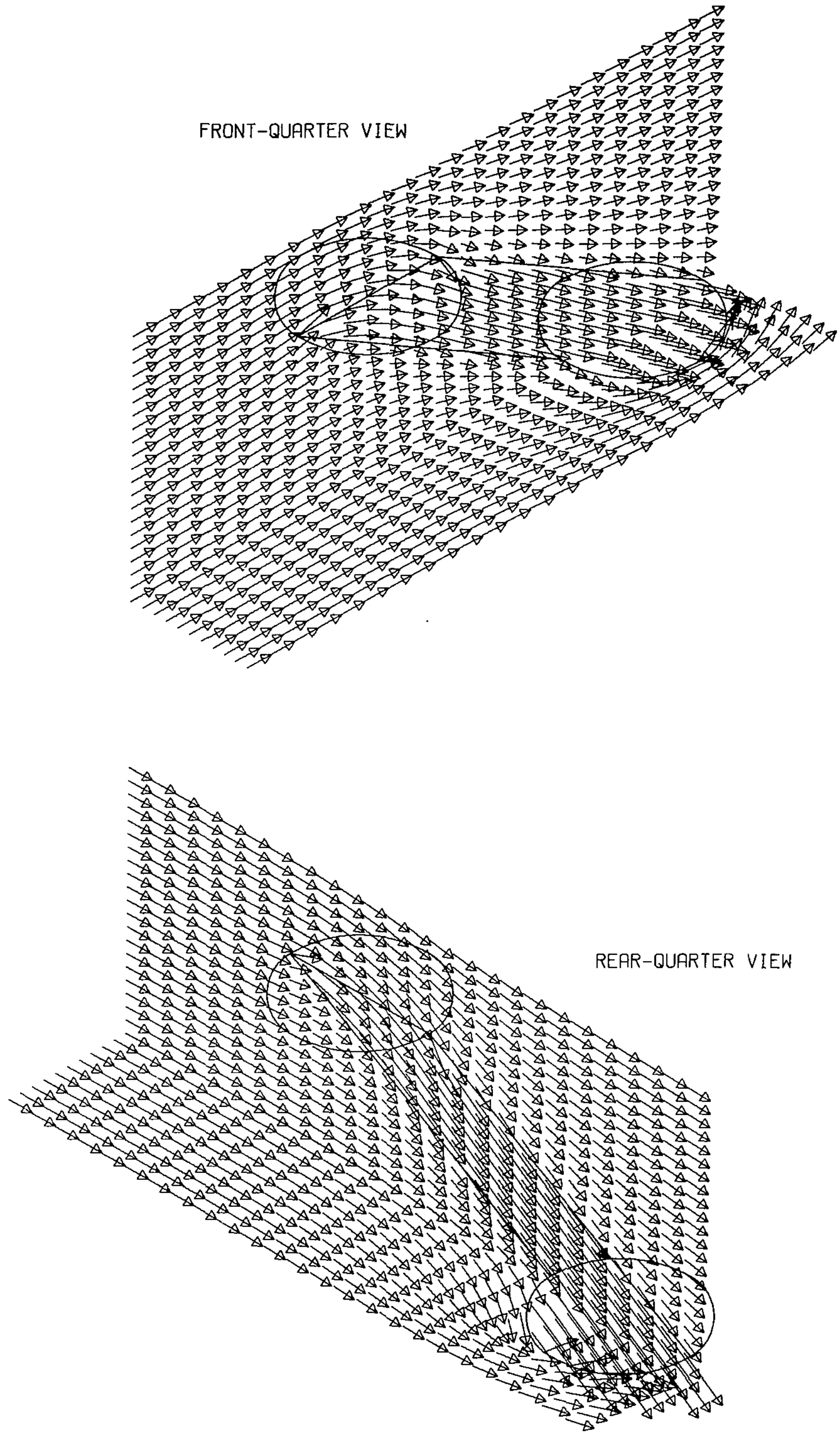

(A).- FREE AIR.

Figure 25.- Isometric views of the flow vectors near a rotor, calculated using vortex cylinders. The rotor and the intersections of the wake with the X-Z plane and the plane of the floor are shown. Because of symmetry, only the vectors in the right-hand half of the plane of the floor are given. $\zeta = 0.769$; $\eta = 1.0$; $\gamma = 1.0$; $\sigma = 0.60$; $\alpha = 0.0^{0}$; $\chi = 60.0^{0}$; uniform loading.

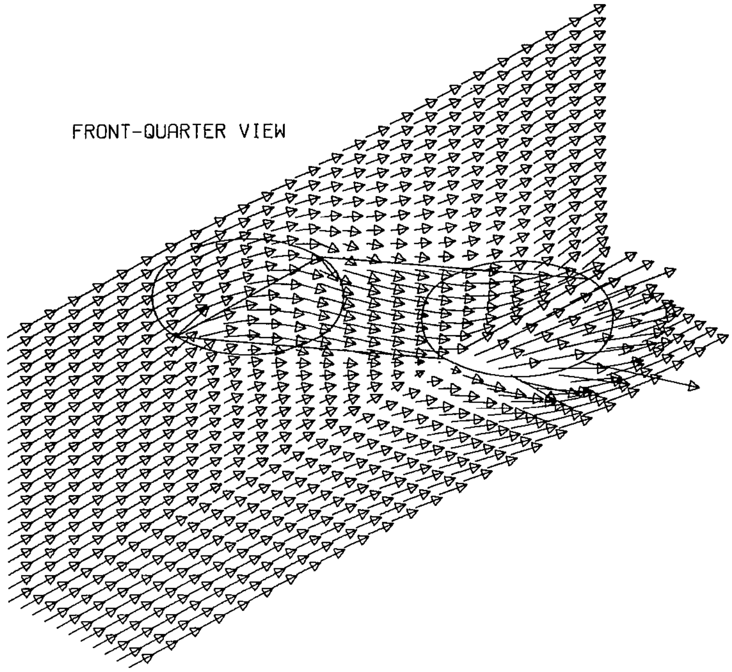

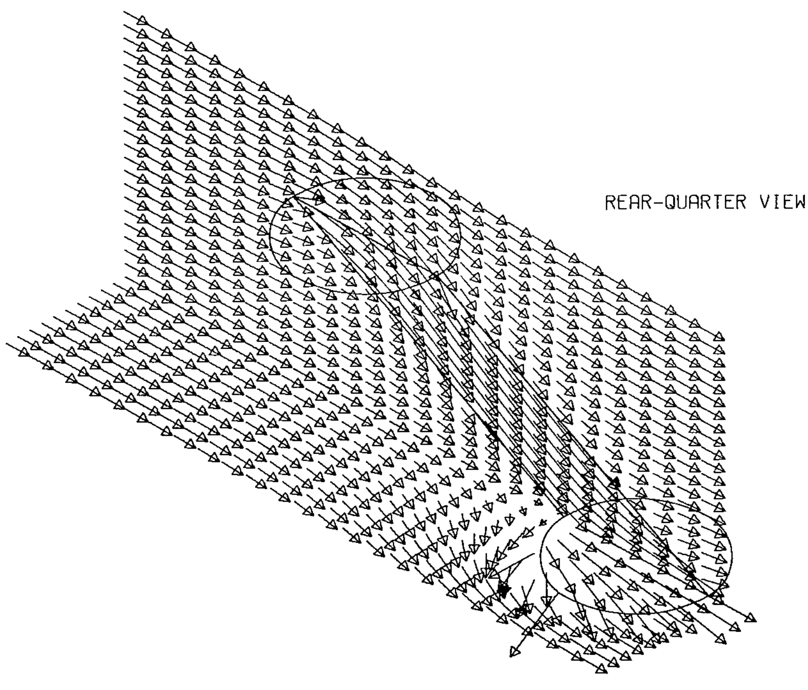

(B).- GROUND EFFECT.

Figure 25.- Continued.

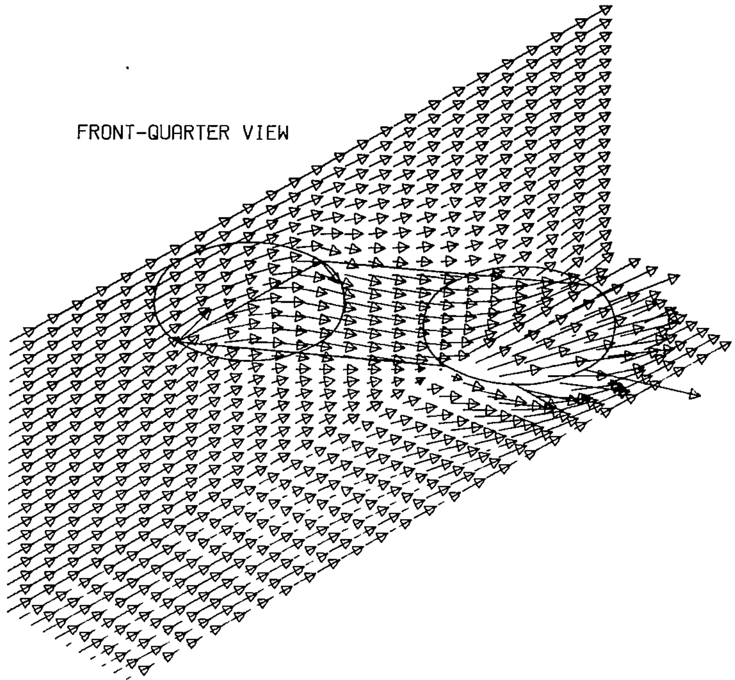

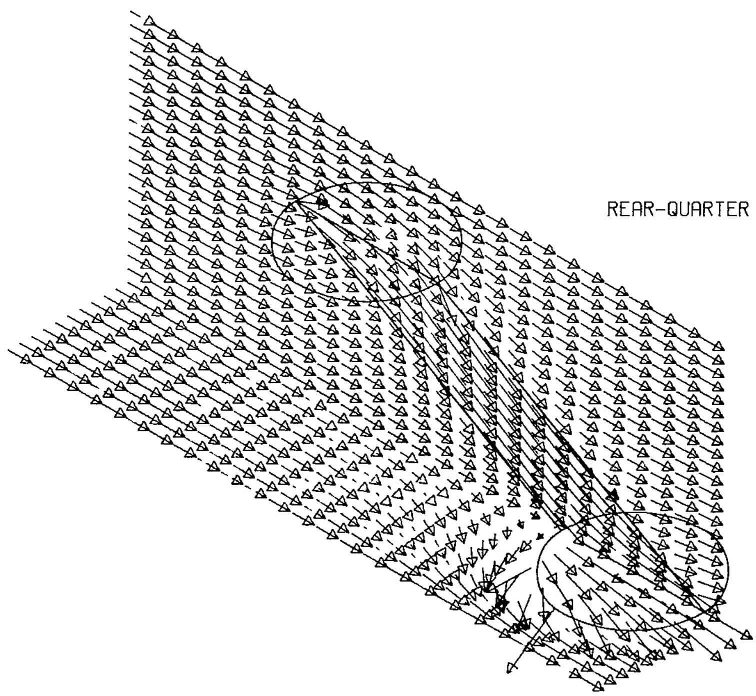

(C).- CLOSED TUNNEL.

Figure 25.- Continued.

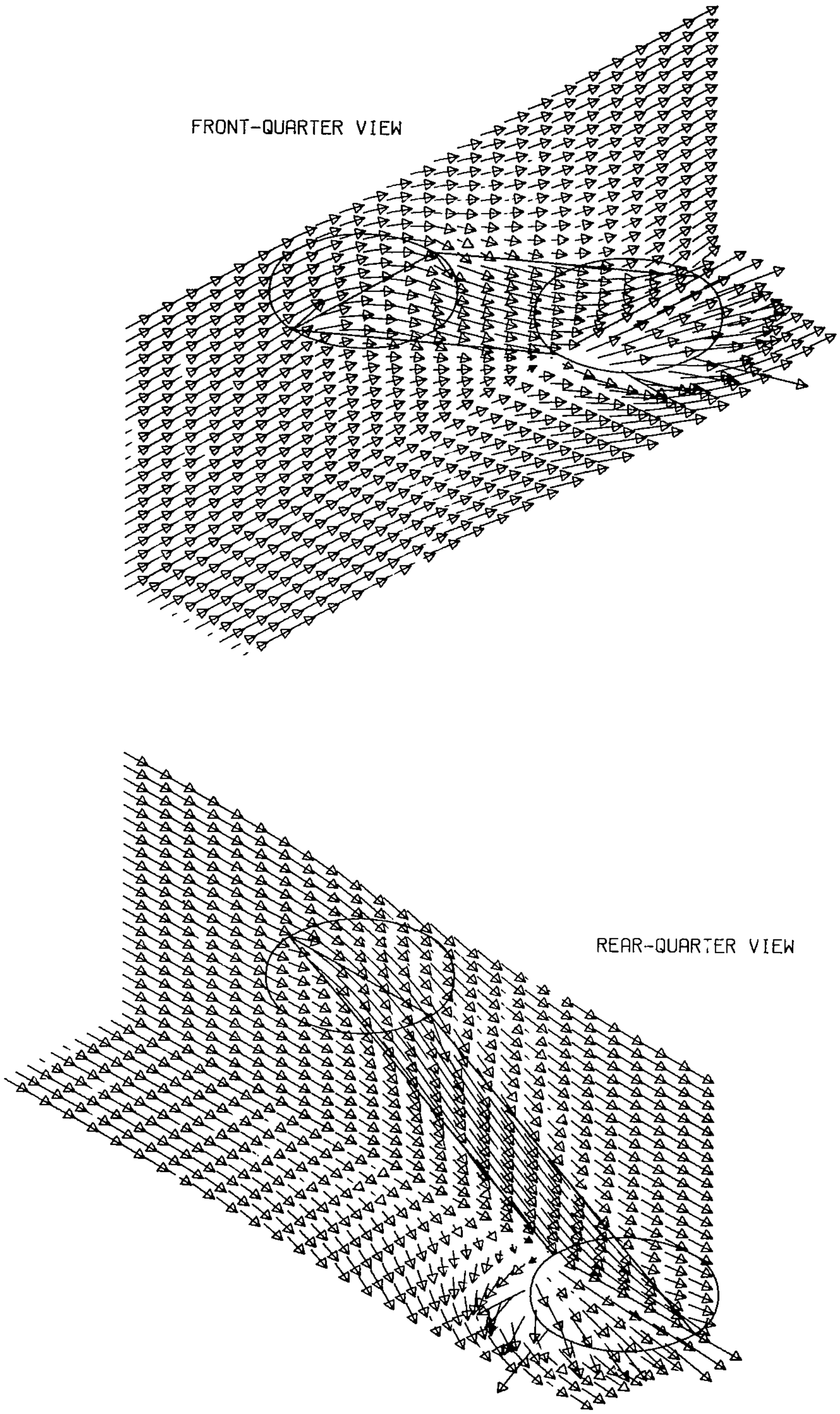

(D).– CLOSED-ON-BOTTOM-ONLY TUNNEL.

Figure 25.- Concluded.

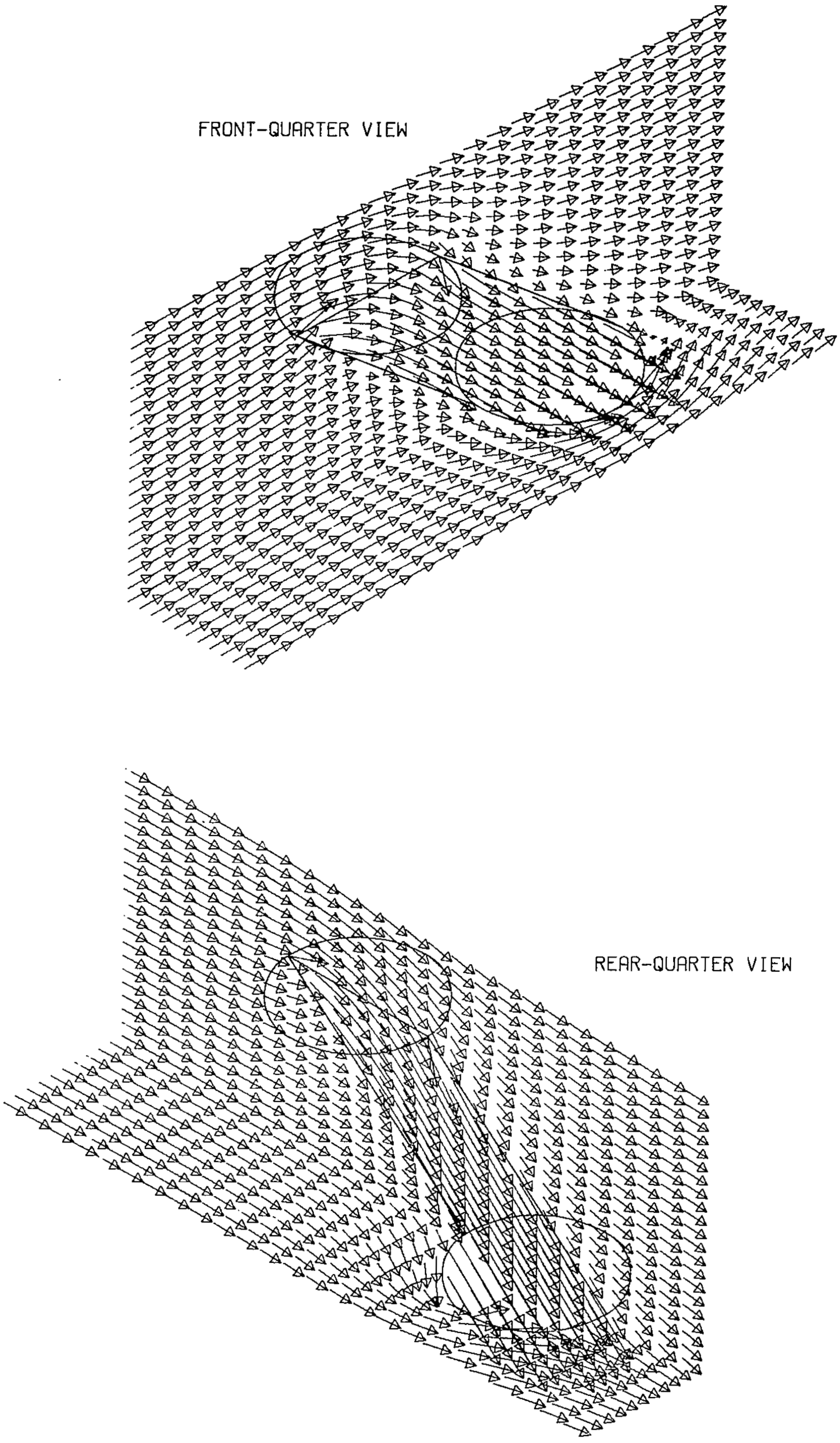

(A).- FREE AIR.

Figure 26.- Isometric views of the flow vectors near a rotor, calculated using vortex cylinders. The rotor and the intersections of the wake with the X-Z plane and the plane of the floor are shown. Because of symmetry, only the vectors in the right-hand half of the plane of the floor are given. $\zeta = 0.769$; $\eta = 1.0$; $\gamma = 1.0$; $\sigma = 0.60$; $\alpha = 0.0^{\circ}$; $\chi = 50.0^{\circ}$; uniform loading.

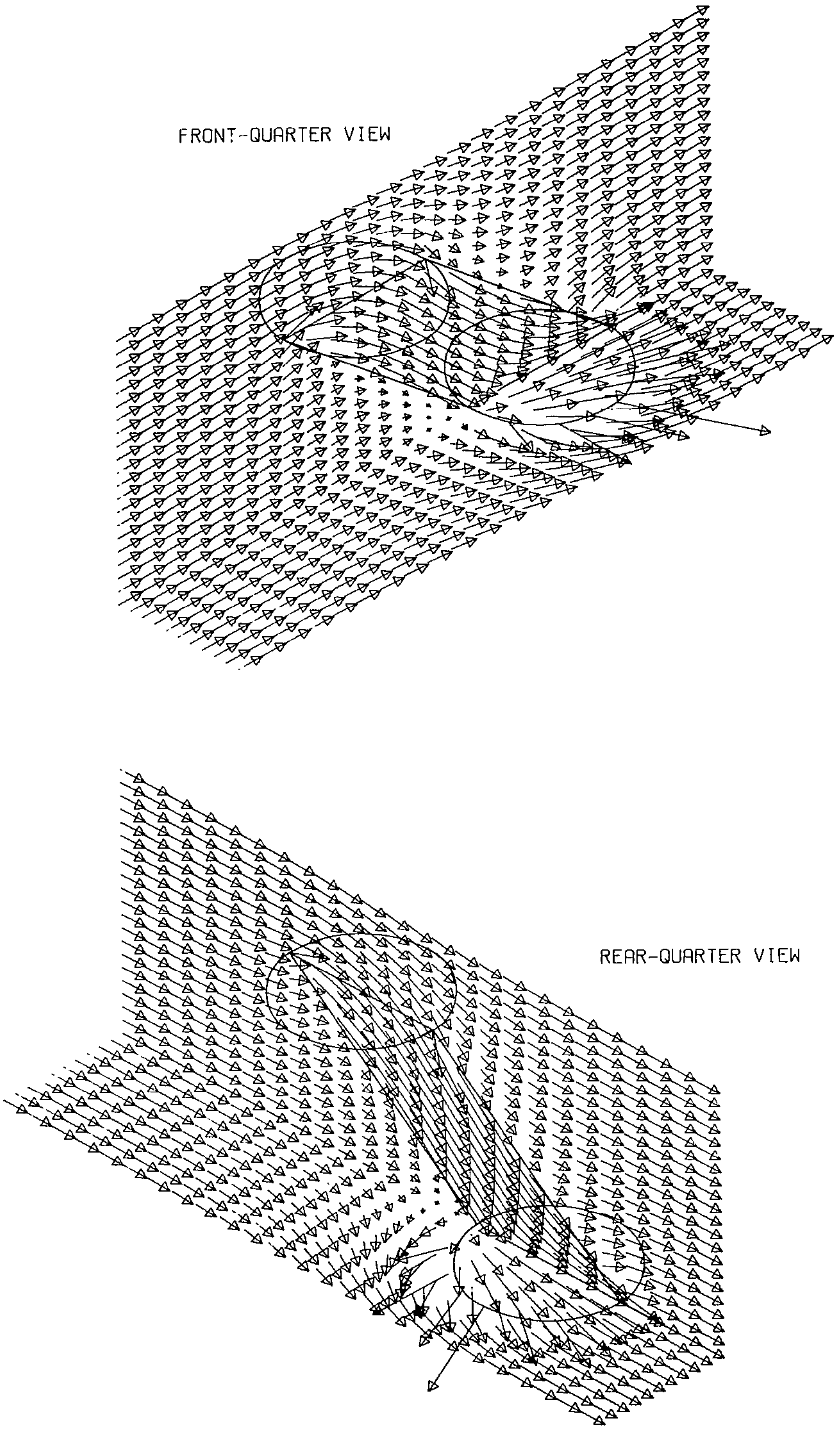

(B).- GROUND EFFECT.

Figure 26.- Continued.

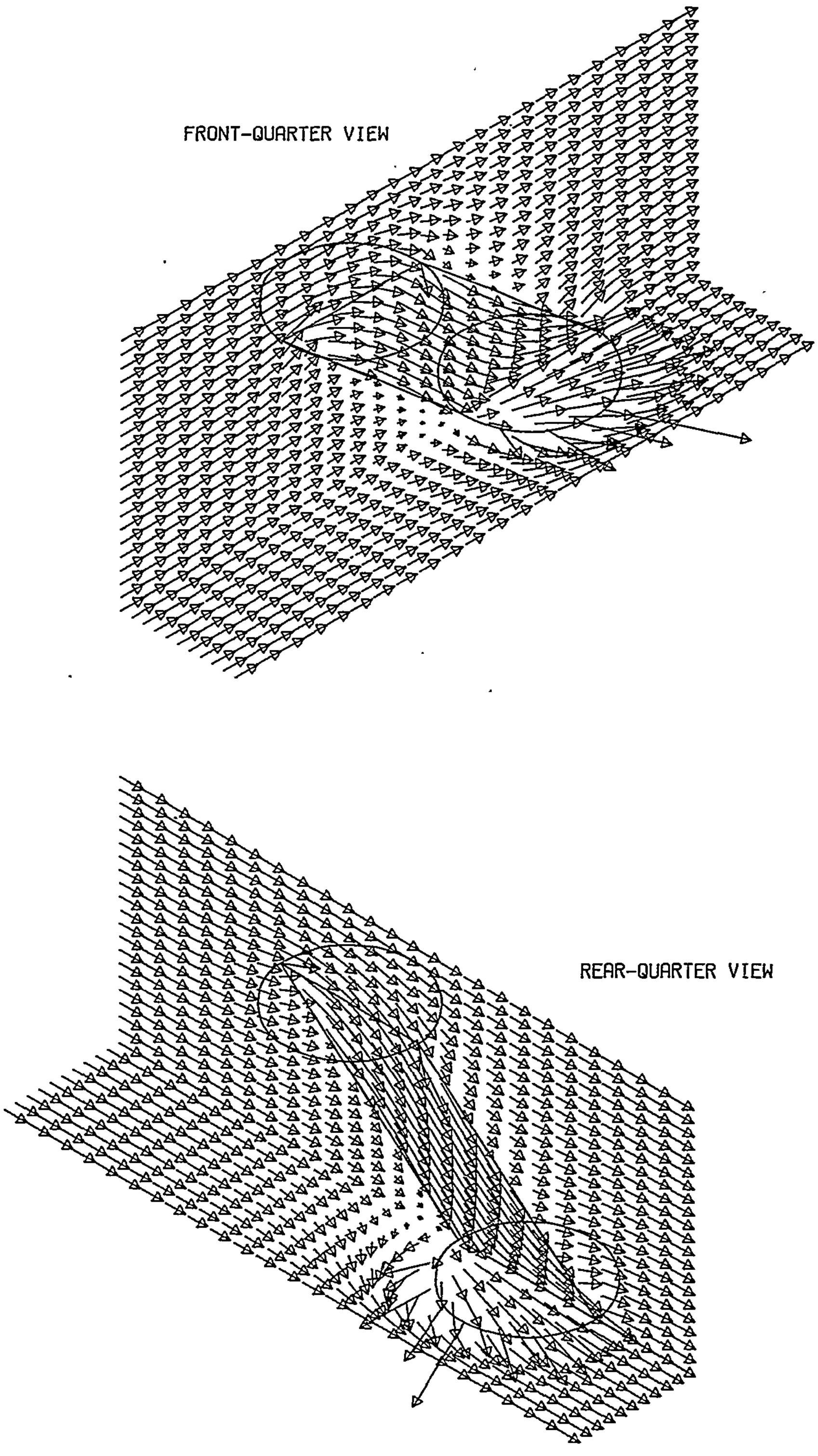

(C).- CLOSED TUNNEL.

Figure 26.- Continued.

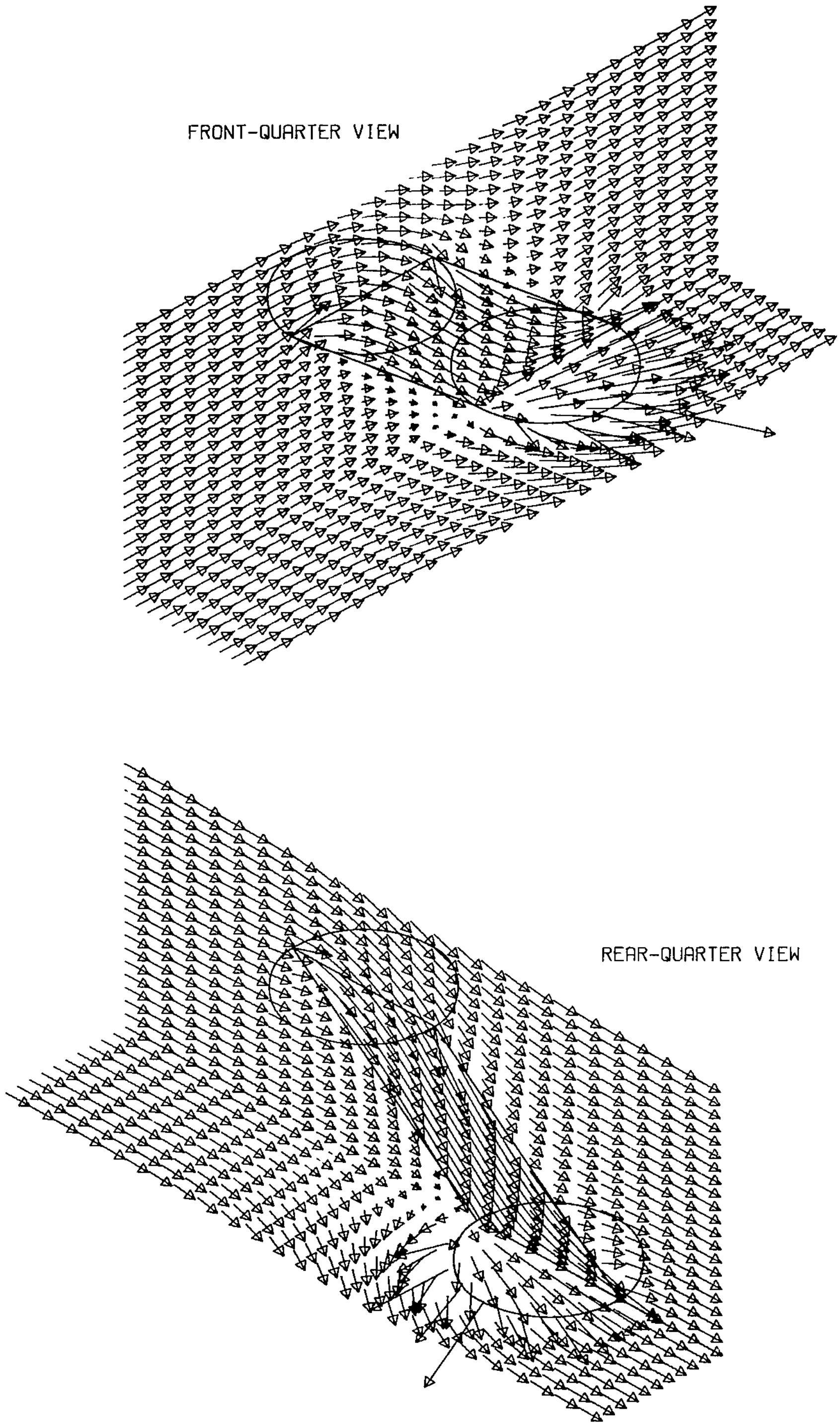

(D).- CLOSED-ON-BOTTOM-ONLY TUNNEL.

Figure 26.- Concluded.

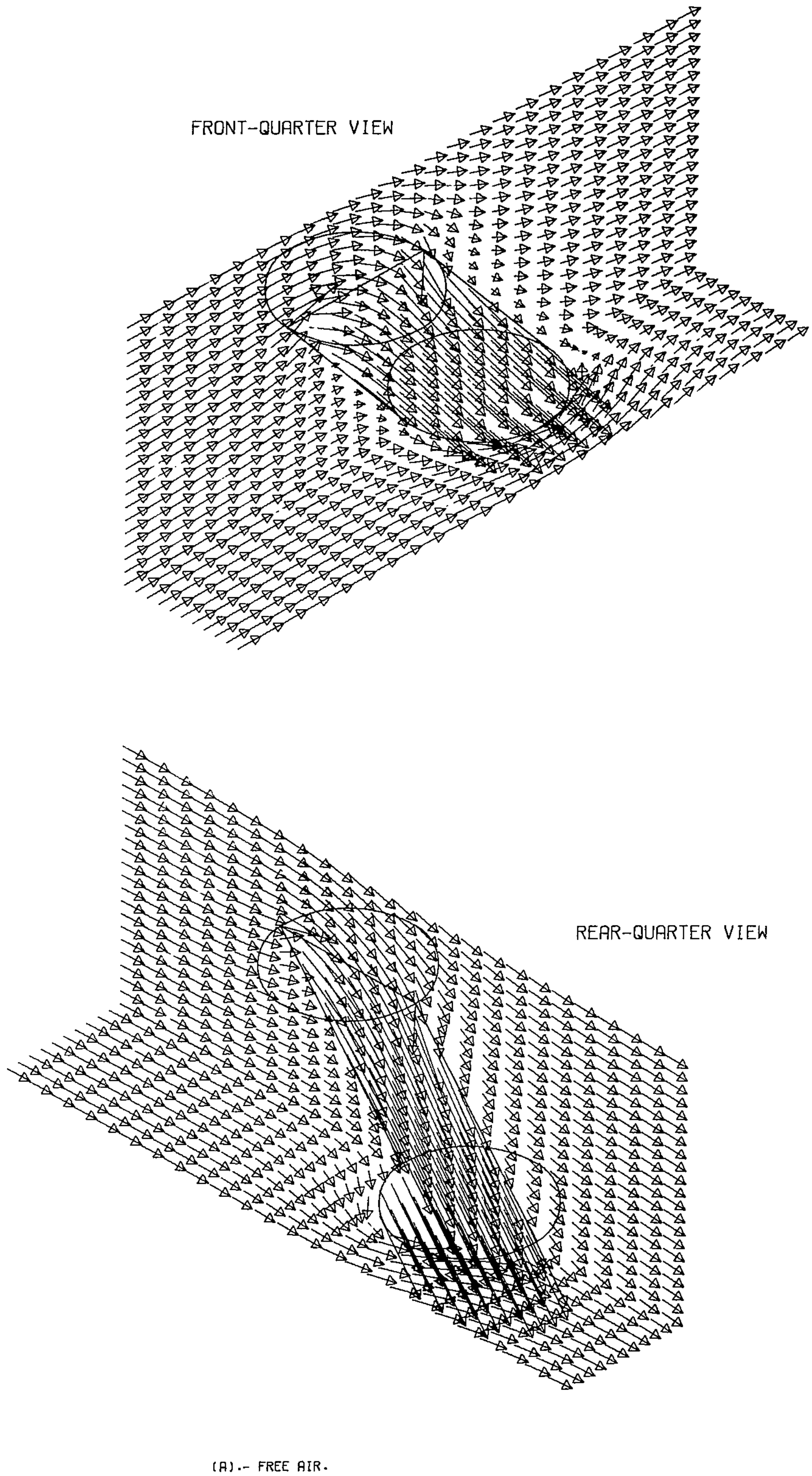

Figure 27.- Isometric views of the flow vectors near a rotor, calculated using vortex cylinders. The rotor and the intersections of the wake with the X-Z plane and the plane of the floor are shown. Because of symmetry, only the vectors in the right-hand half of the plane of the floor are given. $\zeta = 0.769$; $\gamma = 1.0$; $\sigma = 0.60$; $\alpha = 0.0^{\circ}$; $\chi = 40.0^{\circ}$; uniform loading.

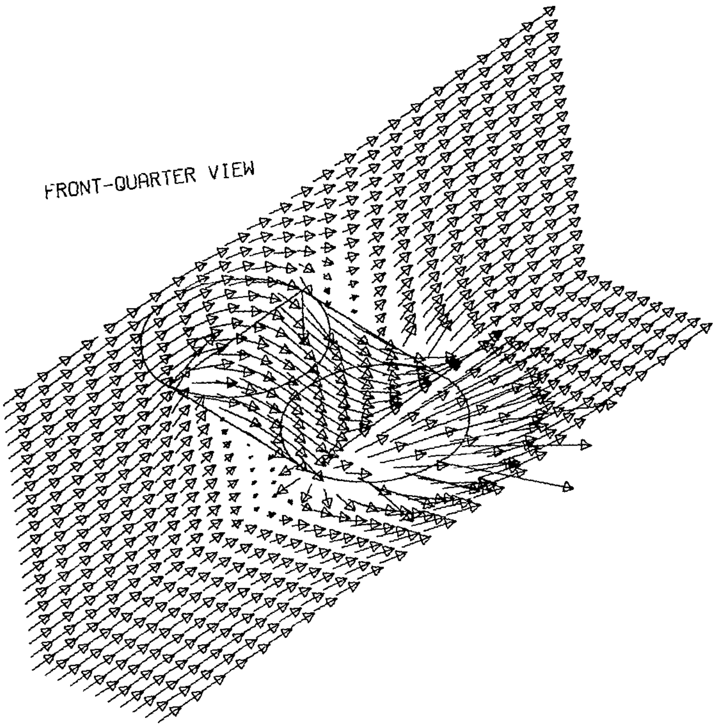

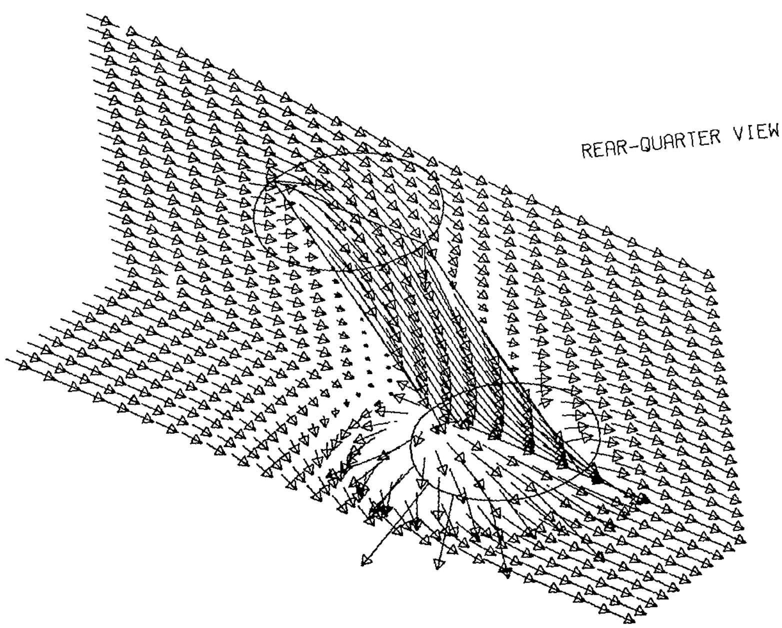

(B).- GROUND EFFECT.

Figure 27.- Continued.

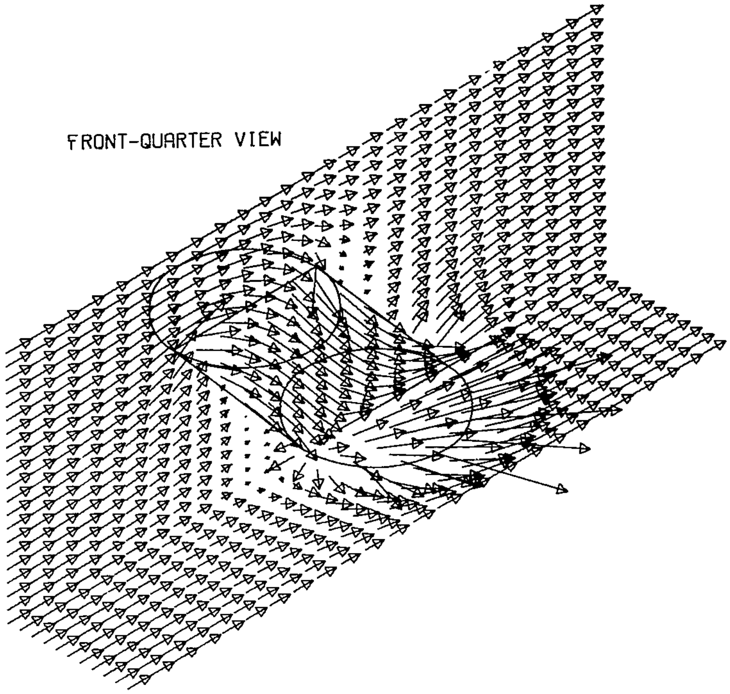

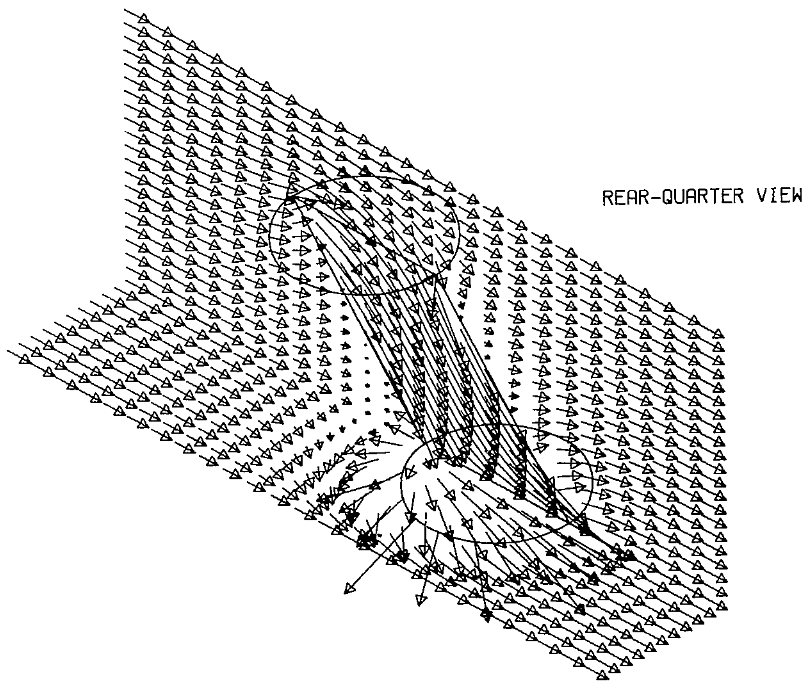

(C).- CLOSED TUNNEL.

Figure 27.- Continued.

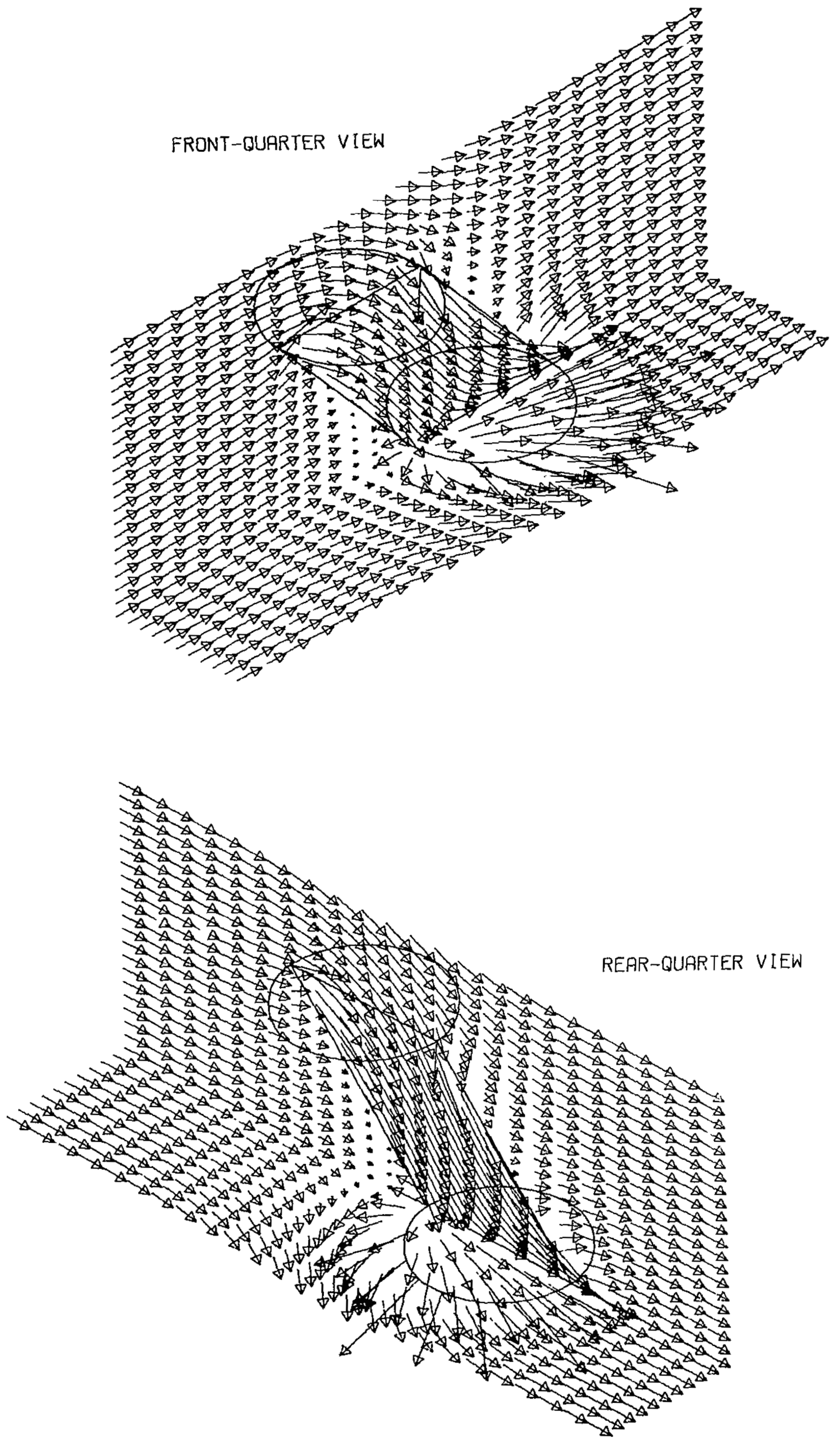

(D).- CLOSED-ON-BOTTOM-ONLY TUNNEL.

Figure 27.- Concluded.

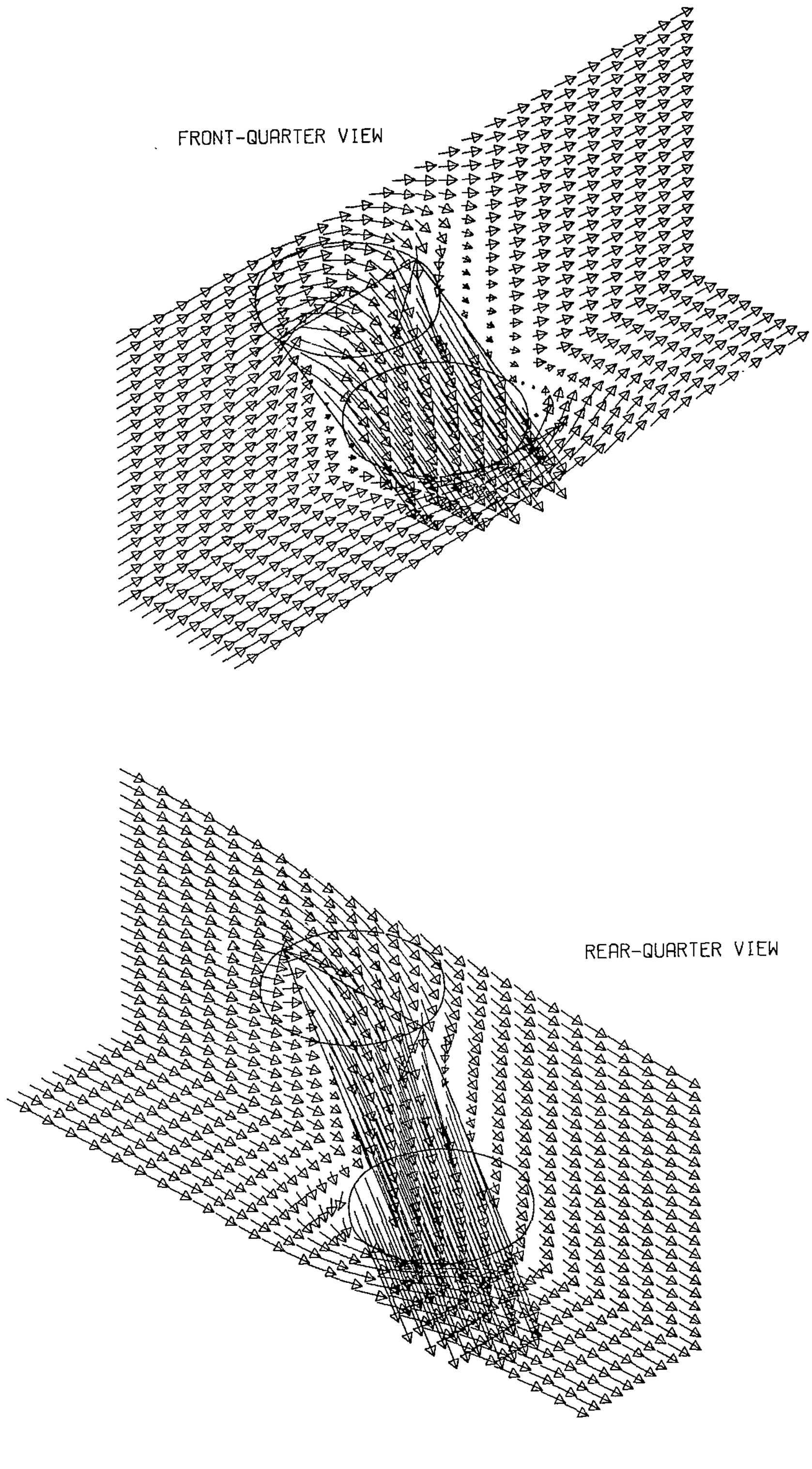

(A).- FREE AIR.

Figure 28.- Isometric views of the flow vectors near a rotor, calculated using vortex cylinders. The rotor and the intersections of the wake with the X-Z plane and the plane of the floor are shown. Because of symmetry, only the vectors in the right-hand half of the plane of the floor are given. ζ = 0.769; γ = 1.0; σ = 0.60; α = 0.0°; χ = 30.0°; uniform loading.

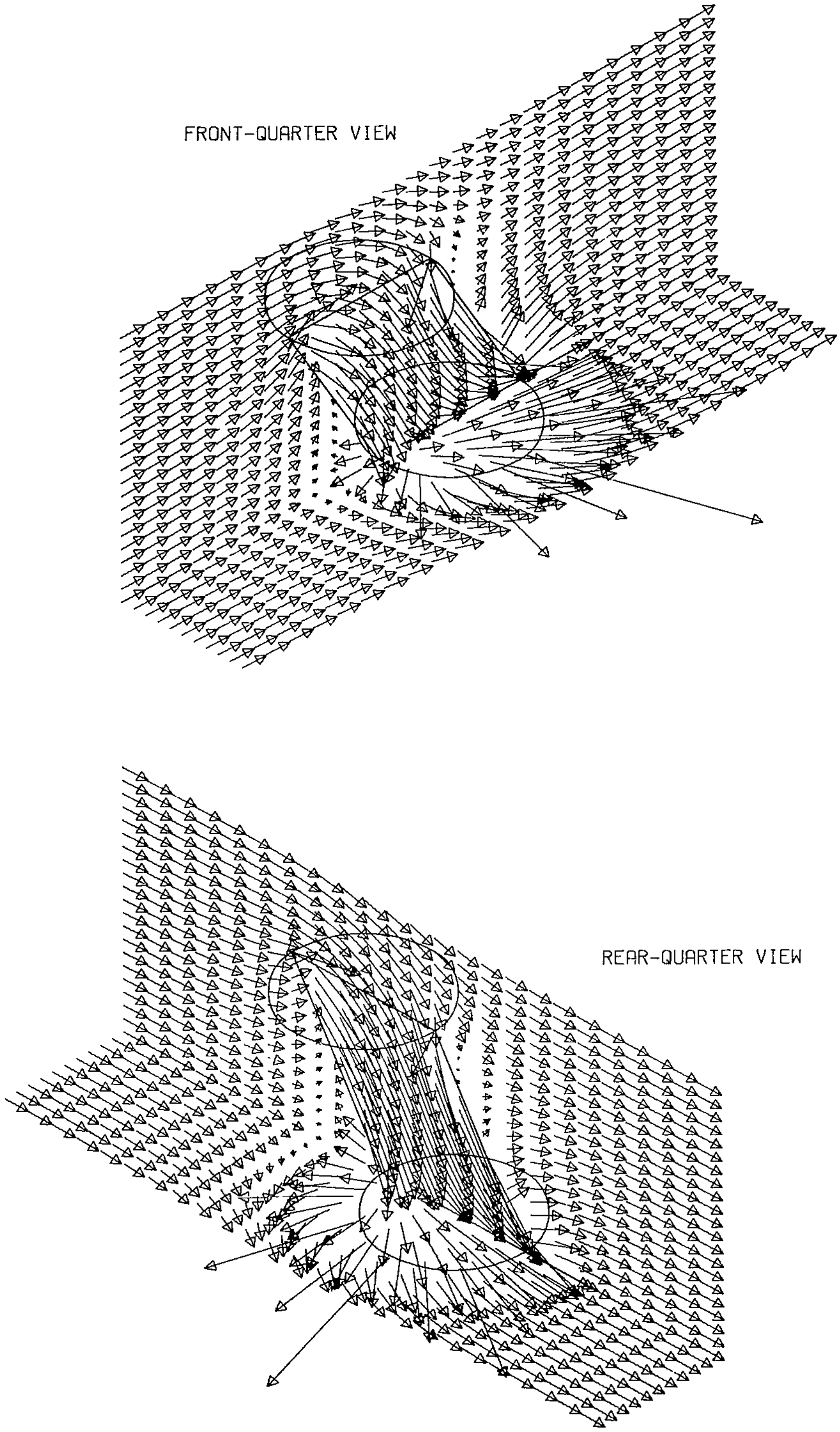

(B).- GROUND EFFECT.

Figure 28.- Continued.

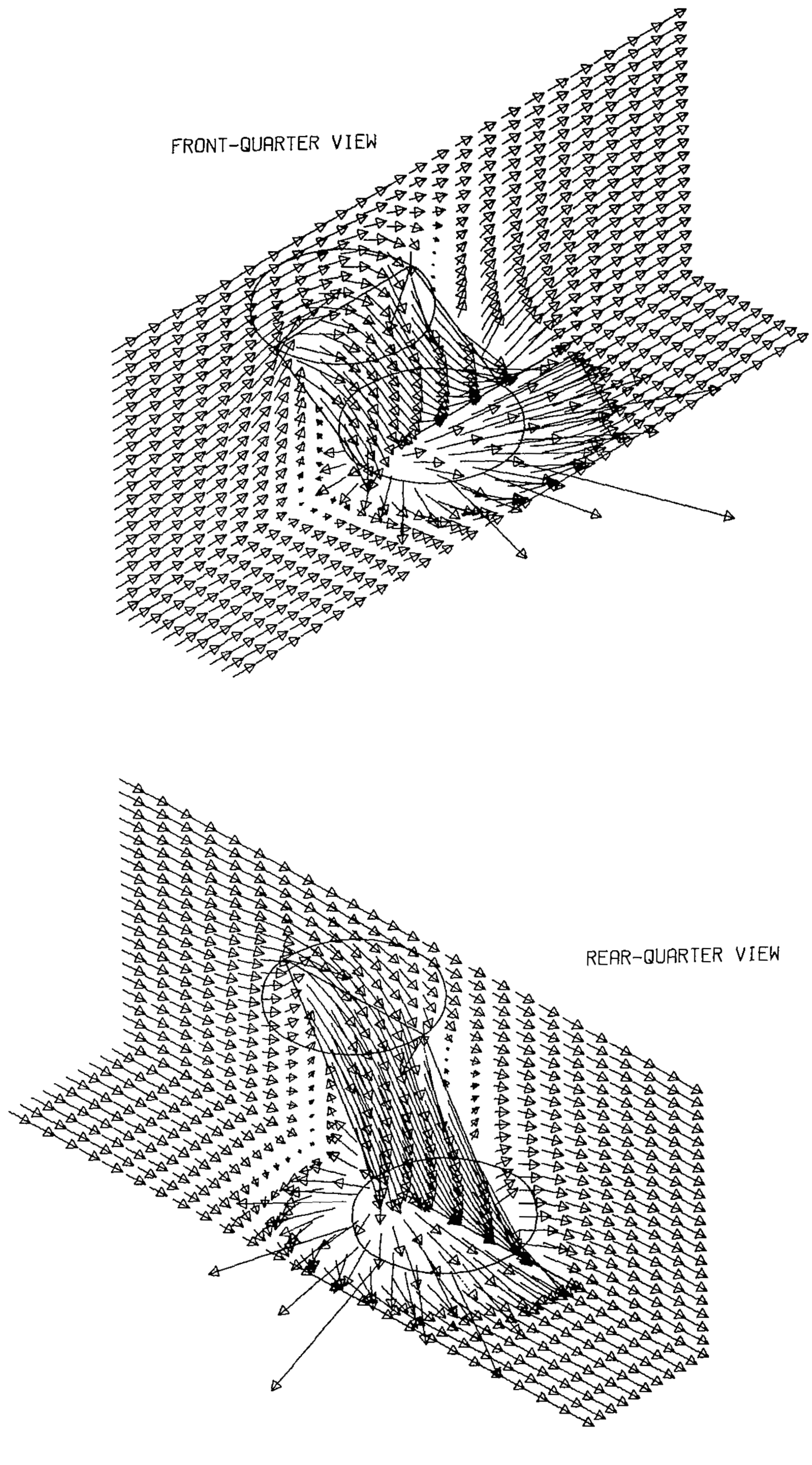

(C).- CLOSED TUNNEL.

Figure 28.- Continued.

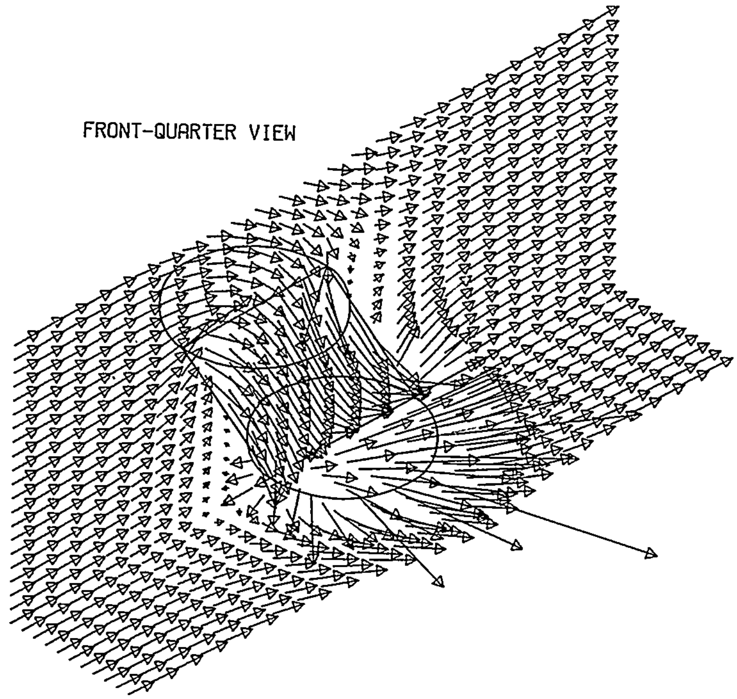

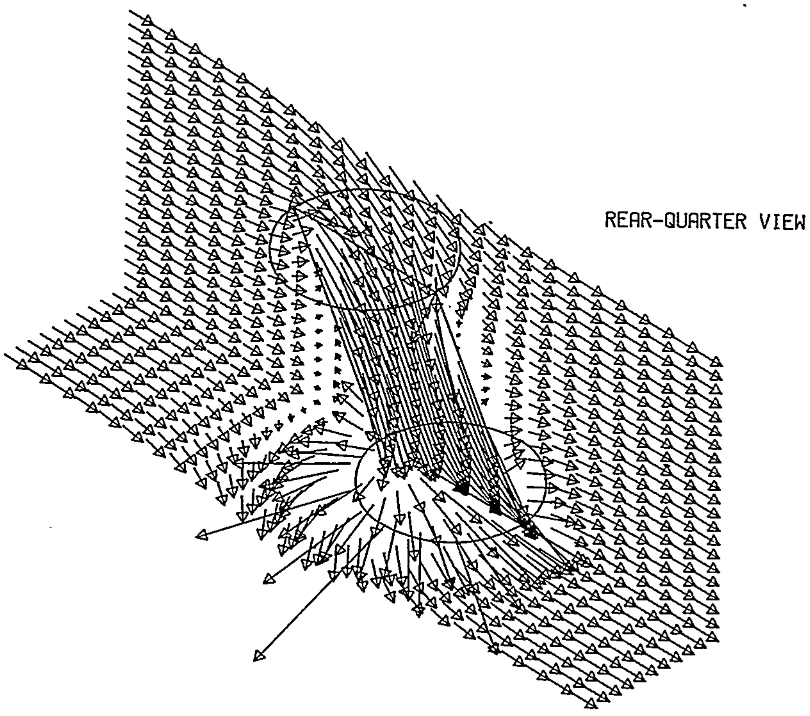

(D).– CLOSED-ON-BOTTOM-ONLY TUNNEL.

Figure 28.- Concluded.

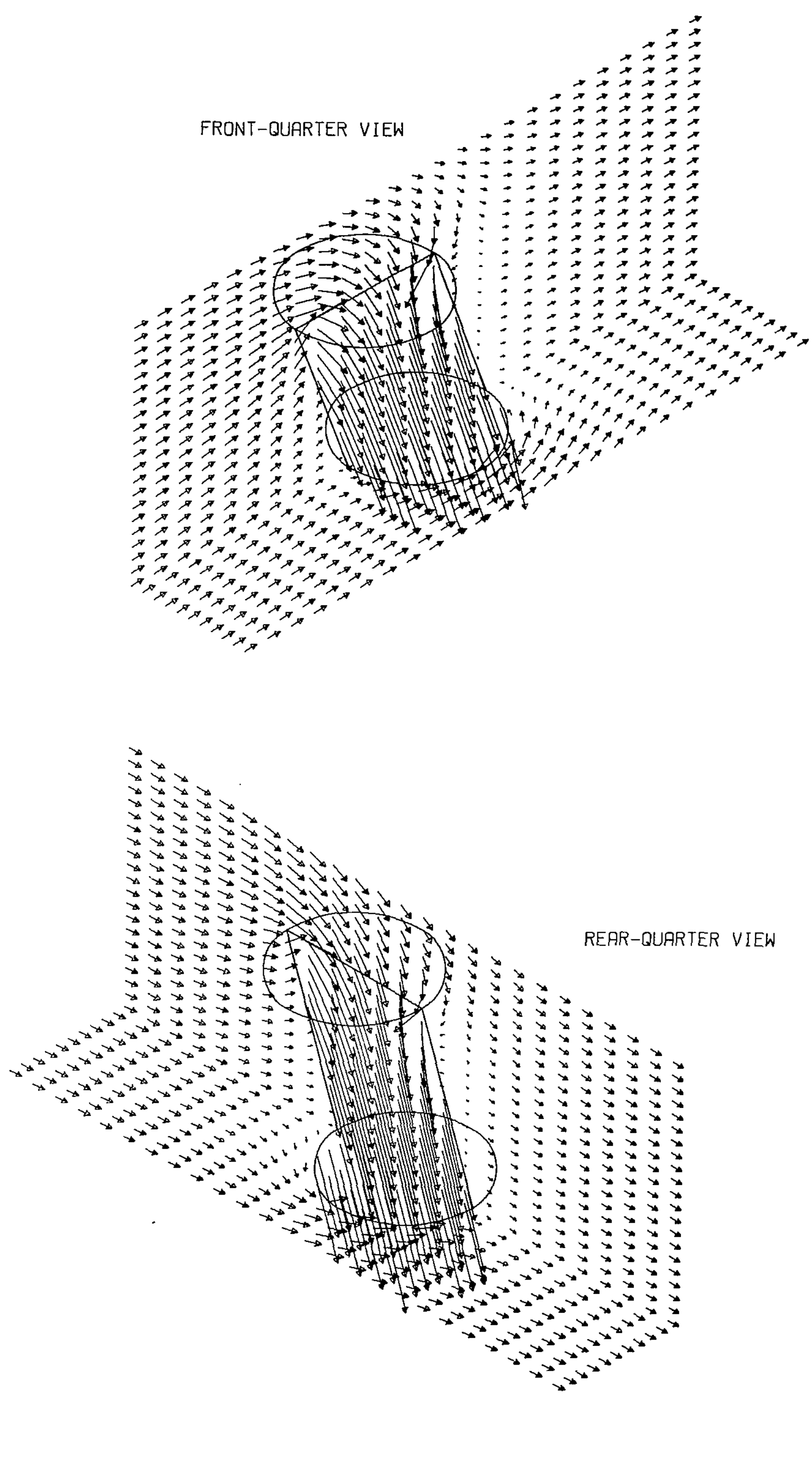

Figure 29.- Isometric views of the flow vectors near a rotor, calculated using vortex cylinders. The rotor and the intersections of the wake with the X-Z plane and the plane of the floor are shown. Because of symmetry, only the vectors in the right-hand half of the plane of the floor are given. ζ = 0.769; η = 1.0; γ = 1.0; σ = 0.60; α = 0.0°; χ = 20.0°; uniform loading.

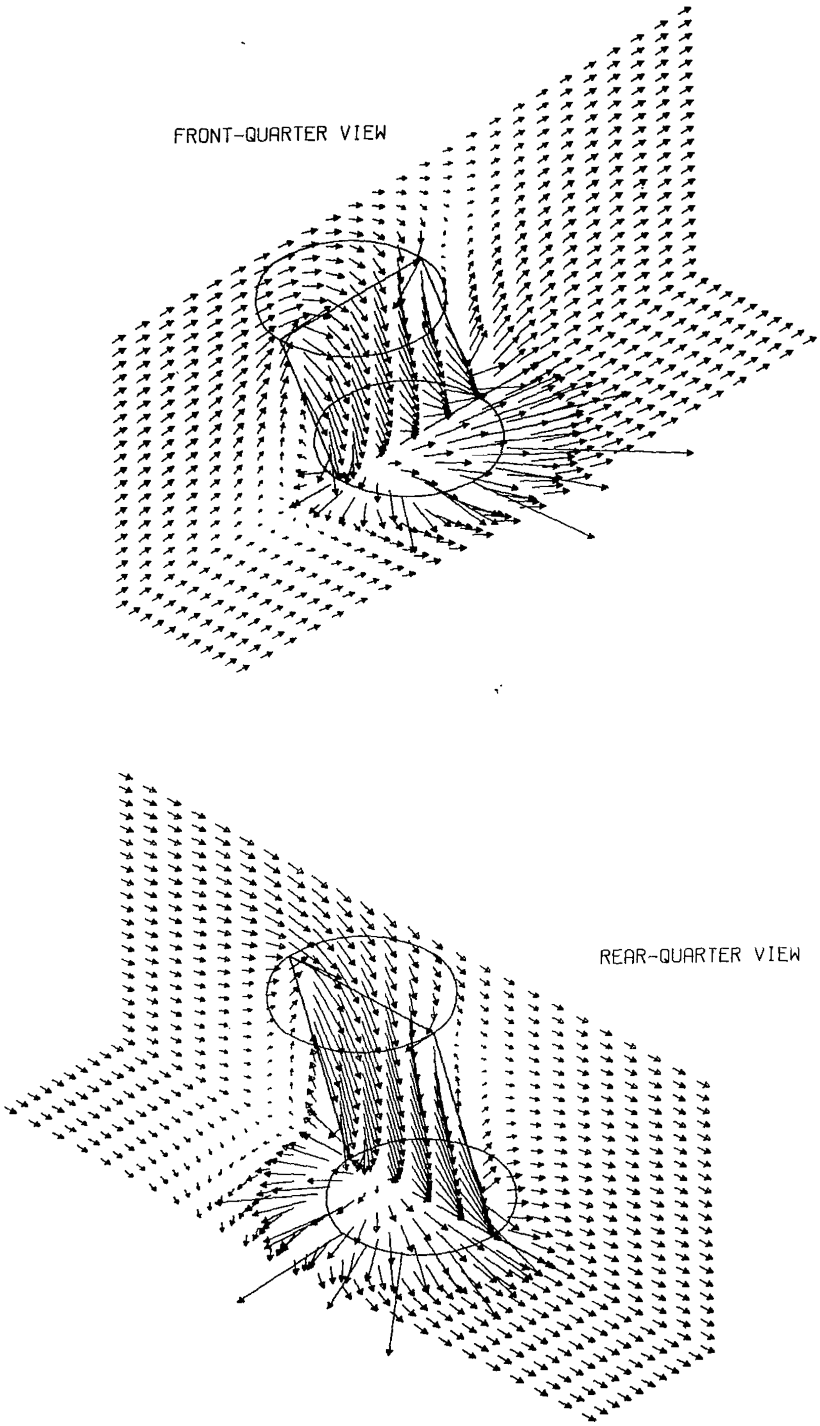

(B).- GROUND EFFECT.

Figure 29 - Continued.

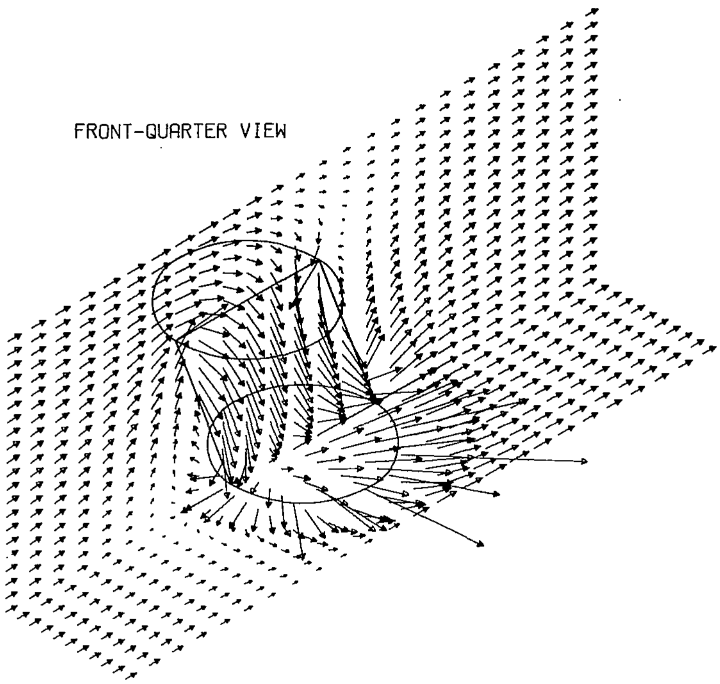

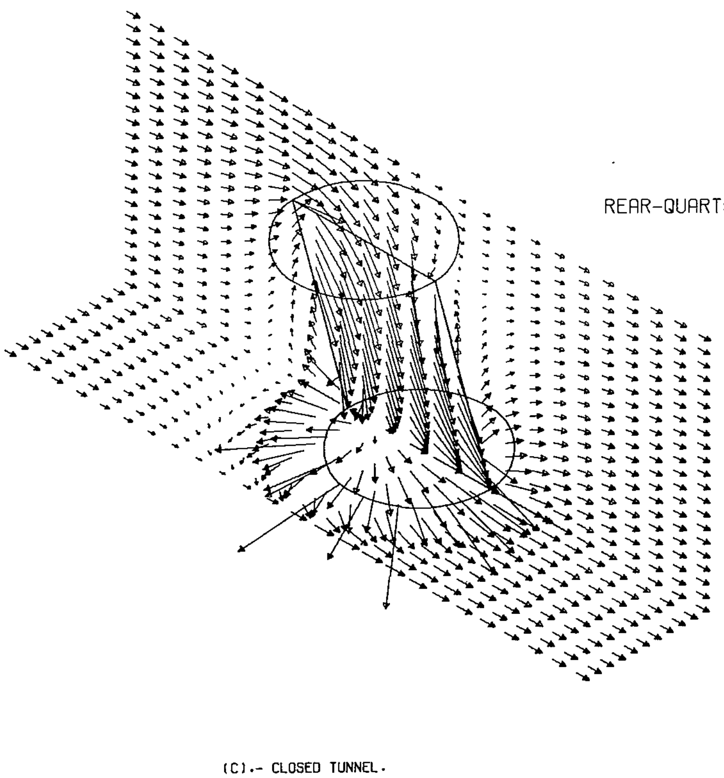

(C).- CLOSED TUNNEL.

Figure 29.- Continued.

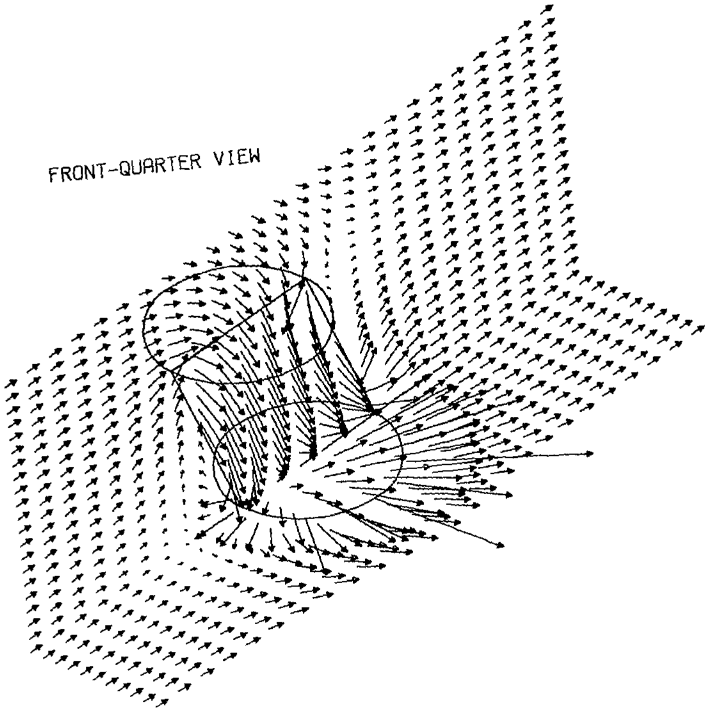

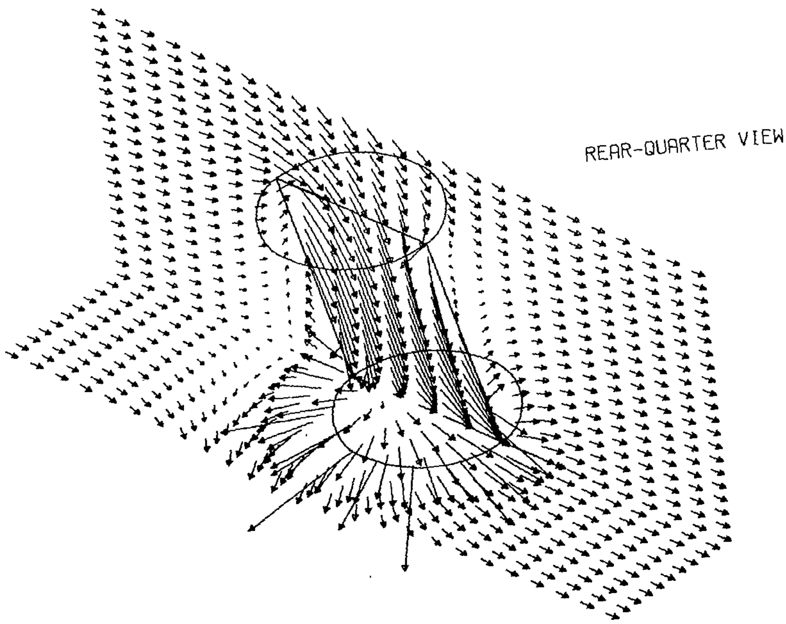

(D).- CLOSED-ON-BOTTOM-ONLY TUNNEL.

Figure 29.- Concluded.

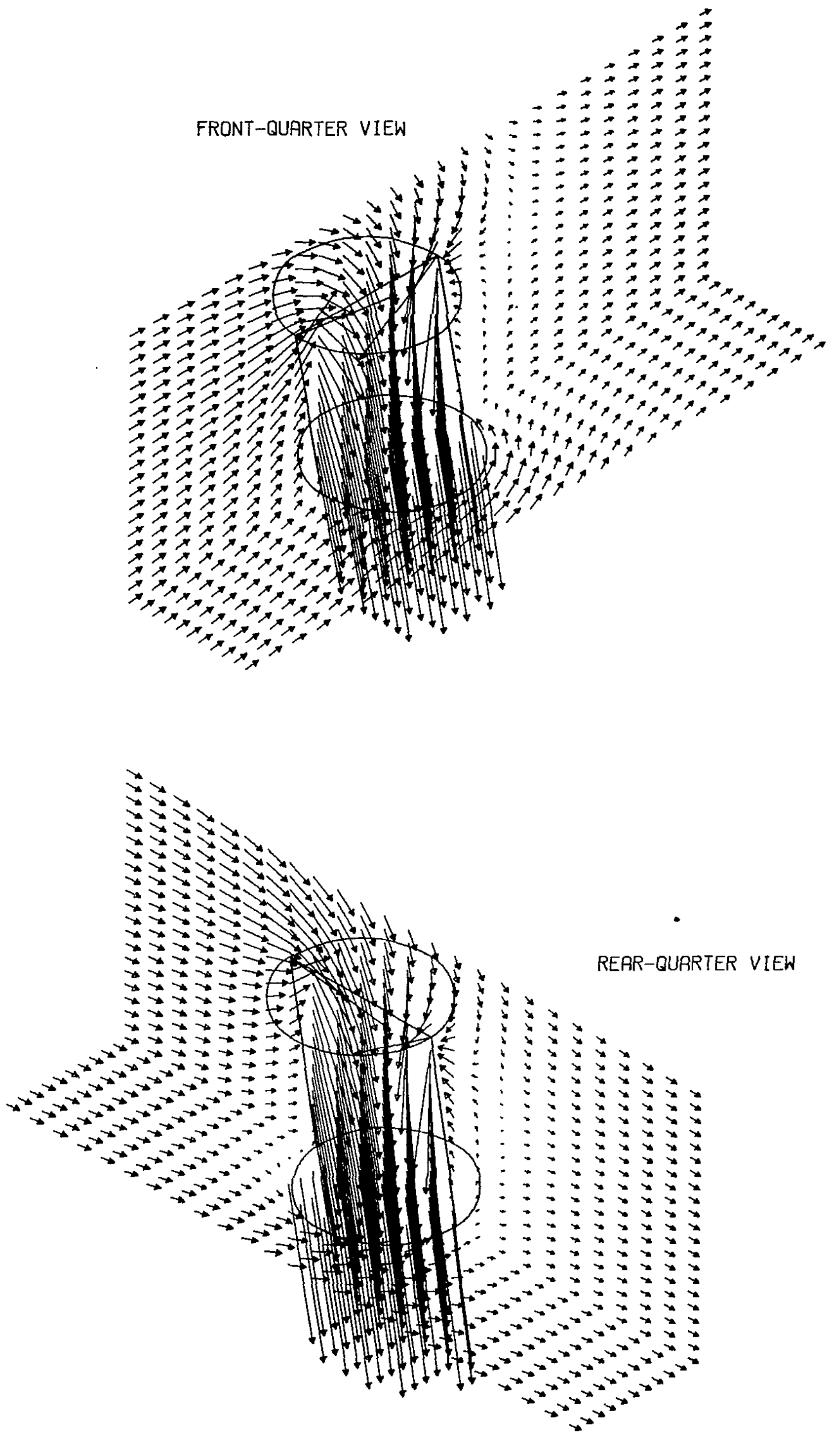

(A).- FREE AIR.

Figure 30.- Isometric views of the flow vectors near a rotor, calculated using vortex cylinders. The rotor and the intersections of the wake with the X-Z plane and the plane of the floor are shown. Because of symmetry, only the vectors in the right-hand half of the plane of the floor are given. $\zeta = 0.769$; $\eta = 1.0$; $\gamma = 1.0$; $\sigma = 0.60$; $\alpha = 0.0^{\circ}$; $\chi = 10.0^{\circ}$; uniform loading.

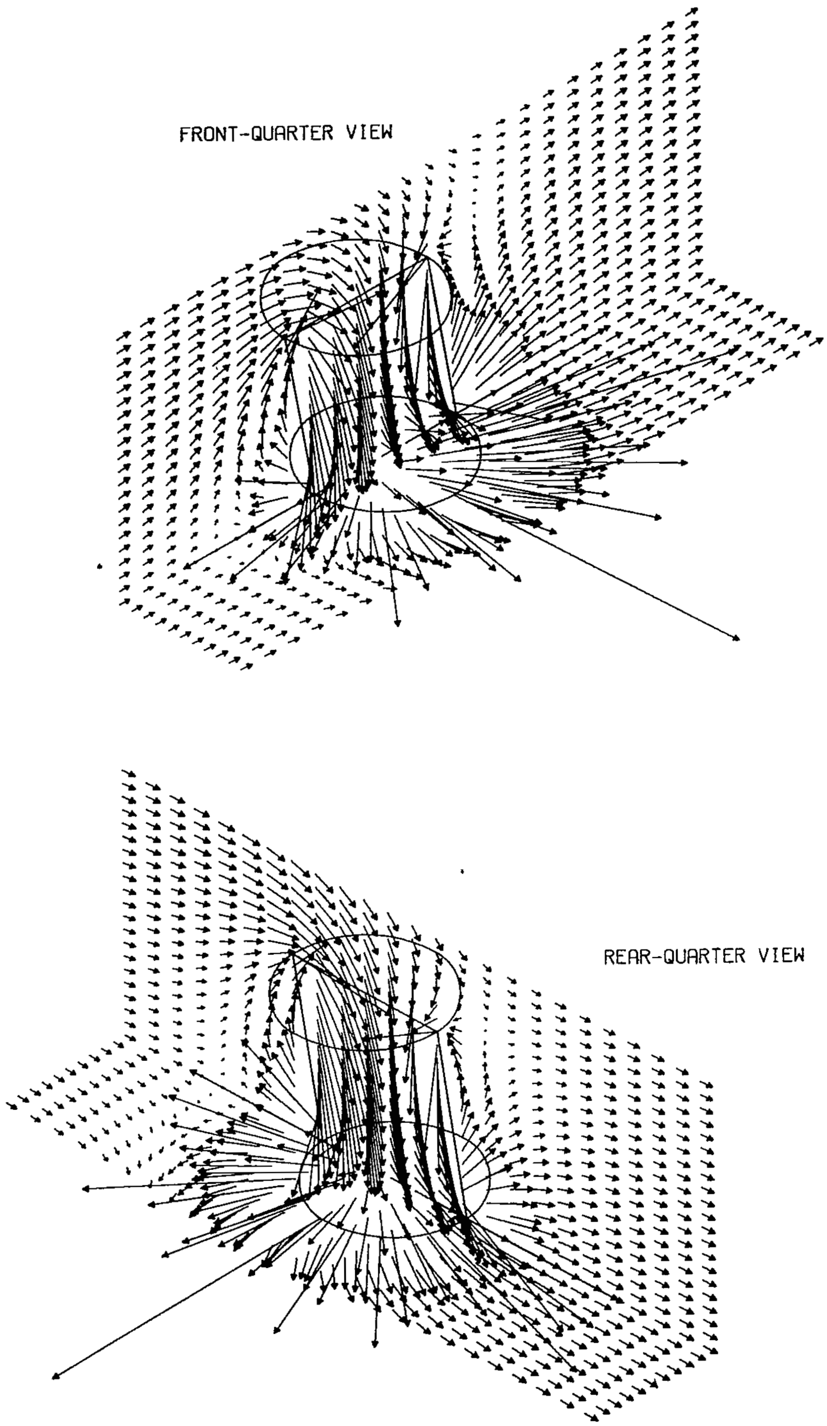

(B).- GROUND EFFECT.

Figure 30.- Continued.

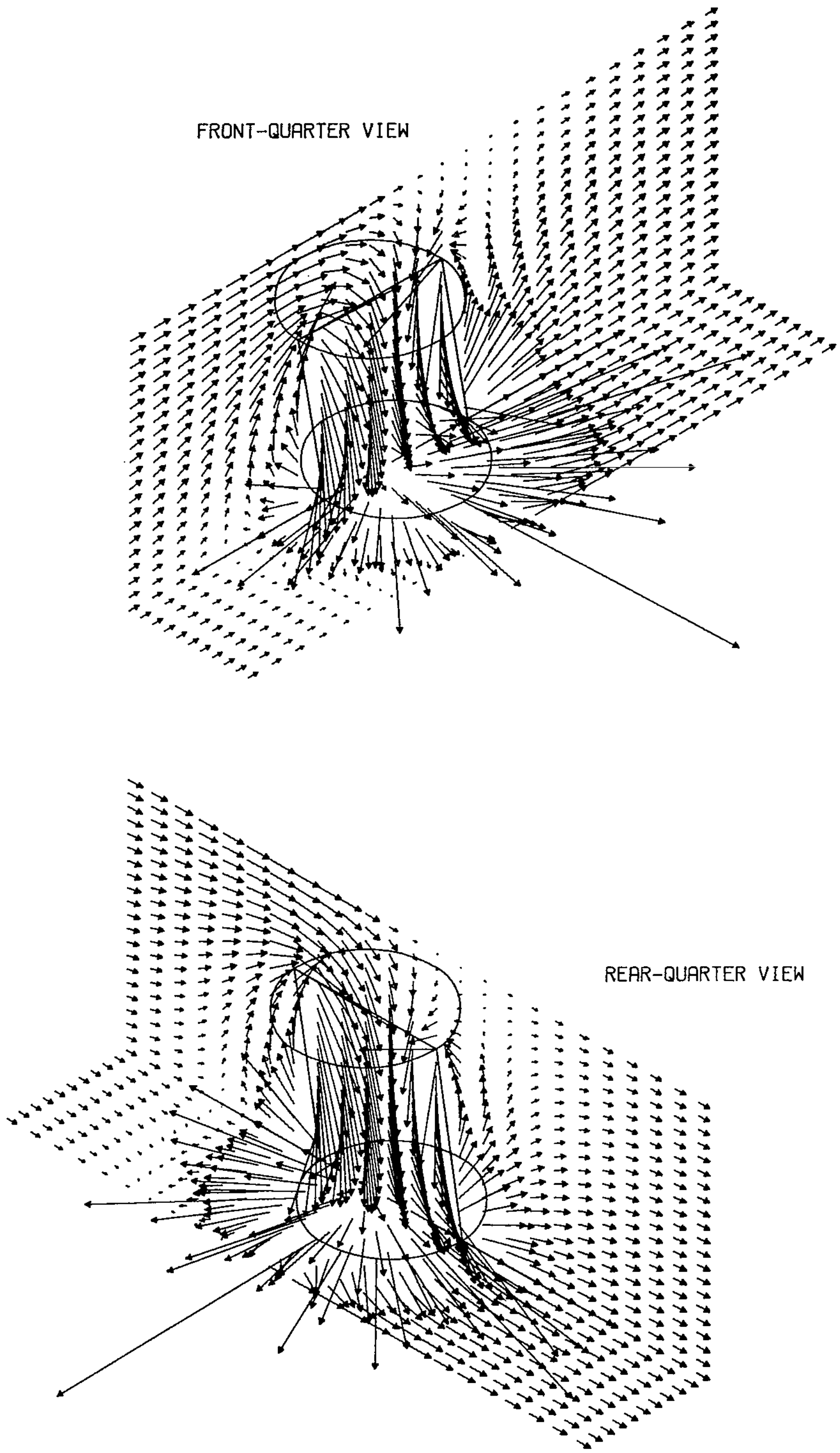

(C).- CLOSED TUNNEL.

Figure 30.- Continued.

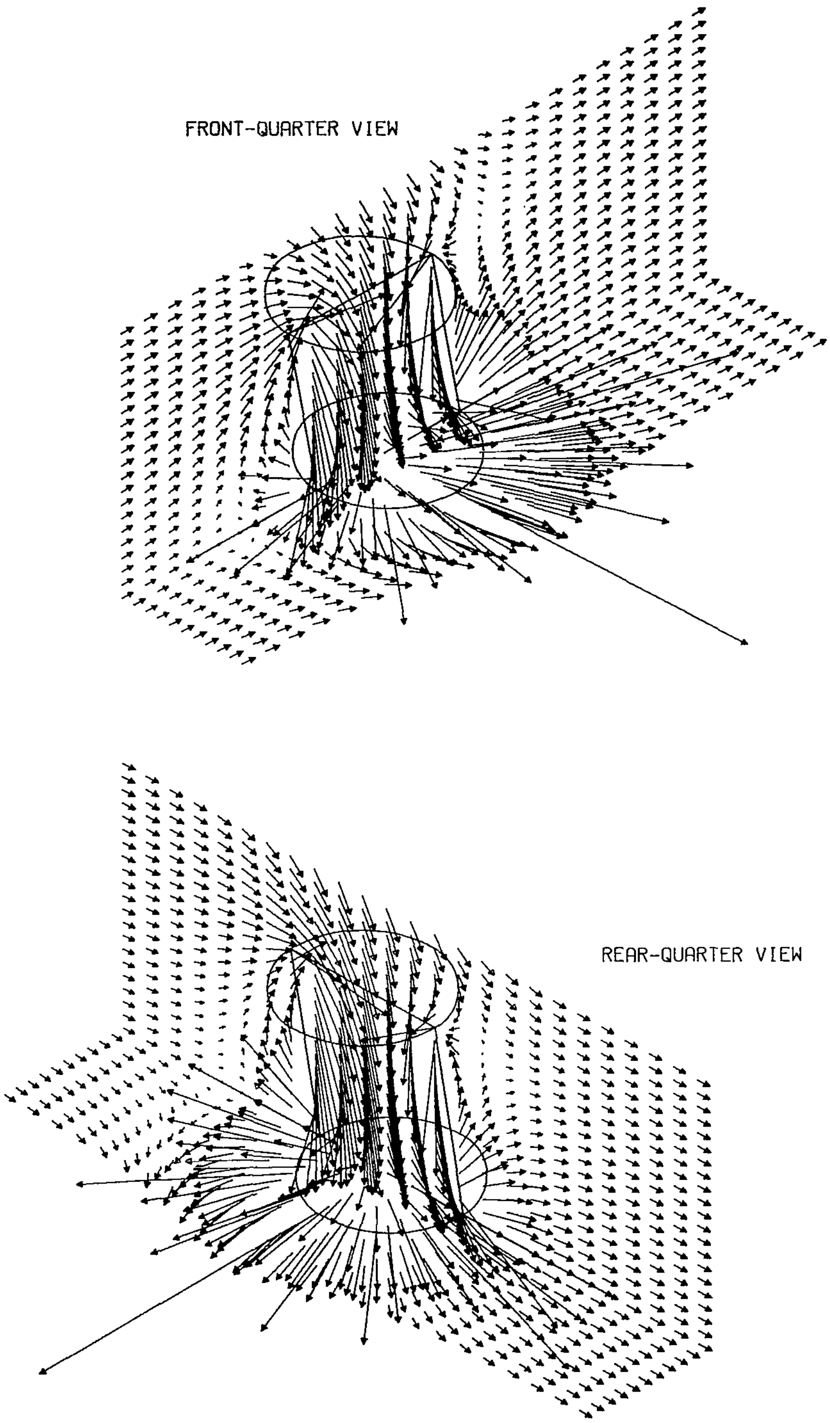

(D).- CLOSED-ON-BOTTOM-ONLY TUNNEL.

Figure 30.- Concluded.

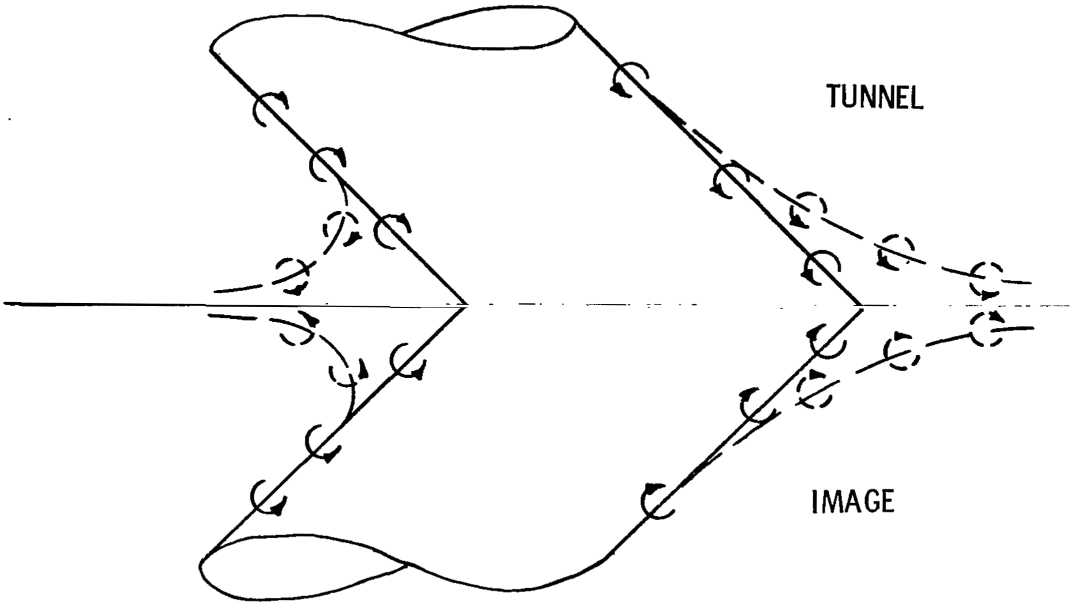

Figure 31.- Sketches of undeformed (solid lines) and deformed (broken lines) wakes near wind-tunnel floor.

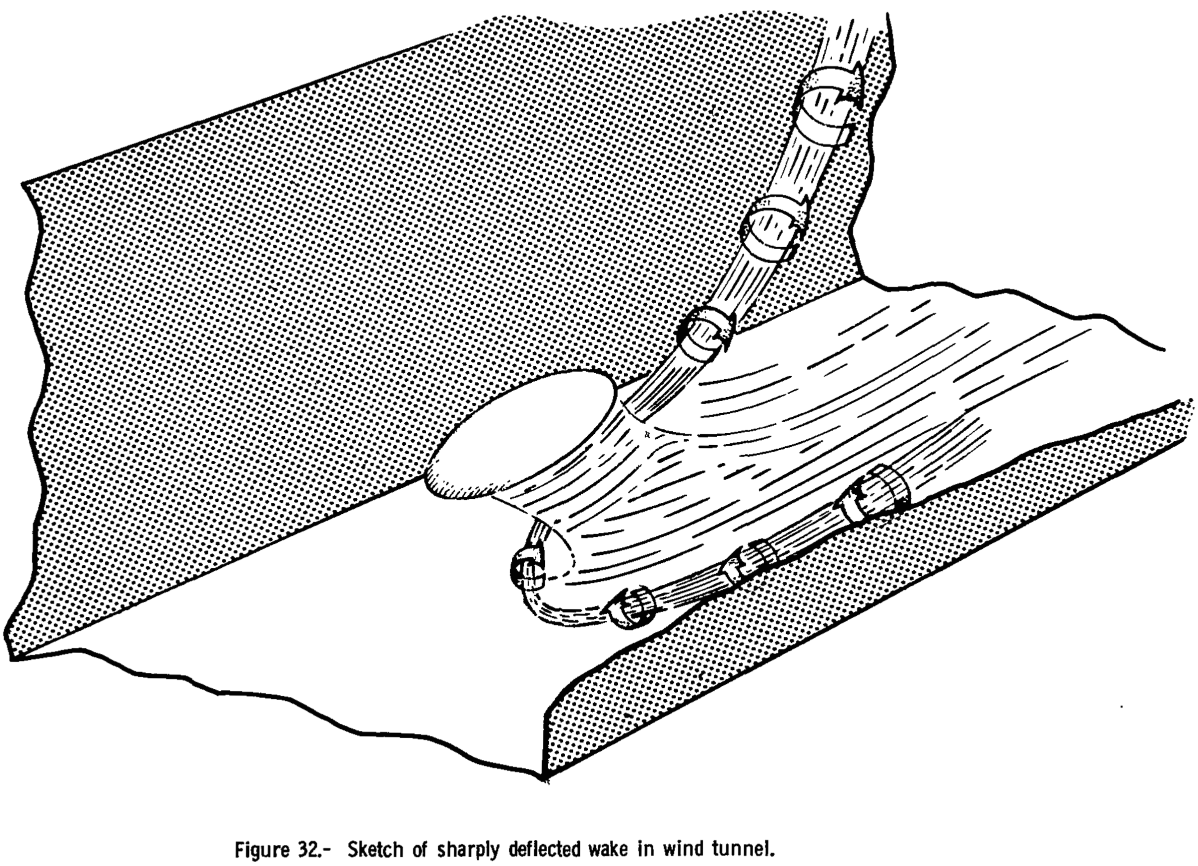

Figure 32.- Sketch of sharply deflected wake in wind tunnel.

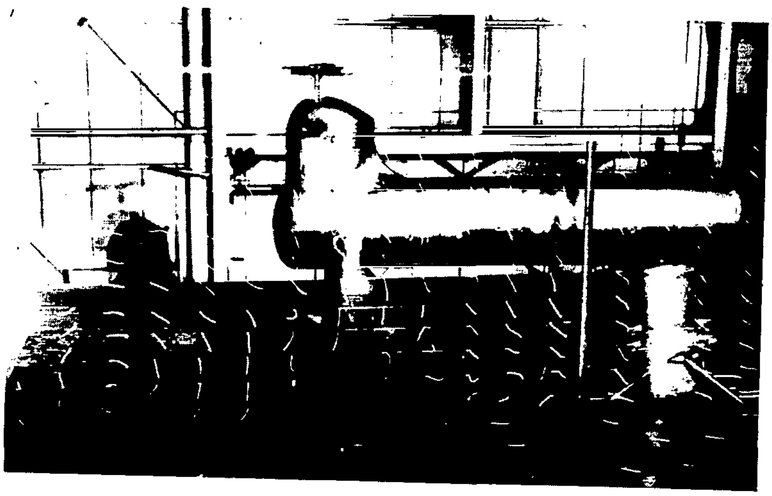

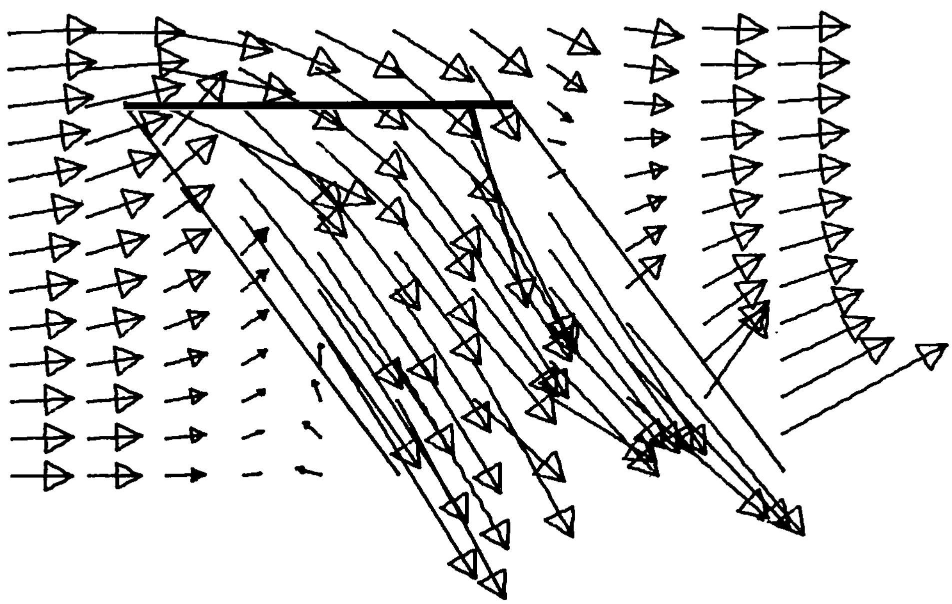

Figure 33.- Comparison of calculated flow field with tuft-grid study in a closed-on-bottom-only tunnel. Calculations are for plane of tuft-grid (0.13H to side of rotor). Calculated flow field assumes triangular disk-load distribution. $\gamma = 2.0$; $\sigma = 0.25$; $\chi \approx 35^{0}$; $\zeta = 1.0$.

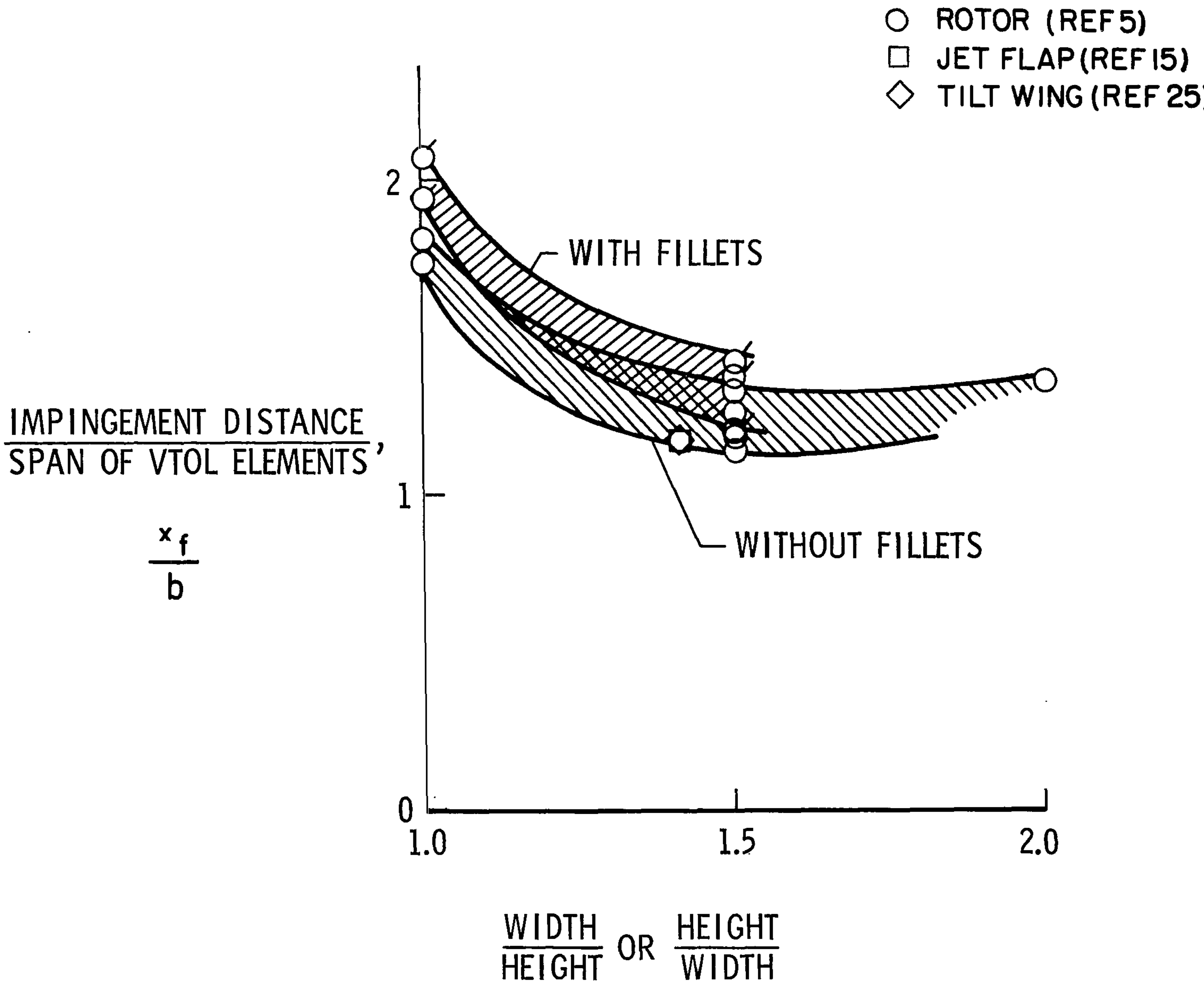

Figure 34.- Minimum-speed limits for V/STOL testing as derived from the data of reference 5.

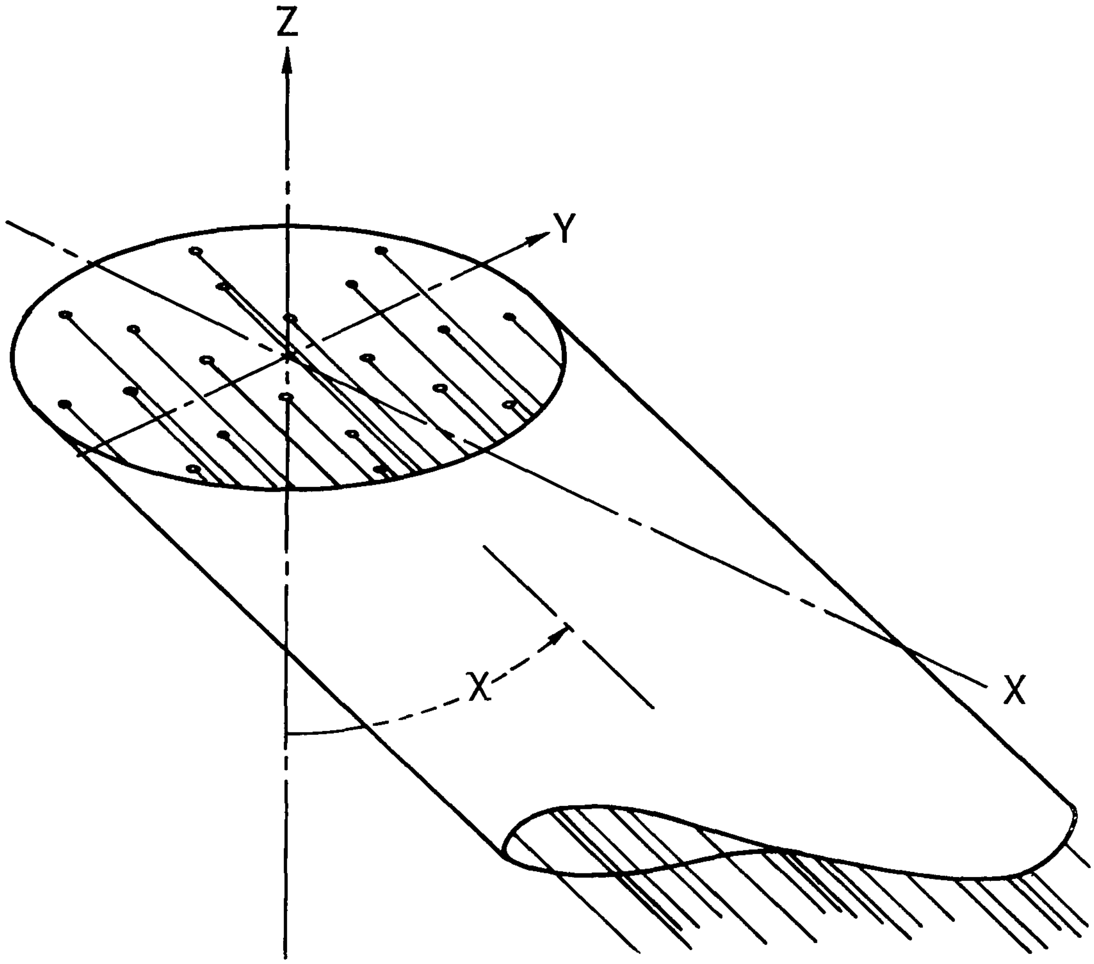

Figure 35.- Sketch of doublet-line system used to represent a rotor in NASA TR R-302 as compared to skewed cylinder of vorticity used to represent a rotor in NASA TN D-394 and NASA TR R-71.

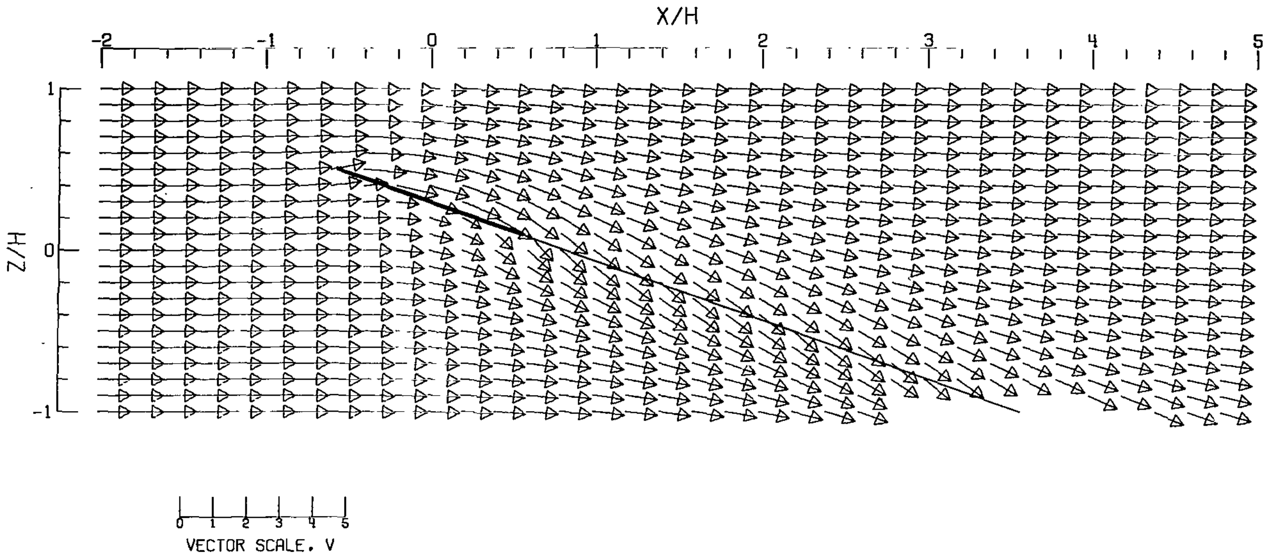

(A).- FREE AIR.

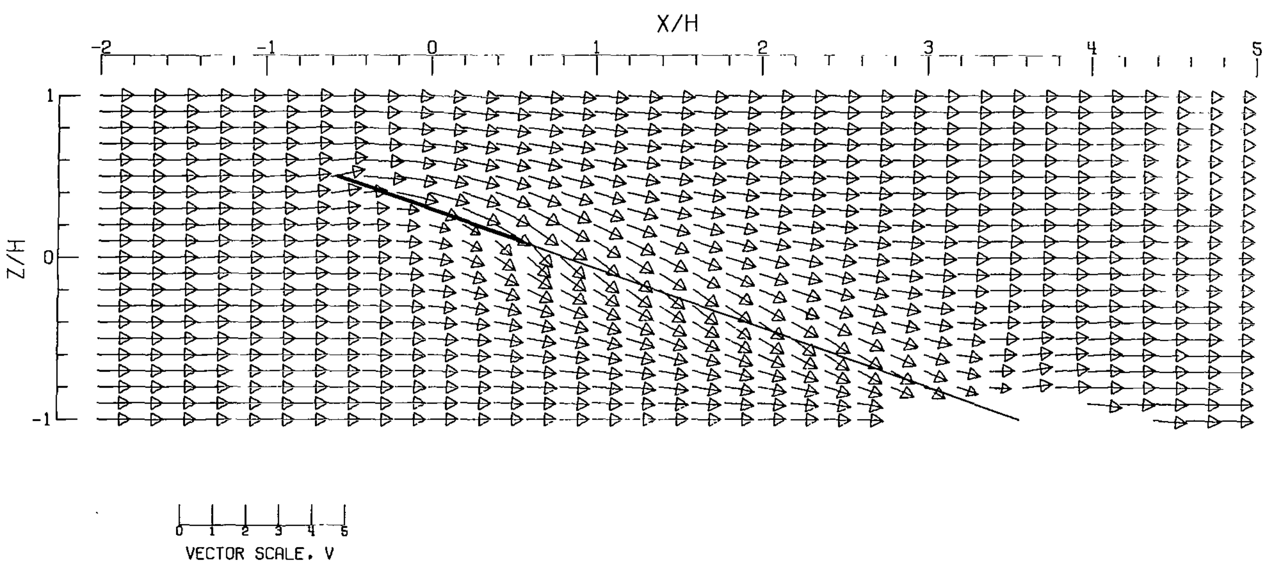

(B).- GROUND EFFECT.

Figure 36.- Flow vectors in the X-Z plane, calculated using doublet strings. The rotor and the edges of the wake are shown. ζ = 0.769; η = 1.000; γ = 1.000; σ = 0.600; α = 20.000°; χ = 70.000°; uniform loading.

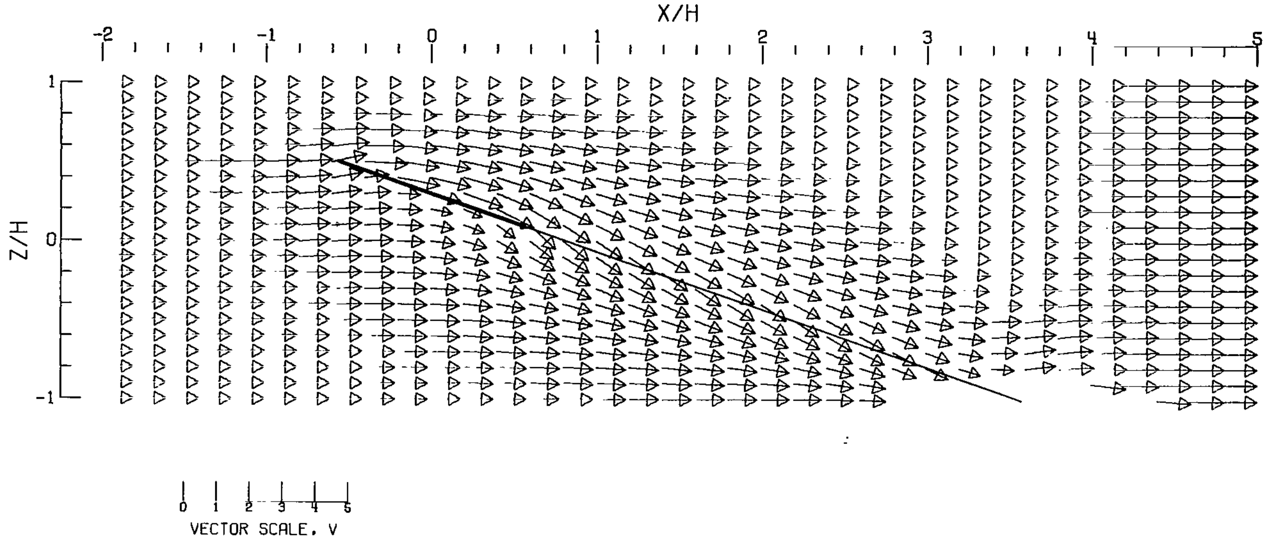

(C).- CLOSED TUNNEL.

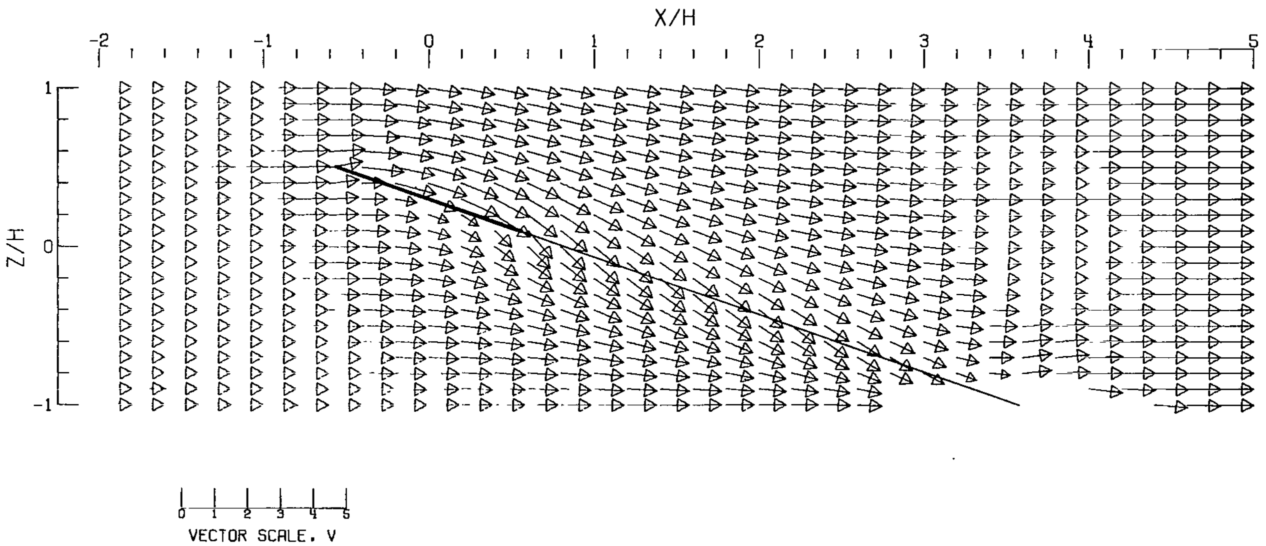

(D).- CLOSED-ON-BOTTOM-ONLY TUNNEL.

Figure 36.- Concluded.

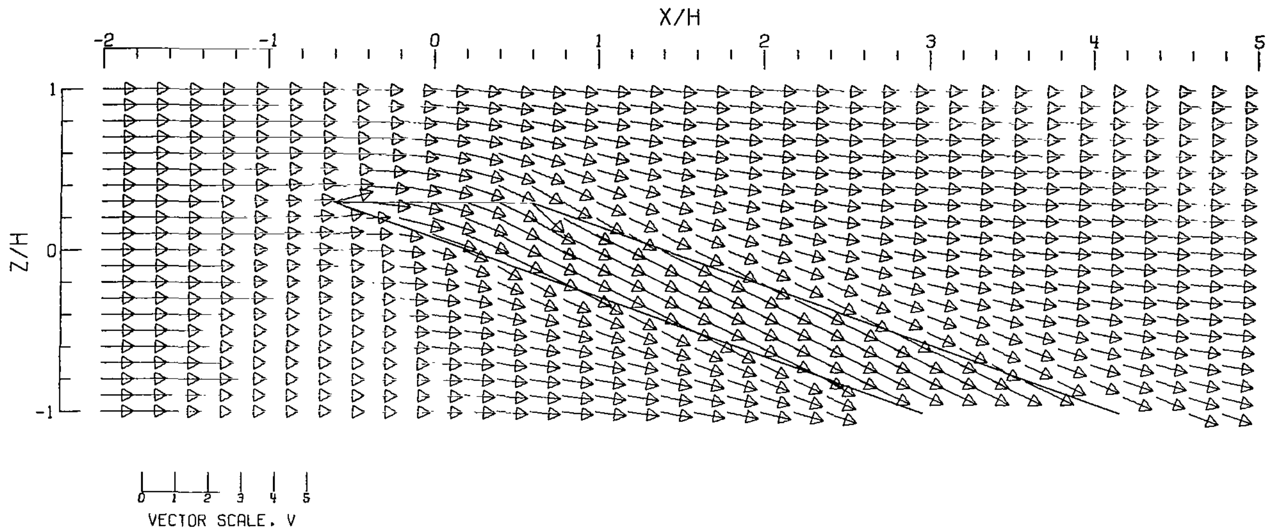

(A).- FREE AIR.

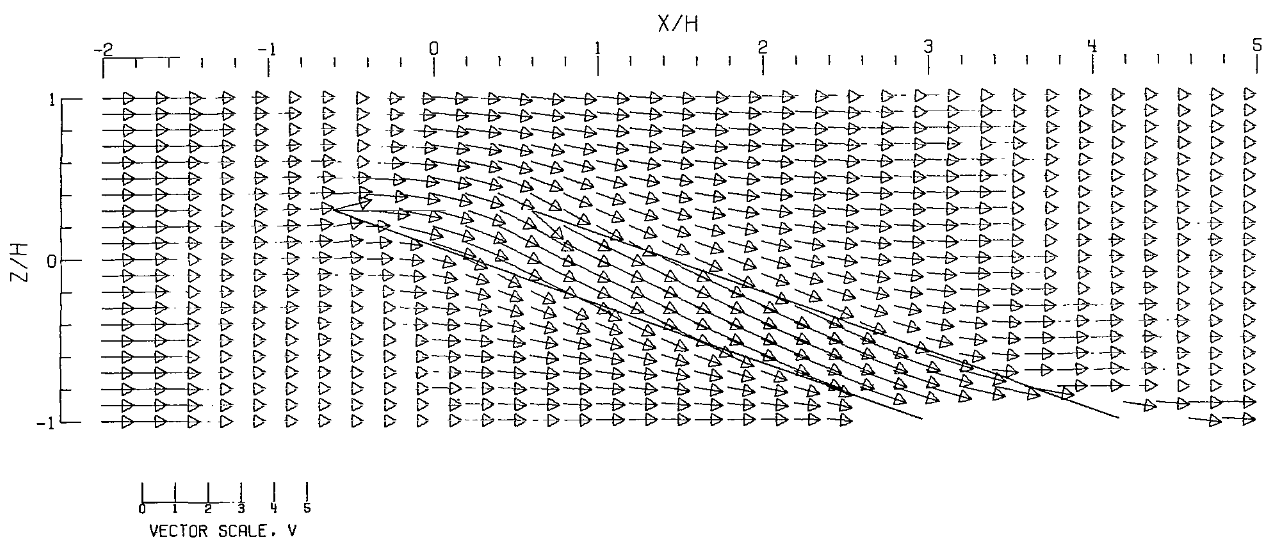

(B).- GROUND EFFECT.

Figure 37.- Flow vectors in the X-Z plane, calculated using doublet strings. The rotor and the edges of the wake are shown. $\zeta = 0.769$; $\eta = 1.000$; $\gamma = 1.000$; $\sigma = 0.600$; $\alpha = 0.000^{\circ}$; $\chi = 70.000^{\circ}$; uniform loading.

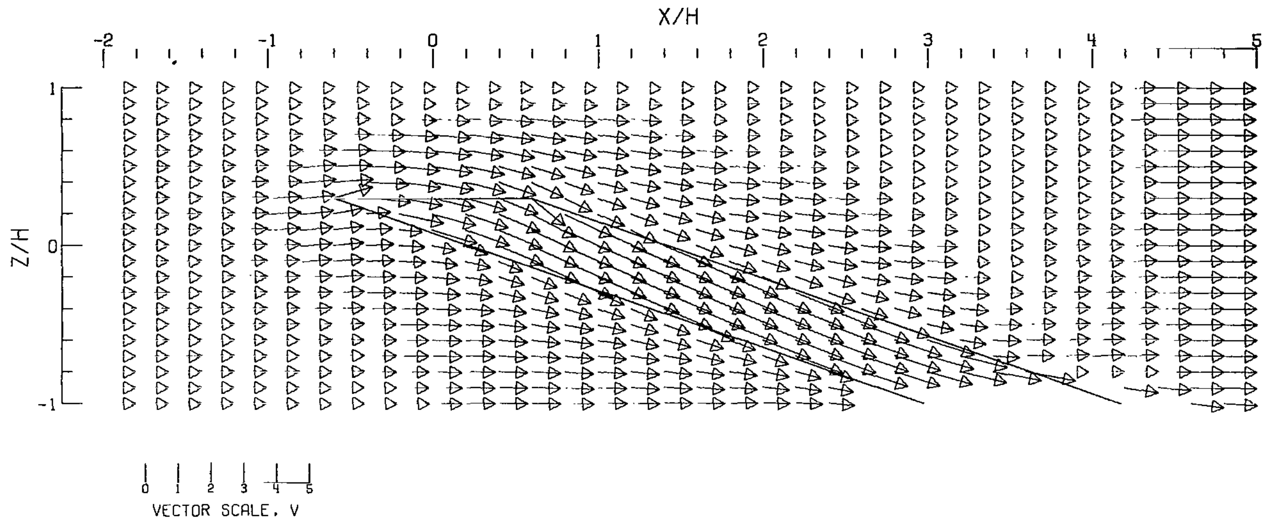

(C).- CLOSED TUNNEL.

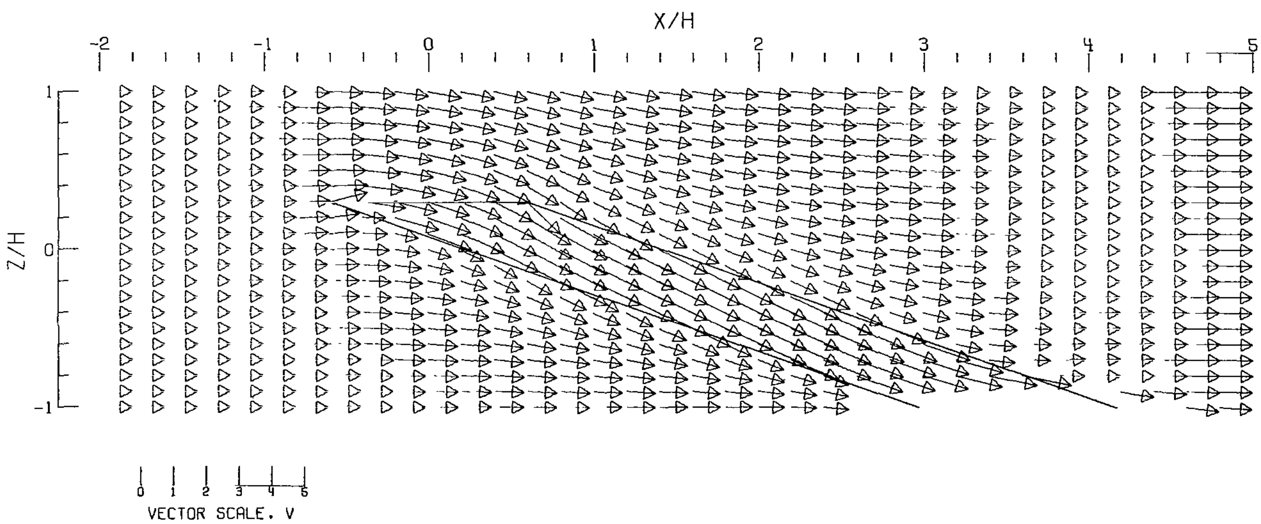

(D).- CLOSED-ON-BOTTOM-ONLY TUNNEL.

Figure 37.- Concluded.

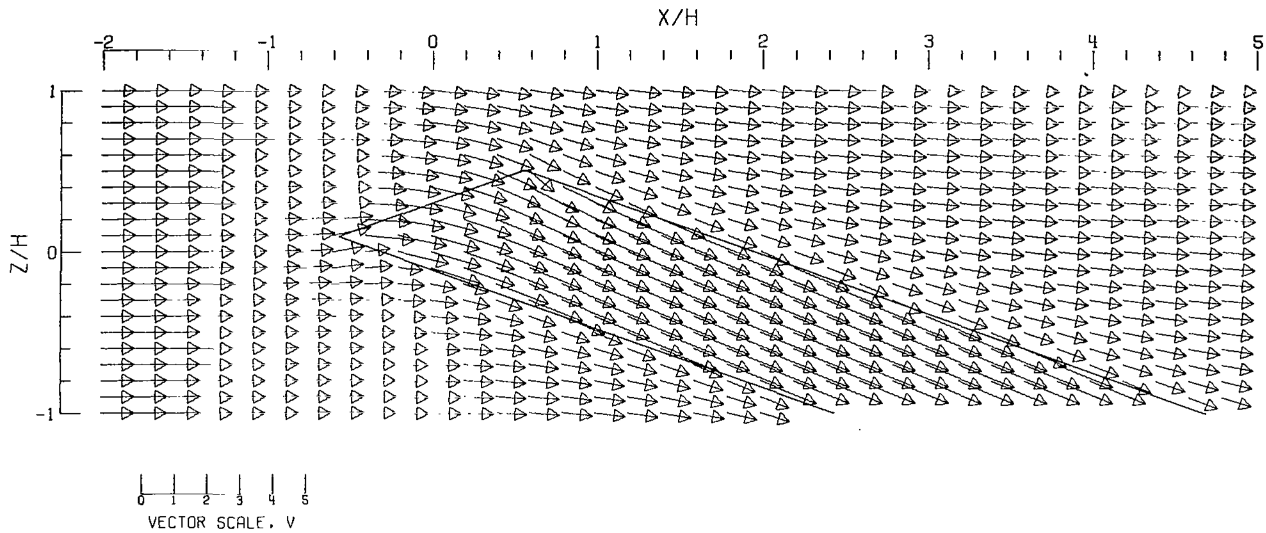

(A).- FREE AIR.

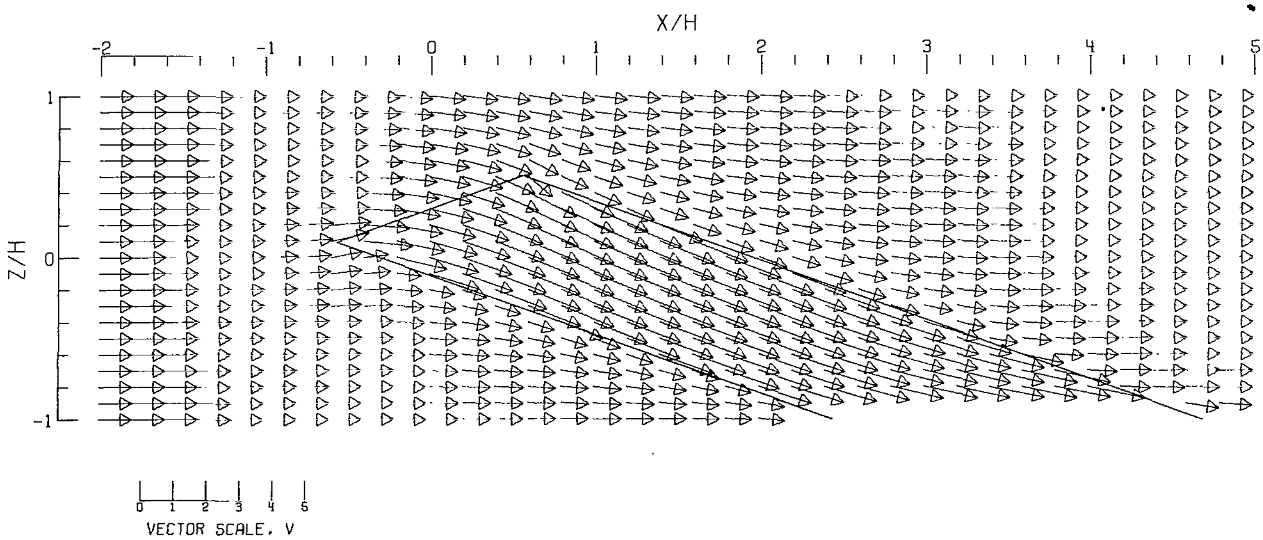

(B).- GROUND EFFECT.

Figure 38.- Flow vectors in the X-Z plane, calculated using doublet strings. The rotor and the edges of the wake are shown. ζ = 0.769; η = 1.000; γ = 1.000; σ = 0.600; α = -20.000°; χ = 70.000°; uniform loading.

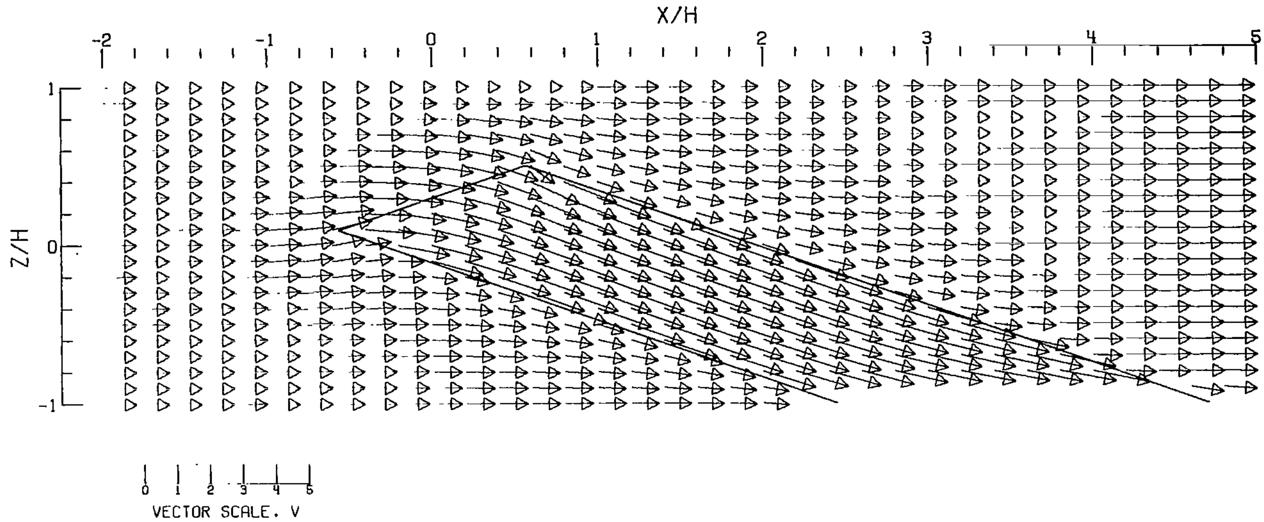

(C).- CLOSED TUNNEL.

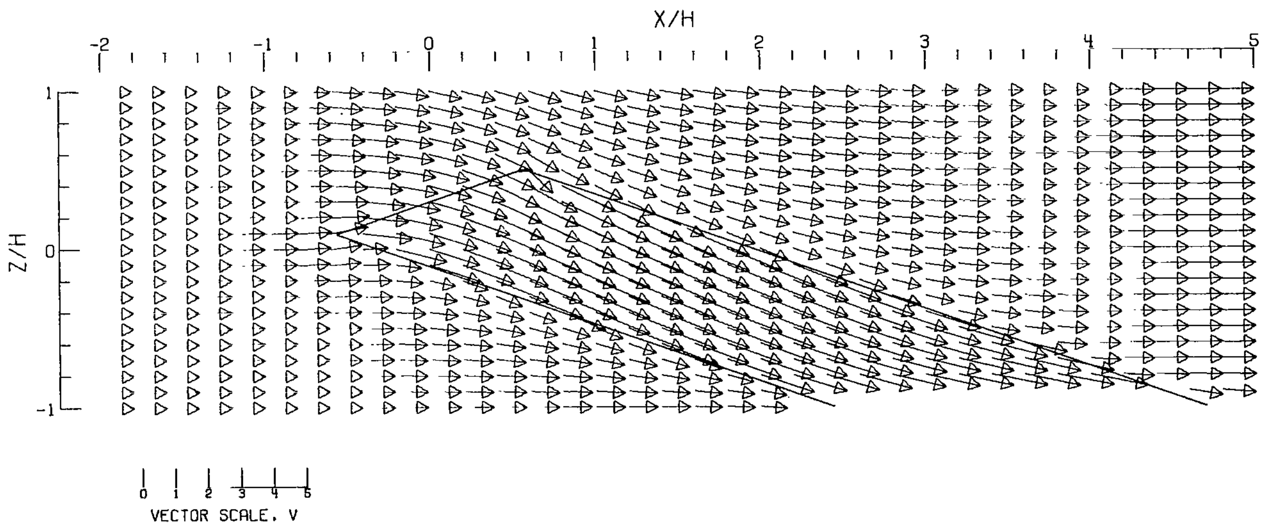

(D).- CLOSED-ON-BOTTOM-ONLY TUNNEL.

Figure 38.- Concluded.

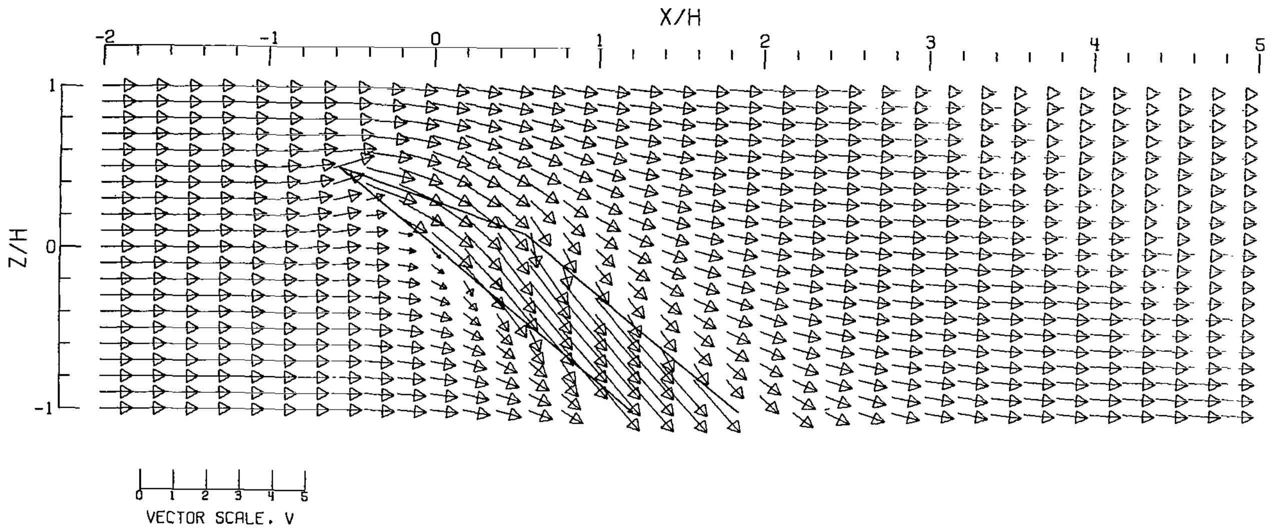

(A).- FREE AIR.

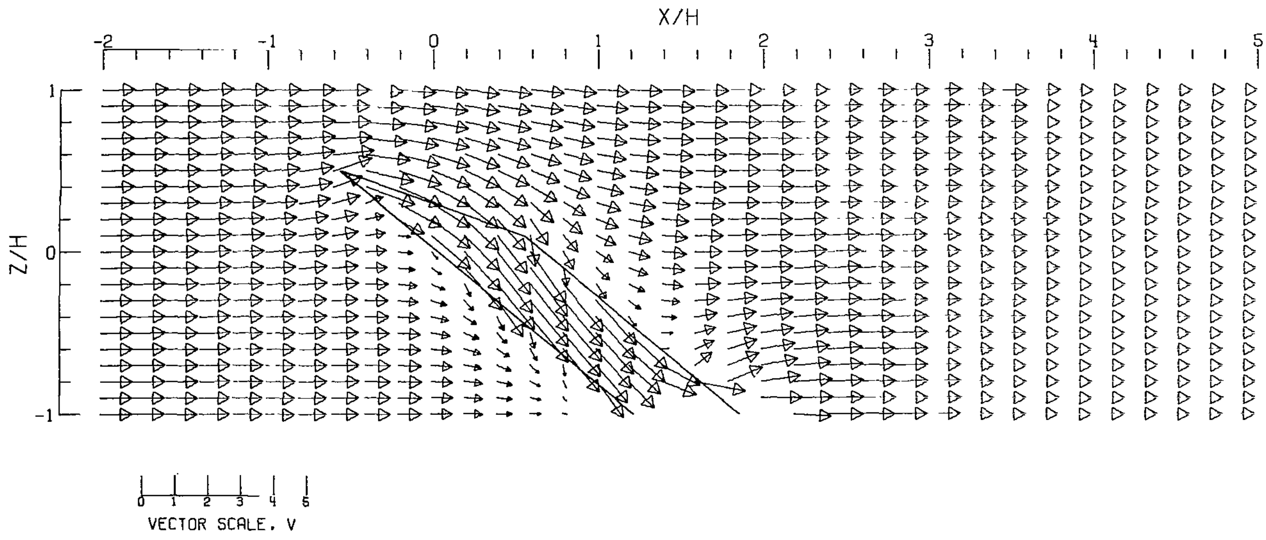

(B).- GROUND EFFECT.

Figure 39.- Flow vectors in the X-Z plane, calculated using doublet strings. The rotor and the edges of the wake are shown. ζ = 0.769; η = 1.000; γ = 1.000; σ = 0.600; α = 20.000°; χ = 50.000°; uniform loading.

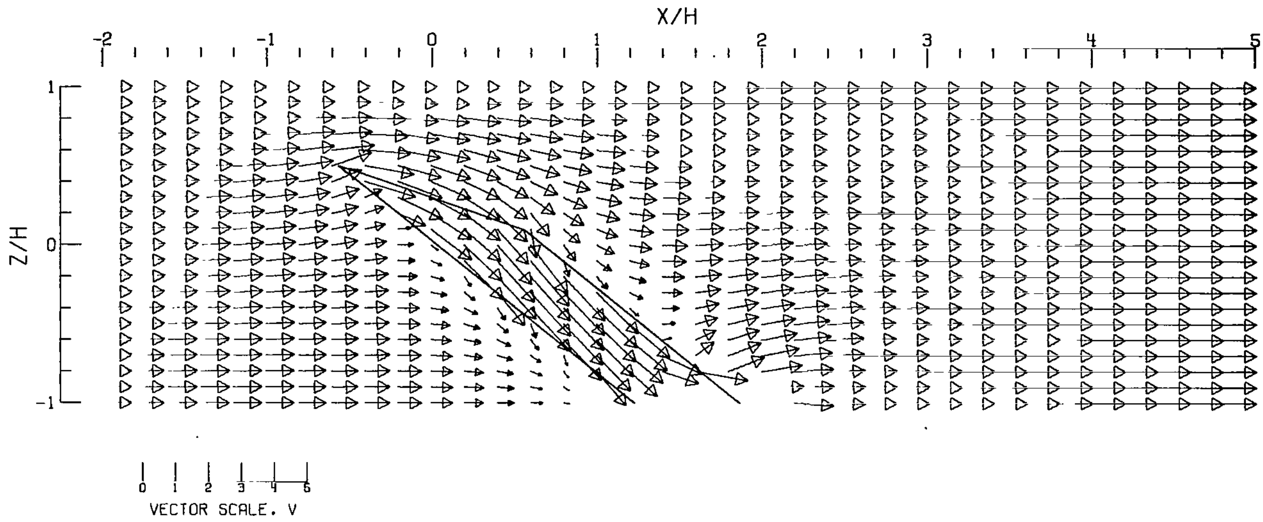

(C).- CLOSED TUNNEL.

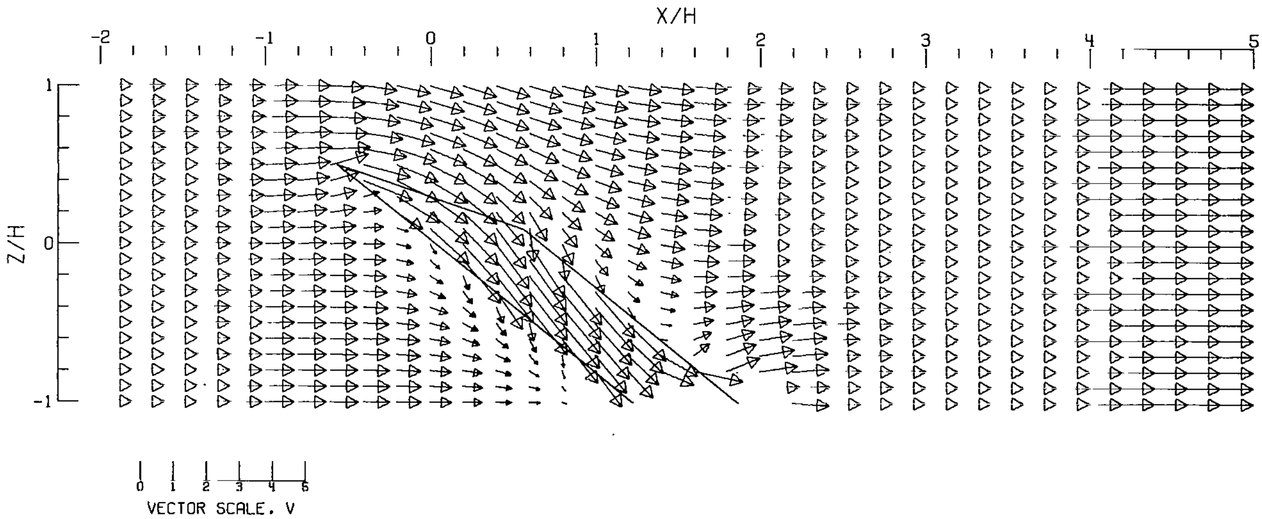

(D).- CLOSED-ON-BOTTOM-ONLY TUNNEL.

Figure 39.- Concluded.

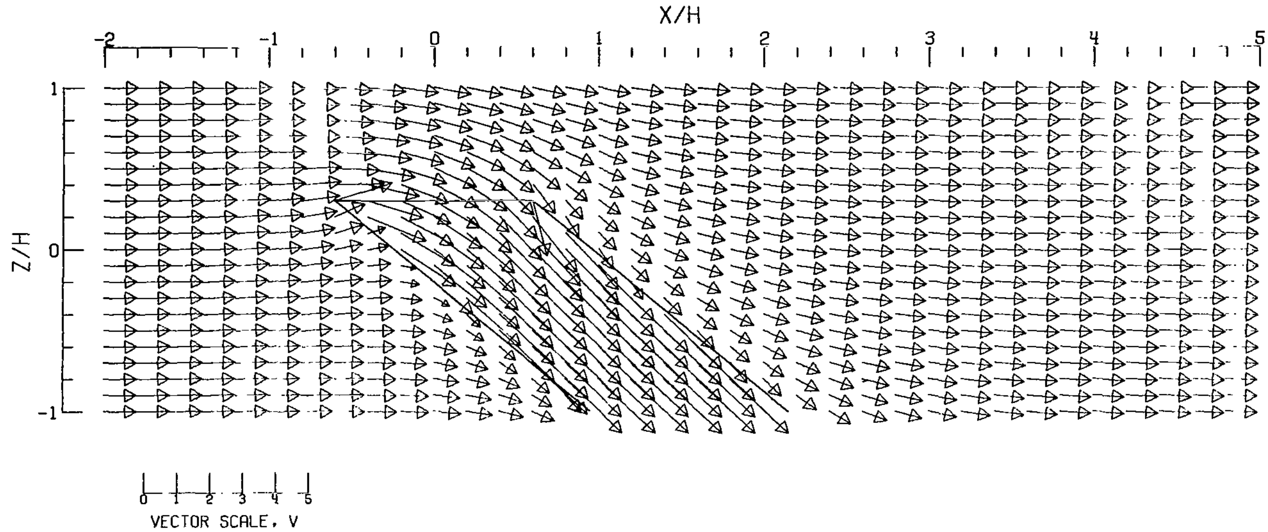

(A).- FREE AIR.

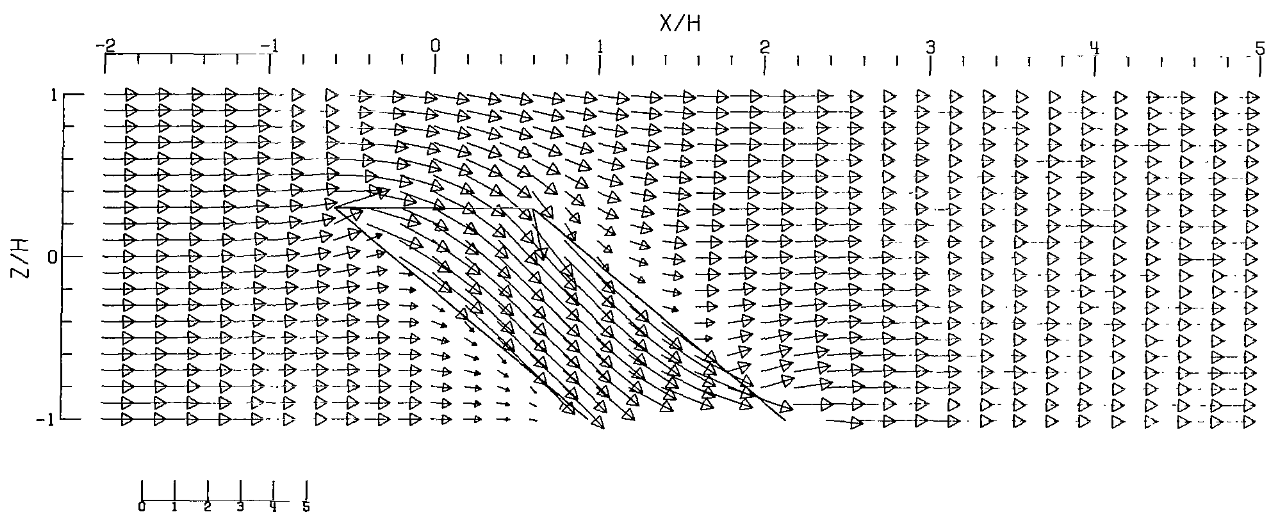

(B).- GROUND EFFECT.

Figure 40.- Flow vectors in the X-Z plane, calculated using doublet strings. The rotor and the edges of the wake are shown. $\zeta = 0.769$; $\eta = 1.000$; $\gamma = 1.000$; $\sigma = 0.600$; $\alpha = 0.000^{\circ}$; $\chi = 50.000^{\circ}$; uniform loading.

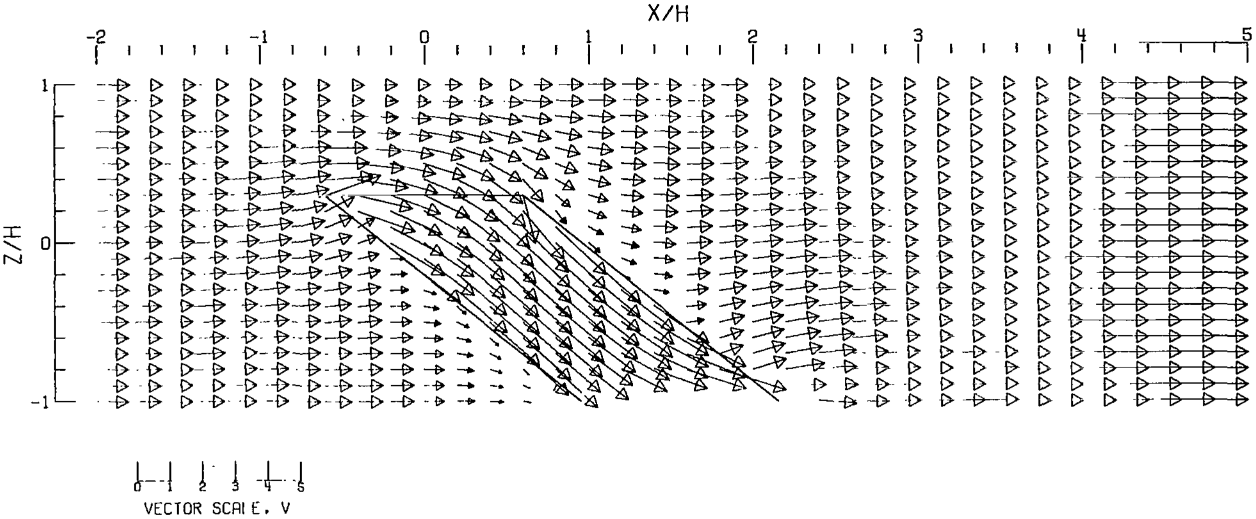

(C).- CLOSED TUNNEL.

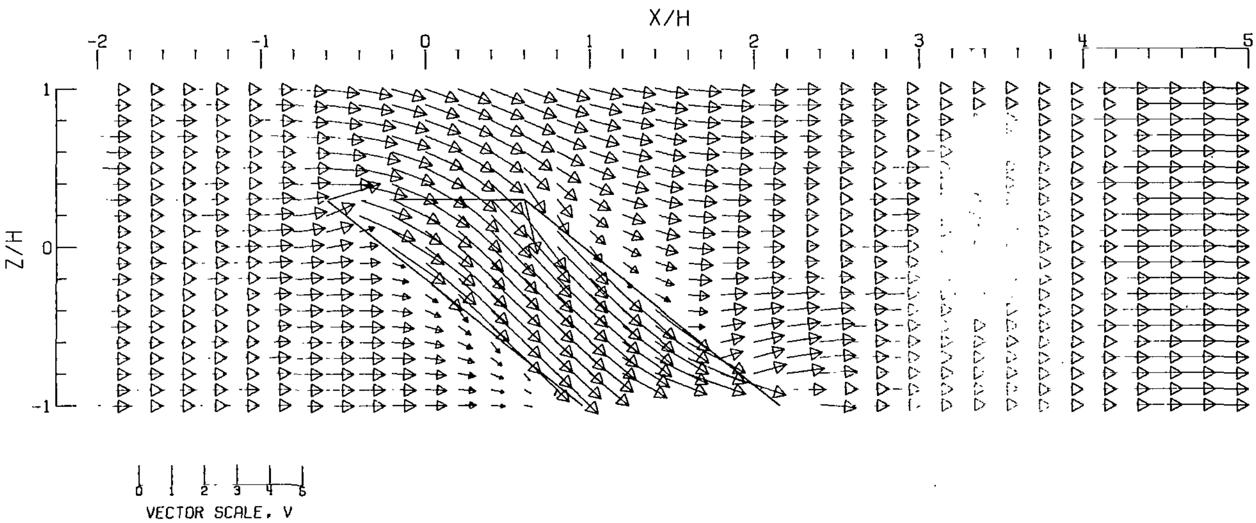

(D).- CLOSED-ON-BOTTOM-ONLY TUNNEL.

Figure 40.- Concluded.

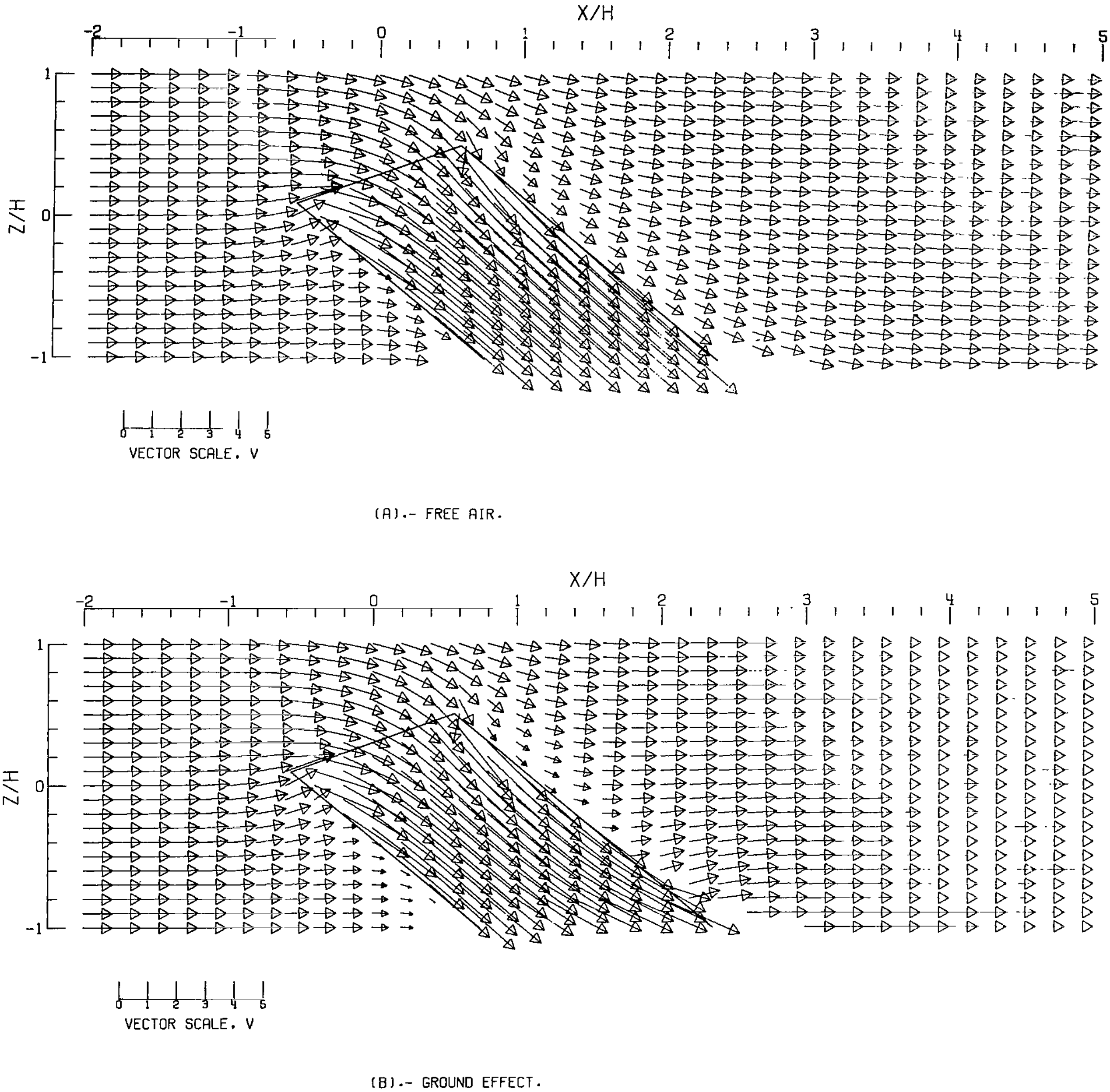

Figure 41.- Flow vectors in the X-Z plane, calculated using doublet strings. The rotor and the edges of the wake are shown. ζ = 0.769; η = 1.000; γ = 1.000; σ = 0.600; α = -20.000°; χ = 50.000°; uniform loading.

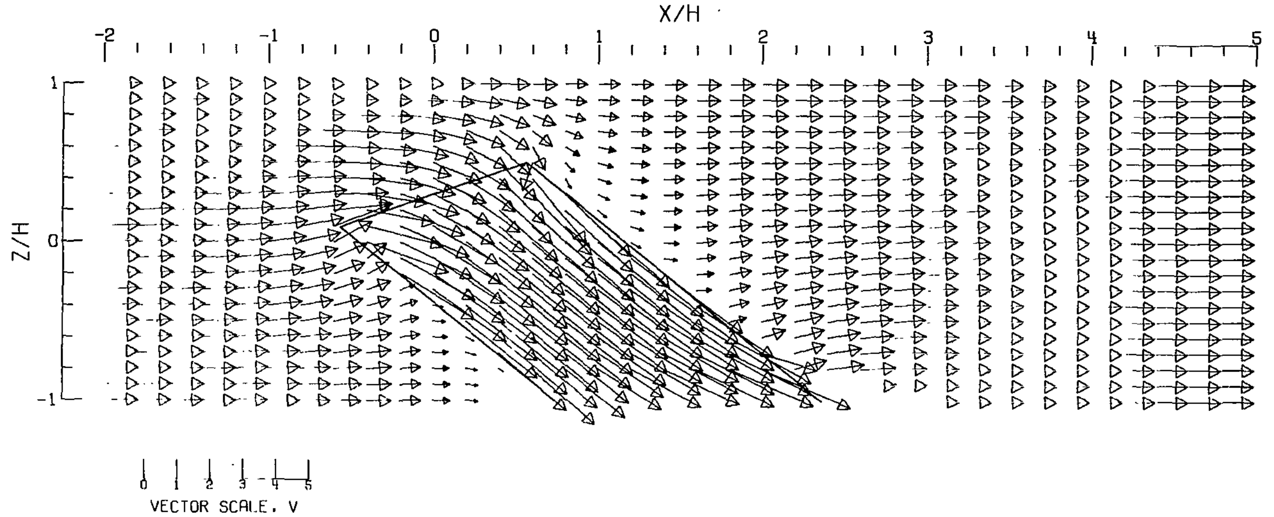

(C).- CLOSED TUNNEL.

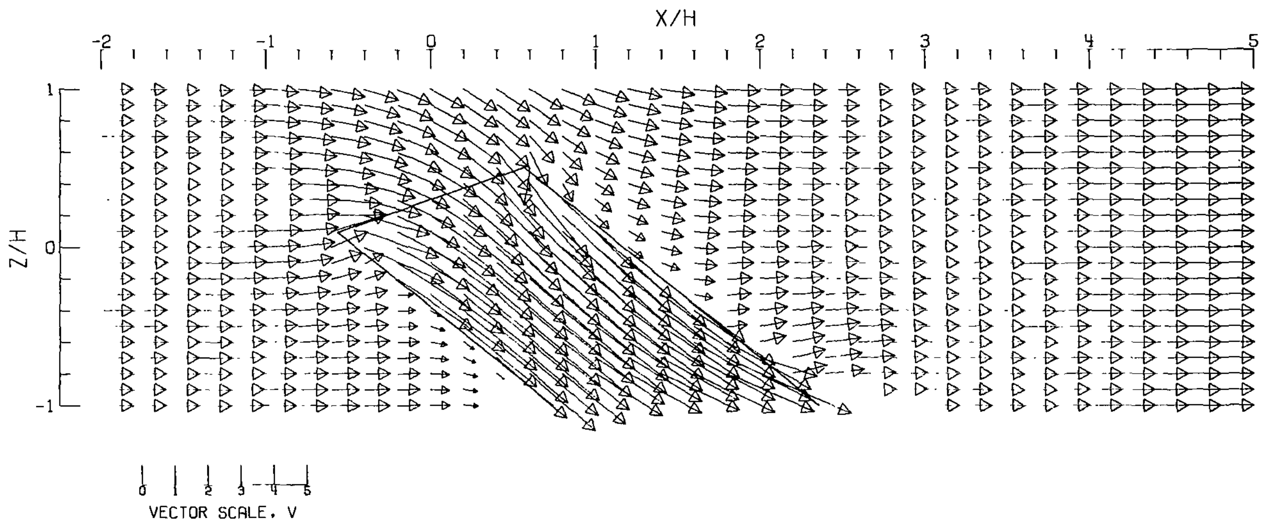

(D).- CLOSED-ON-BOTTOM-ONLY TUNNEL.

Figure 41.- Concluded.

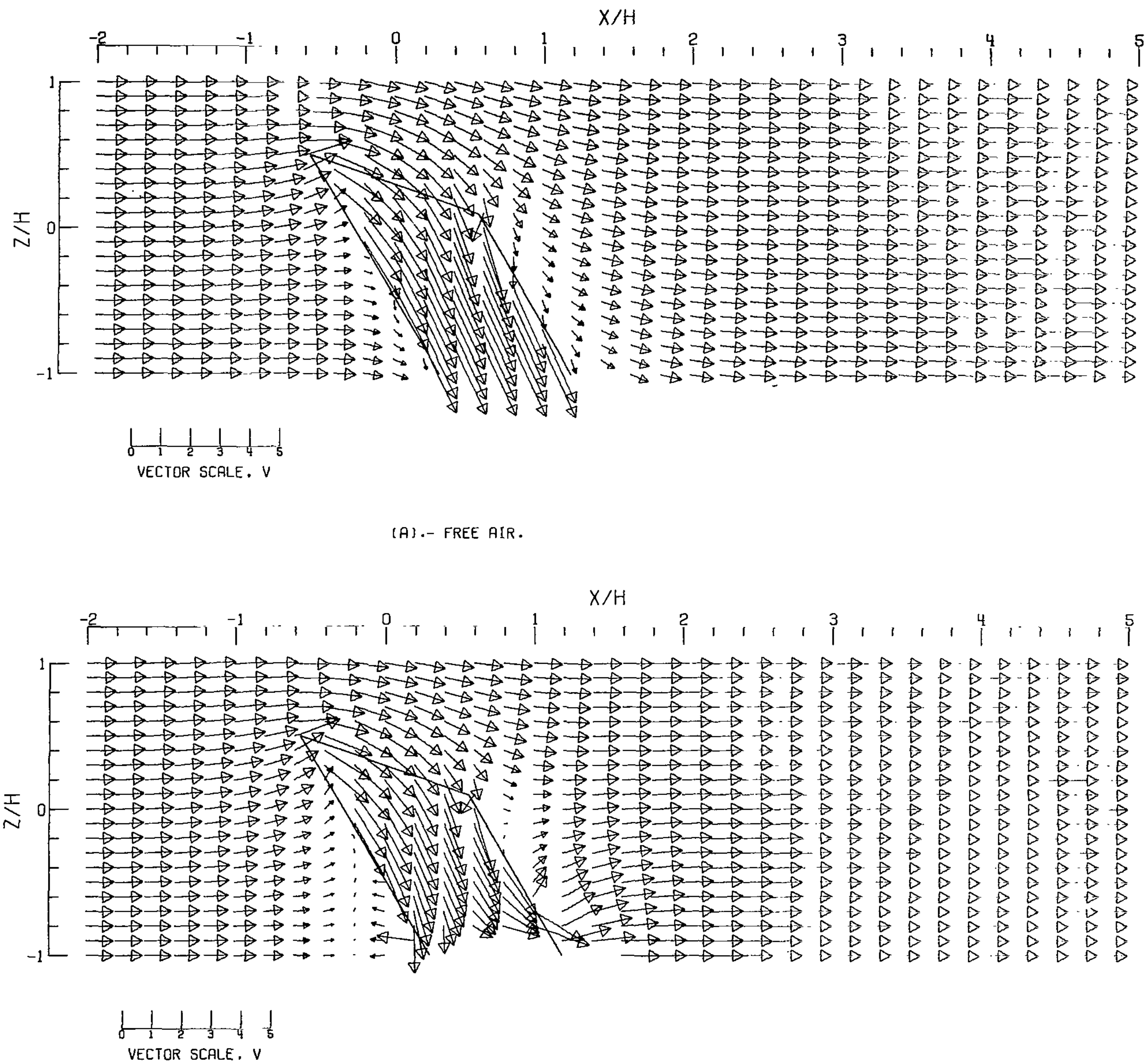

(A).- FREE AIR.

(B).- GROUND EFFECT.

Figure 42.- Flow vectors in the X-Z plane, calculated using doublet strings. The rotor and the edges of the wake are shown. ζ = 0.769; η = 1.000; γ = 1.000; σ = 0.600; α = 20.000°; χ = 30.000°; uniform loading.

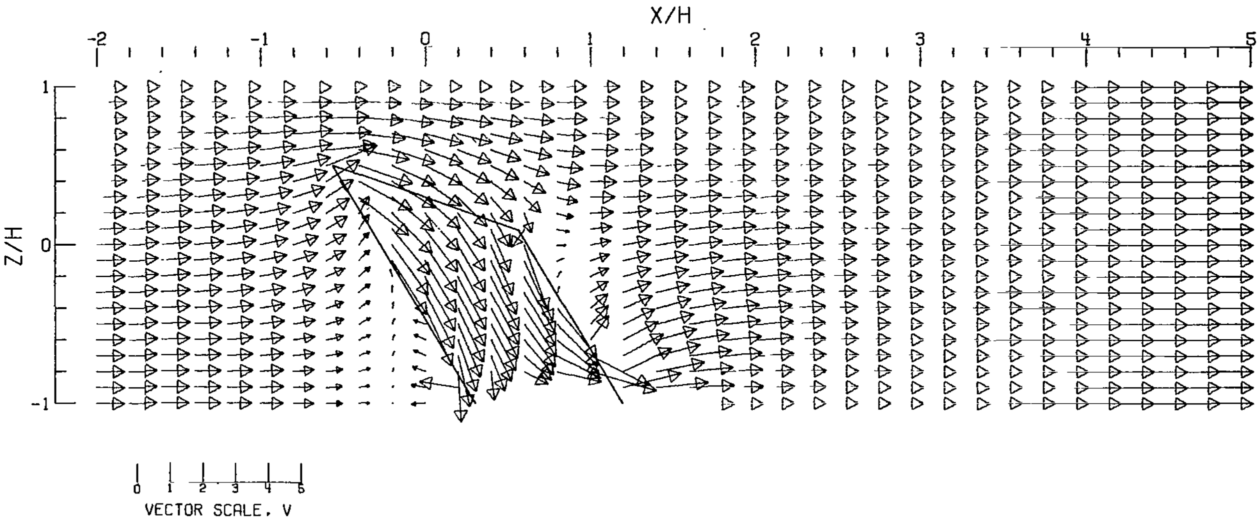

(C).- CLOSED TUNNEL.

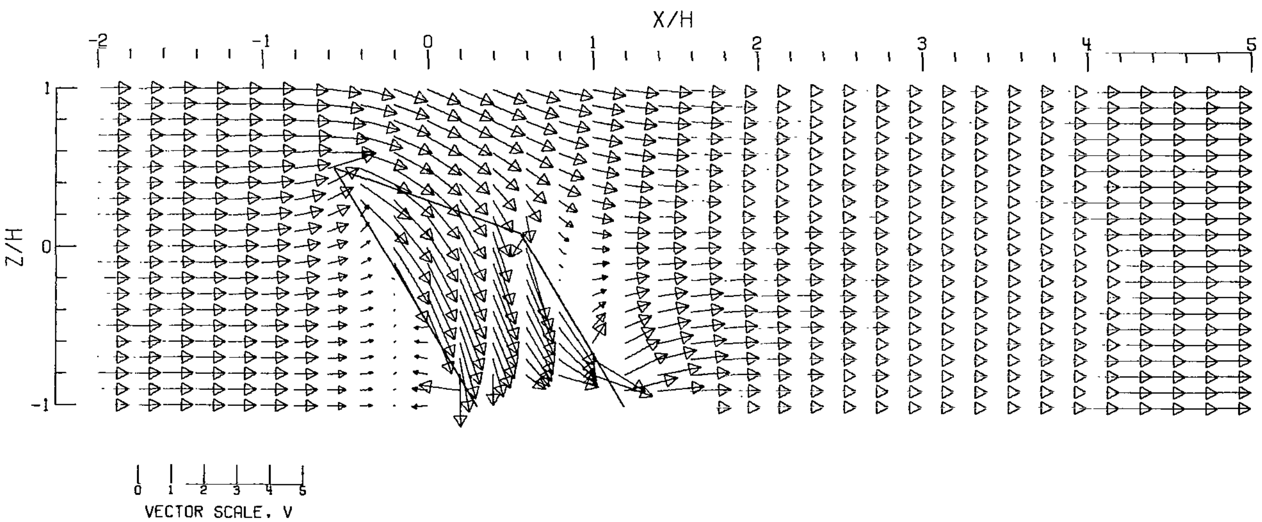

(D).- CLOSED-ON-BOTTOM-ONLY TUNNEL.

Figure 42.- Concluded.

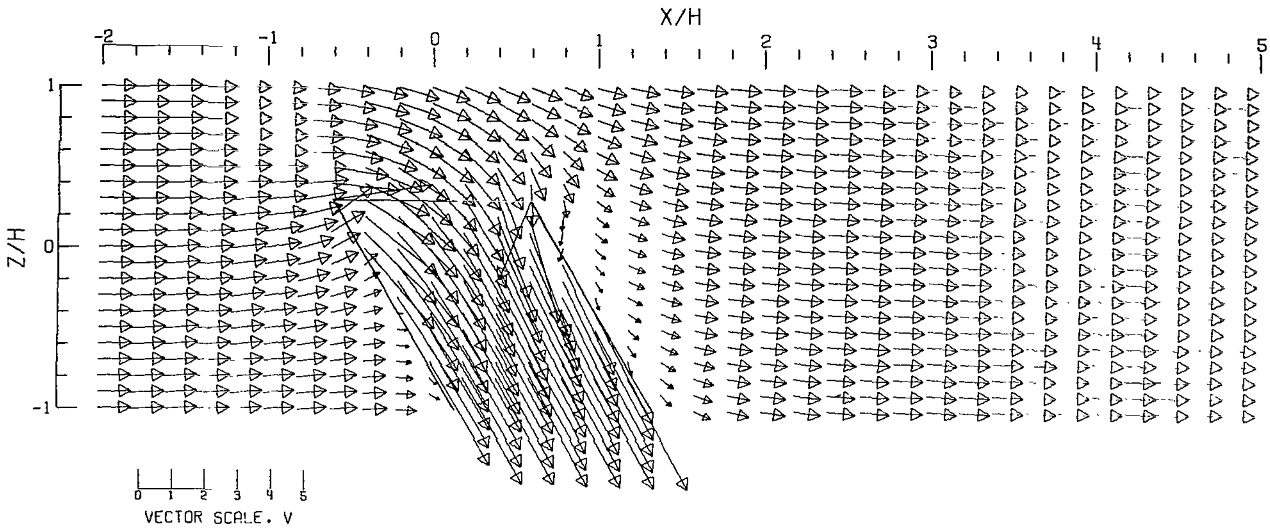

(A).- FREE AIR.

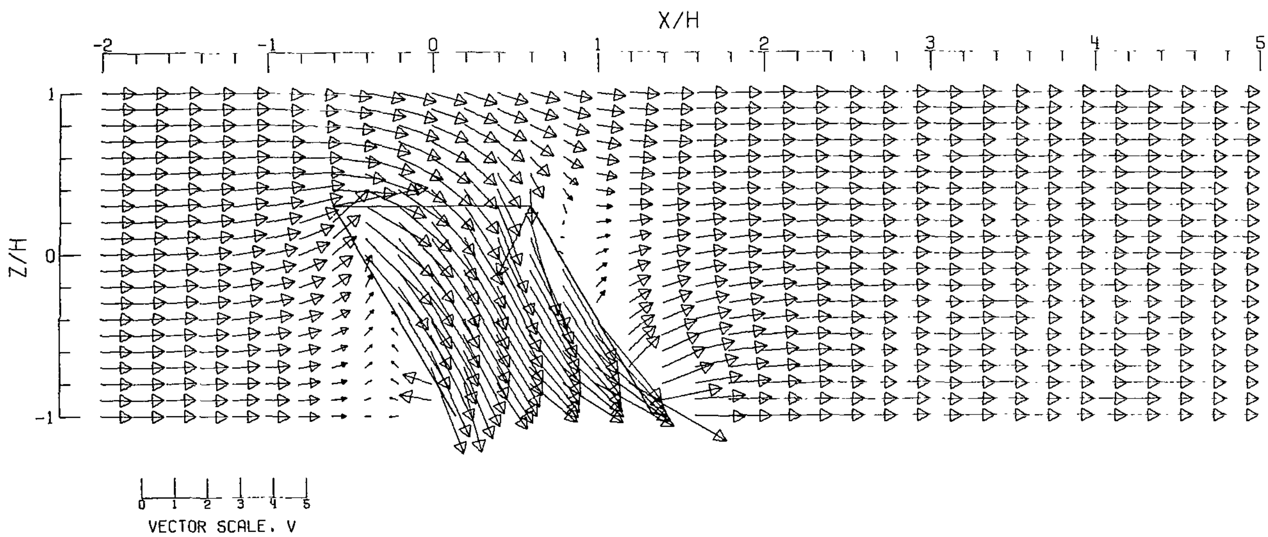

(B).- GROUND EFFECT.

Figure 43.- Flow vectors in the X-Z plane, calculated using doublet strings. The rotor and the edges of the wake are shown. ζ = 0.769; η = 1.000; γ = 1.000; σ = 0.600; α = 0.000°; χ = 30.000°; uniform loading.

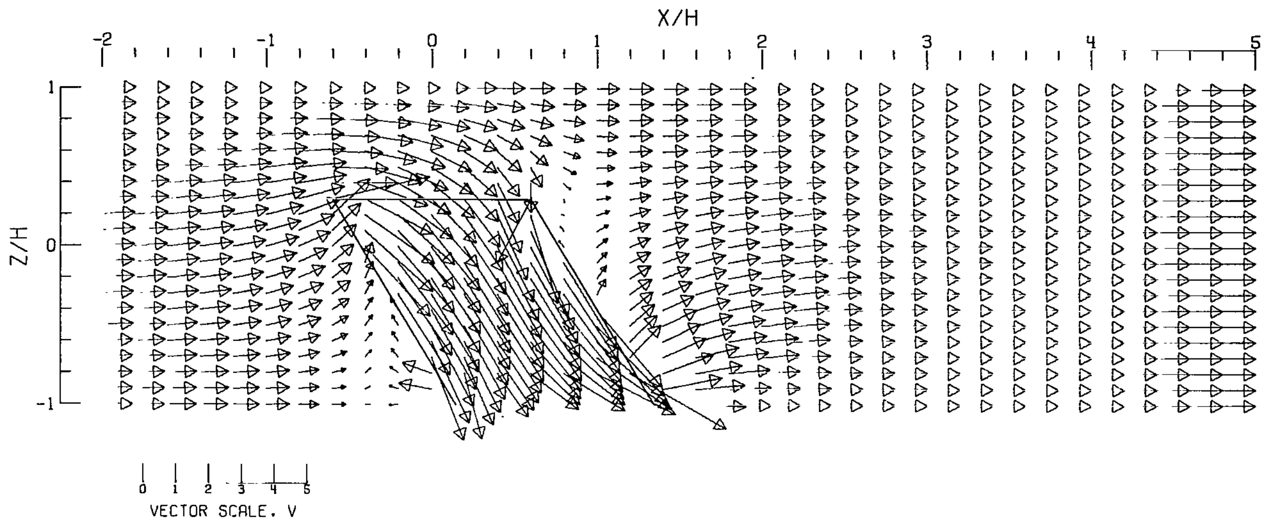

(C).- CLOSED TUNNEL.

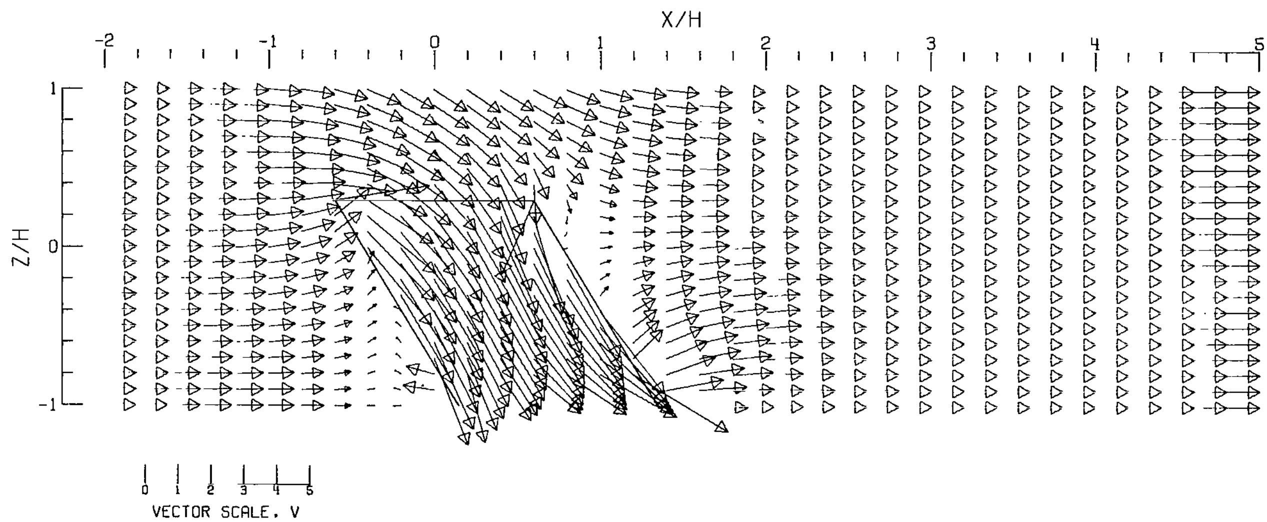

(D).- CLOSED-ON-BOTTOM-ONLY TUNNEL.

Figure 43.- Concluded.

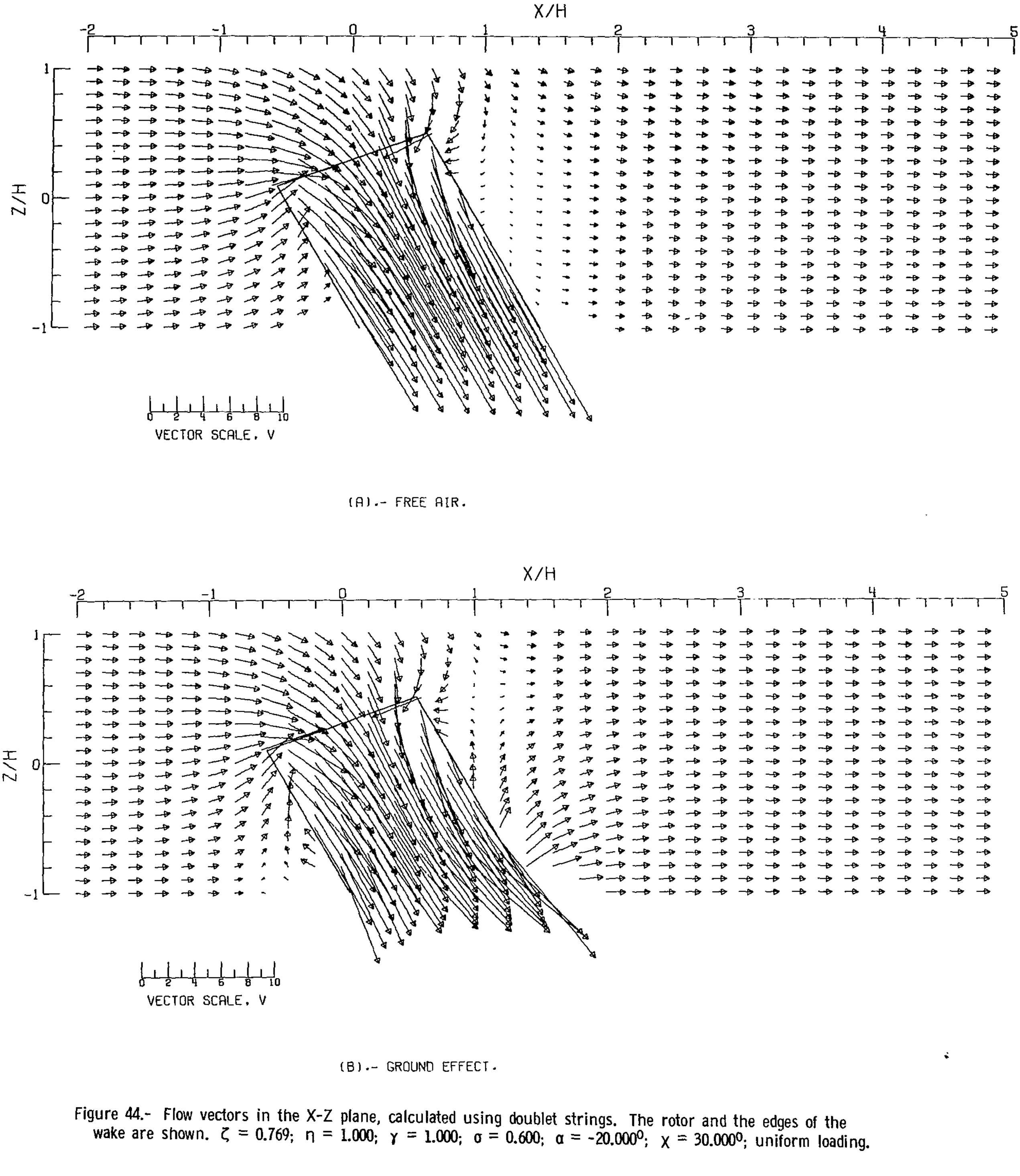

(A).- FREE AIR.

(B).- GROUND EFFECT.

Figure 44.- Flow vectors in the X-Z plane, calculated using doublet strings. The rotor and the edges of the wake are shown. ζ = 0.769; η = 1.000; γ = 1.000; σ = 0.600; α = -20.000°; χ = 30.000°; uniform loading.

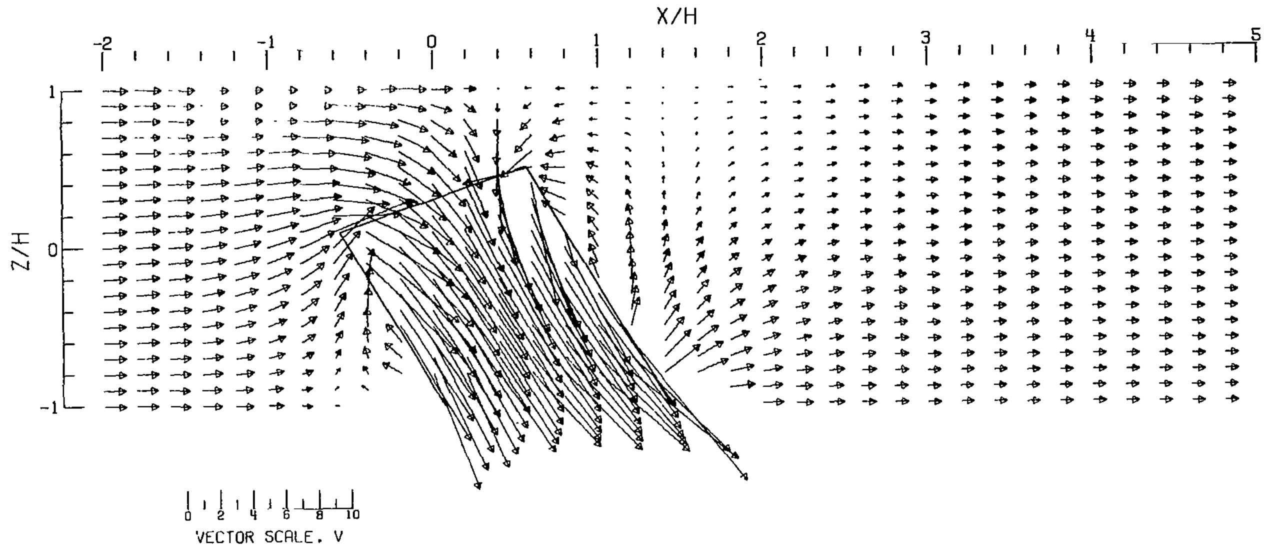

(C).- CLOSED TUNNEL.

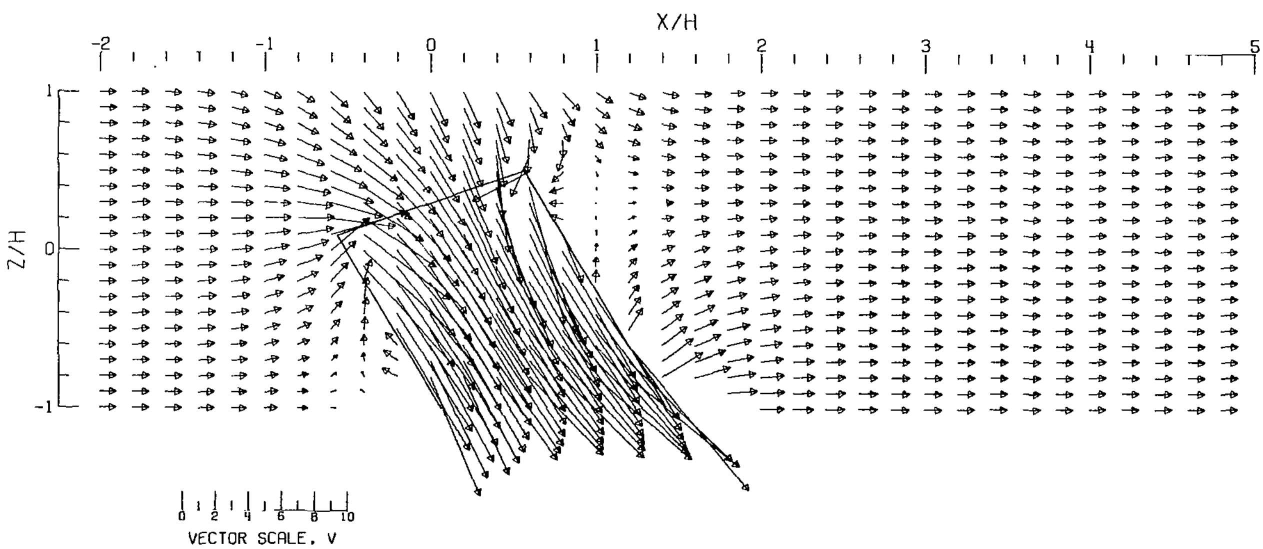

(D).- CLOSED-ON-BOTTOM-ONLY TUNNEL.

Figure 44.- Concluded.

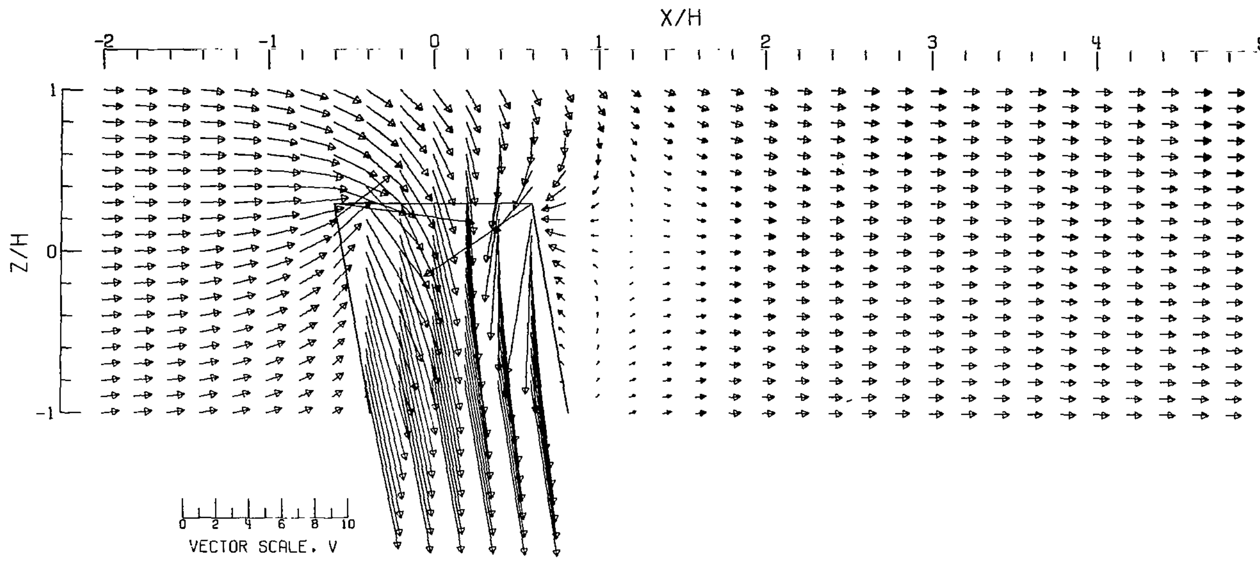

(A).- FREE AIR.

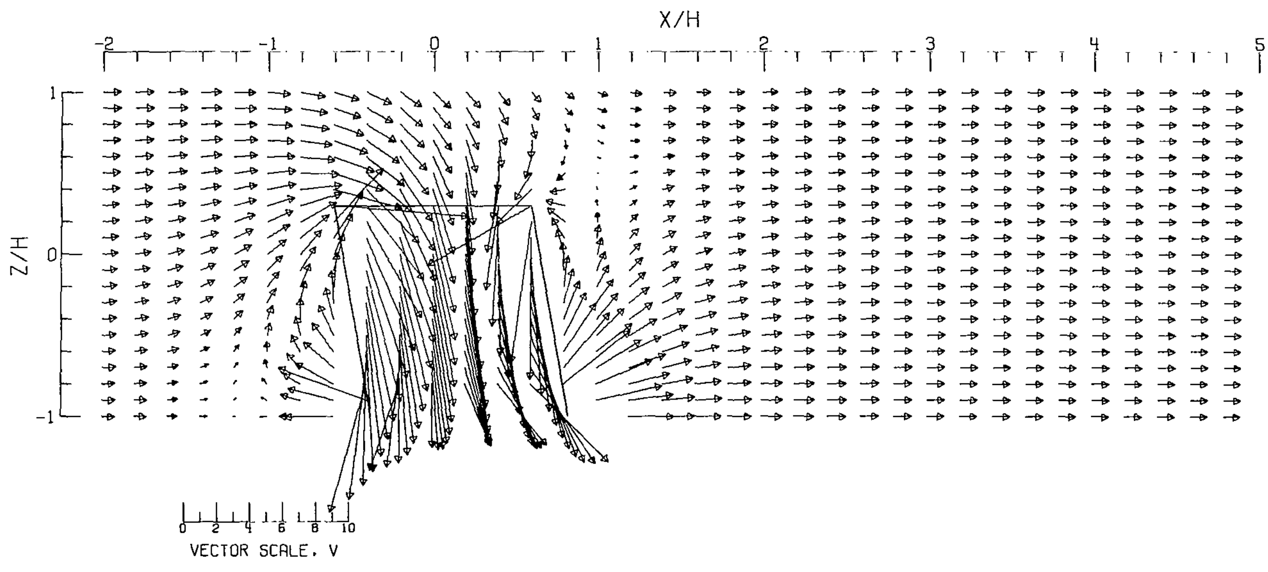

(B).- GROUND EFFECT.

Figure 45.- Flow vectors in the X-Z plane, calculated using doublet strings. The rotor and the edges of the wake are shown. ζ = 0.769; η = 1.000; γ = 1.000; σ = 0.600; α = 0.000°; χ = 10.000°; uniform loading.

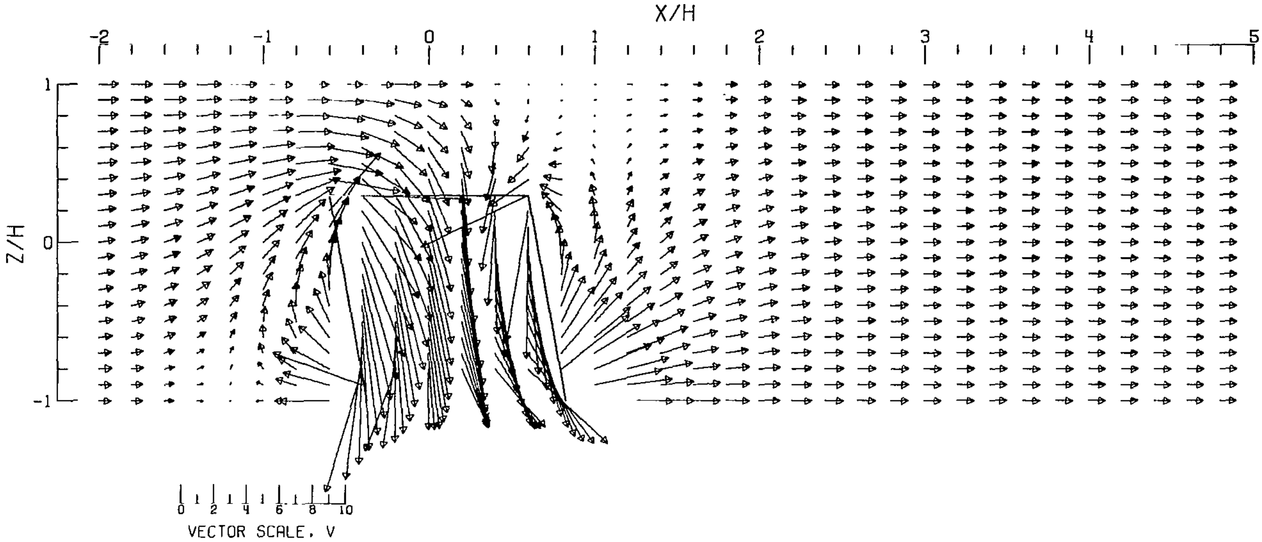

(C).- CLOSED TUNNEL.

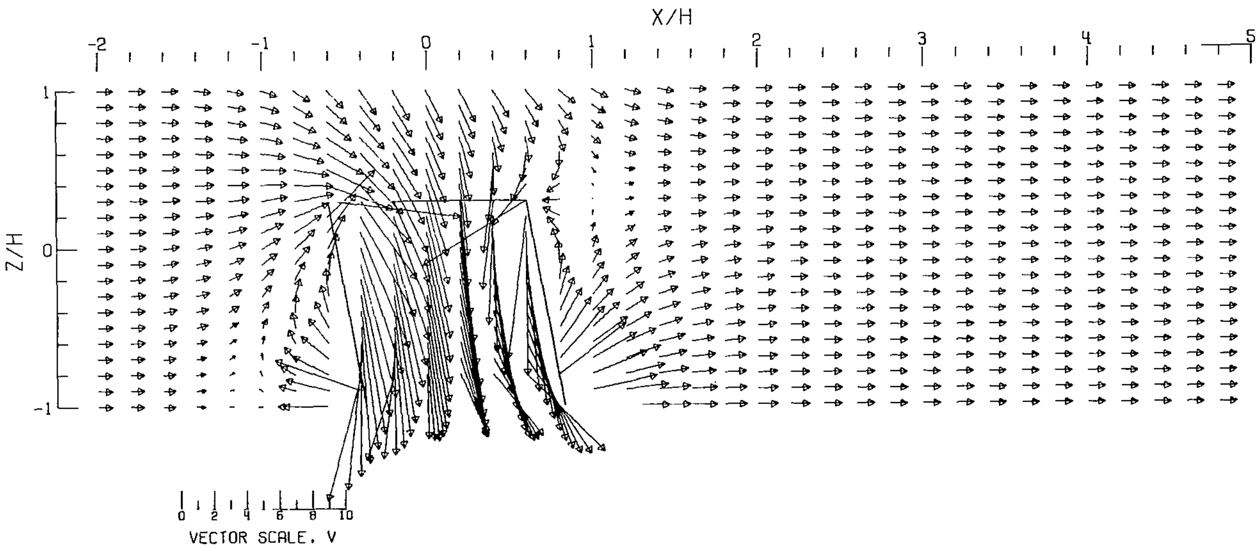

(D).- CLOSED-ON-BOTTOM-ONLY TUNNEL.

Figure 45.- Concluded.

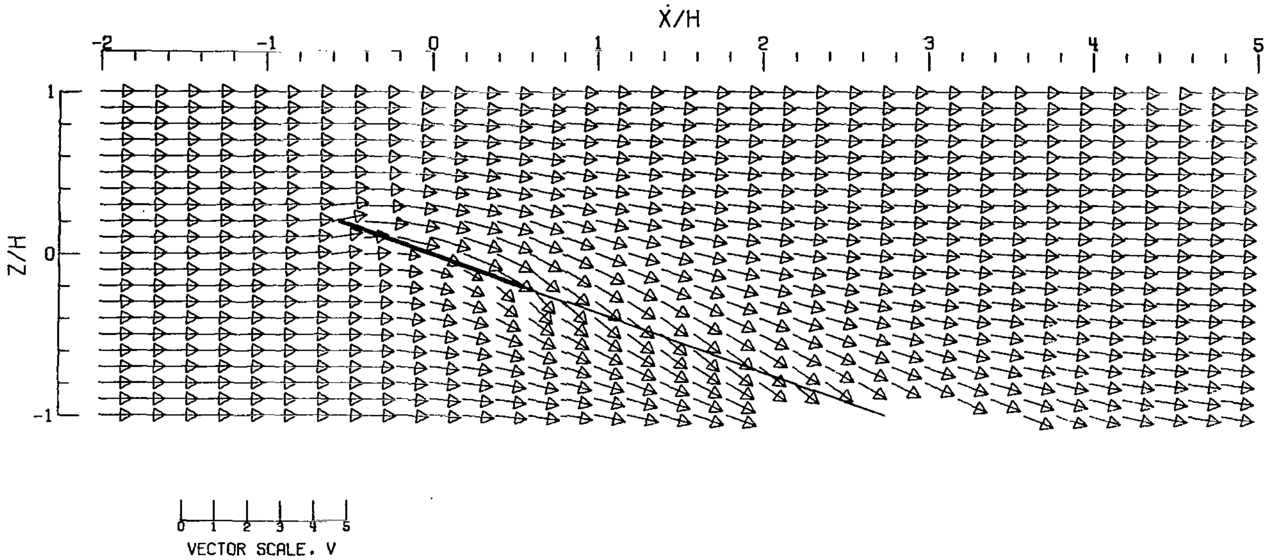

(A).- FREE AIR.

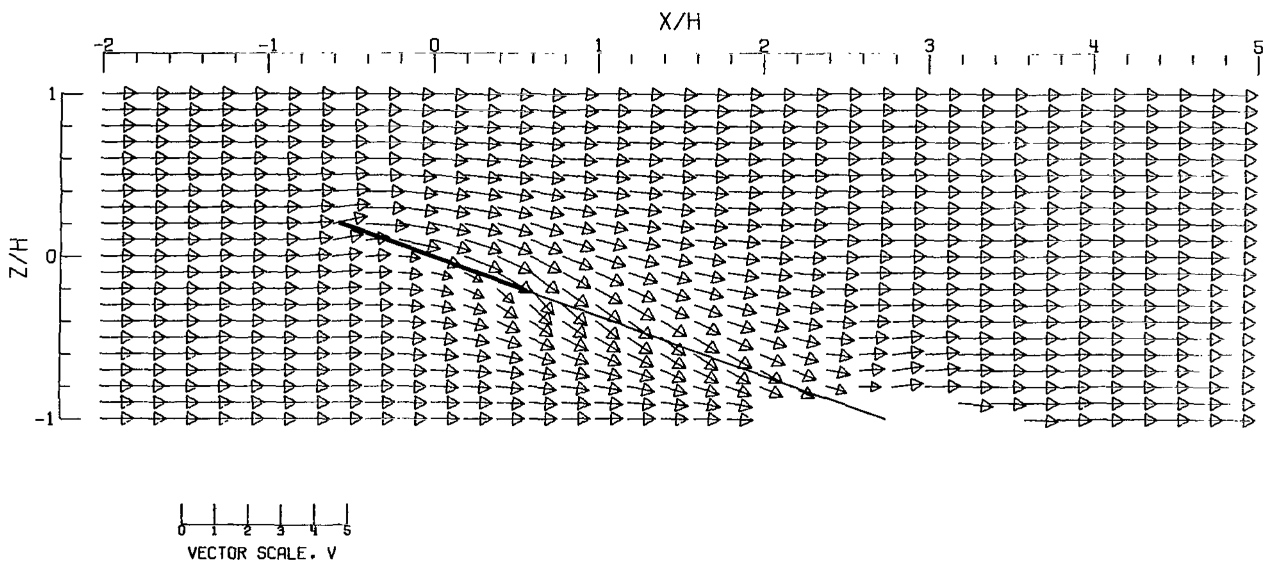

(B).- GROUND EFFECT.

Figure 46.- Flow vectors in the X-Z plane, calculated using doublet strings. The rotor and the edges of the wake are shown. ζ = 1.000; η = 1.000; γ = 1.000; σ = 0.600; α = 20.000°; χ = 70.000°; uniform loading.

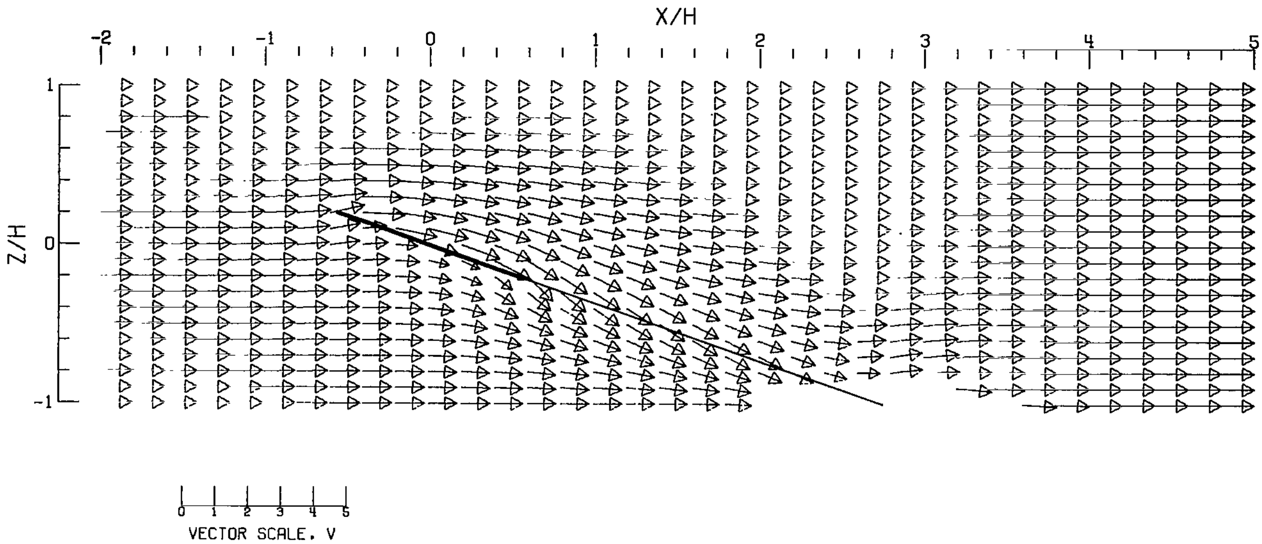

(C).- CLOSED TUNNEL.

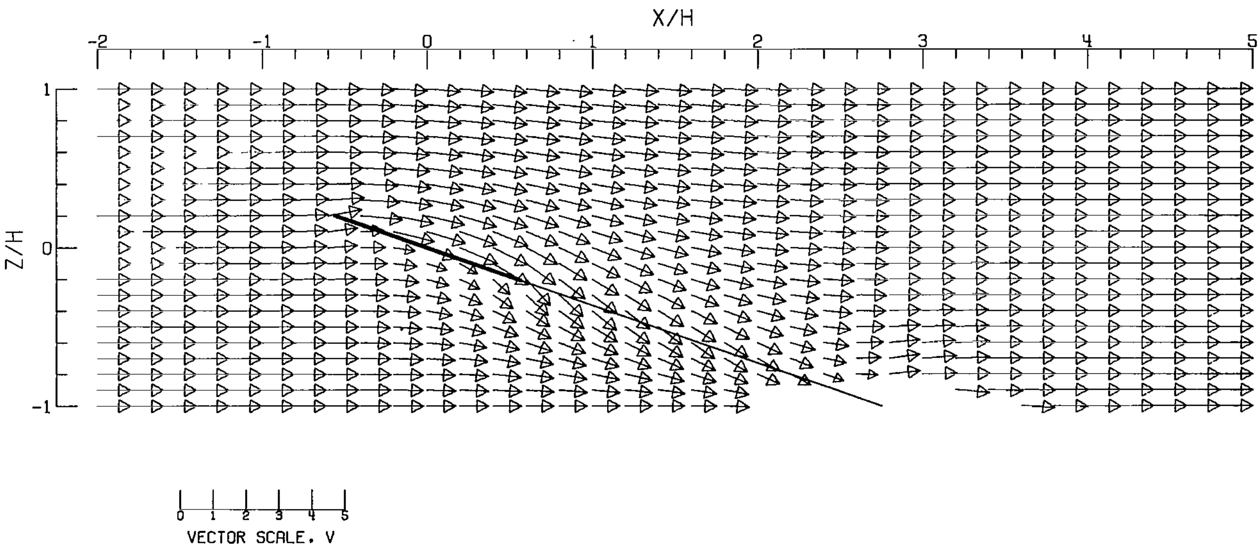

(D).- CLOSED-ON-BOTTOM-ONLY TUNNEL.

Figure 46.- Concluded.

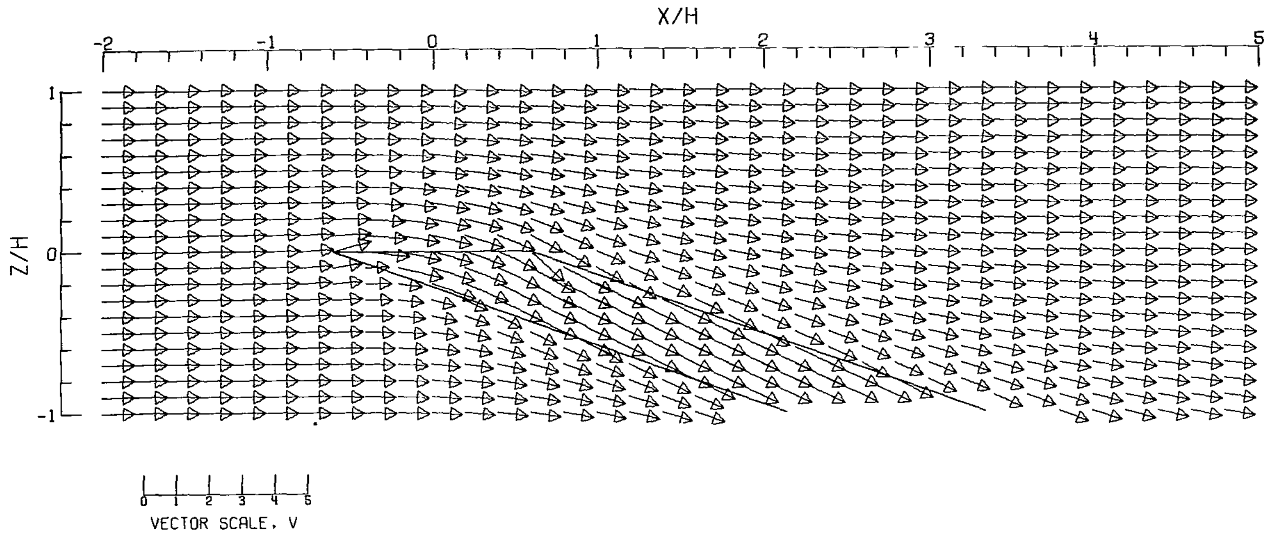

(A).- FREE AIR.

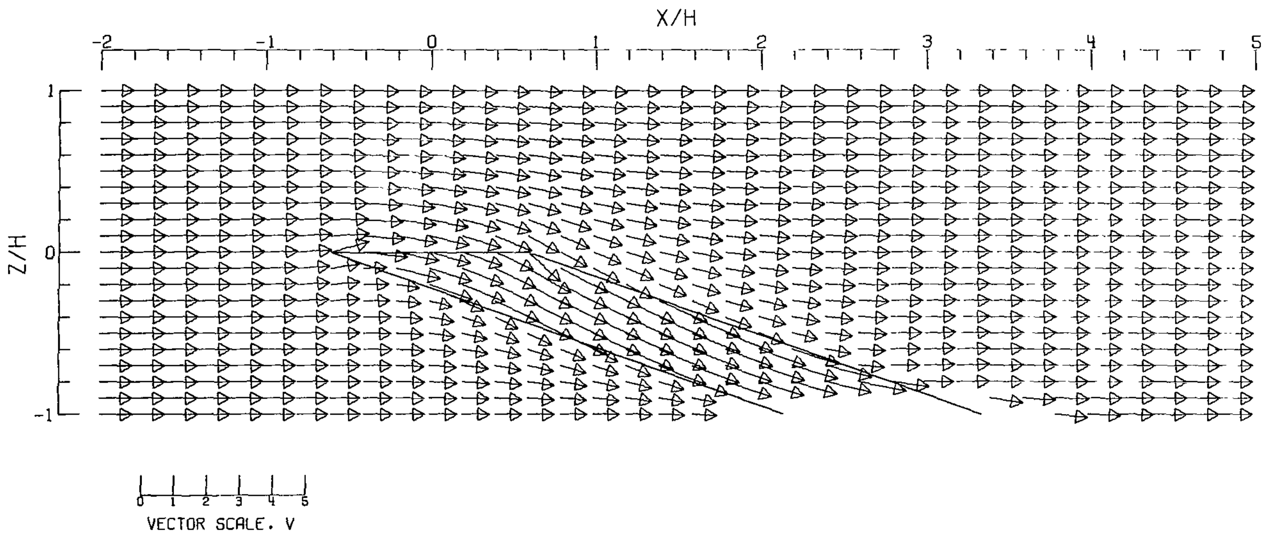

(B).- GROUND EFFECT.

Figure 47.- Flow vectors in the X-Z plane, calculated using doublet strings. The rotor and the edges of the wake are shown. ζ = 1.000; η = 1.000; γ = 1.000; σ = 0.600; α = 0.000°; χ = 70.000°; uniform loading.

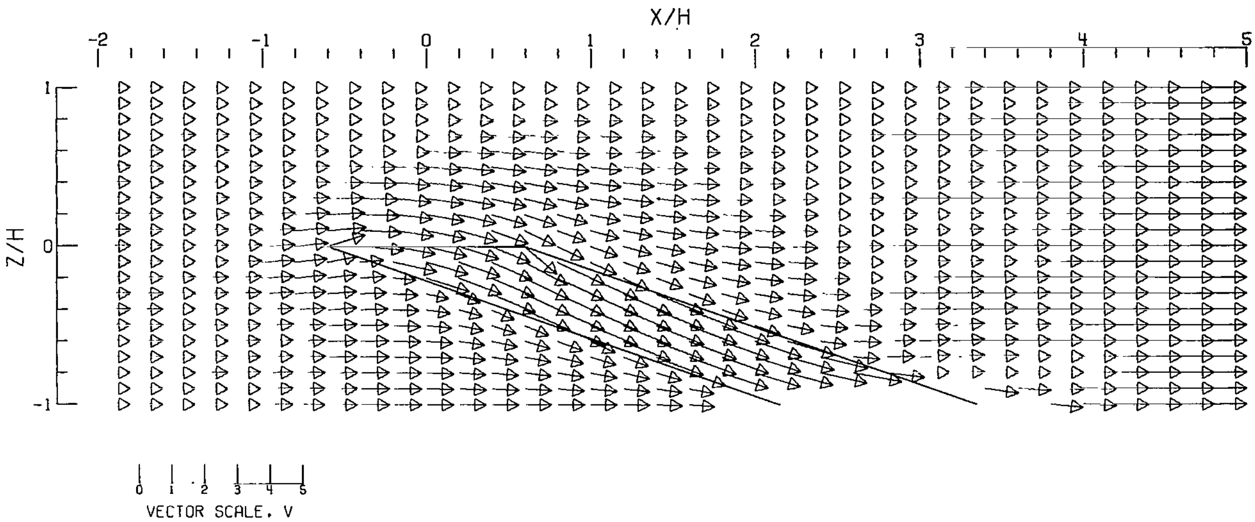

(C).- CLOSED TUNNEL.

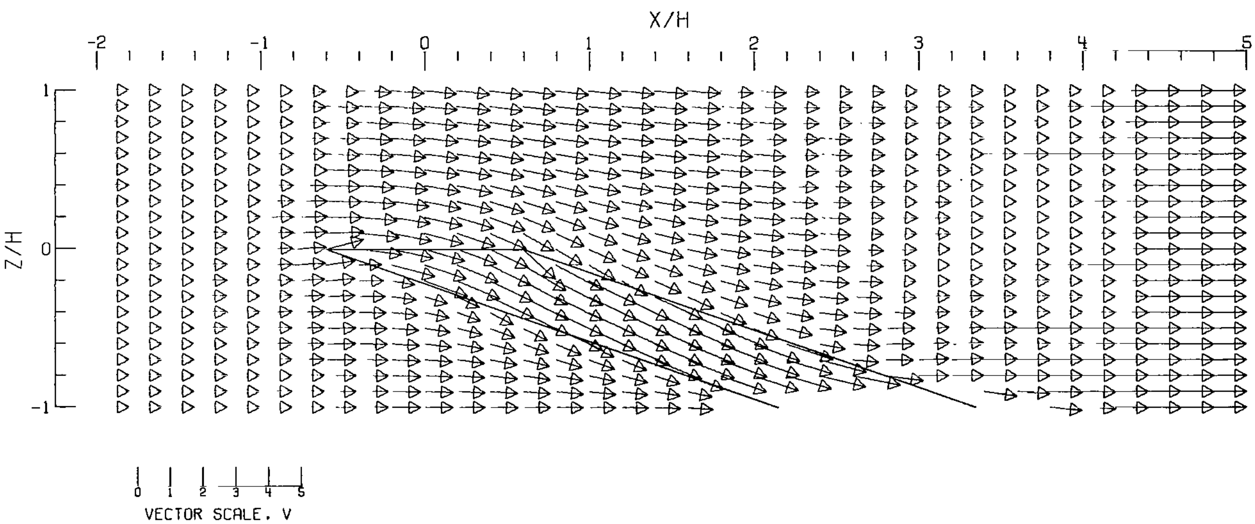

(D).- CLOSED-ON-BOTTOM-ONLY TUNNEL.

Figure 47.- Concluded.

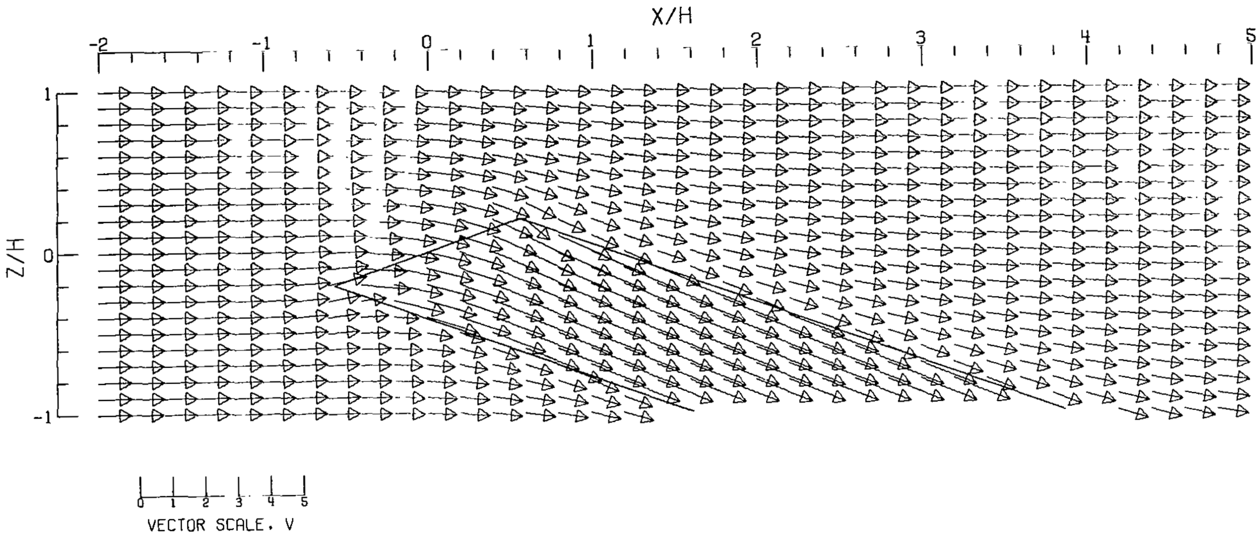

(A).- FREE AIR.

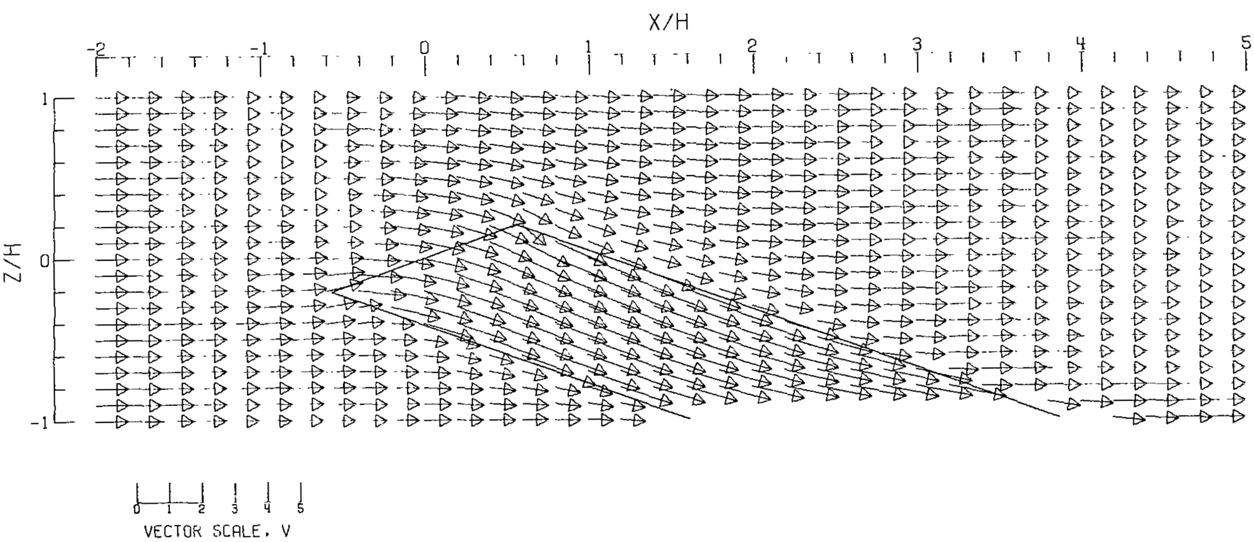

(B).- GROUND EFFECT.

Figure 48.- Flow vectors in the X-Z plane, calculated using doublet strings. The rotor and the edges of the wake are shown. ζ = 1.000; η = 1.000; γ = 1.000; σ = 0.600; α = -20.000°; χ = 70.000°; uniform loading.

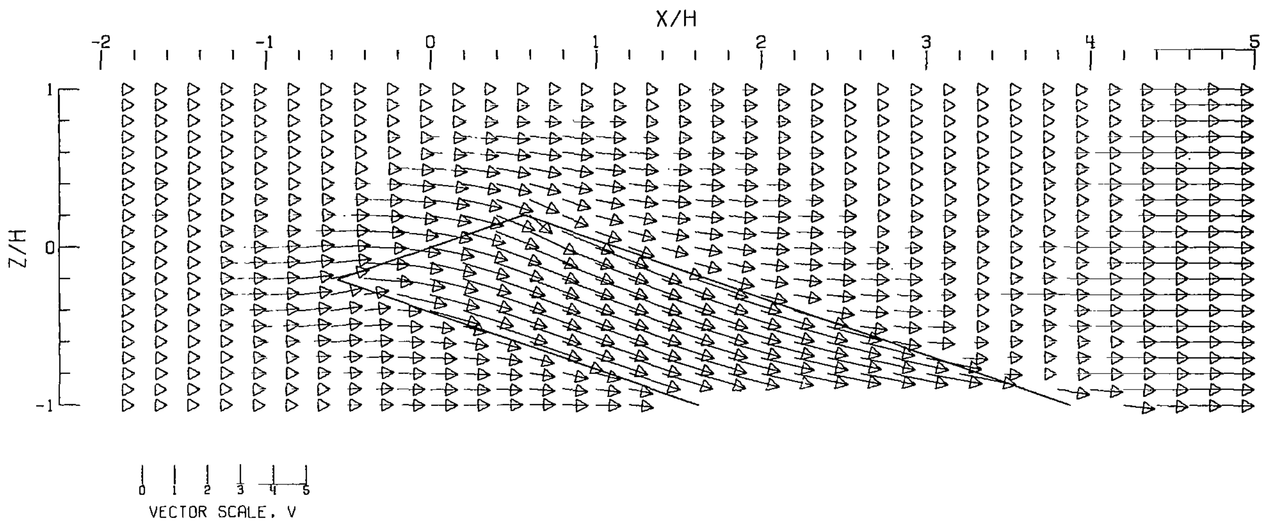

(C).- CLOSED TUNNEL.

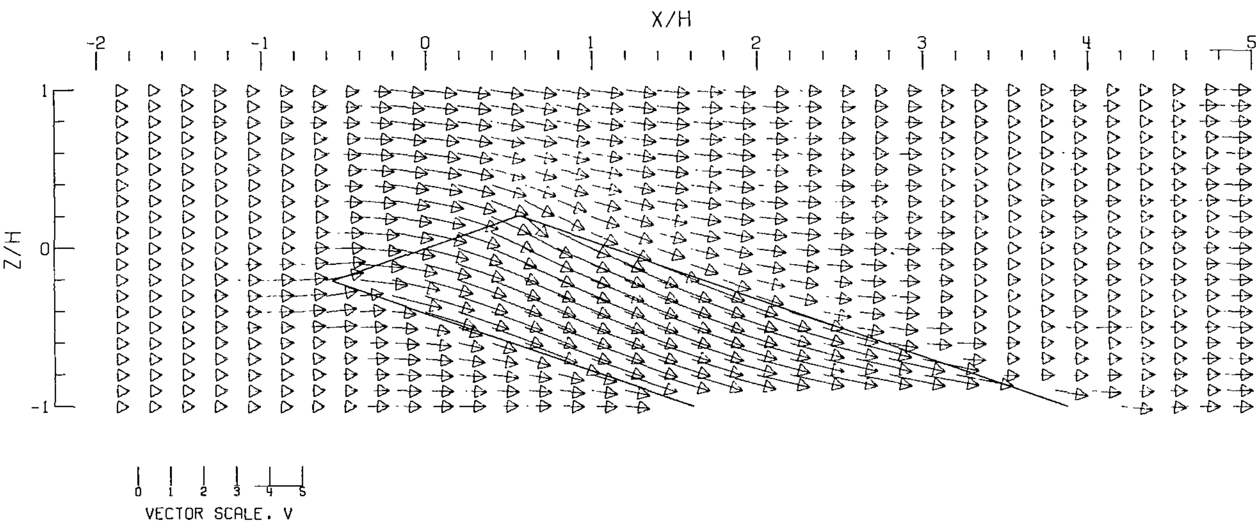

(D).- CLOSED-ON-BOTTOM-ONLY TUNNEL.

Figure 48.- Concluded.

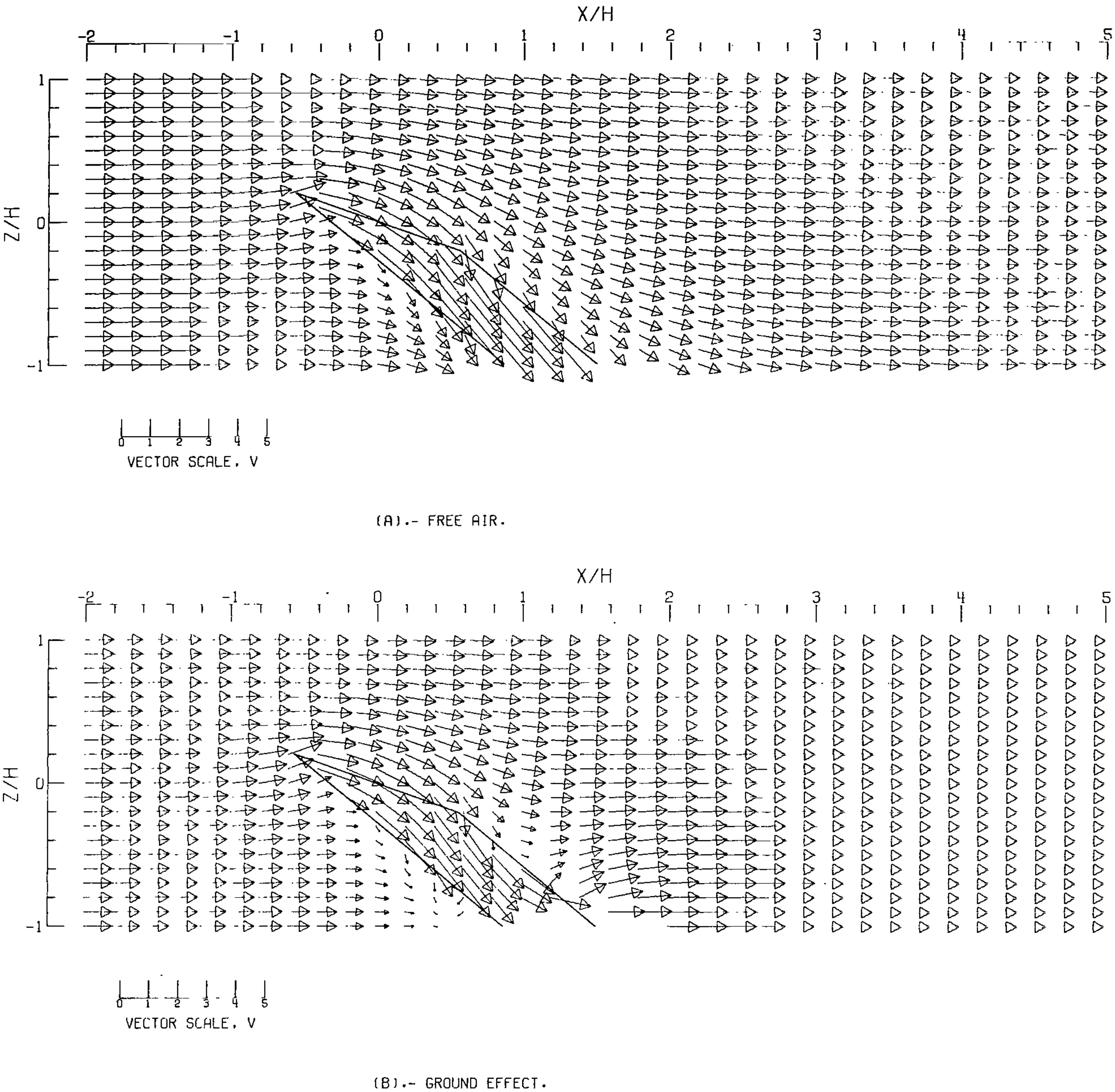

Figure 49.- Flow vectors in the X-Z plane, calculated using doublet strings. The rotor and the edges of the wake are shown. $\zeta = 1.000$; $\eta = 1.000$; $\gamma = 1.000$; $\sigma = 0.600$; $\alpha = 20.000^{\circ}$; $\chi = 50.000^{\circ}$; uniform loading.

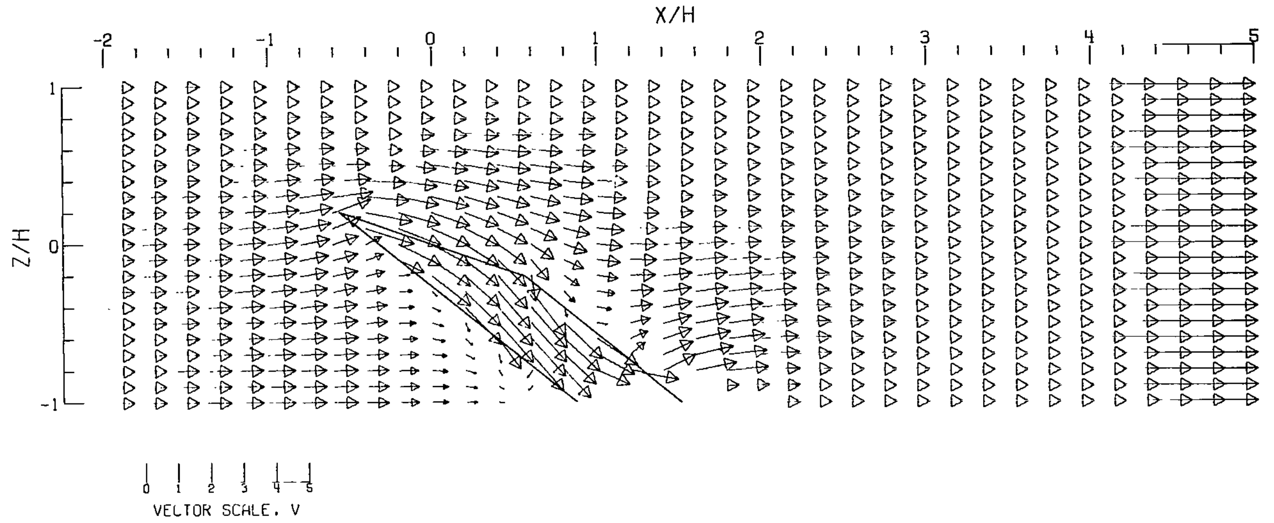

(C).- CLOSED TUNNEL.

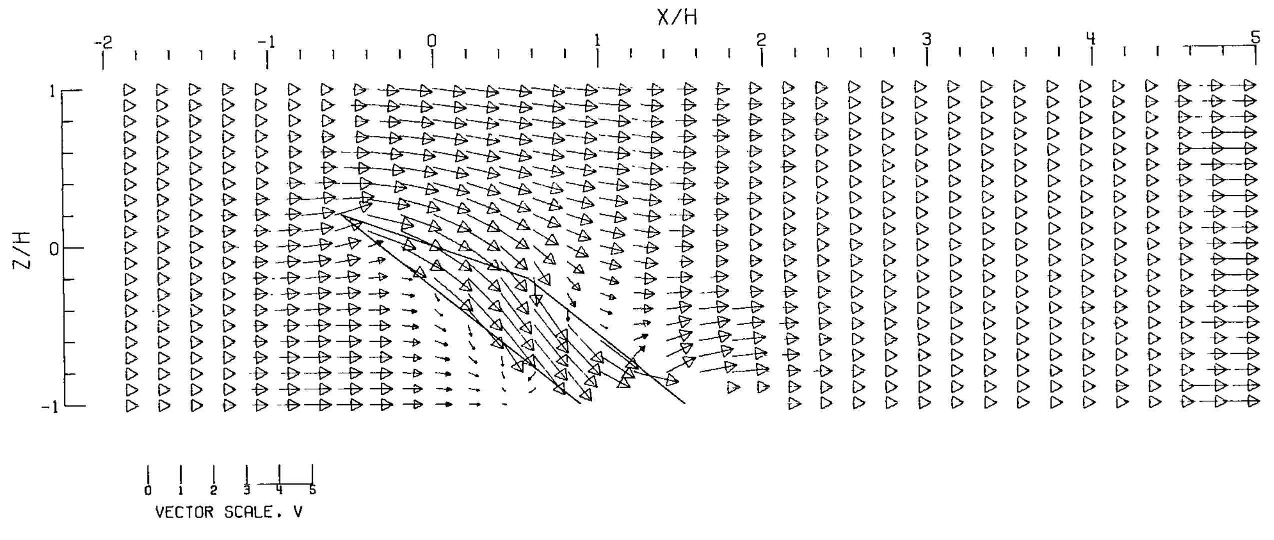

(D).- CLOSED-ON-BOTTOM-ONLY TUNNEL.

Figure 49.- Concluded.

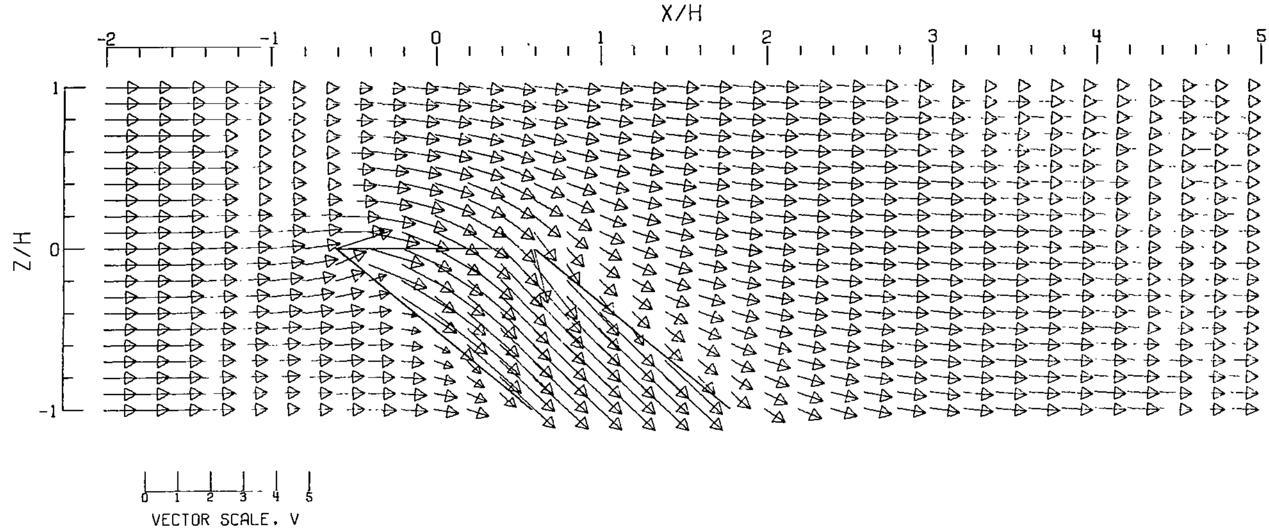

(A).- FREE AIR.

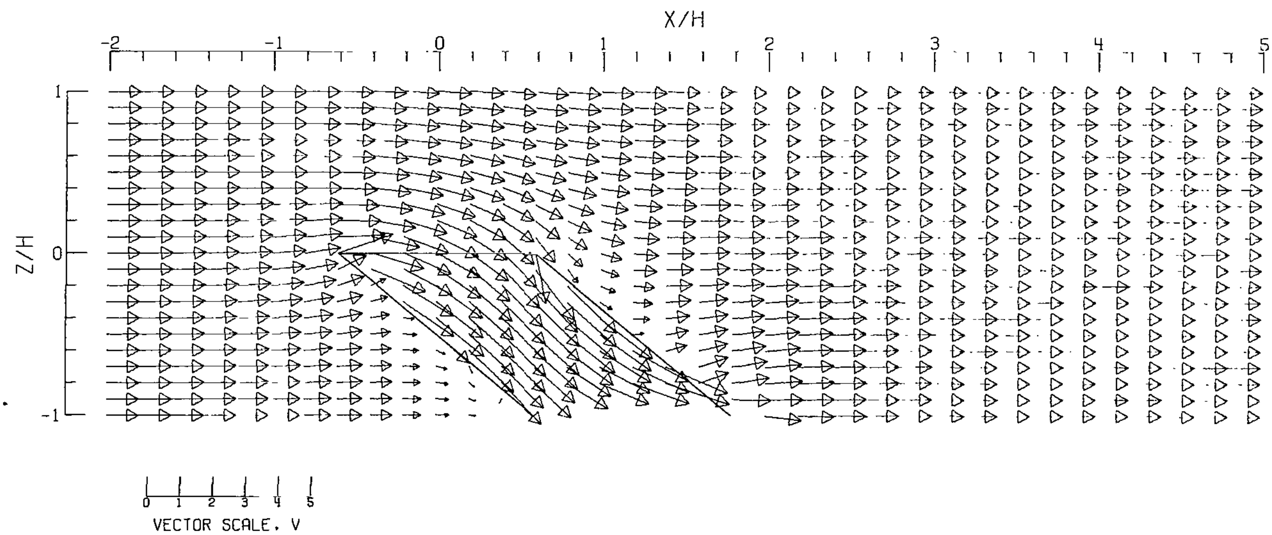

(B).- GROUND EFFECT.

Figure 50.- Flow vectors in the X-Z plane, calculated using doublet strings. The rotor and the edges of the wake are shown. ζ = 1.000; η = 1.000; γ = 1.000; σ = 0.600; α = 0.000°; χ = 50.000°; uniform loading.

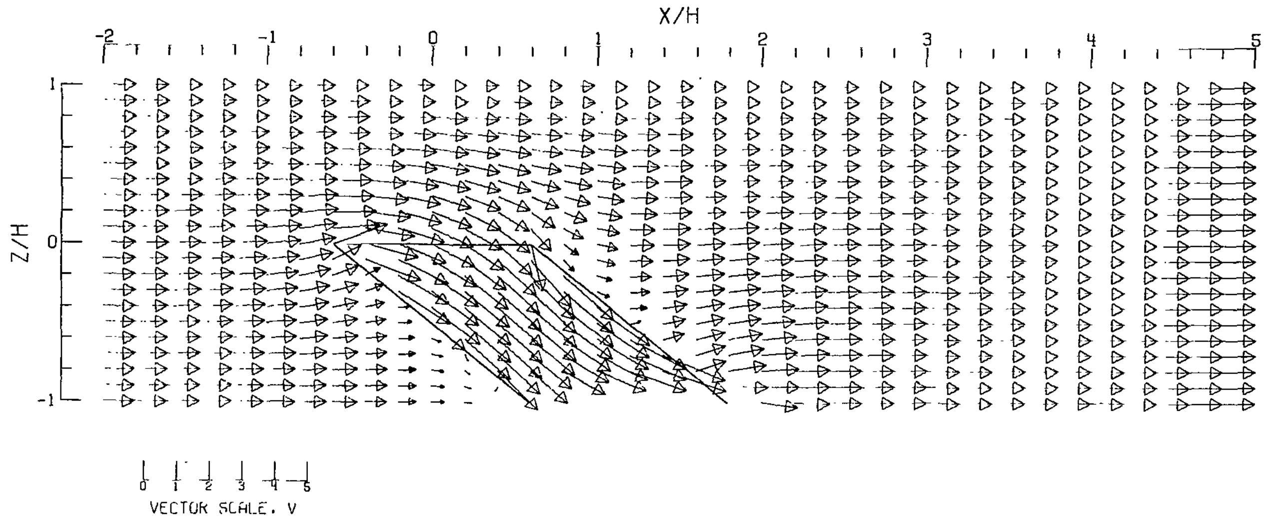

(C).- CLOSED TUNNEL.

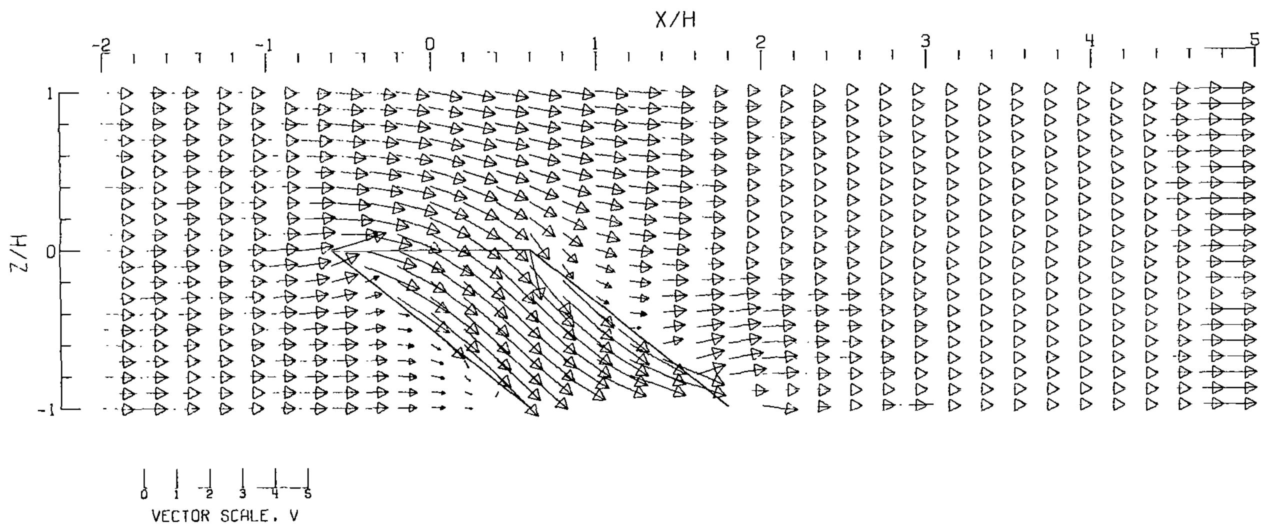

(D).- CLOSED-ON-BOTTOM-ONLY TUNNEL.

Figure 50.- Concluded.

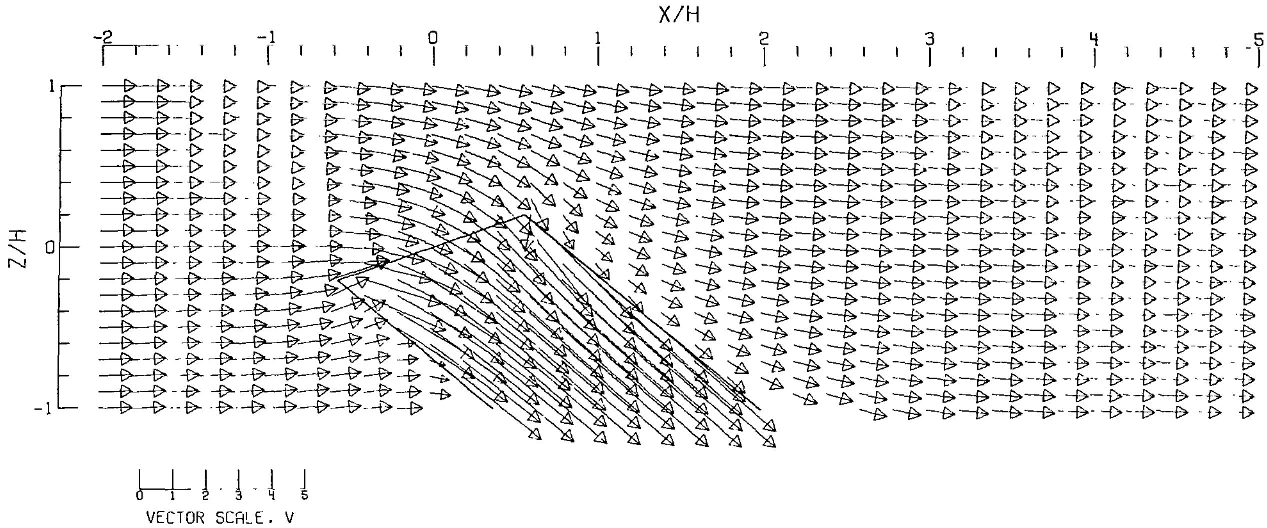

(A).- FREE AIR.

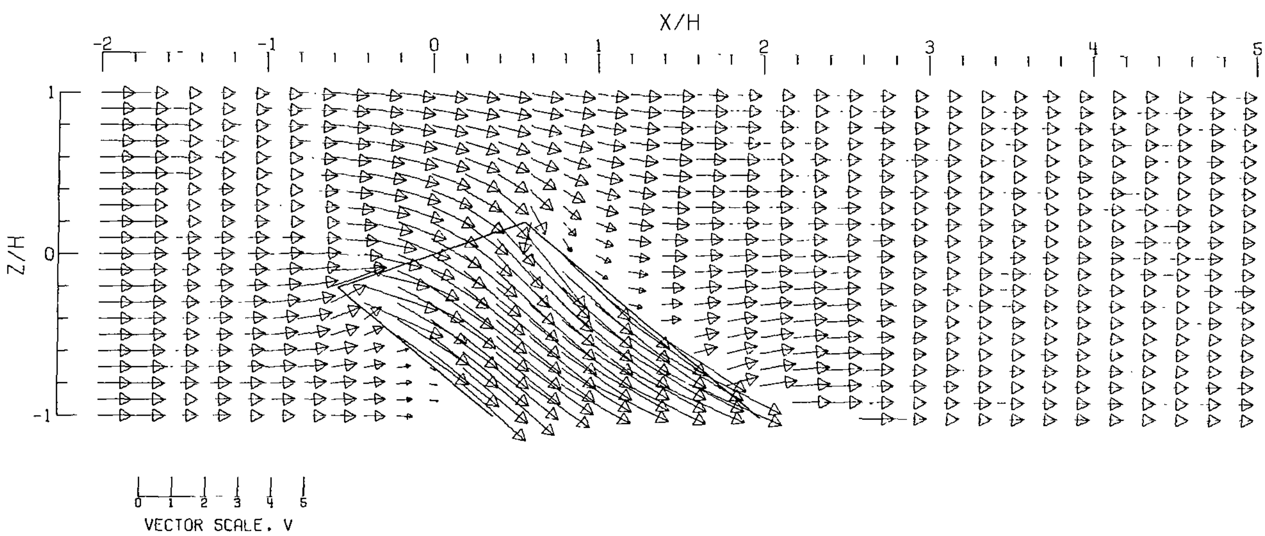

(B).- GROUND EFFECT.

Figure 51.- Flow vectors in the X-Z plane, calculated using doublet strings. The rotor and the edges of the wake are shown. $\zeta = 1.000$; $\eta = 1.000$; $\gamma = 1.000$; $\sigma = 0.600$; $\alpha = -20.000^0$; $\chi = 50.000^0$; uniform loading.

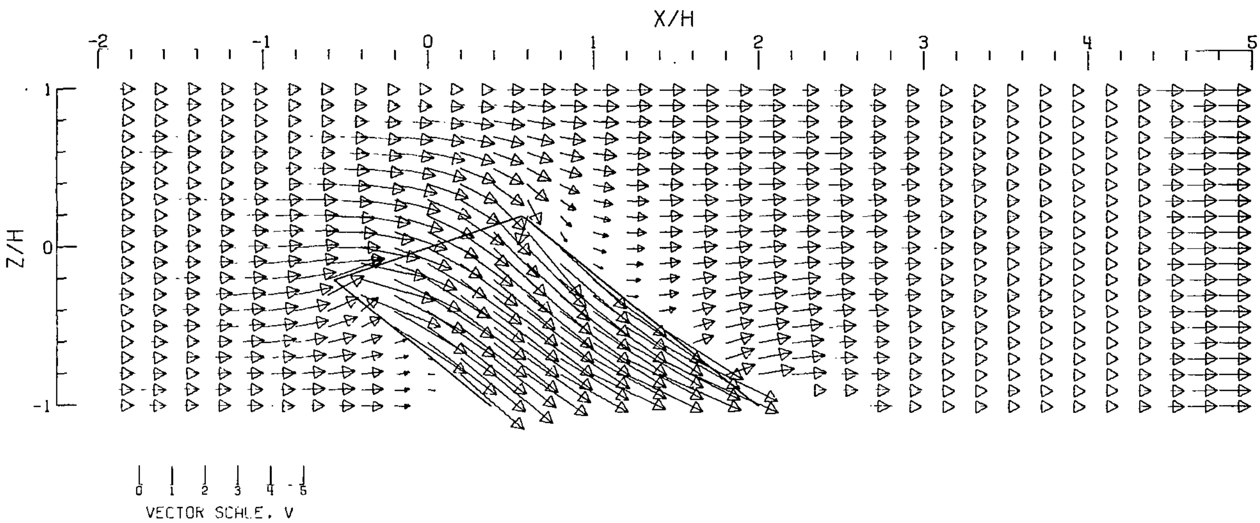

(C).- CLOSED TUNNEL.

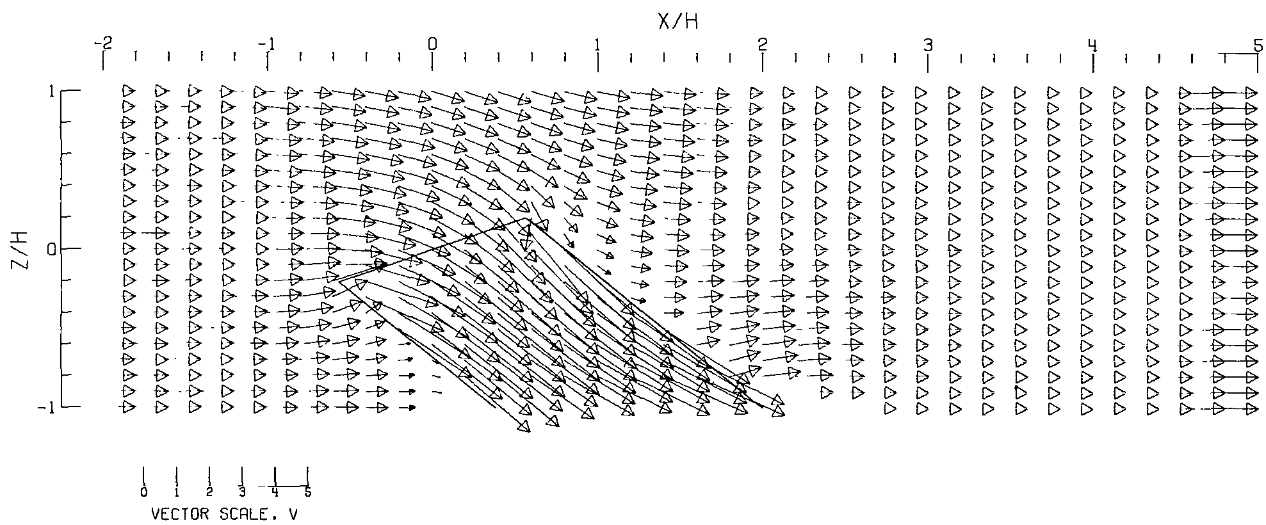

(D).- CLOSED-ON-BOTTOM-ONLY TUNNEL.

Figure 51.- Concluded.

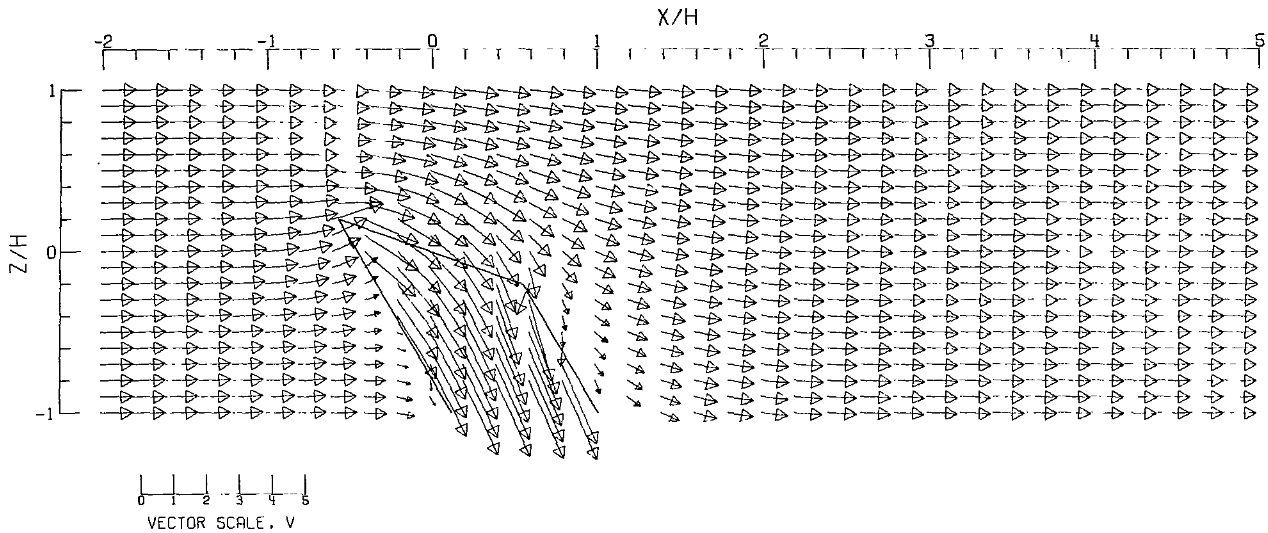

(A).- FREE AIR.

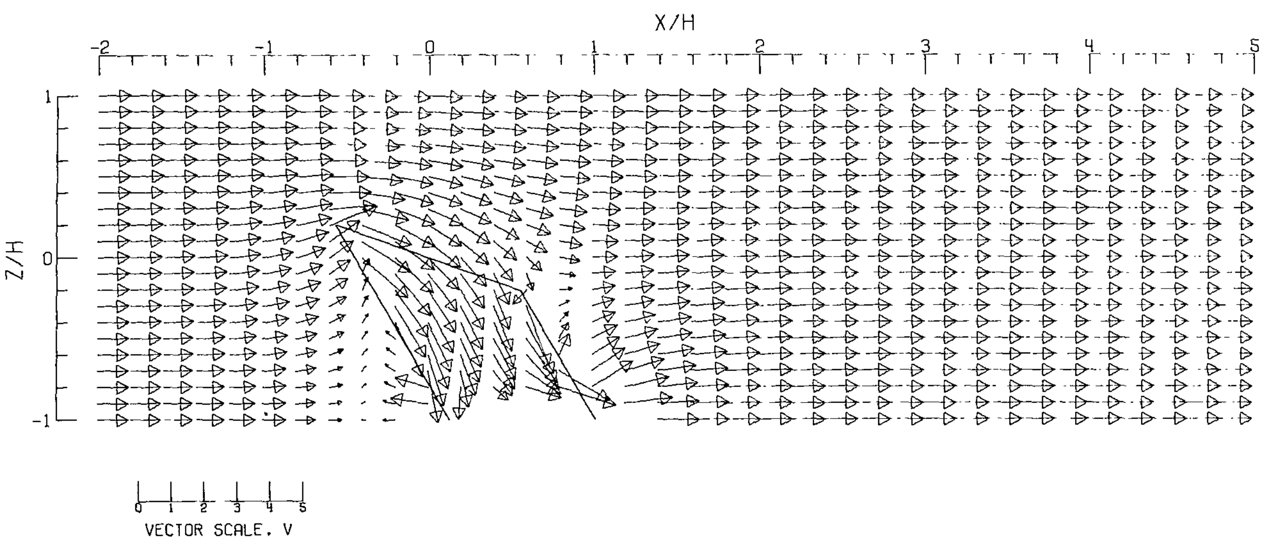

(B).- GROUND EFFECT.

Figure 52.- Flow vectors in the X-Z plane, calculated using doublet strings. The rotor and the edges of the wake are shown. ζ = 1.000; η = 1.000; γ = 1.000; σ = 0.600; α = 20.000°; χ = 30.000°; uniform loading.

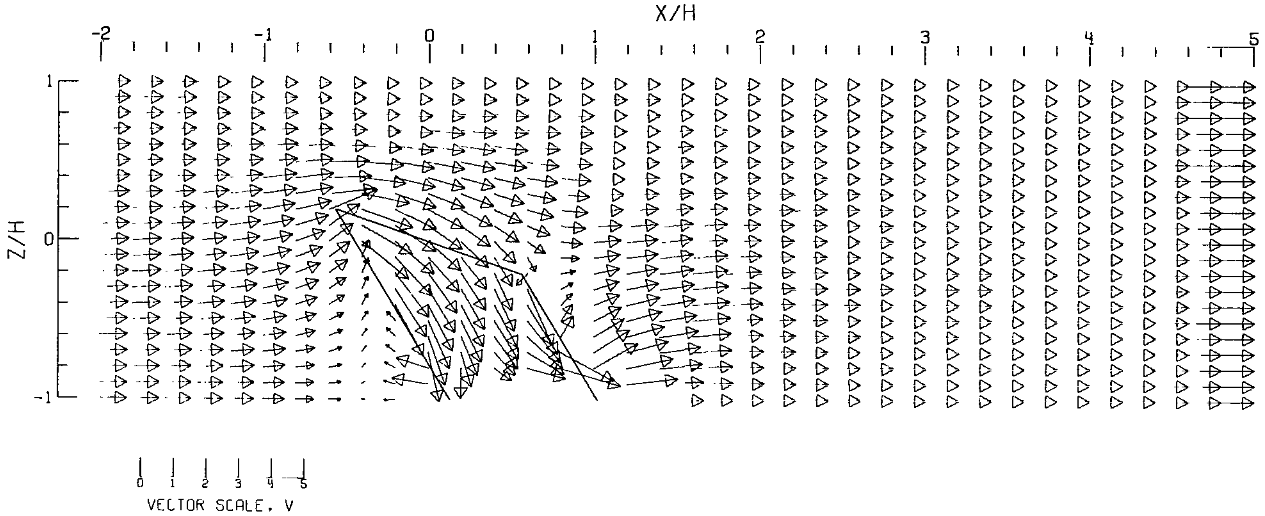

(C).- CLOSED TUNNEL.

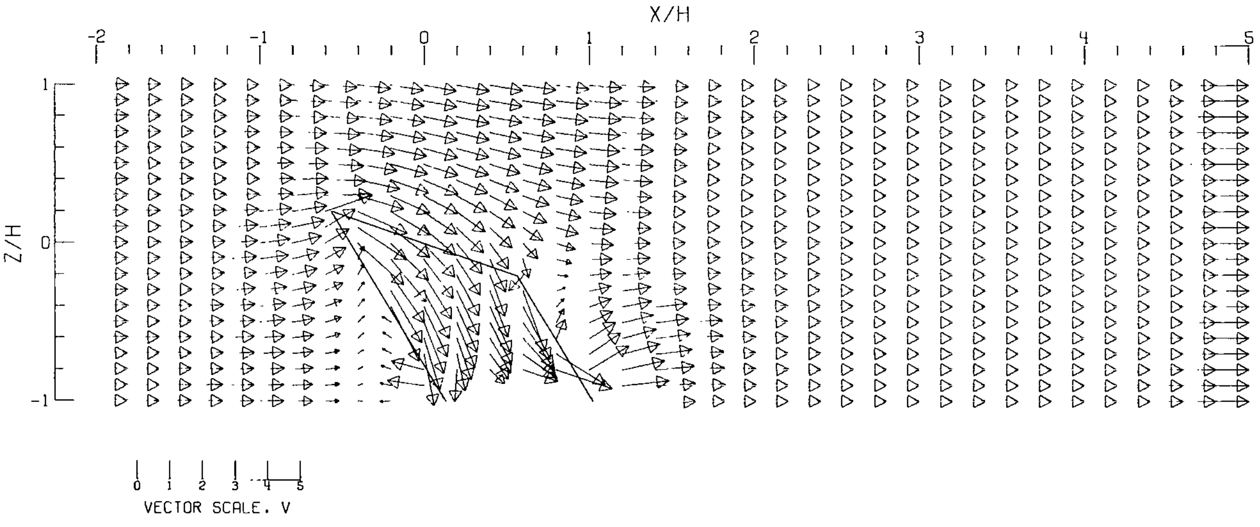

(D).- CLOSED-ON-BOTTOM-ONLY TUNNEL.

Figure 52.- Concluded.

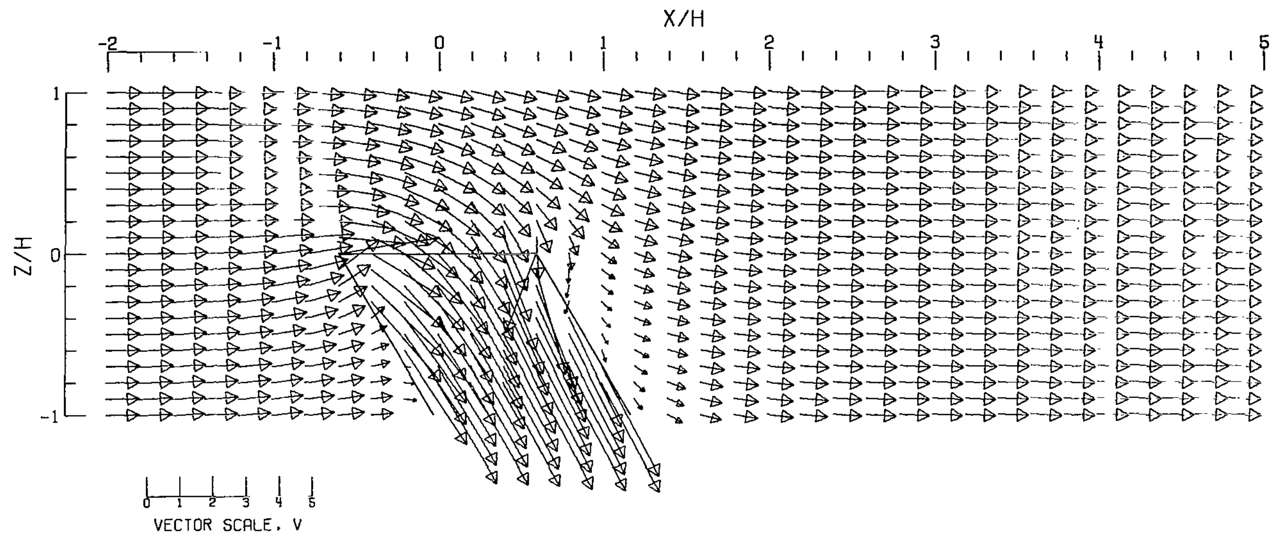

(A).- FREE AIR.

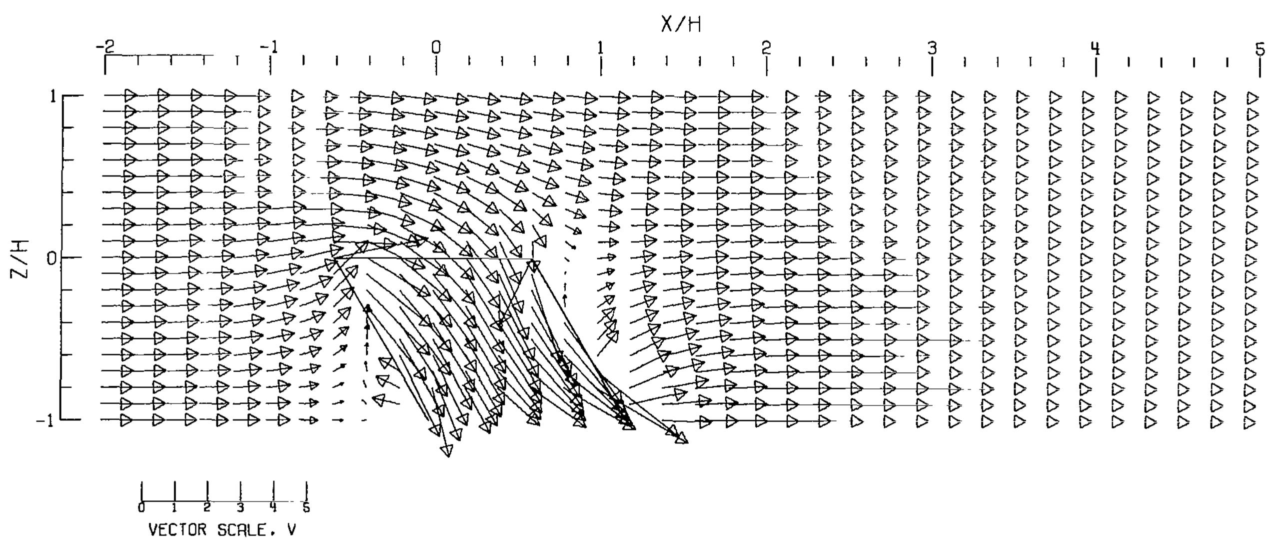

(B).- GROUND EFFECT.

Figure 53.- Flow vectors in the X-Z plane, calculated using doublet strings. The rotor and the edges of the wake are shown. ζ = 1.000; η = 1.000; γ = 1.000; σ = 0.600; α = 0.000°; χ = 30.000°; uniform loading.

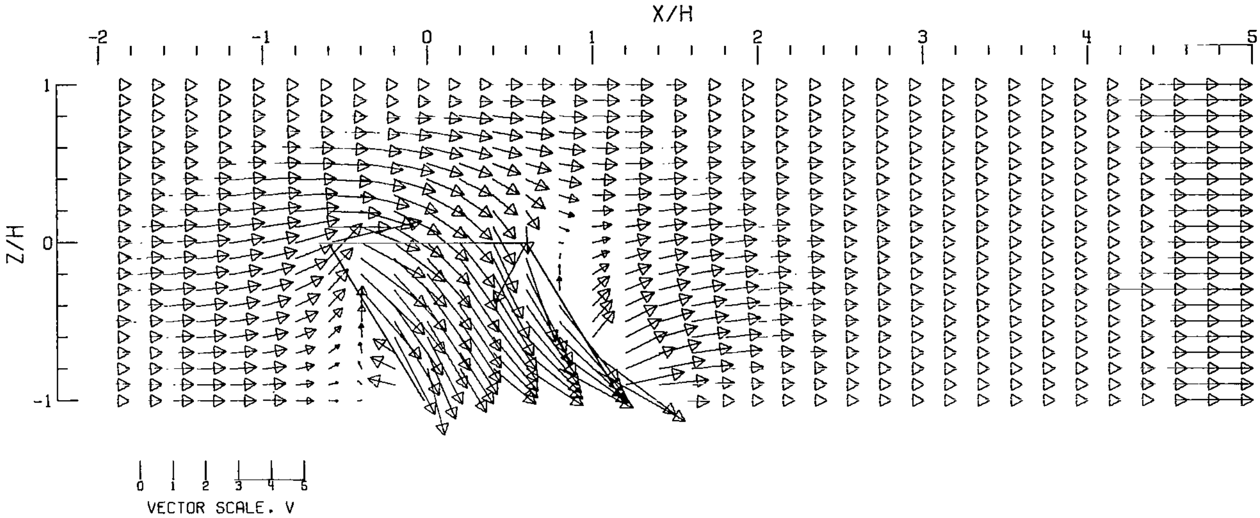

(C).- CLOSED TUNNEL.

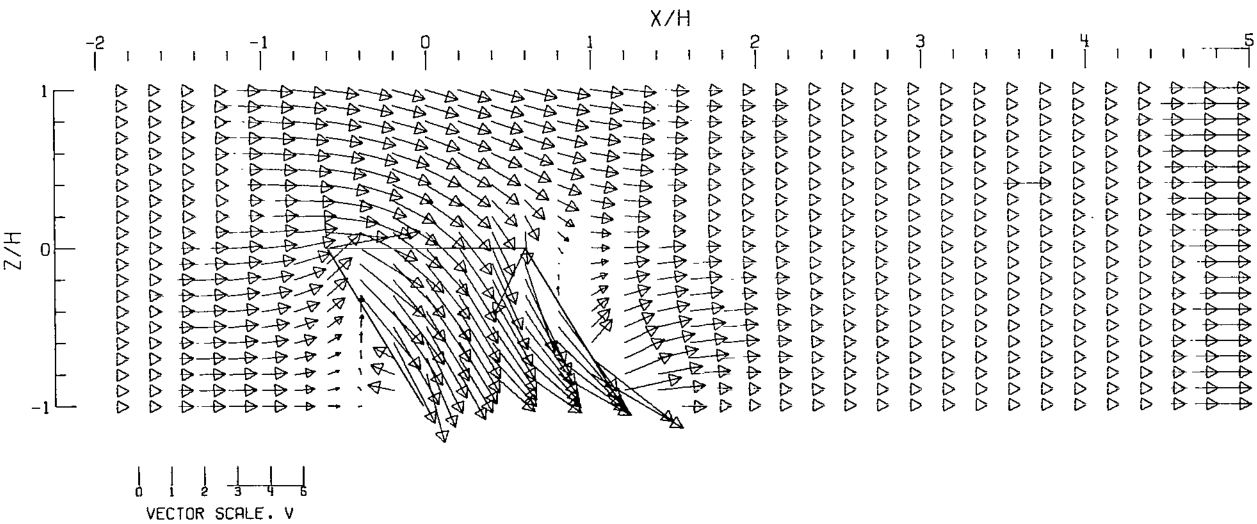

(D).- CLOSED-ON-BOTTOM-ONLY TUNNEL.

Figure 53.- Concluded.

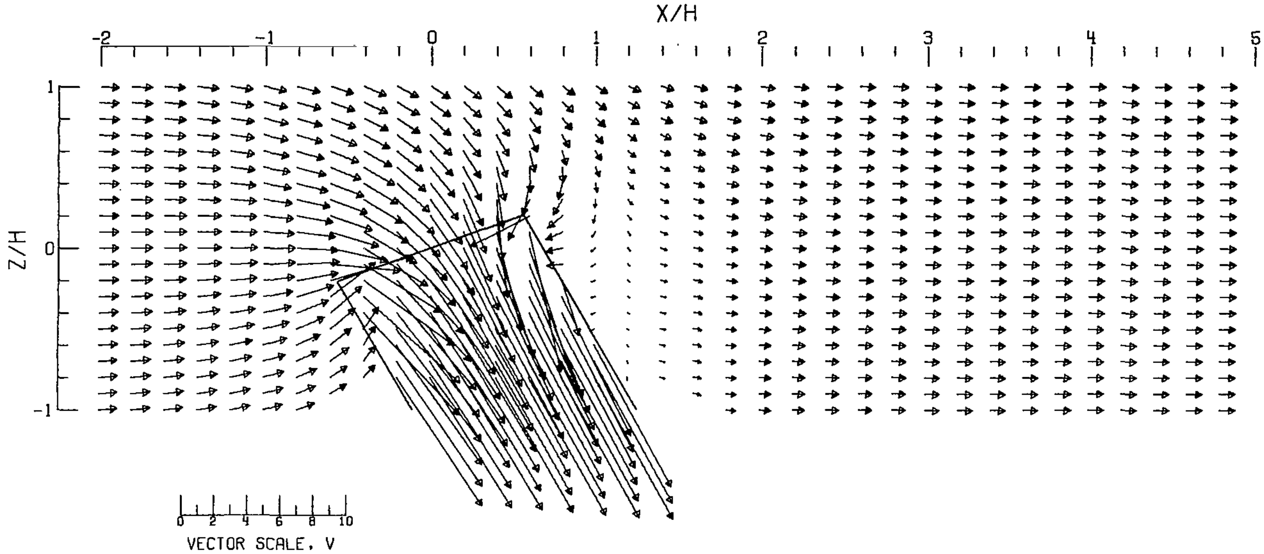

(A).- FREE AIR.

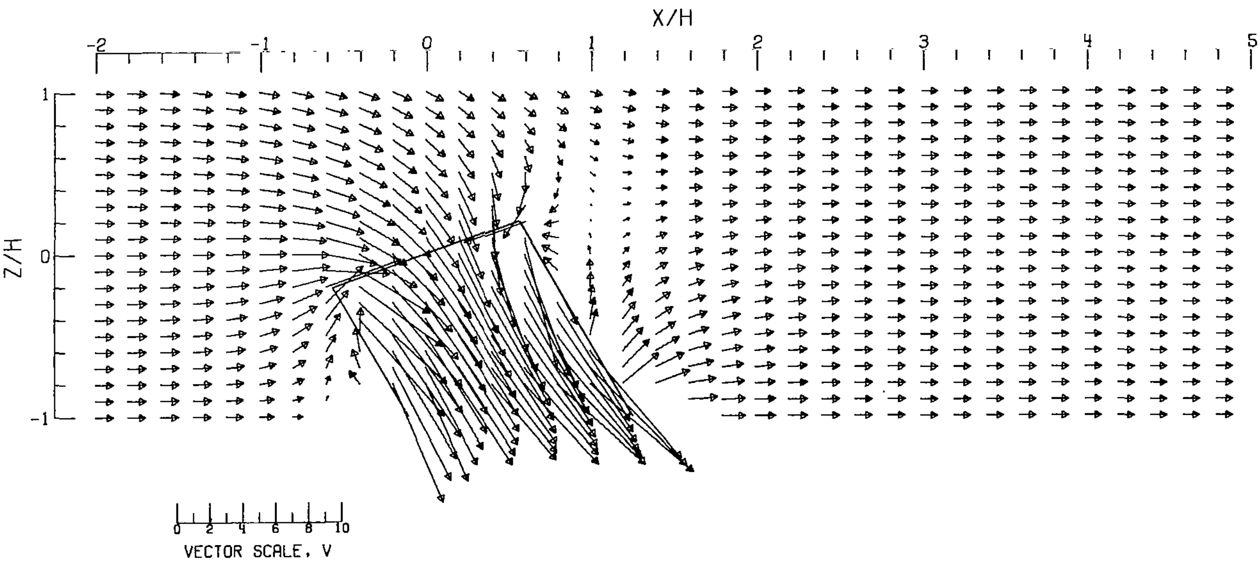

(B).- GROUND EFFECT.

Figure 54.- Flow vectors in the X-Z plane, calculated using doublet strings. The rotor and the edges of the wake are shown. ζ = 1.000; η = 1.000; γ = 1.000; σ = 0.600; α = -20.000°; χ = 30.000°; uniform loading.

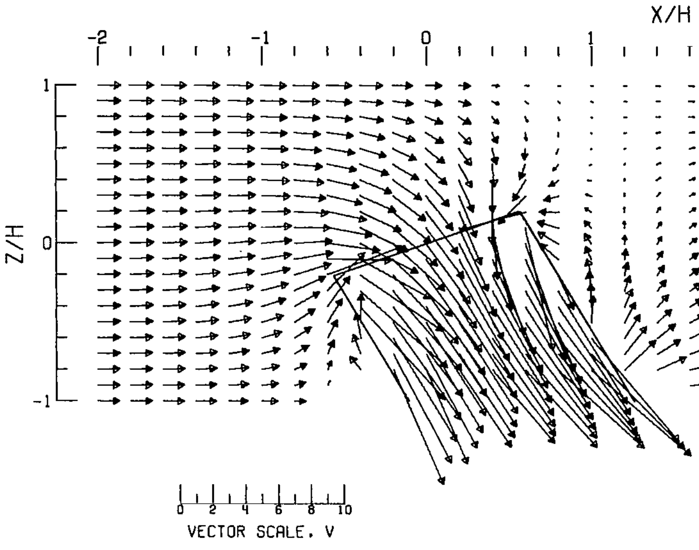

(C).- CLOSED TUNNEL.

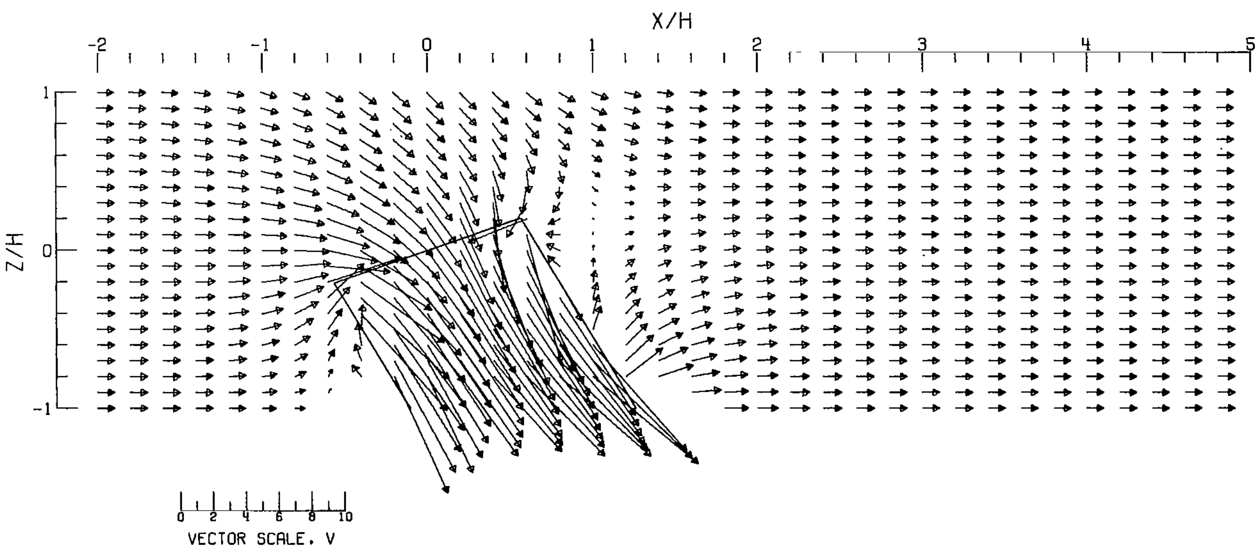

(D).- CLOSED-ON-BOTTOM-ONLY TUNNEL.

Figure 54.- Concluded.

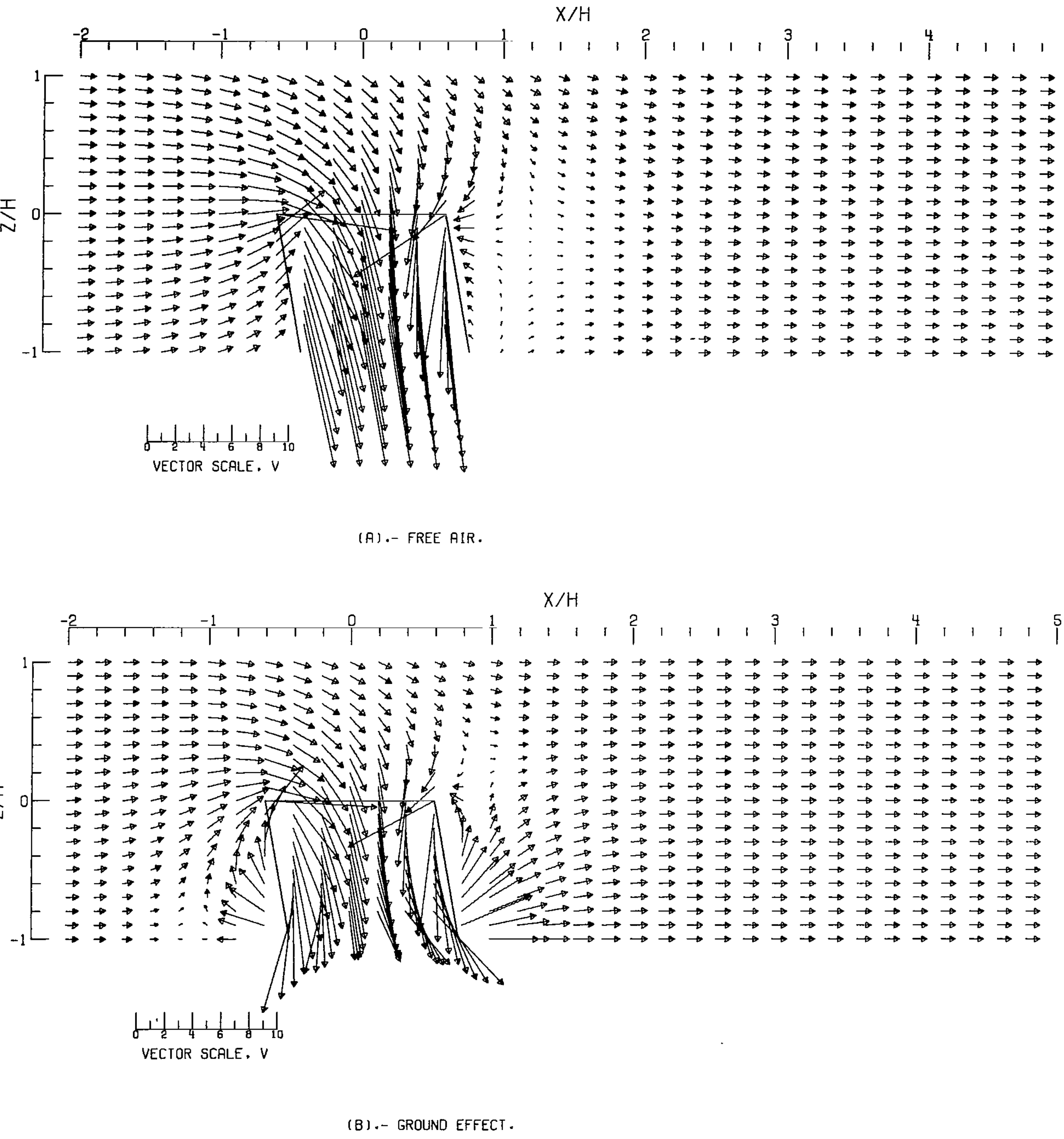

Figure 55.- Flow vectors in the X-Z plane, calculated using doublet strings. The rotor and the edges of the wake are shown. ζ = 1.000; η = 1.000; γ = 1.000; σ = 0.600; α = 0.000°; χ = 10.000°; uniform loading.

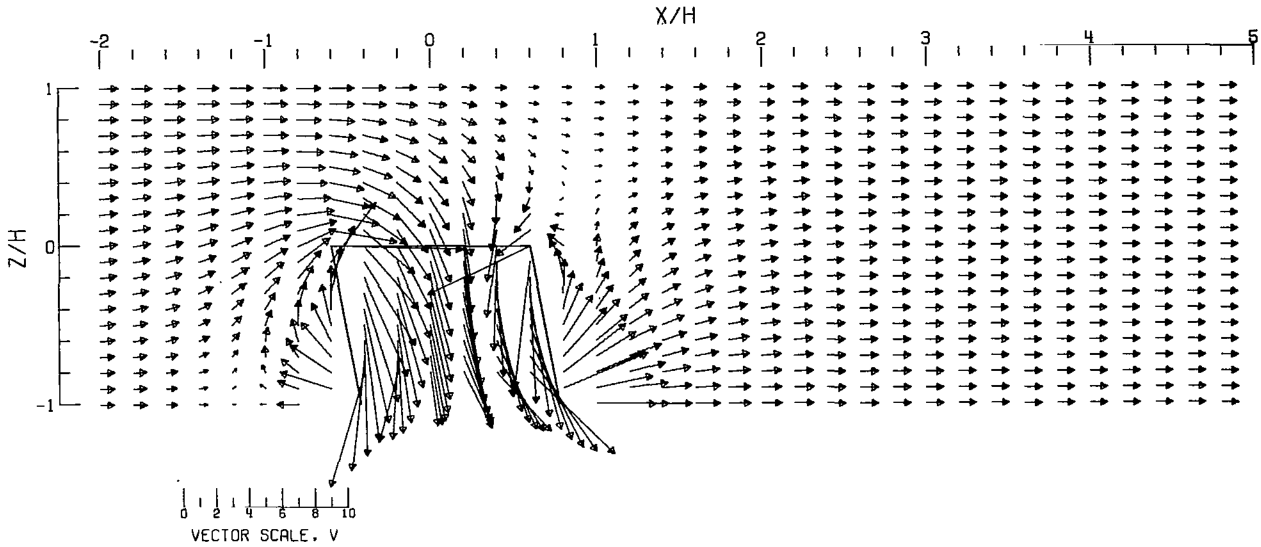

(C).- CLOSED TUNNEL.

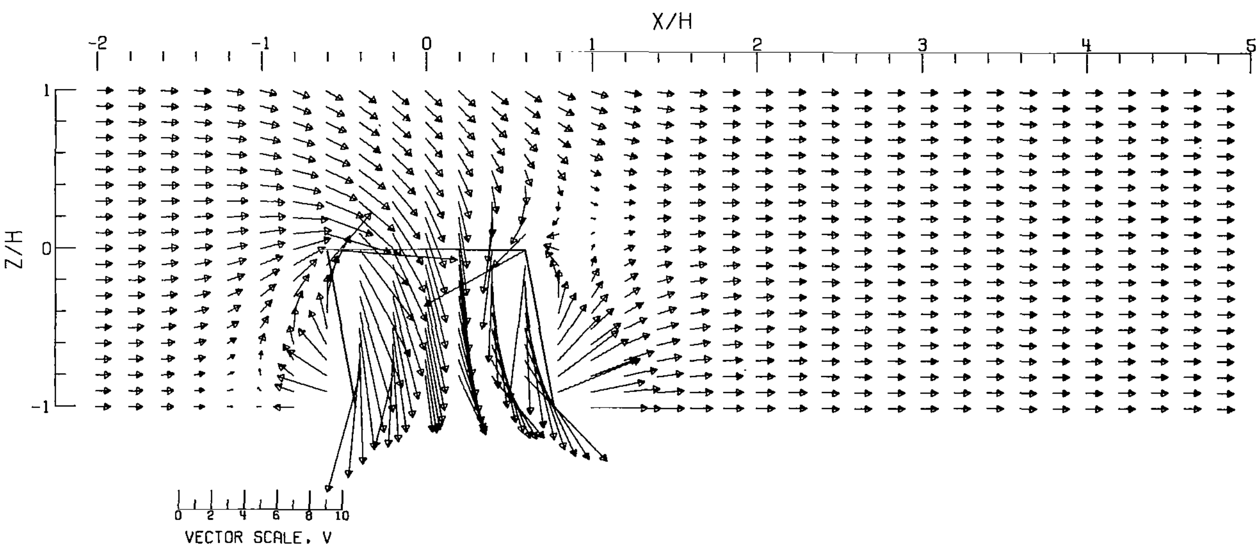

(D).- CLOSED-ON-BOTTOM-ONLY TUNNEL.

Figure 55.- Concluded.

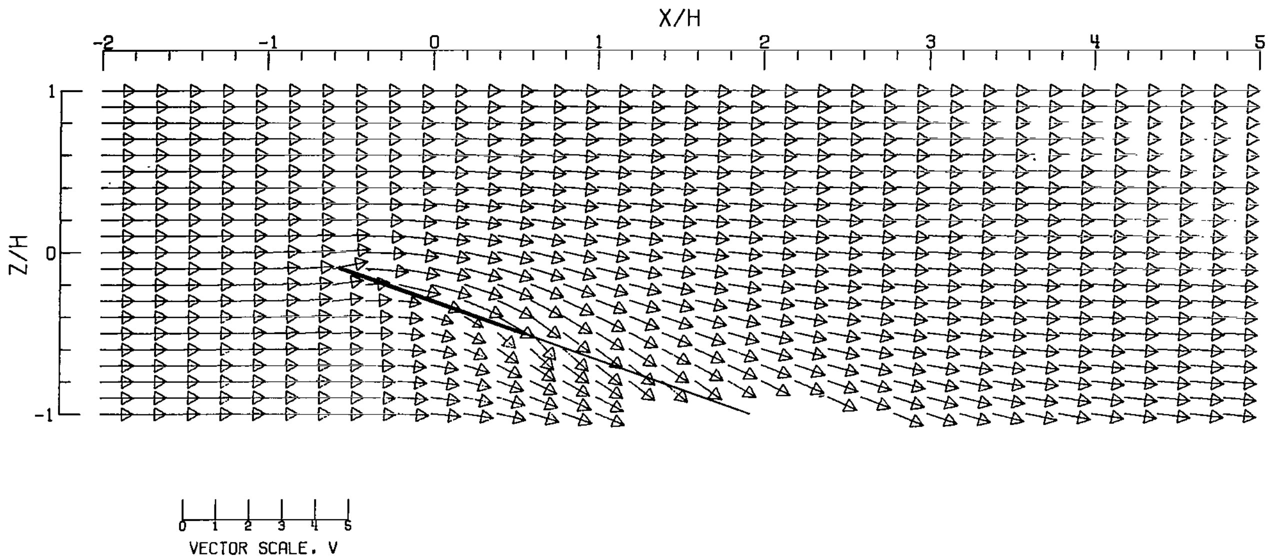

(A).- FREE AIR.

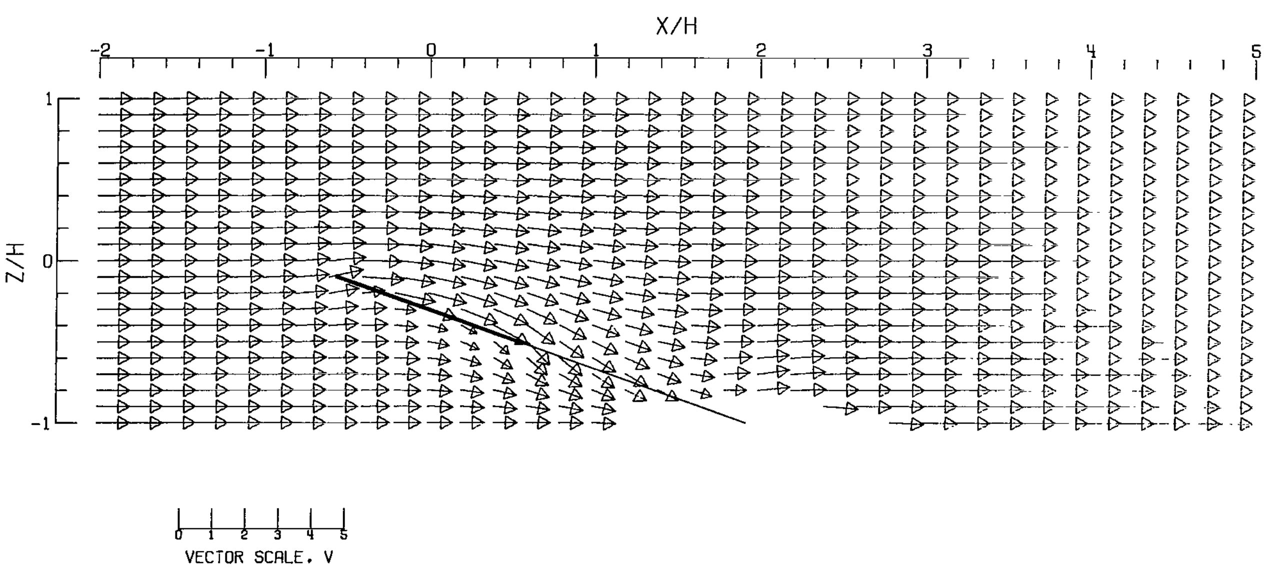

(B).- GROUND EFFECT.

Figure 56.- Flow vectors in the X-Z plane, calculated using doublet strings. The rotor and the edges of the wake are shown. ζ = 1.428; η = 1.0; γ = 1.0; σ = 0.600; α = 20.0°; χ = 70.0°; uniform loading.

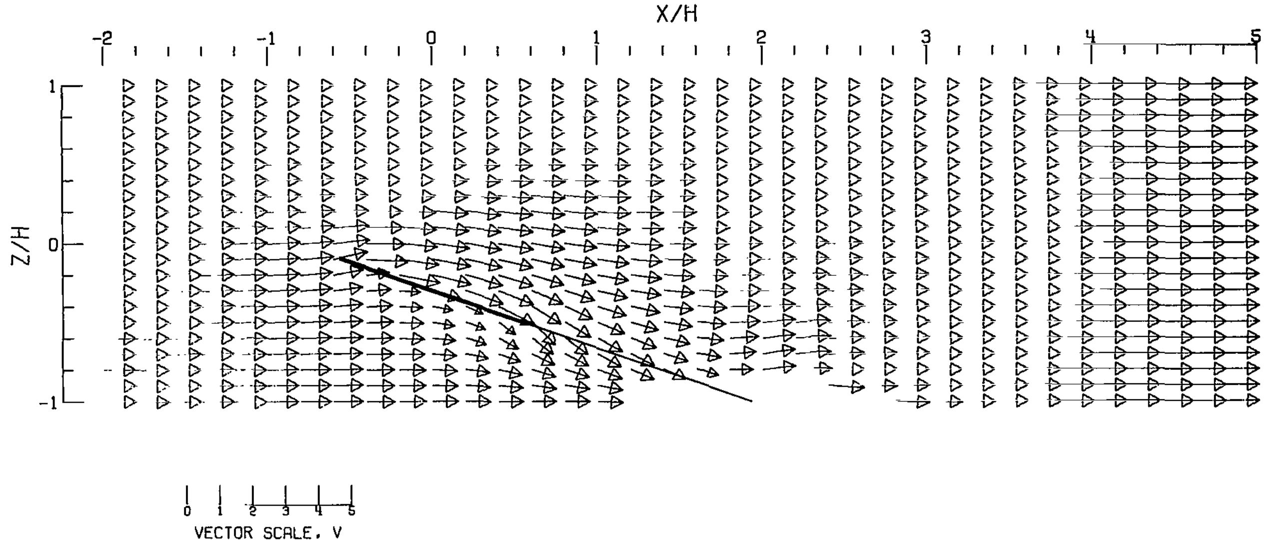

(C).- CLOSED TUNNEL.

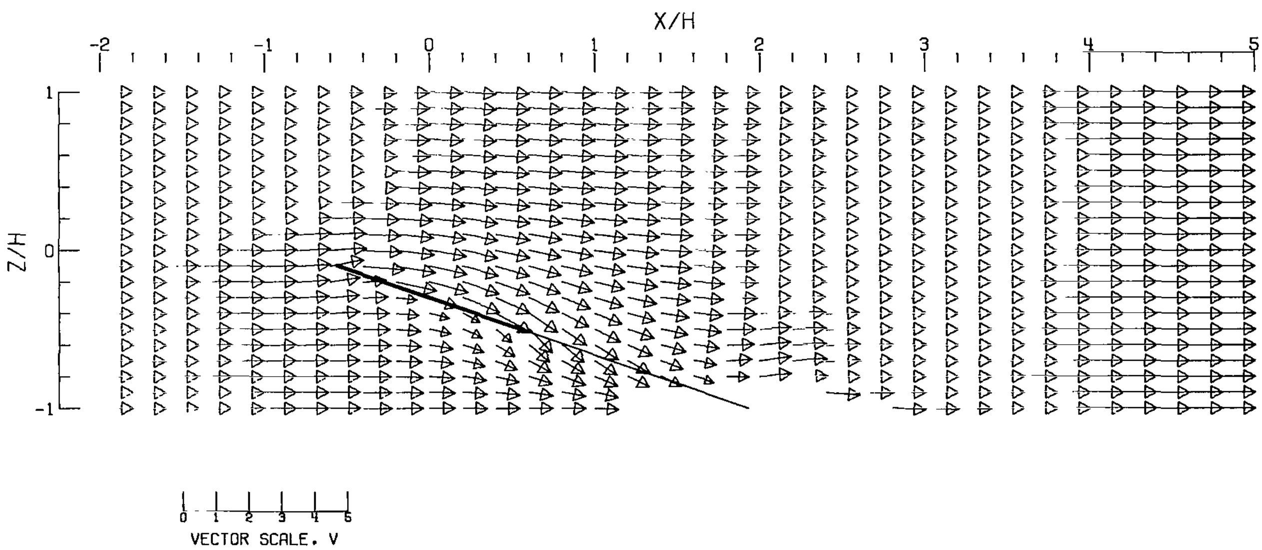

(D).- CLOSED-ON-BOTTOM-ONLY TUNNEL.

Figure 56.- Concluded.

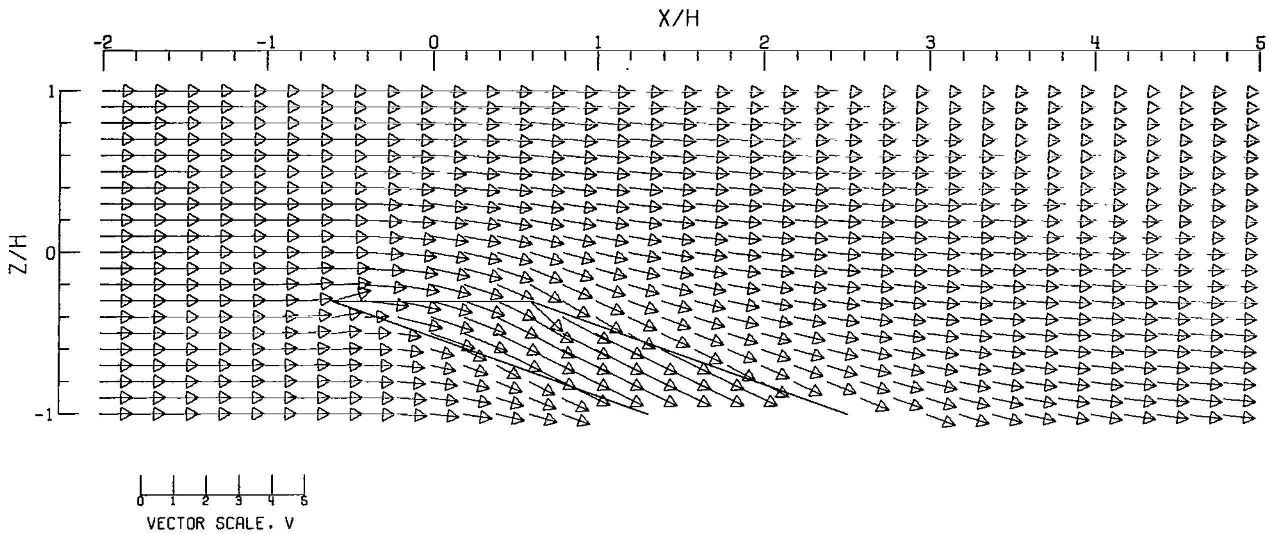

(A).- FREE AIR.

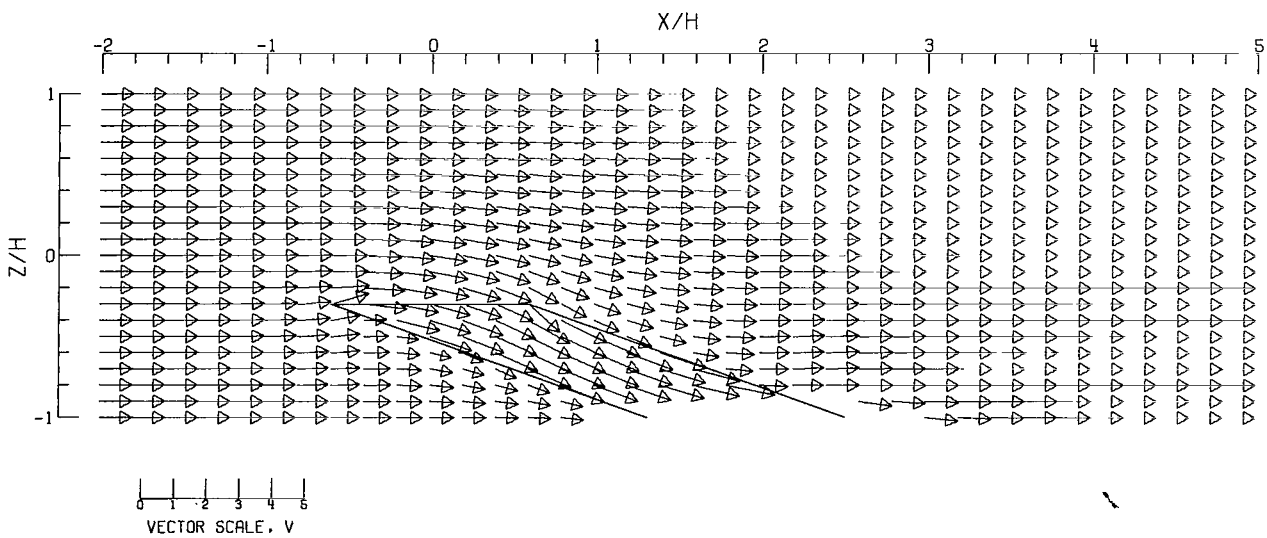

(B).- GROUND EFFECT.

Figure 57.- Flow vectors in the X-Z plane, calculated using doublet strings. The rotor and the edges of the wake are shown. ζ = 1.428; η = 1.0; γ = 1.0; σ = 0.600; α = 0.0^{o}; χ = 70.0^{o}; uniform loading.

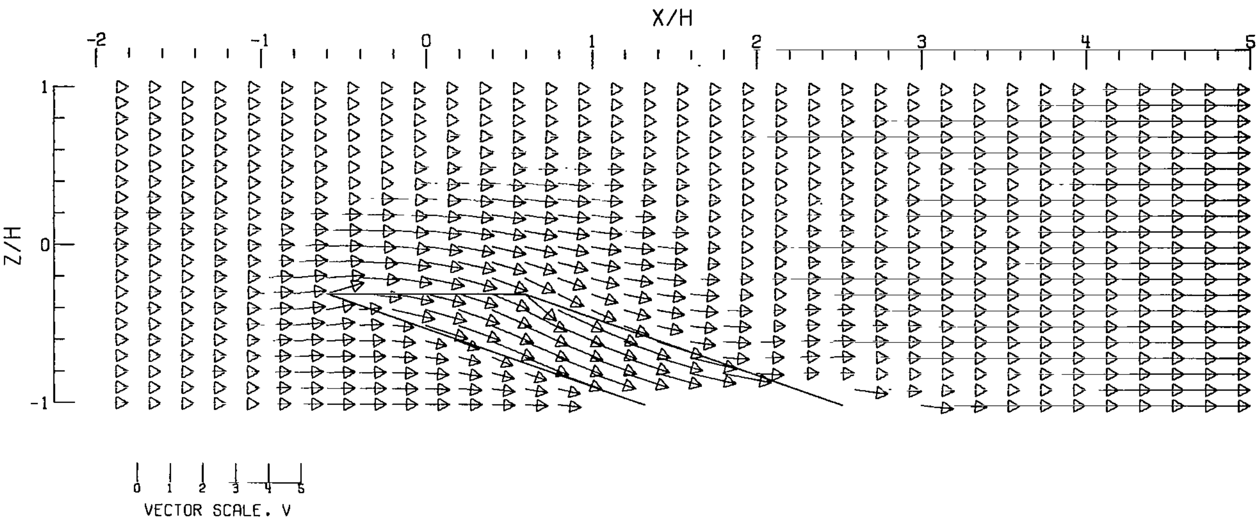

(C).- CLOSED TUNNEL.

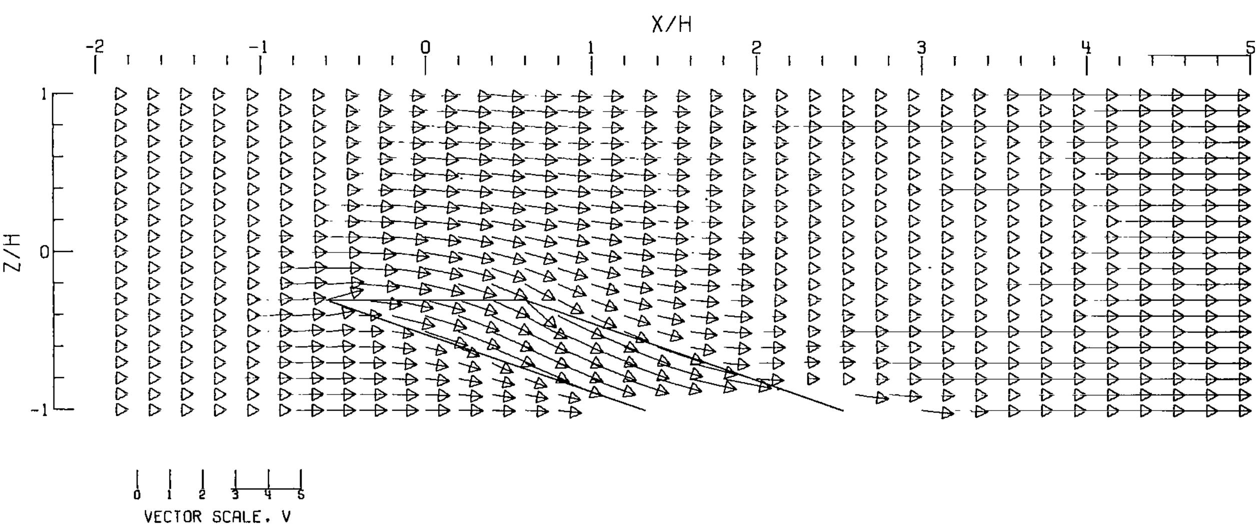

(D).- CLOSED-ON-BOTTOM-ONLY TUNNEL.

Figure 57.- Concluded.

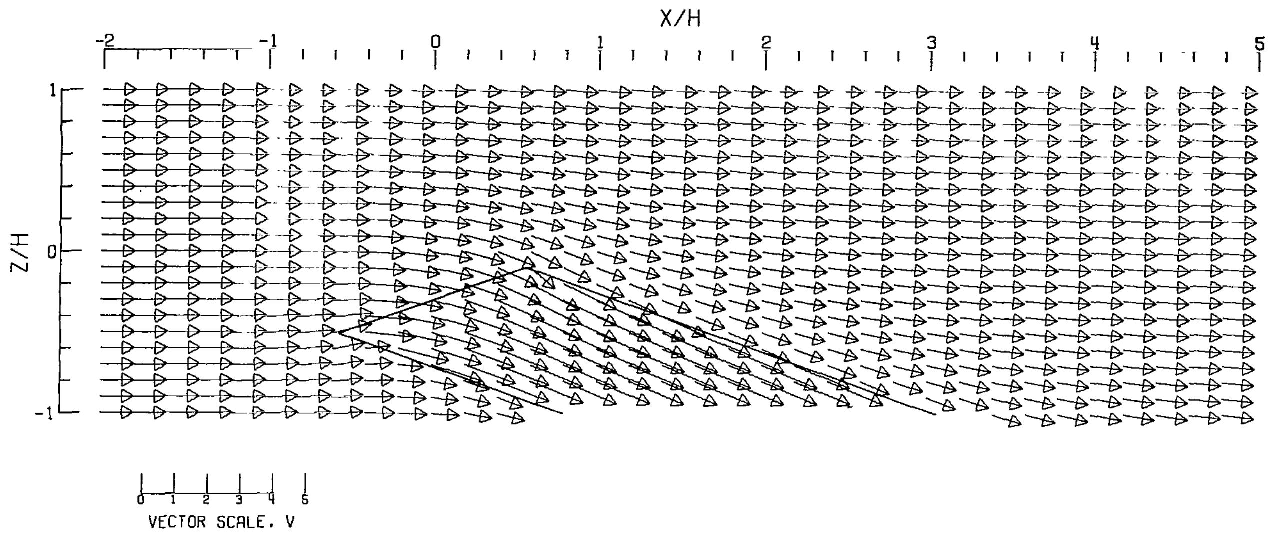

(A).- FREE AIR.

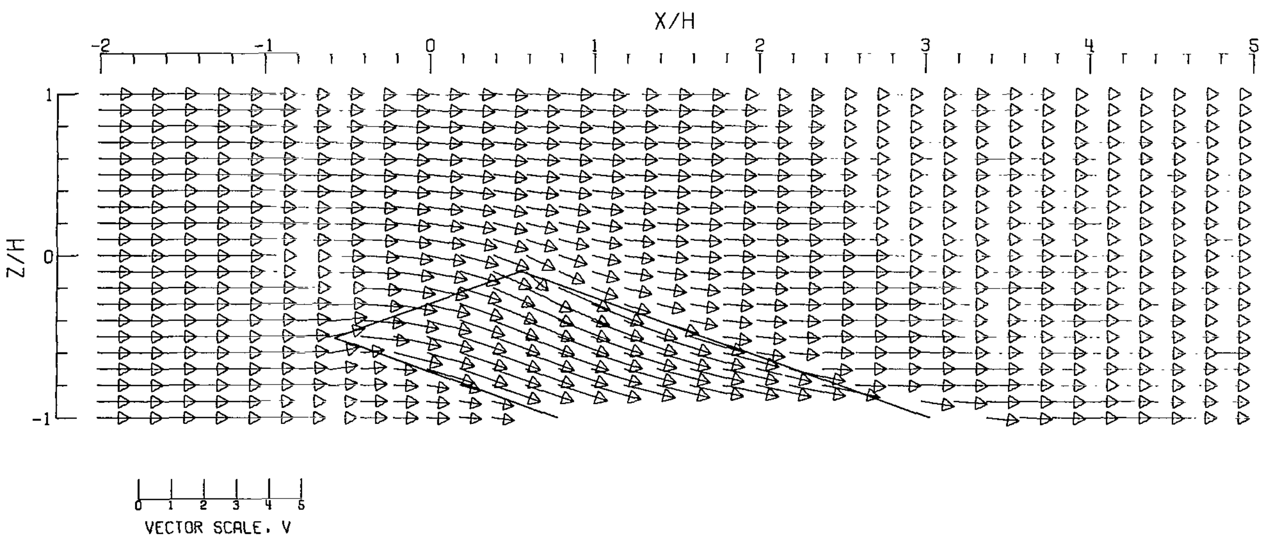

(B).- GROUND EFFECT.

Figure 58.- Flow vectors in the X-Z plane, calculated using doublet strings. The rotor and the edges of the wake are shown. ζ = 1.428; η = 1.0; γ = 1.0; σ = 0.600; α = -20.0°; χ = 70.0°; uniform loading.

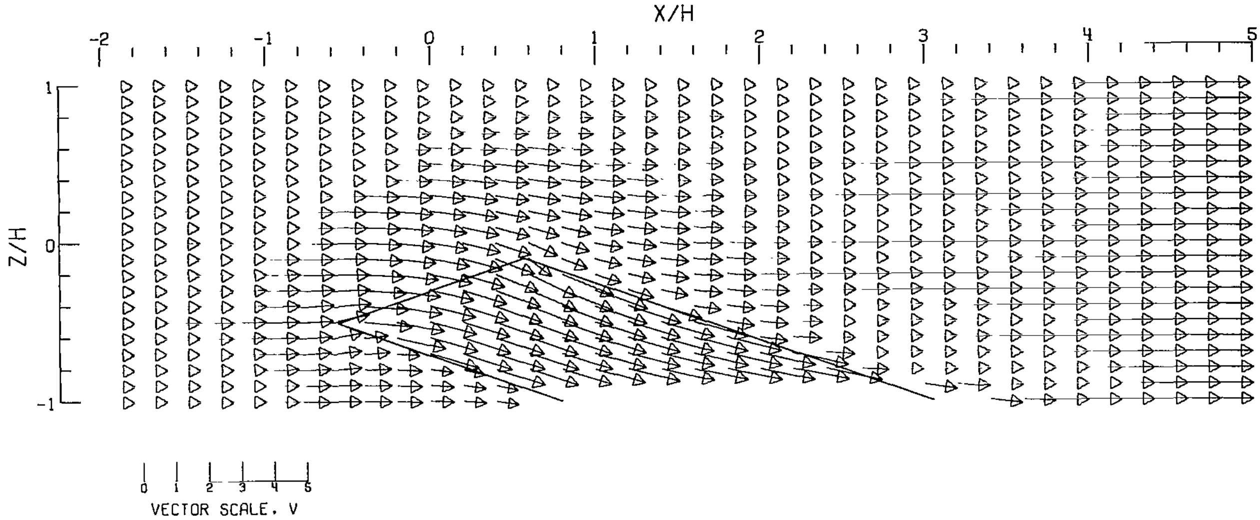

(C).- CLOSED TUNNEL.

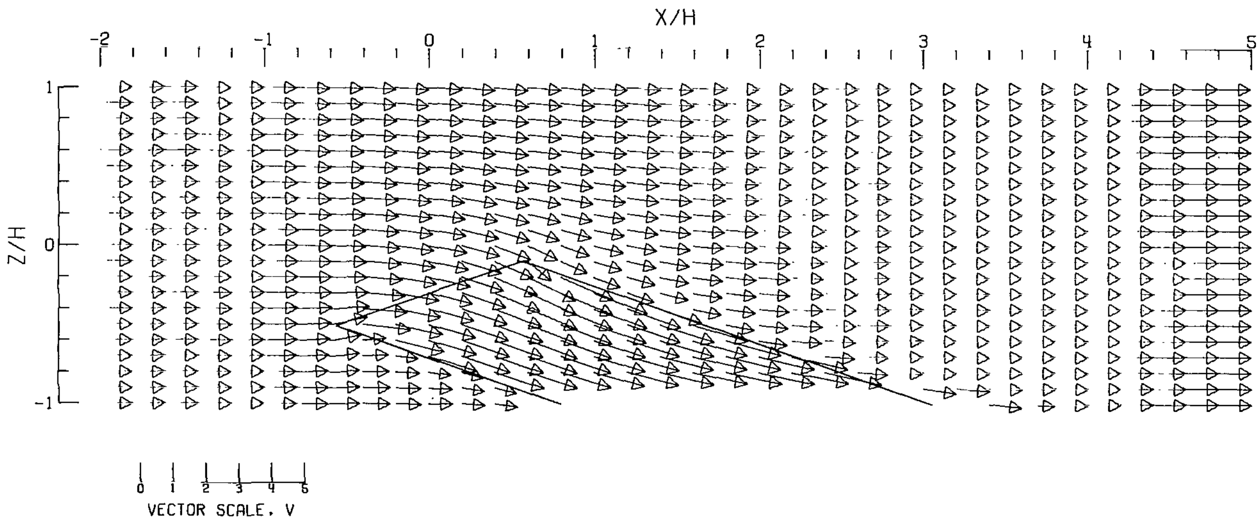

(D).- CLOSED-ON-BOTTOM-ONLY TUNNEL.

Figure 58.- Concluded.

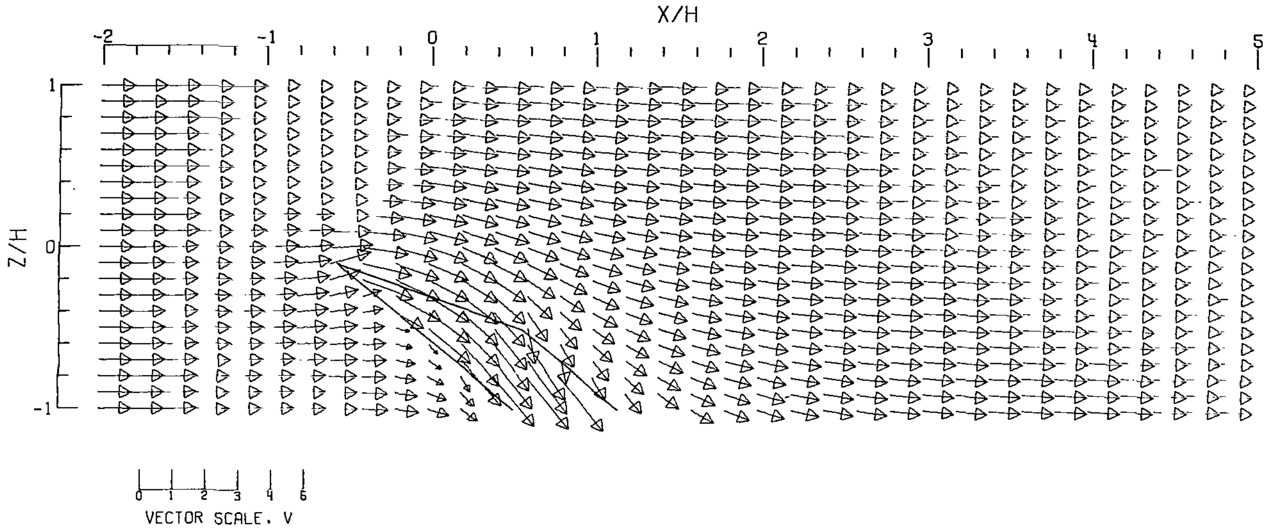

(A).- FREE AIR.

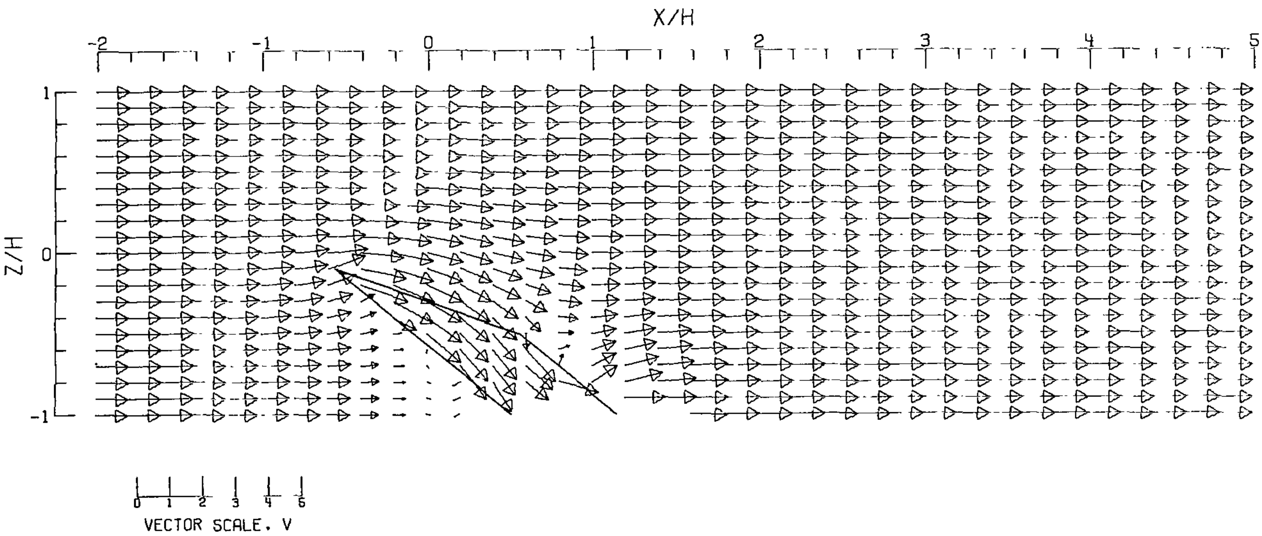

(B).- GROUND EFFECT.

Figure 59.- Flow vectors in the X-Z plane, calculated using doublet strings. The rotor and the edges of the wake are shown. ζ = 1.428; η = 1.0; γ = 1.0; σ = 0.600; α = 20.0^0; χ = 50.0^0; uniform loading.

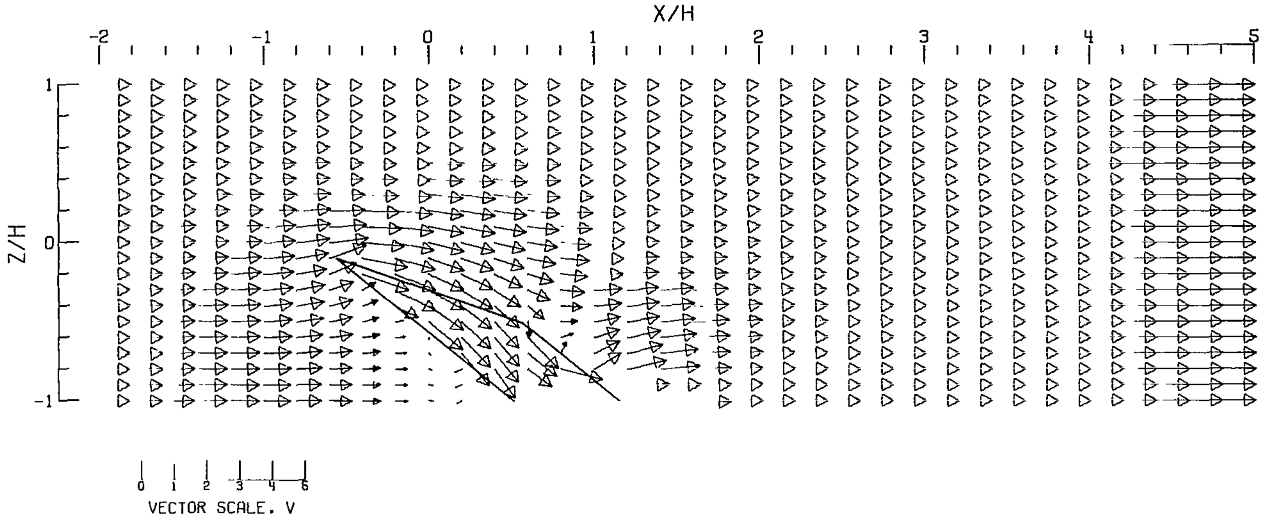

(C).- CLOSED TUNNEL.

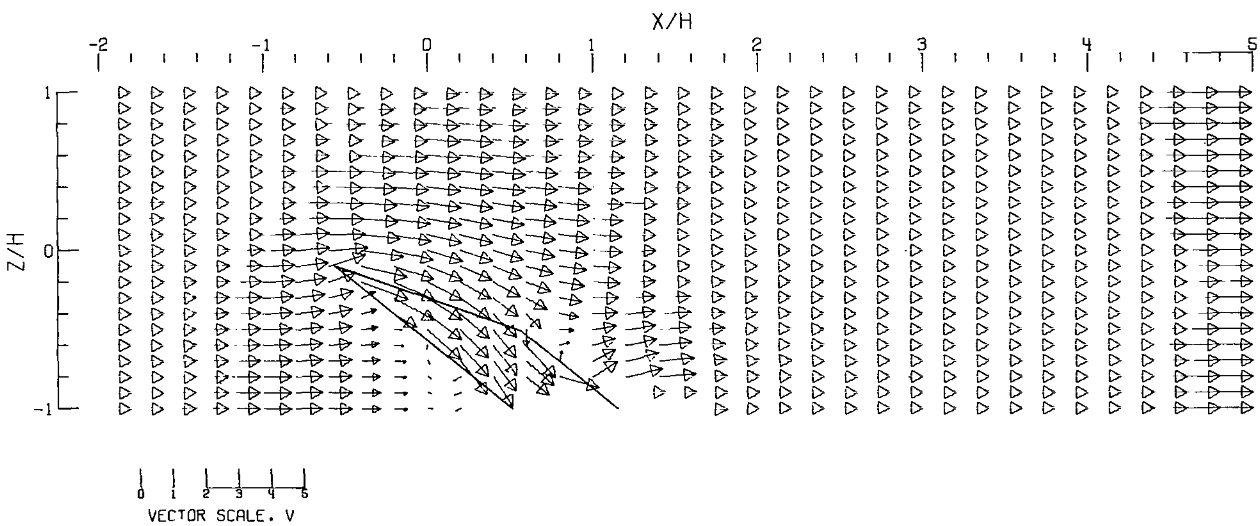

(D).- CLOSED-ON-BOTTOM-ONLY TUNNEL.

Figure 59.- Concluded.

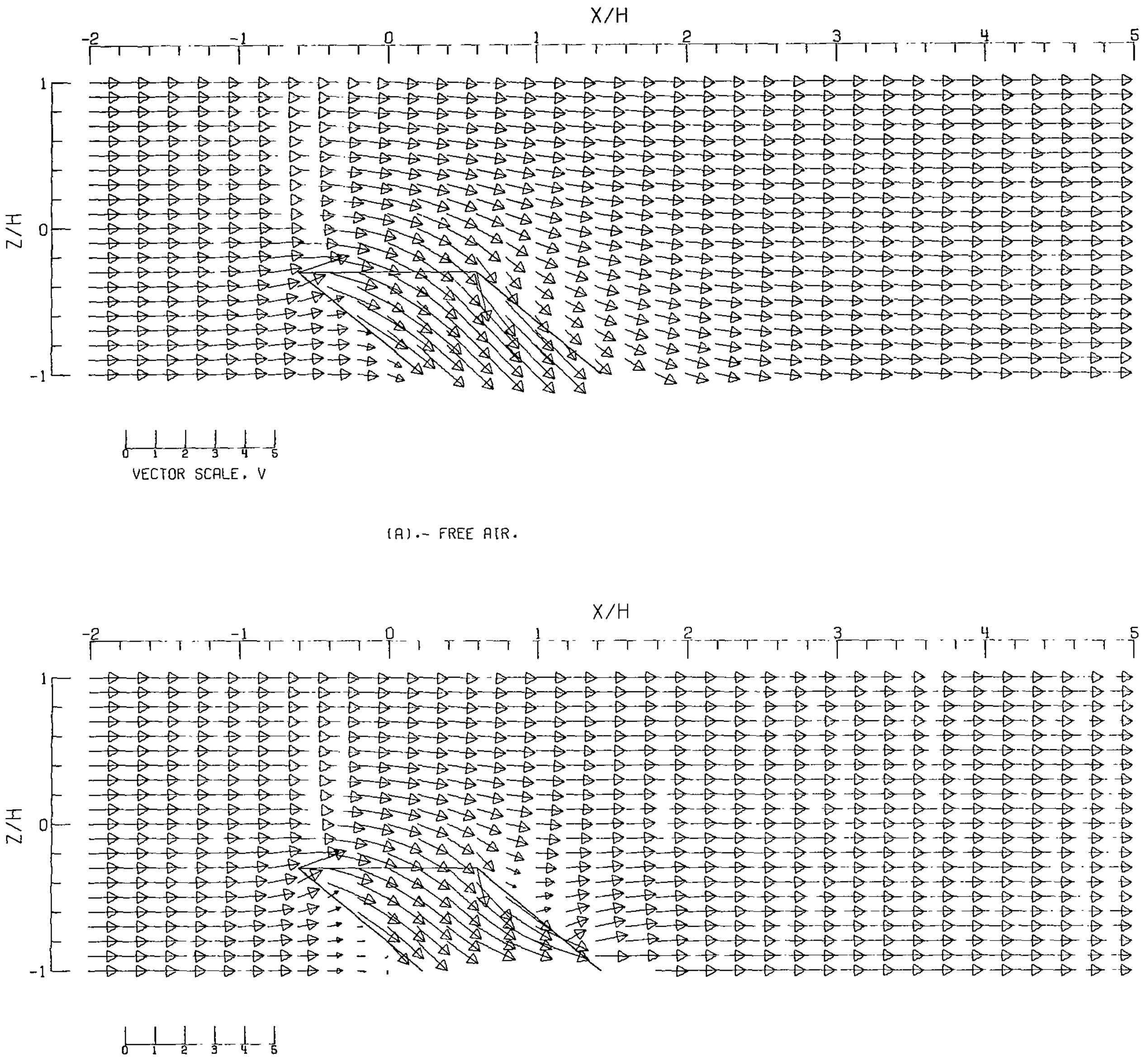

(A).- FREE AIR.

(B).- GROUND EFFECT.

Figure 60.- Flow vectors in the X-Z plane, calculated using doublet strings. The rotor and the edges of the wake are shown. $\zeta = 1.428$; $\eta = 1.0$; $\gamma = 1.0$; $\sigma = 0.600$; $\alpha = 0.0^{0}$; $\chi = 50.0^{0}$; uniform loading.

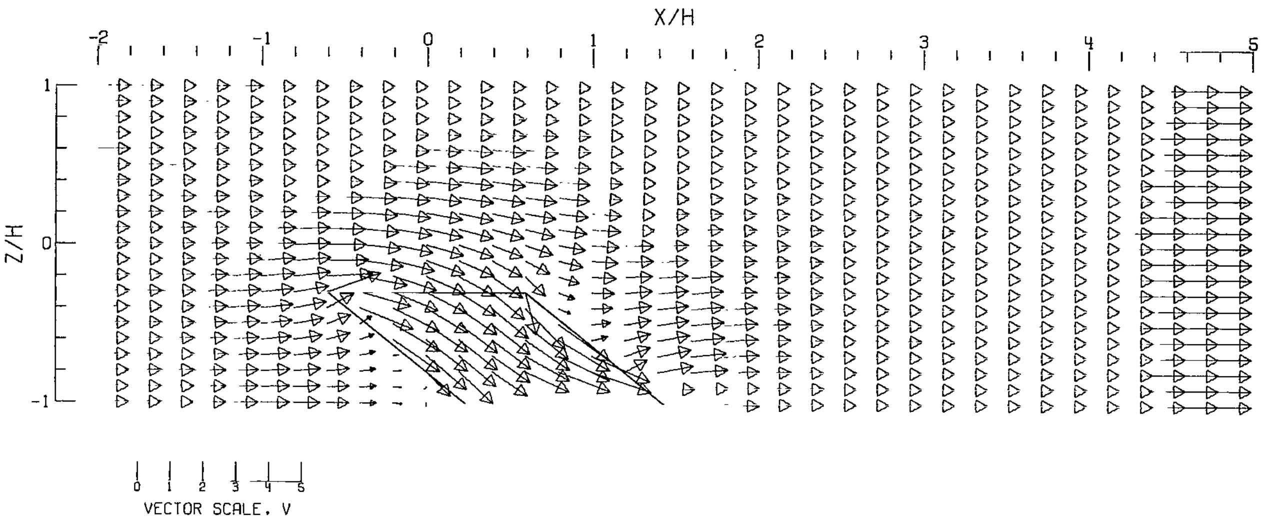

(C).- CLOSED TUNNEL.

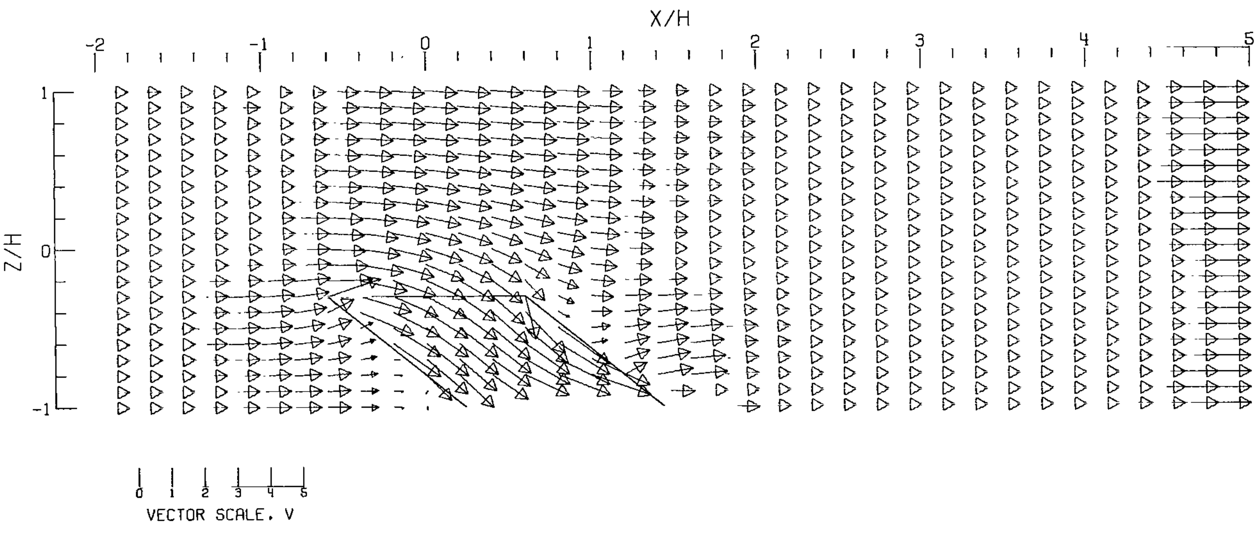

(D).- CLOSED-ON-BOTTOM-ONLY TUNNEL.

Figure 60.- Concluded.

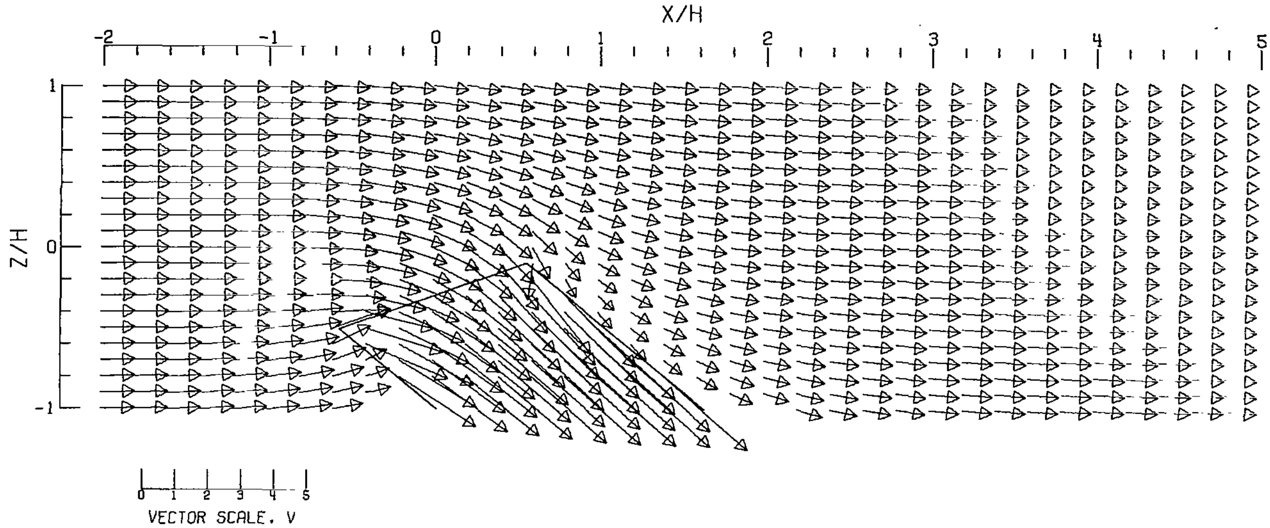

(A).- FREE AIR.

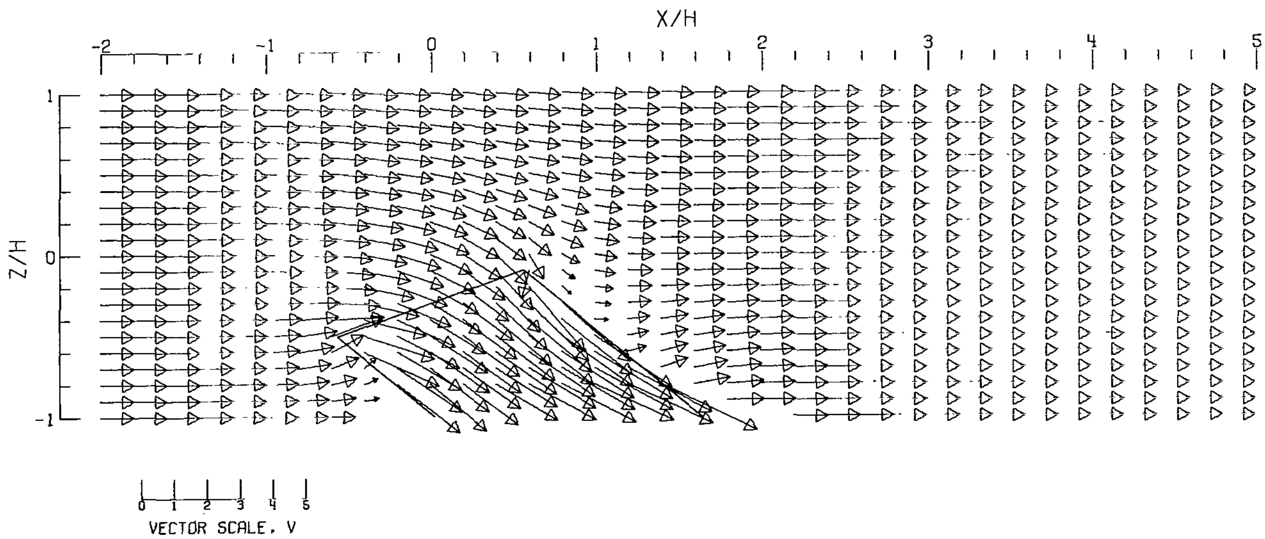

(B).- GROUND EFFECT.

Figure 61.- Flow vectors in the X-Z plane, calculated using doublet strings. The rotor and the edges of the wake are shown. ζ = 1.428; η = 1.0; γ = 1.0; σ = 0.600; α = -20.0°; χ = 50.0°; uniform loading.

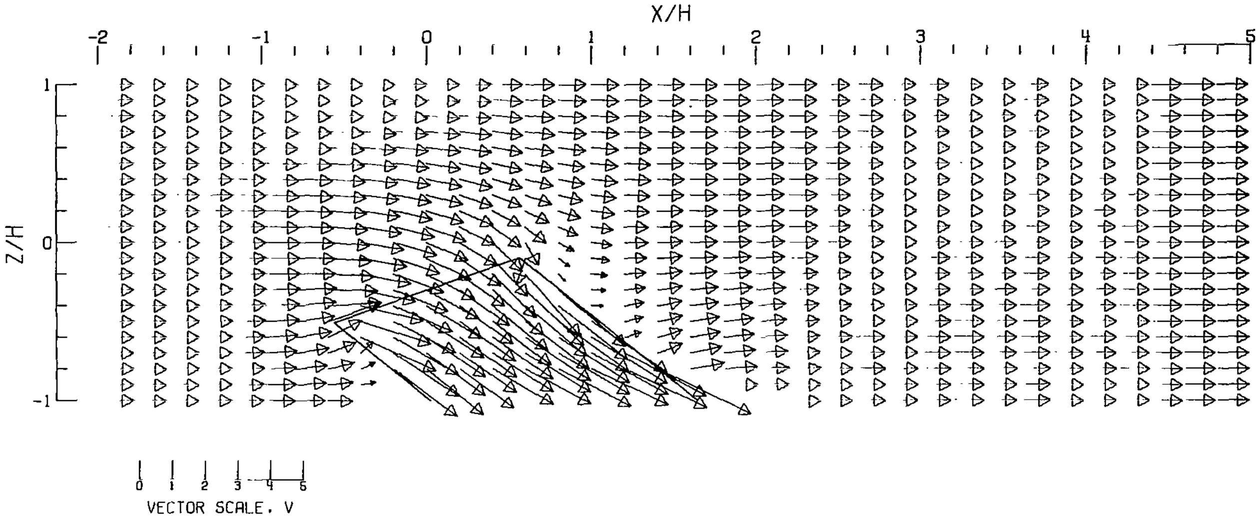

(C).- CLOSED TUNNEL.

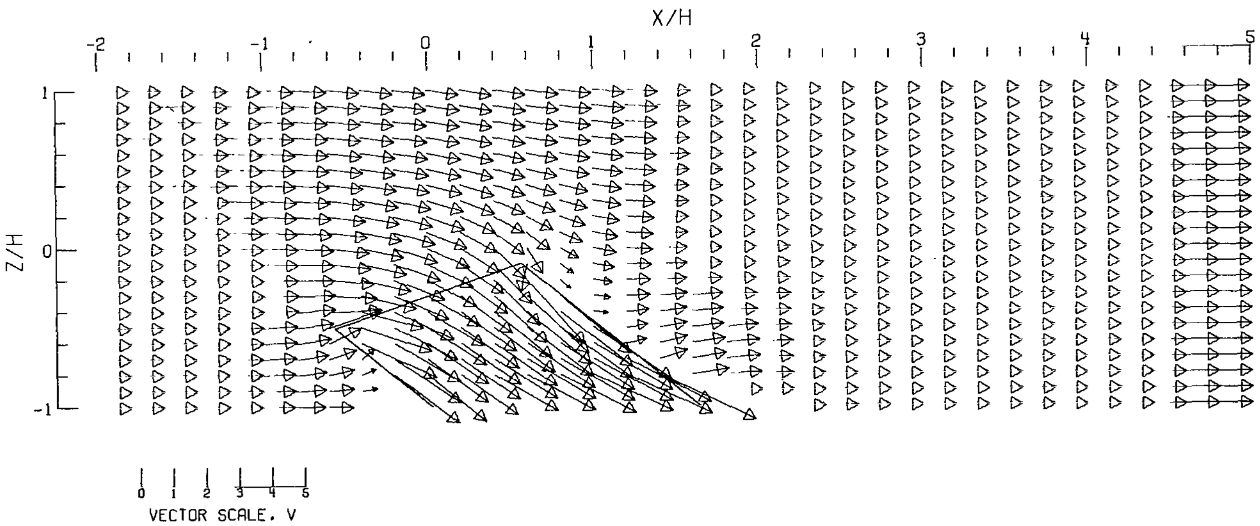

(D).- CLOSED-ON-BOTTOM-ONLY TUNNEL.

Figure 61.- Concluded.

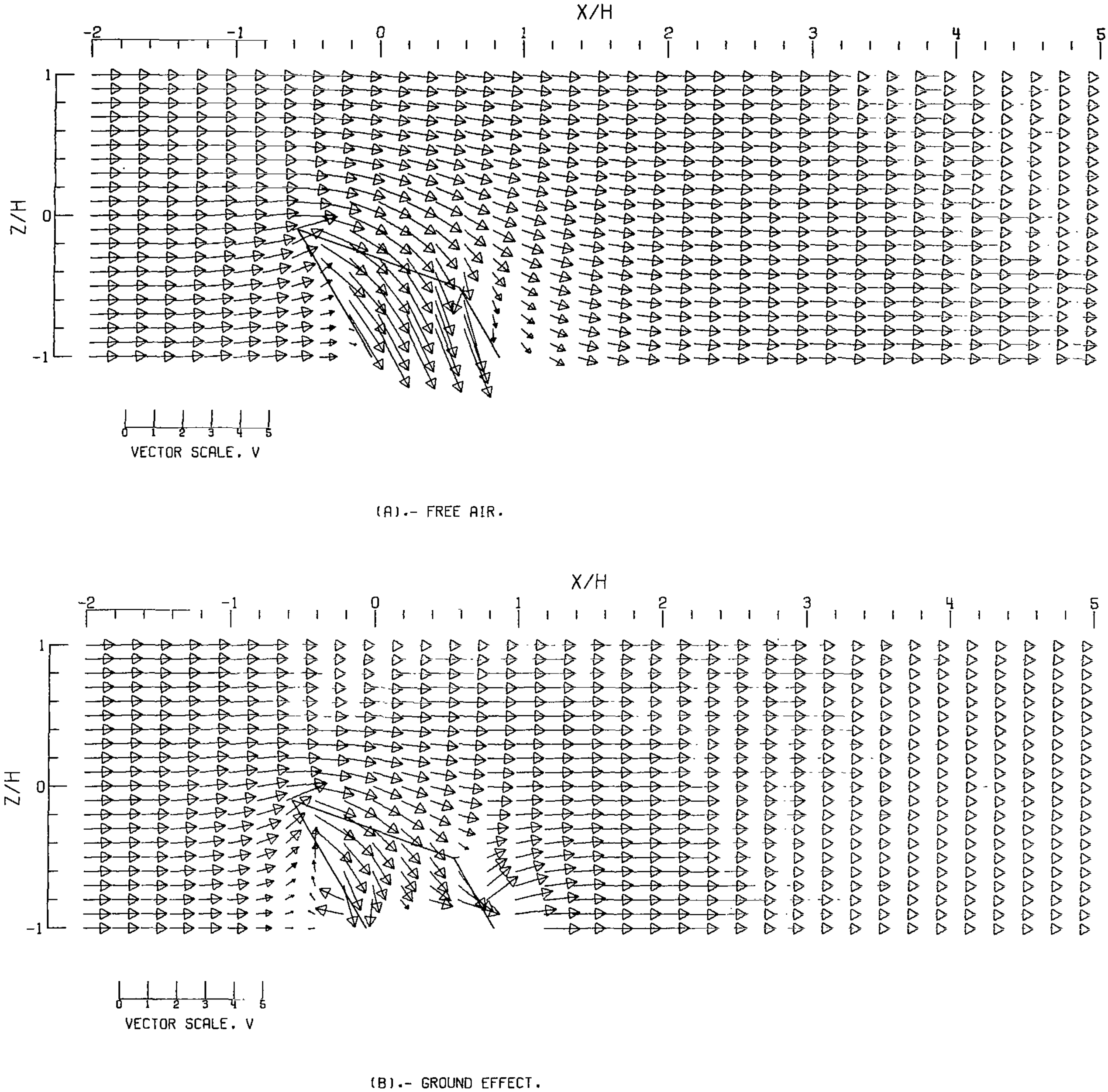

Figure 62.- Flow vectors in the X-Z plane, calculated using doublet strings. The rotor and the edges of the wake are shown. ζ = 1.428; η = 1.0; γ = 1.0; σ = 0.600; α = 20.0°; χ = 30.0°; uniform loading.

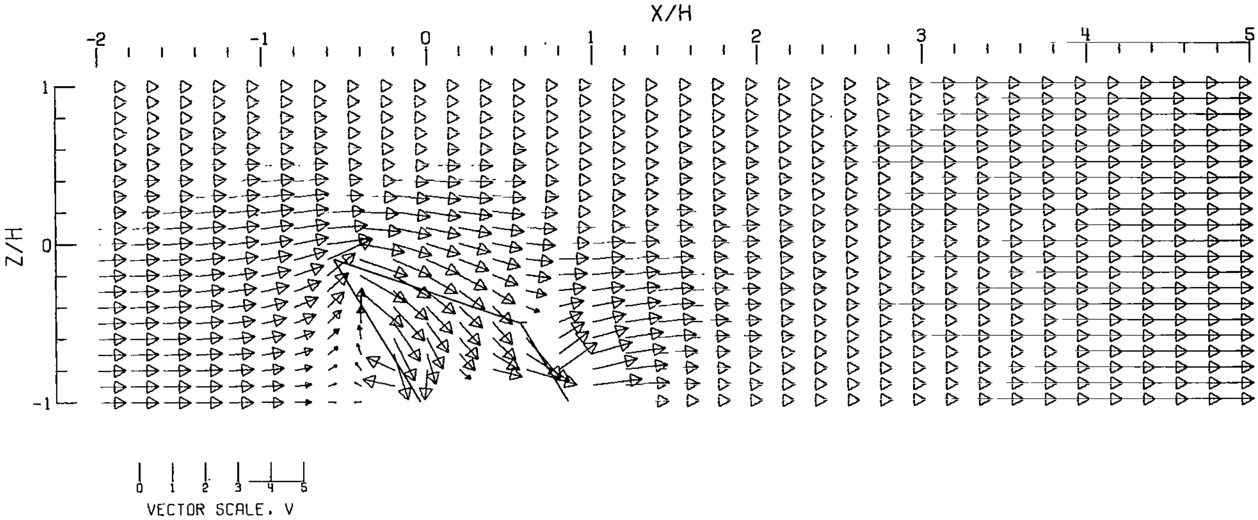

(C).- CLOSED TUNNEL.

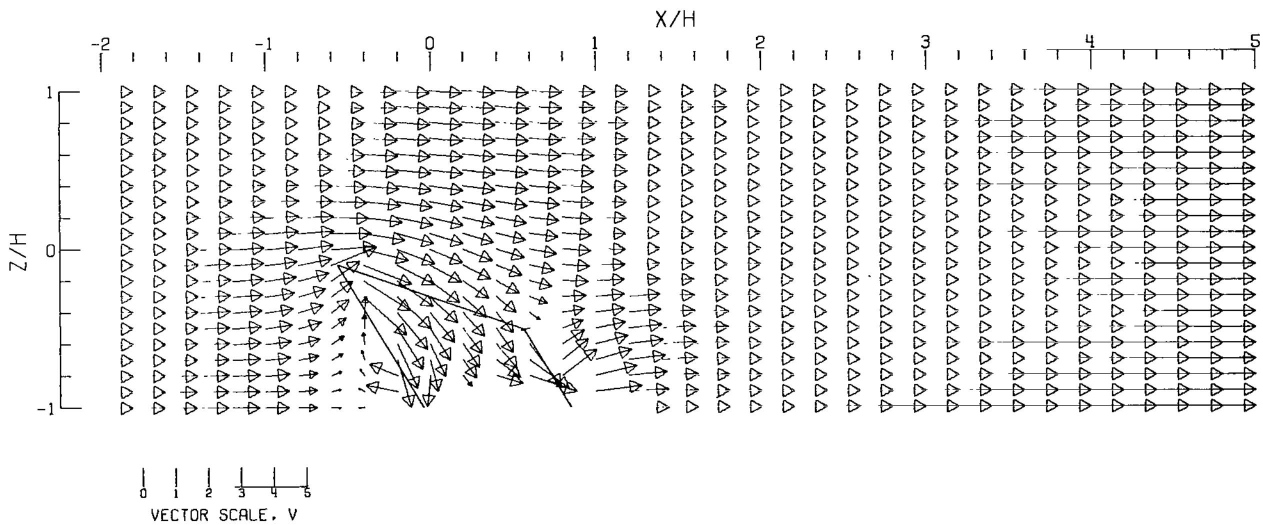

(D).- CLOSED-ON-BOTTOM-ONLY TUNNEL.

Figure 62.- Concluded.

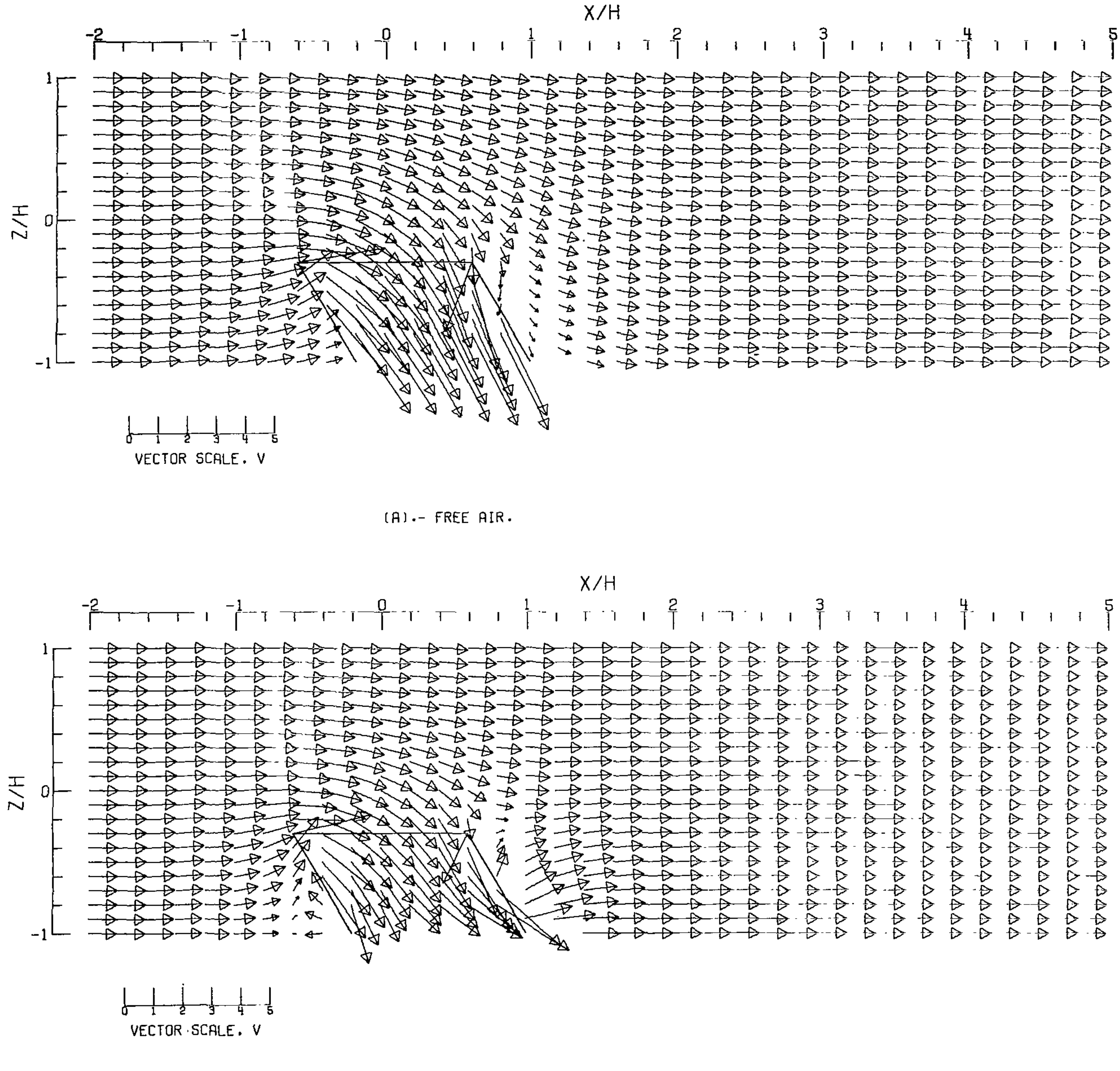

Figure 63.- Flow vectors in the X-Z plane, calculated using doublet strings. The rotor and the edges of the wake are shown. ζ = 1.428; η = 1.0; γ = 1.0; σ = 0.600; α = 0.0°; χ = 30.0°; uniform loading.

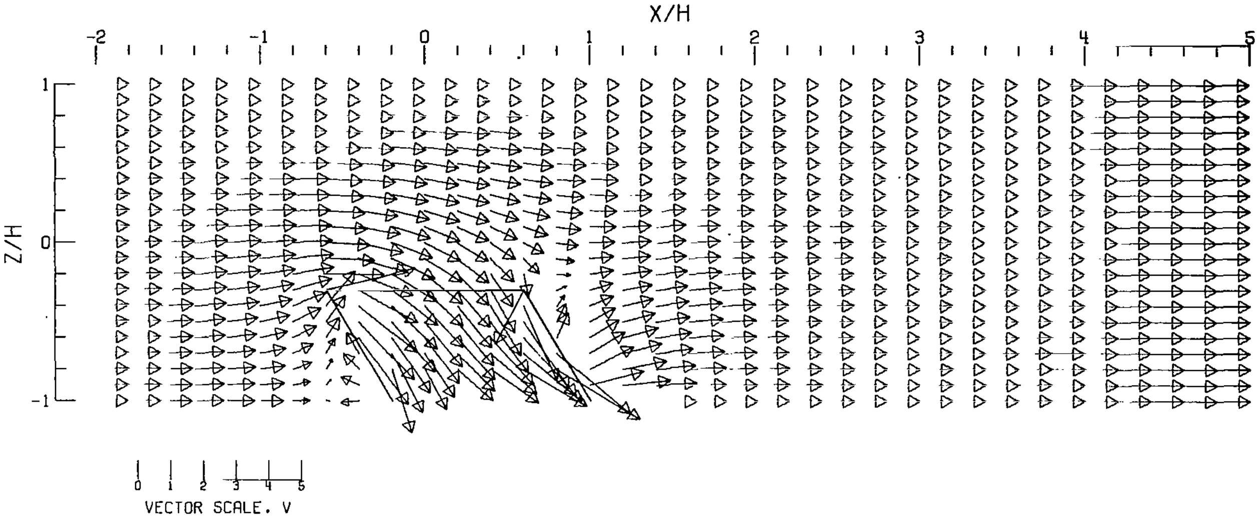

(C).- CLOSED TUNNEL.

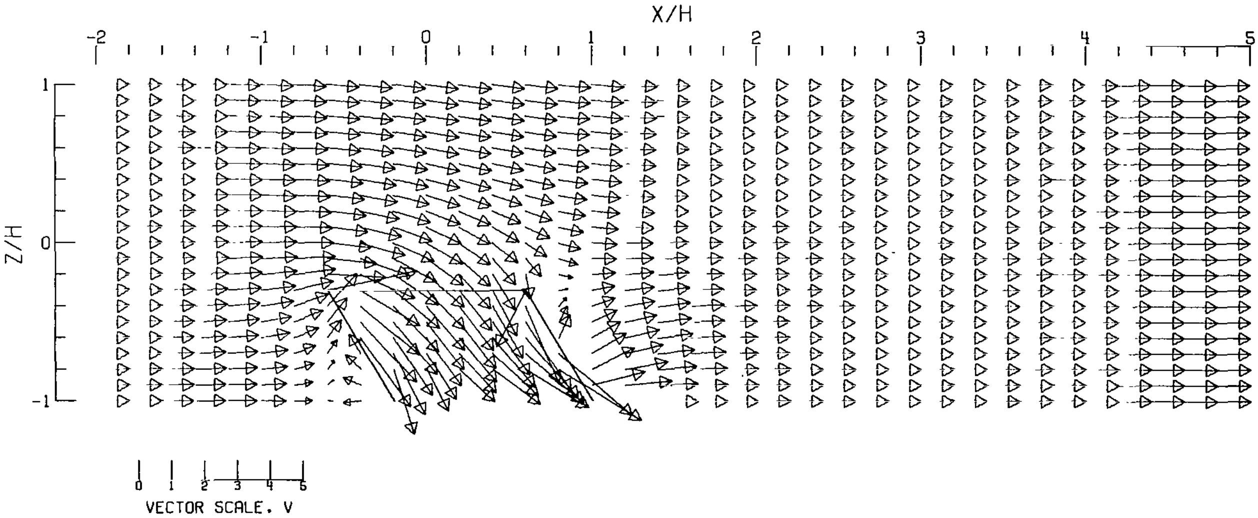

(D).- CLOSED-ON-BOTTOM-ONLY TUNNEL.

Figure 63.- Concluded.

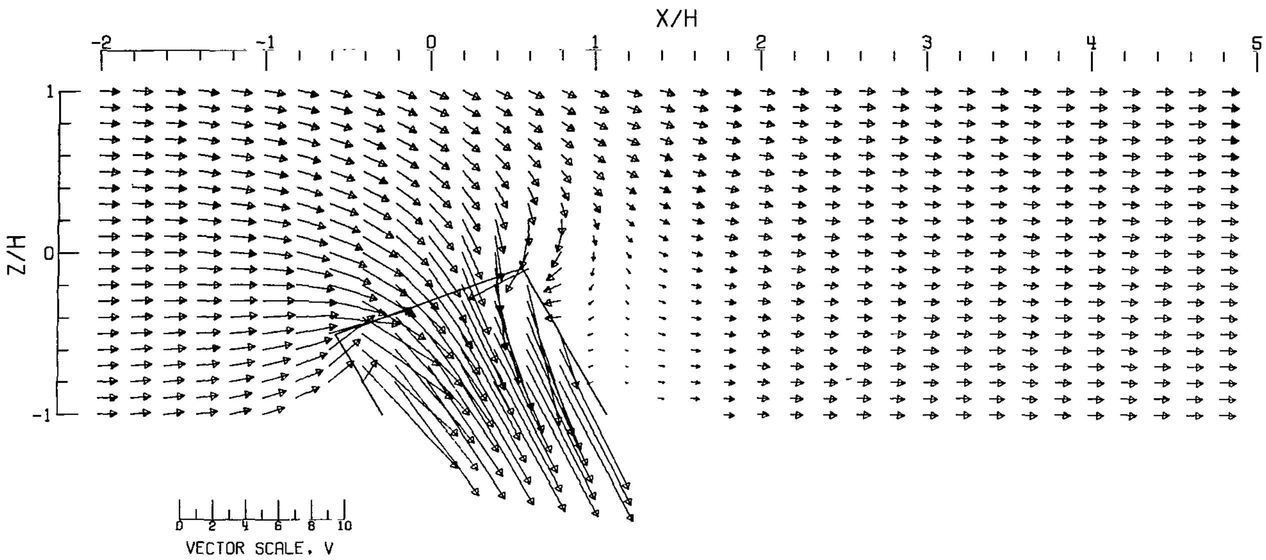

(A).- FREE AIR.

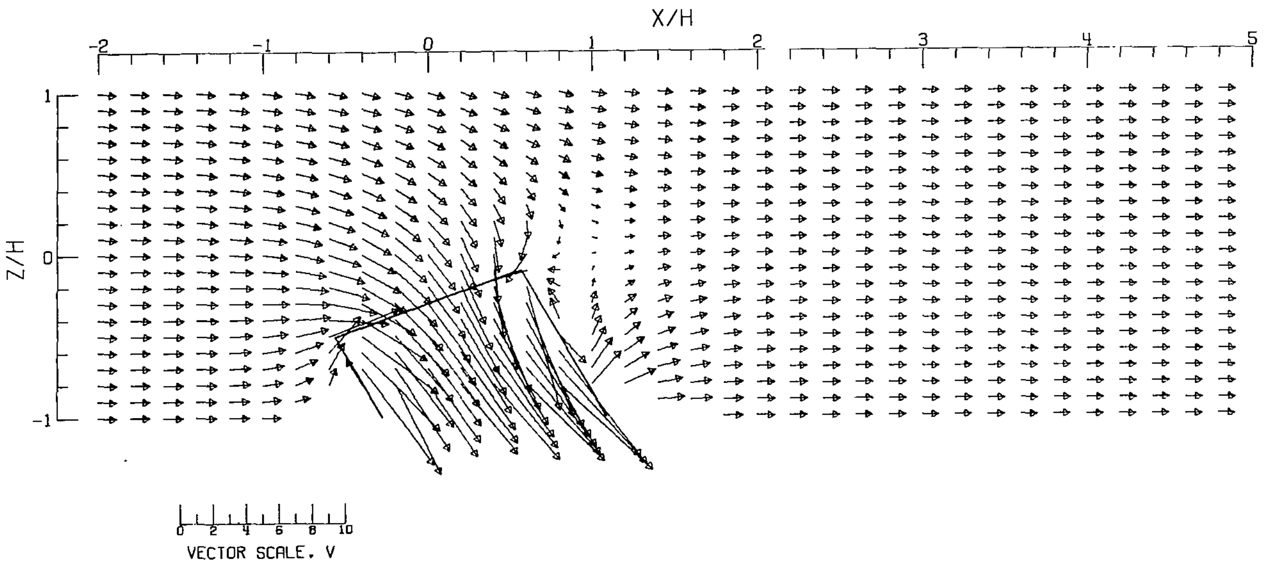

(B).- GROUND EFFECT.

Figure 64.- Flow vectors in the X-Z plane, calculated using doublet strings. The rotor and the edges of the wake are shown. ζ = 1.428; η = 1.0; γ = 1.0; σ = 0.600; α = -20.0°; χ = 30.0°; uniform loading.

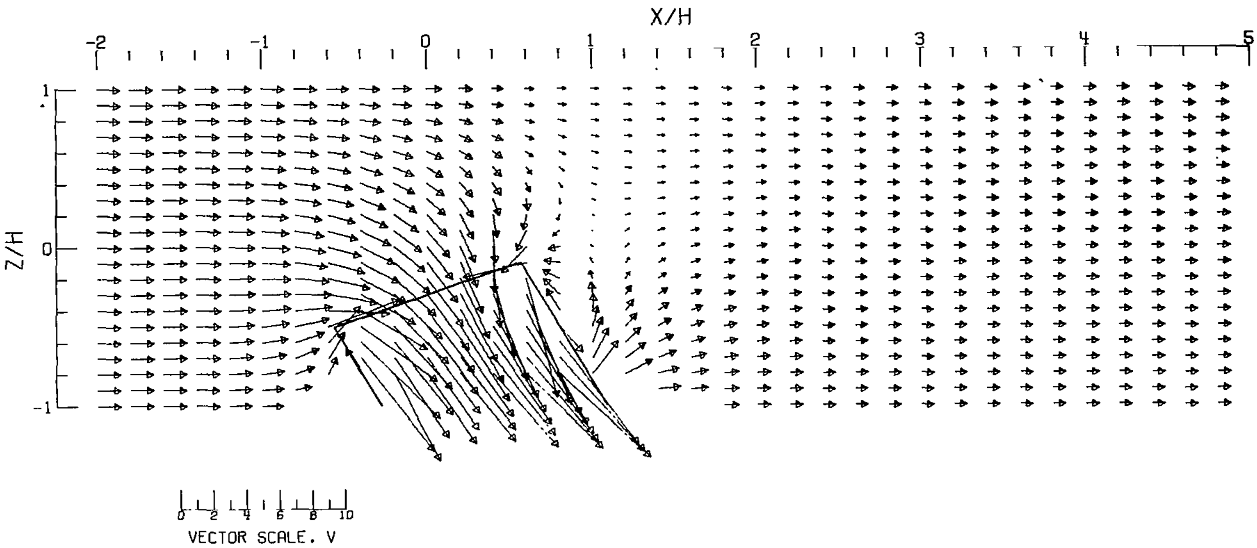

(C).- CLOSED TUNNEL.

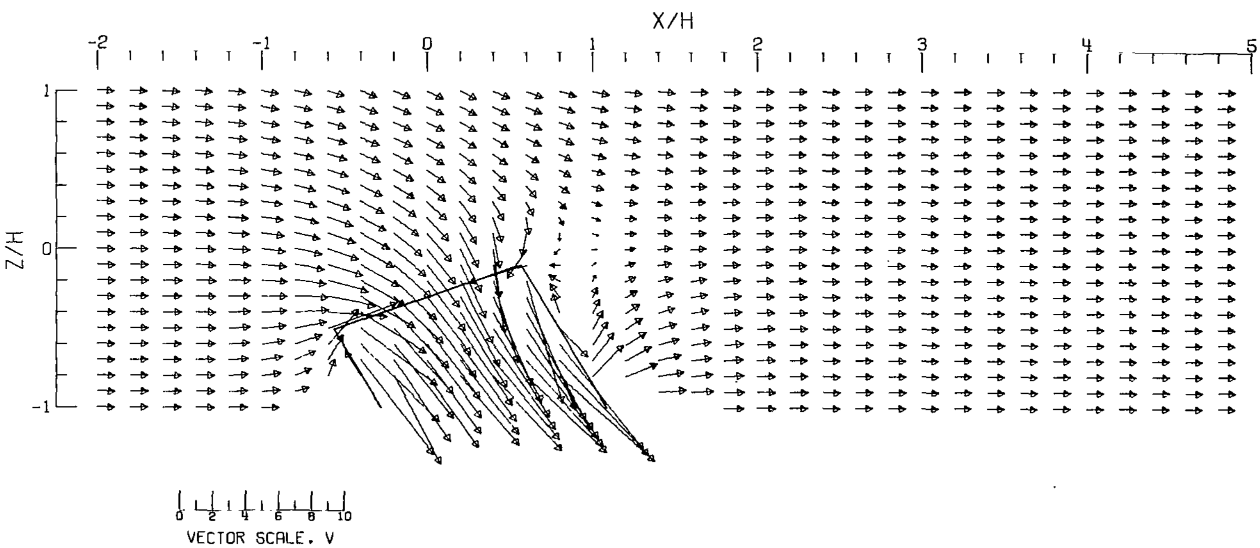

(D).- CLOSED-ON-BOTTOM-ONLY TUNNEL.

Figure 64.- Concluded.

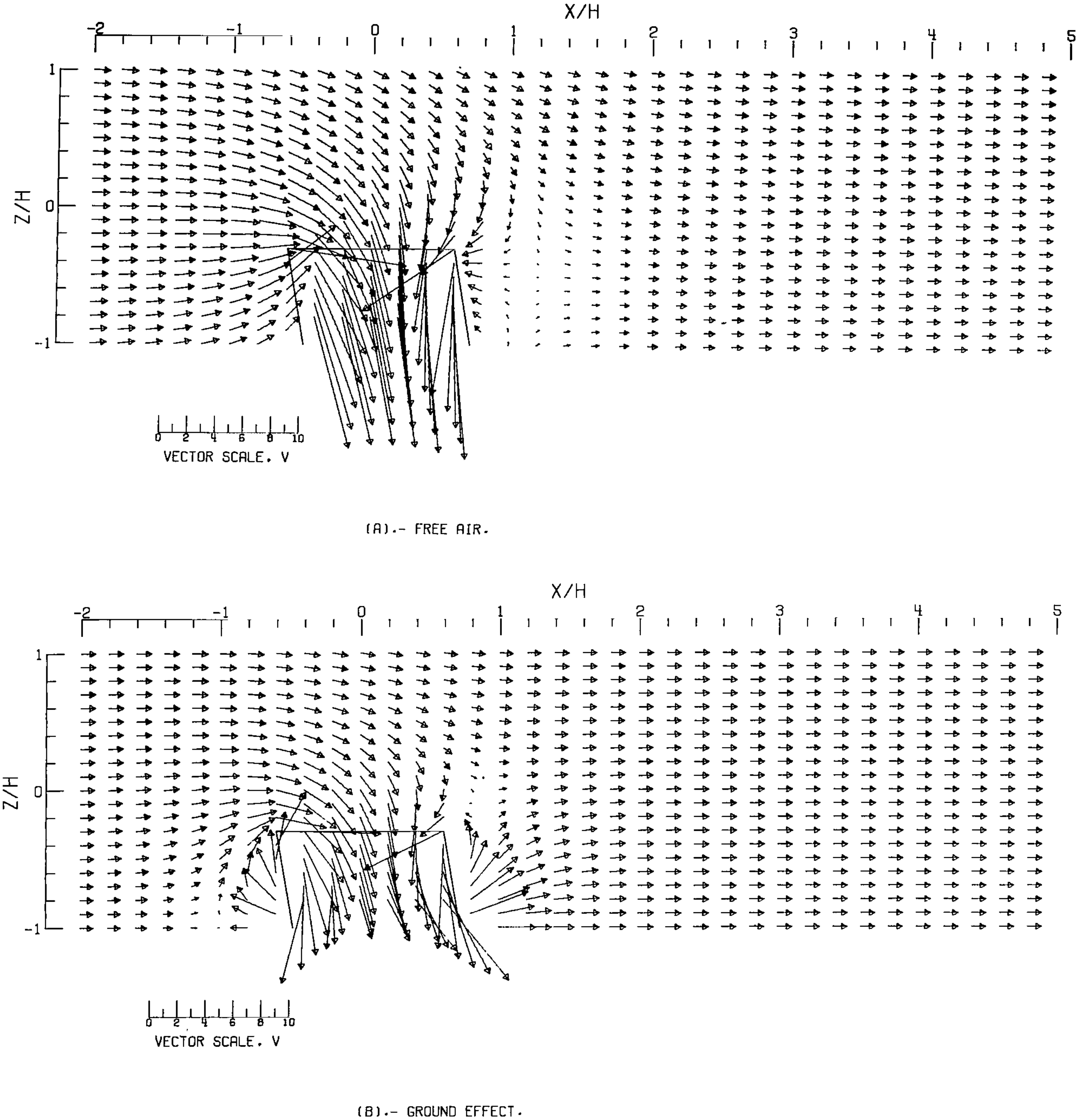

Figure 65.- Flow vectors in the X-Z plane, calculated using doublet strings. The rotor and the edges of the wake are shown. ζ = 1.428; η = 1.0; γ = 1.0; σ = 0.600; α = 0.0°; χ = 10.0°; uniform loading.

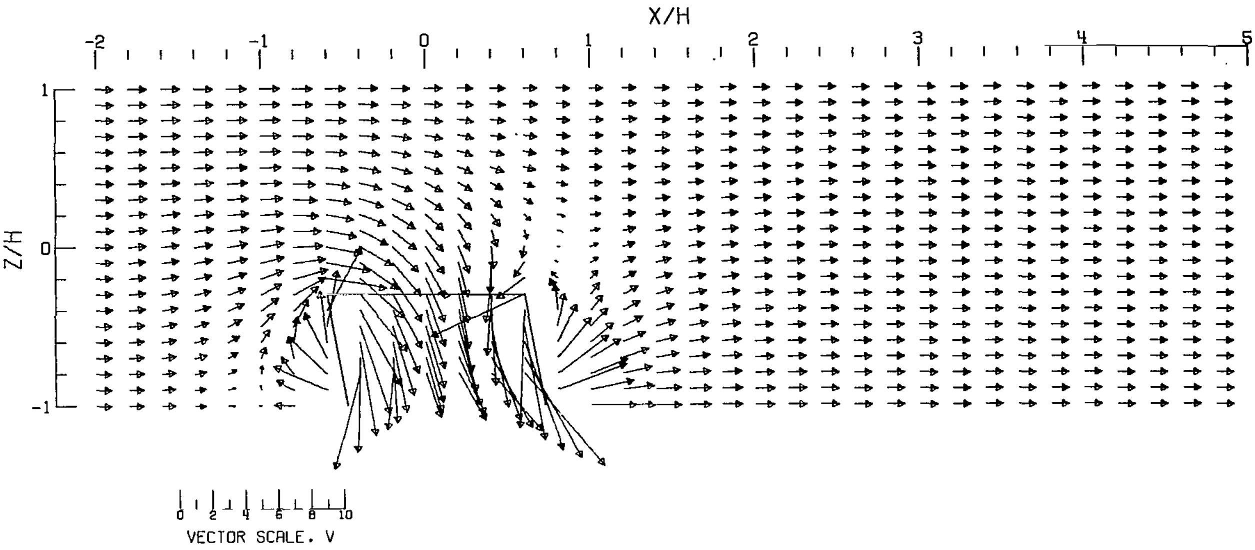

(C).- CLOSED TUNNEL.

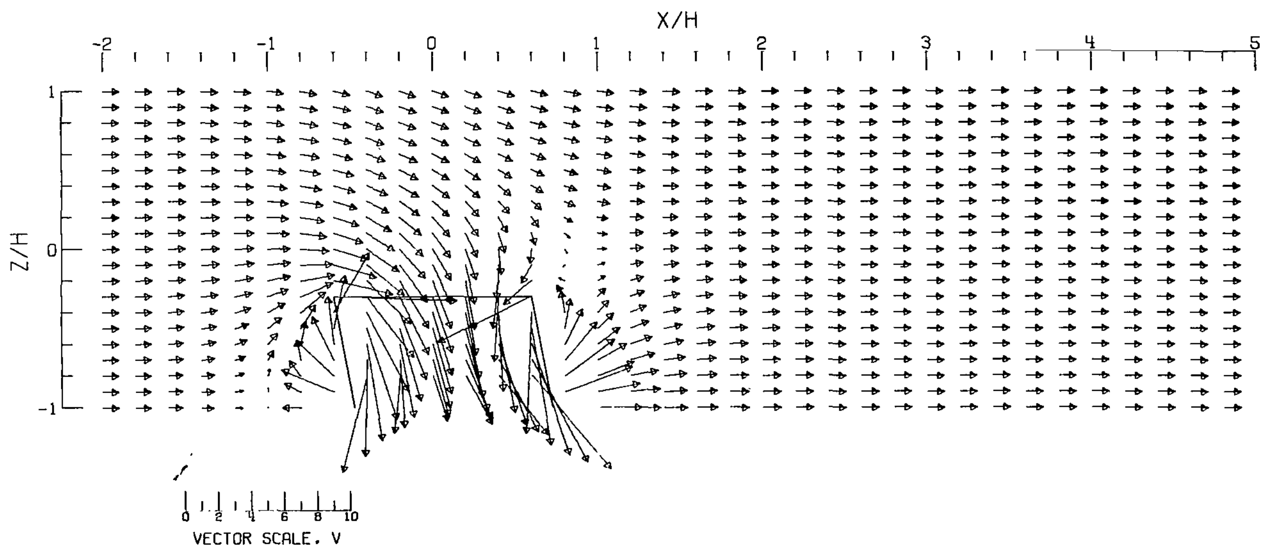

(D).- CLOSED-ON-BOTTOM-ONLY TUNNEL.

Figure 65.- Concluded.

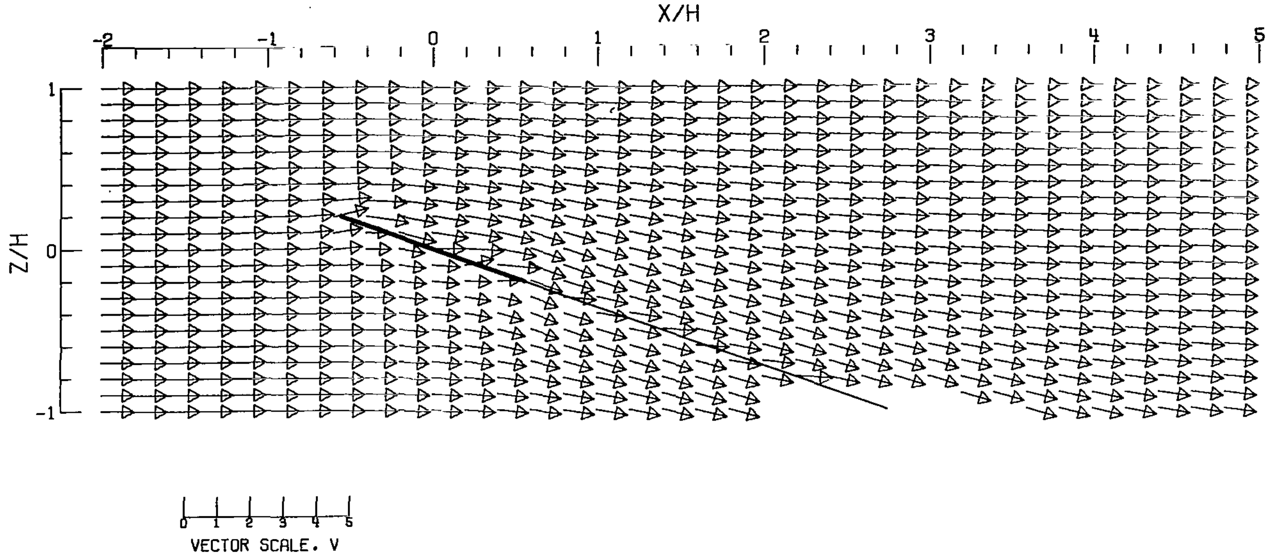

(A).– FREE AIR.

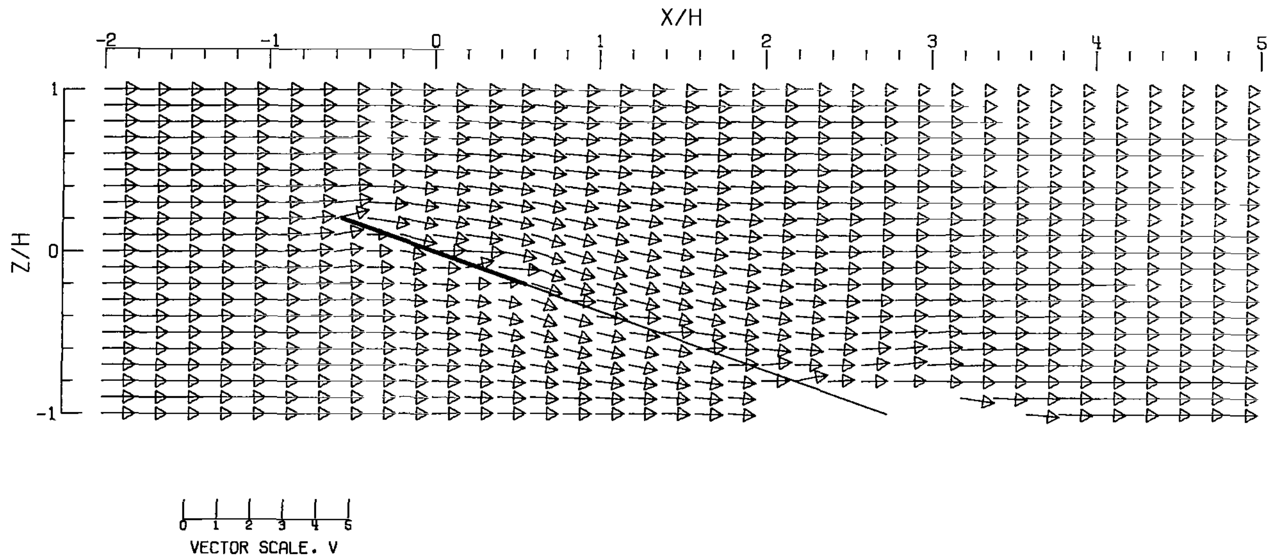

(B).– GROUND EFFECT.

Figure 66.- Flow vectors in the X-Z plane, calculated using doublet strings. The rotor and the edges of the wake are shown. $\zeta = 1.000$; $\eta = 1.000$; $\gamma = 1.000$; $\sigma = 0.600$; $\alpha = 20.000^{\circ}$; $\chi = 70.000^{\circ}$; triangular loading.

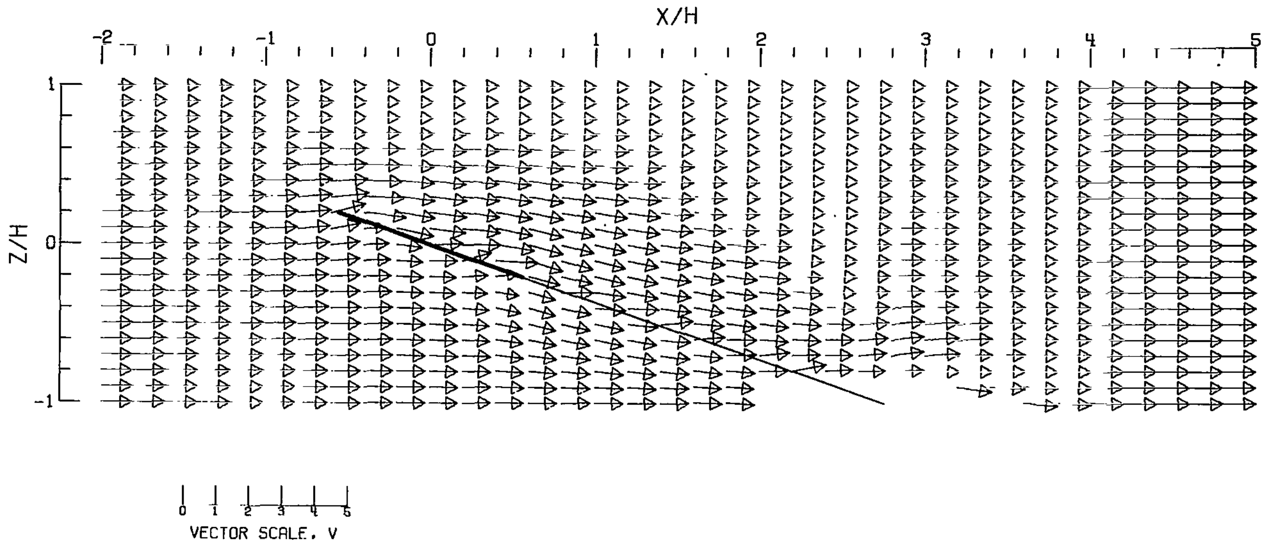

(C).- CLOSED TUNNEL.

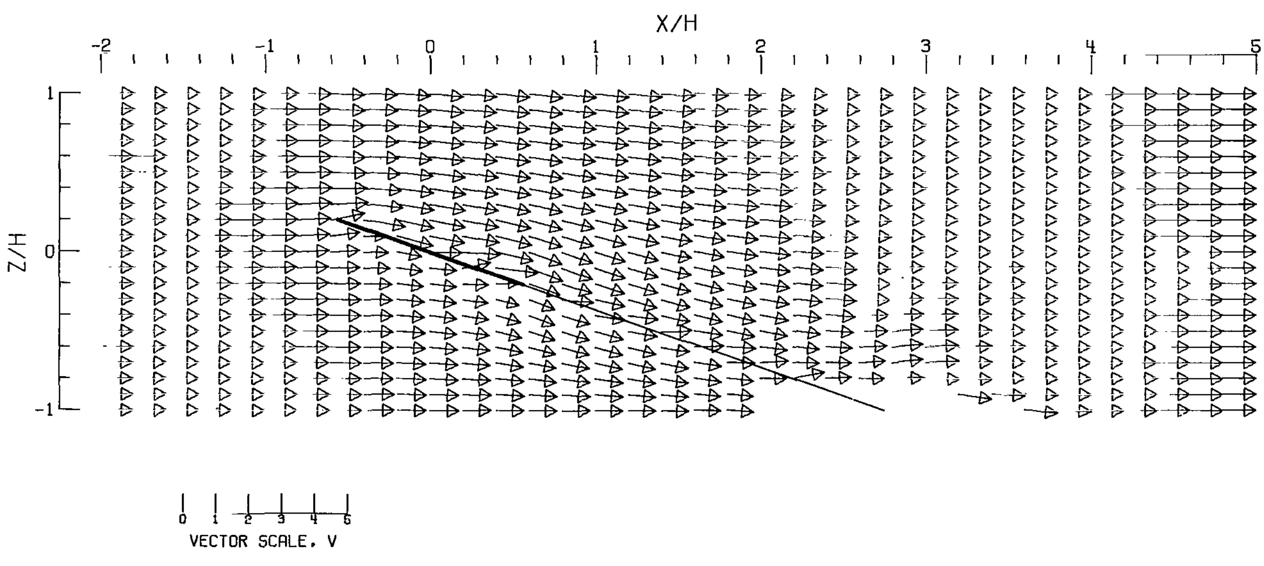

(D).- CLOSED-ON-BOTTOM-ONLY TUNNEL.

Figure 66.- Concluded.

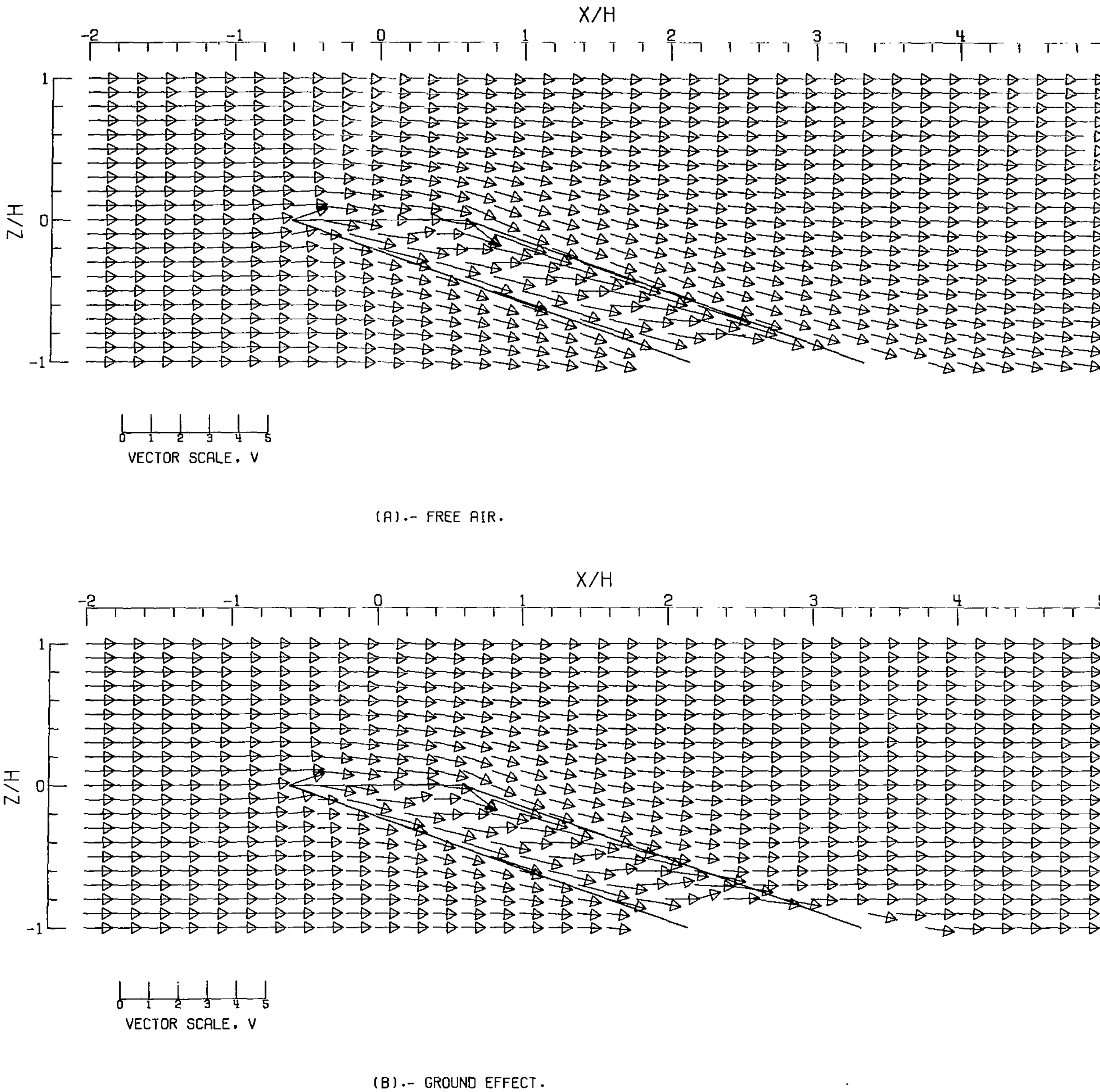

Figure 67.- Flow vectors in the X-Z plane, calculated using doublet strings. The rotor and the edges of the wake are shown. ζ = 1.000; η = 1.000; γ = 1.000; σ = 0.600; α = 0.000°; χ = 70.000°; triangular loading.

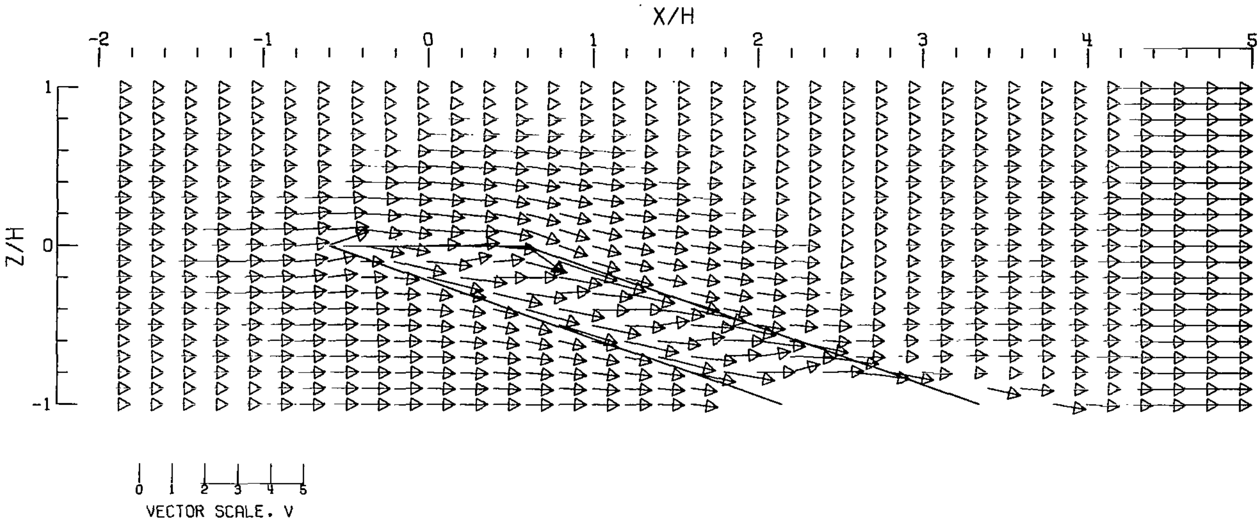

(C).- CLOSED TUNNEL.

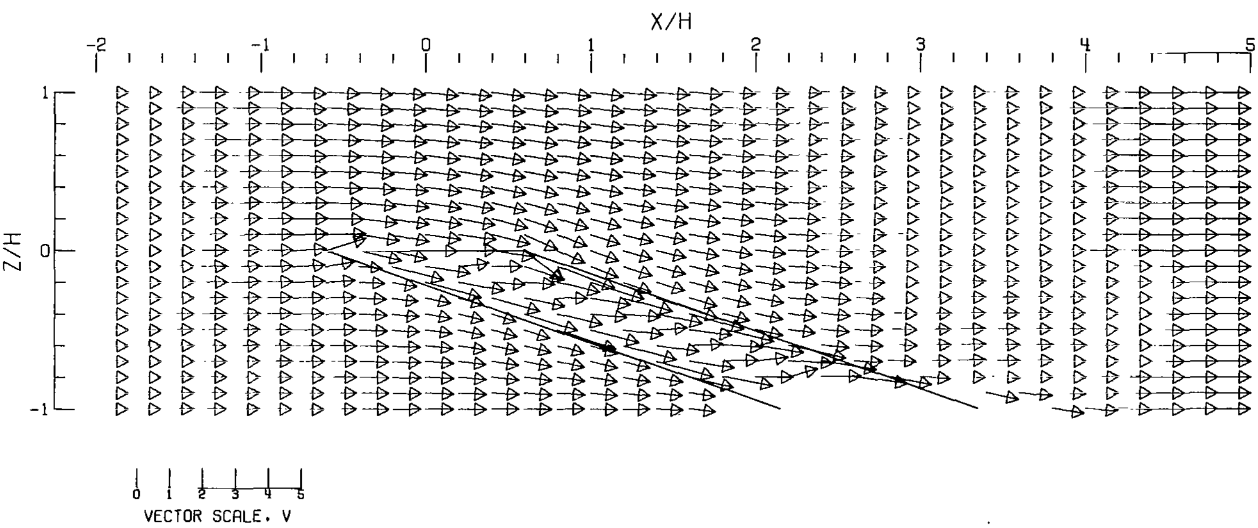

(D).- CLOSED-ON-BOTTOM-ONLY TUNNEL.

Figure 67.- Concluded.

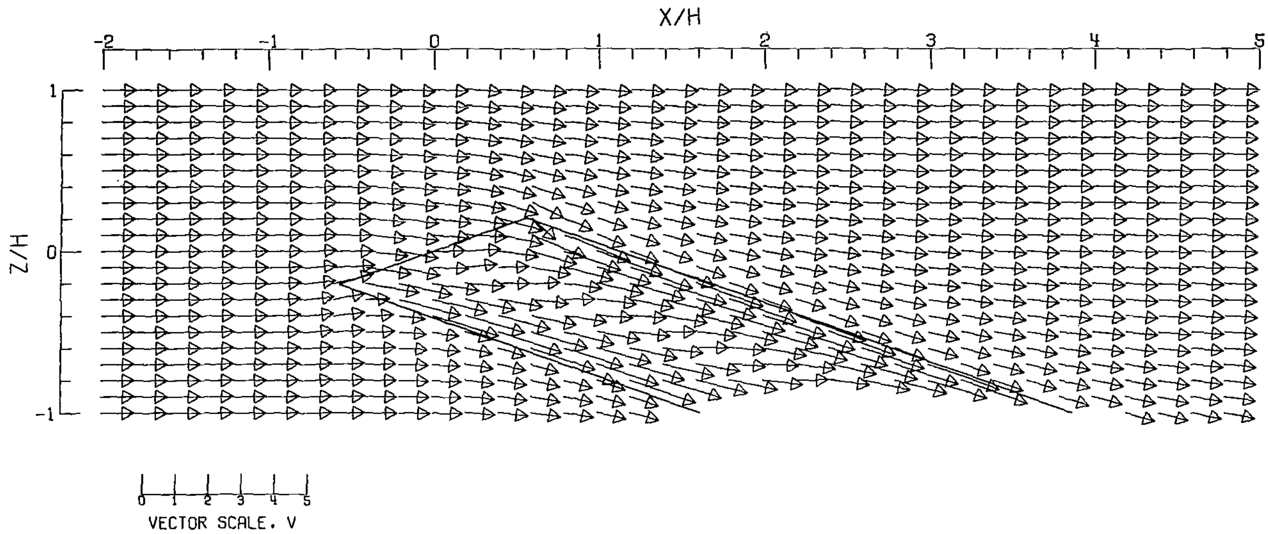

(A).- FREE AIR.

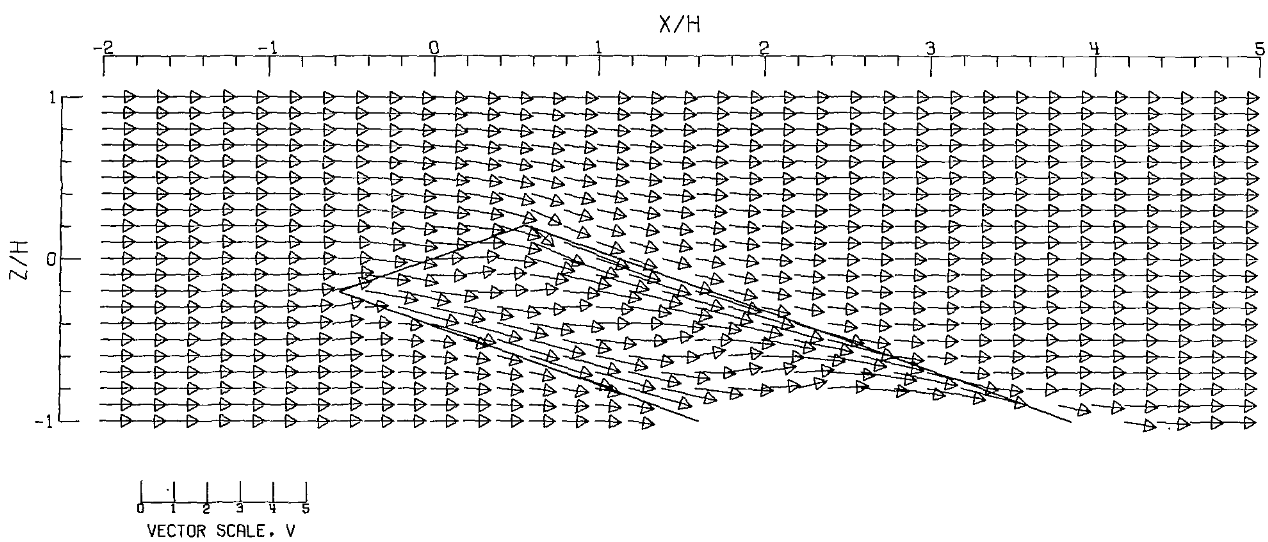

(B).- GROUND EFFECT.

Figure 68.- Flow vectors in the X-Z plane, calculated using doublet strings. The rotor and the edges of the wake are shown. ζ = 1.000; η = 1.000; γ = 1.000; σ = 0.600; α = -20.000°; χ = 70.000°; triangular loading.

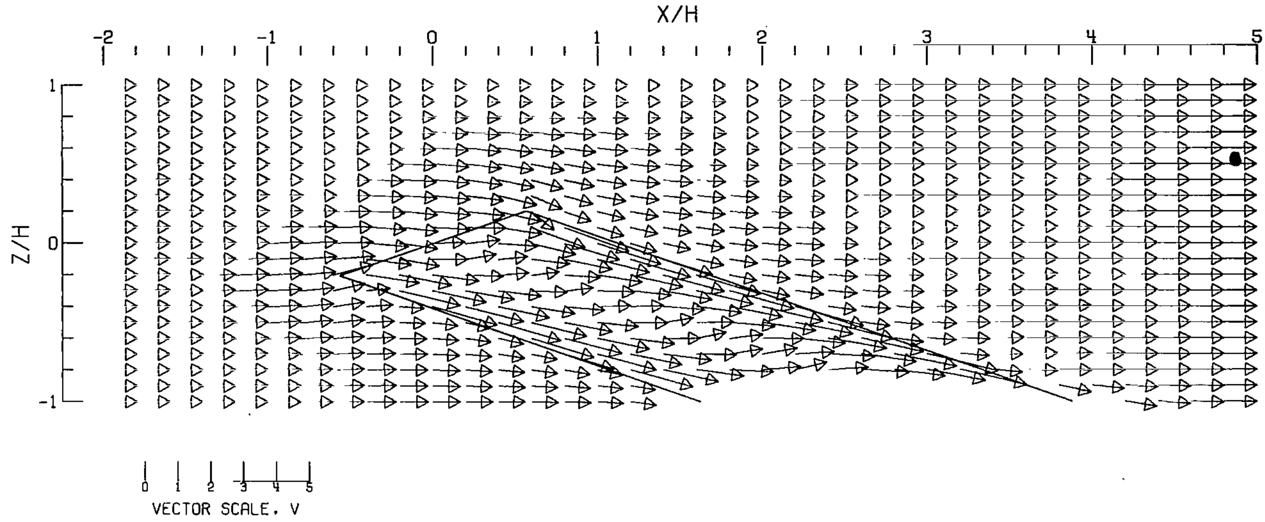

(C).- CLOSED TUNNEL.

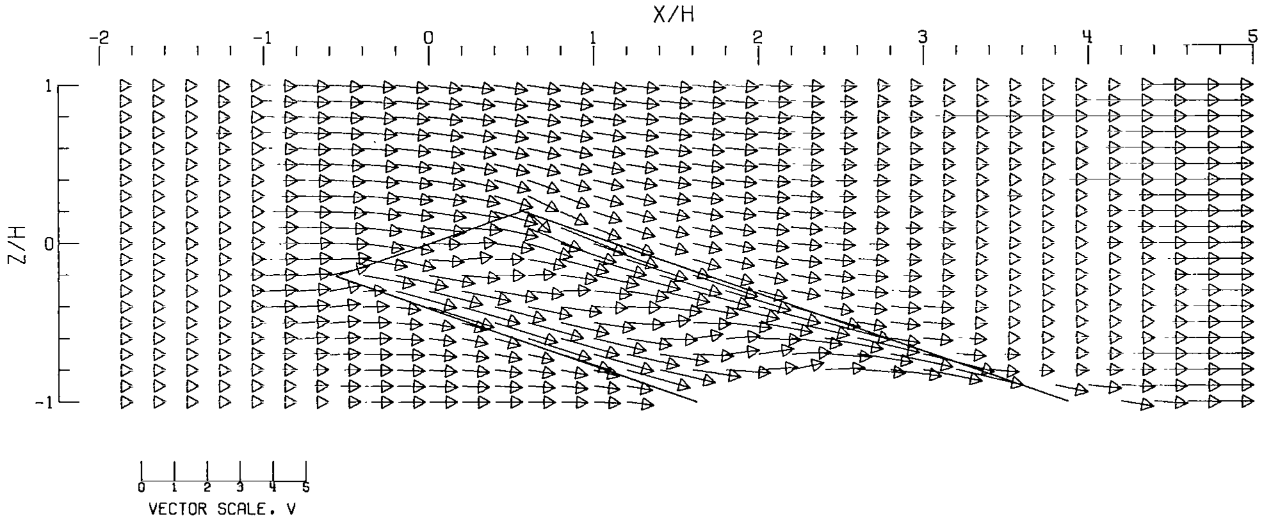

(D).- CLOSED-ON-BOTTOM-ONLY TUNNEL.

Figure 68.- Concluded.

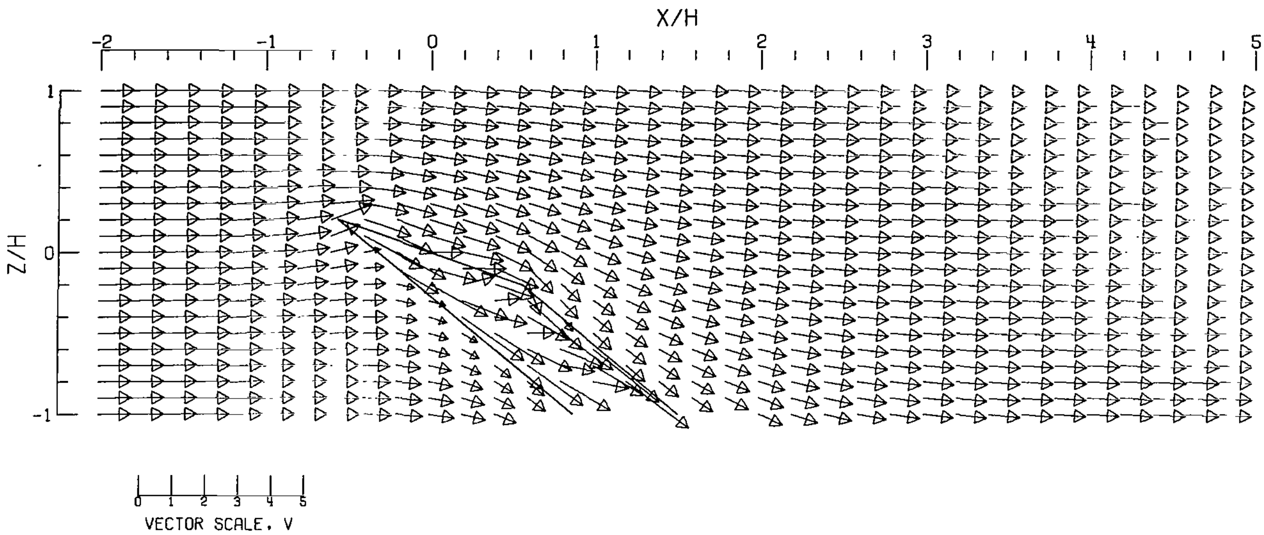

(A).- FREE AIR.

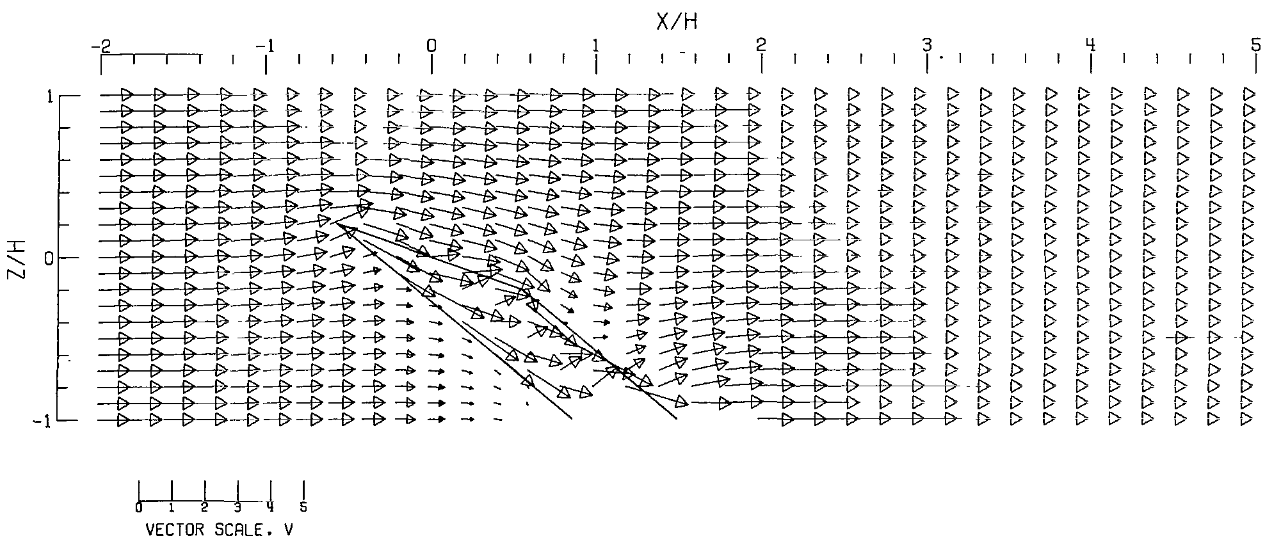

(B).- GROUND EFFECT.

Figure 69.- Flow vectors in the X-Z plane, calculated using doublet strings. The rotor and the edges of the wake are shown. $\zeta = 1.000$; $\eta = 1.000$; $\gamma = 1.000$; $\sigma = 0.600$; $\alpha = 20.000^{\circ}$; $\chi = 50.000^{\circ}$; triangular loading.

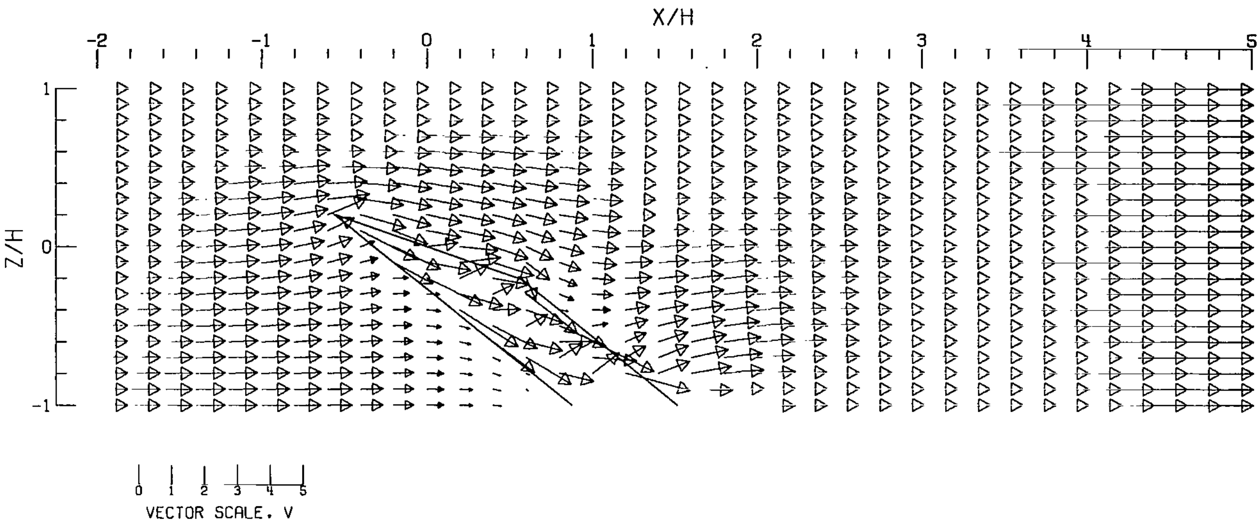

(C).- CLOSED TUNNEL.

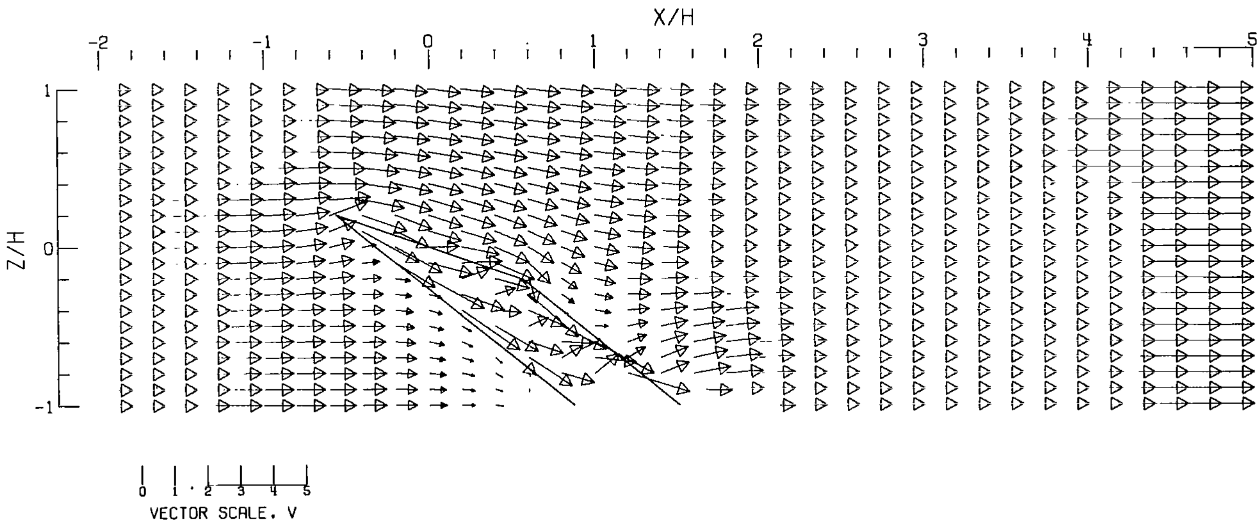

(D).- CLOSED-ON-BOTTOM-ONLY TUNNEL.

Figure 69.- Concluded.

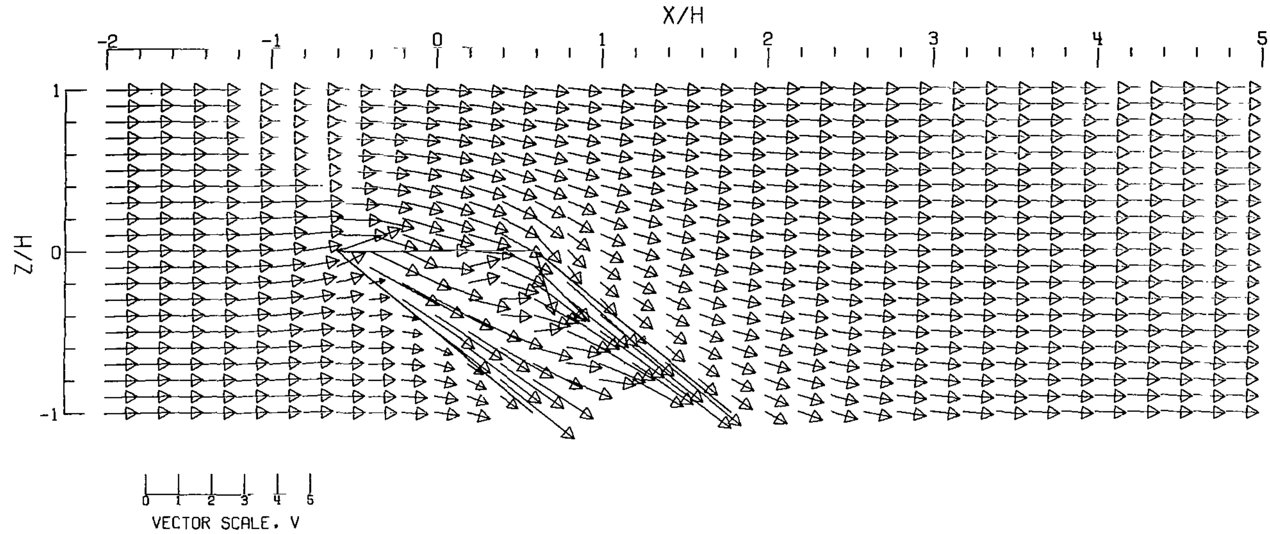

(A).- FREE AIR.

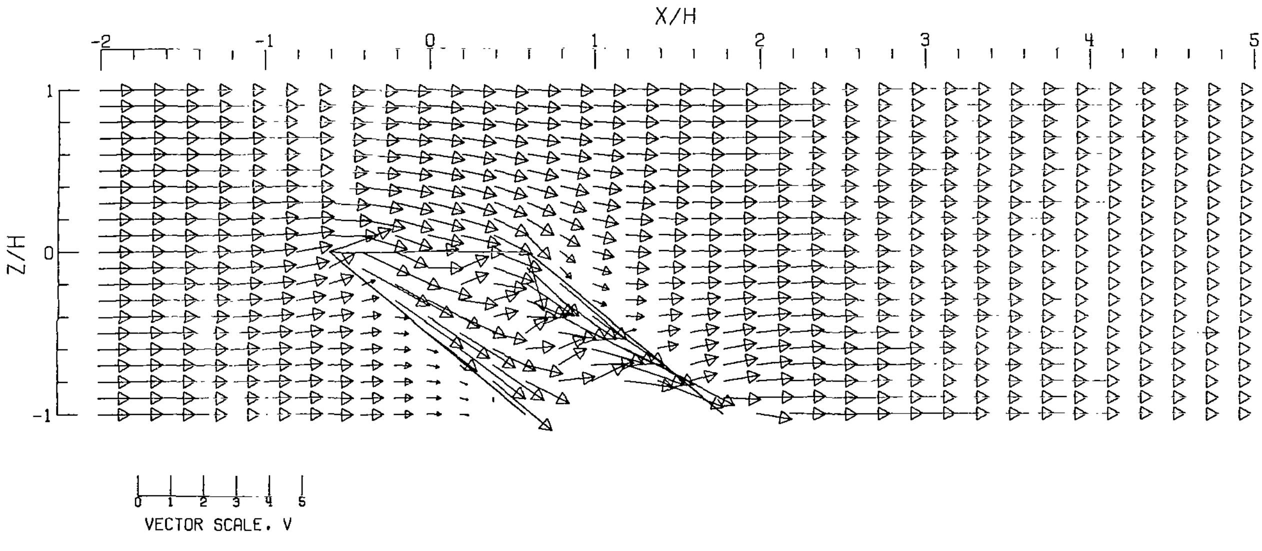

(B).- GROUND EFFECT.

Figure 70.- Flow vectors in the X-Z plane, calculated using doublet strings. The rotor and the edges of the wake are shown. ζ = 1.000; η = 1.0; γ = 1.0; σ = 0.600; α = 0.0°; χ = 50.0°; triangular loading.

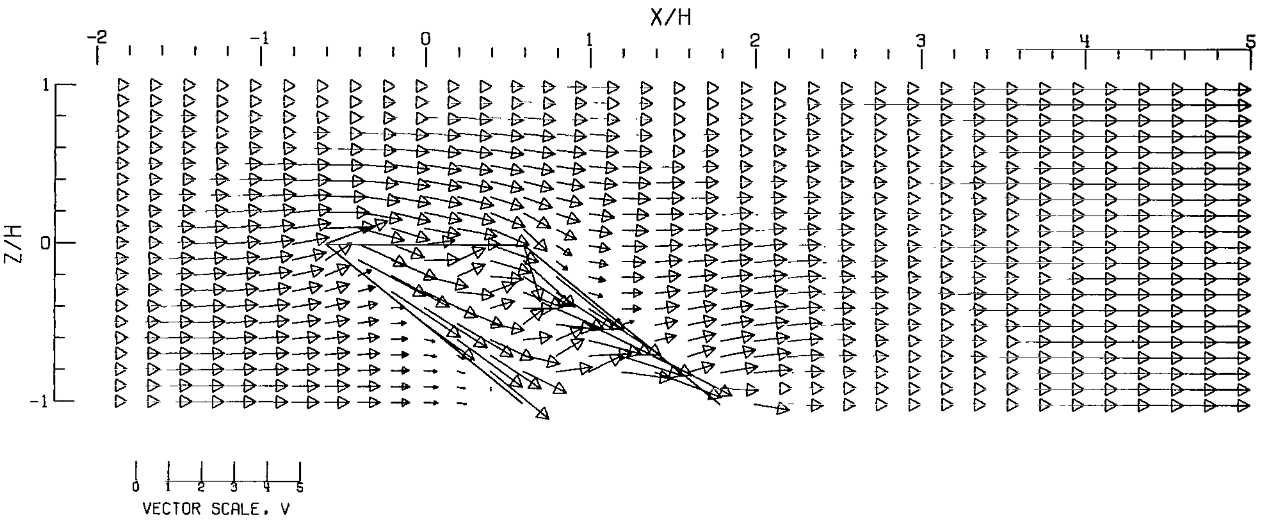

(C).- CLOSED TUNNEL.

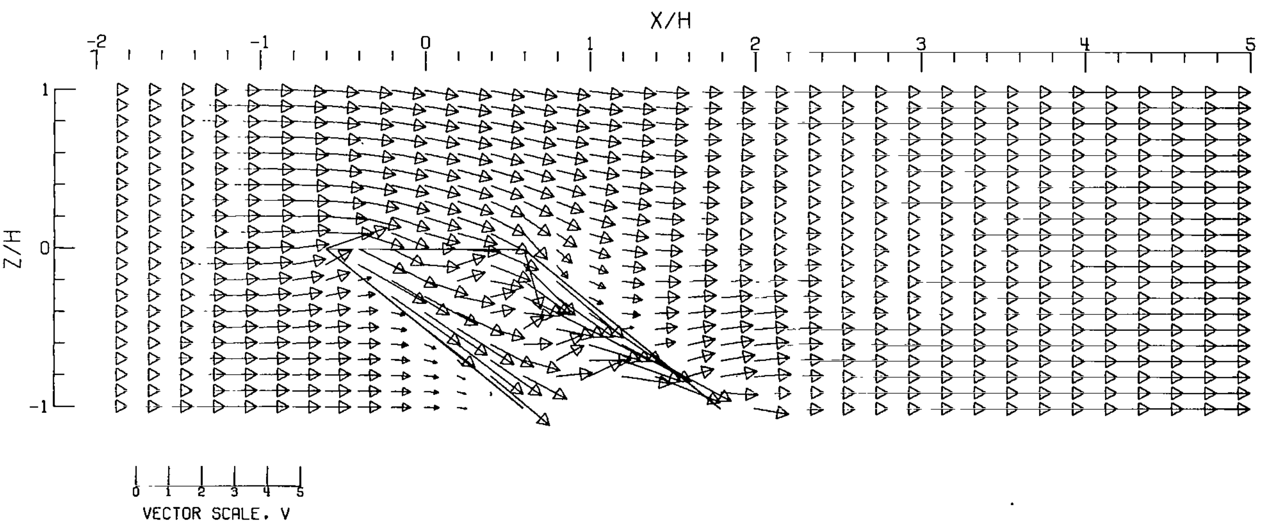

(D).- CLOSED-ON-BOTTOM-ONLY TUNNEL.

Figure 70.- Concluded.

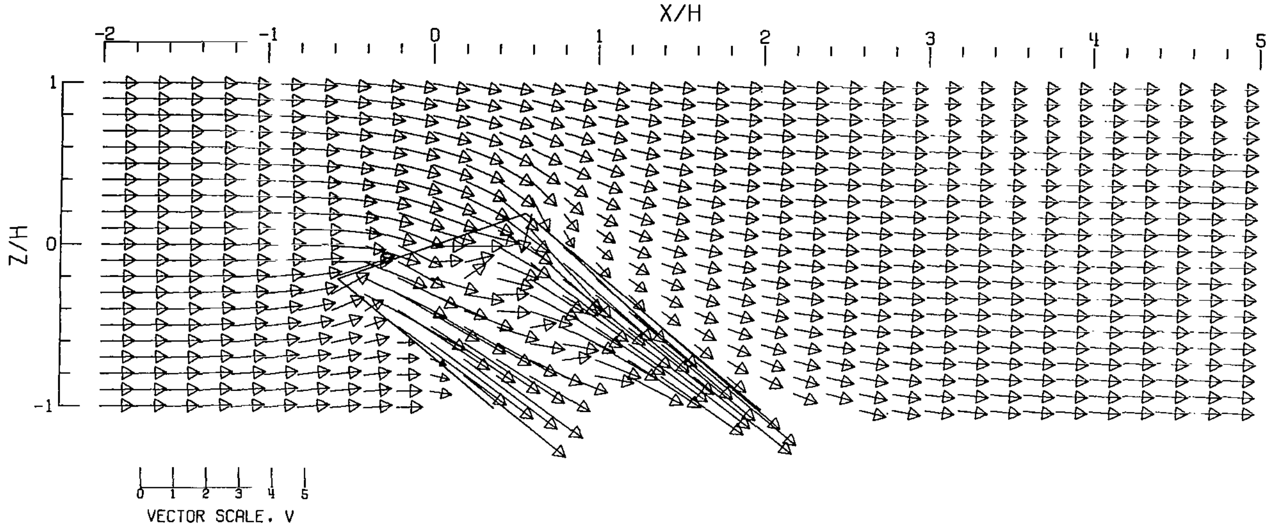

(A).- FREE AIR.

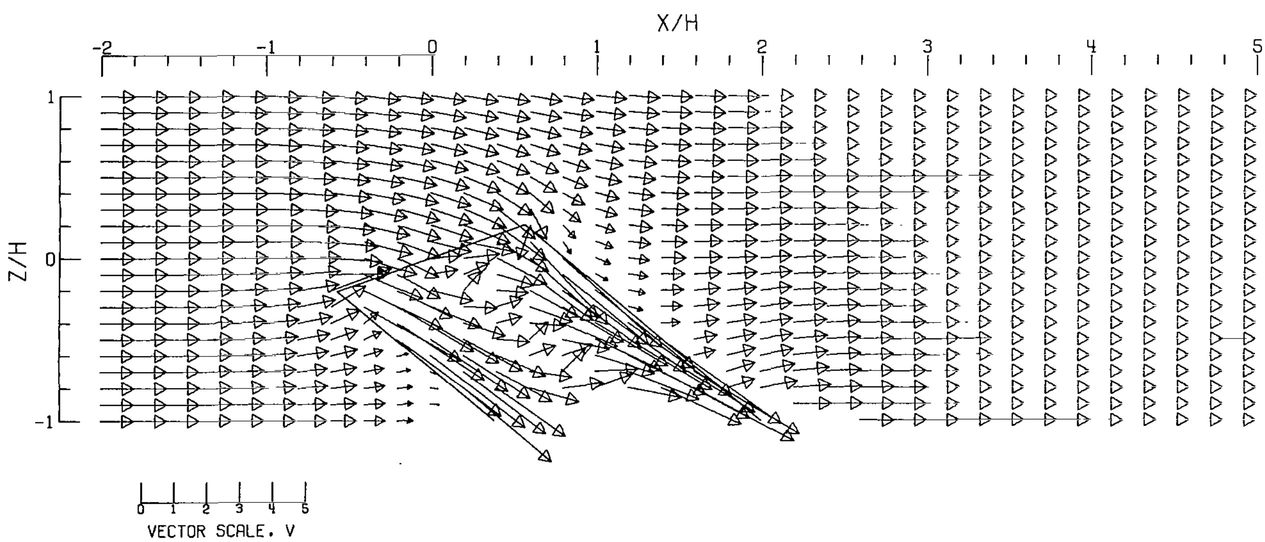

(B).- GROUND EFFECT.

Figure 71.- Flow vectors in the X-Z plane, calculated using doublet strings. The rotor and the edges of the wake are shown. ζ = 1.000; η = 1.000; γ = 1.000; σ = 0.600; α = -20.000°; χ = 50.000°; triangular loading.

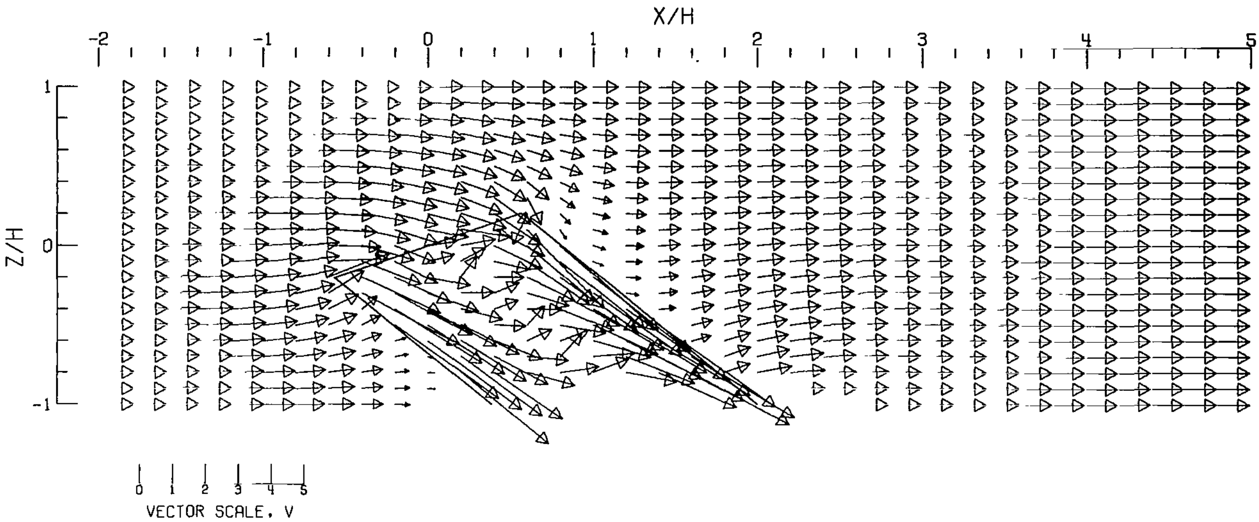

(C).- CLOSED TUNNEL.

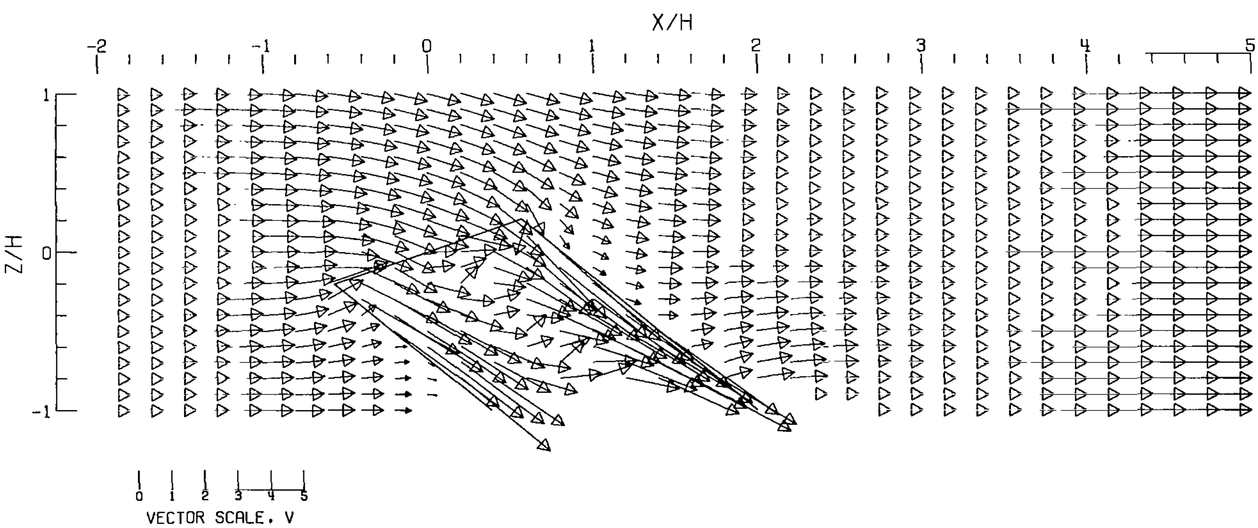

(D).- CLOSED-ON-BOTTOM-ONLY TUNNEL.

Figure 71.- Concluded.

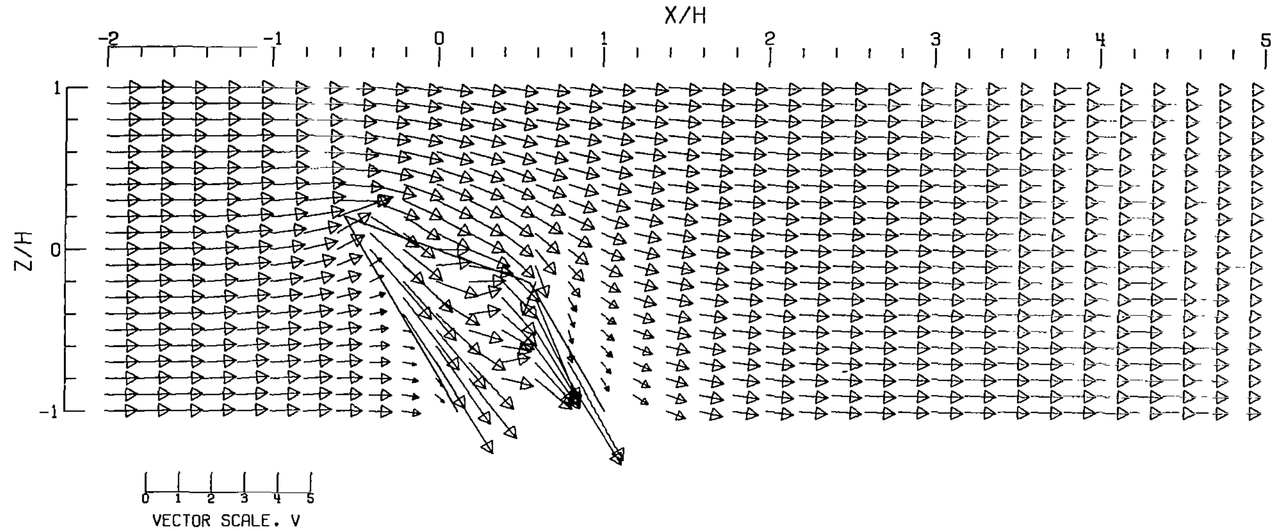

(A).- FREE AIR.

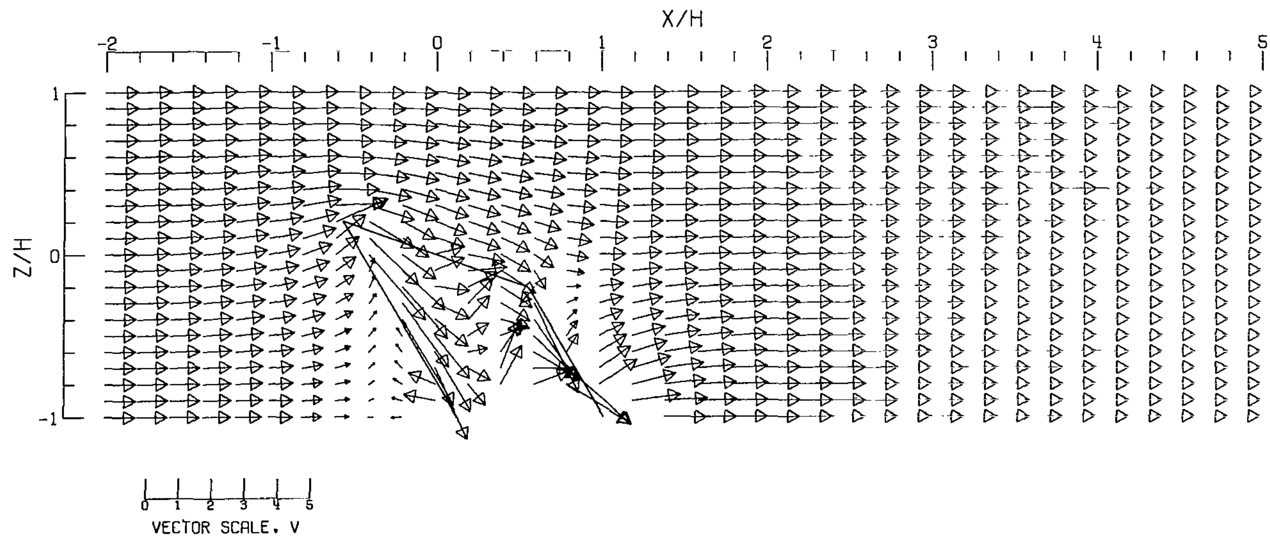

(B).- GROUND EFFECT.

Figure 72.- Flow vectors in the X-Z plane, calculated using doublet strings. The rotor and the edges of the wake are shown. ζ = 1.000; η = 1.000; γ = 1.000; σ = 0.600; α = 20.000°; χ = 30.000°; triangular loading.

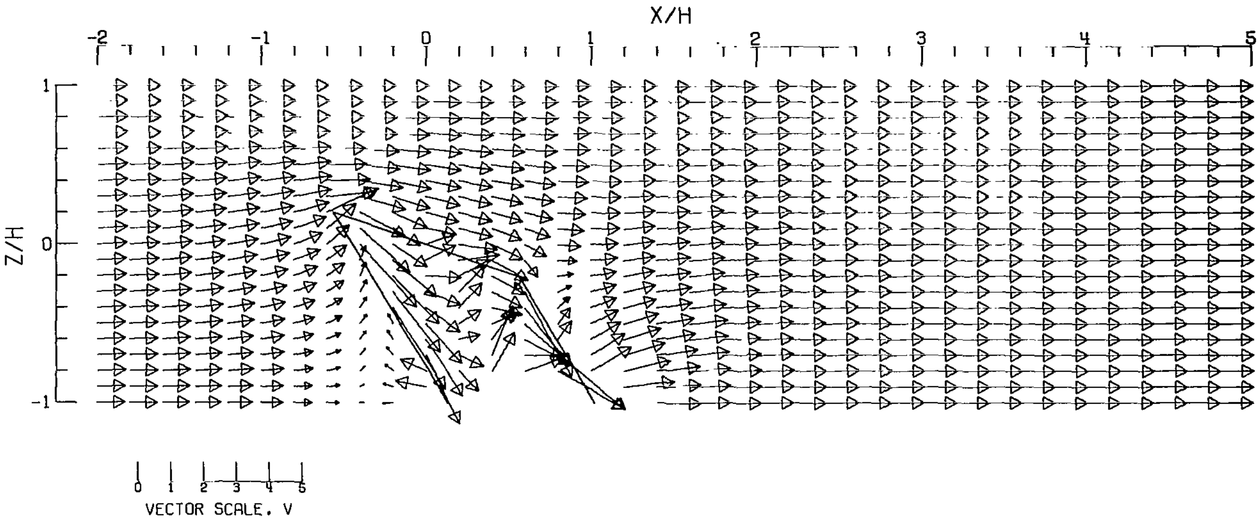

(C).- CLOSED TUNNEL.

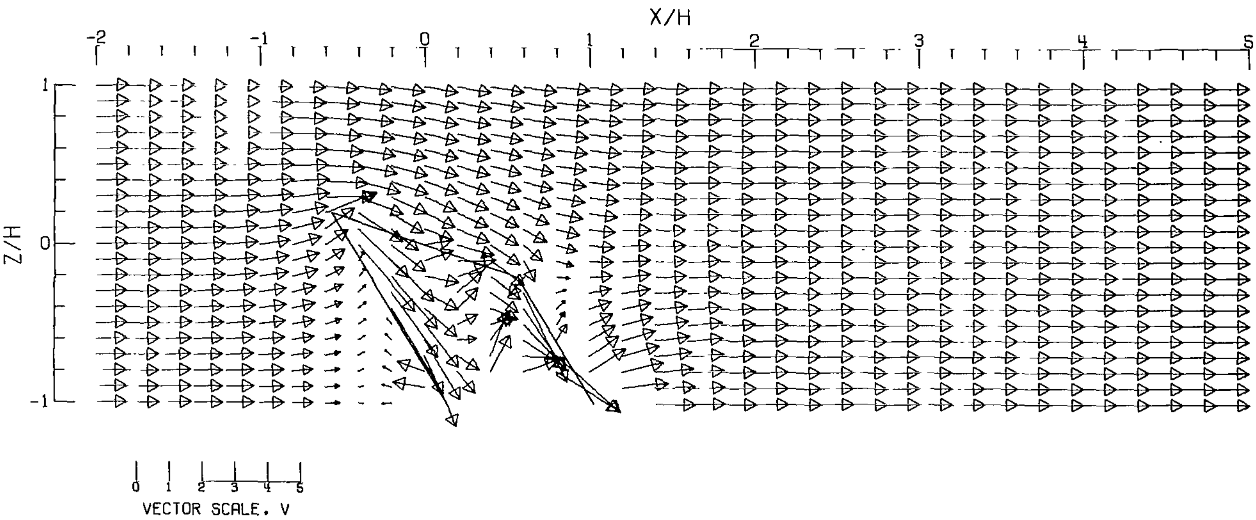

(D).- CLOSED-ON-BOTTOM-ONLY TUNNEL.

Figure 72.- Concluded.

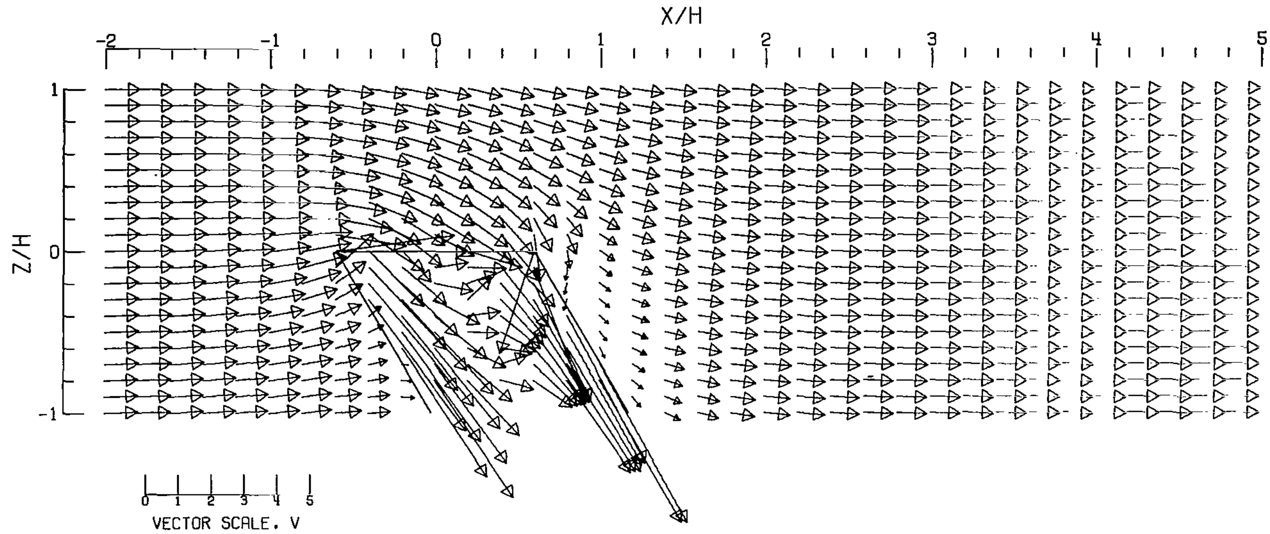

(A).– FREE AIR.

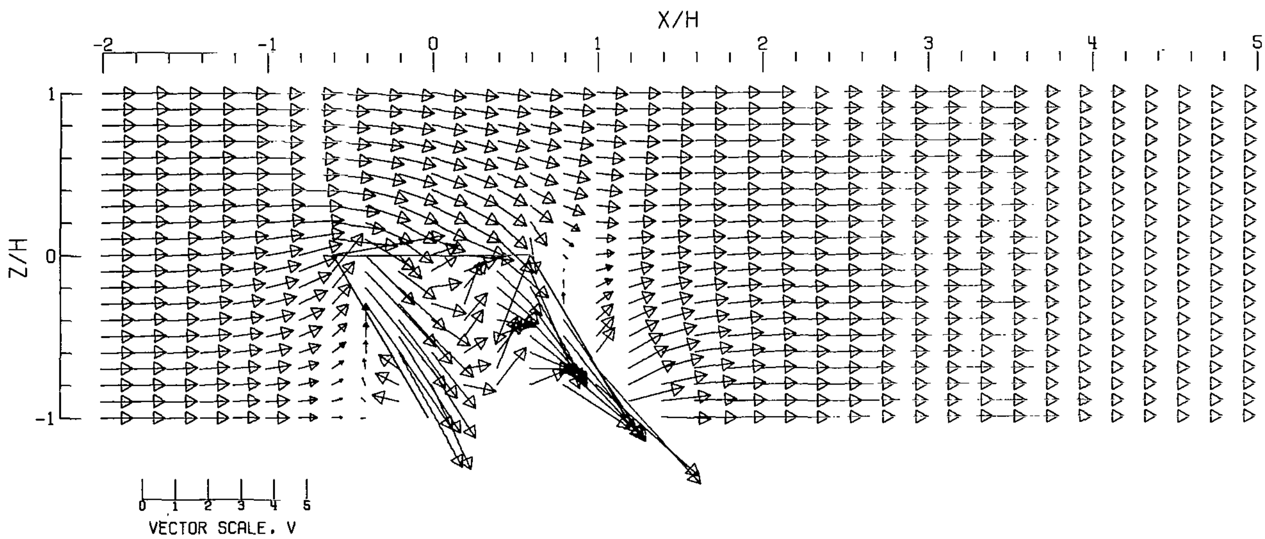

(B).– GROUND EFFECT.

Figure 73.- Flow vectors in the X-Z plane, calculated using doublet strings. The rotor and the edges of the wake are shown. ζ = 1.000; η = 1.000; γ = 1.000; σ = 0.600; α = 0.000°; χ = 30.000°; triangular loading.

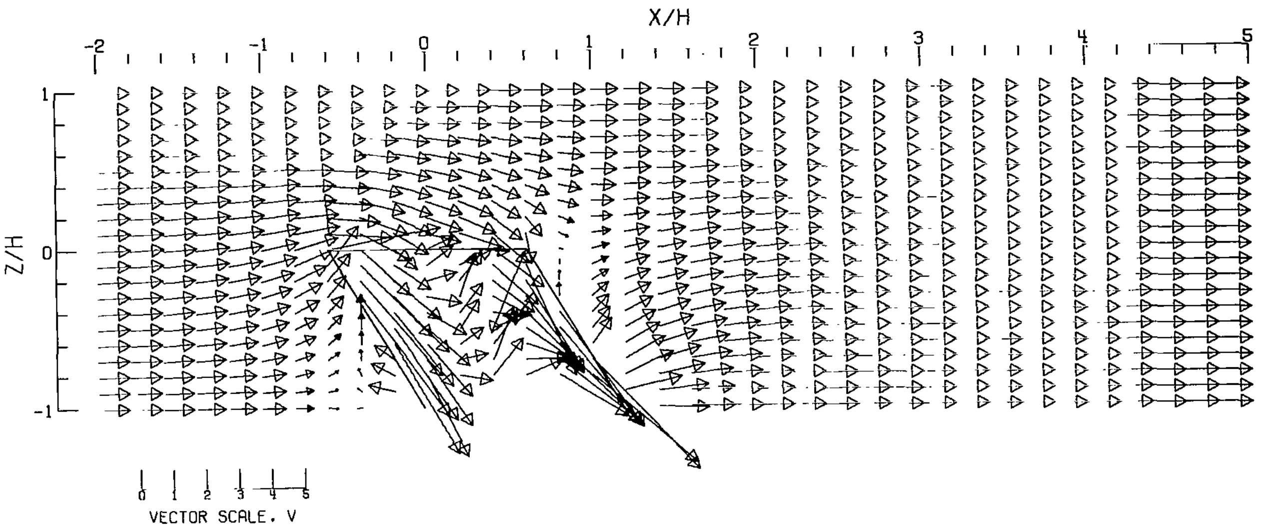

(C).- CLOSED TUNNEL.

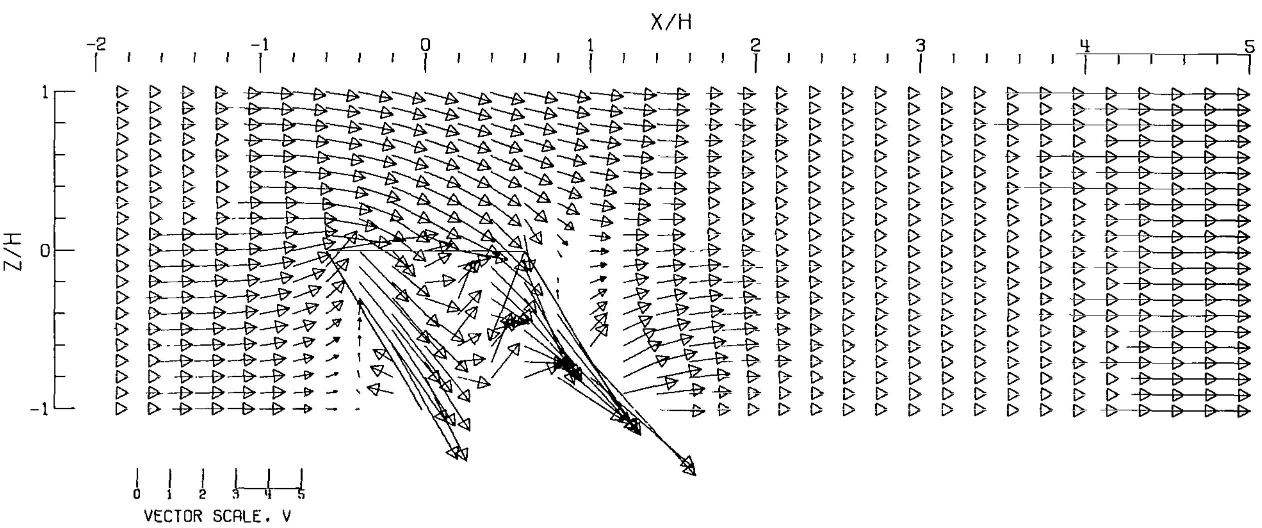

(D).- CLOSED-ON-BOTTOM-ONLY TUNNEL.

Figure 73.- Concluded.

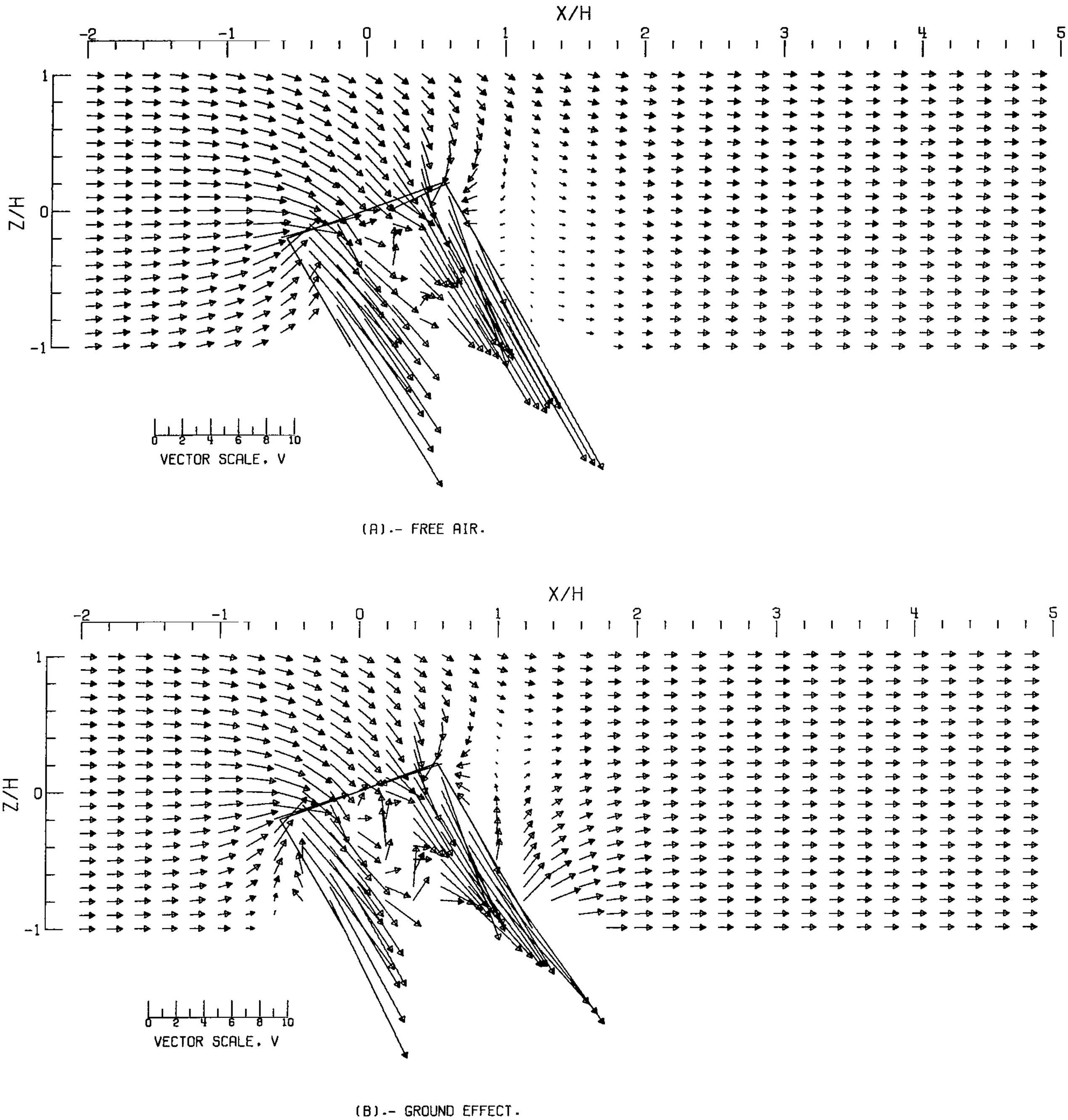

Figure 74.- Flow vectors in the X-Z plane, calculated using doublet strings. The rotor and the edges of the wake are shown. ζ = 1.000; η = 1.000; γ = 1.000; σ = 0.600; α = -20.000^0; χ = 30.000^0; triangular loading.

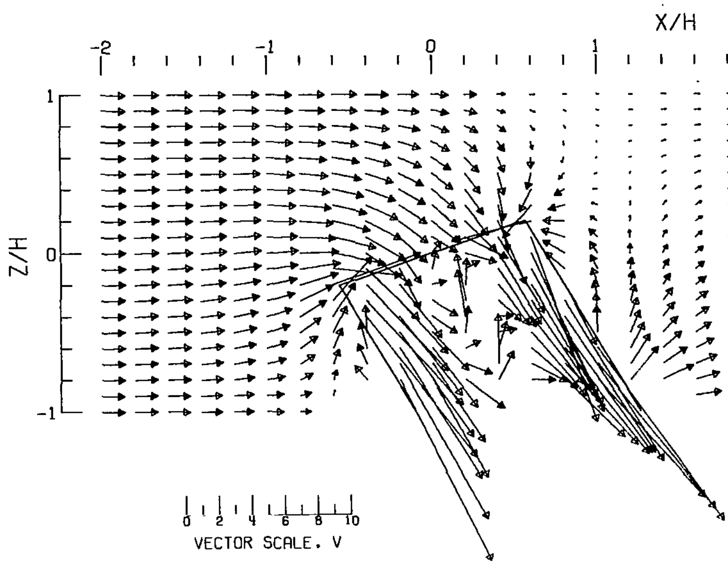

(C).- CLOSED TUNNEL.

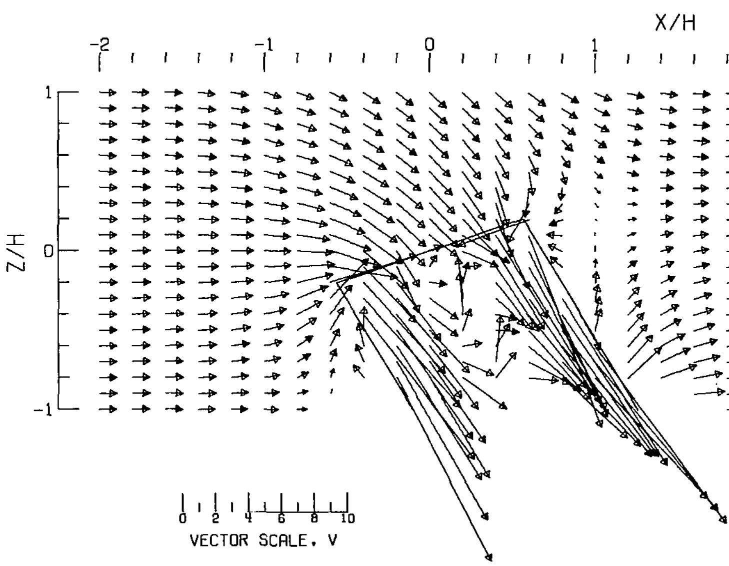

(D).- CLOSED-ON-BOTTOM-ONLY TUNNEL.

Figure 74.- Concluded.

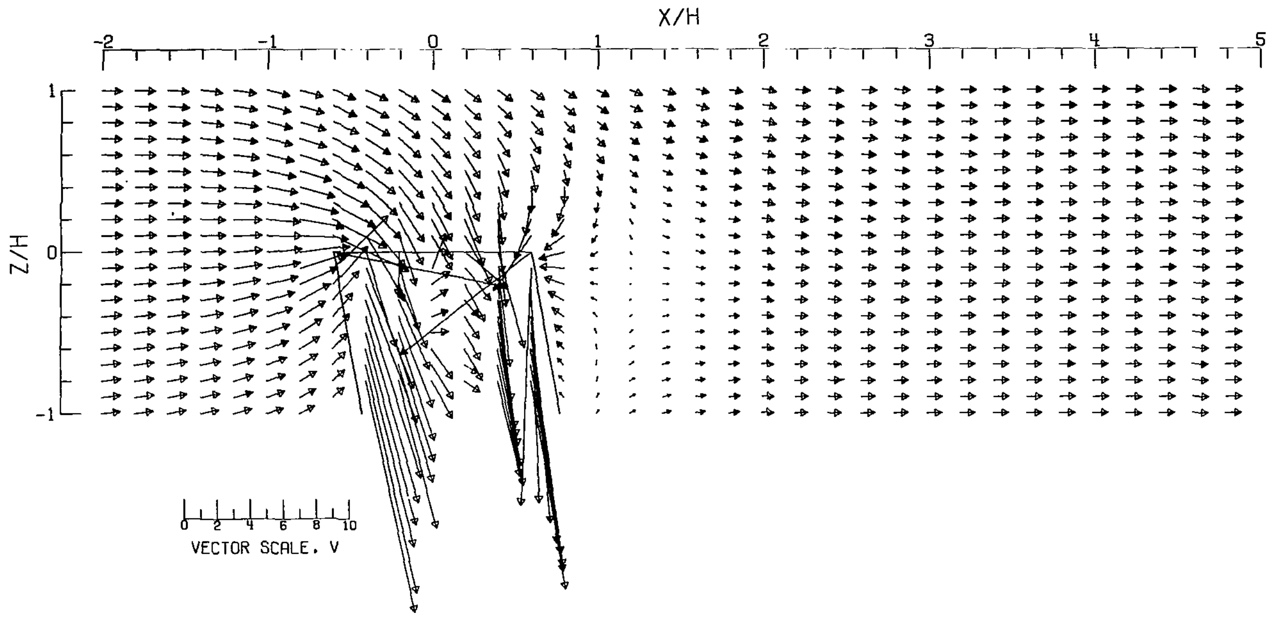

(A).- FREE AIR.

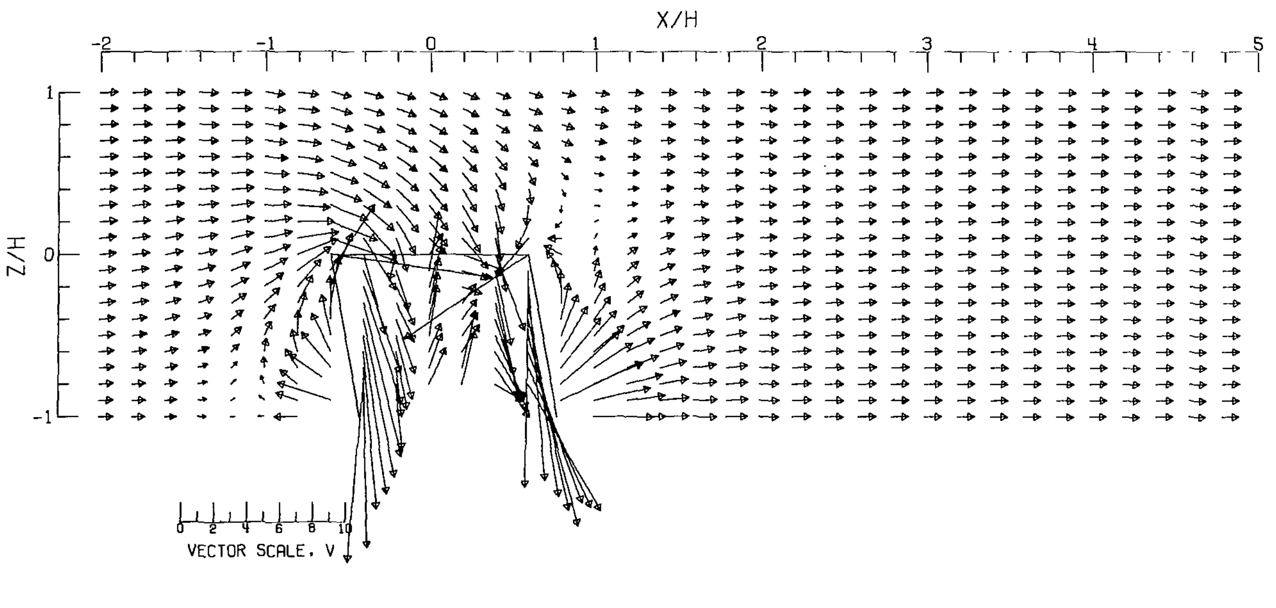

(B).- GROUND EFFECT.

Figure 75.- Flow vectors in the X-Z plane, calculated using doublet strings. The rotor and the edges of the wake are shown. $\zeta = 1.000$; $\eta = 1.000$; $\gamma = 1.000$; $\sigma = 0.600$; $\alpha = 0.000^{\circ}$; $\chi = 10.000^{\circ}$; triangular loading.

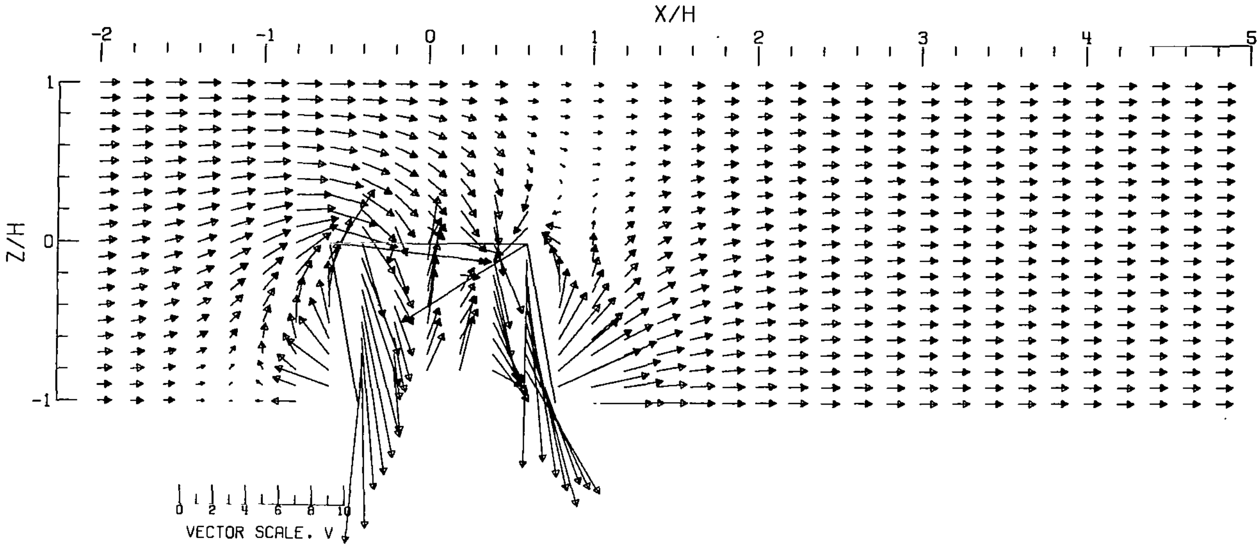

(C).- CLOSED TUNNEL.

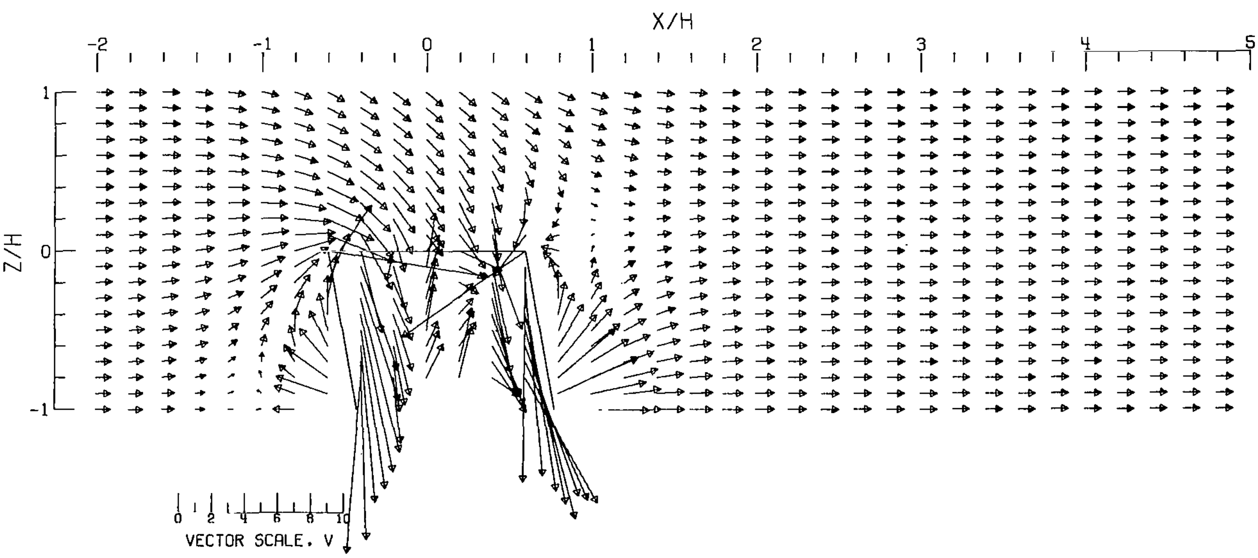

(D).- CLOSED-ON-BOTTOM-ONLY TUNNEL.

Figure 75.- Concluded.

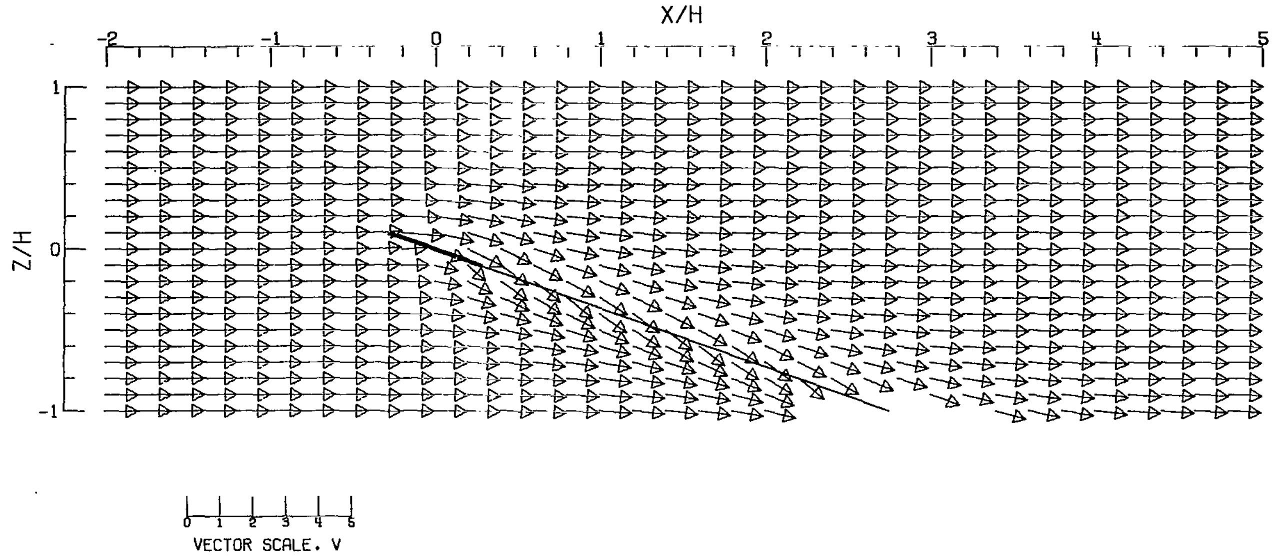

(A).- FREE AIR.

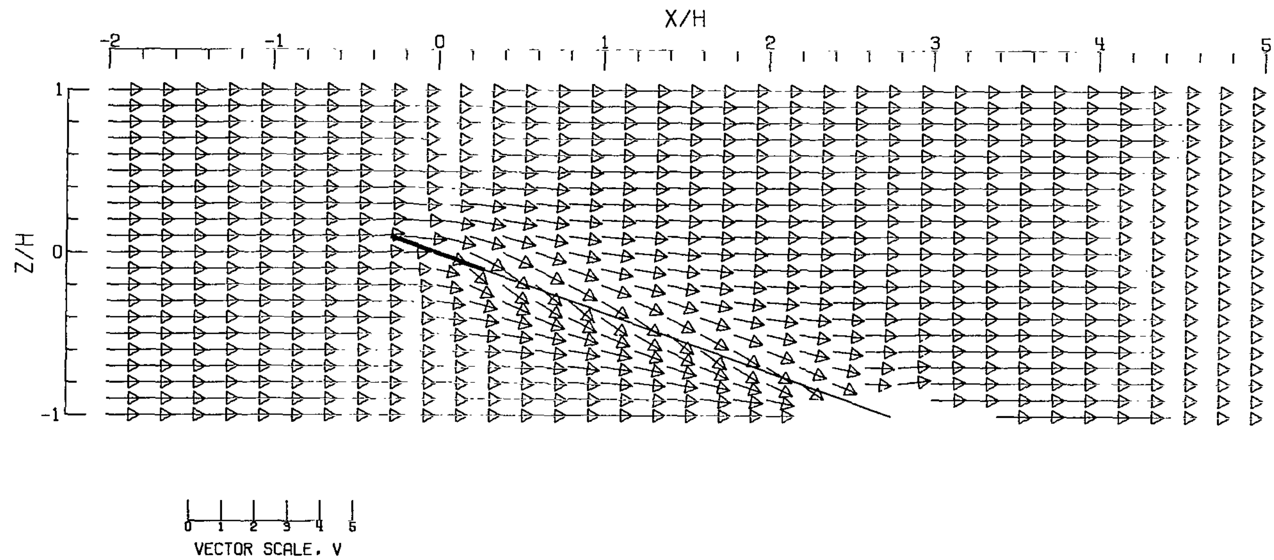

(B).- GROUND EFFECT.

Figure 76.- Flow vectors in the X-Z plane, calculated using doublet strings. The rotor and the edges of the wake are shown. $\zeta = 1.000$; $\eta = 1.000$; $\gamma = 1.000$; $\sigma = 0.300$; $\alpha = 20.000^{\circ}$; $\chi = 70.000^{\circ}$; uniform loading.

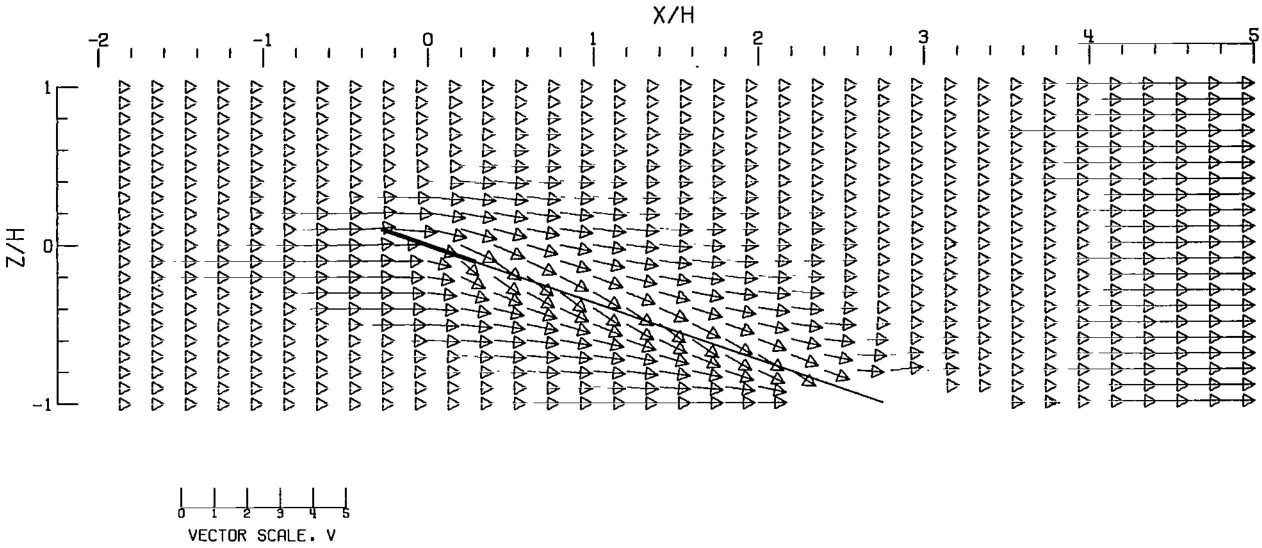

(C).- CLOSED TUNNEL.

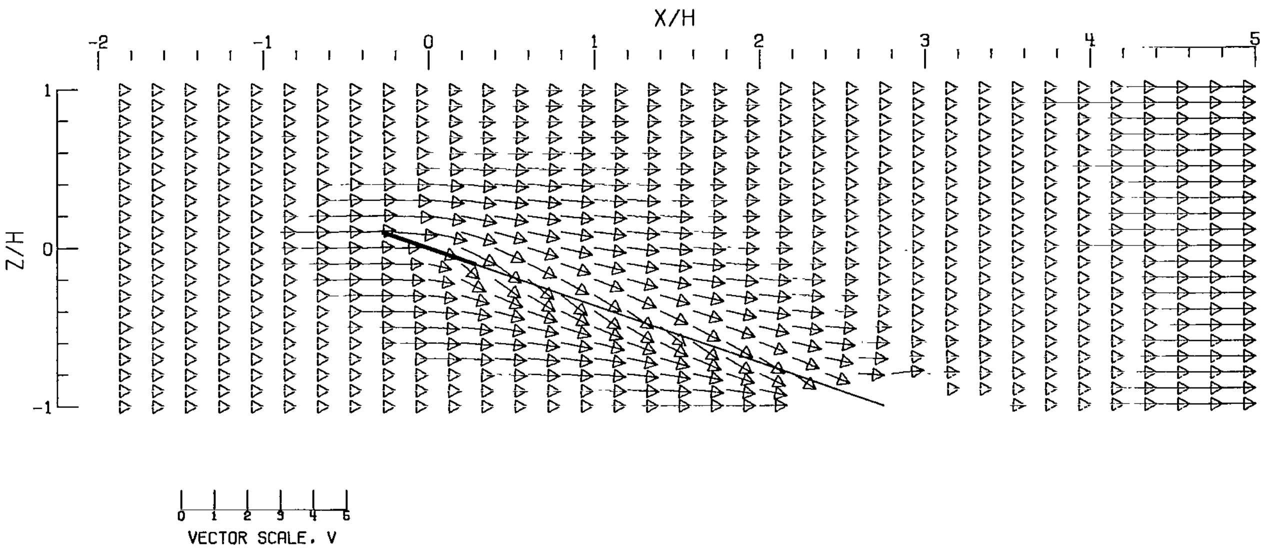

(D).- CLOSED-ON-BOTTOM-ONLY TUNNEL.

Figure 76.- Concluded.

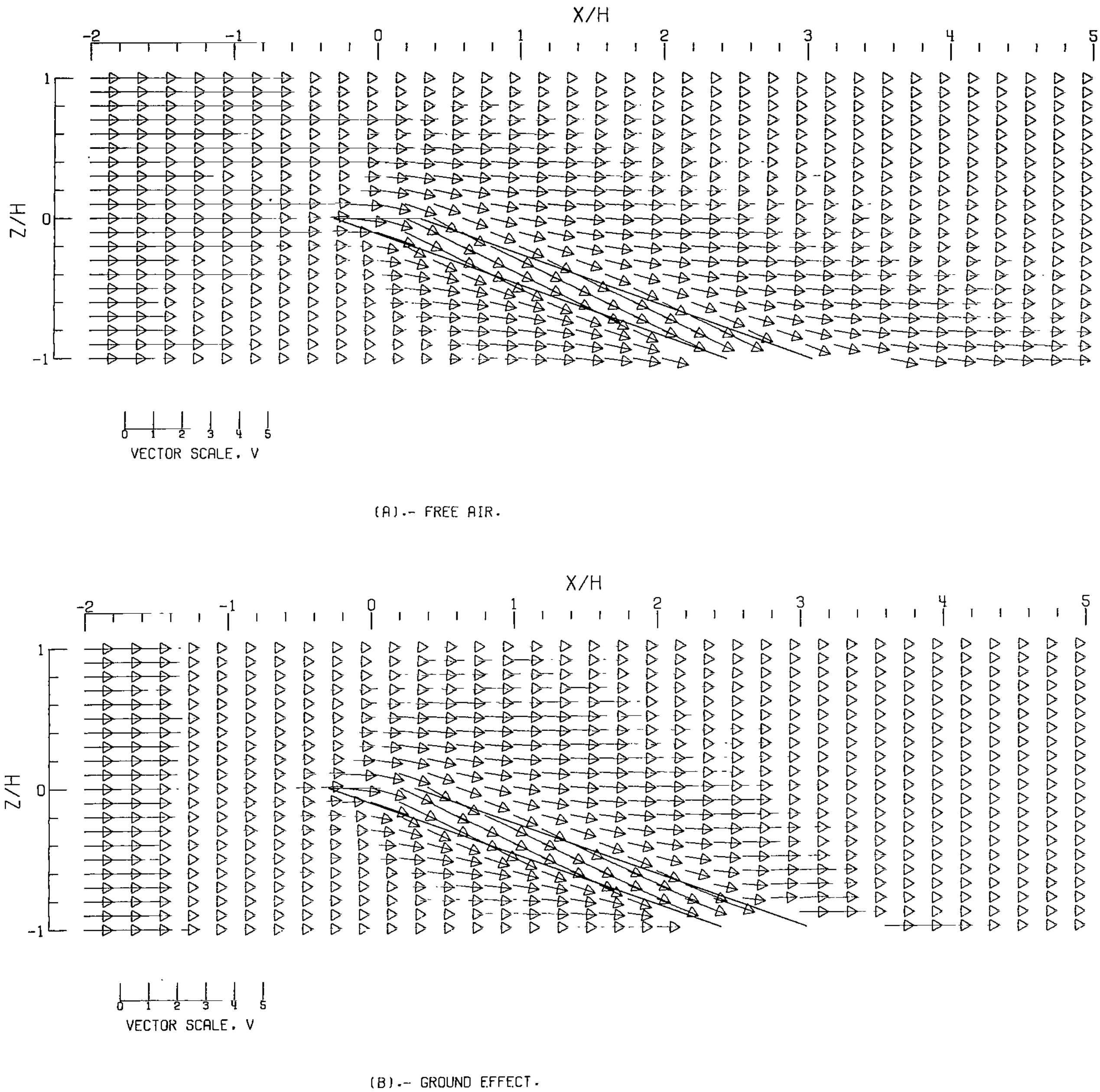

Figure 77.- Flow vectors in the X-Z plane, calculated using doublet strings. The rotor and the edges of the wake are shown. ζ = 1.000; η = 1.000; γ = 1.000; σ = 0.300; α = 0.000°; χ = 70.000°; uniform loading.

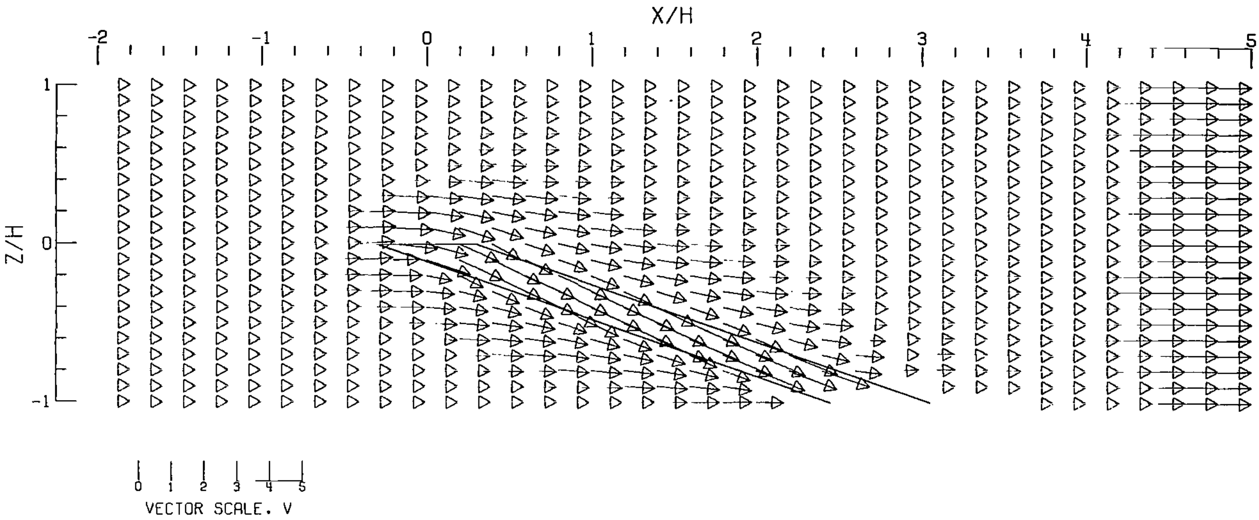

(C).- CLOSED TUNNEL.

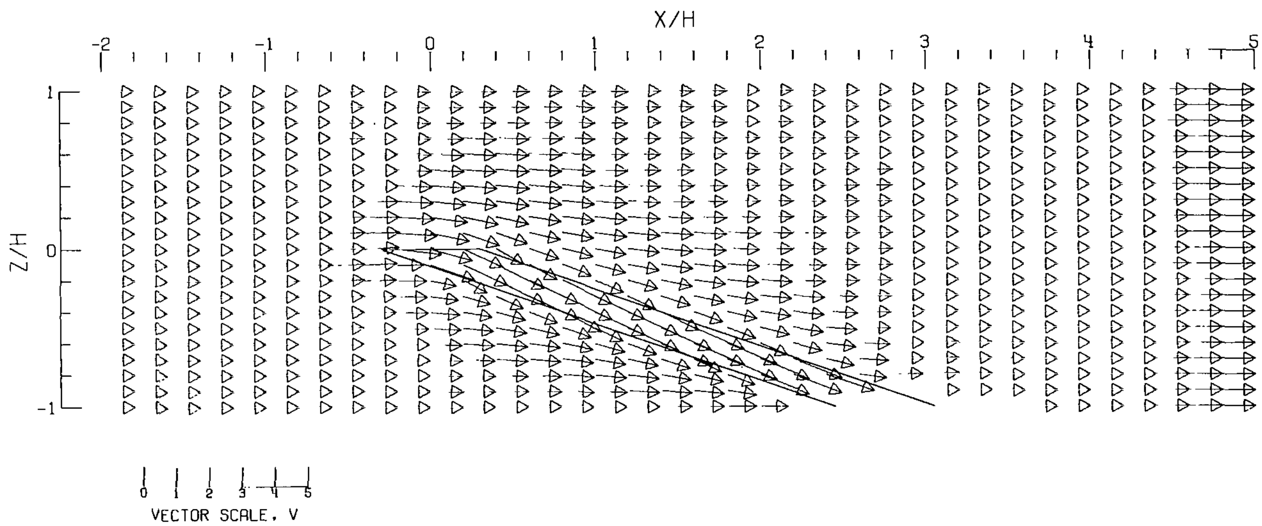

(D).- CLOSED-ON-BOTTOM-ONLY TUNNEL.

Figure 77.- Concluded.

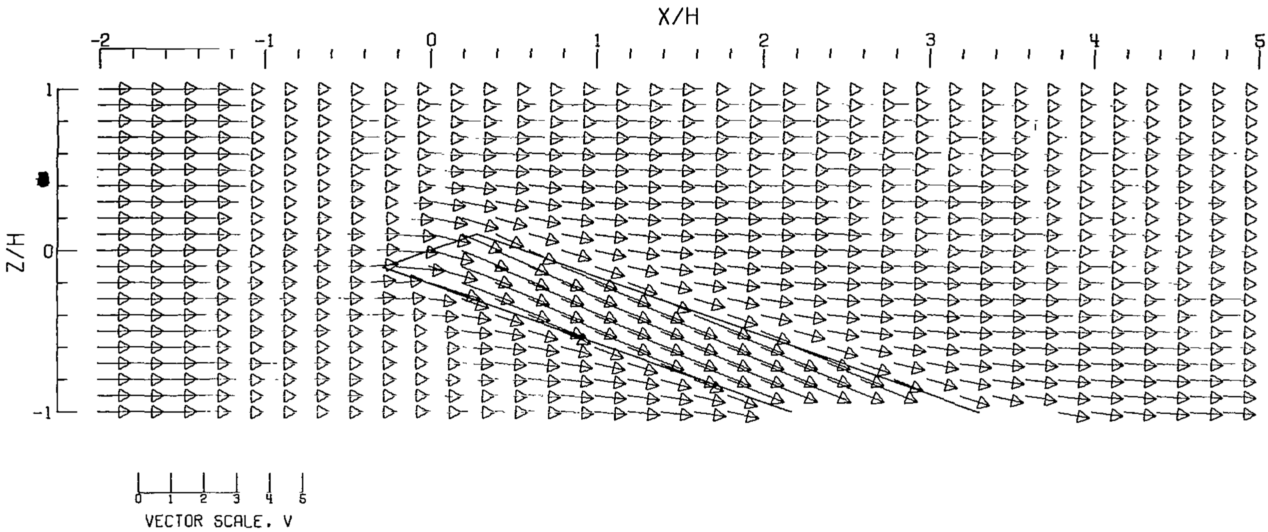

(A).- FREE AIR.

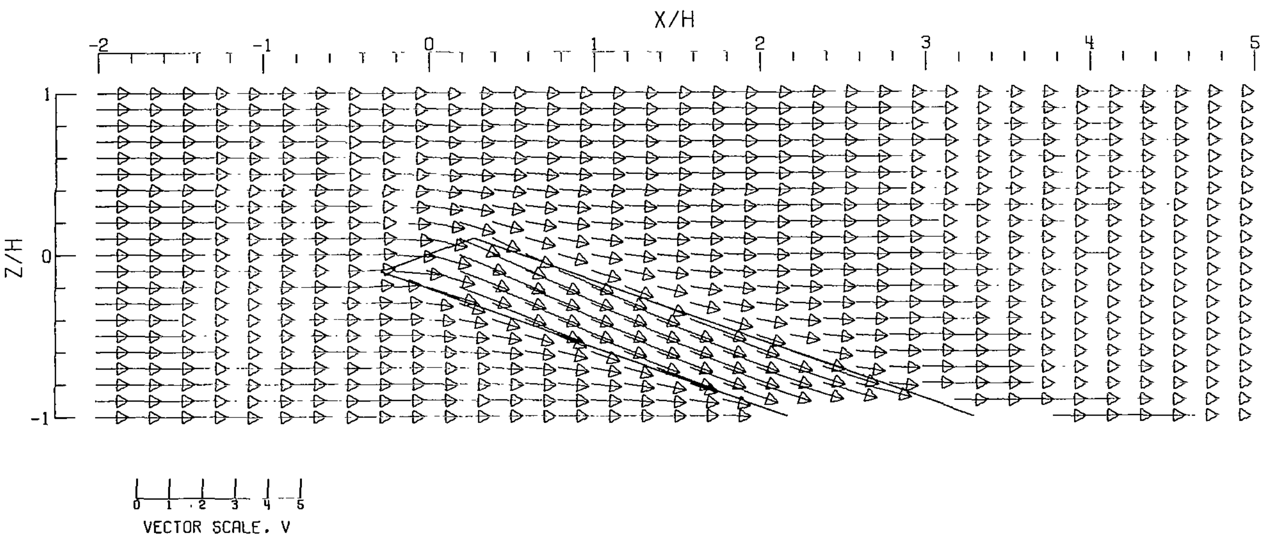

(B).- GROUND EFFECT.

Figure 78.- Flow vectors in the X-Z plane, calculated using doublet strings. The rotor and the edges of the wake are shown. ζ = 1.000; η = 1.000; γ = 1.000; σ = 0.300; α = -20.000°; χ = 70.000°; uniform loading.

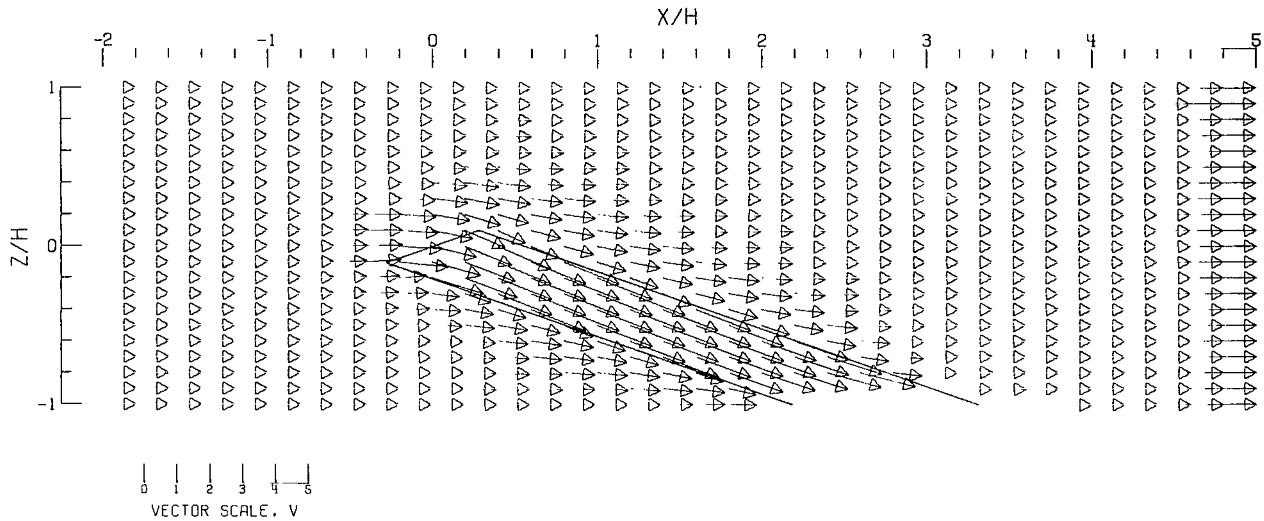

(C).- CLOSED TUNNEL.

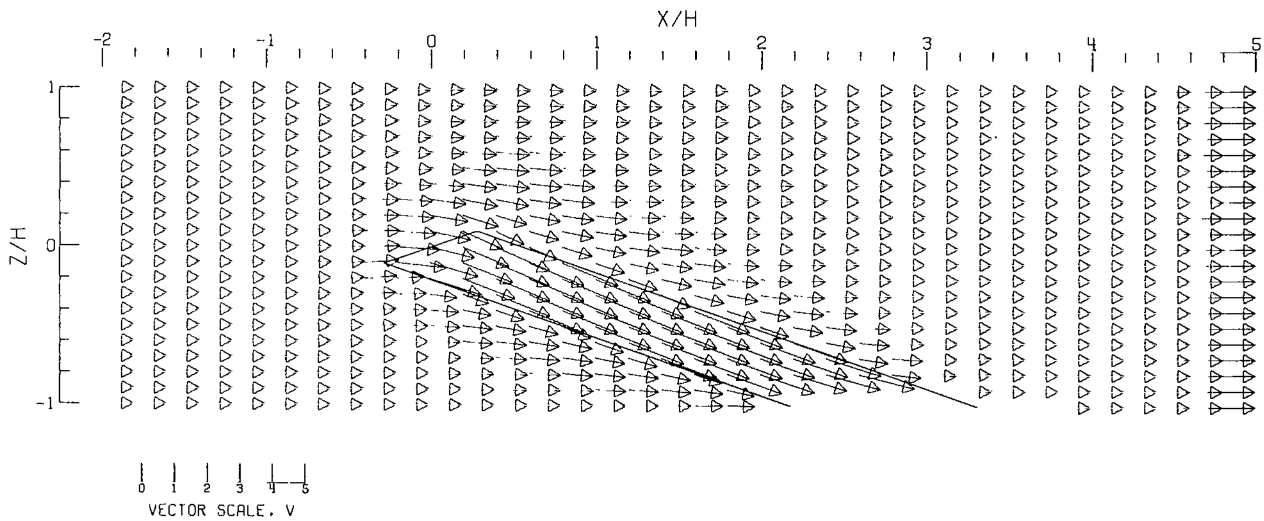

(D).- CLOSED-ON-BOTTOM-ONLY TUNNEL.

Figure 78.- Concluded.

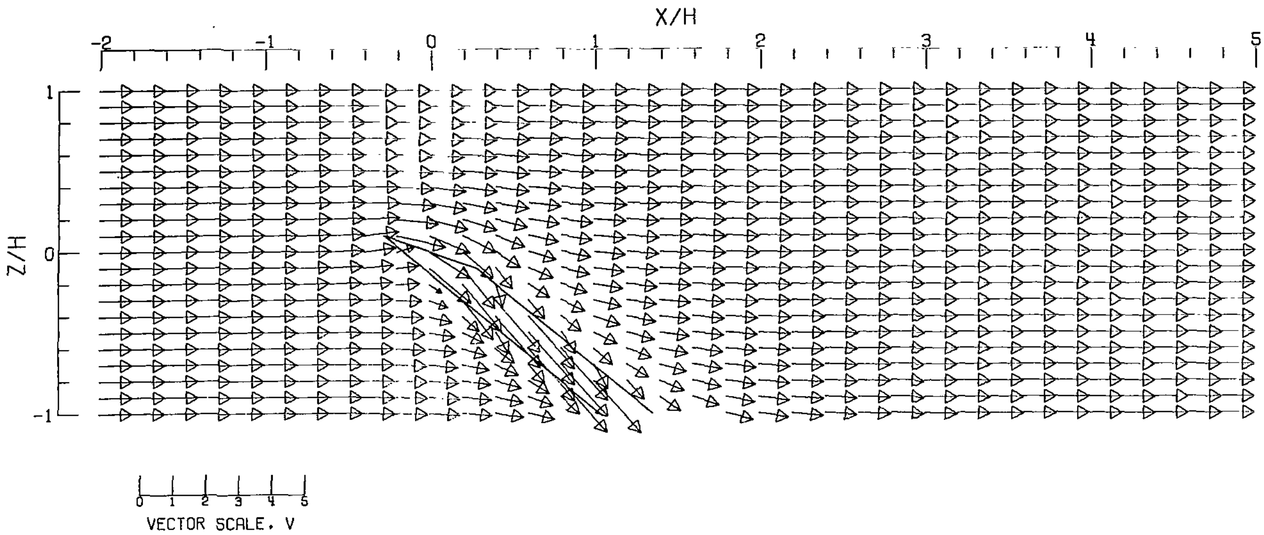

(A).- FREE AIR.

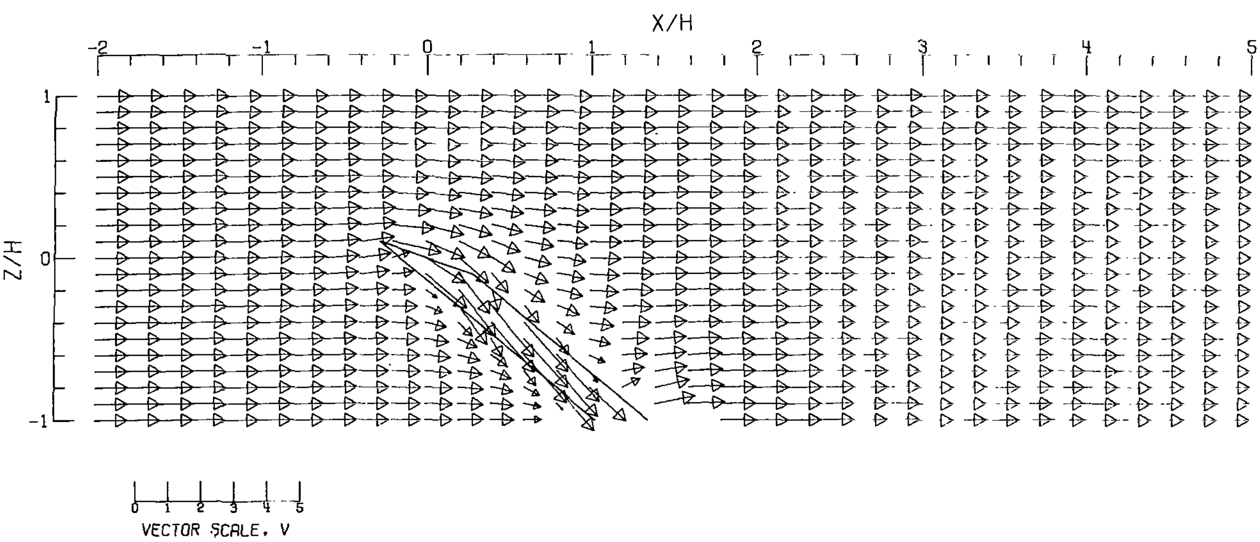

(B).- GROUND EFFECT.

Figure 79.- Flow vectors in the X-Z plane, calculated using doublet strings. The rotor and the edges of the wake are shown. ζ = 1.000; η = 1.0; γ = 1.0; σ = 0.300; α = 20.0°; χ = 50.0°; uniform loading.

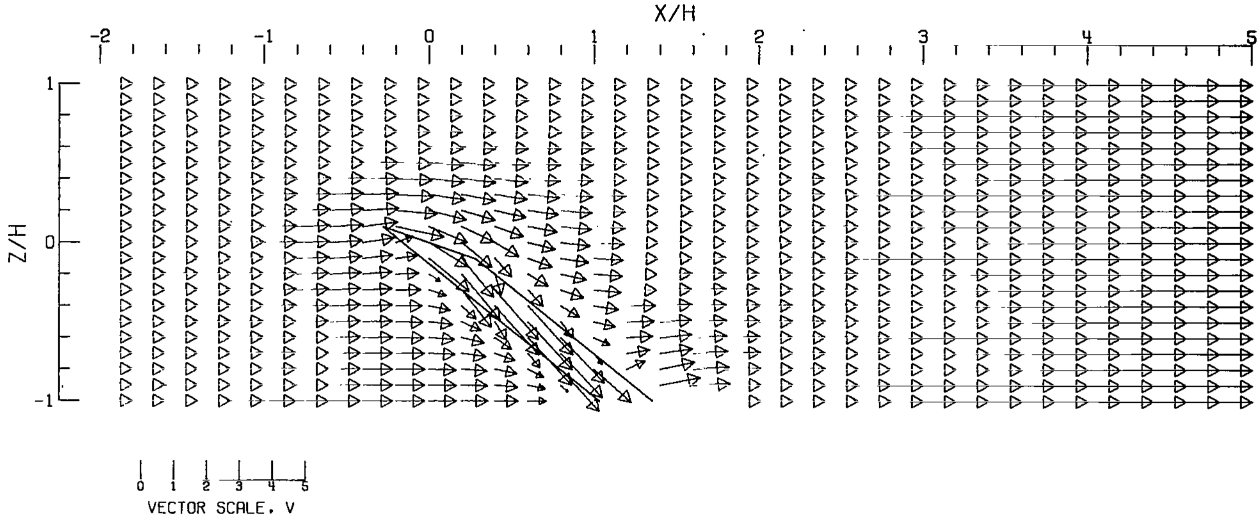

(C).- CLOSED TUNNEL.

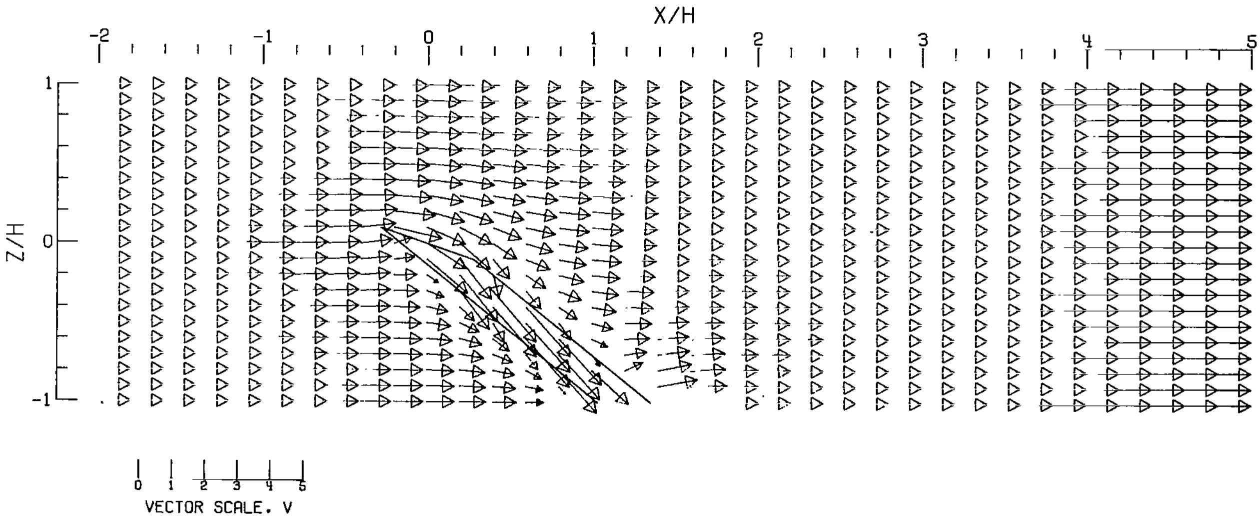

(D).- CLOSED-ON-BOTTOM-ONLY TUNNEL.

Figure 79.- Concluded.

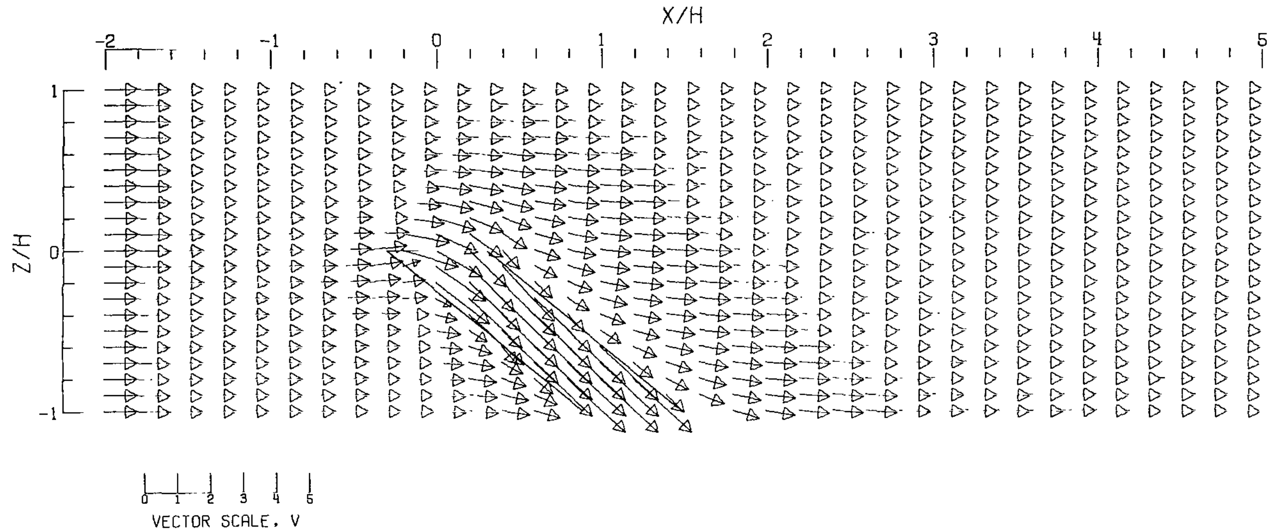

(A).- FREE AIR.

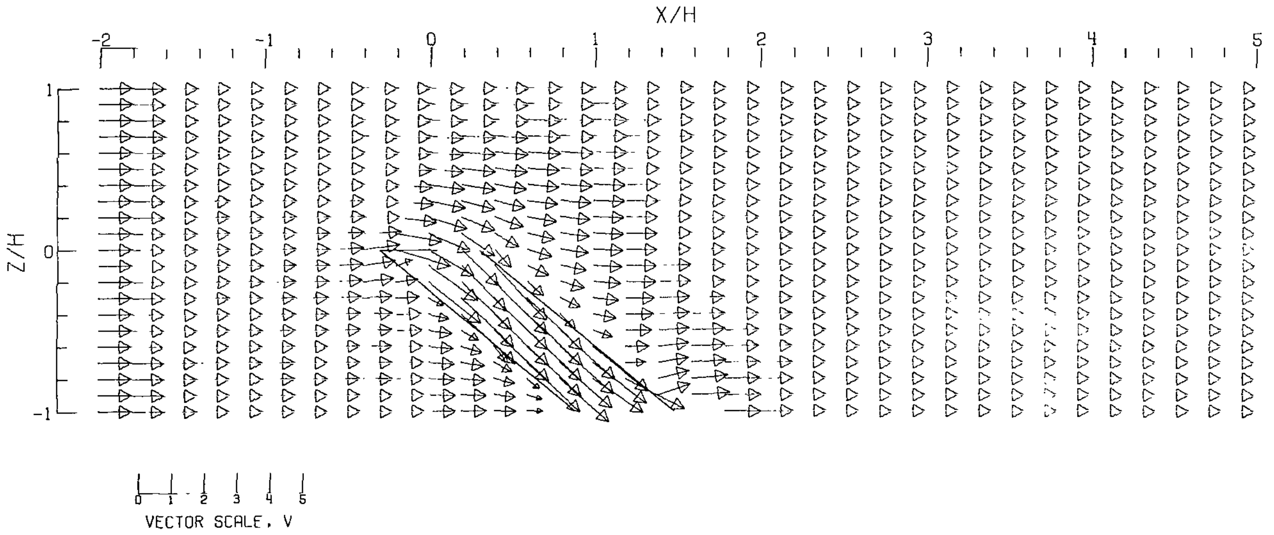

(B).- GROUND EFFECT.

Figure 80.- Flow vectors in the X-Z plane, calculated using doublet strings. The rotor and the edges of the wake are shown. $\zeta = 1.000$; $\eta = 1.000$; $\gamma = 1.000$; $\sigma = 0.300$; $\alpha = 0.000^{\circ}$; $\chi = 50.000^{\circ}$; uniform loading.

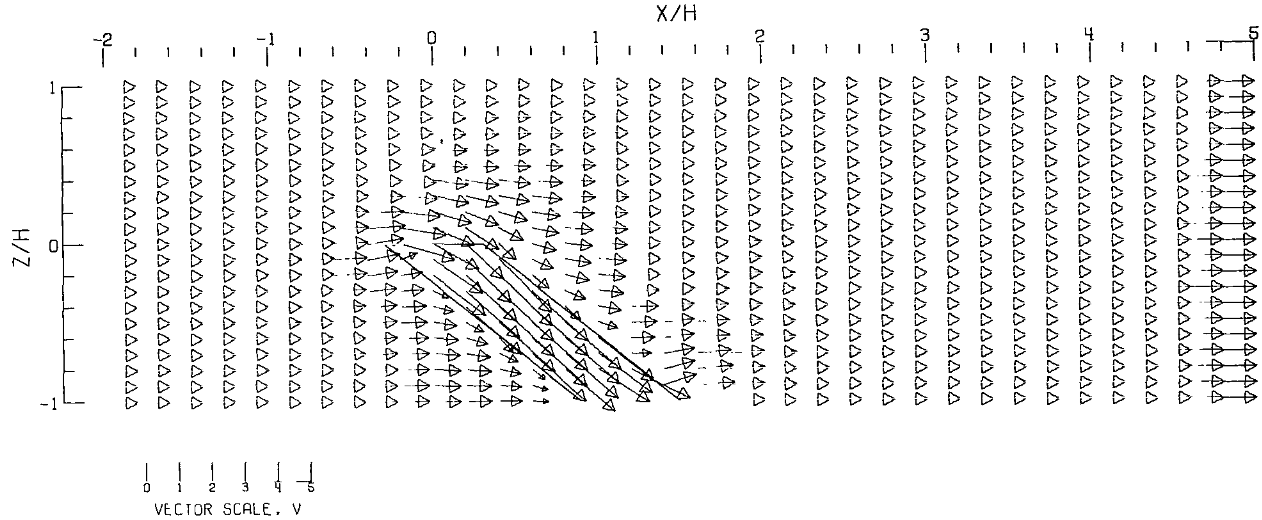

(C).- CLOSED TUNNEL.

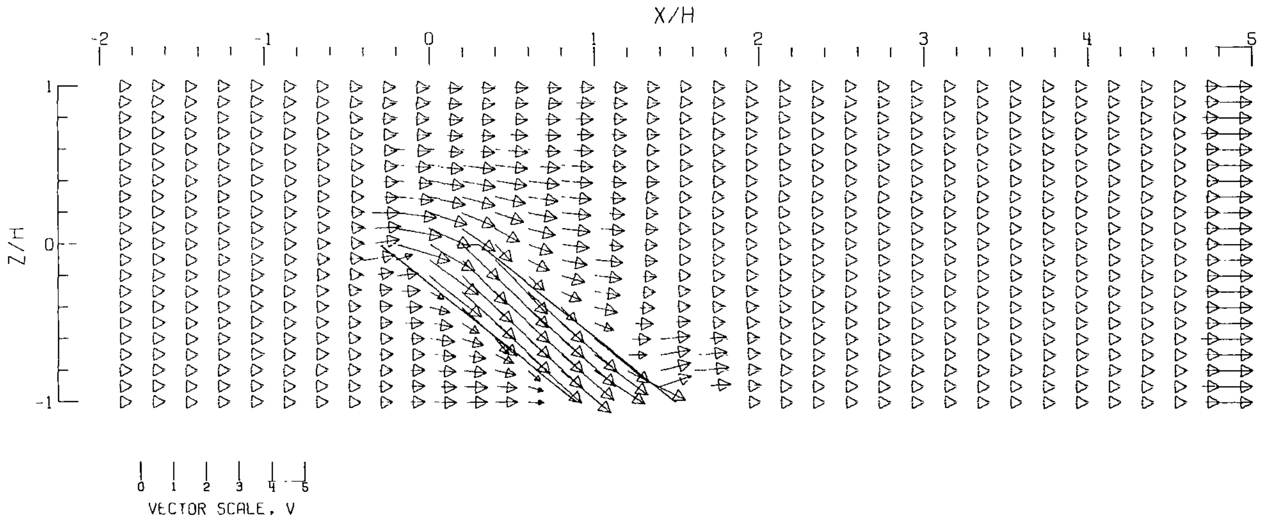

(D).- CLOSED-ON-BOTTOM-ONLY TUNNEL.

Figure 80.- Concluded.

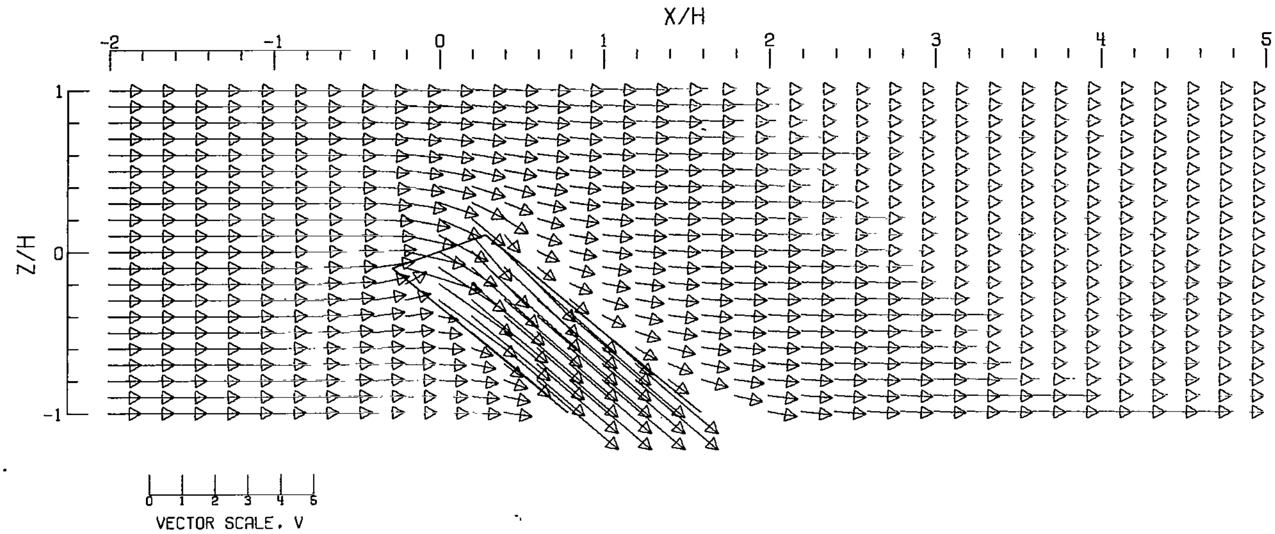

(A).- FREE AIR.

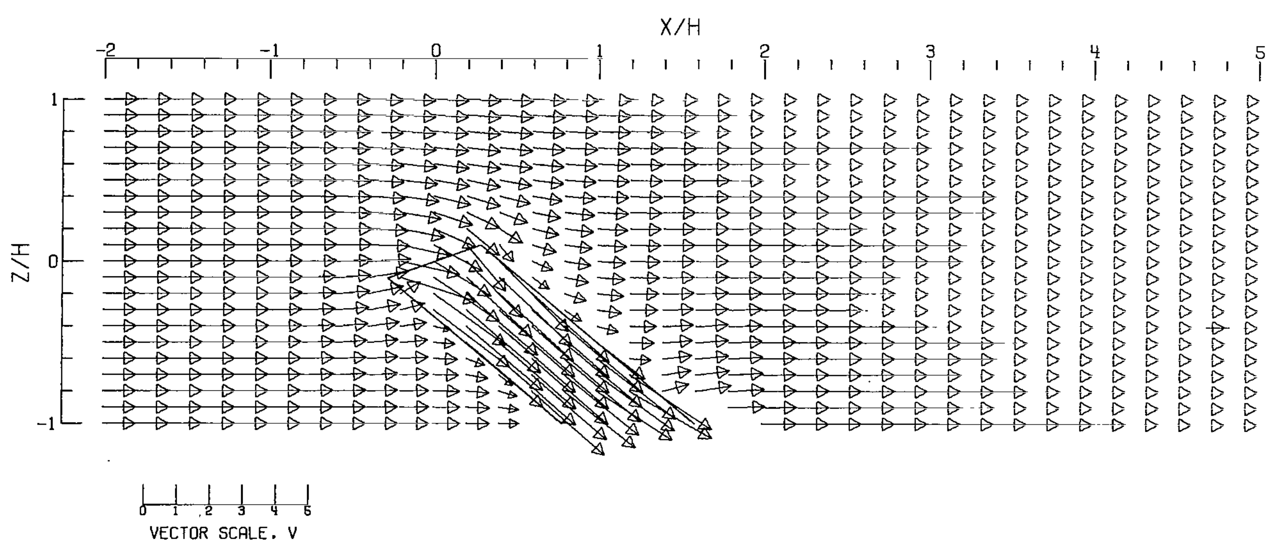

(B).- GROUND EFFECT.

Figure 81.- Flow vectors in the X-Z plane, calculated using doublet strings. The rotor and the edges of the wake are shown. ζ = 1.000; η = 1.0; γ = 1.0; σ = 0.300; α = -20.0°; χ = 50.0°; uniform loading.

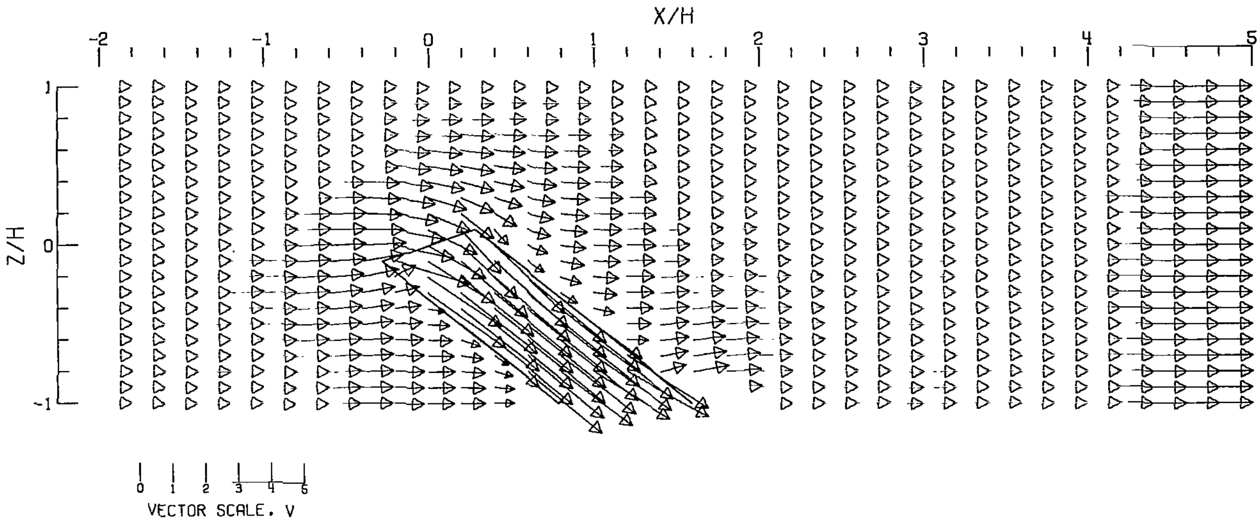

(C).- CLOSED TUNNEL.

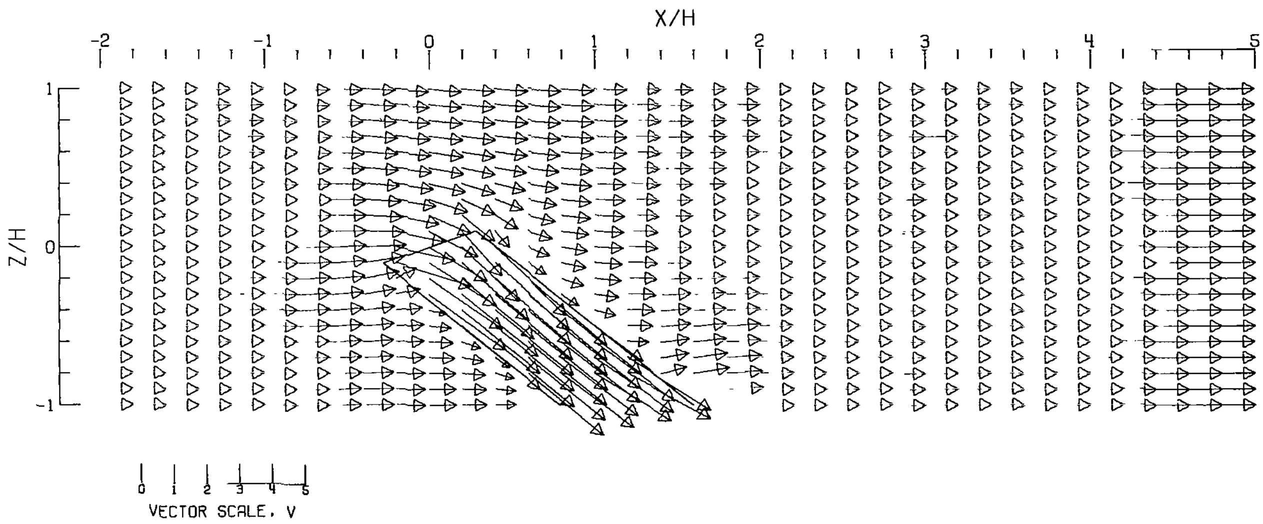

(D).- CLOSED-ON-BOTTOM-ONLY TUNNEL.

Figure 81.- Concluded.

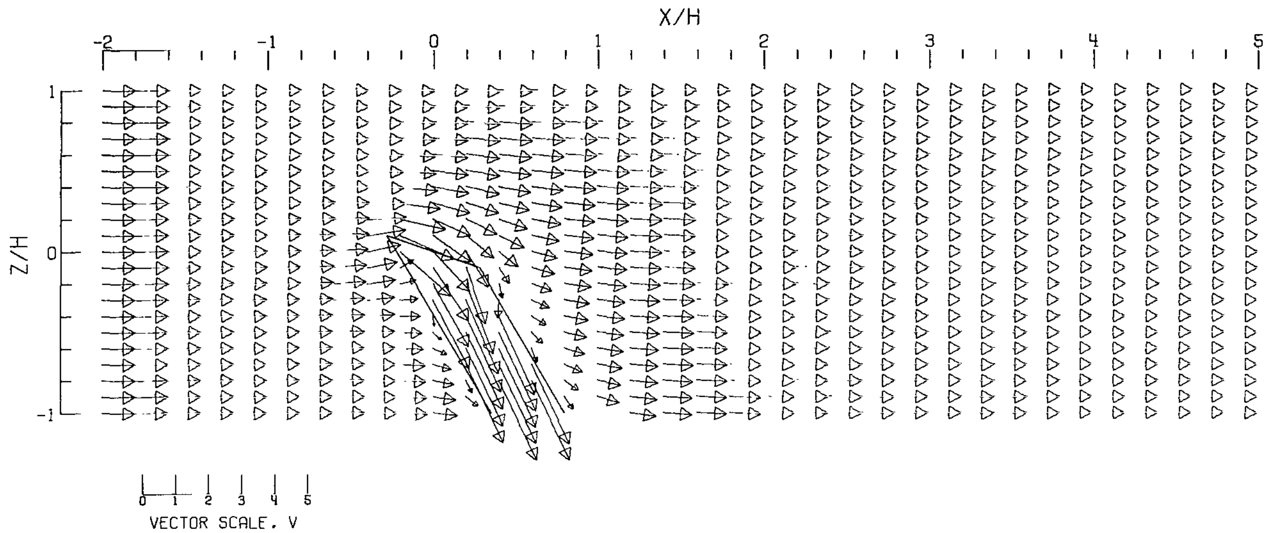

(A).- FREE AIR.

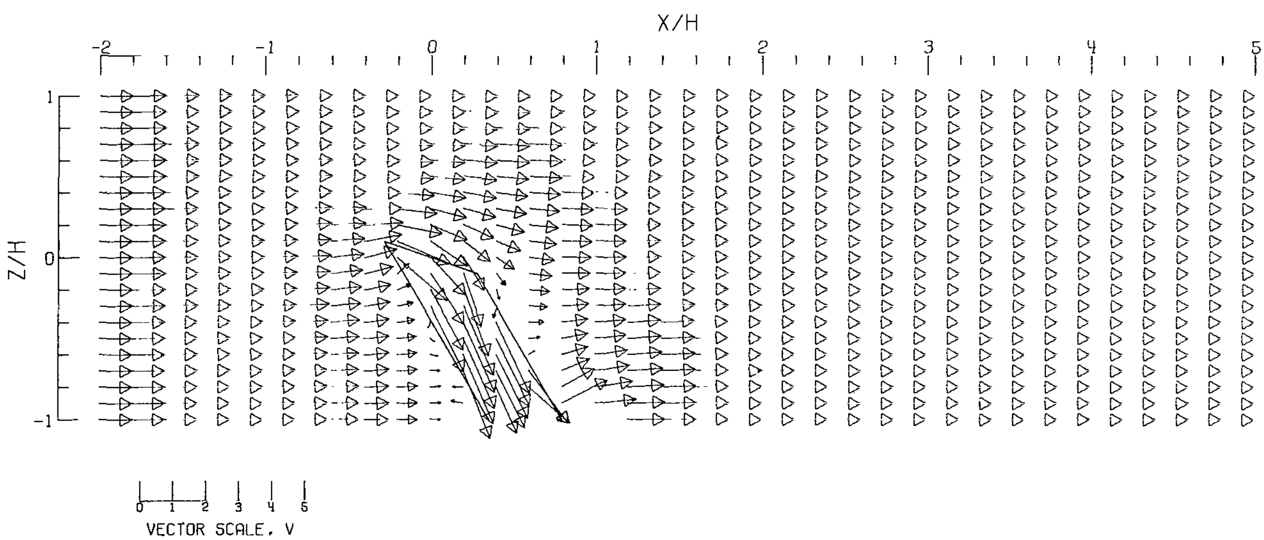

(B).- GROUND EFFECT.

Figure 82.- Flow vectors in the X-Z plane, calculated using doublet strings. The rotor and the edges of the wake are shown. ζ = 1.000; η = 1.000; γ = 1.000; σ = 0.300; α = 20.000°; χ = 30.000°; uniform loading.

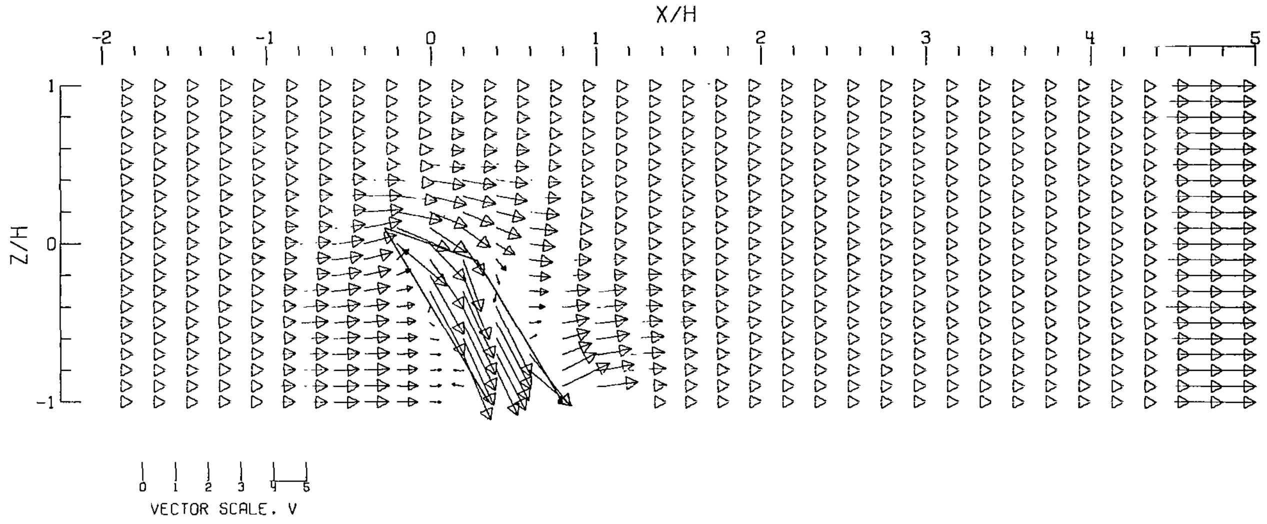

(C).- CLOSED TUNNEL.

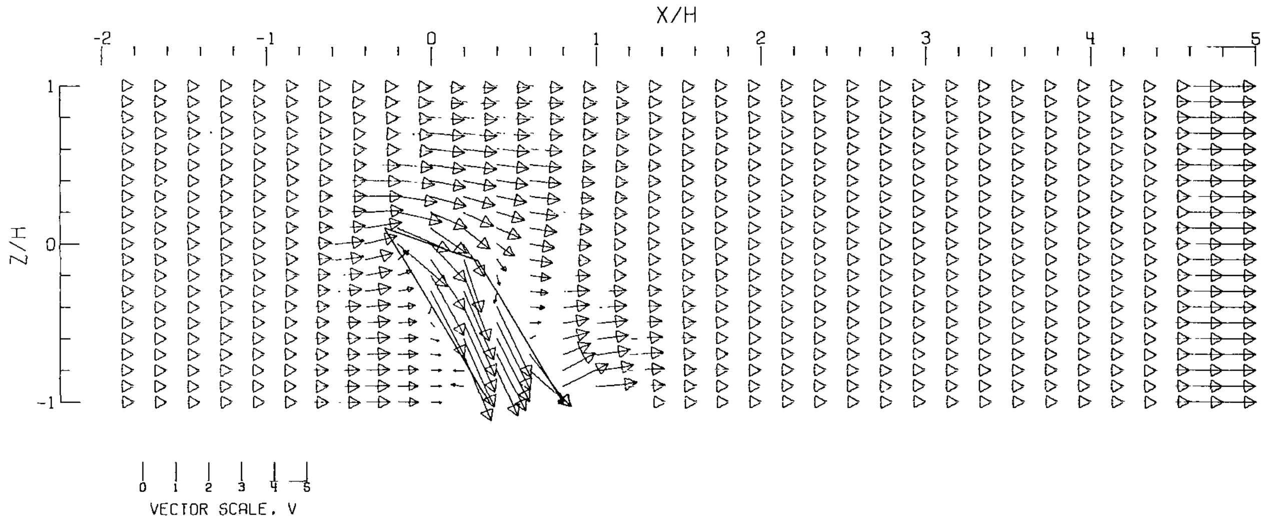

(D).- CLOSED-ON-BOTTOM-ONLY TUNNEL.

Figure 82.- Concluded.

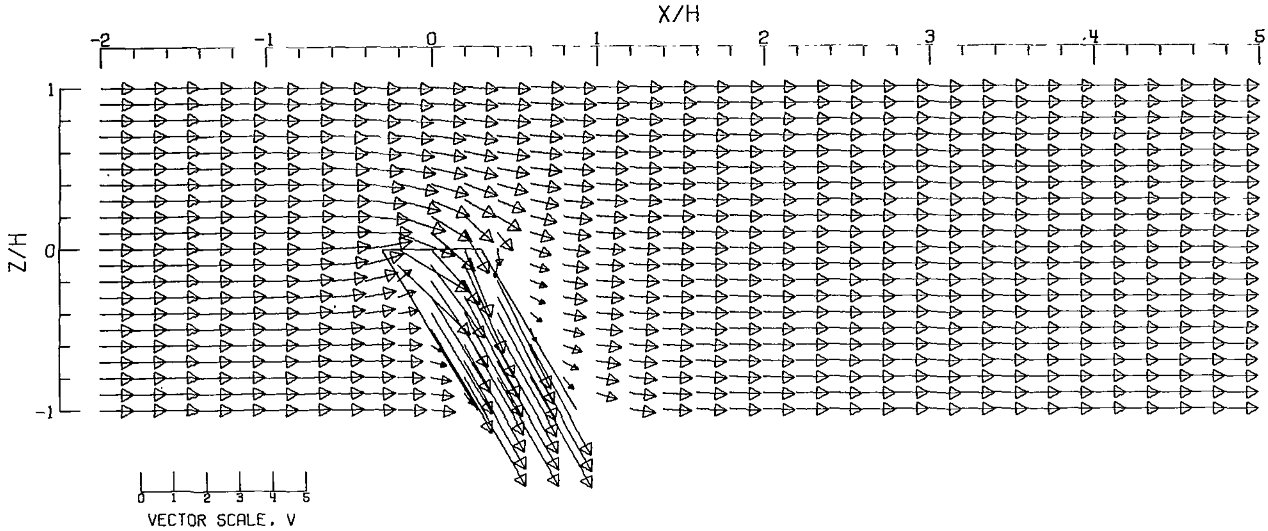

(A).- FREE AIR.

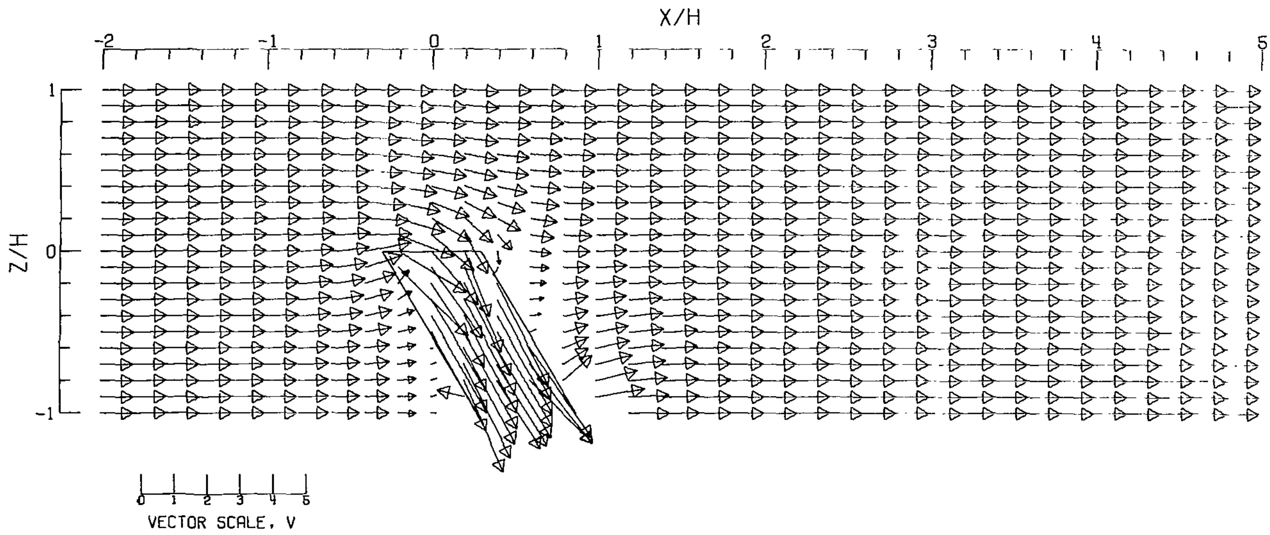

(B).- GROUND EFFECT.

Figure 83.- Flow vectors in the X-Z plane, calculated using doublet strings. The rotor and the edges of the wake are shown. ζ = 1.000; η = 1.000; γ = 1.000; σ = 0.300; α = 0.000°; χ = 30.000°; uniform loading.

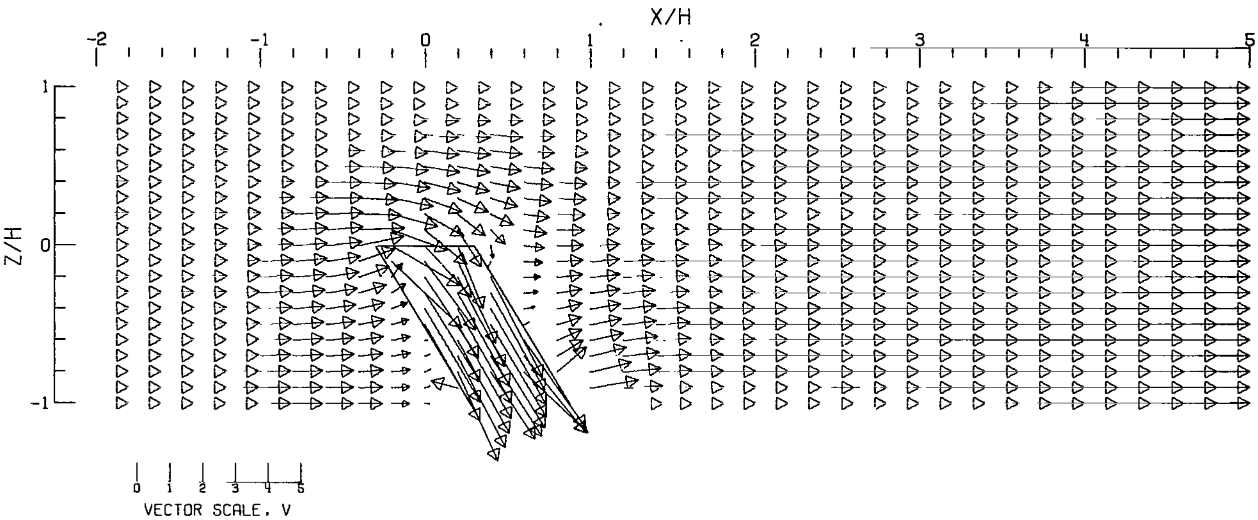

(C).- CLOSED TUNNEL.

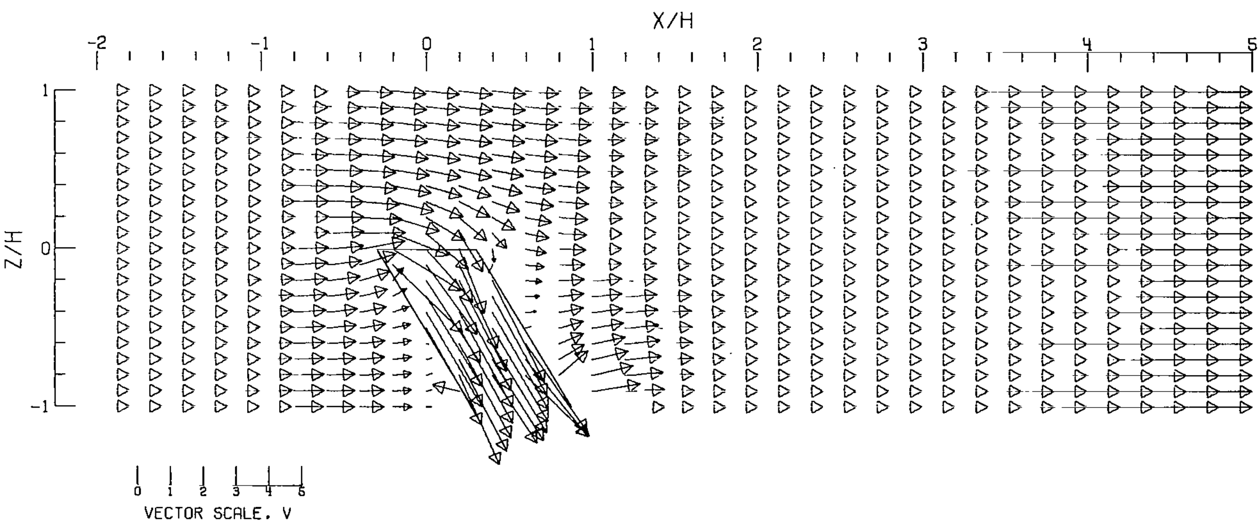

(D).- CLOSED-ON-BOTTOM-ONLY TUNNEL.

Figure 83.- Concluded.

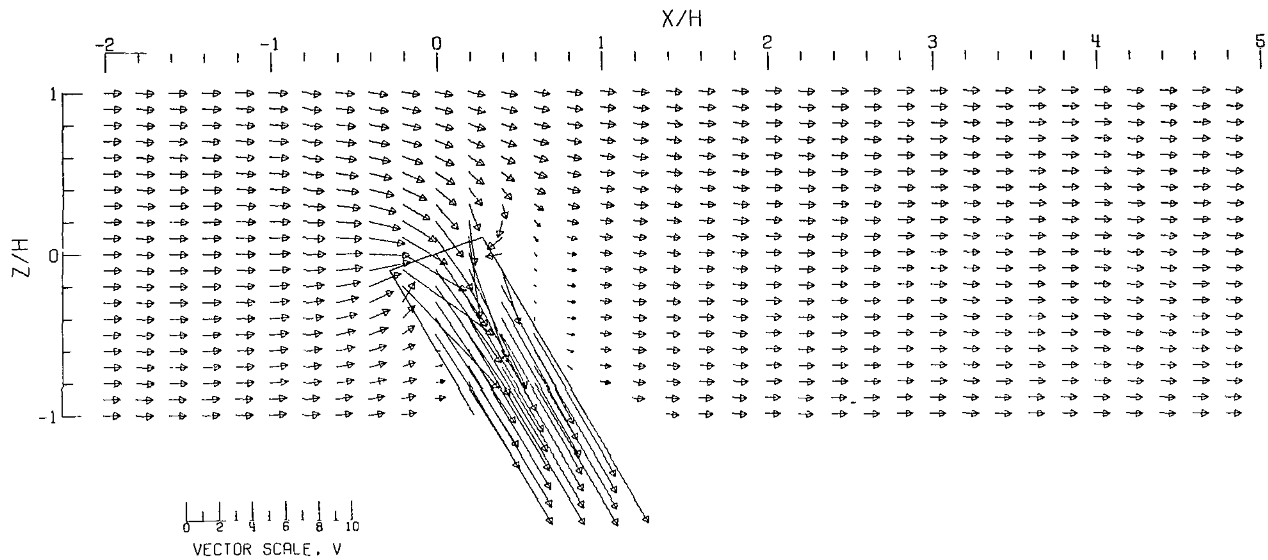

(A).- FREE AIR.

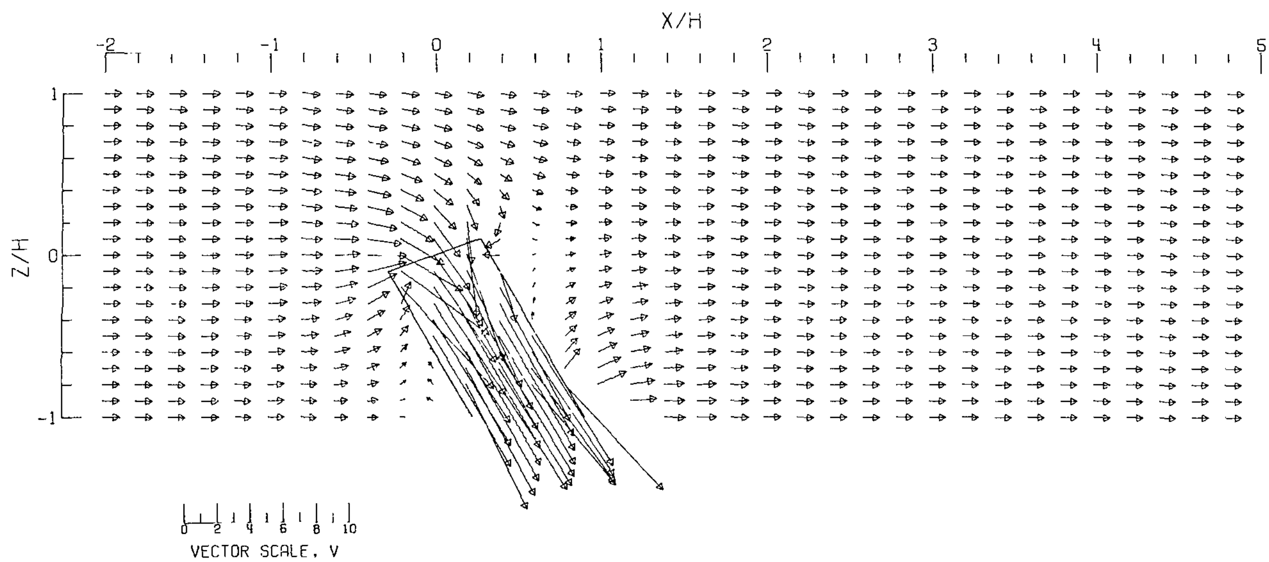

(B).- GROUND EFFECT.

Figure 84.- Flow vectors in the X-Z plane, calculated using doublet strings. The rotor and the edges of the wake are shown. ζ = 1.000; η = 1.000; γ = 1.000; σ = 0.300; α = -20.000°; χ = 30.000°; uniform loading.

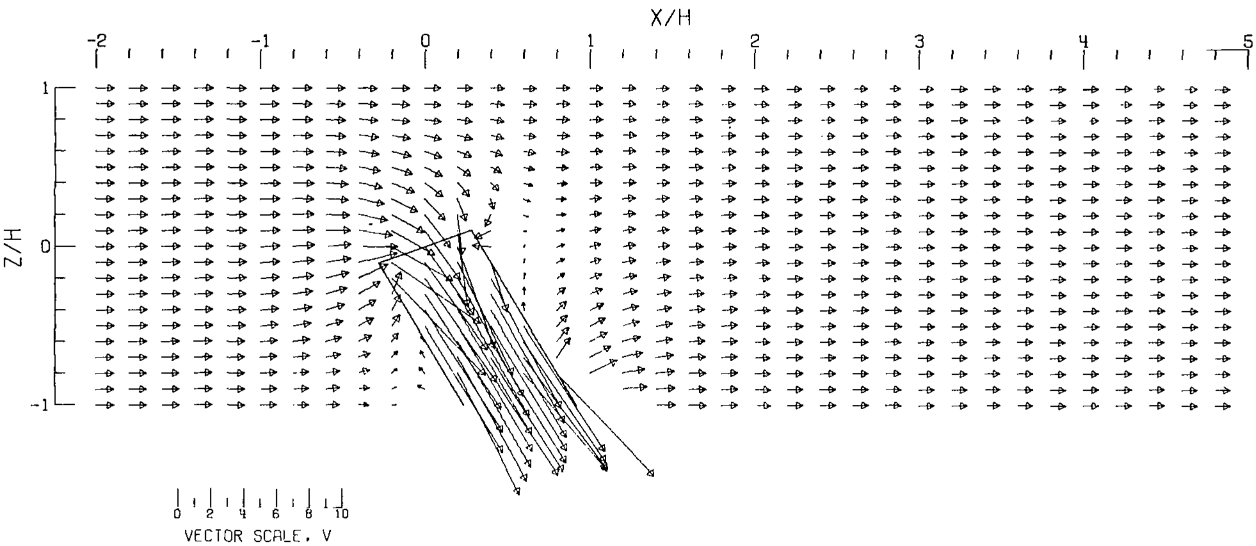

(C).- CLOSED TUNNEL.

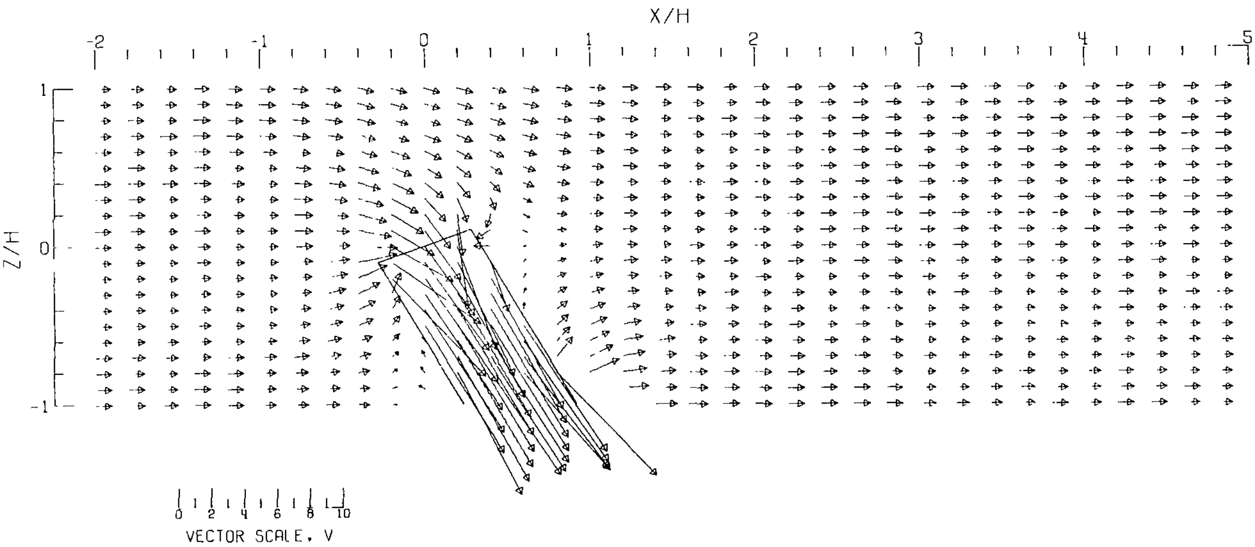

(D).- CLOSED-ON-BOTTOM-ONLY TUNNEL.

Figure 84.- Concluded.

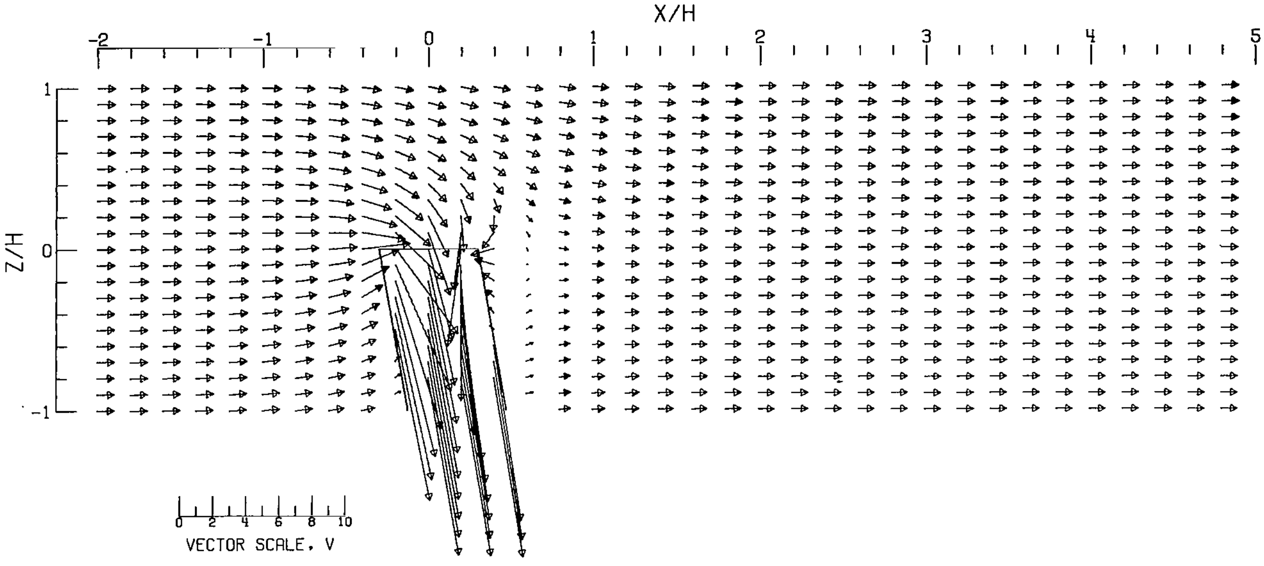

(A).- FREE AIR.

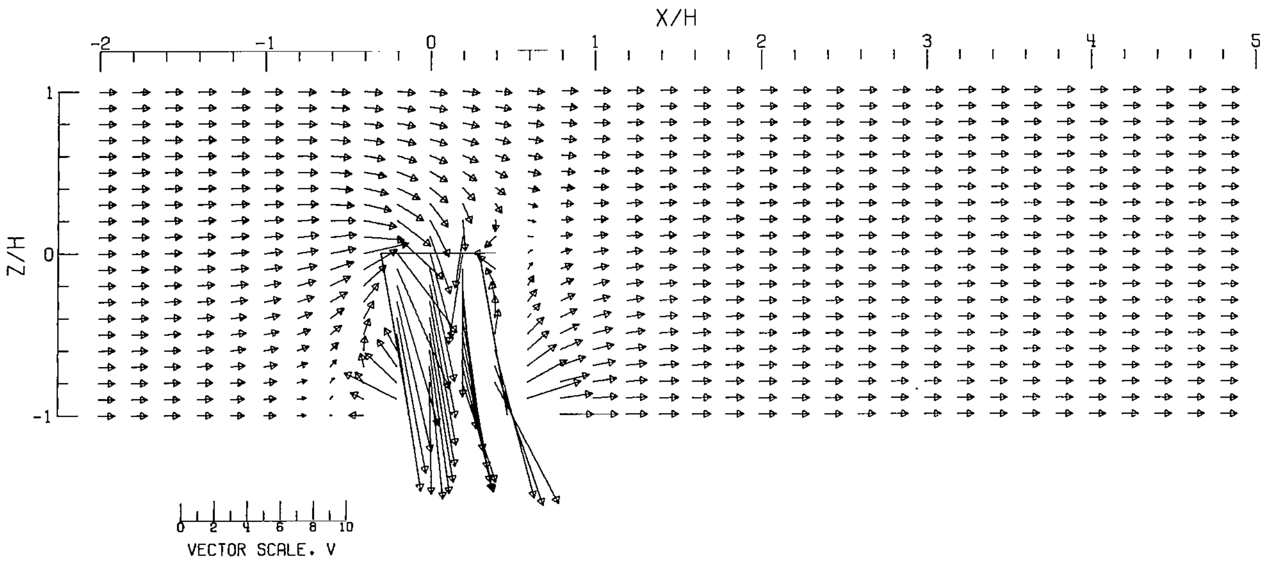

(B).- GROUND EFFECT.

Figure 85.- Flow vectors in the X-Z plane, calculated using doublet strings. The rotor and the edges of the wake are shown. ζ = 1.000; η = 1.000; γ = 1.000; σ = 0.300; α = 0.000°; χ = 10.000°; uniform loading.

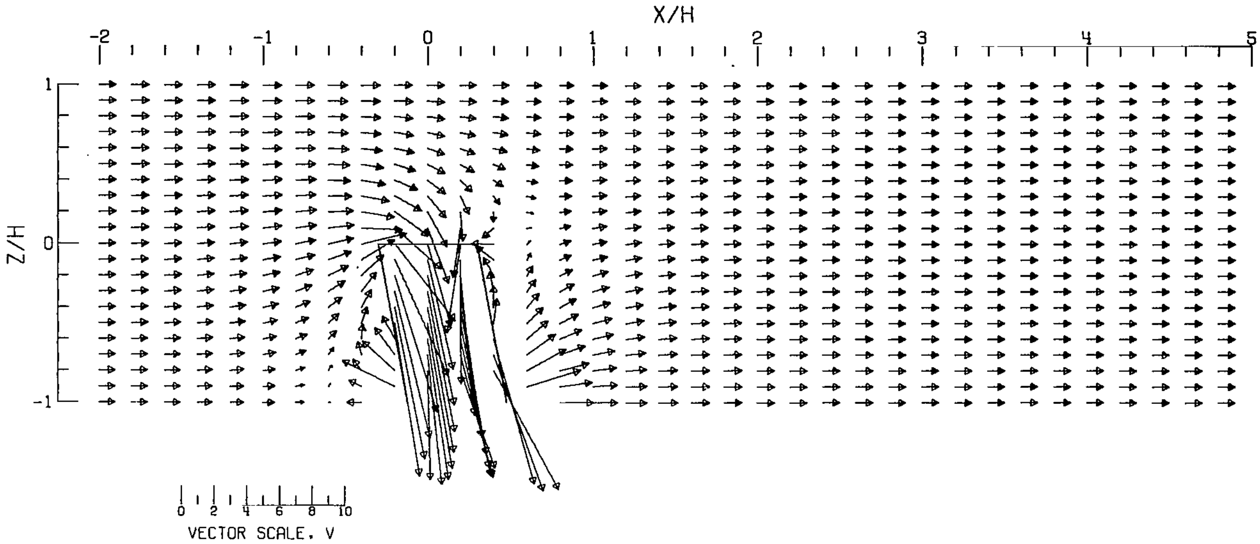

(C).- CLOSED TUNNEL.

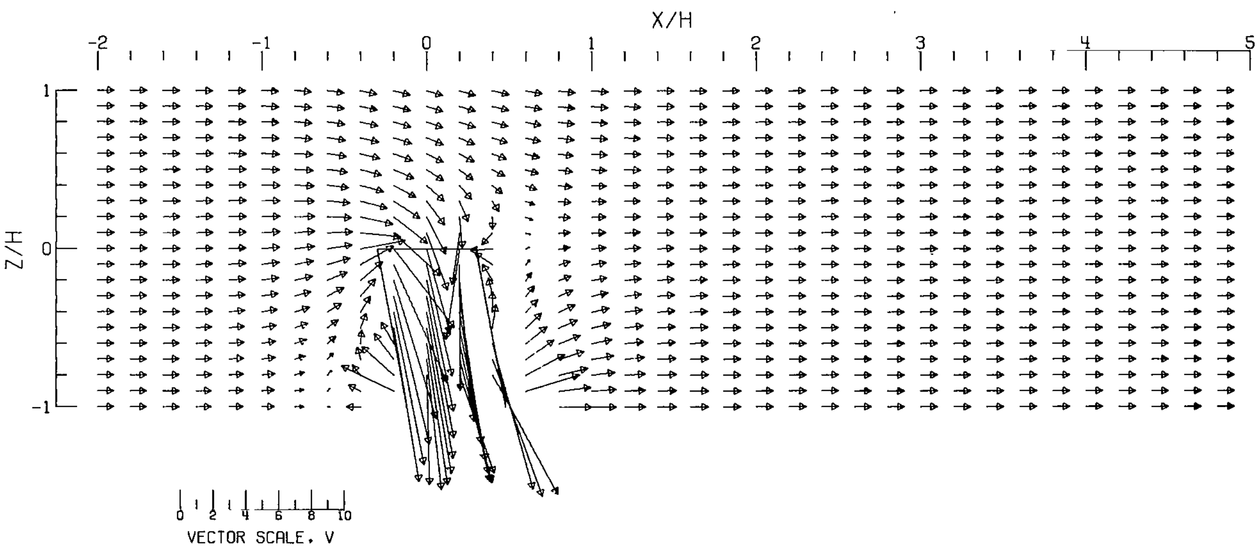

(D).- CLOSED-ON-BOTTOM-ONLY TUNNEL.

Figure 85.- Concluded.

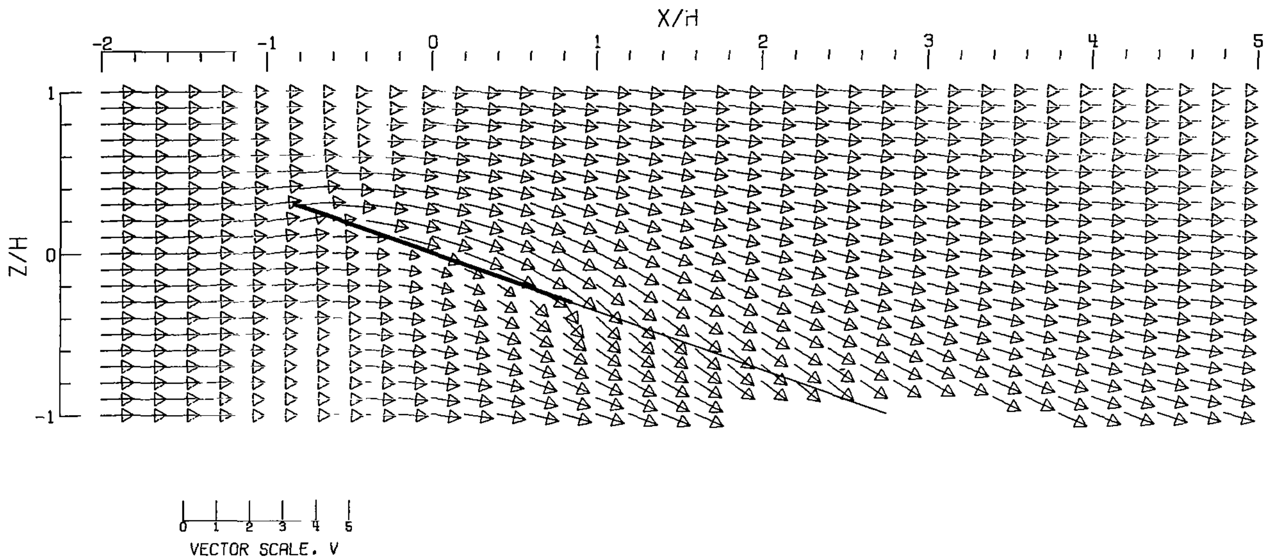

(A).- FREE AIR.

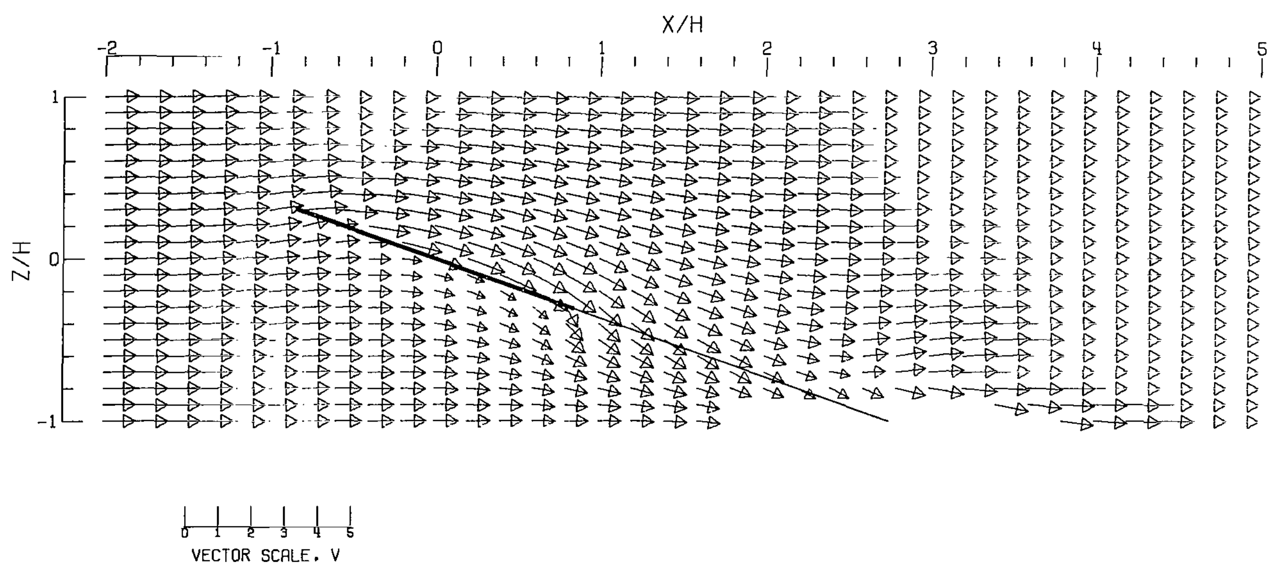

(B).- GROUND EFFECT.

Figure 86.- Flow vectors in the X-Z plane, calculated using doublet strings. The rotor and the edges of the wake are shown. ζ = 1.000; η = 1.0; γ = 1.0; σ = 0.900; α = 20.0°; χ = 70.0°; uniform loading.

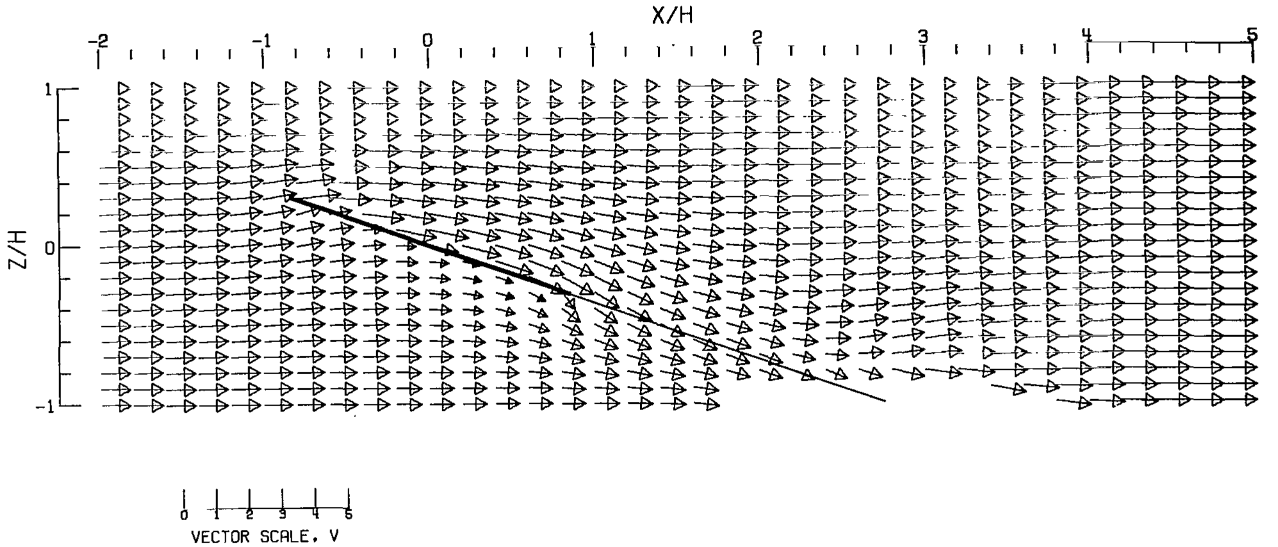

(C).- CLOSED TUNNEL.

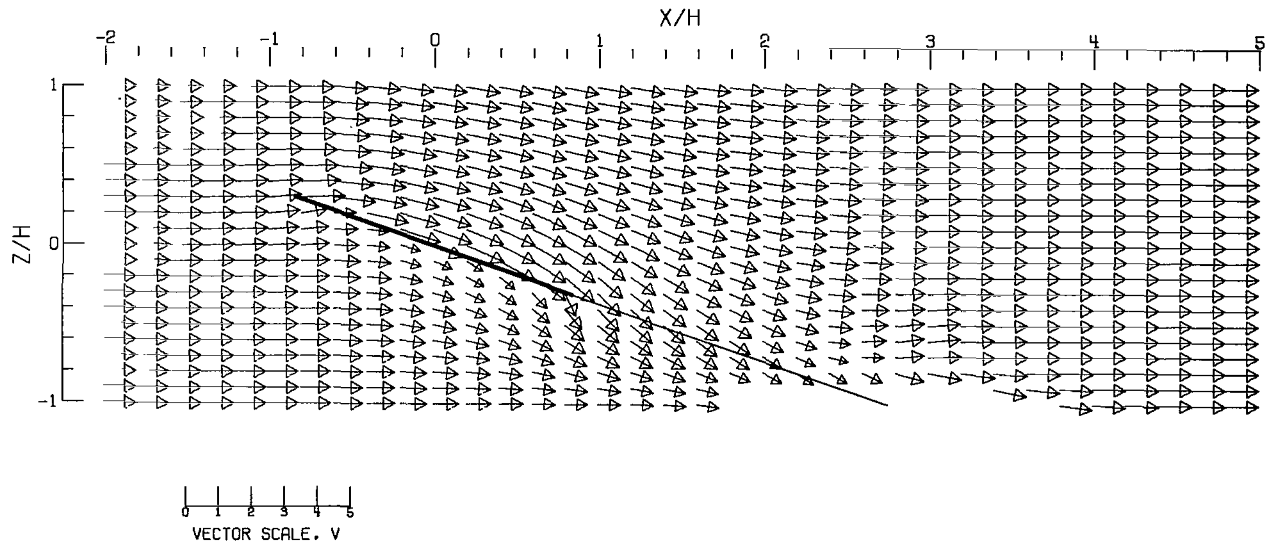

(D).- CLOSED-ON-BOTTOM-ONLY TUNNEL.

Figure 86.- Concluded.

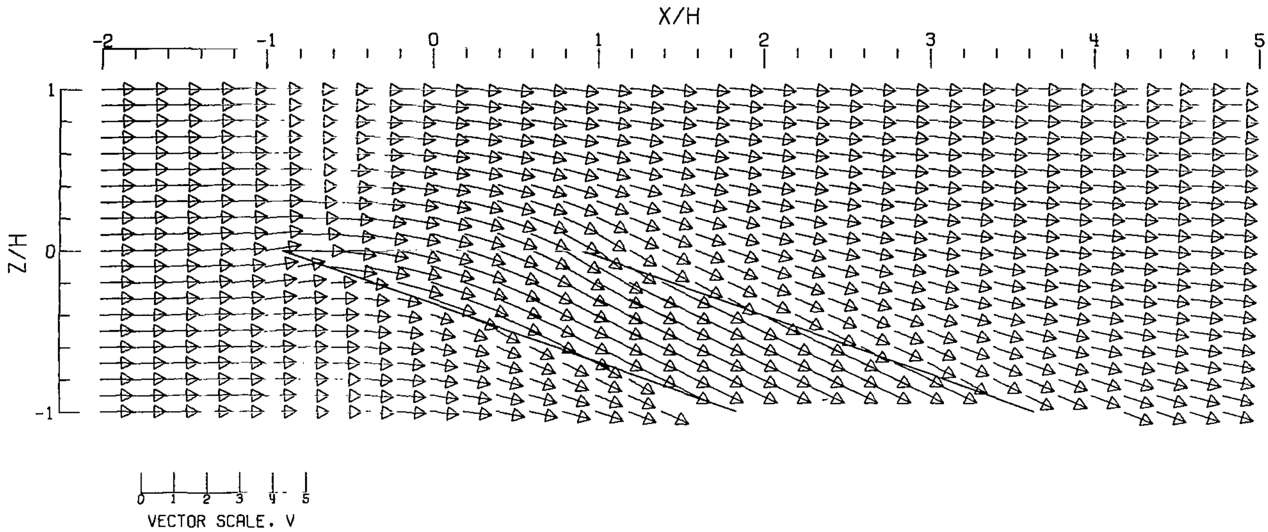

(A).- FREE AIR.

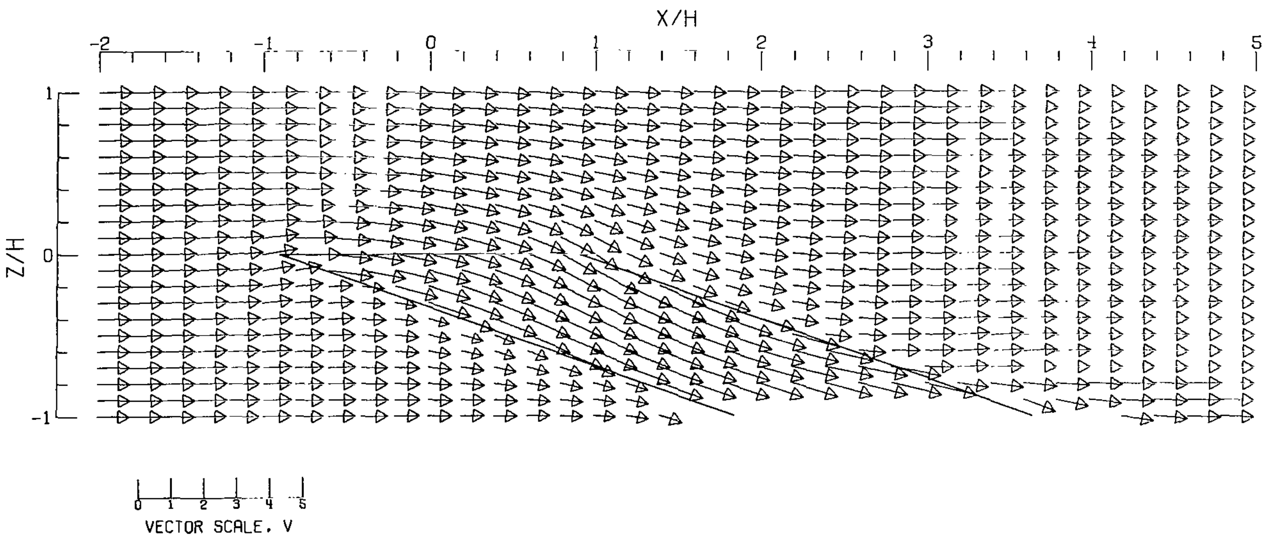

(B).- GROUND EFFECT.

Figure 87.- Flow vectors in the X-Z plane, calculated using doublet strings. The rotor and the edges of the wake are shown. ζ = 1.000; η = 1.0; γ = 1.0; σ = 0.900; α = 0.0°; χ = 70.0°; uniform loading.

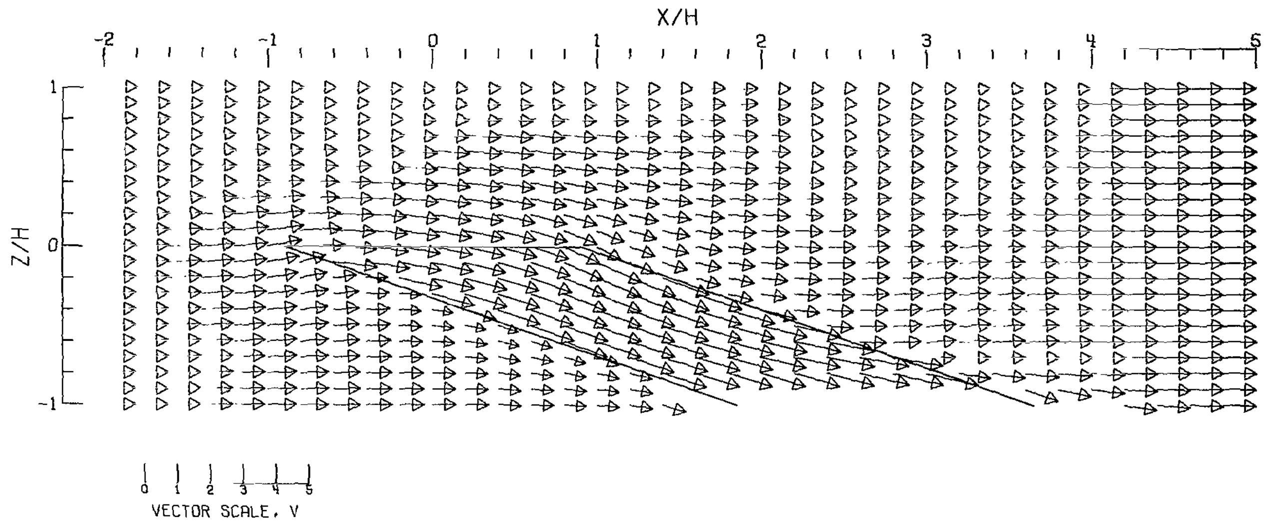

(C).- CLOSED TUNNEL.

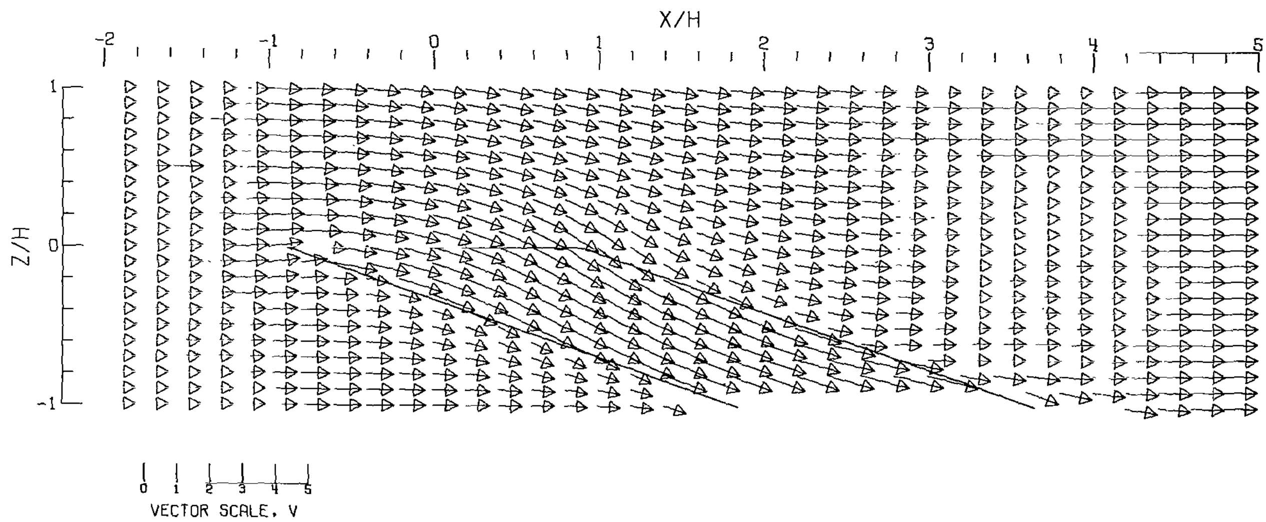

(D).- CLOSED-ON-BOTTOM-ONLY TUNNEL.

Figure 87.- Concluded.

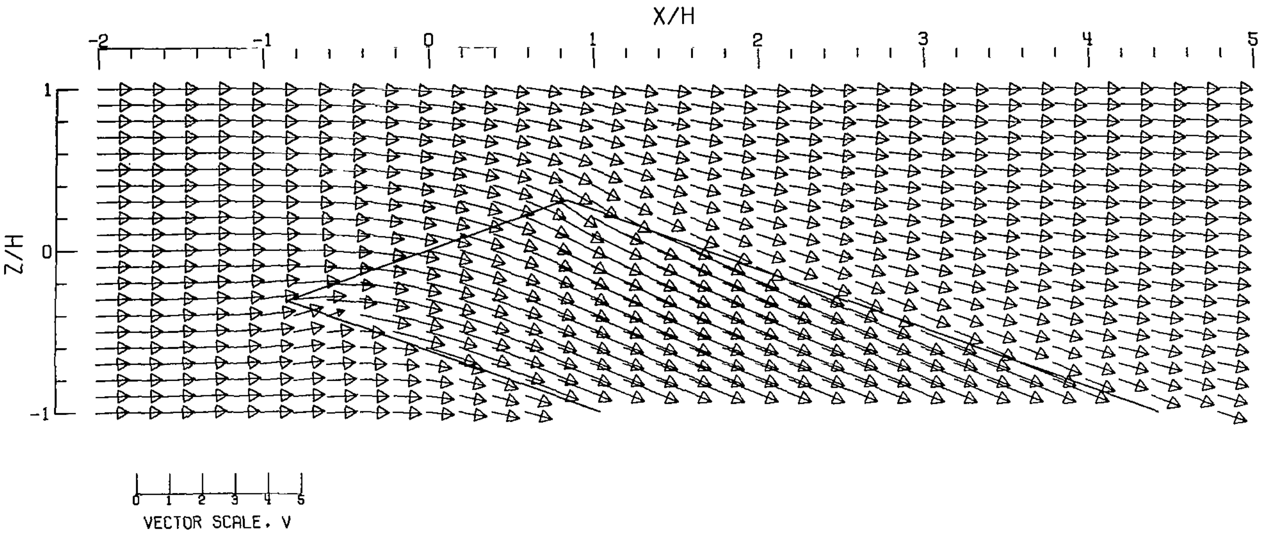

(A).- FREE AIR.

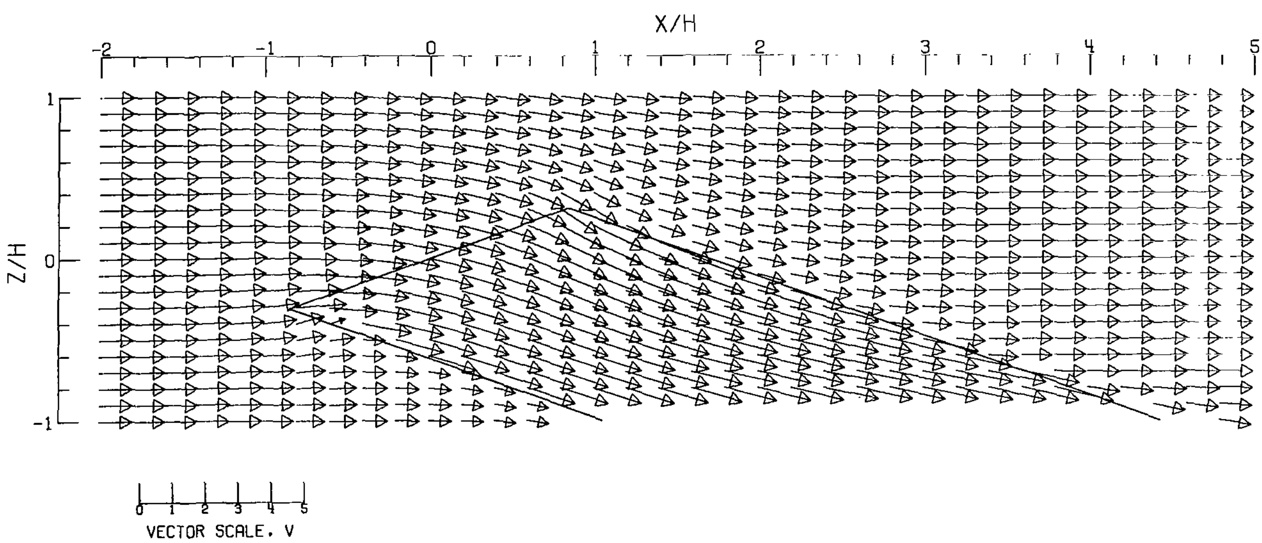

(B).- GROUND EFFECT.

Figure 88.- Flow vectors in the X-Z plane, calculated using doublet strings. The rotor and the edges of the wake are shown. ζ = 1.000; η = 1.0; γ = 1.0; σ = 0.900; α = -20.0°; χ = 70.0°; uniform loading.

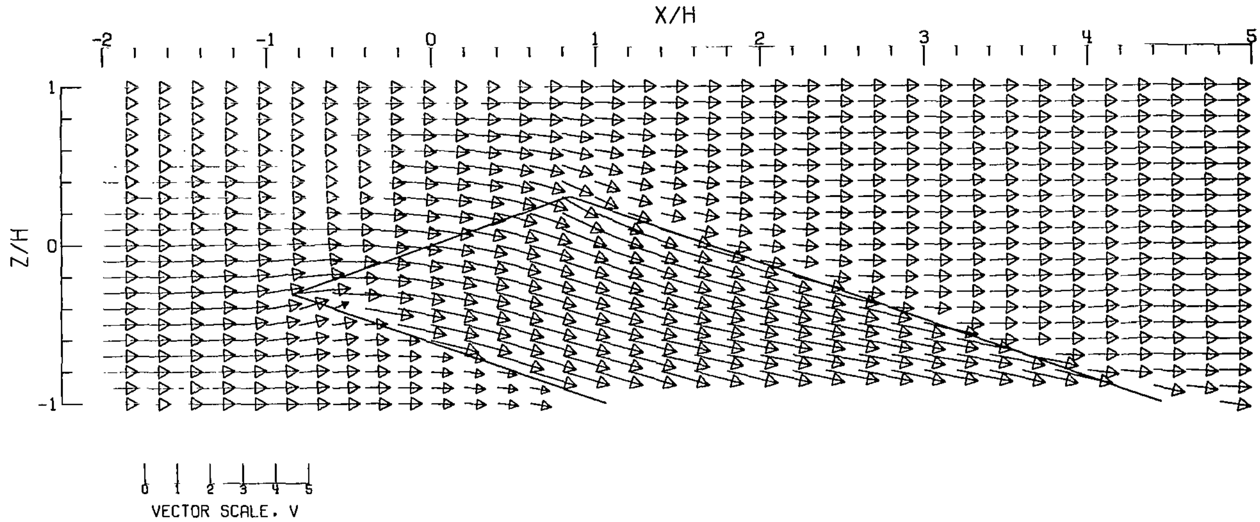

(C).- CLOSED TUNNEL.

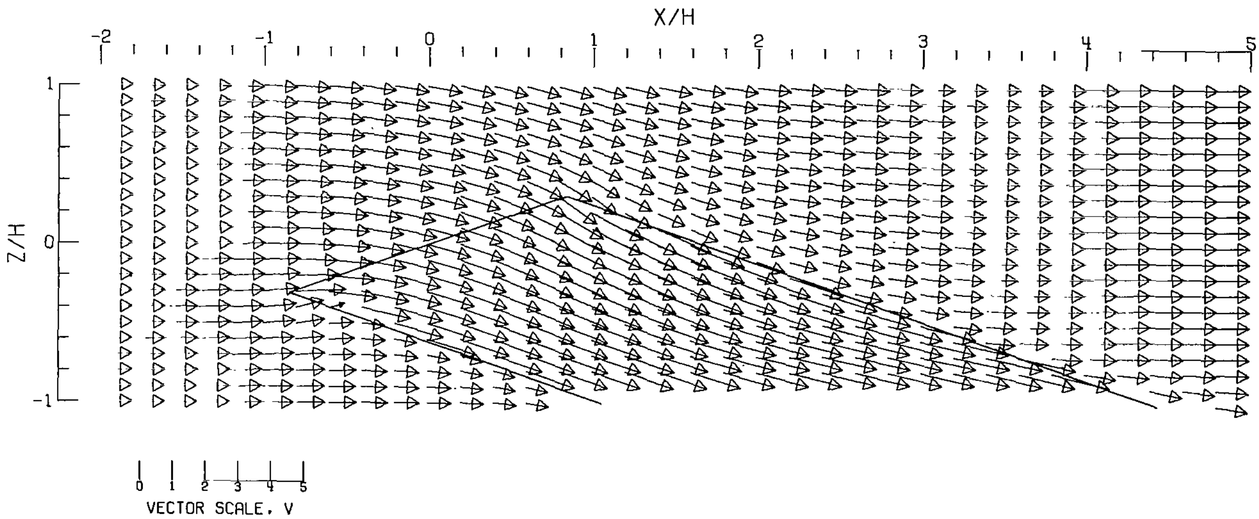

(D).- CLOSED-ON-BOTTOM-ONLY TUNNEL.

Figure 88.- Concluded.

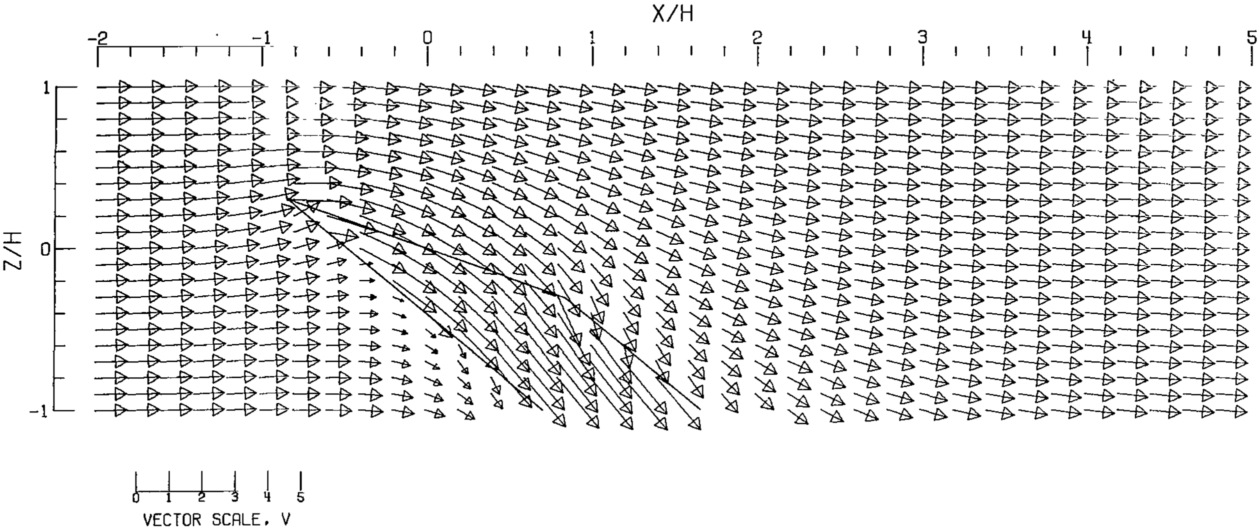

(A).- FREE AIR.

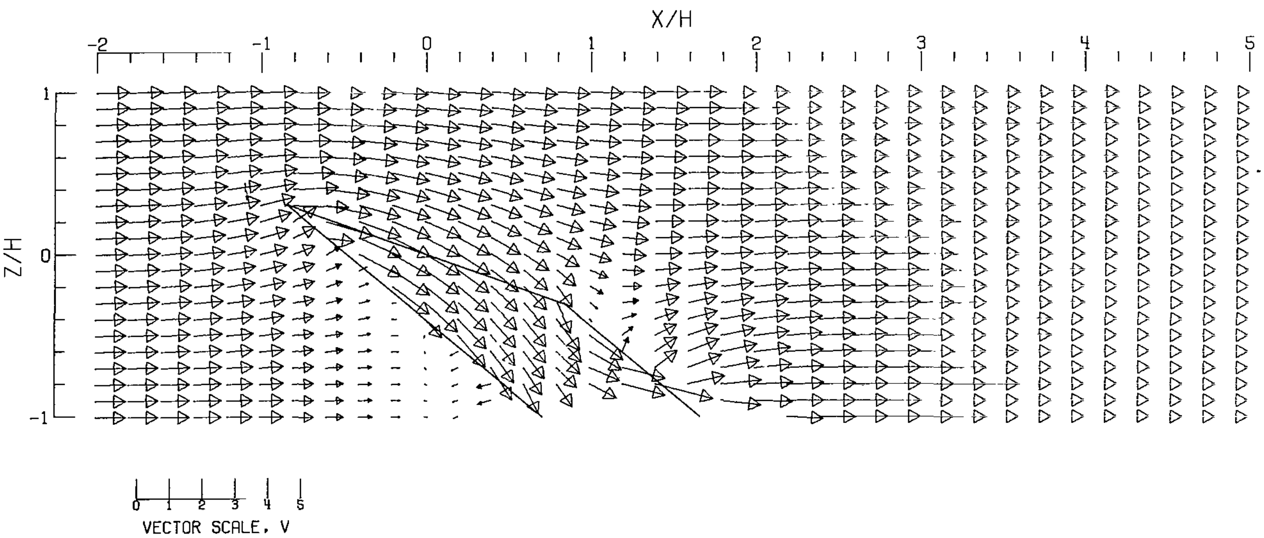

(B).- GROUND EFFECT.

Figure 89.- Flow vectors in the X-Z plane, calculated using doublet strings. The rotor and the edges of the wake are shown. ζ = 1.000; η = 1.0; γ = 1.0; σ = 0.900; $\alpha = 20.0^{0}$; $\chi = 50.0^{0}$; uniform loading.

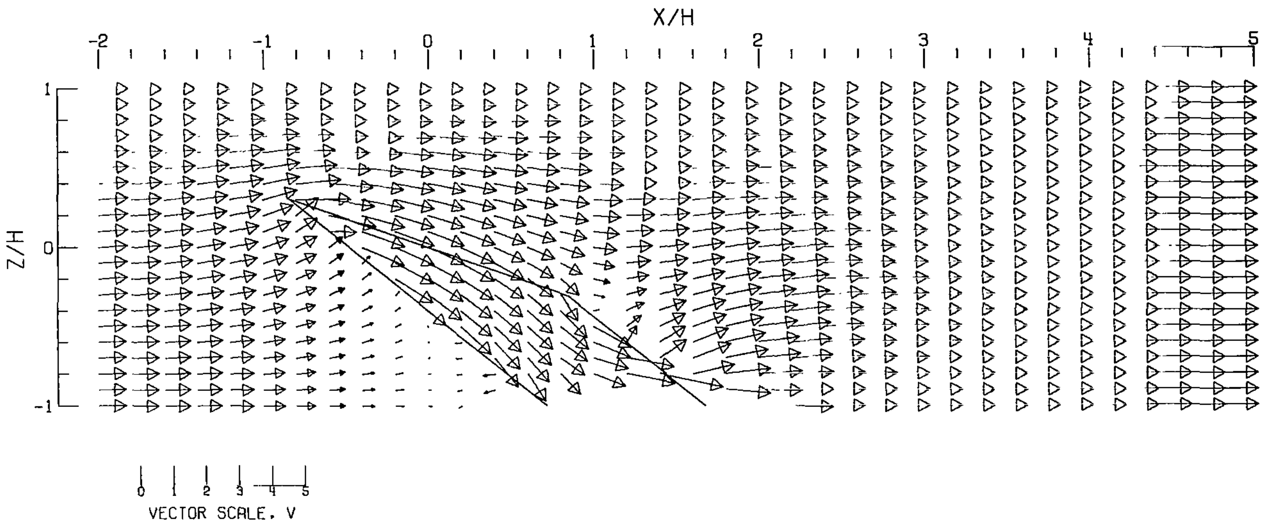

(C).- CLOSED TUNNEL.

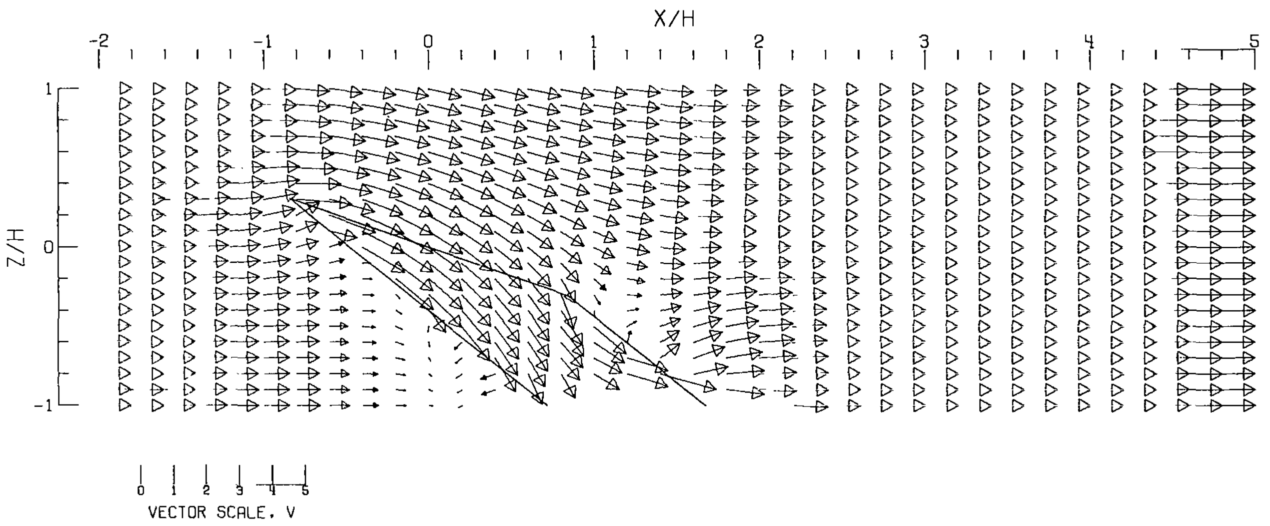

(D).- CLOSED-ON-BOTTOM-ONLY TUNNEL.

Figure 89.- Concluded.

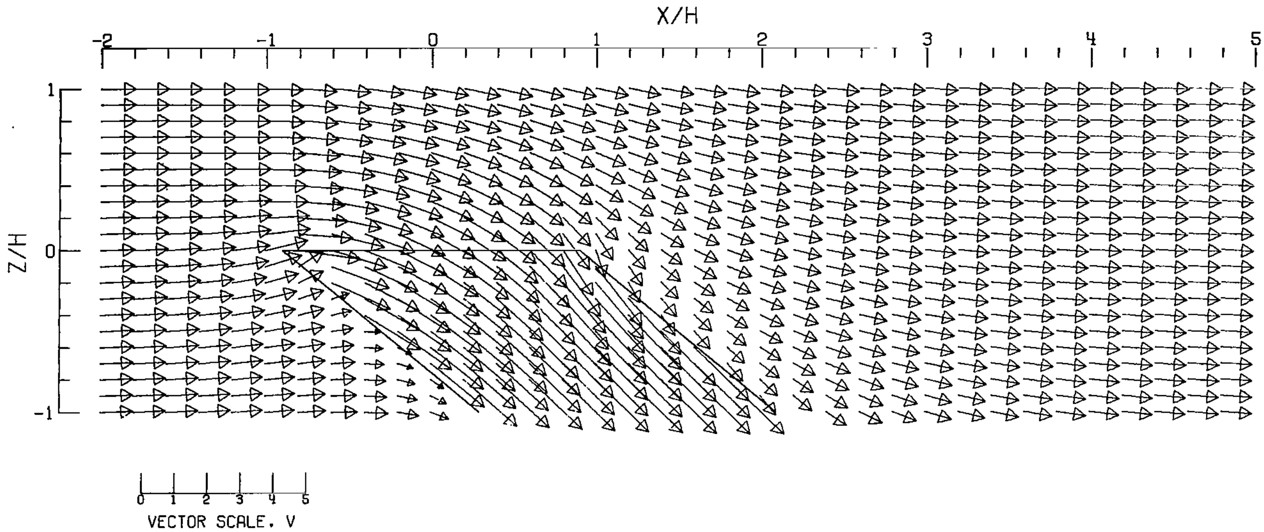

(A).- FREE AIR.

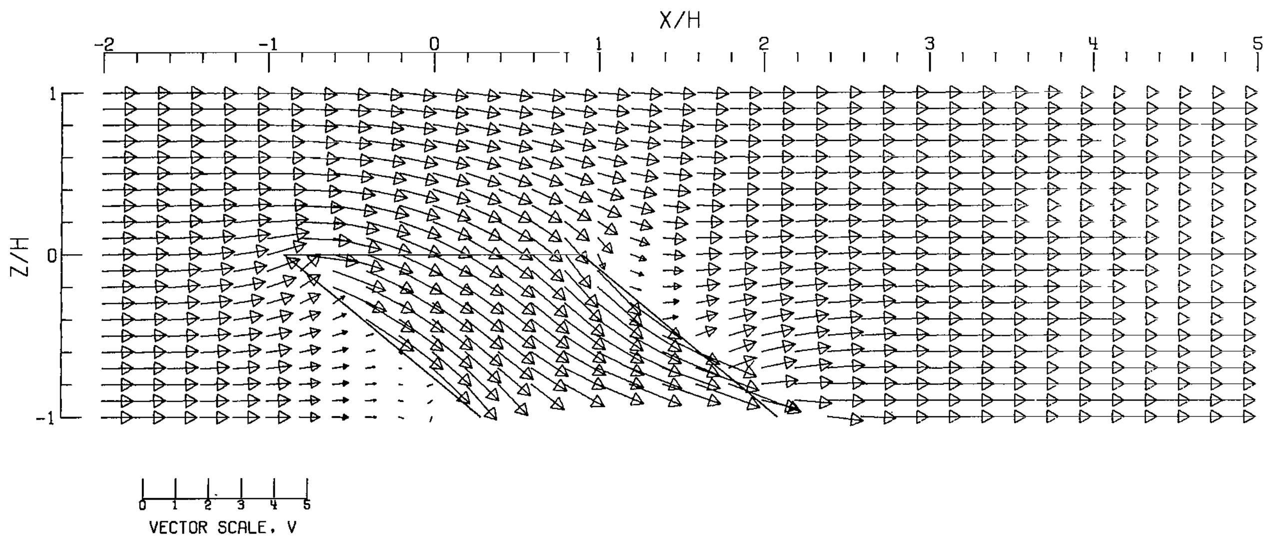

(B).- GROUND EFFECT.

Figure 90.- Flow vectors in the X-Z plane, calculated using doublet strings. The rotor and the edges of the wake are shown. $\zeta = 1.000$; $\eta = 1.000$; $\gamma = 1.000$; $\sigma = 0.900$; $\alpha = 0.000^{0}$; $\chi = 50.000^{0}$; uniform loading.

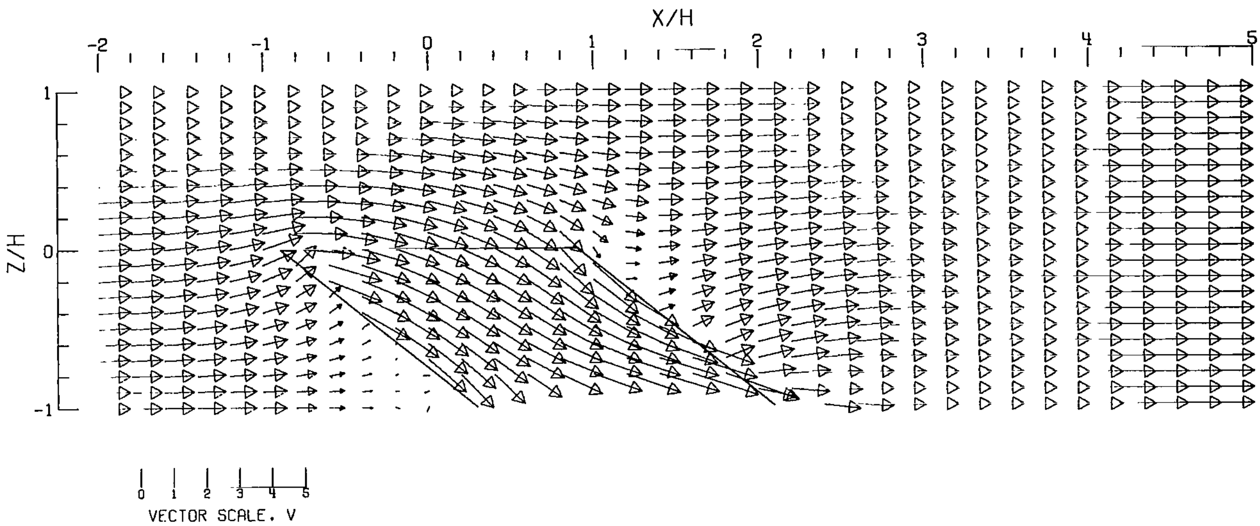

(C).- CLOSED TUNNEL.

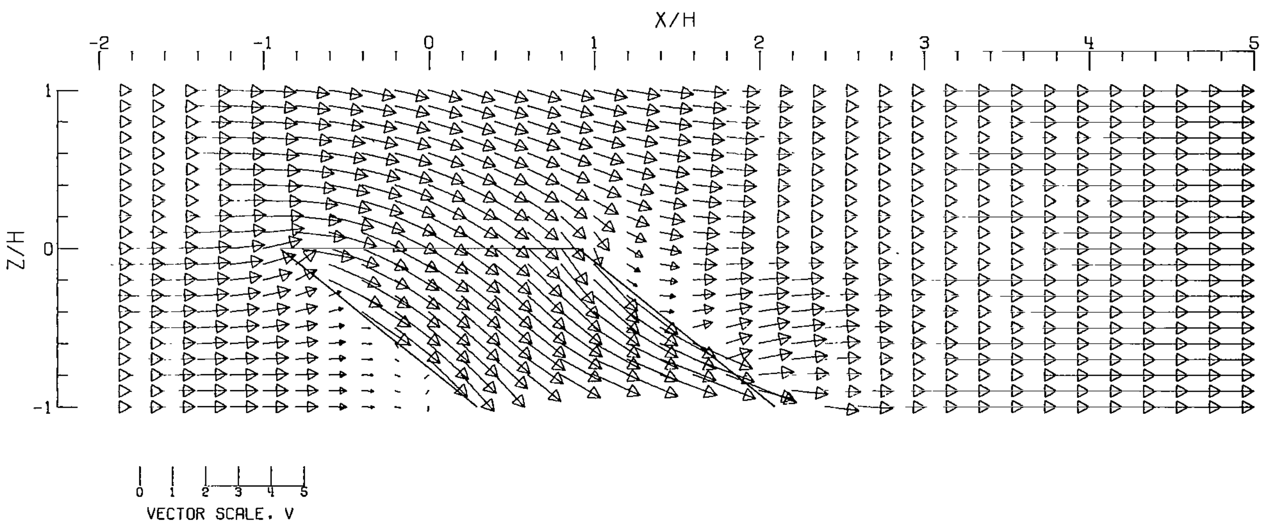

(D).- CLOSED-ON-BOTTOM-ONLY TUNNEL.

Figure 90.- Concluded.

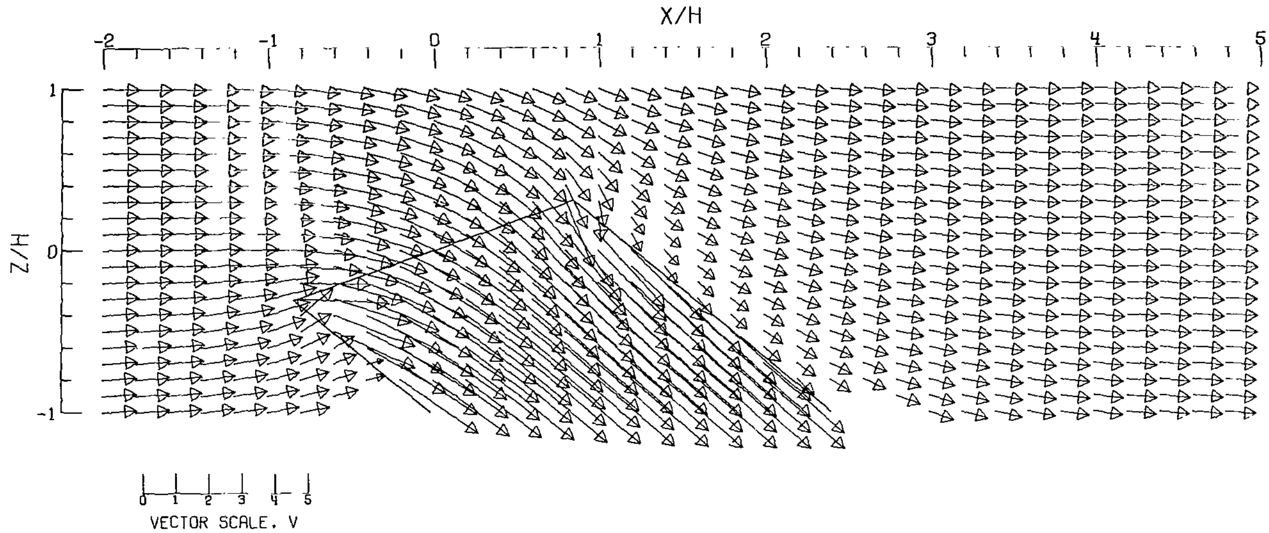

(A).- FREE AIR.

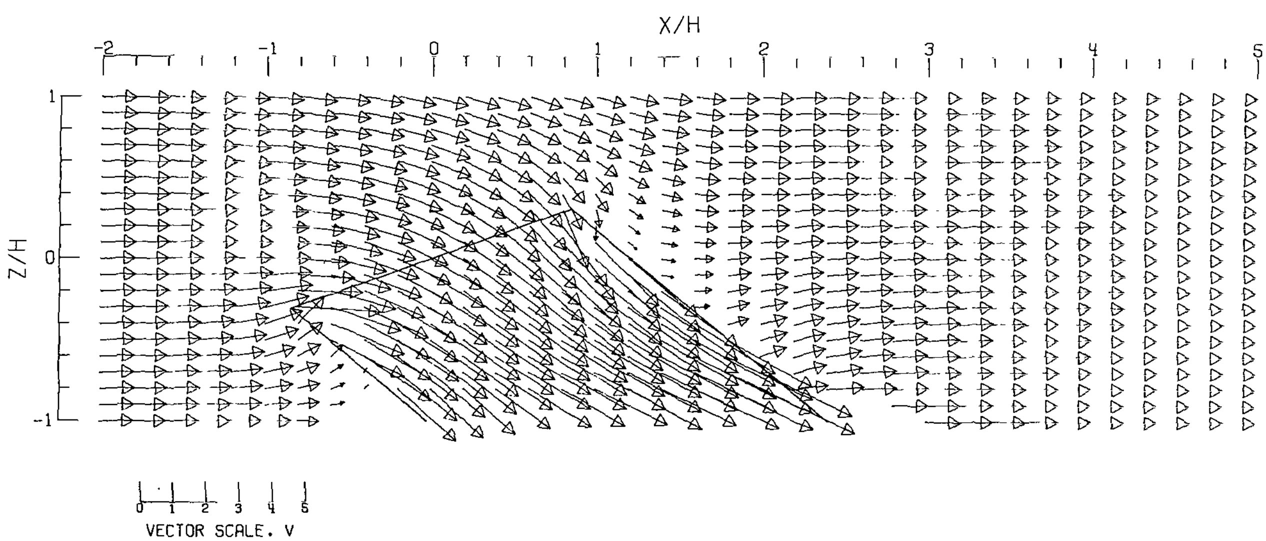

(B).- GROUND EFFECT.

Figure 91.- Flow vectors in the X-Z plane, calculated using doublet strings. The rotor and the edges of the wake are shown. ζ = 1.000; η = 1.0; γ = 1.0; σ = 0.900; α = -20.0°; χ = 50.0°; uniform loading.

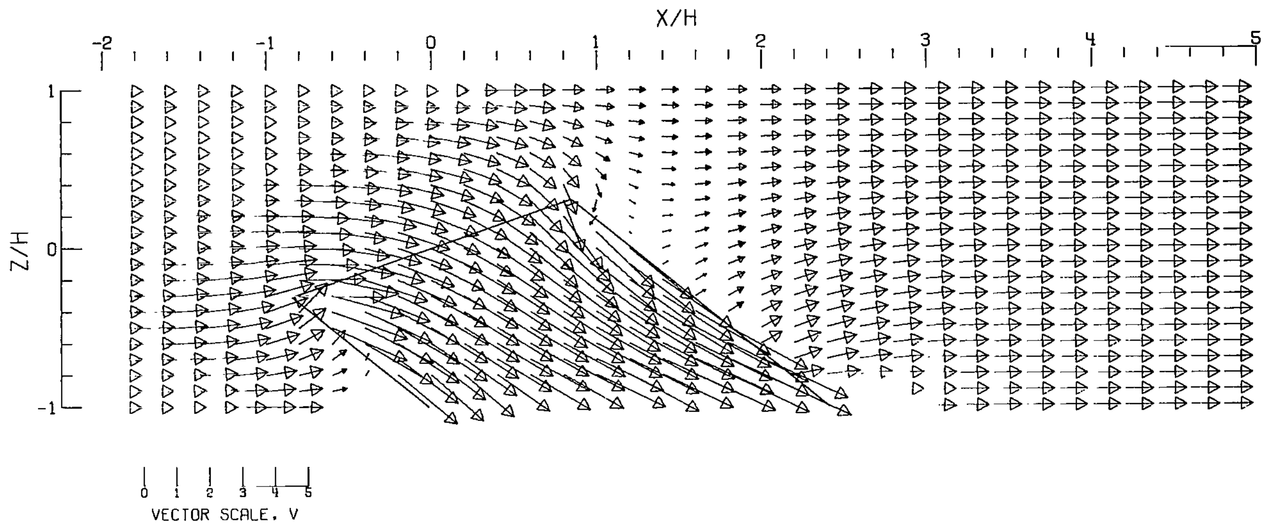

(C).- CLOSED TUNNEL.

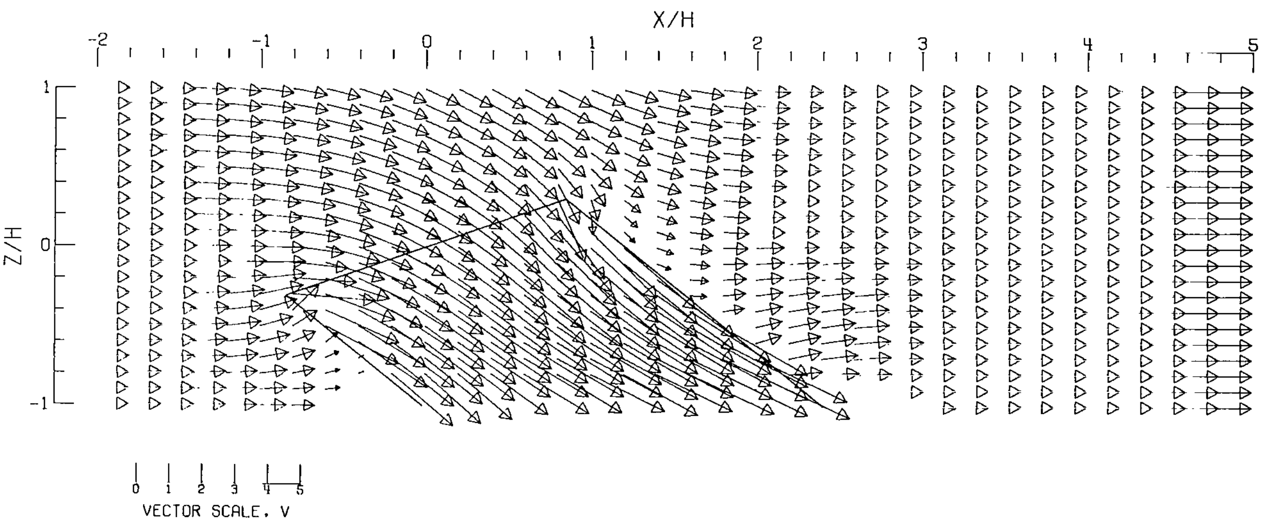

(D).- CLOSED-ON-BOTTOM-ONLY TUNNEL.

Figure 91.- Concluded.

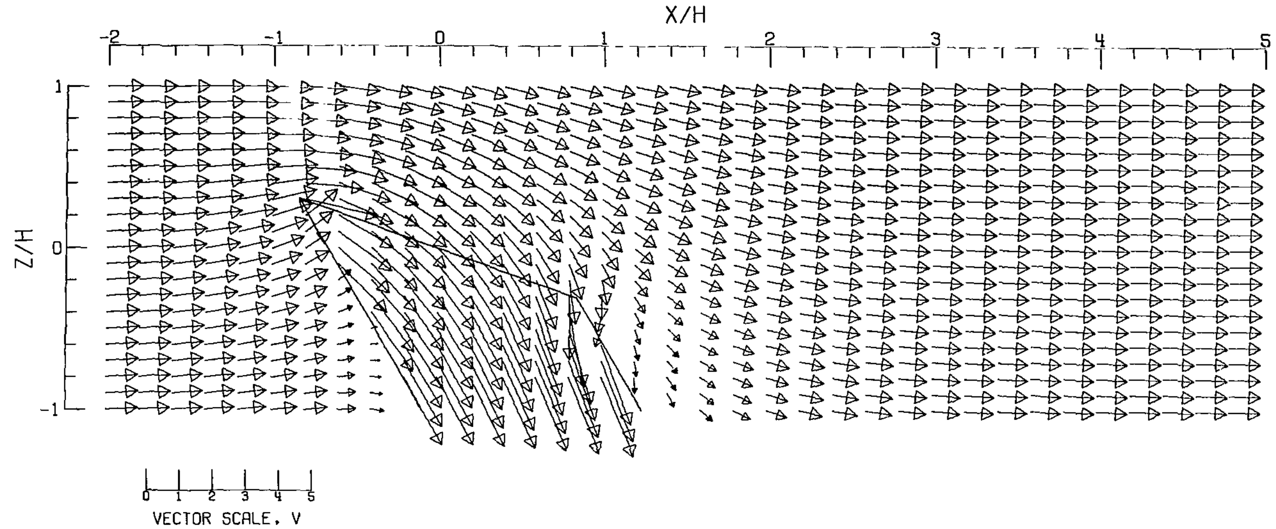

(A).- FREE AIR.

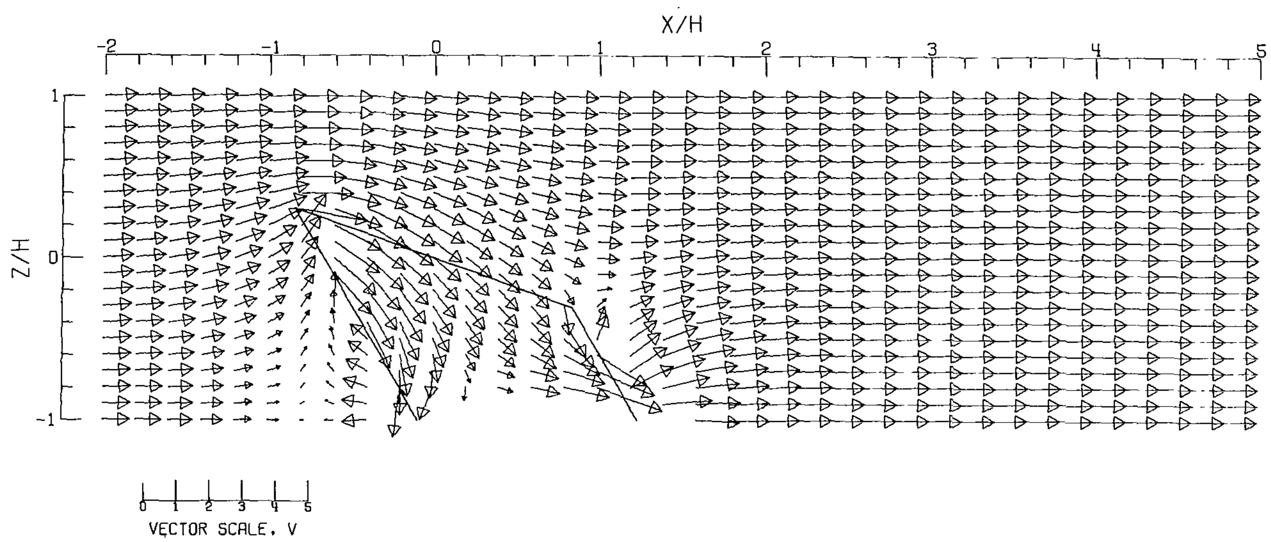

(B).- GROUND EFFECT.

Figure 92.- Flow vectors in the X-Z plane, calculated using doublet strings. The rotor and the edges of the wake are shown. ζ = 1.000; η = 1.000; γ = 1.000; σ = 0.900; α = 20.000°; χ = 30.000°; uniform loading.

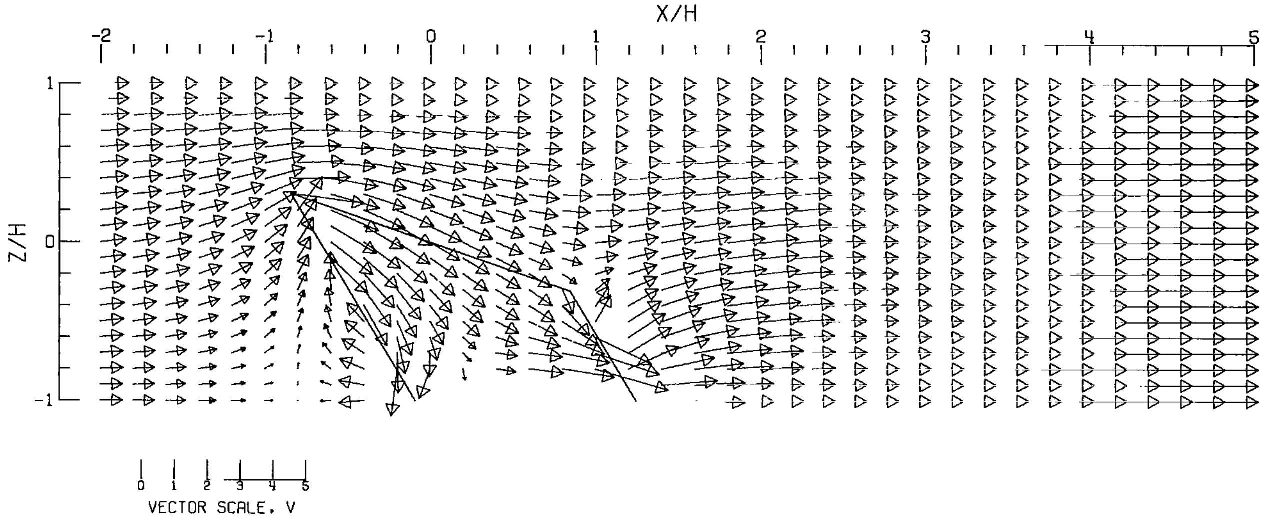

(C).- CLOSED TUNNEL.

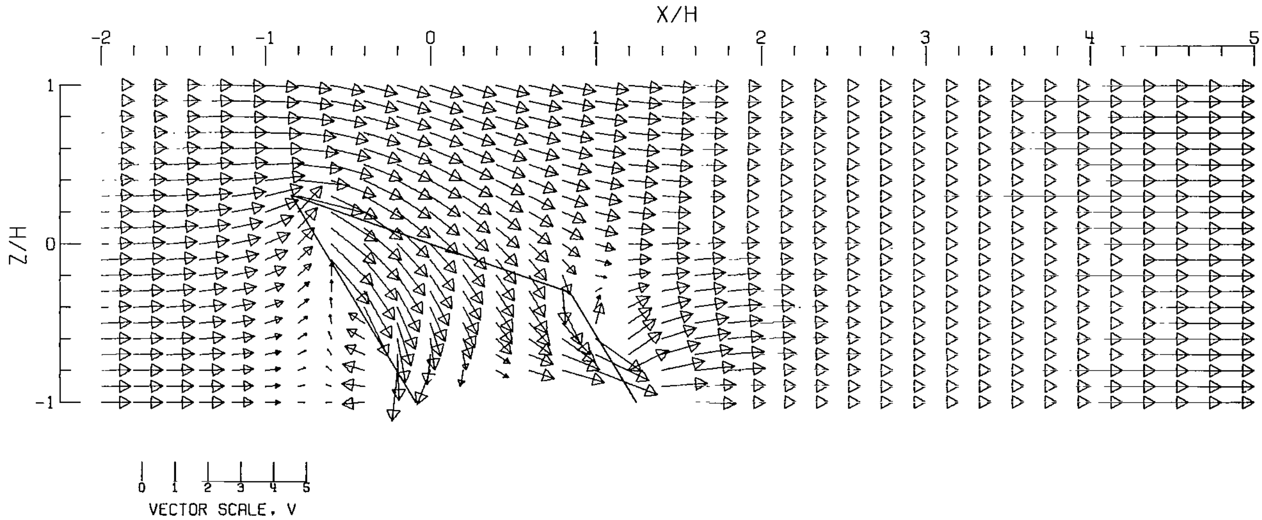

(D).- CLOSED-ON-BOTTOM-ONLY TUNNEL.

Figure 92.- Concluded.

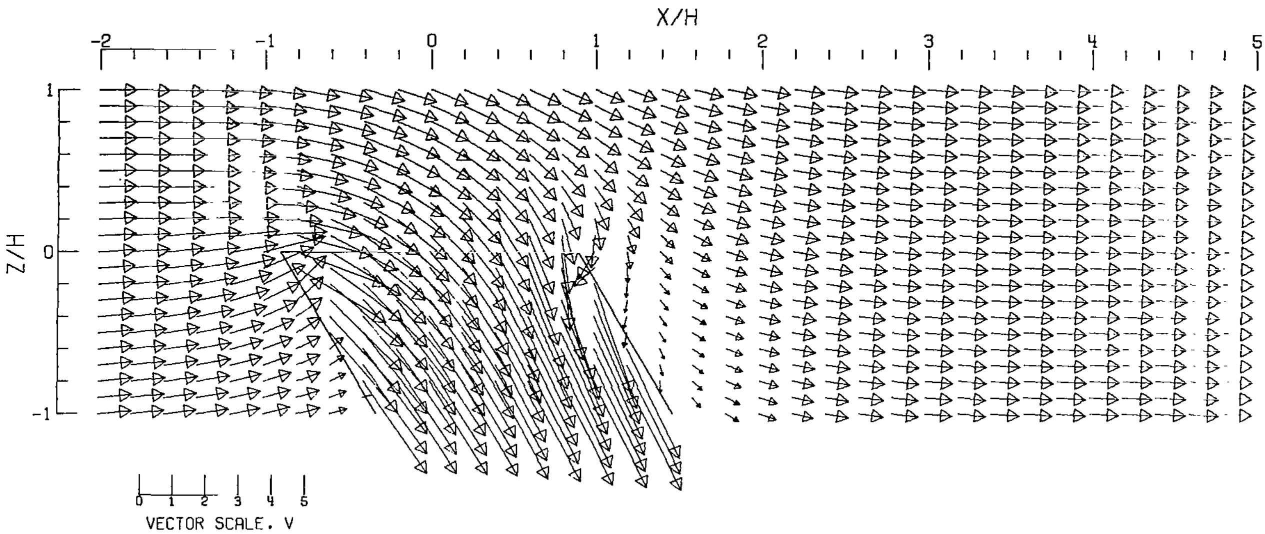

(A).– FREE AIR.

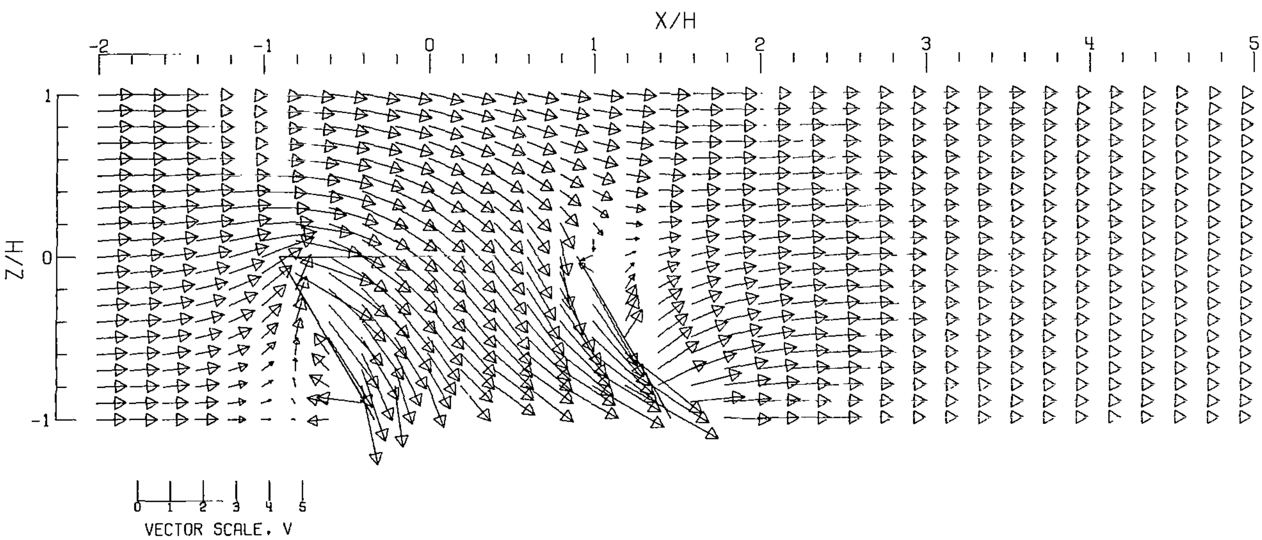

(B).– GROUND EFFECT.

Figure 93.- Flow vectors in the X-Z plane, calculated using doublet strings. The rotor and the edges of the wake are shown. ζ = 1.000; η = 1.000; γ = 1.000; σ = 0.900; α = 0.000°; χ = 30.000°; uniform loading.

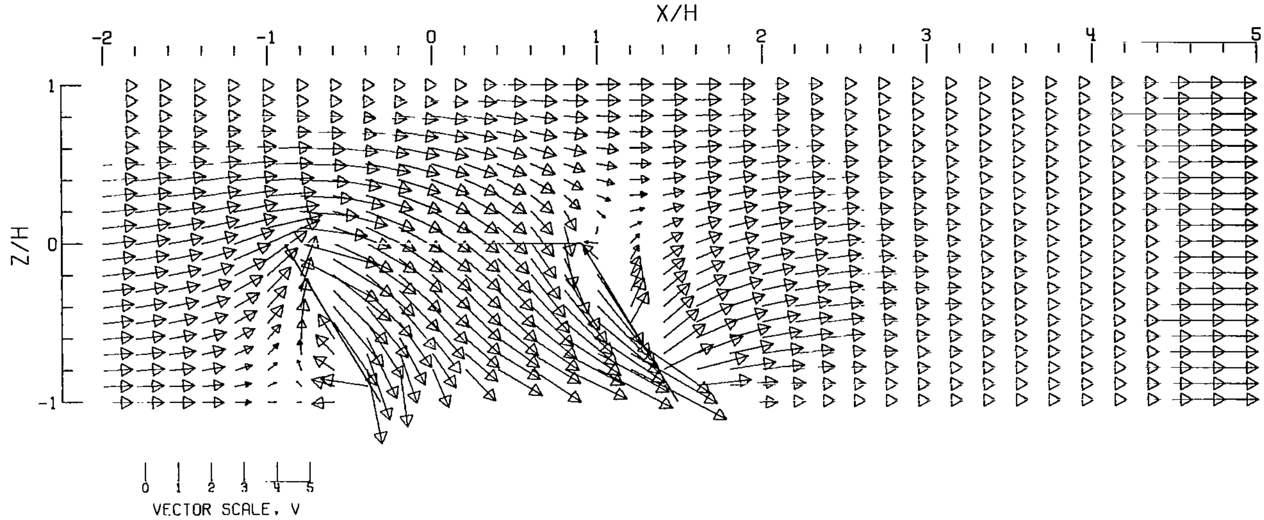

(C).- CLOSED TUNNEL.

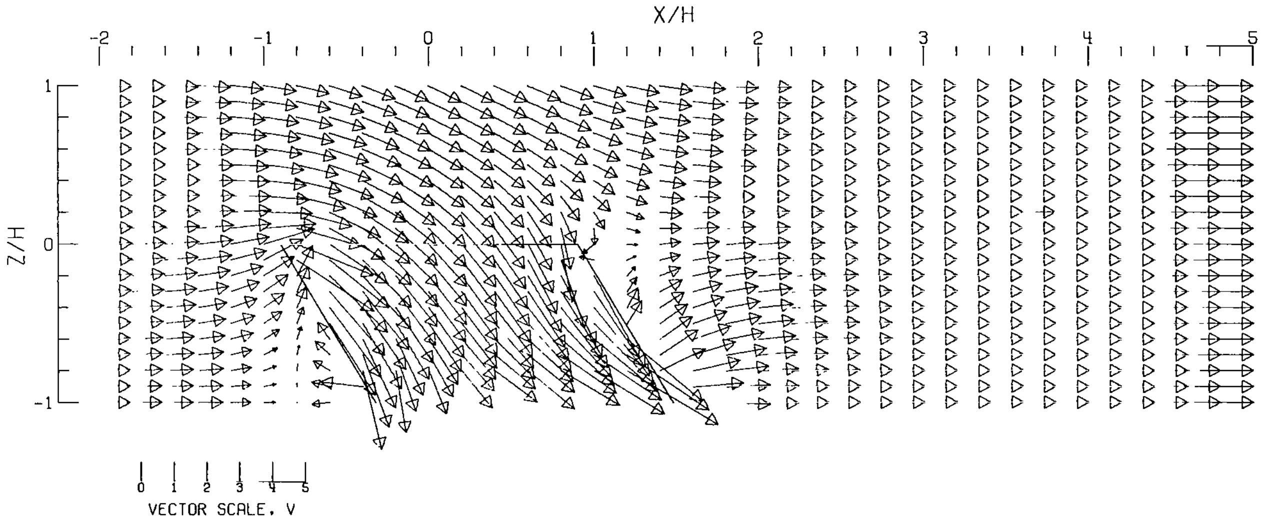

(D).- CLOSED-ON-BOTTOM-ONLY TUNNEL.

Figure 93.- Concluded.

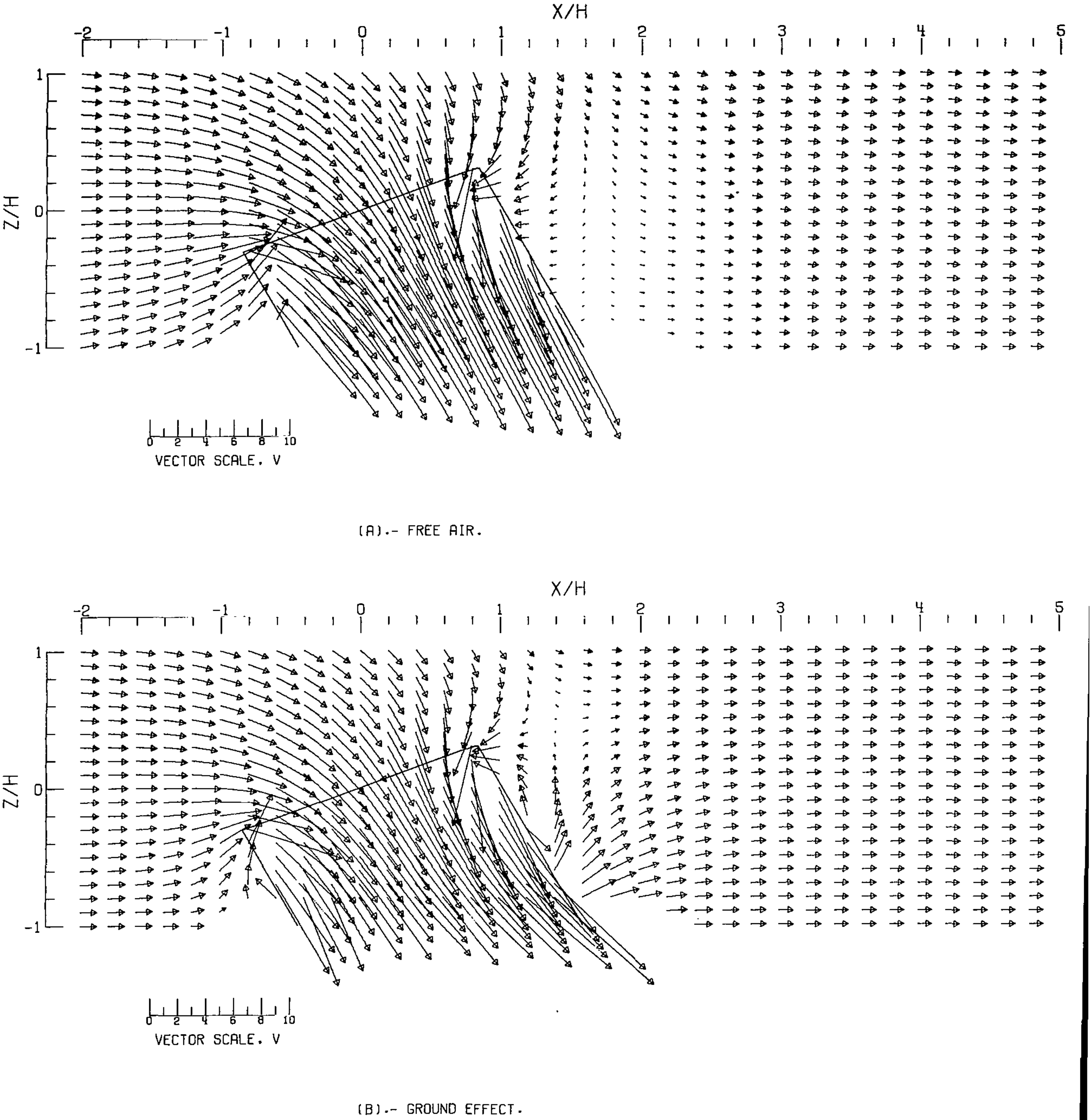

Figure 94.- Flow vectors in the X-Z plane, calculated using doublet strings. The rotor and the edges of the wake are shown. ζ = 1.000; η = 1.000; γ = 1.000; σ = 0.900; α = -20.000°; χ = 30.000°; uniform loading.

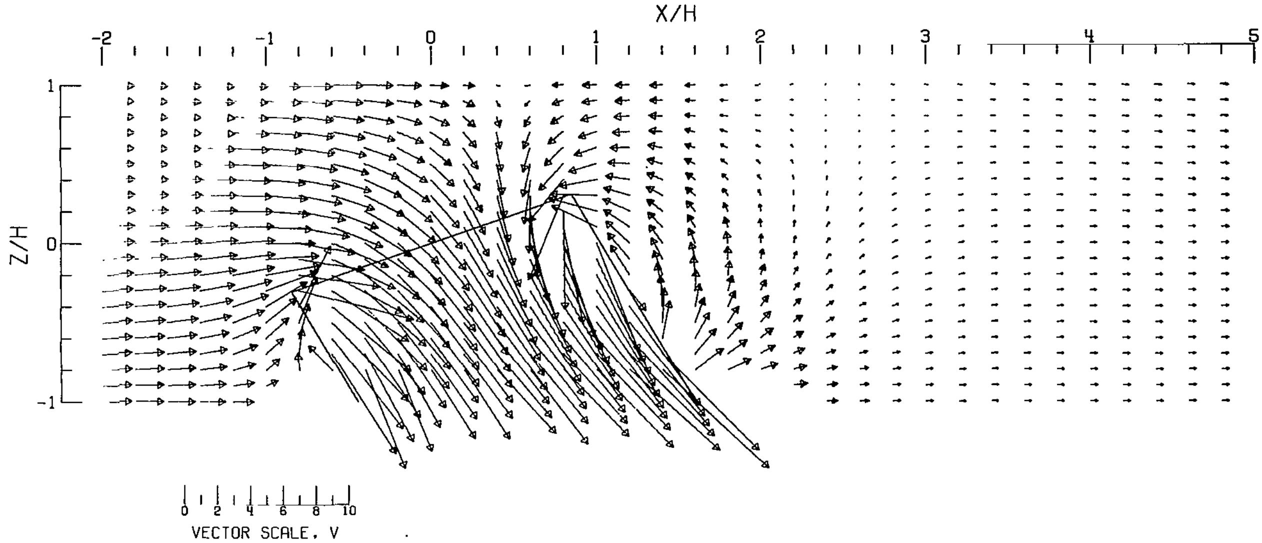

(C).– CLOSED TUNNEL.

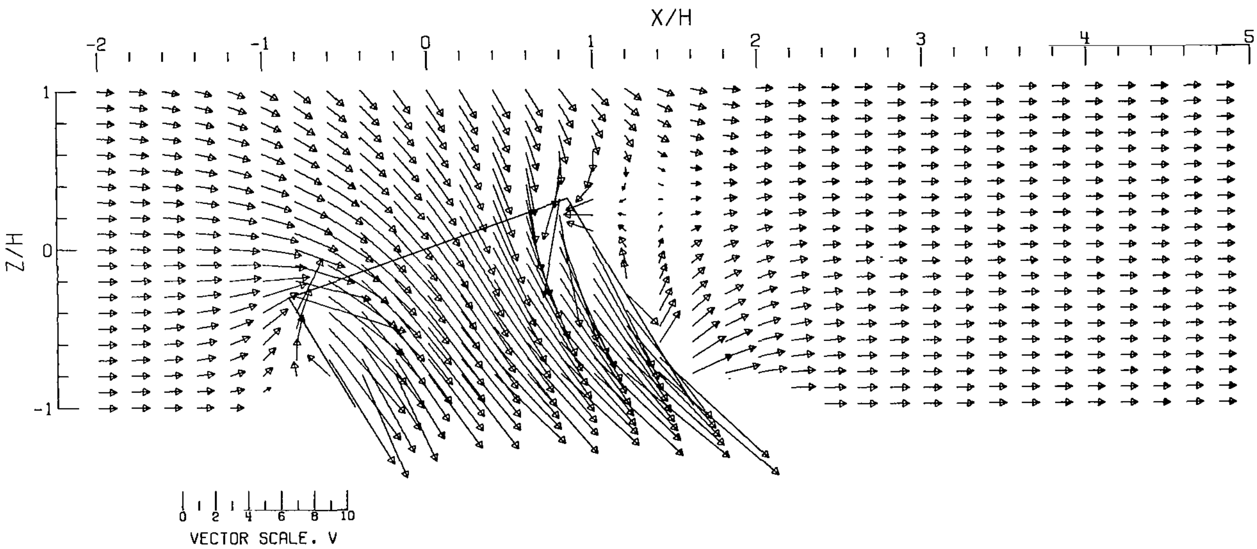

(D).– CLOSED-ON-BOTTOM-ONLY TUNNEL.

Figure 94.- Concluded.

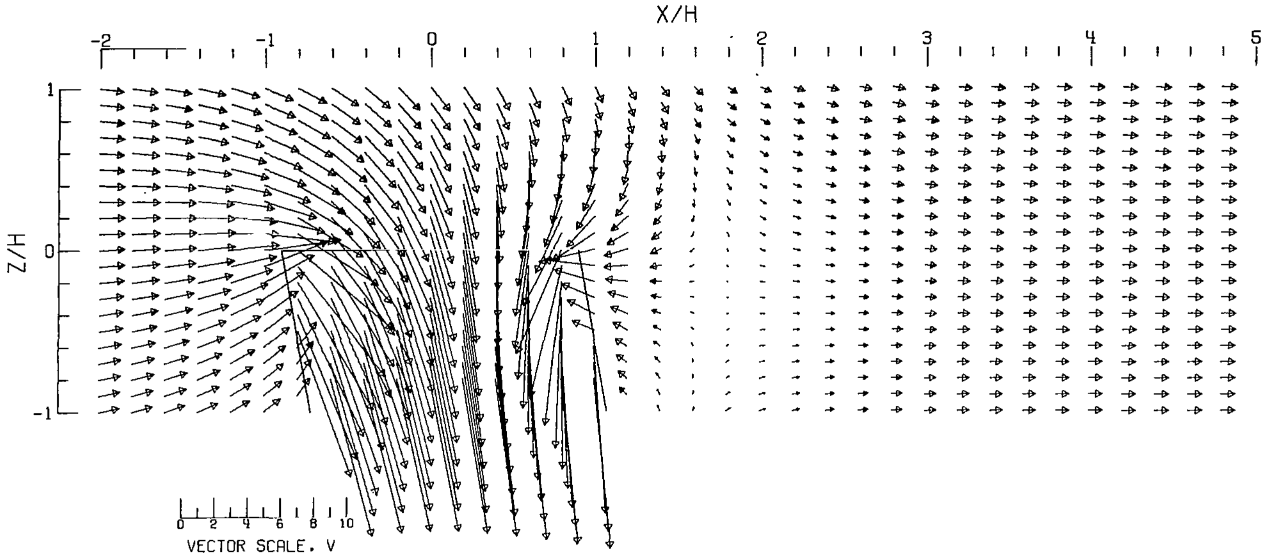

(A).- FREE AIR.

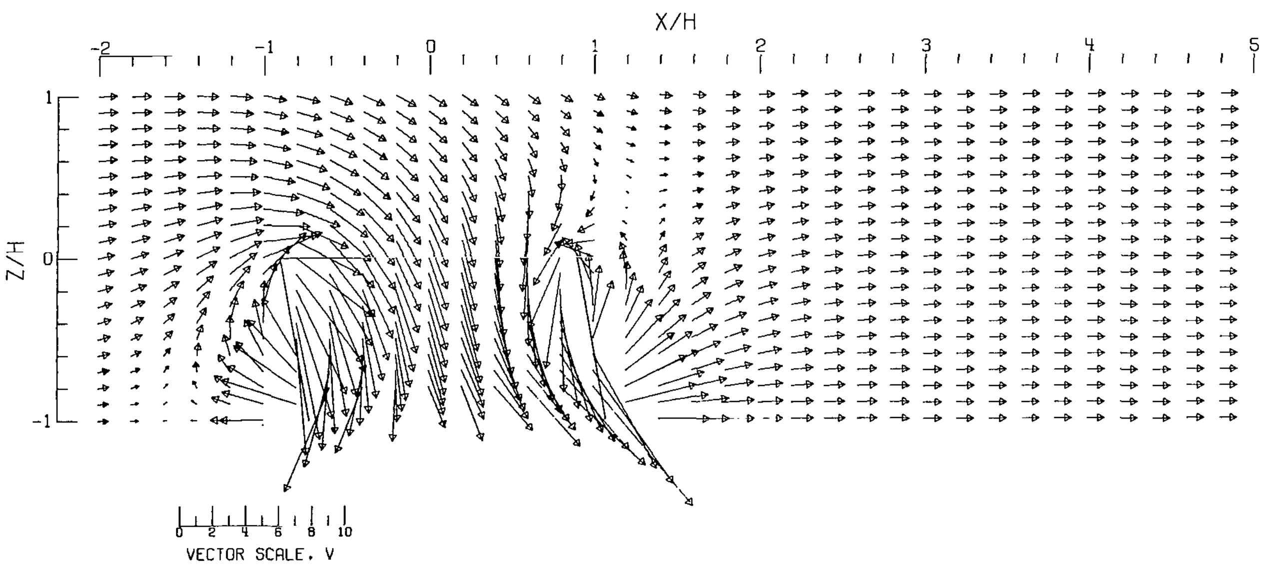

(B).- GROUND EFFECT.

Figure 95.- Flow vectors in the X-Z plane, calculated using doublet strings. The rotor and the edges of the wake are shown. ζ = 1.000; η = 1.000; γ = 1.000; σ = 0.900; α = 0.000°; χ = 10.000°; uniform loading.

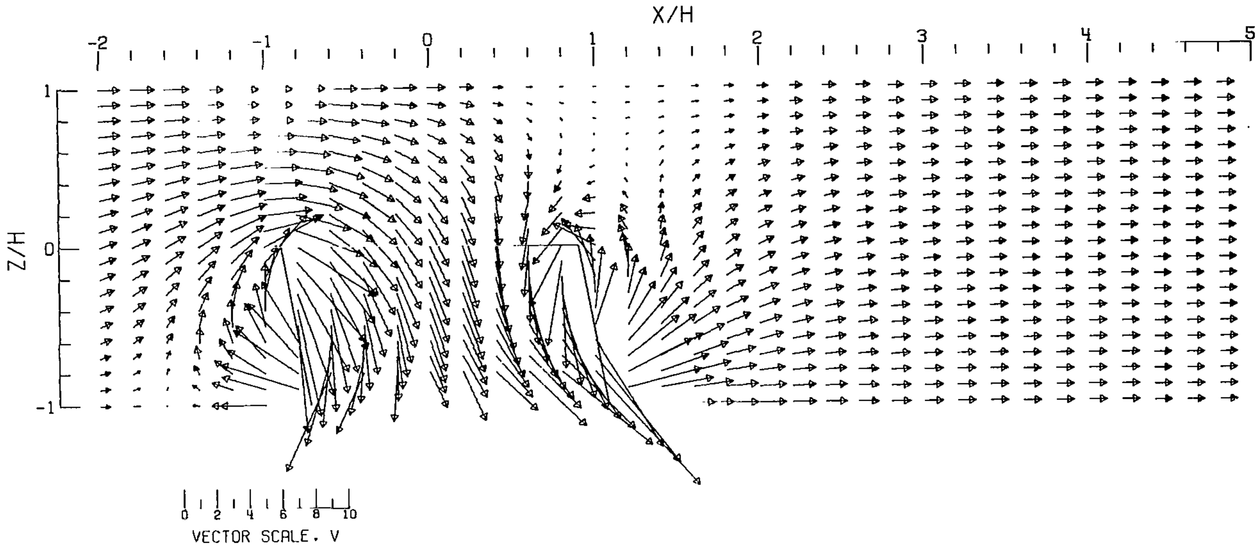

(C).-- CLOSED TUNNEL.

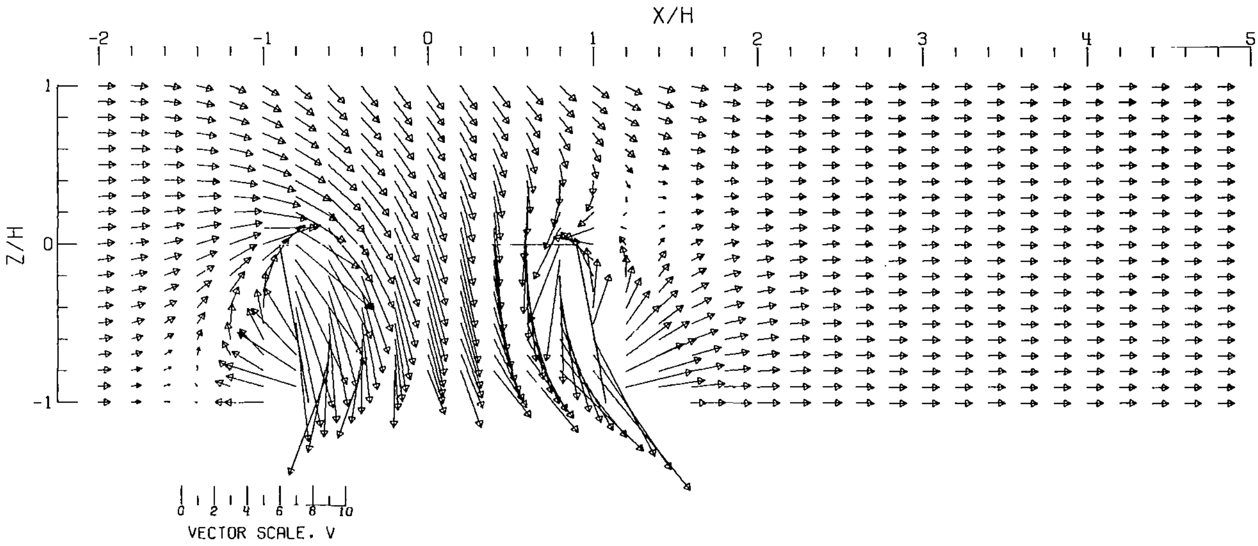

(D).-- CLOSED-ON-BOTTOM-ONLY TUNNEL.

Figure 95.- Concluded.

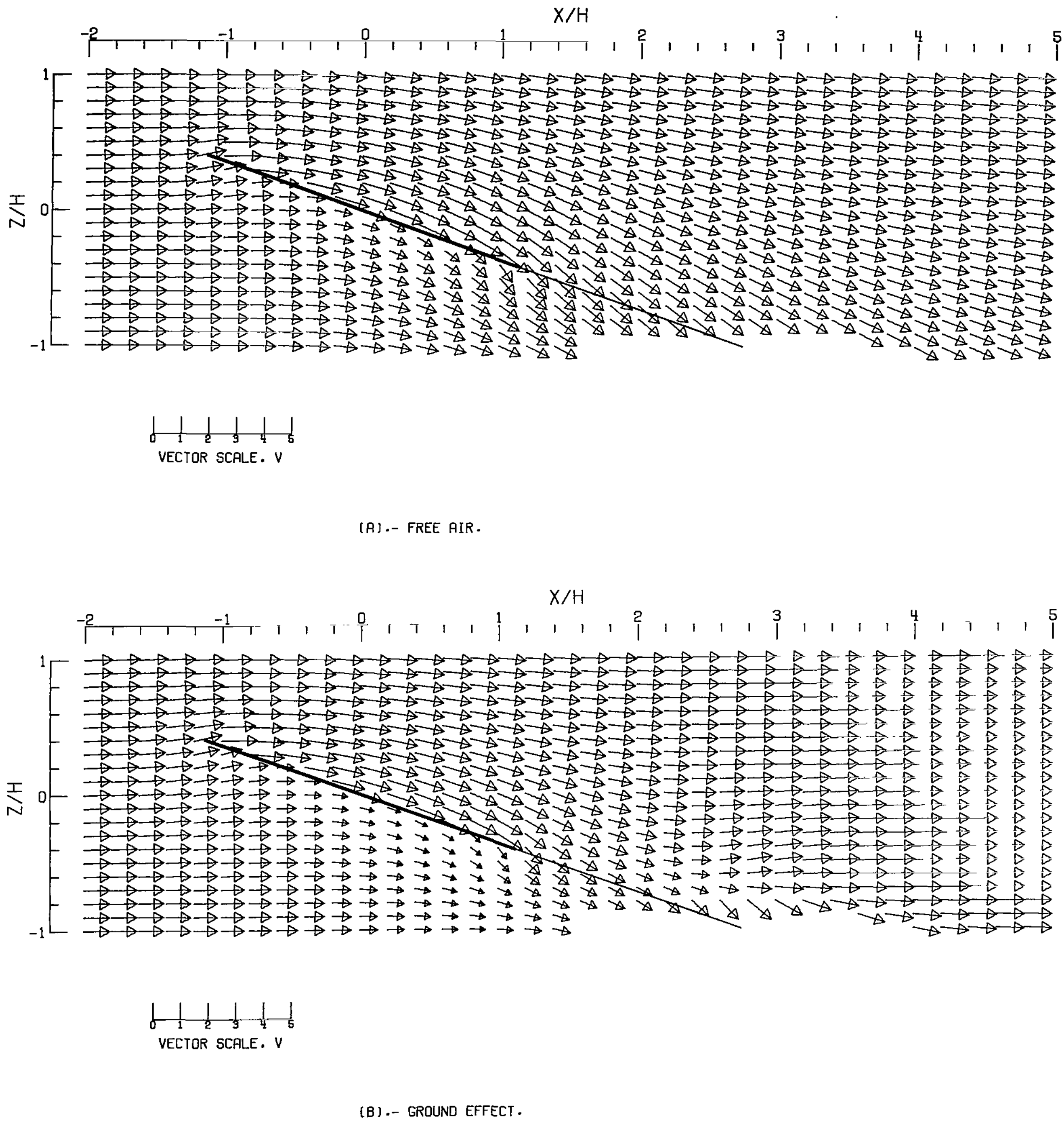

Figure 96.- Flow vectors in the X-Z plane, calculated using doublet strings. The rotor and the edges of the wake are shown. $\zeta = 1.000$; $\eta = 1.0$; $\gamma = 2.0$; $\sigma = 0.600$; $\alpha = 20.0^{\circ}$; $\chi = 70.0^{\circ}$; uniform loading.

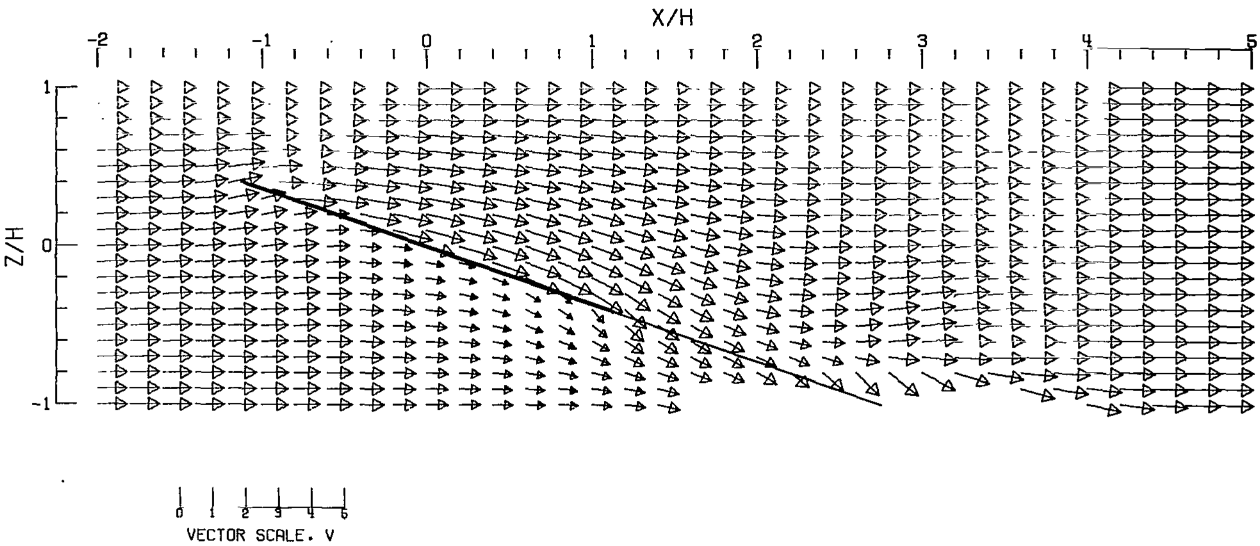

(C).– CLOSED TUNNEL.

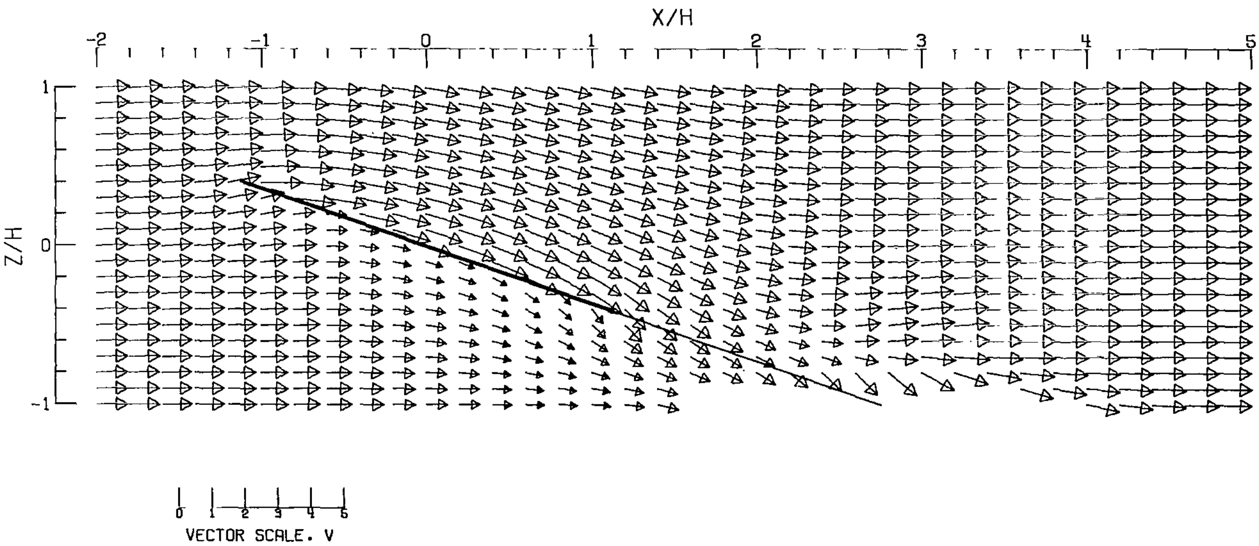

(D).– CLOSED-ON-BOTTOM-ONLY TUNNEL.

Figure 96.- Concluded.

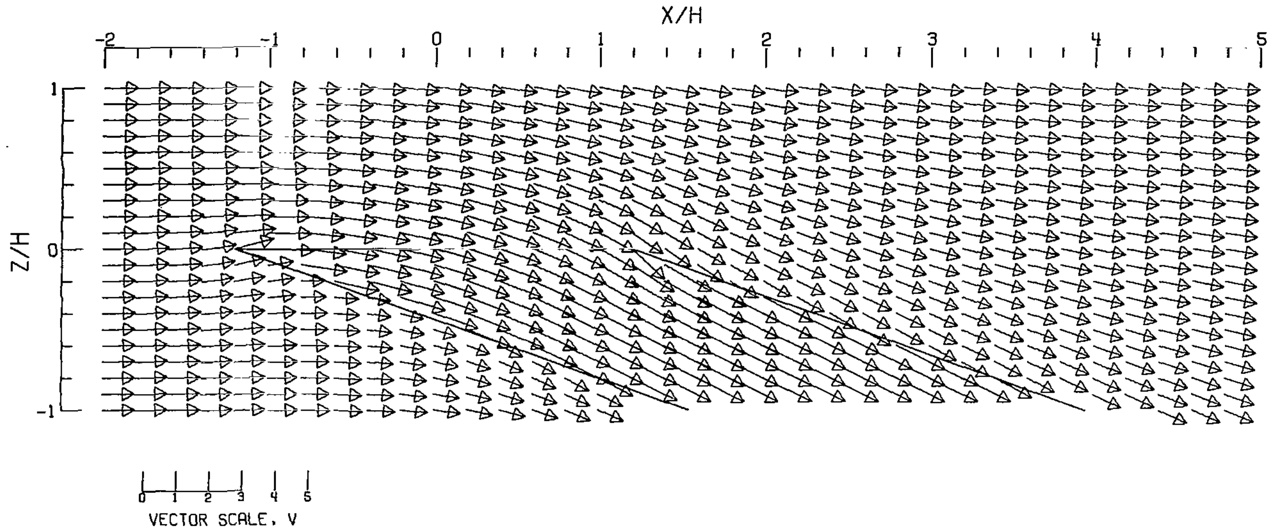

(A).- FREE AIR.

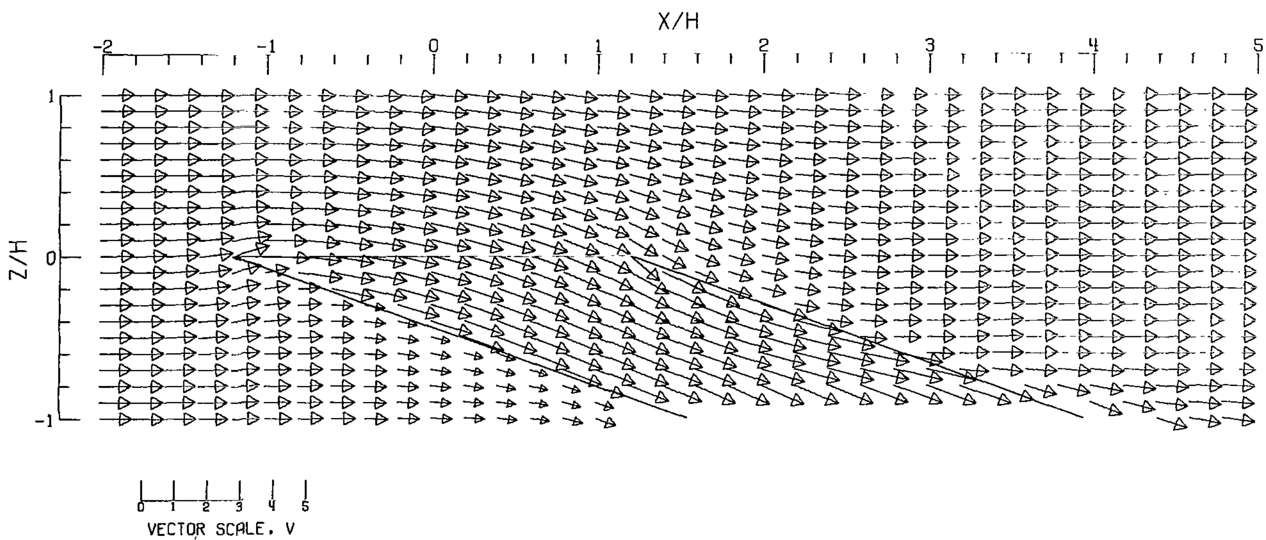

(B).- GROUND EFFECT.

Figure 97.- Flow vectors in the X-Z plane, calculated using doublet strings. The rotor and the edges of the wake are shown. ζ = 1.000; η = 1.0; γ = 2.0; σ = 0.600; α = 0.0°; χ = 70.0°; uniform loading.

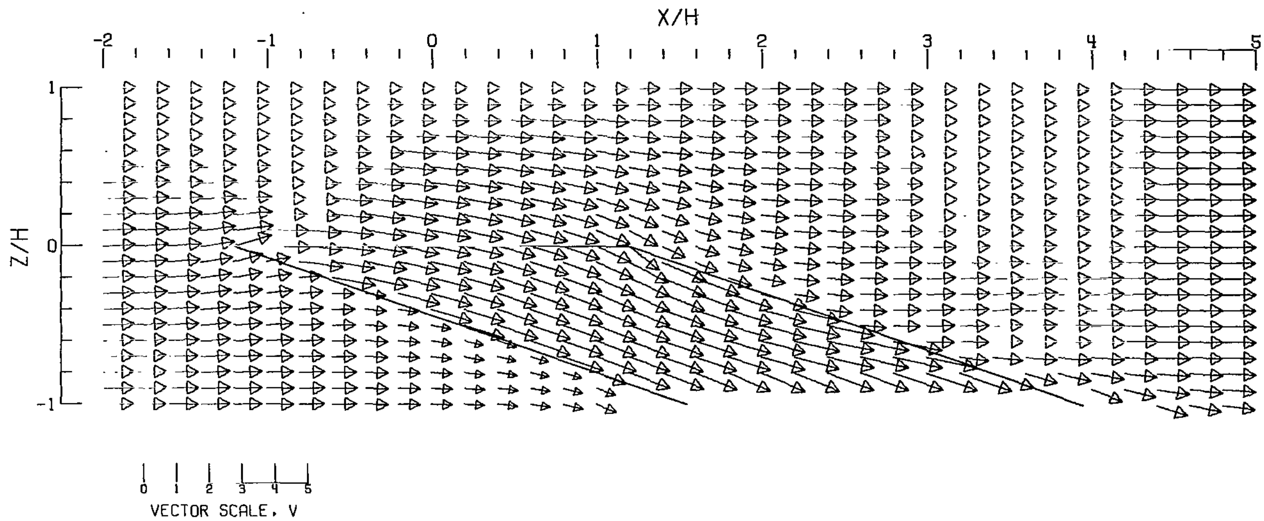

(C).- CLOSED TUNNEL.

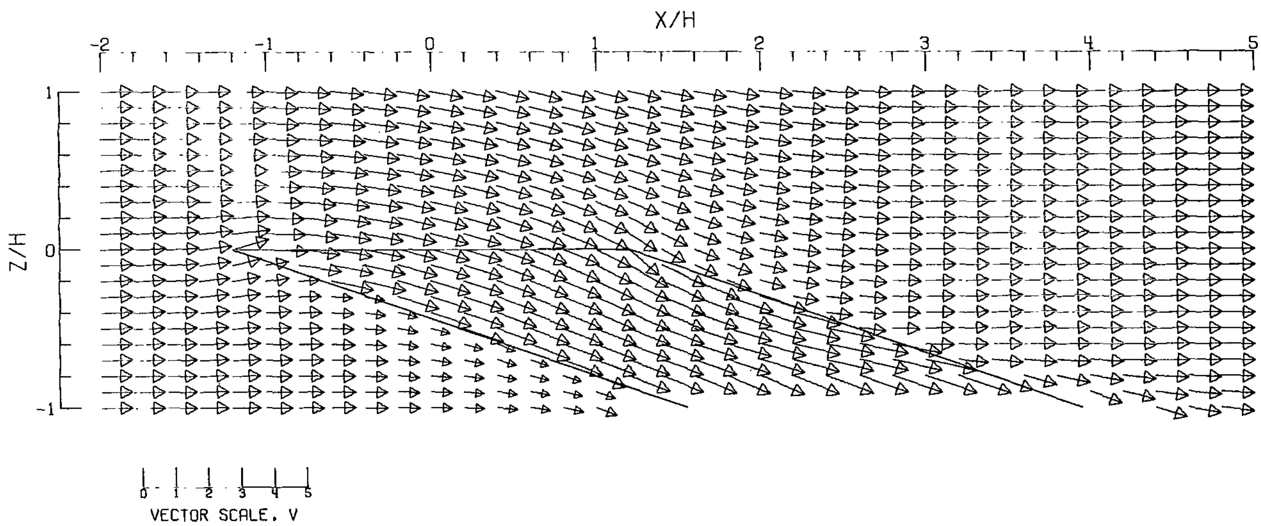

(D).- CLOSED-ON-BOTTOM-ONLY TUNNEL.

Figure 97.- Concluded.

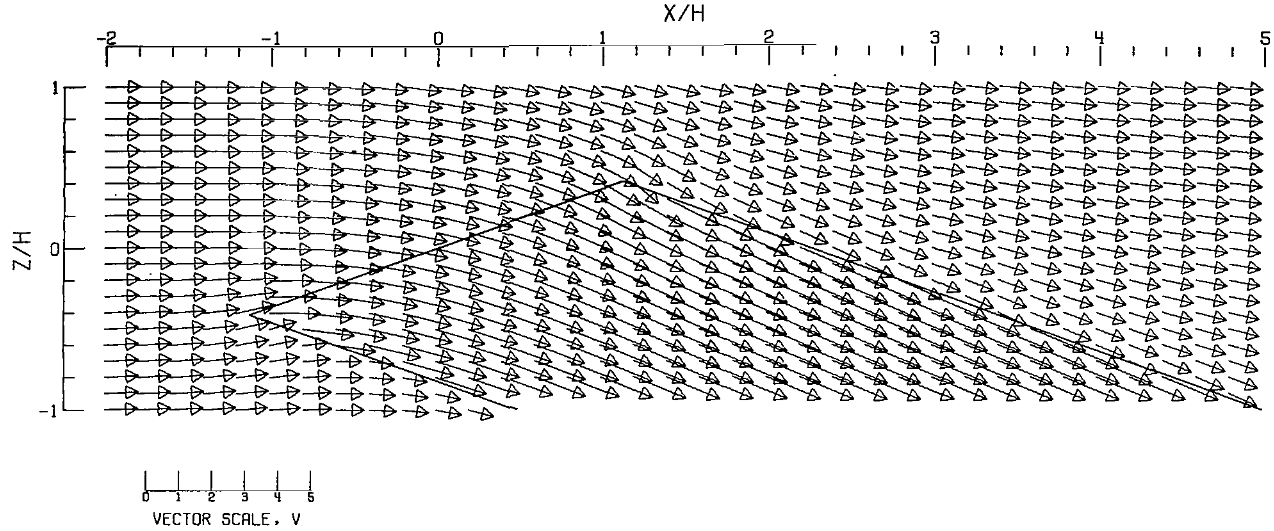

(A).- FREE AIR.

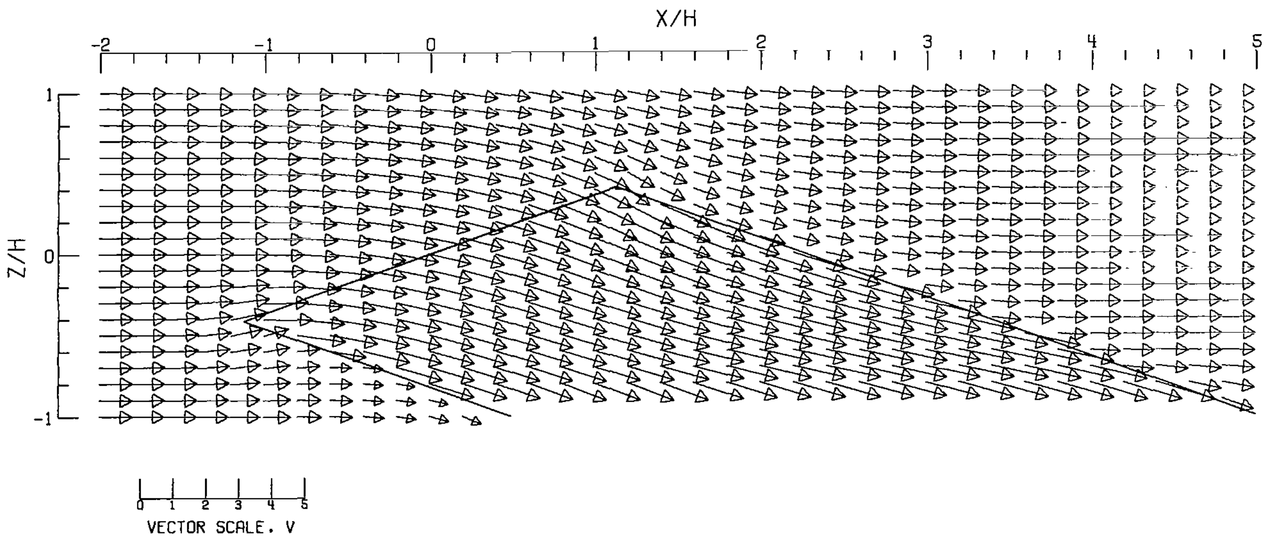

(B).- GROUND EFFECT.

Figure 98.- Flow vectors in the X-Z plane, calculated using doublet strings. The rotor and the edges of the wake are shown. ζ = 1.000; η = 1.0; γ = 2.0; σ = 0.600; α = -20.0°; χ = 70.0°; uniform loading.

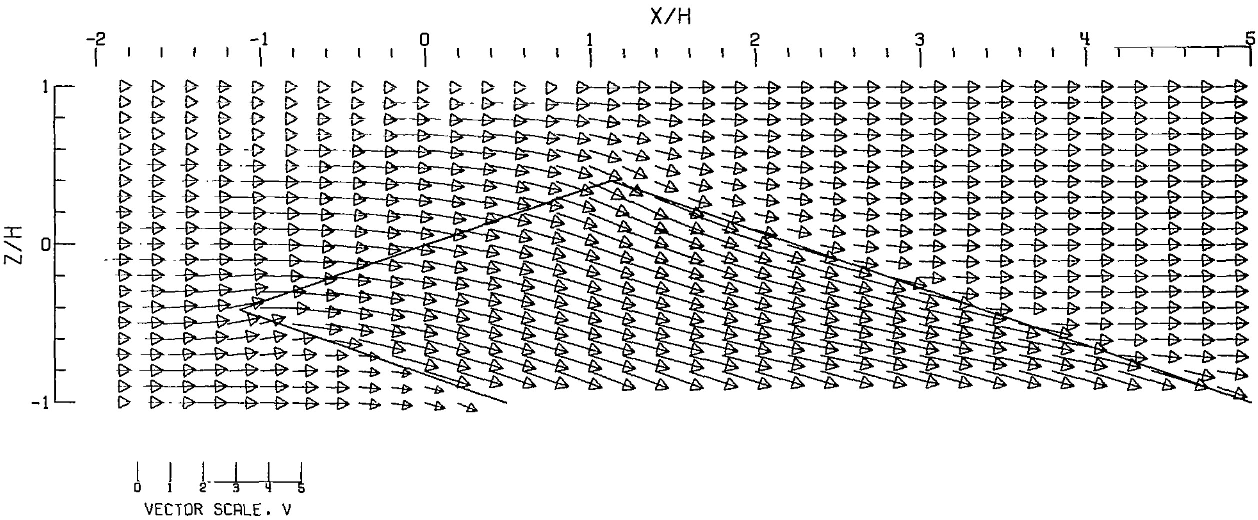

(C).- CLOSED TUNNEL.

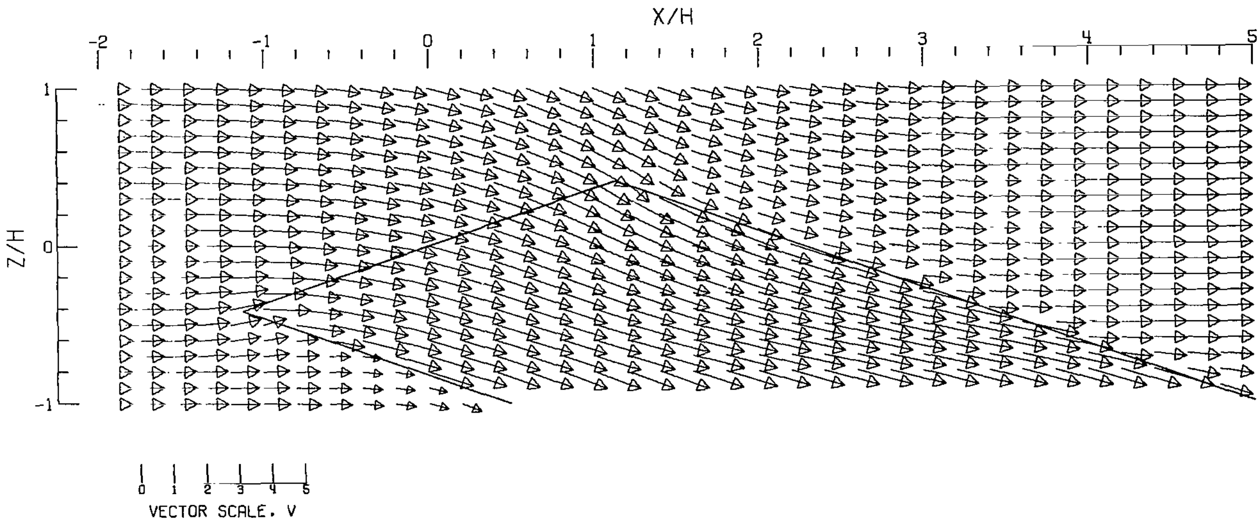

(D).- CLOSED-ON-BOTTOM-ONLY TUNNEL.

Figure 98.- Concluded.

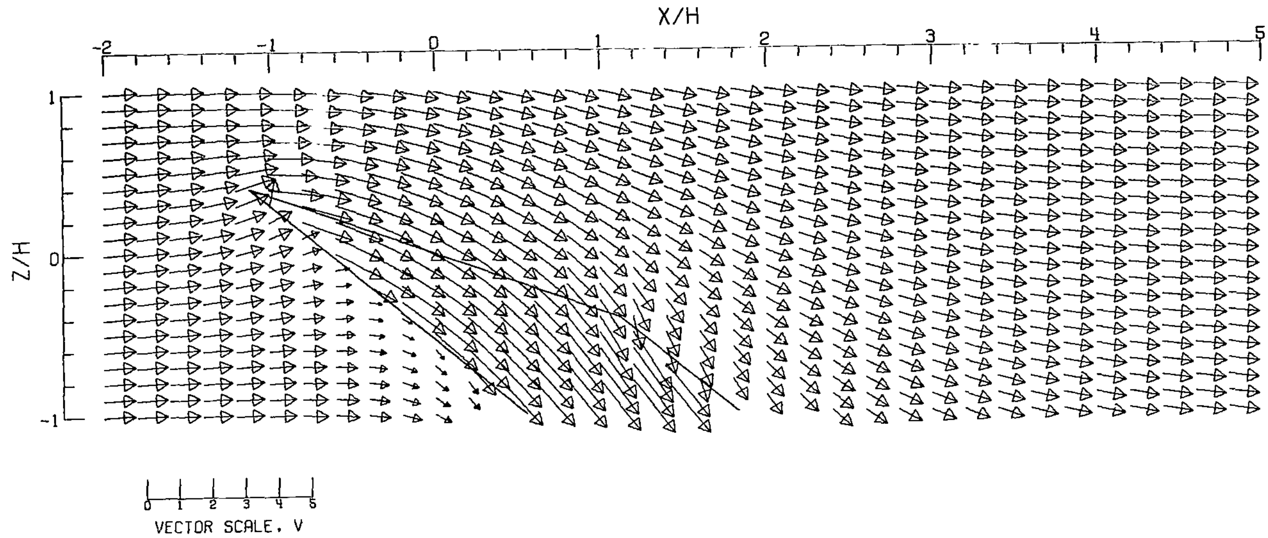

(A).- FREE AIR.

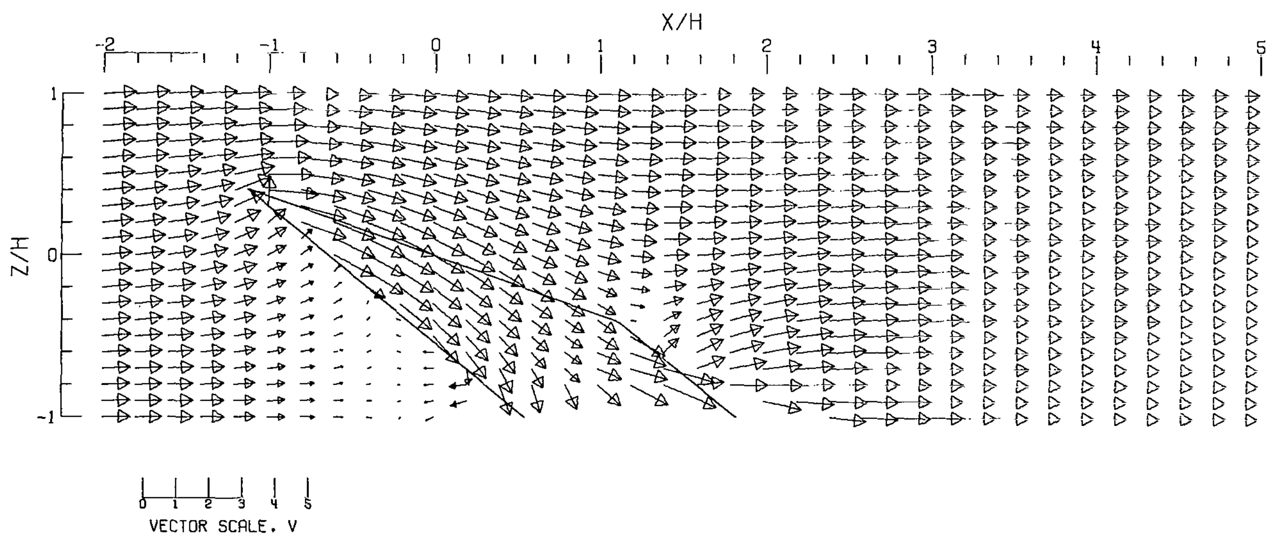

(B).- GROUND EFFECT.

Figure 99.- Flow vectors in the X-Z plane, calculated using doublet strings. The rotor and the edges of the wake are shown. ζ = 1.000; η = 1.0; γ = 2.0; σ = 0.600; α = 20.0°; χ = 50.0°; uniform loading.

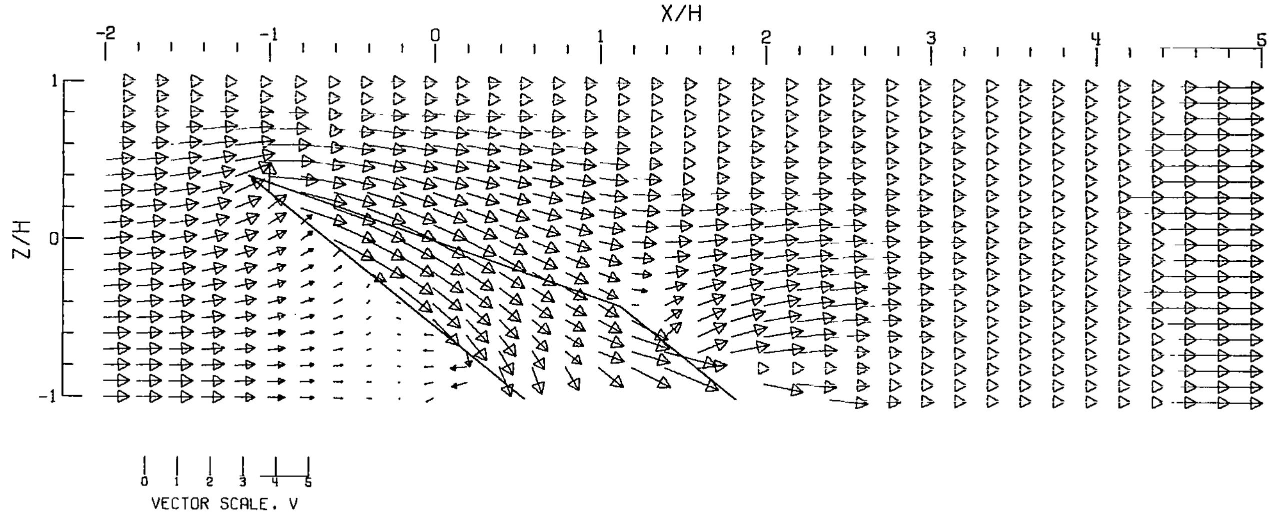

(C).- CLOSED TUNNEL.

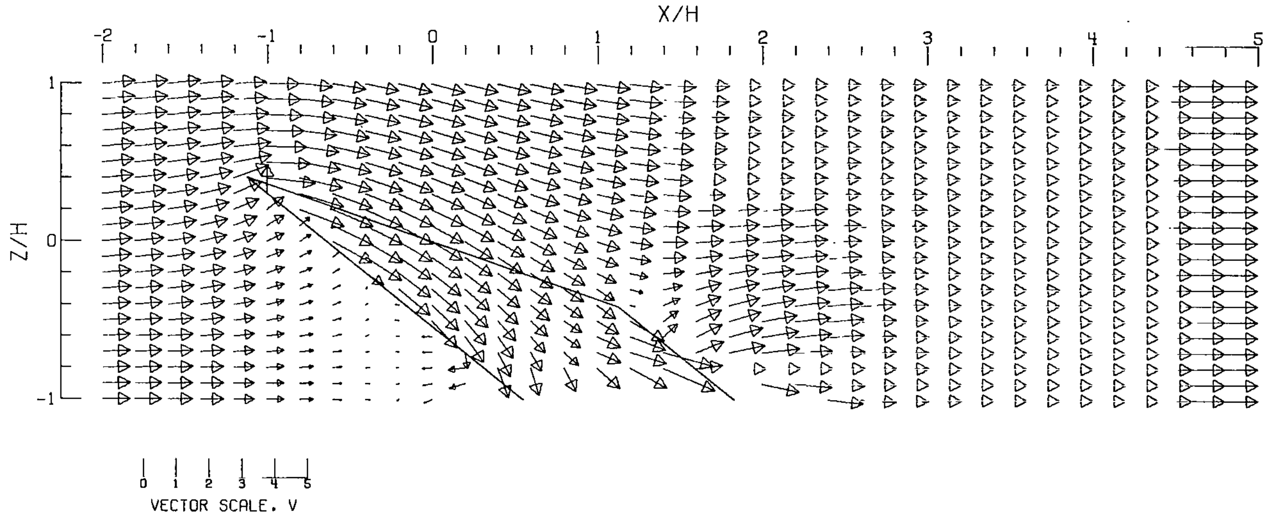

(D).- CLOSED-ON-BOTTOM-ONLY TUNNEL.

Figure 99.- Concluded.

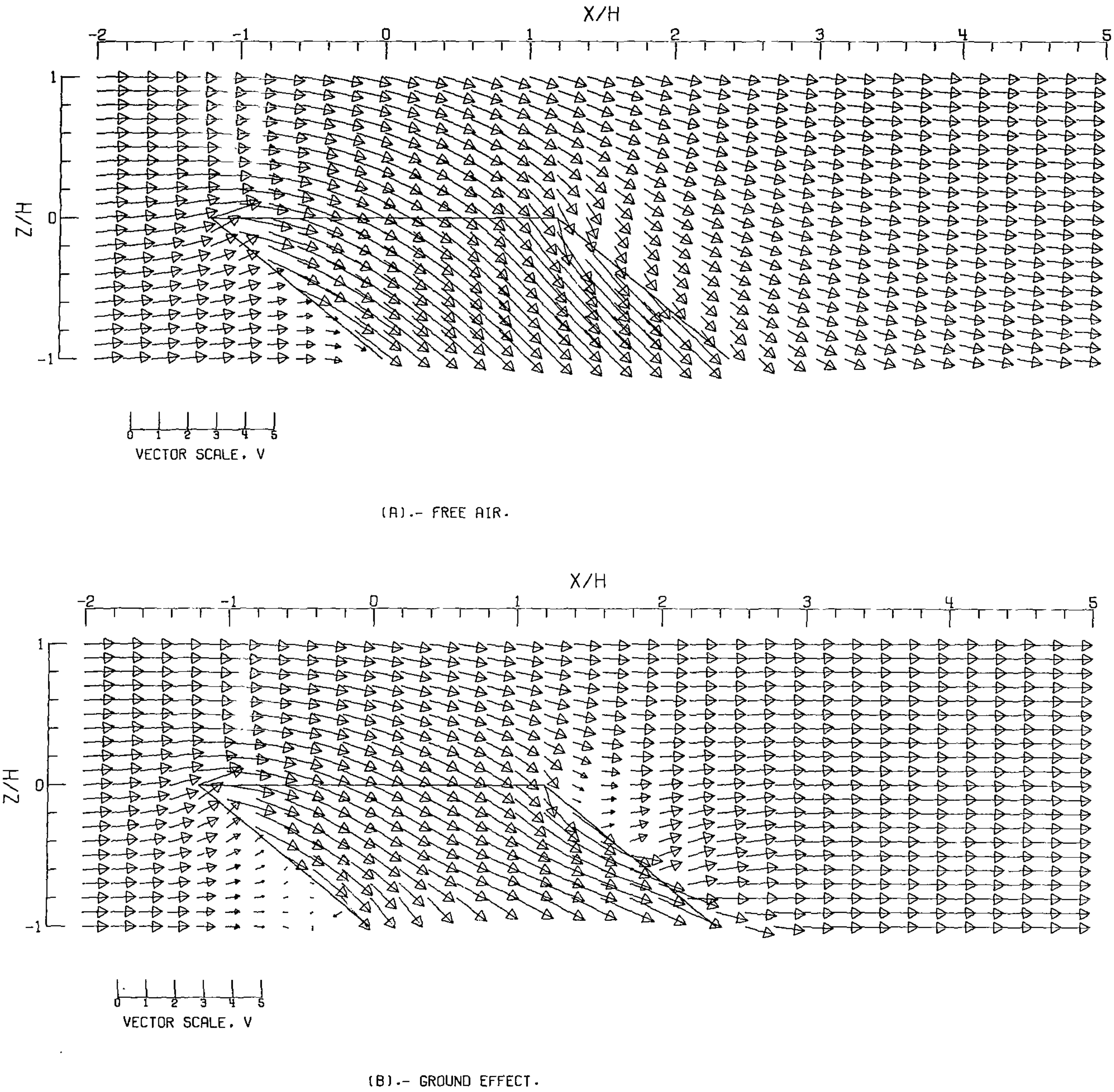

Figure 100.- Flow vectors in the X-Z plane, calculated using doublet strings. The rotor and the edges of the wake are shown. ζ = 1.000; η = 1.0; γ = 2.0; σ = 0.600; α = 0.0°; χ = 50.0°; uniform loading.

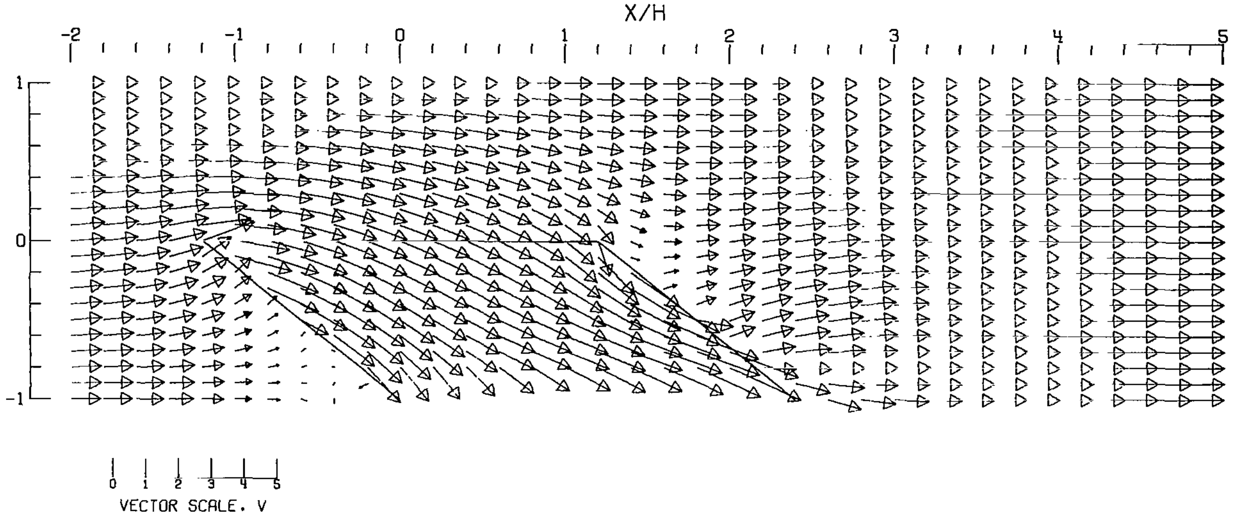

(C).- CLOSED TUNNEL.

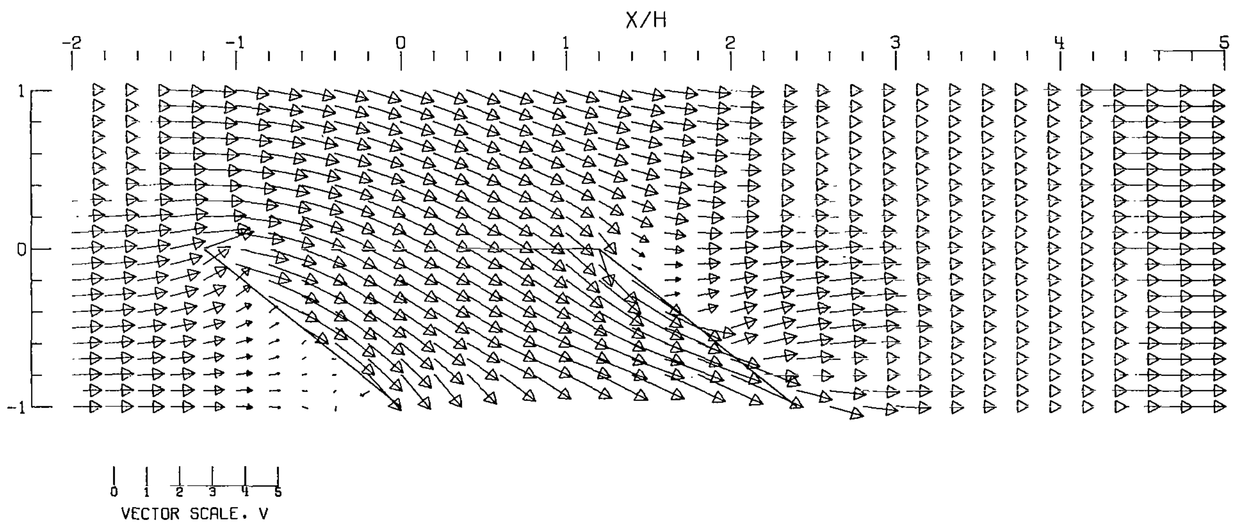

(D).- CLOSED-ON-BOTTOM-ONLY TUNNEL.

Figure 100.- Concluded.

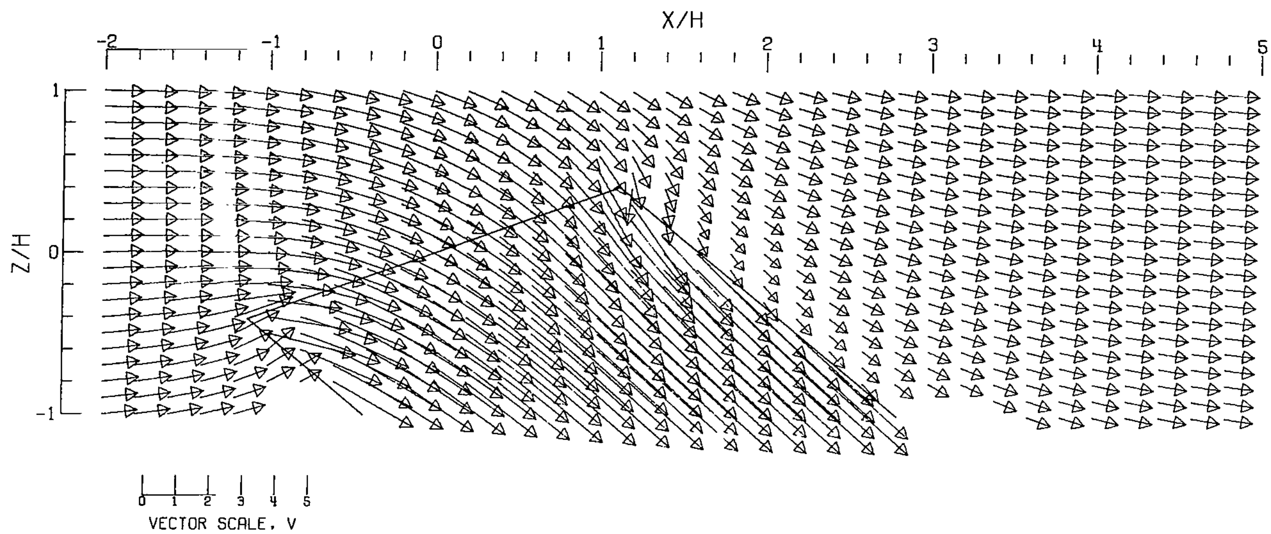

(A).- FREE AIR.

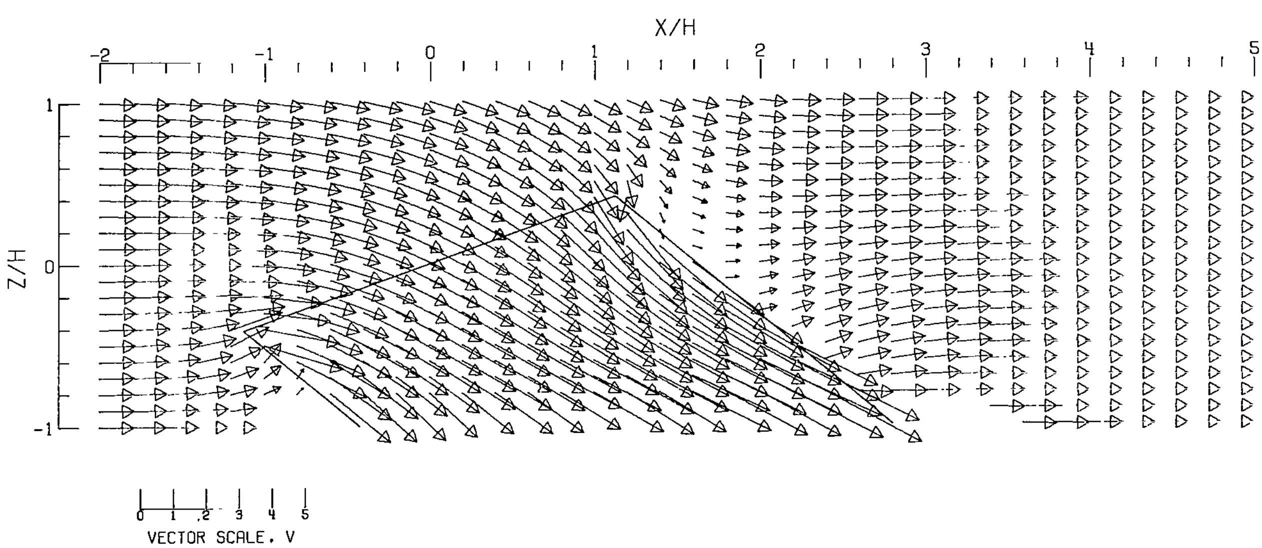

(B).- GROUND EFFECT.

Figure 101.- Flow vectors in the X-Z plane, calculated using doublet strings. The rotor and the edges of the wake are shown. ζ = 1.000; η = 1.0; γ = 2.0; σ = 0.600; α = -20.0^0; χ = 50.0^0; uniform loading.

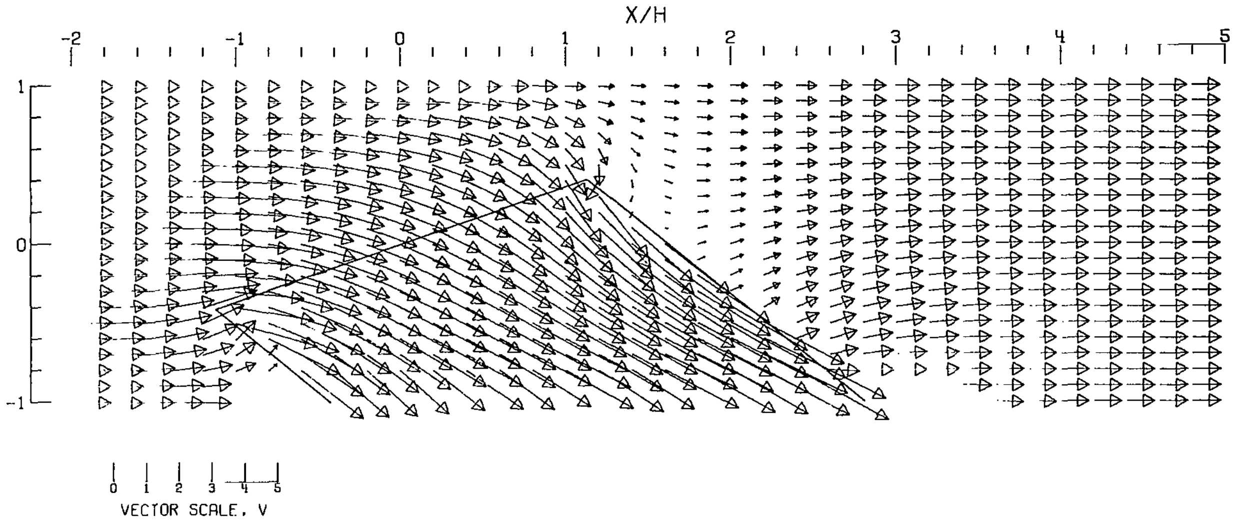

(C).- CLOSED TUNNEL.

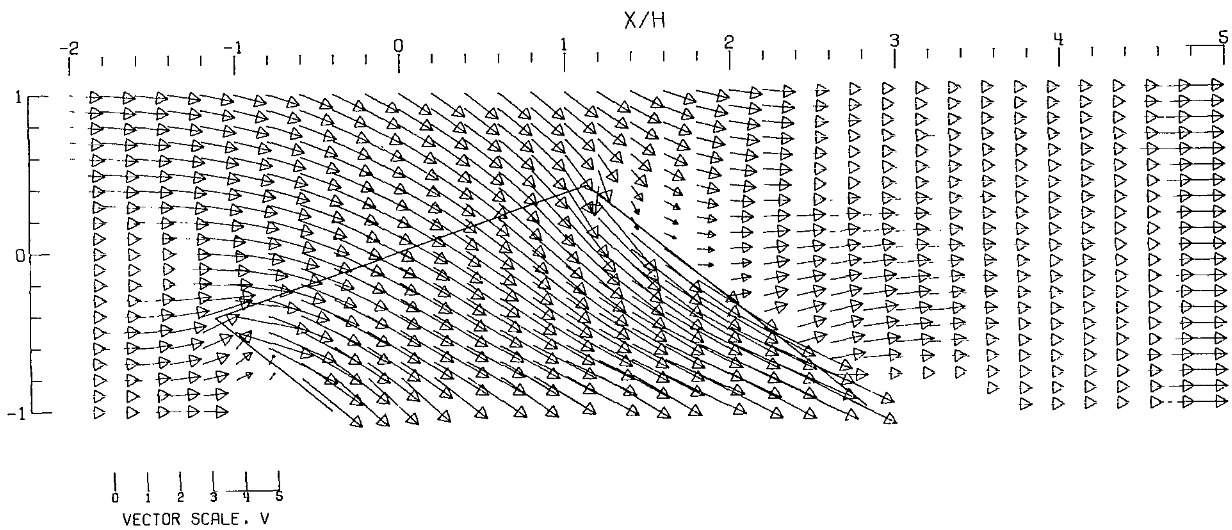

(D).- CLOSED-ON-BOTTOM-ONLY TUNNEL.

Figure 101.- Concluded.

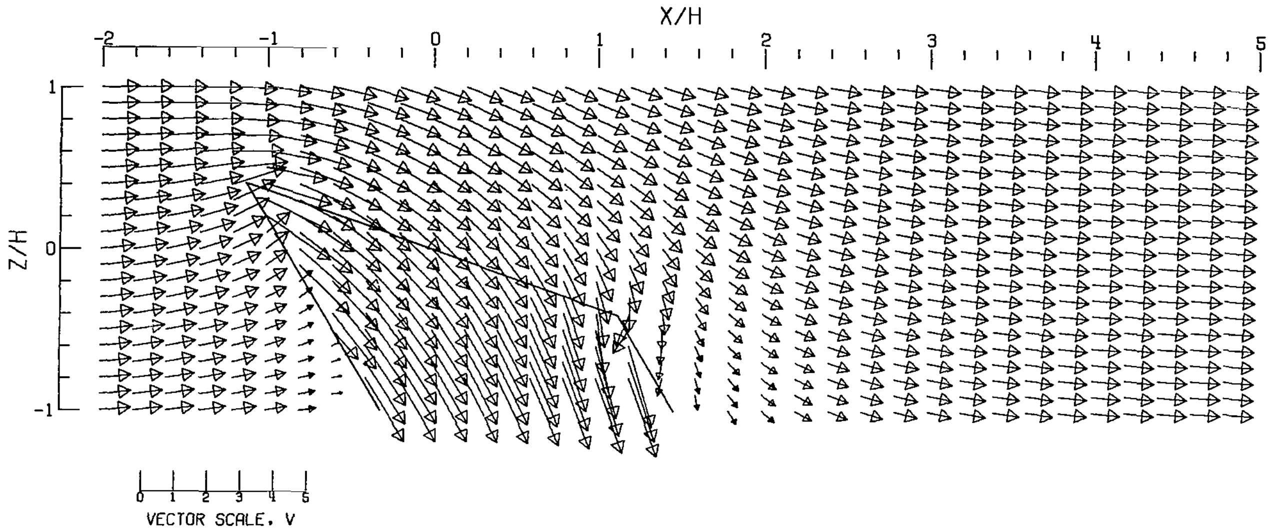

(A).- FREE AIR.

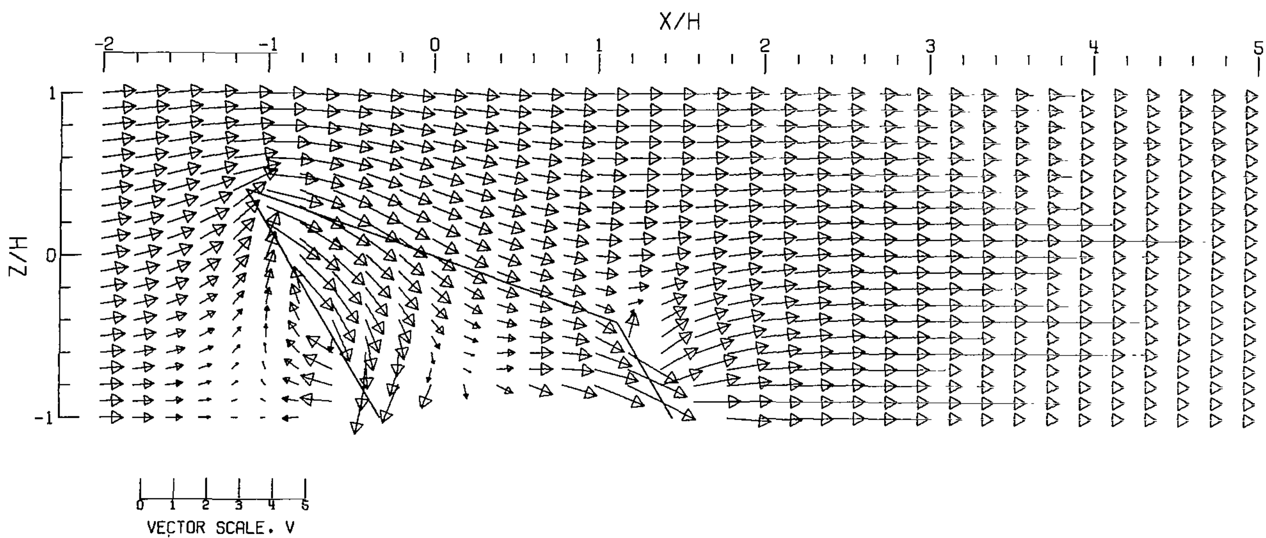

(B).- GROUND EFFECT.

Figure 102.- Flow vectors in the X-Z plane, calculated using doublet strings. The rotor and the edges of the wake are shown. $\zeta = 1.000$; $\eta = 1.0$; $\gamma = 2.0$; $\sigma = 0.600$; $\alpha = 20.0^{\circ}$; $\chi = 30.0^{\circ}$; uniform loading.

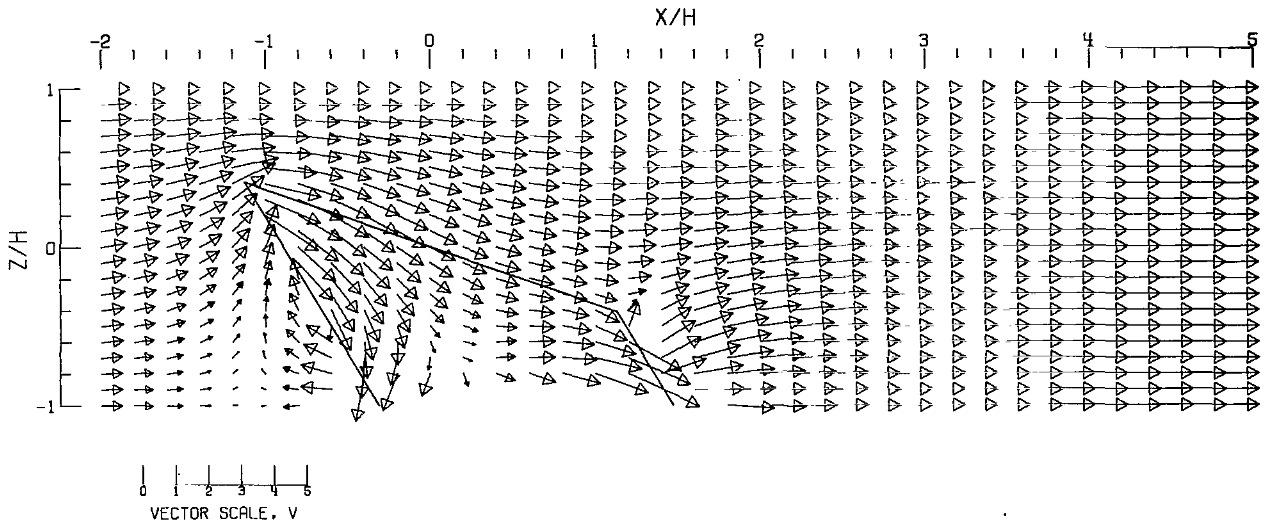

(C).- CLOSED TUNNEL.

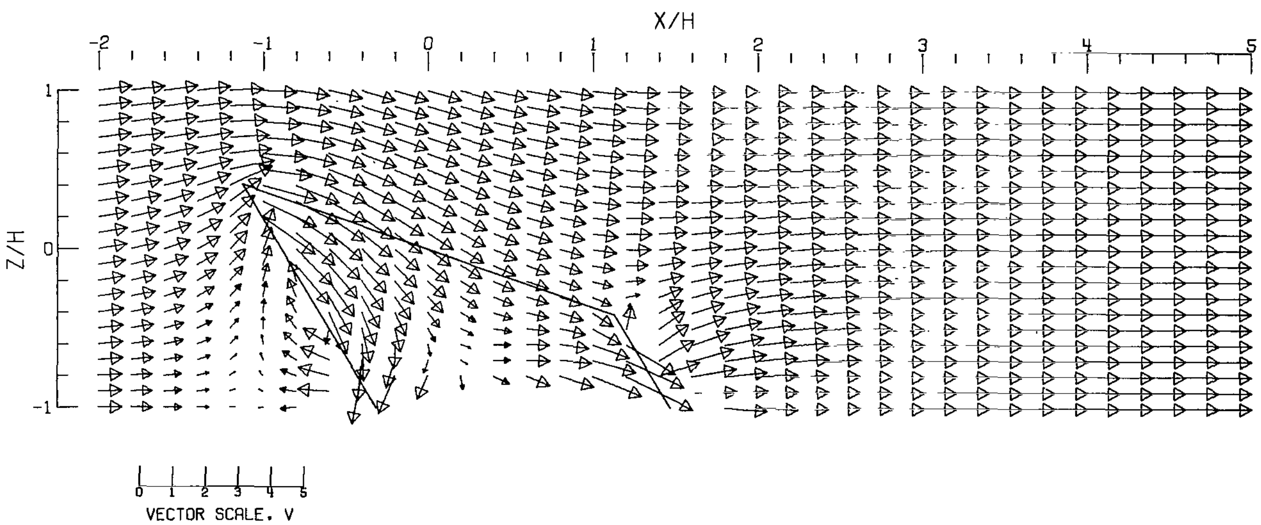

(D).- CLOSED-ON-BOTTOM-ONLY TUNNEL.

Figure 102.- Concluded.

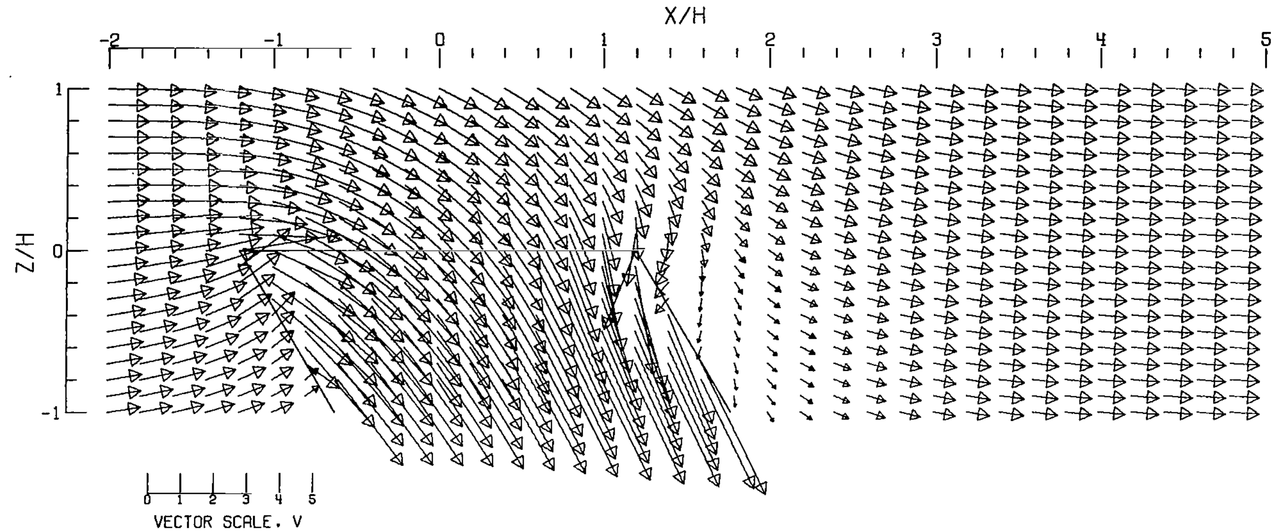

(A).- FREE AIR.

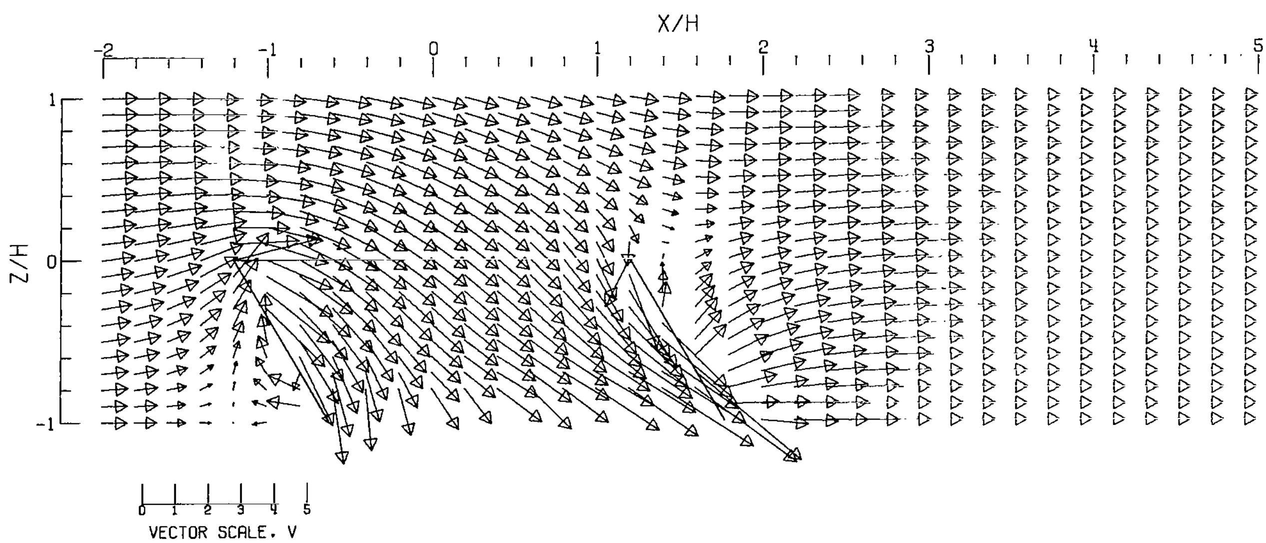

(B).- GROUND EFFECT.

Figure 103.- Flow vectors in the X-Z plane, calculated using doublet strings. The rotor and the edges of the wake are shown. ζ = 1.000; η = 1.0; γ = 2.0; σ = 0.600; α = 0.0°; χ = 30.0°; uniform loading.

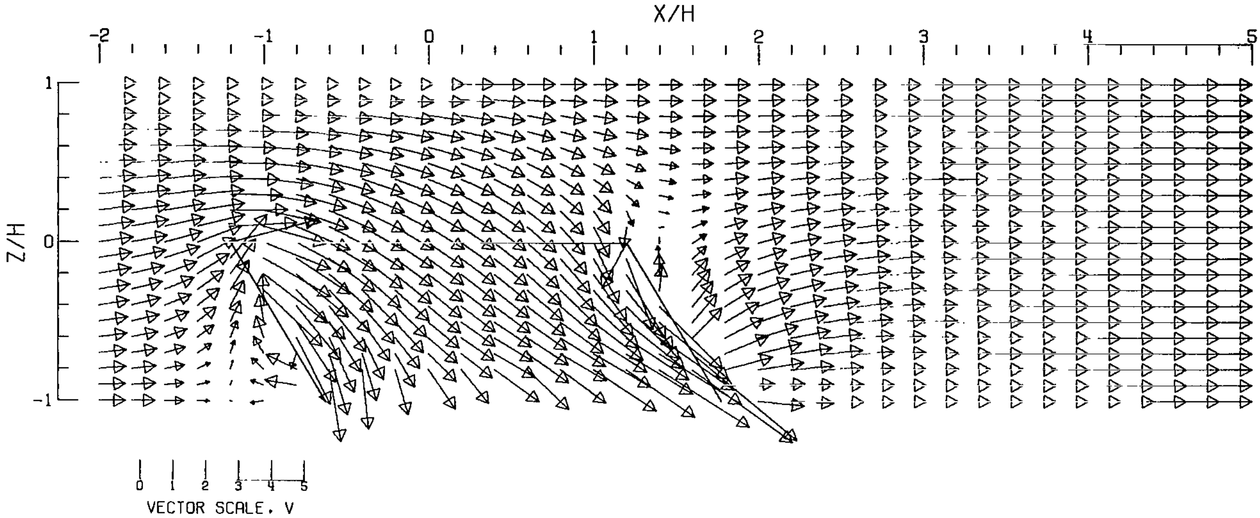

(C).- CLOSED TUNNEL.

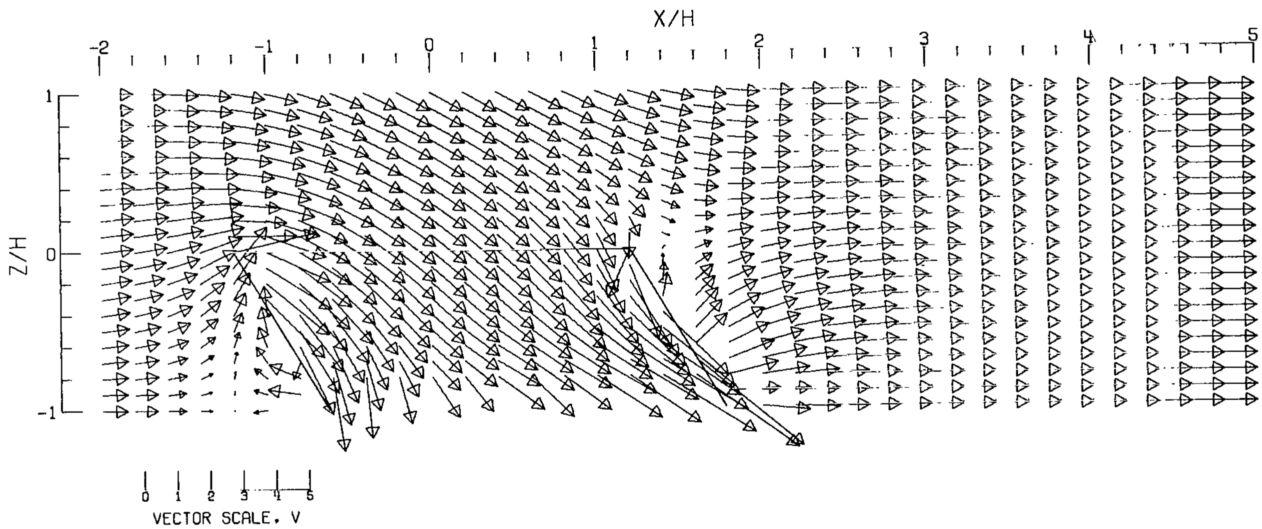

(D).- CLOSED-ON-BOTTOM-ONLY TUNNEL.

Figure 103.- Concluded.

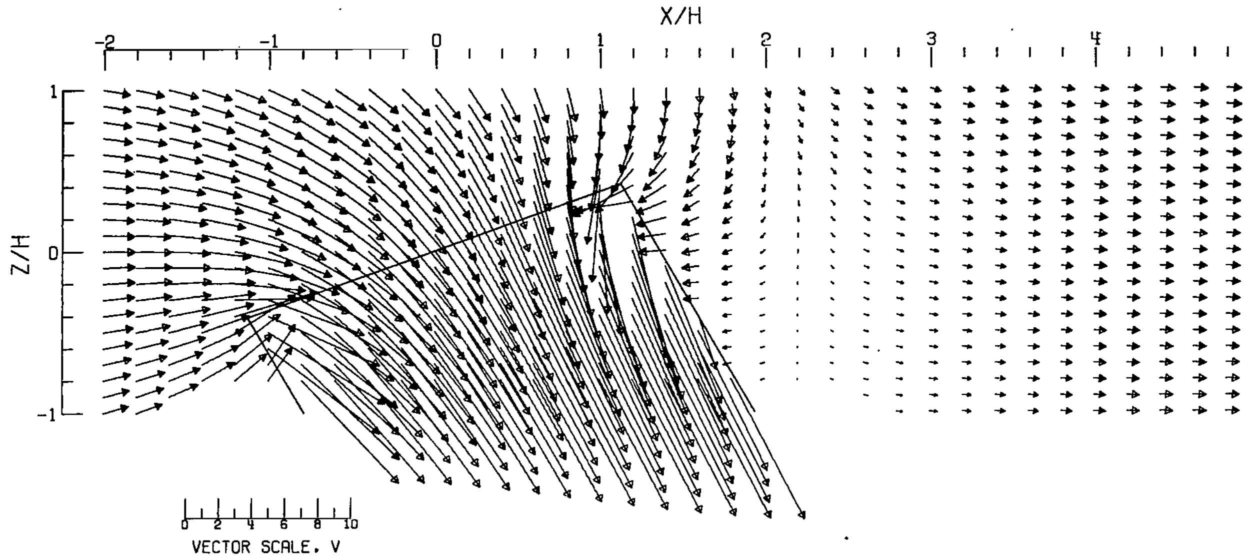

(A).- FREE AIR.

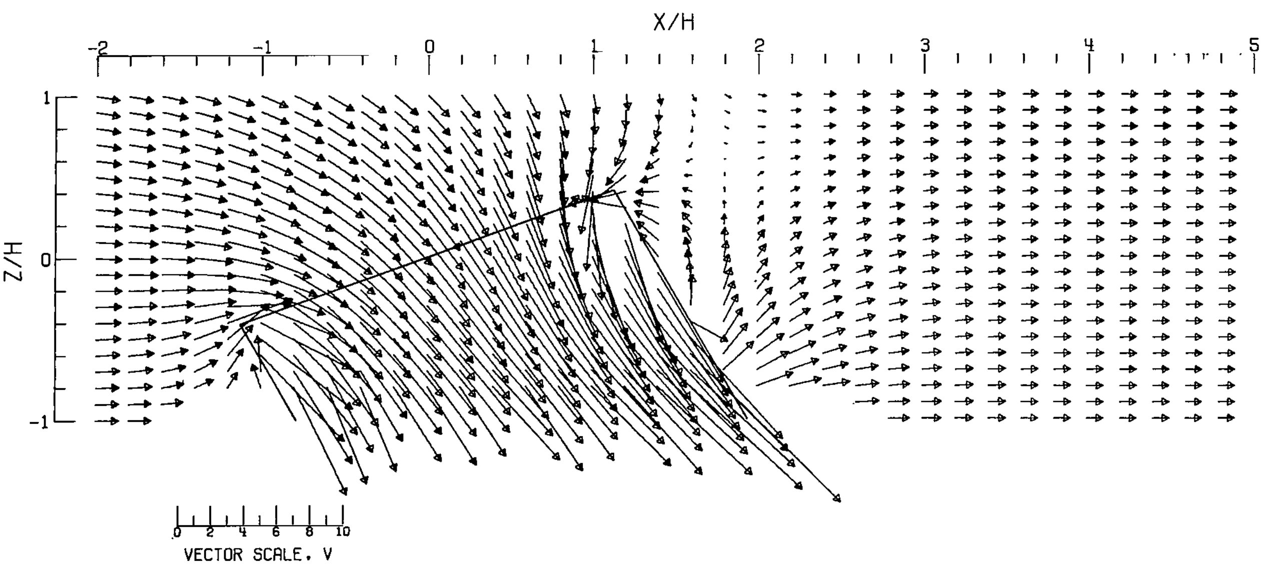

(B).- GROUND EFFECT.

Figure 104.- Flow vectors in the X-Z plane, calculated using doublet strings. The rotor and the edges of the wake are shown. ζ = 1.000; η = 1.0; γ = 2.0; σ = 0.600; α = -20.0°; χ = 30.0°; uniform loading.

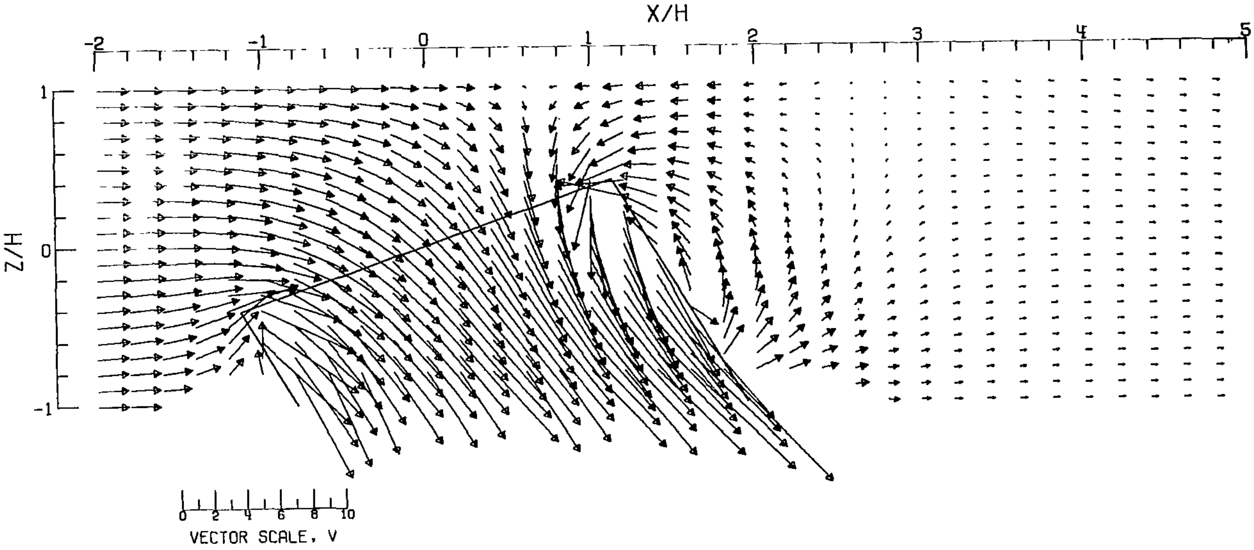

(C).- CLOSED TUNNEL.

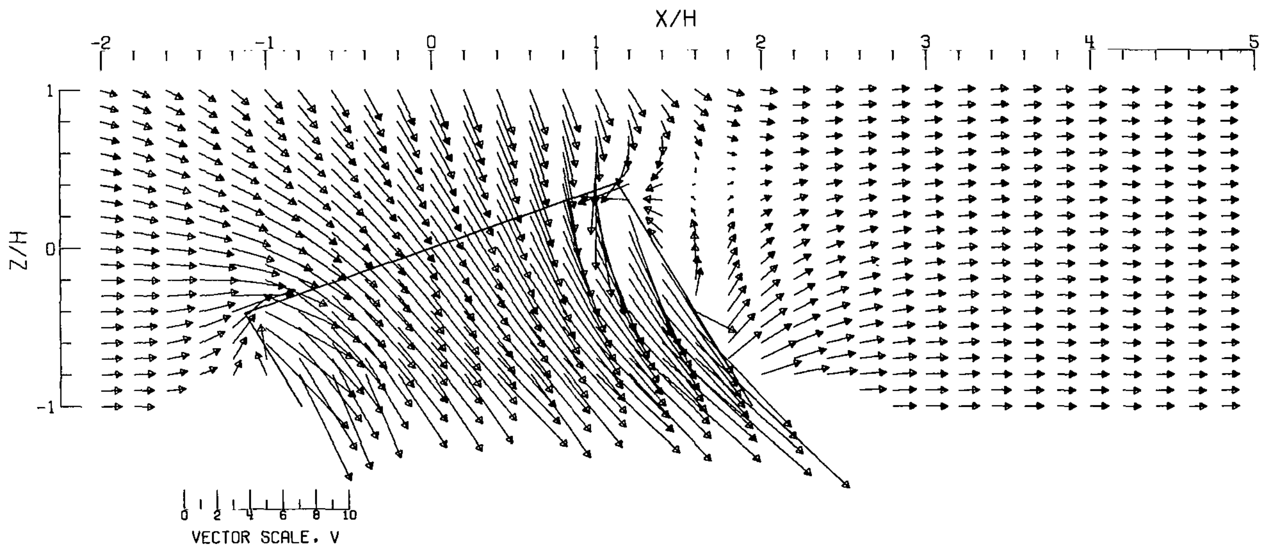

(D).- CLOSED-ON-BOTTOM-ONLY TUNNEL.

Figure 104.- Concluded.

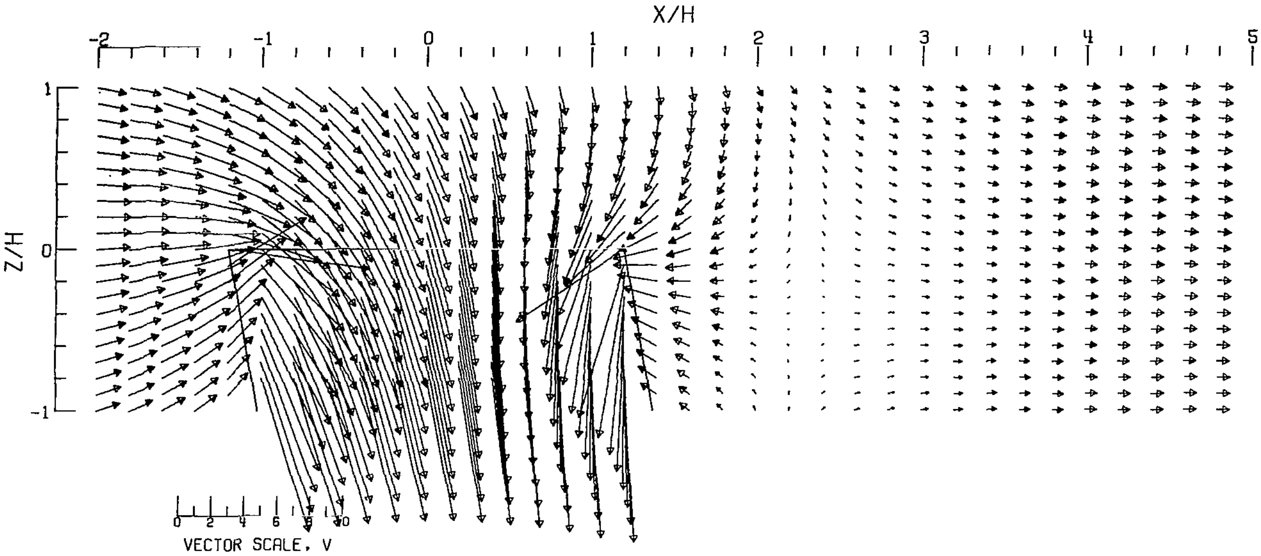

(A).- FREE AIR.

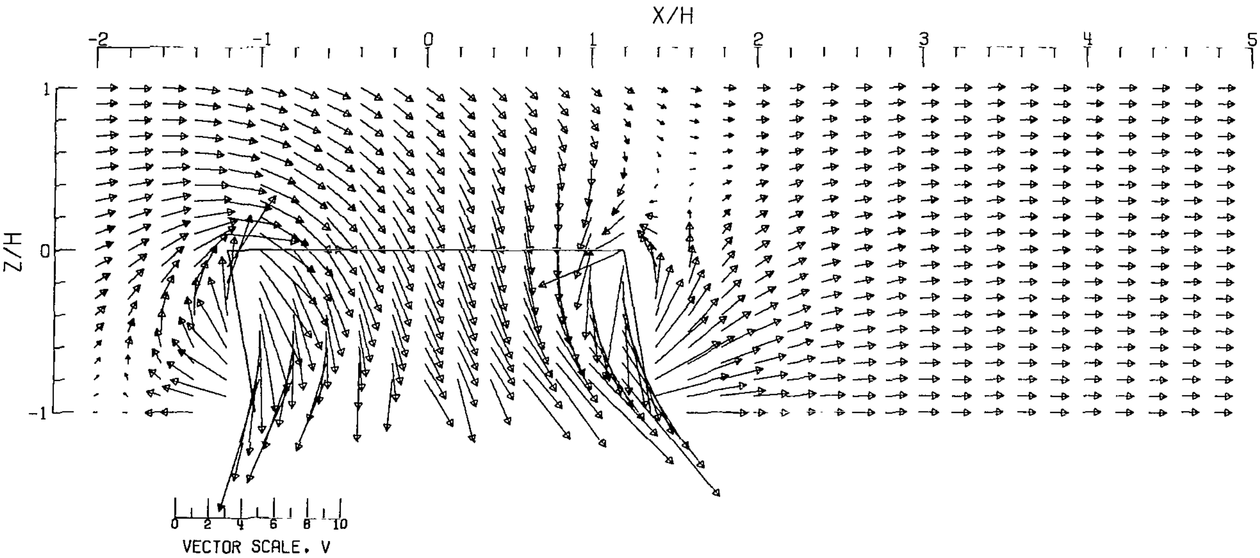

(B).- GROUND EFFECT.

Figure 105.- Flow vectors in the X-Z plane, calculated using doublet strings. The rotor and the edges of the wake are shown. ζ = 1.000; η = 1.0; γ = 2.0; σ = 0.600; $\alpha = 0.0^0$; $\chi = 10.0^0$; uniform loading.

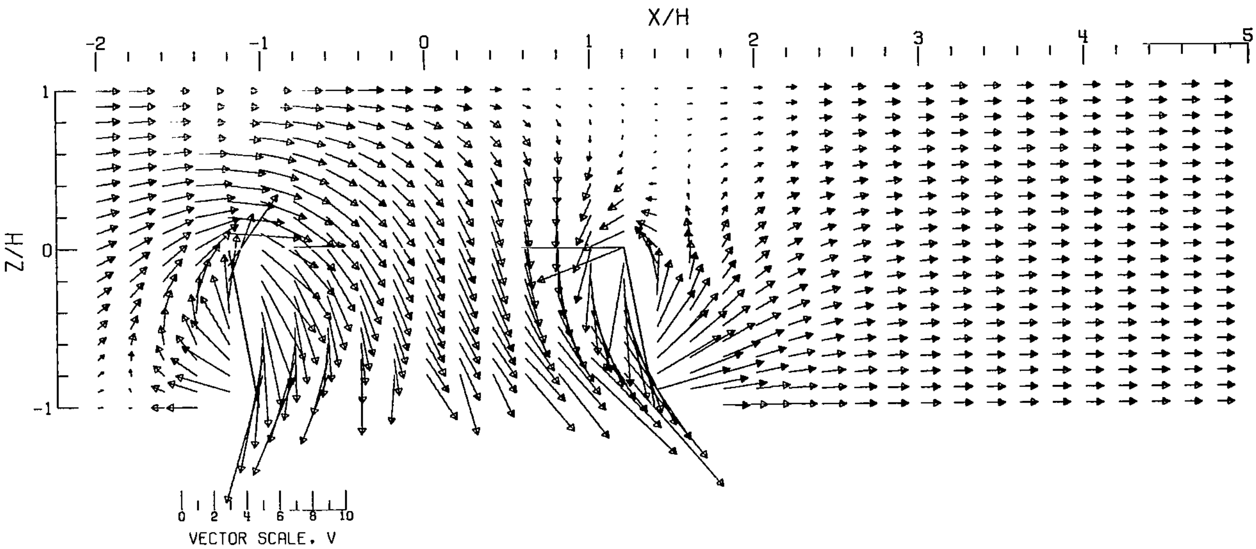

(C).- CLOSED TUNNEL.

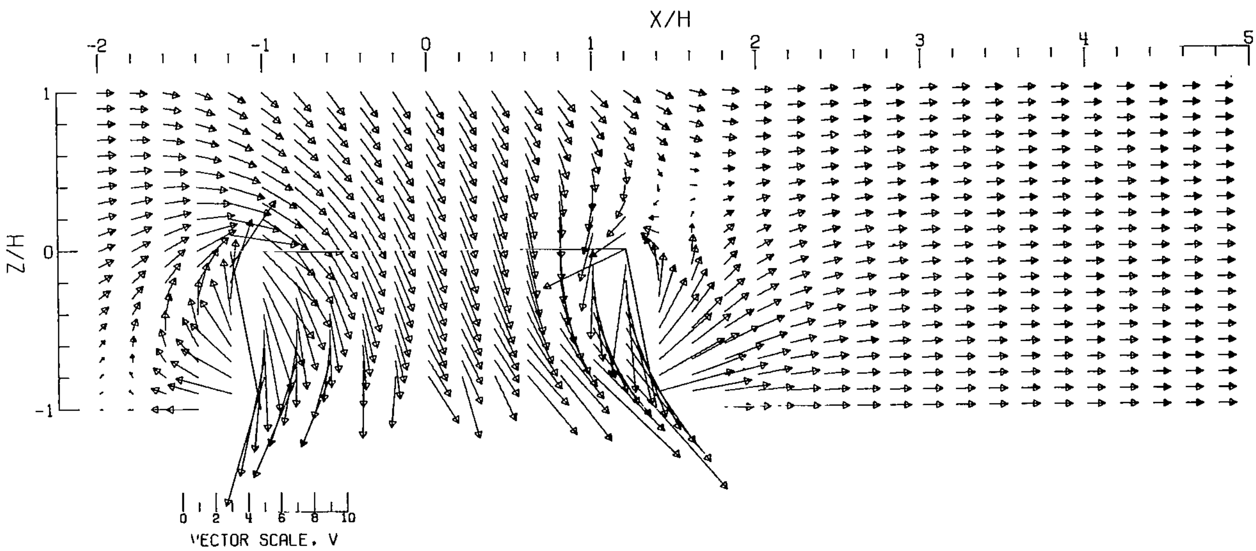

(D).- CLOSED-ON-BOTTOM-ONLY TUNNEL.

Figure 105.- Concluded.

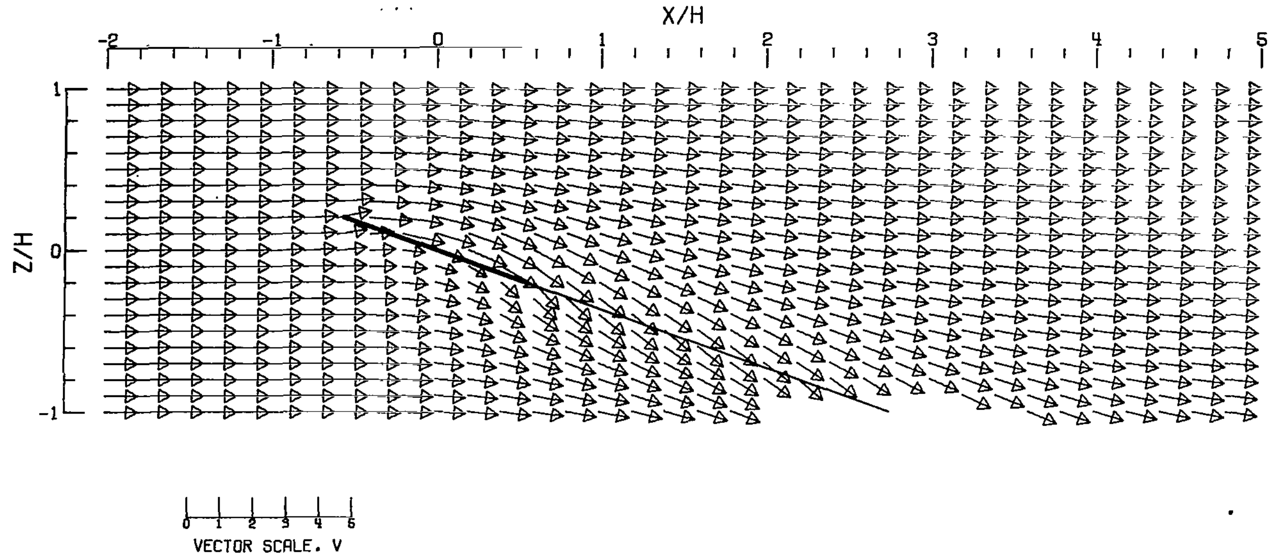

(A).- FREE AIR.

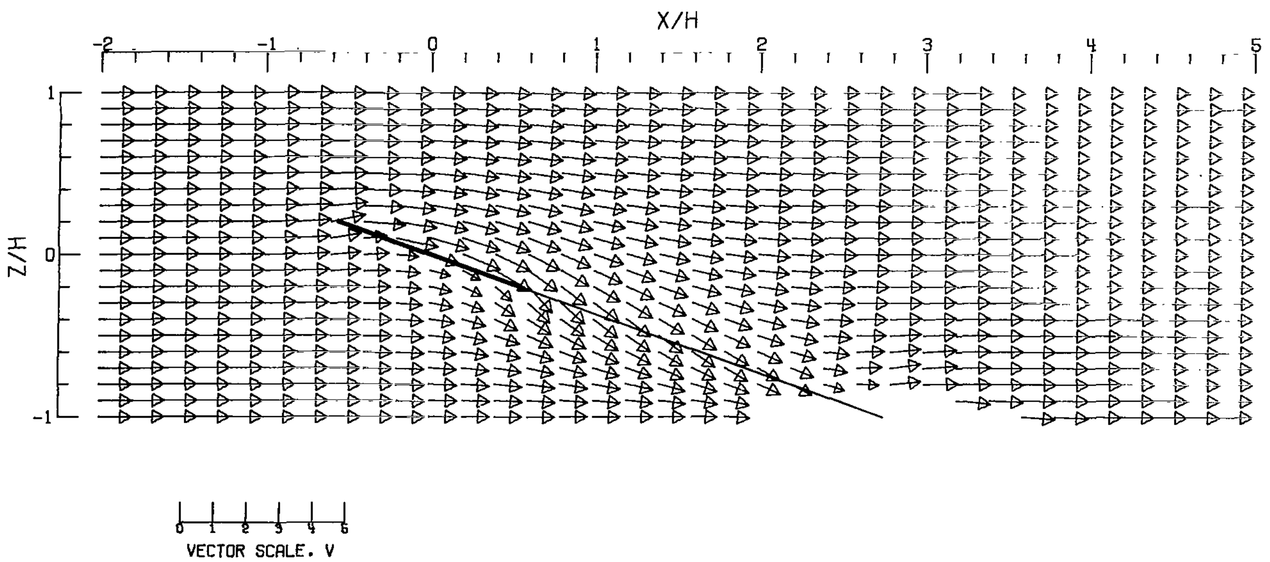

(B).- GROUND EFFECT.

Figure 106.- Flow vectors in the X-Z plane, calculated using doublet strings. The rotor and the edges of the wake are shown. ζ = 1.000; η = 1.0; γ = 2.0; σ = 0.300; α = 20.0^{0}; χ = 70.0^{0}; uniform loading.

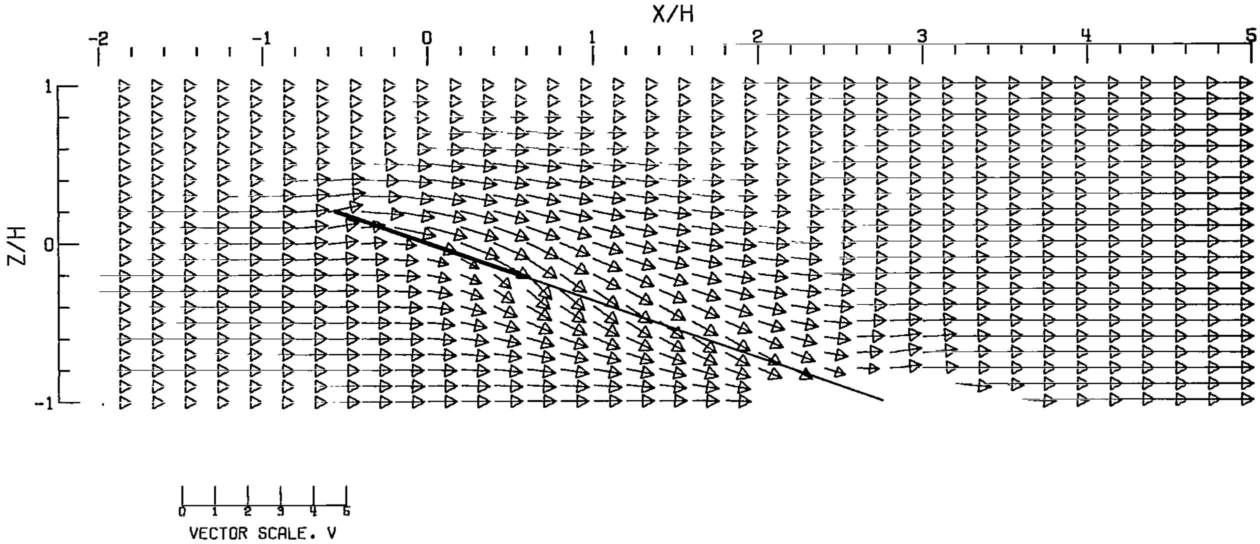

(C).- CLOSED TUNNEL.

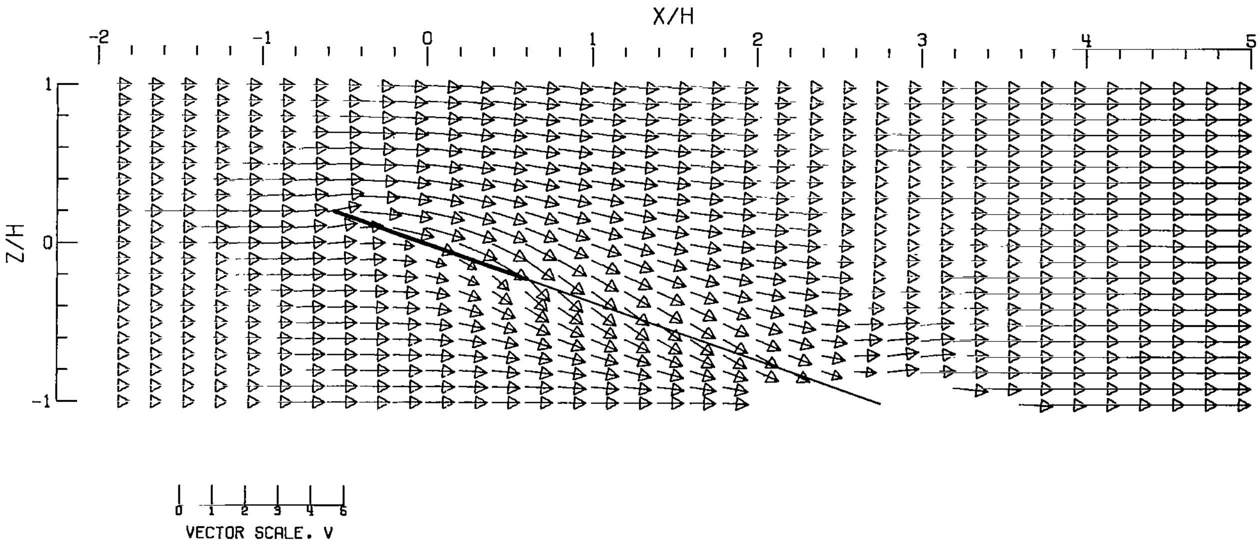

(D).- CLOSED-ON-BOTTOM-ONLY TUNNEL.

Figure 106.- Concluded.

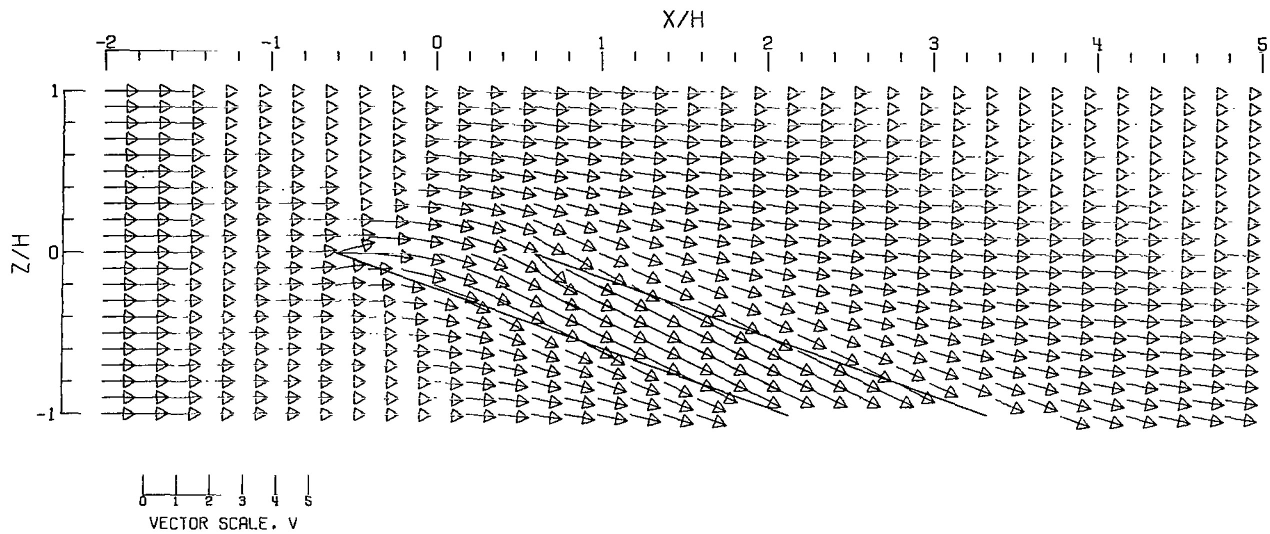

(A).- FREE AIR.

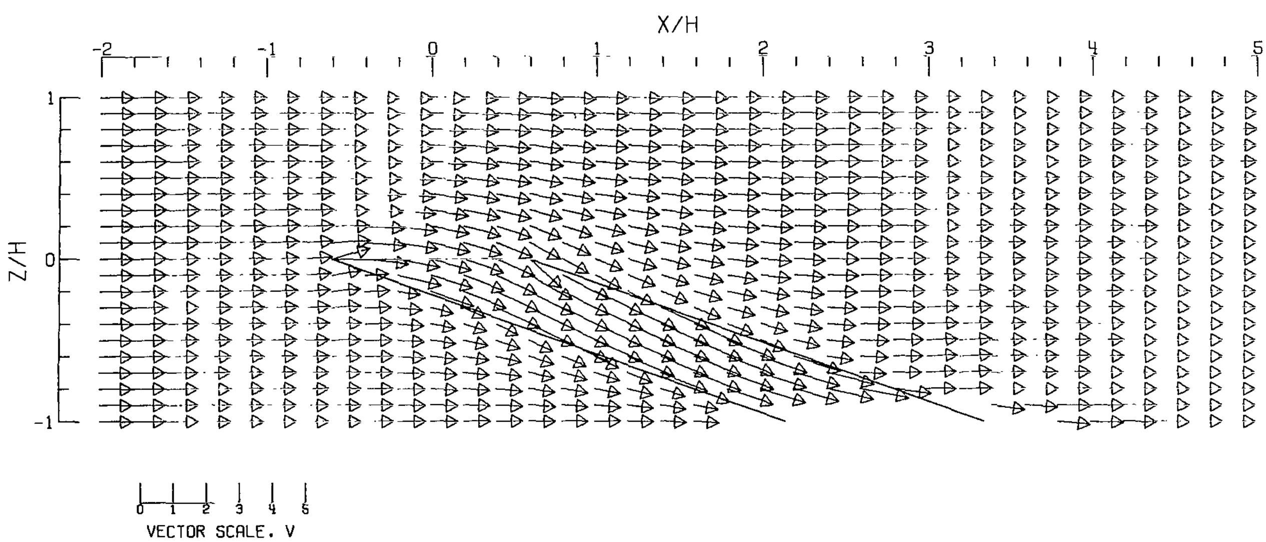

(B).- GROUND EFFECT.

Figure 107.- Flow vectors in the X-Z plane, calculated using doublet strings. The rotor and the edges of the wake are shown. $\zeta = 1.000$; $\eta = 1.0$; $\gamma = 2.0$; $\sigma = 0.300$; $\alpha = 0.0^{0}$; $\chi = 70.0^{0}$; uniform loading.

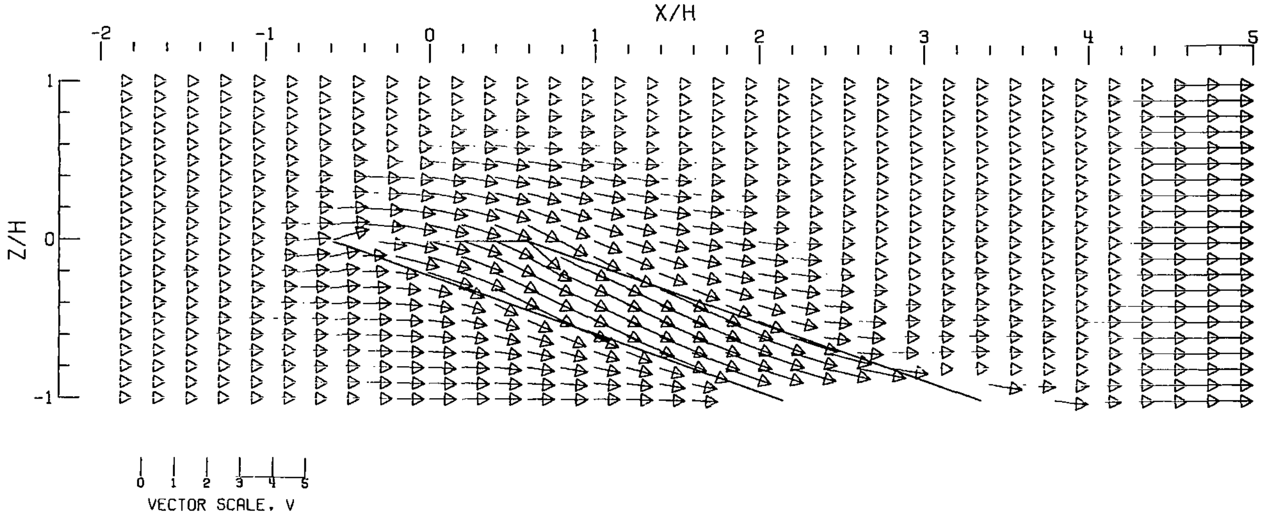

(C).- CLOSED TUNNEL.

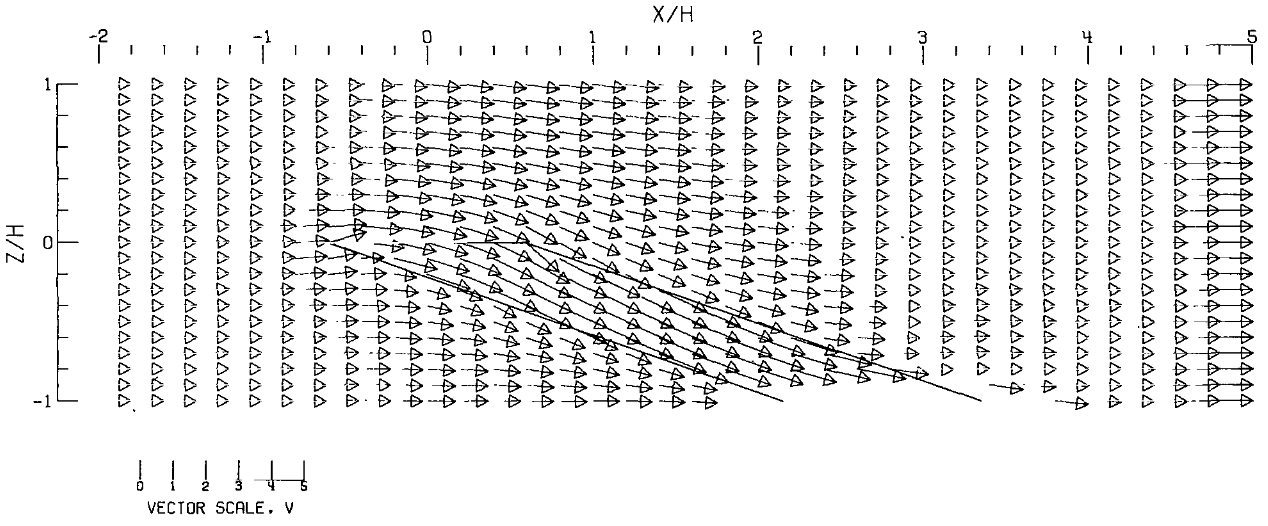

(D).- CLOSED-ON-BOTTOM-ONLY TUNNEL.

Figure 107.- Concluded.

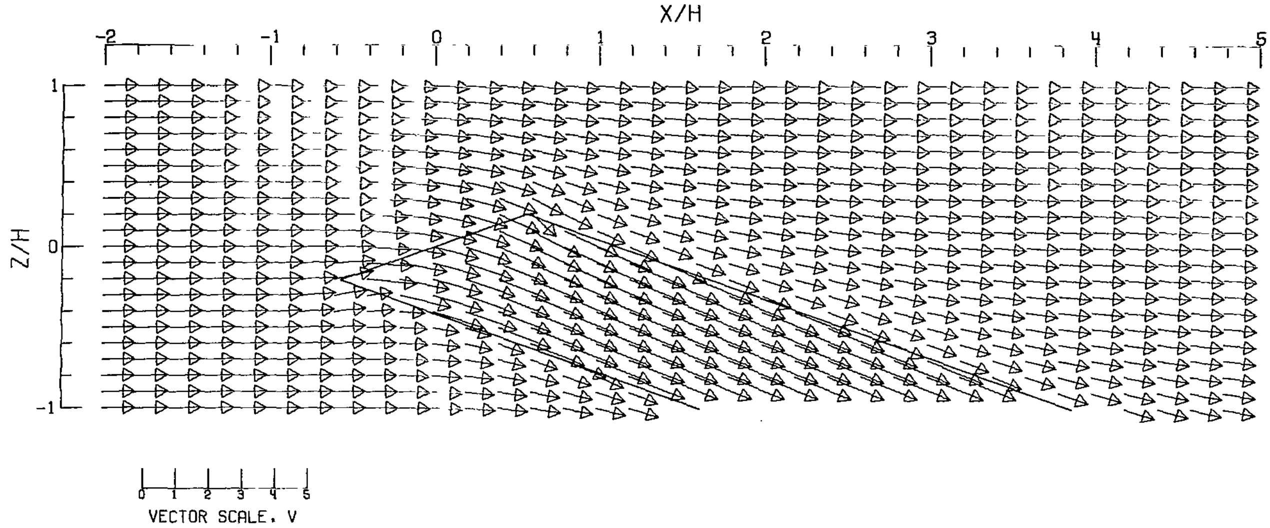

(A).- FREE AIR.

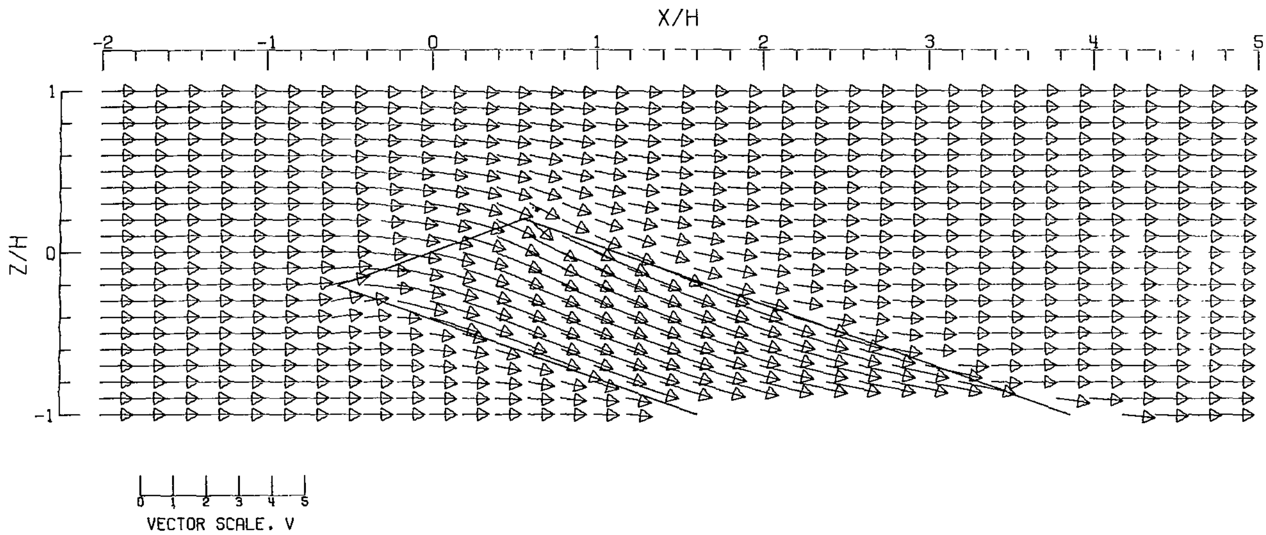

(B).- GROUND EFFECT.

Figure 108.- Flow vectors in the X-Z plane, calculated using doublet strings. The rotor and the edges of the wake are shown. ζ = 1.000; η = 1.0; γ = 2.0; σ = 0.300; α = -20.0°; χ = 70.0°; uniform loading.

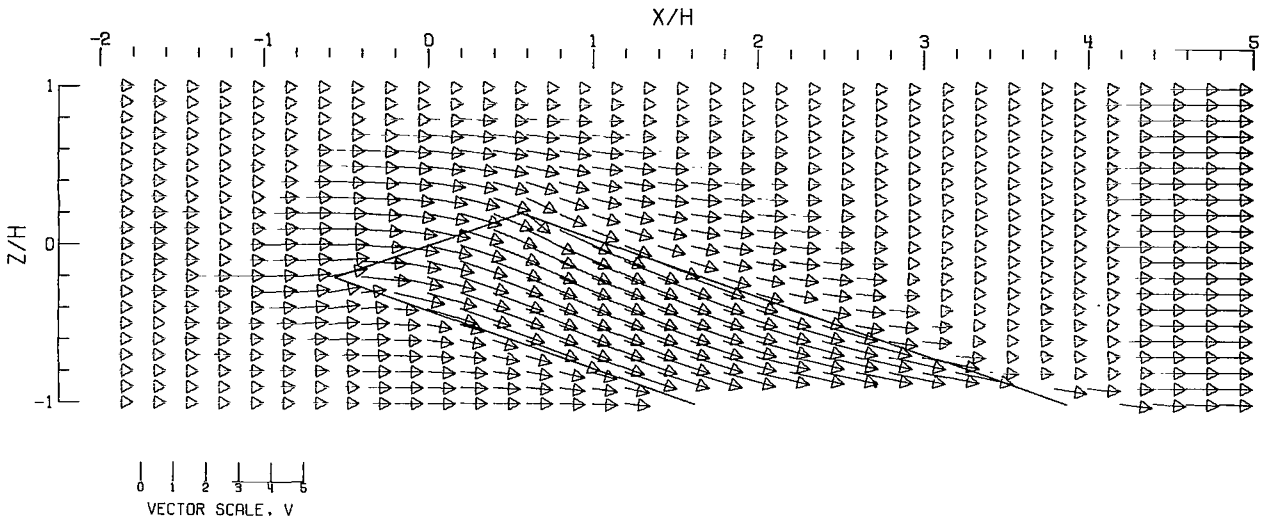

(C).- CLOSED TUNNEL.

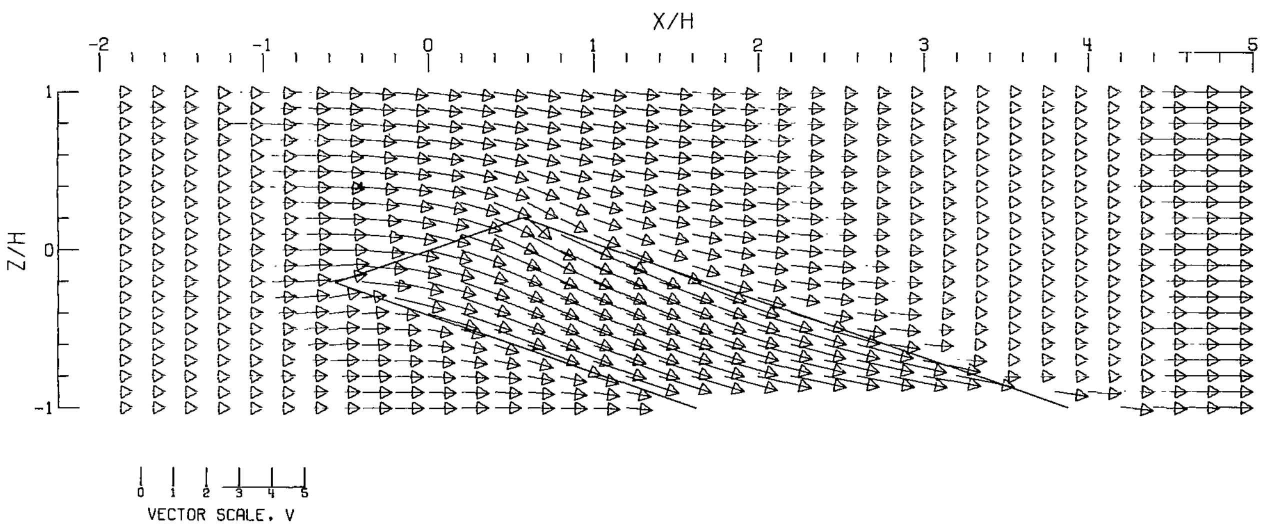

(D).- CLOSED-ON-BOTTOM-ONLY TUNNEL.

Figure 108.- Concluded.

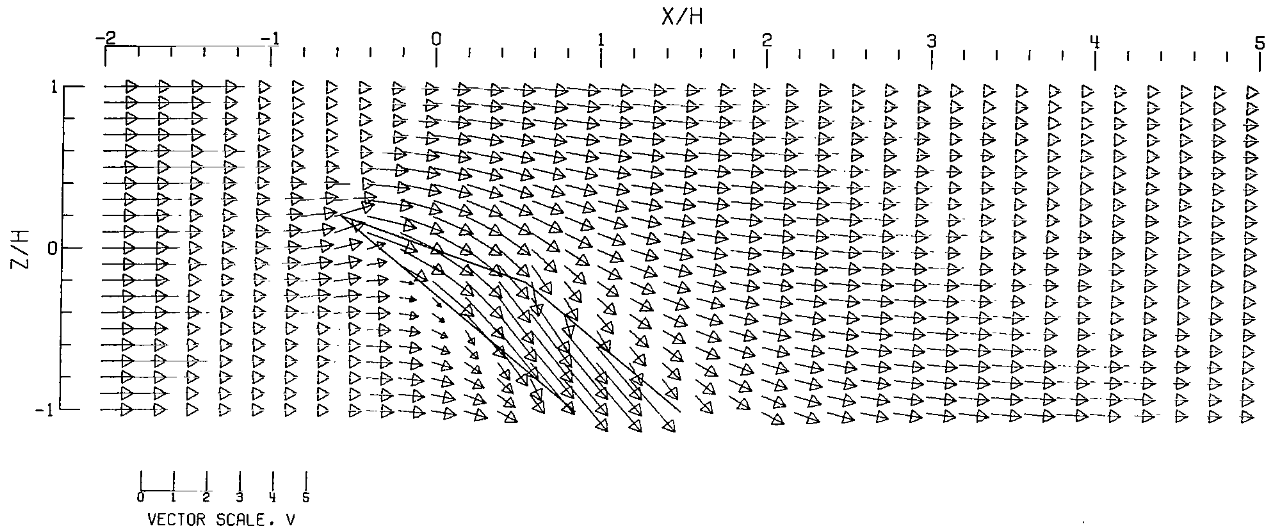

(A).- FREE AIR.

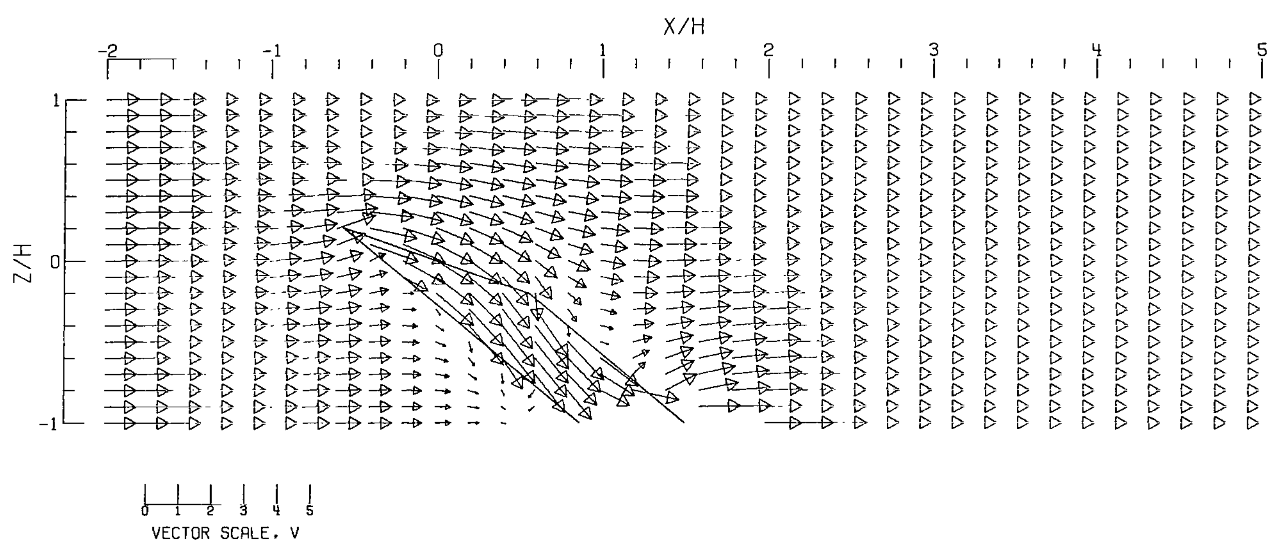

(B).- GROUND EFFECT.

Figure 109.- Flow vectors in the X-Z plane, calculated using doublet strings. The rotor and the edges of the wake are shown. ζ = 1.000; η = 1.0; γ = 2.0; σ = 0.300; α = 20.0°; χ = 50.0°; uniform loading.

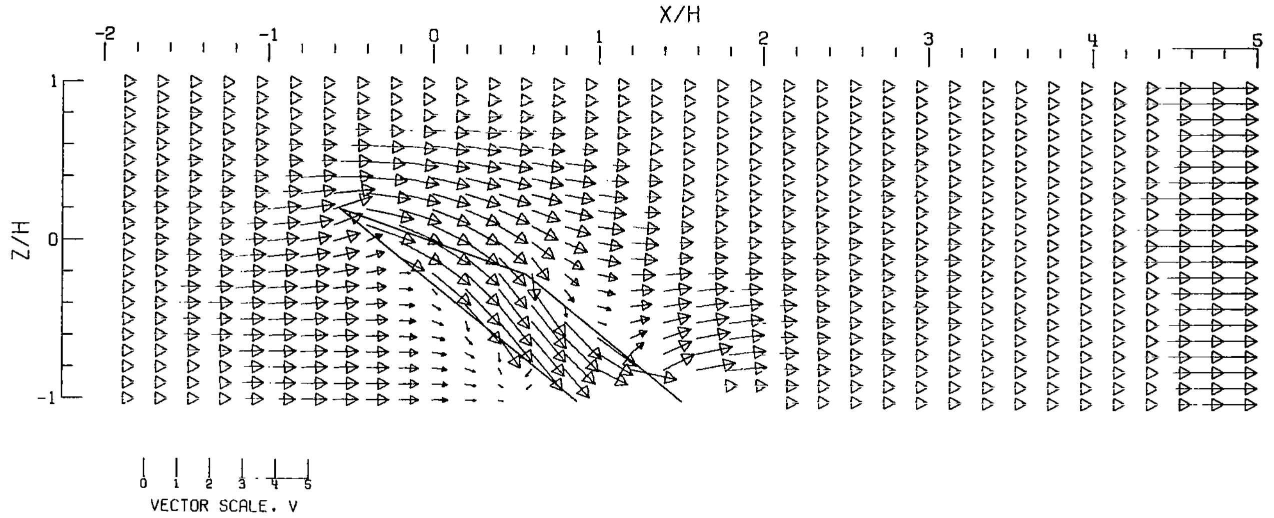

(C).- CLOSED TUNNEL.

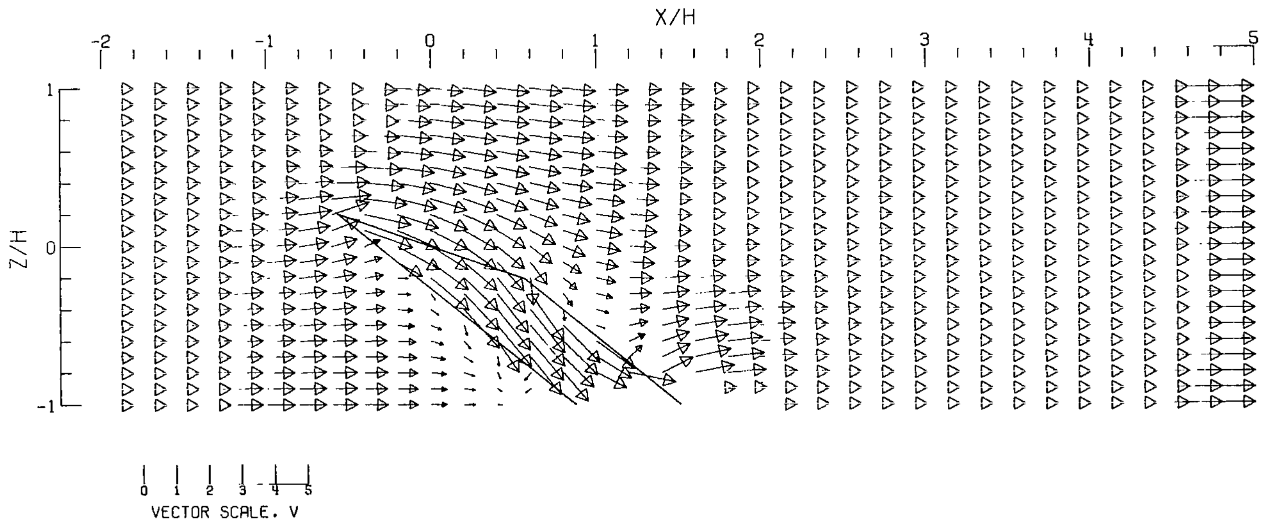

(D).- CLOSED-ON-BOTTOM-ONLY TUNNEL.

Figure 109.- Concluded.

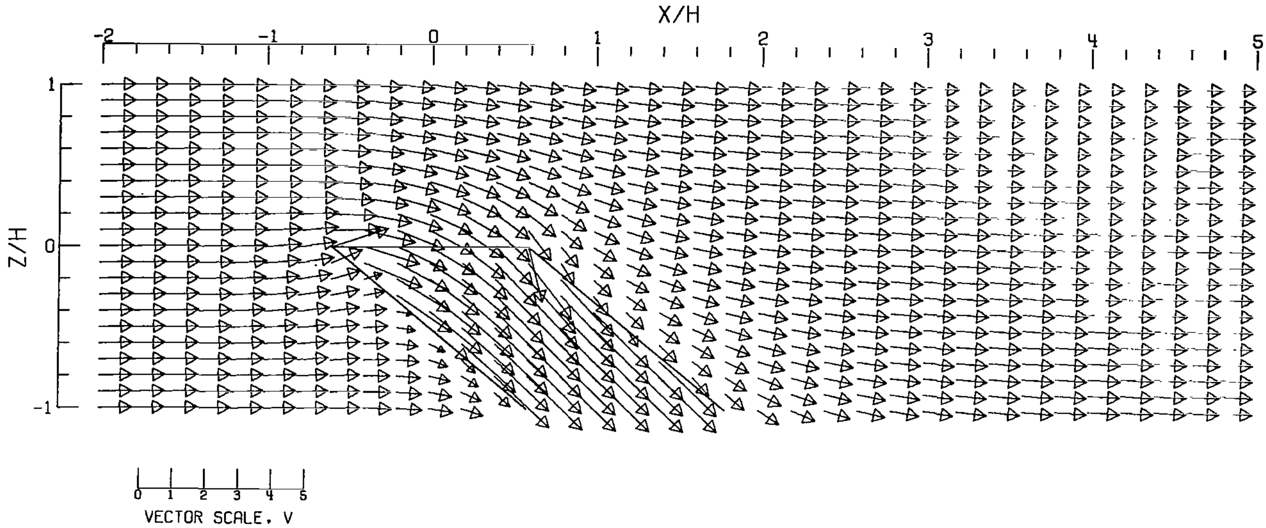

(A).- FREE AIR.

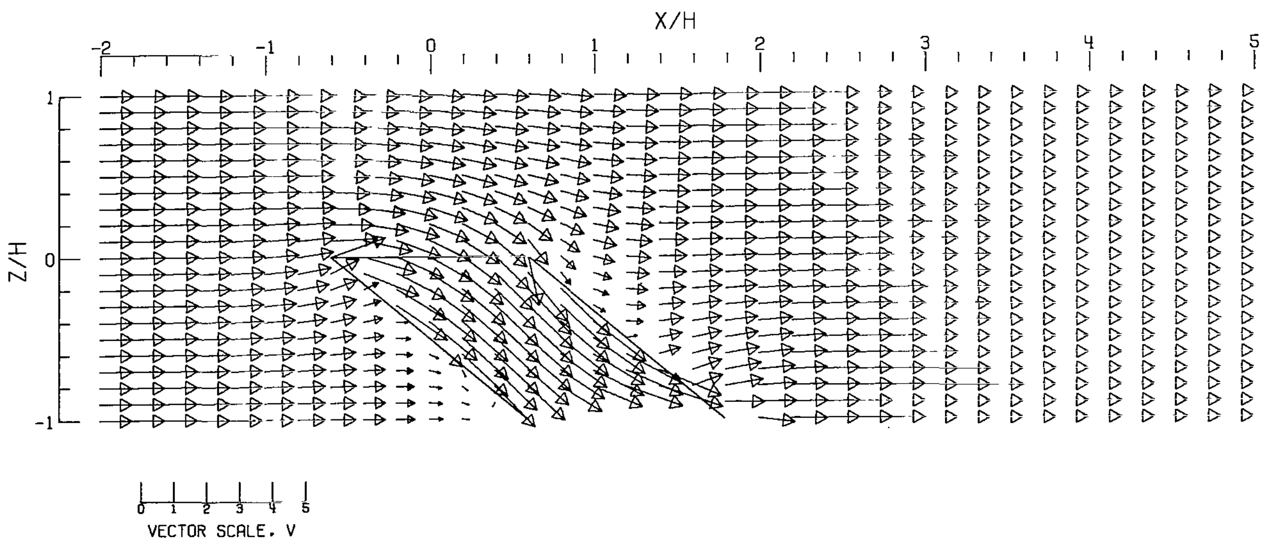

(B).- GROUND EFFECT.

Figure 110.- Flow vectors in the X-Z plane, calculated using doublet strings. The rotor and the edges of the wake are shown. ζ = 1.000; η = 1.0; γ = 2.0; σ = 0.300; α = 0.0°; χ = 50.0°; uniform loading.

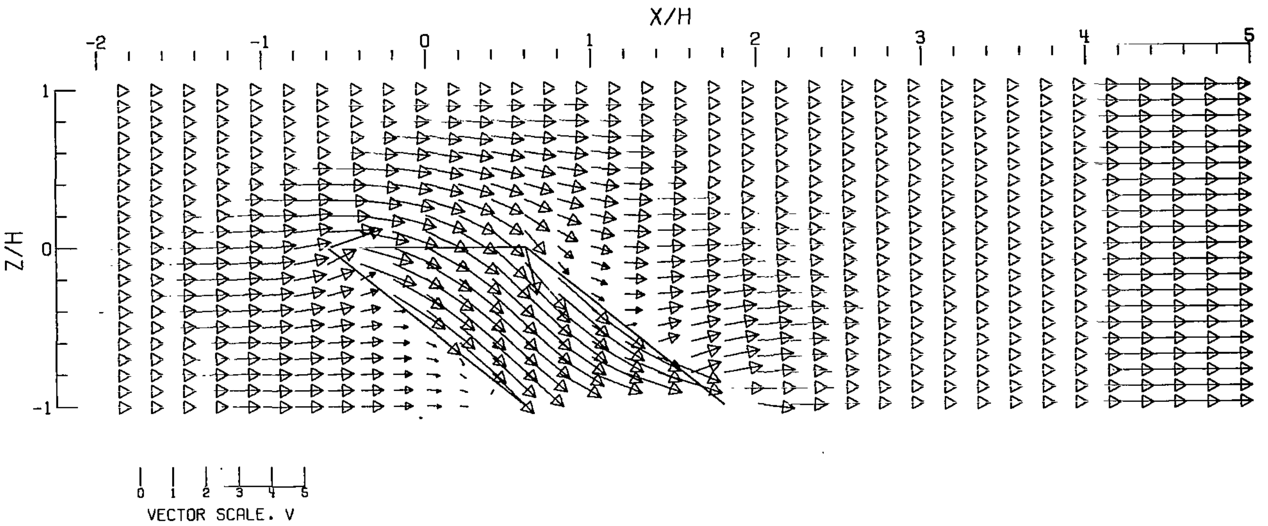

(C).- CLOSED TUNNEL.

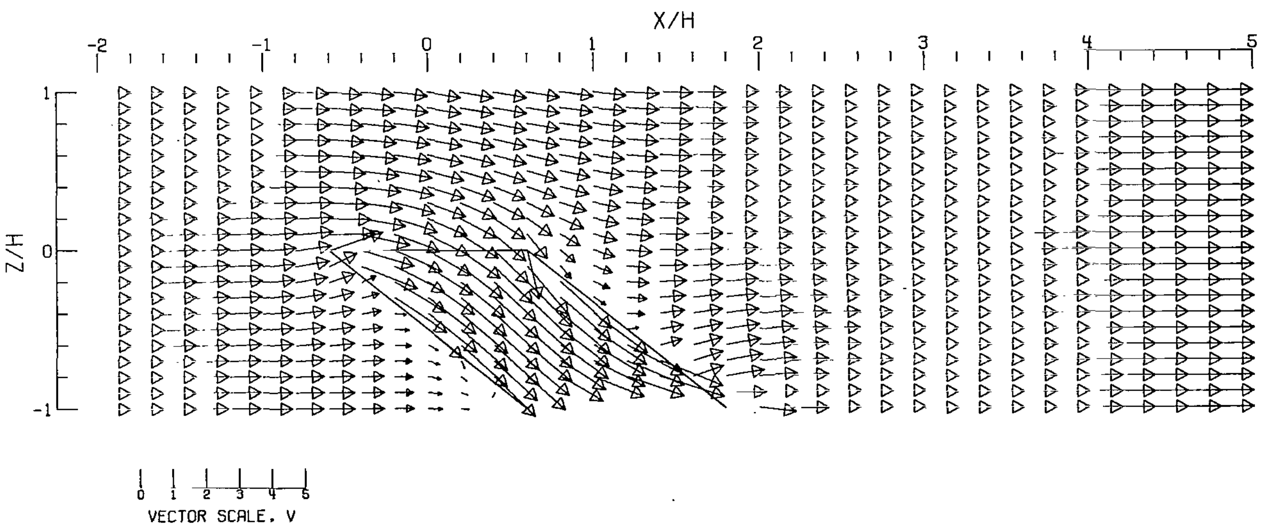

(D).- CLOSED-ON-BOTTOM-ONLY TUNNEL.

Figure 110.- Concluded.

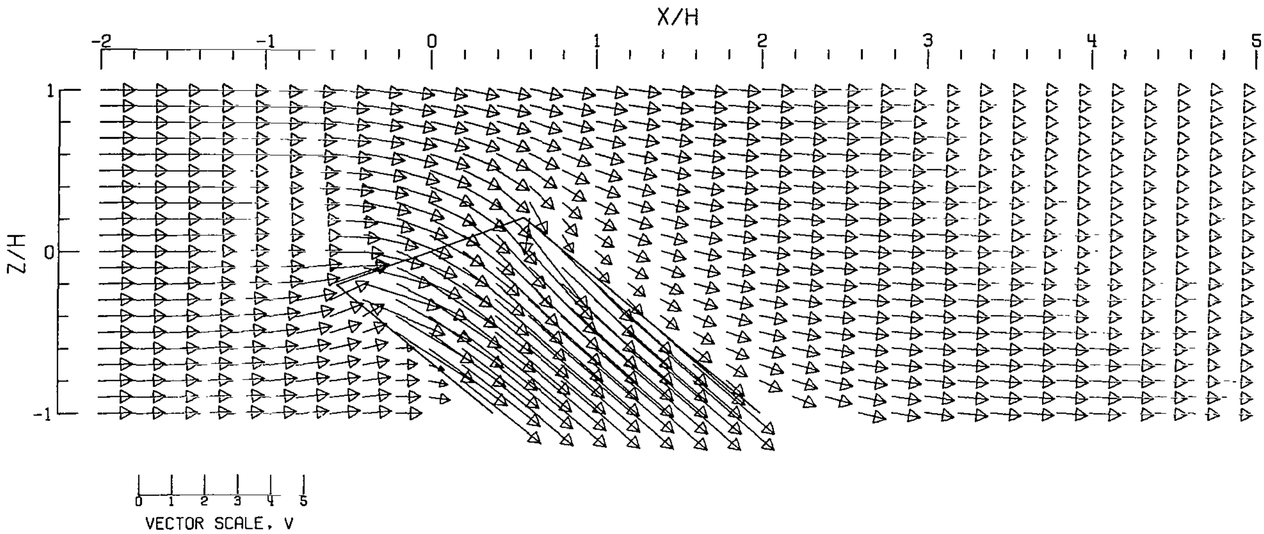

(A).- FREE AIR.

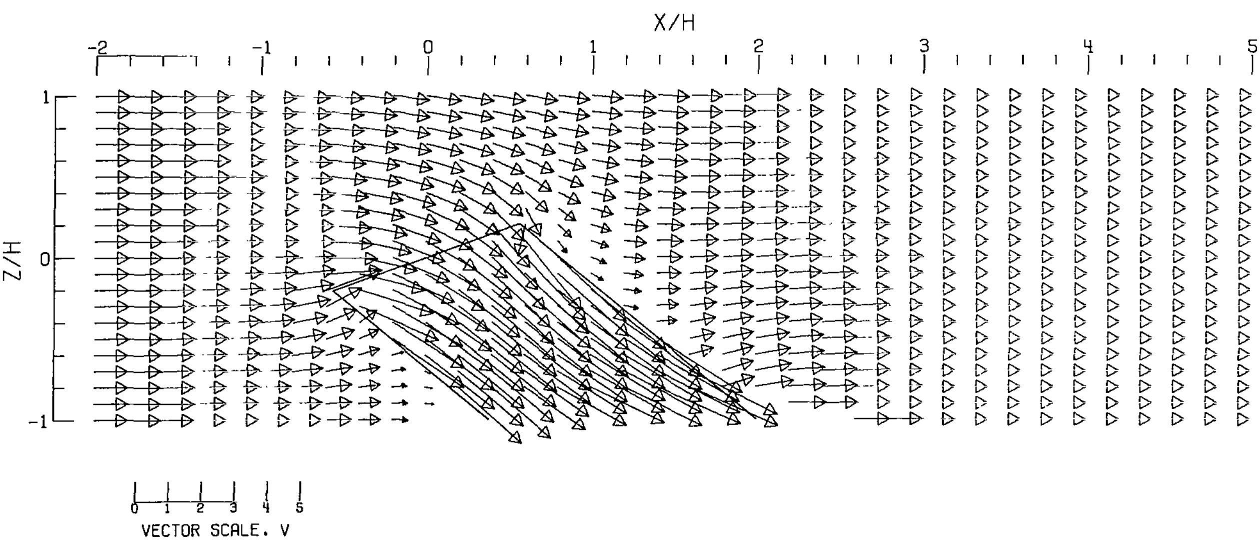

(B).- GROUND EFFECT.

Figure 111.- Flow vectors in the X-Z plane, calculated using doublet strings. The rotor and the edges of the wake are shown. ζ = 1.000; η = 1.0; γ = 2.0; σ = 0.300; α = -20.0^0; χ = 50.0^0; uniform loading.

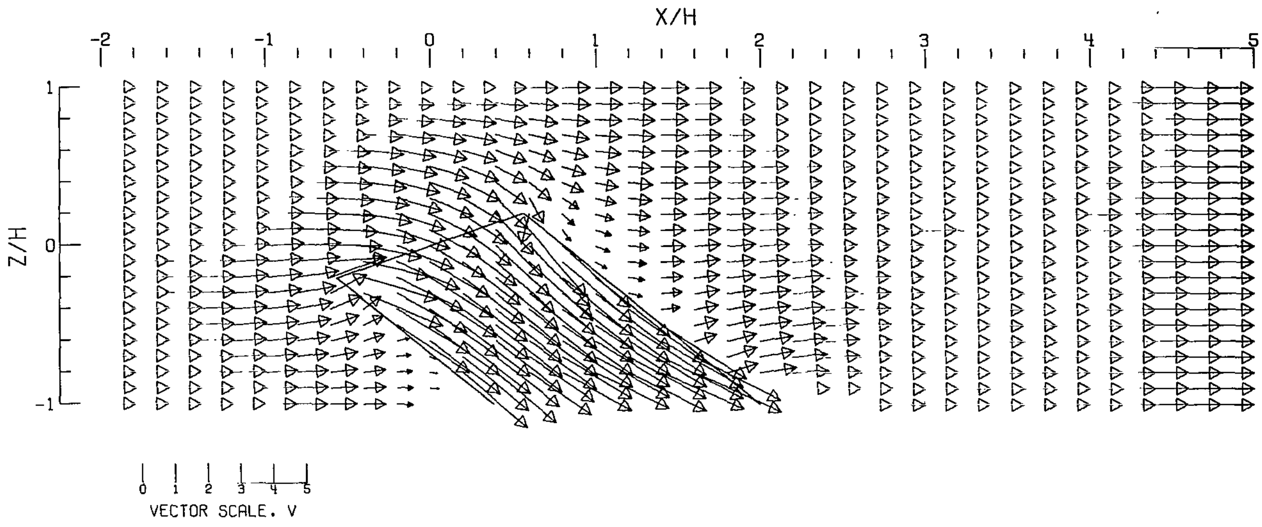

(C).- CLOSED TUNNEL.

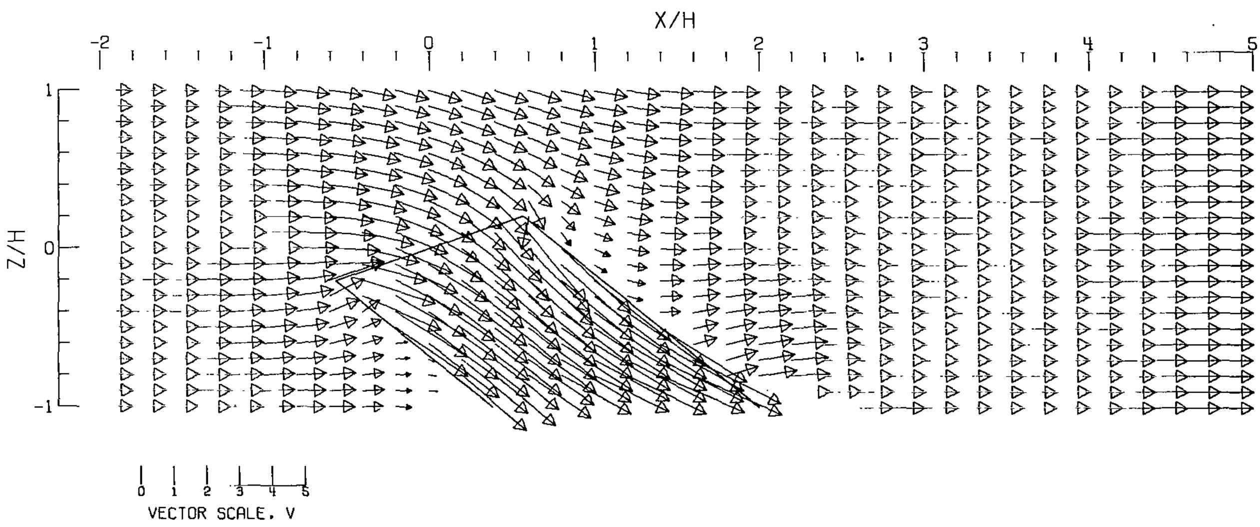

(D).- CLOSED-ON-BOTTOM-ONLY TUNNEL.

Figure 111.- Concluded.

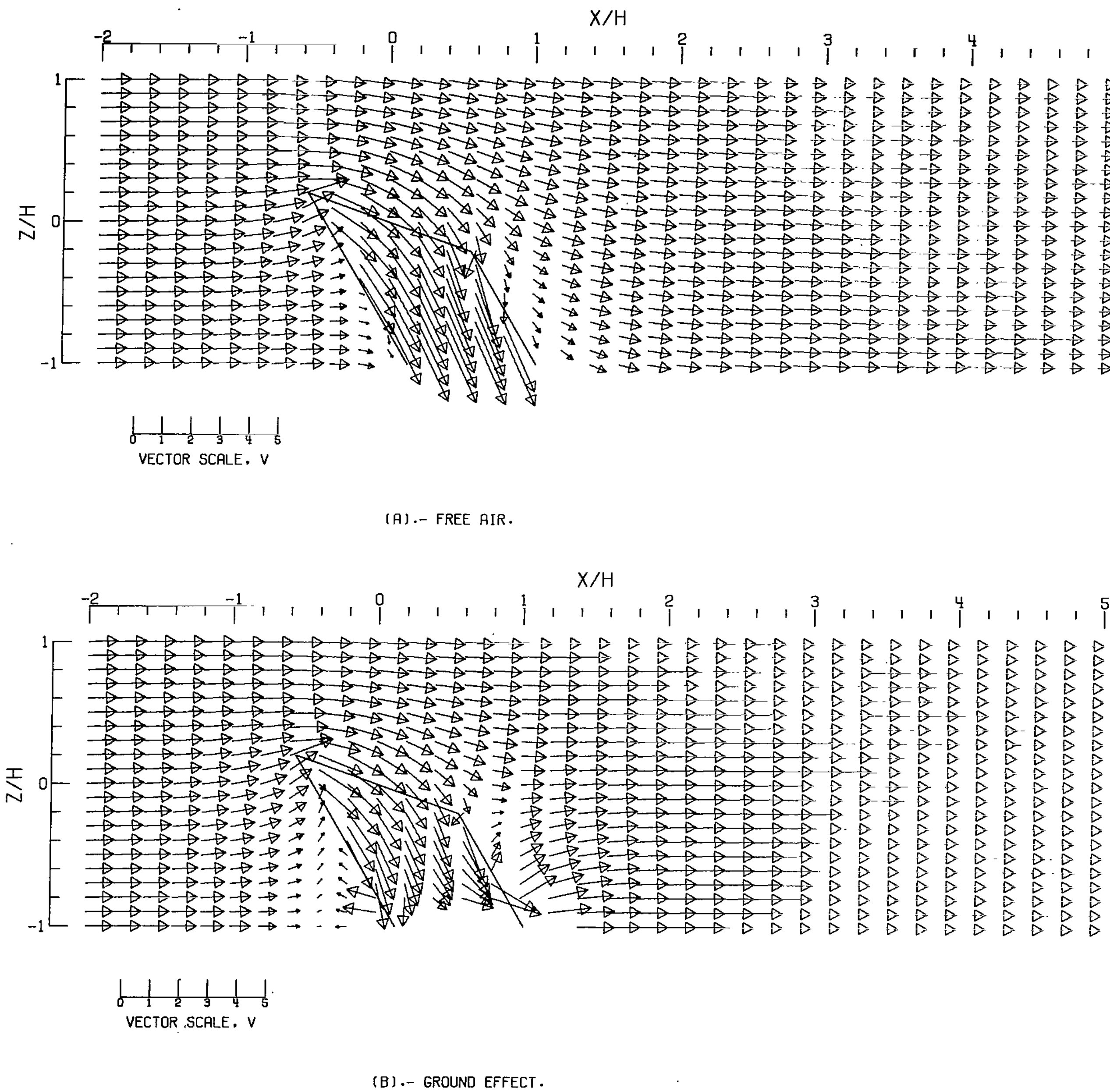

Figure 112.- Flow vectors in the X-Z plane, calculated using doublet strings. The rotor and the edges of the wake are shown. ζ = 1.000; η = 1.0; γ = 2.0; σ = 0.300; α = 20.0°; χ = 30.0°; uniform loading.

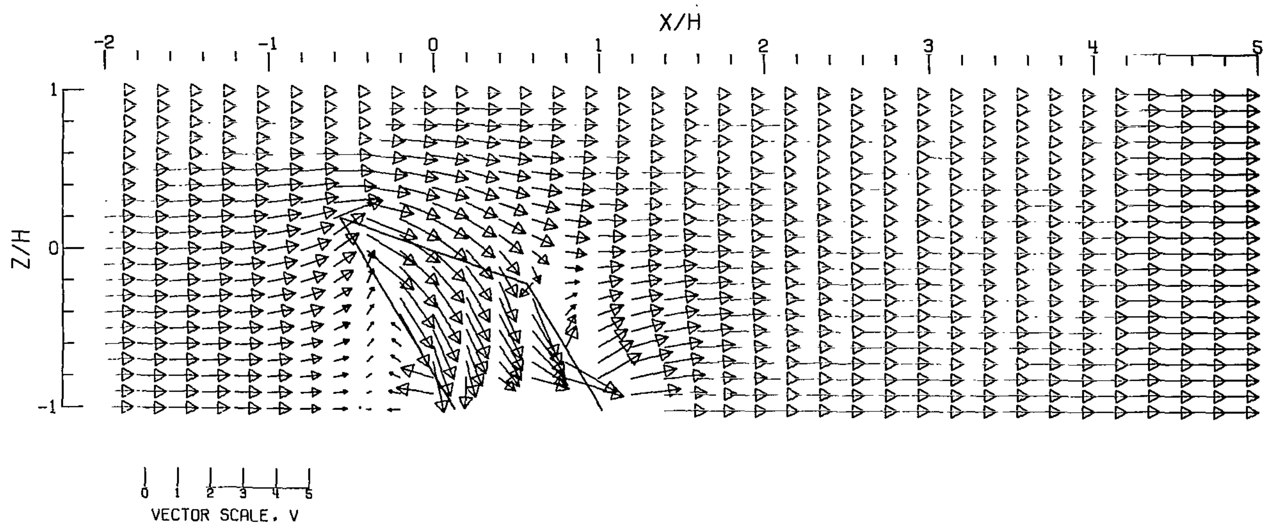

(C).- CLOSED TUNNEL.

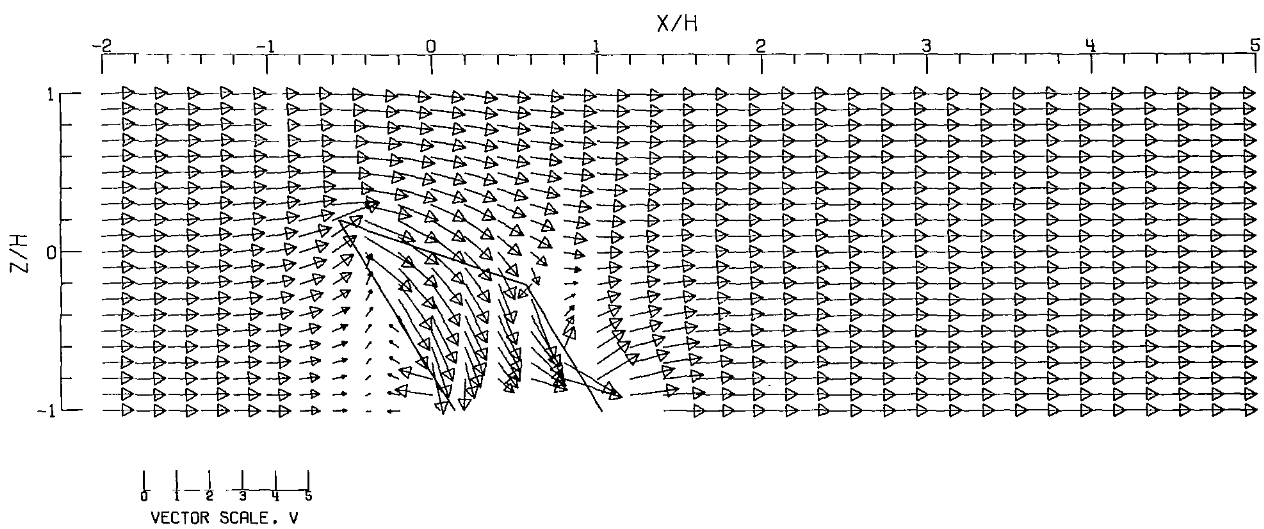

(D).- CLOSED-ON-BOTTOM-ONLY TUNNEL.

Figure 112.- Concluded.

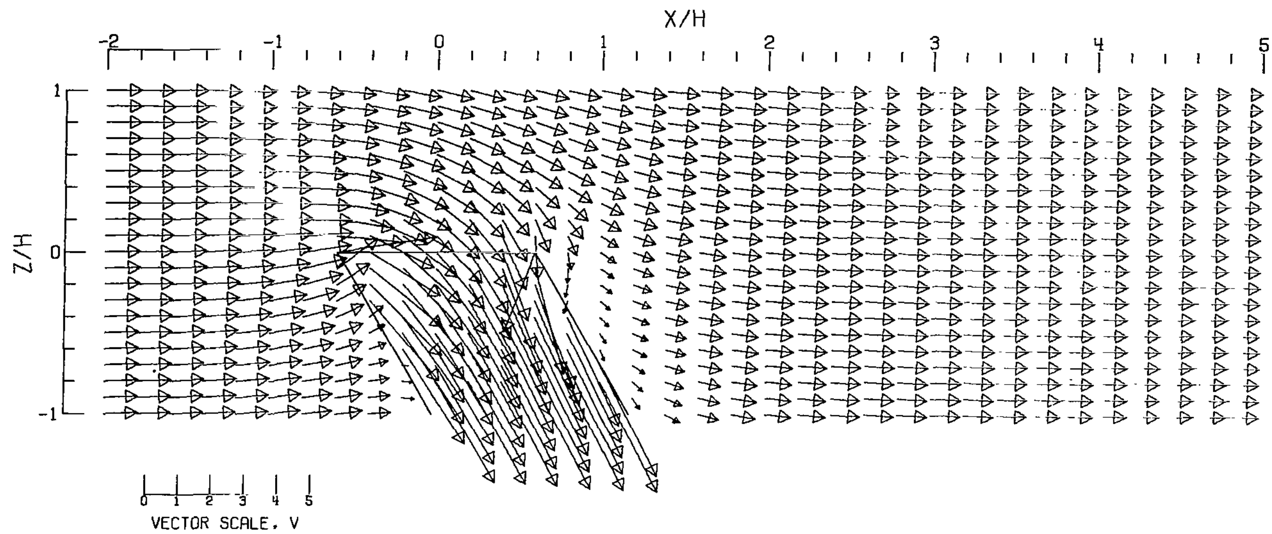

(A).- FREE AIR.

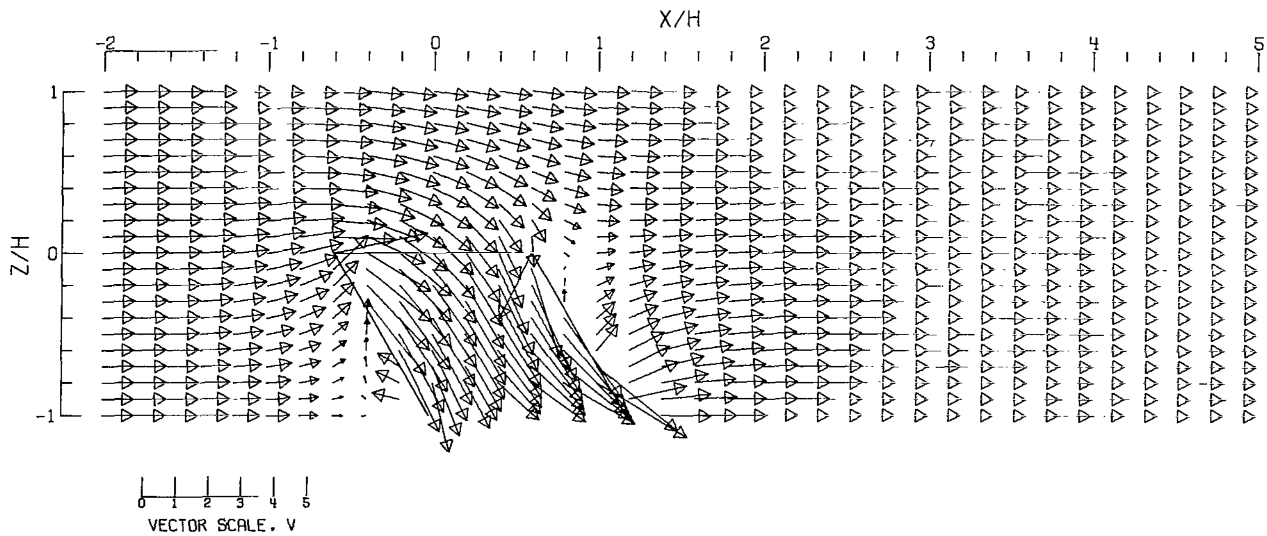

(B).- GROUND EFFECT.

Figure 113.- Flow vectors in the X-Z plane, calculated using doublet strings. The rotor and the edges of the wake are shown. ζ = 1.000; η = 1.0; γ = 2.0; σ = 0.300; α = 0.0°; χ = 30.0°; uniform loading.

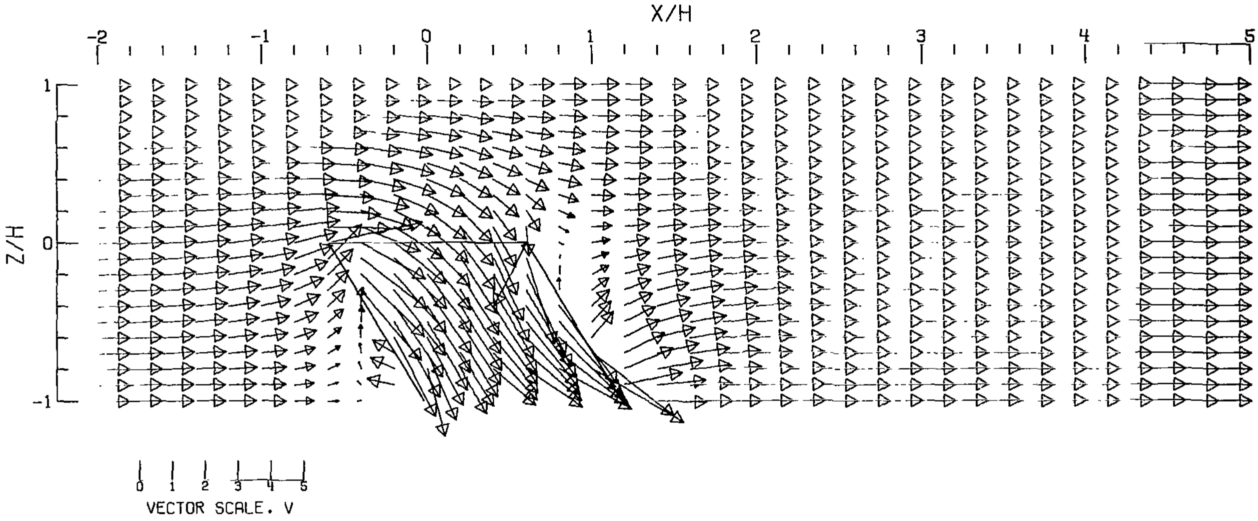

(C).- CLOSED TUNNEL.

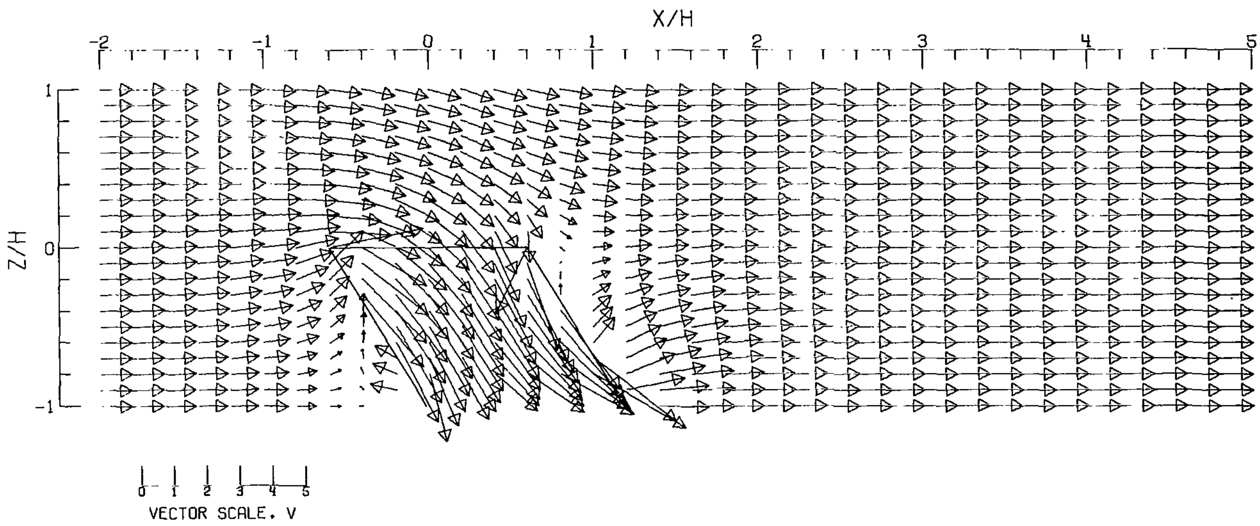

(D).- CLOSED-ON-BOTTOM-ONLY TUNNEL.

Figure 113.- Concluded.

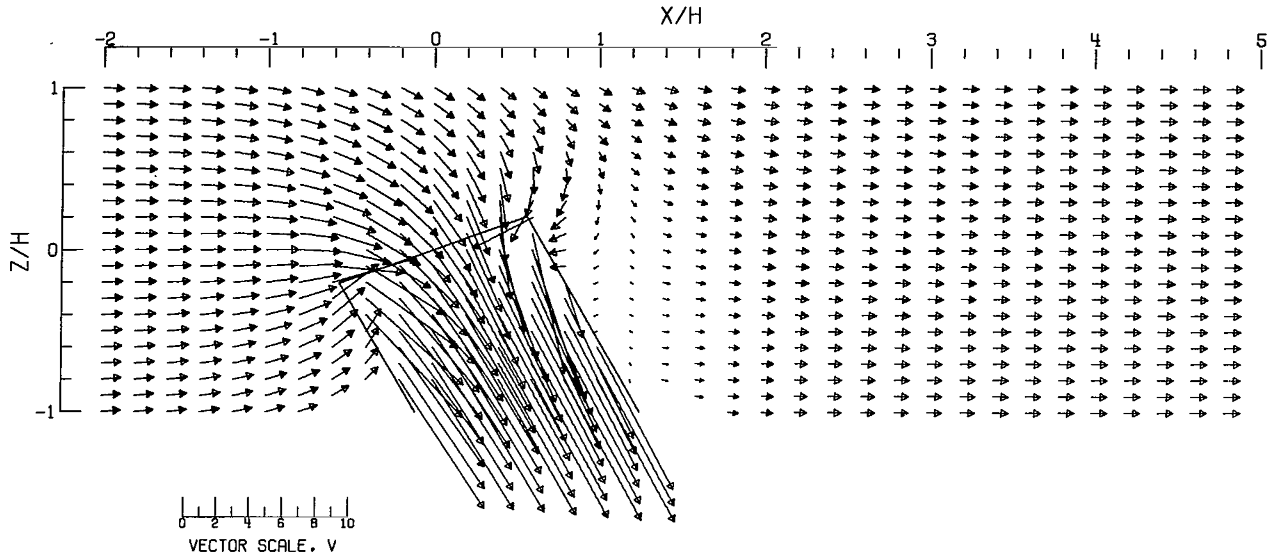

(A).- FREE AIR.

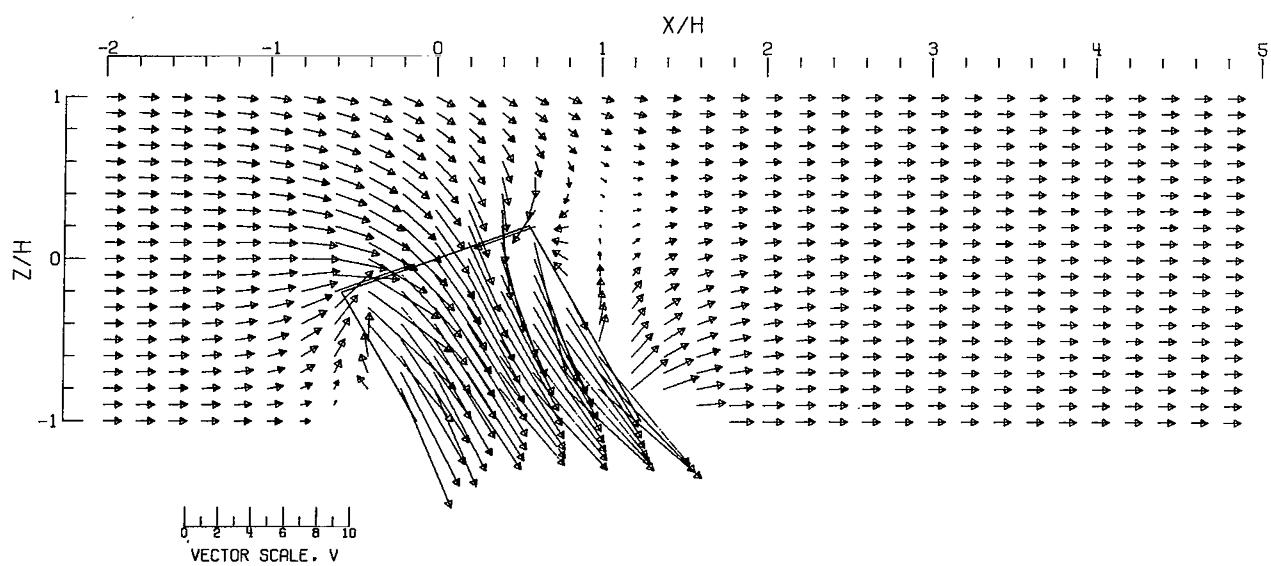

(B).- GROUND EFFECT.

Figure 114.- Flow vectors in the X-Z plane, calculated using doublet strings. The rotor and the edges of the wake are shown. ζ = 1.000; η = 1.0; γ = 2.0; σ = 0.300; α = -20.0°; χ = 30.0°; uniform loading.

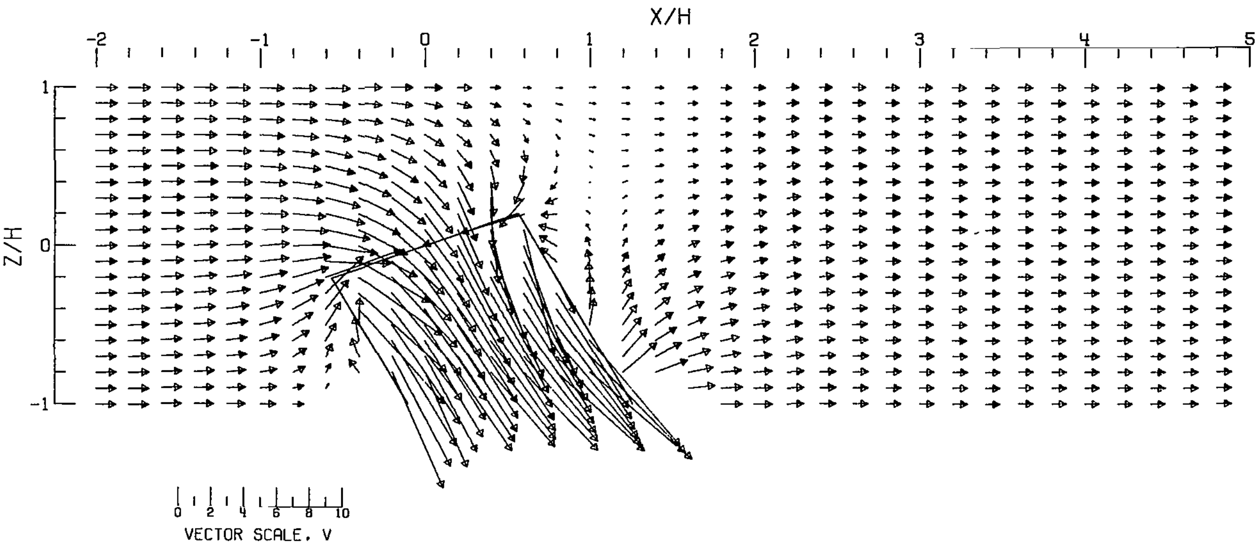

(C).- CLOSED TUNNEL.

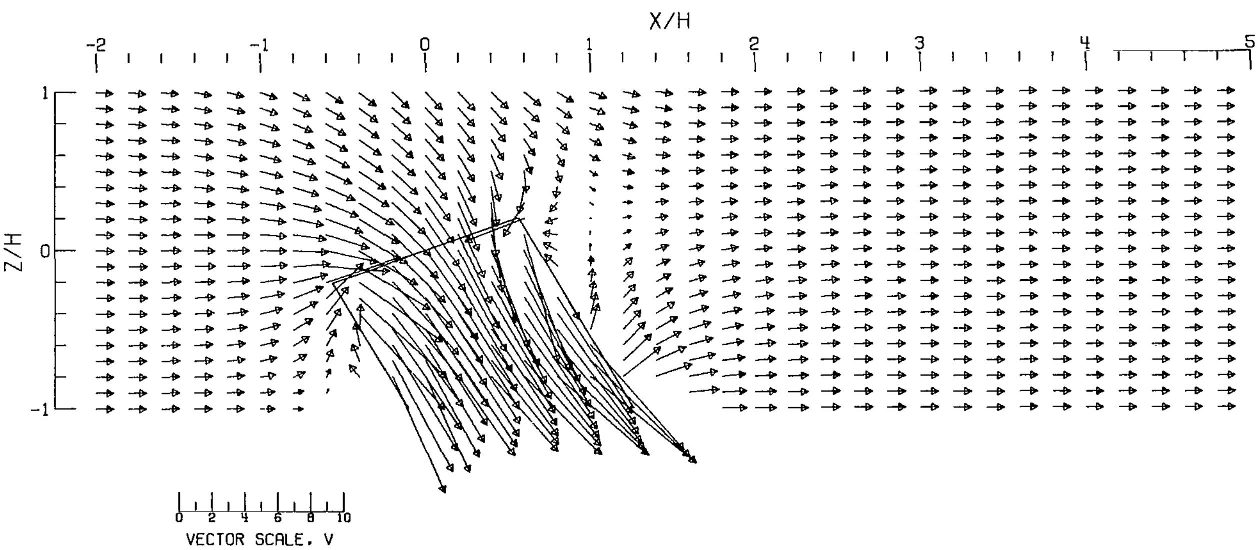

(D).- CLOSED-ON-BOTTOM-ONLY TUNNEL.

Figure 114.- Concluded.

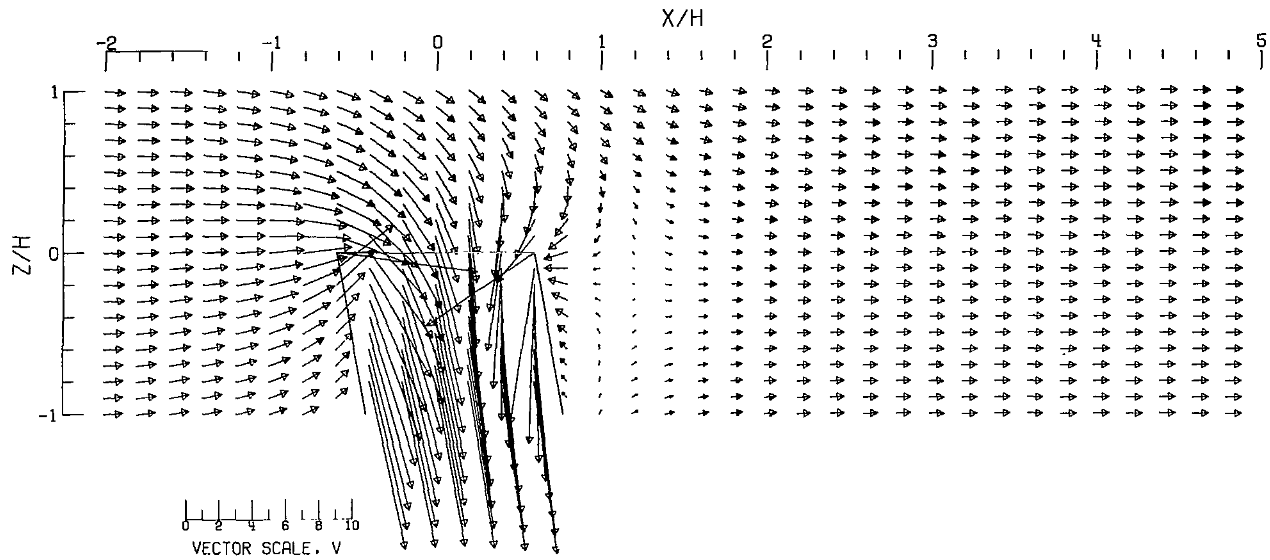

(A).- FREE AIR.

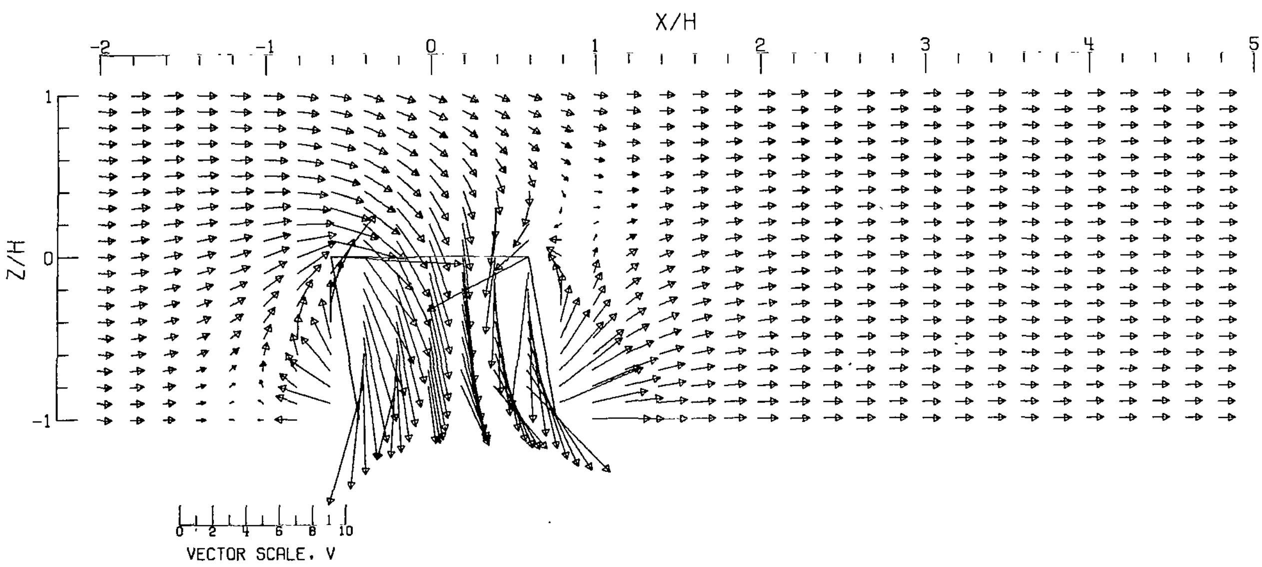

(B).- GROUND EFFECT.

Figure 115.- Flow vectors in the X-Z plane, calculated using doublet strings. The rotor and the edges of the wake are shown. ζ = 1.000; η = 1.0; γ = 2.0; σ = 0.300; α = 0.0°; χ = 10.0°; uniform loading.

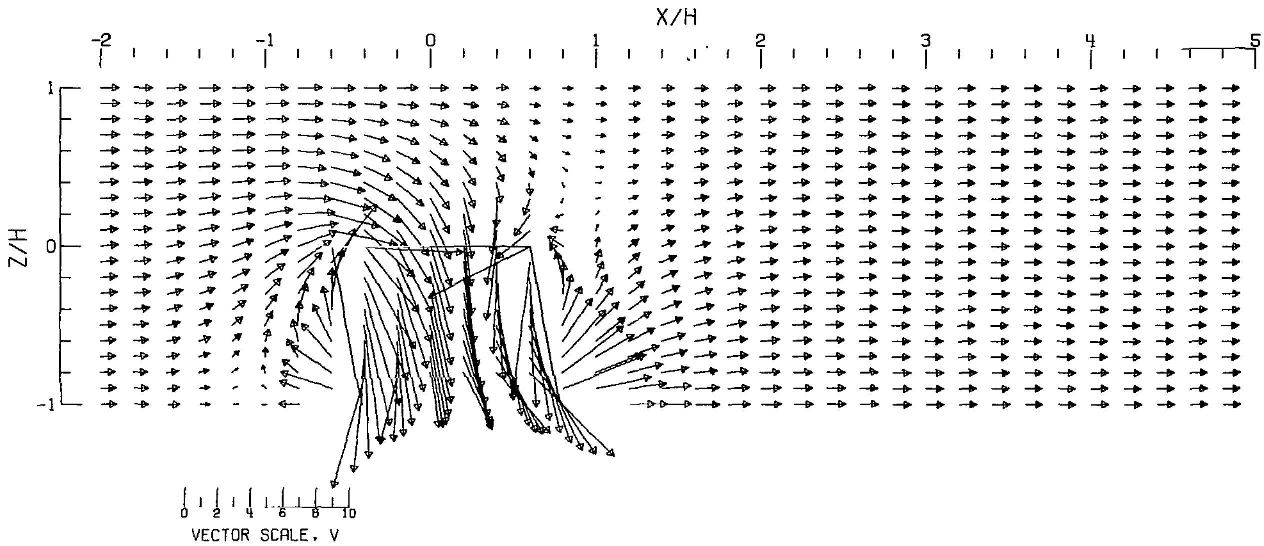

(C).- CLOSED TUNNEL.

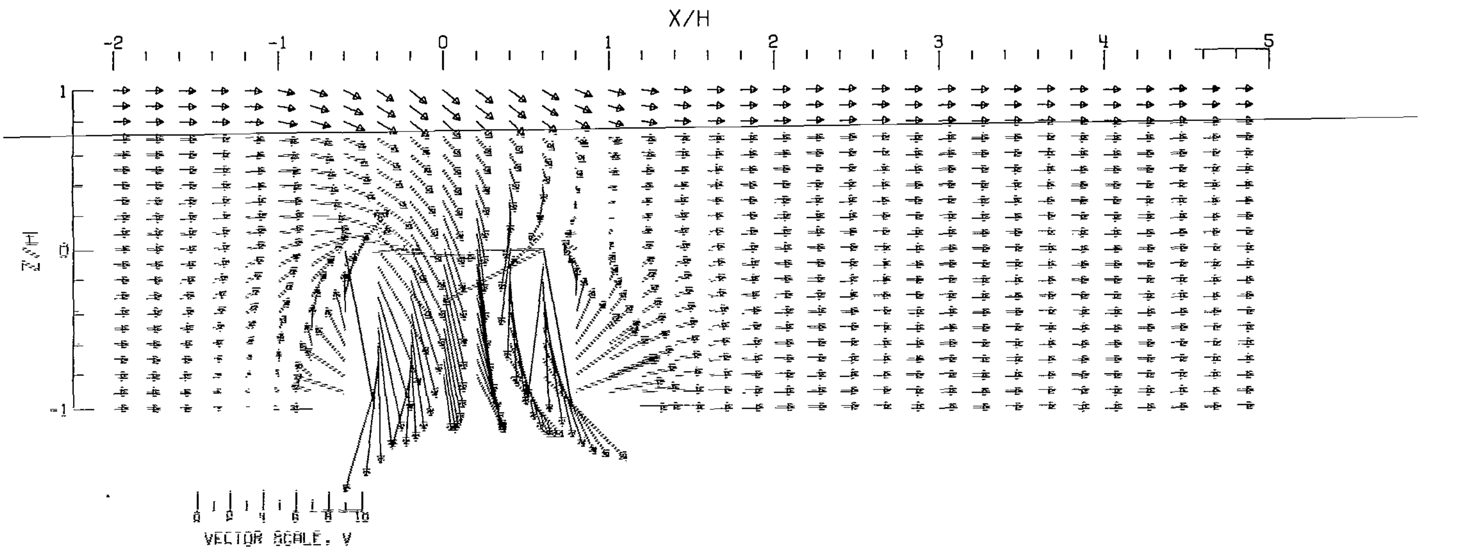

(D).- CLOSED-ON-BOTTOM-ONLY TUNNEL.

Figure 115.- Concluded.

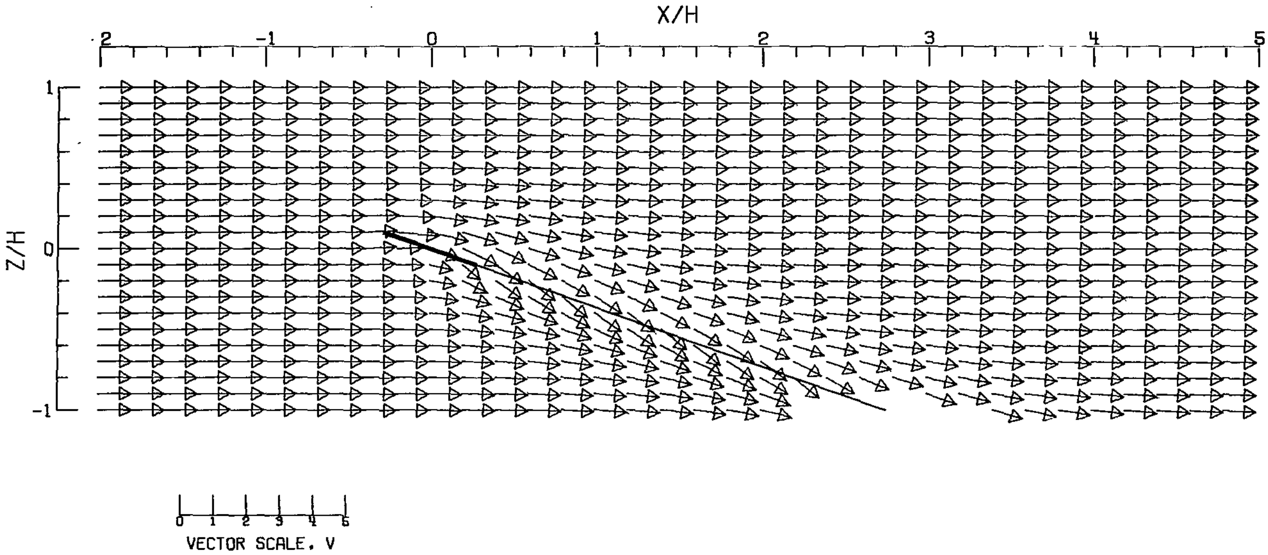

(A).– FREE AIR.

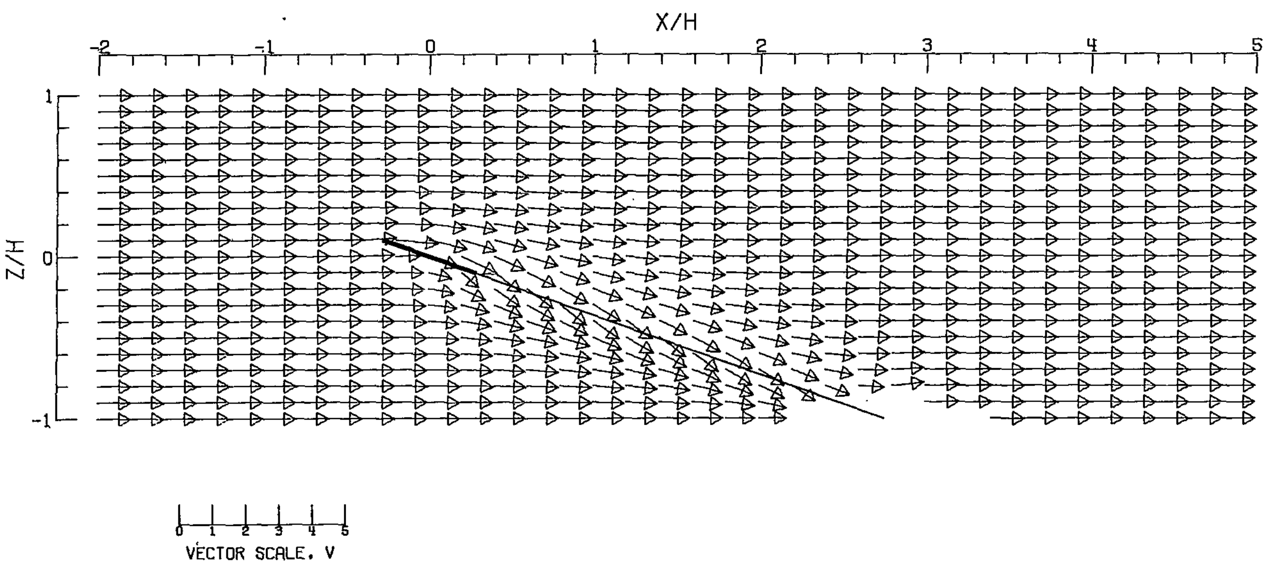

(B).– GROUND EFFECT.

Figure 116.- Flow vectors in the X-Z plane, calculated using doublet strings. The rotor and the edges of the wake are shown. ζ = 1.000; η = 1.0; γ = 0.5; σ = 0.600; α = 20.0°; χ = 70.0°; uniform loading.

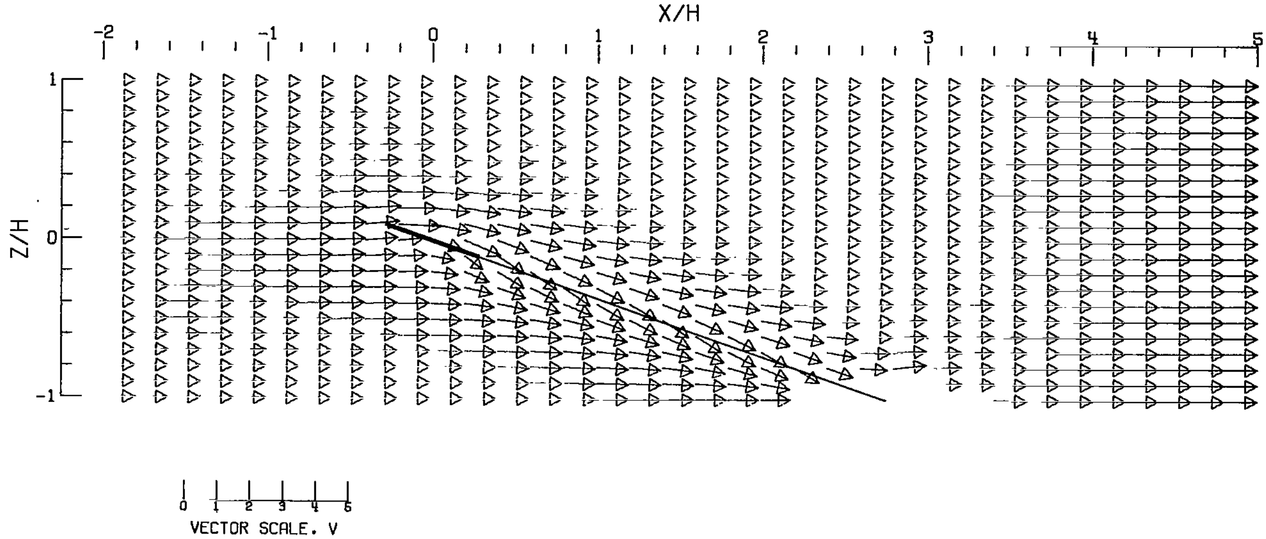

(C).- CLOSED TUNNEL.

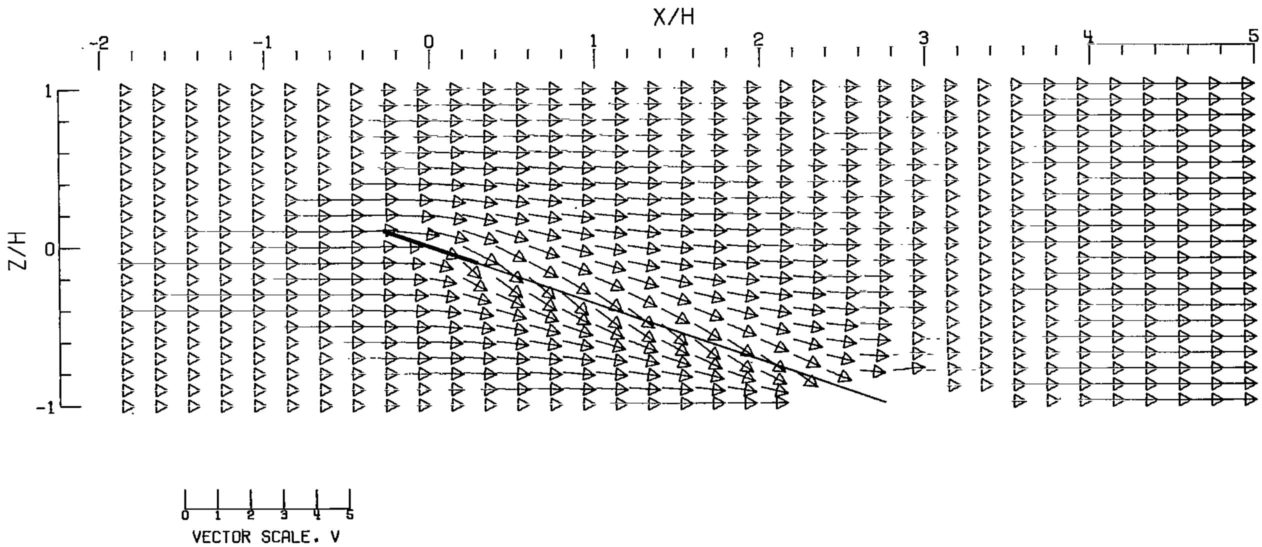

(D).- CLOSED-ON-BOTTOM-ONLY TUNNEL.

Figure 116.- Concluded.

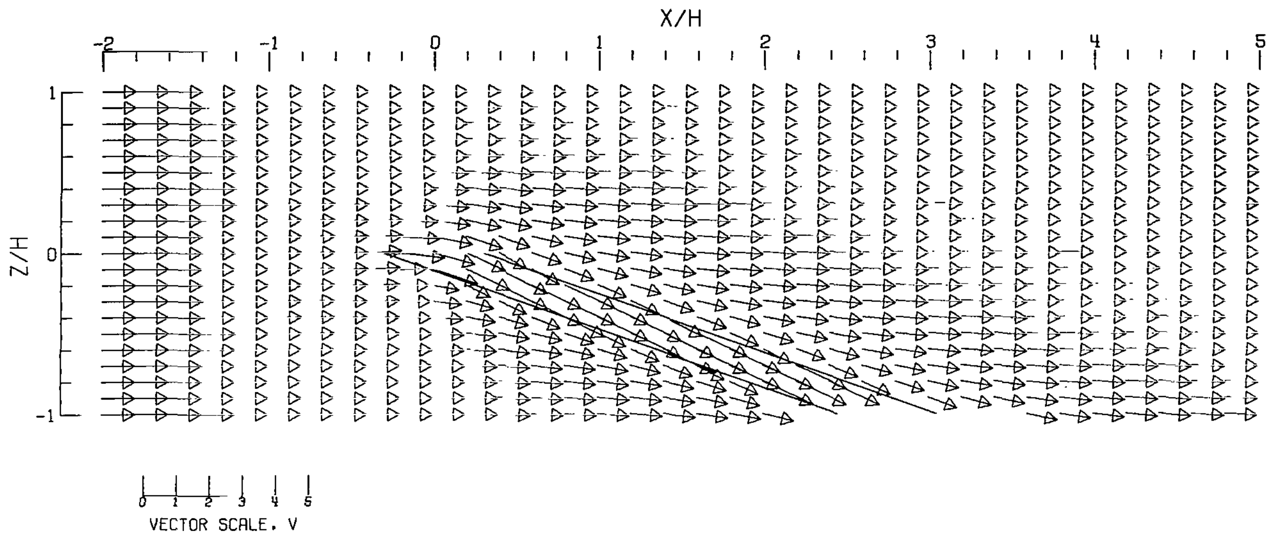

(A).- FREE AIR.

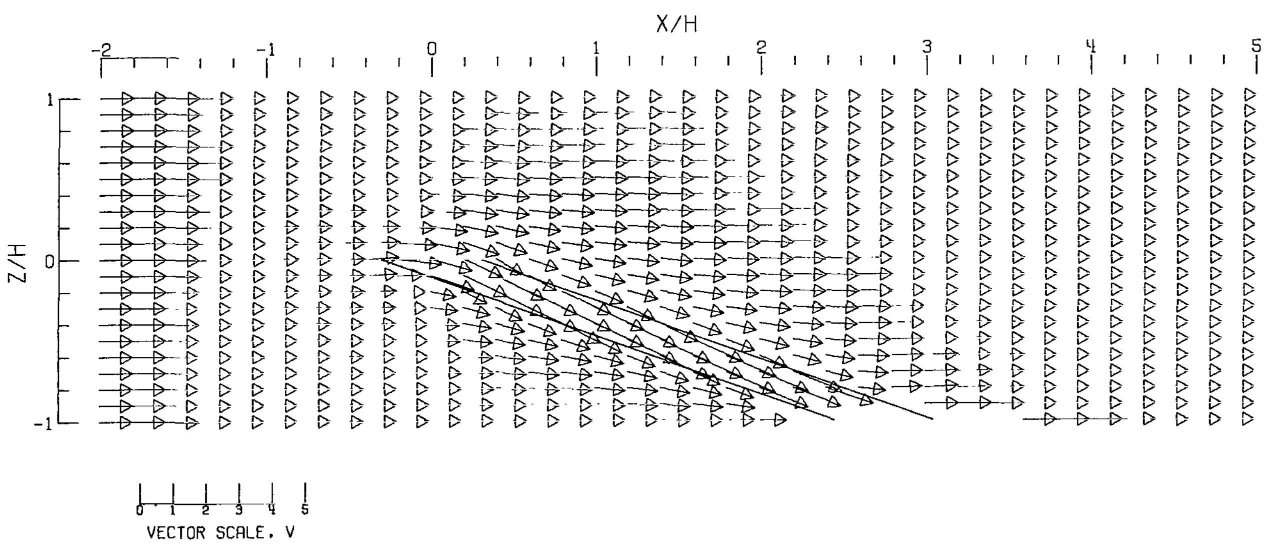

(B).- GROUND EFFECT.

Figure 117.- Flow vectors in the X-Z plane, calculated using doublet strings. The rotor and the edges of the wake are shown. ζ = 1.000; η = 1.0; γ = 0.5; σ = 0.600; α = 0.0°; χ = 70.0°; uniform loading.

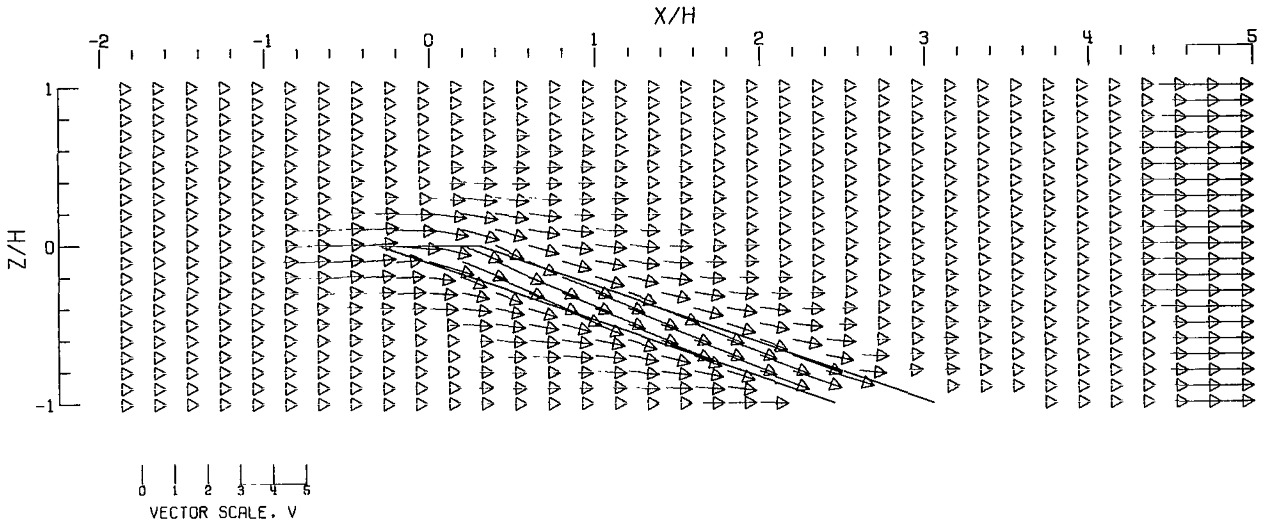

(C).- CLOSED TUNNEL.

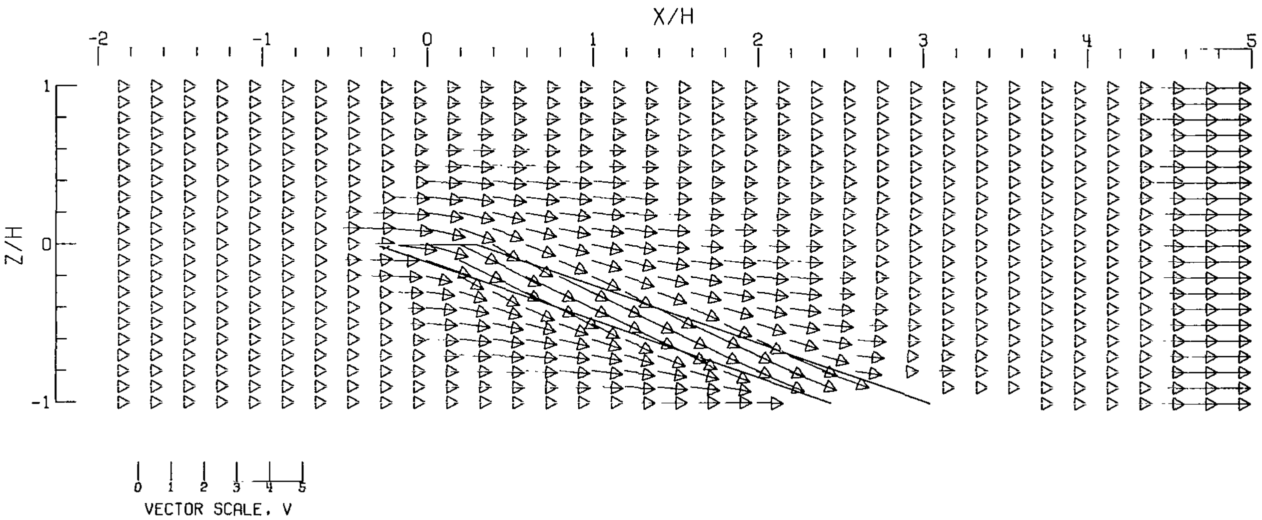

(D).- CLOSED-ON-BOTTOM-ONLY TUNNEL.

Figure 117.- Concluded.

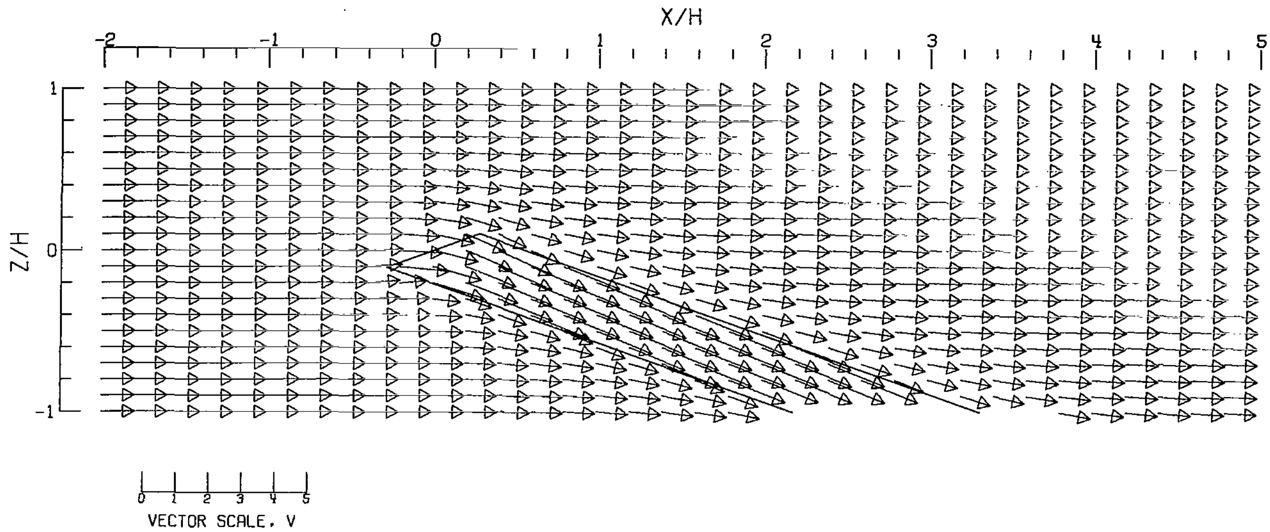

(A).- FREE AIR.

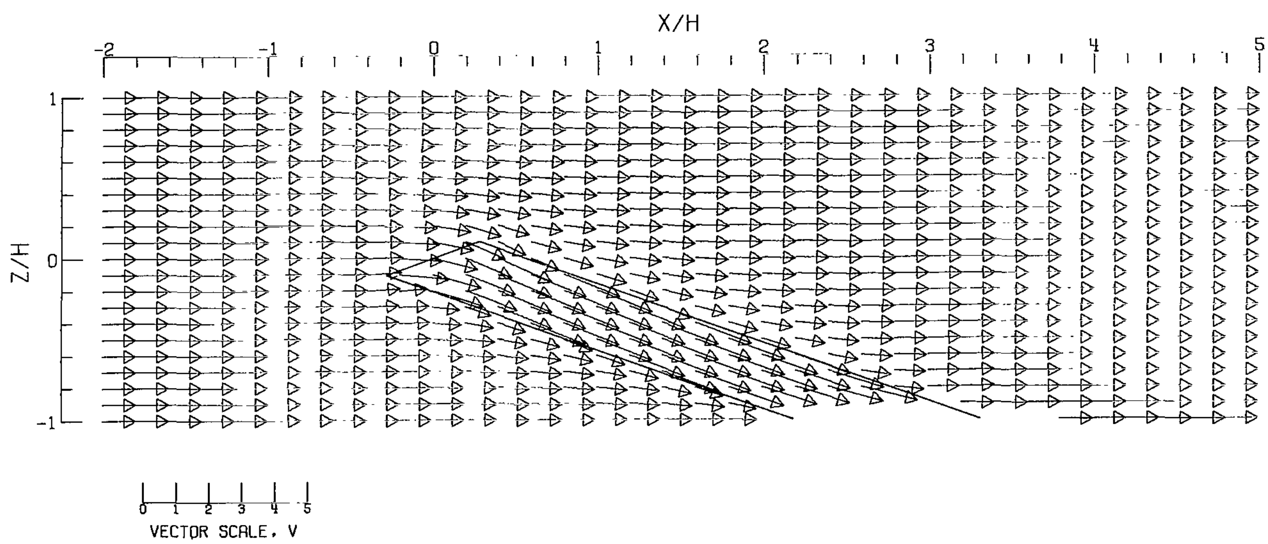

(B).- GROUND EFFECT.

Figure 118.- Flow vectors in the X-Z plane, calculated using doublet strings. The rotor and the edges of the wake are shown. $\zeta = 1.000$; $\eta = 1.0$; $\gamma = 0.5$; $\sigma = 0.600$; $\alpha = -20.0^{\circ}$; $\chi = 70.0^{\circ}$; uniform loading.

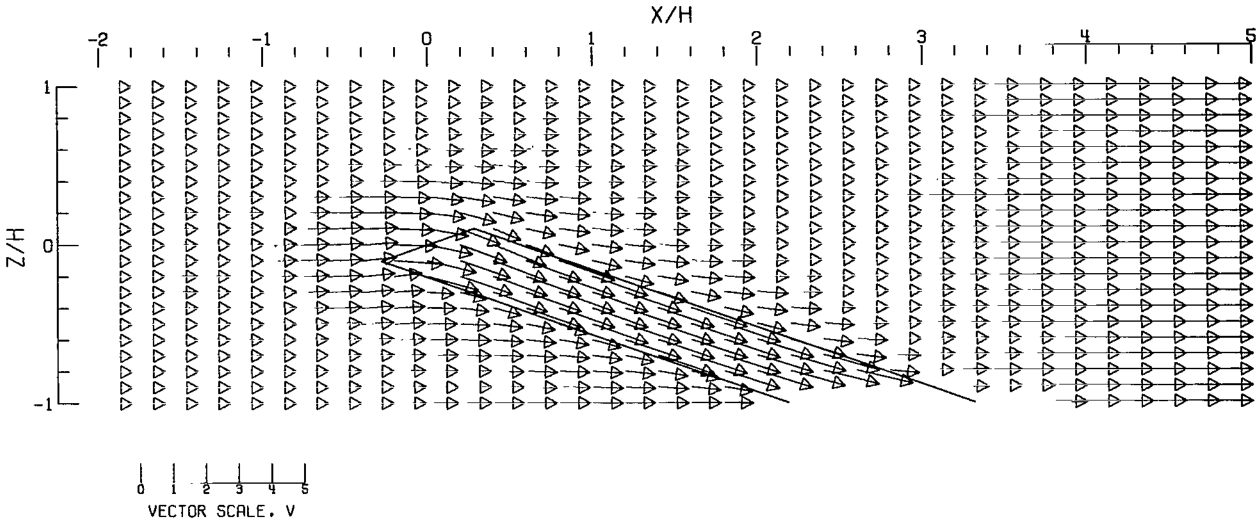

(C).– CLOSED TUNNEL.

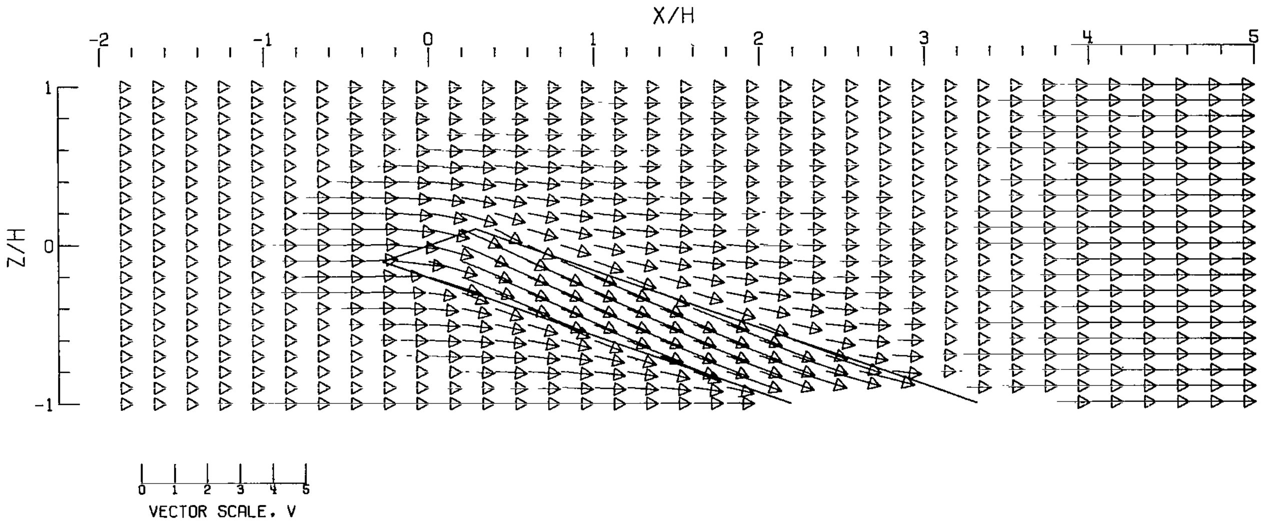

(D).– CLOSED-ON-BOTTOM-ONLY TUNNEL.

Figure 118.- Concluded.

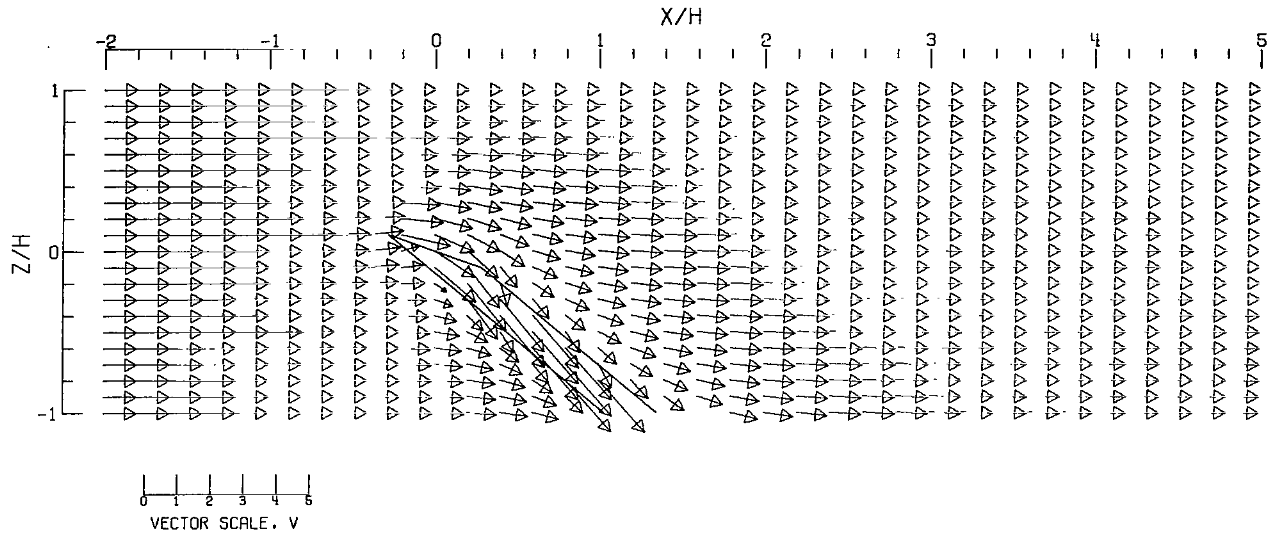

(A).- FREE AIR.

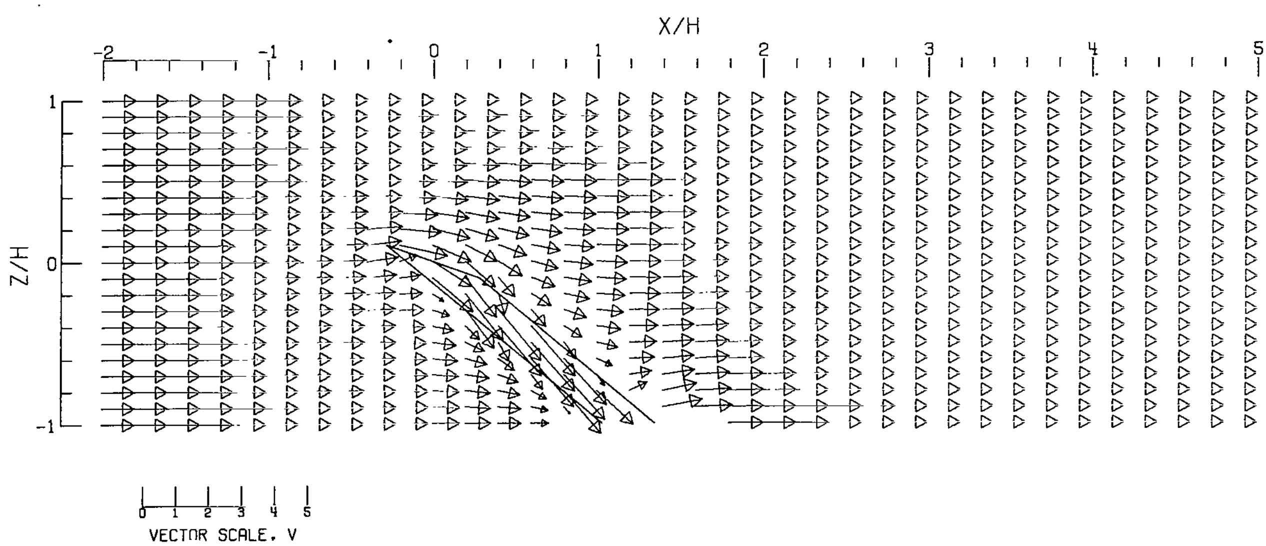

(B).- GROUND EFFECT.

Figure 119.- Flow vectors in the X-Z plane, calculated using doublet strings. The rotor and the edges of the wake are shown. ζ = 1.000; η = 1.0; γ = 0.5; σ = 0.600; α = 20.0°; χ = 50.0°; uniform loading.

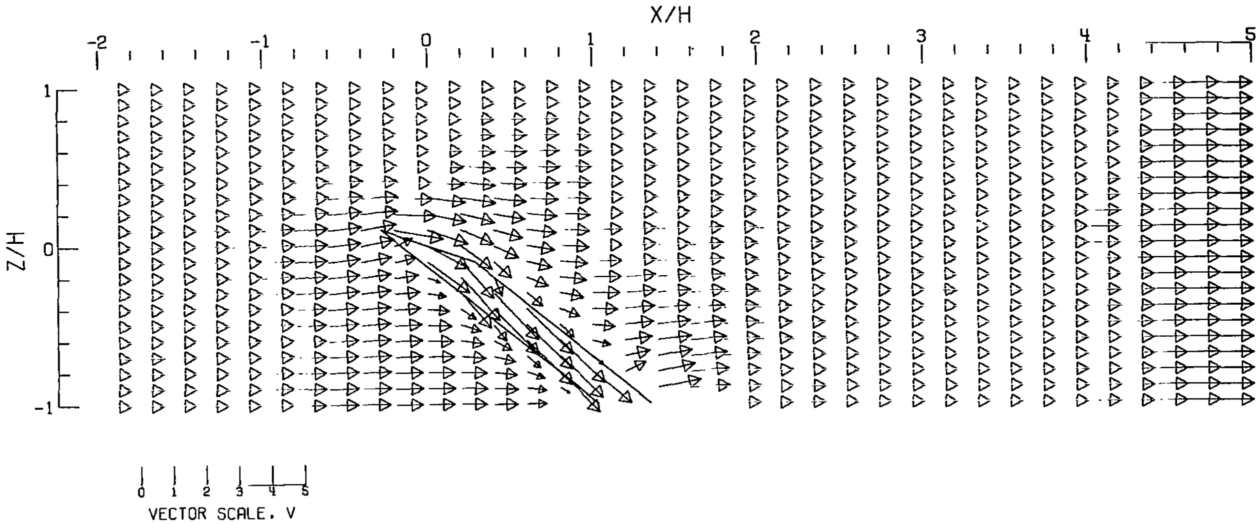

(C).- CLOSED TUNNEL.

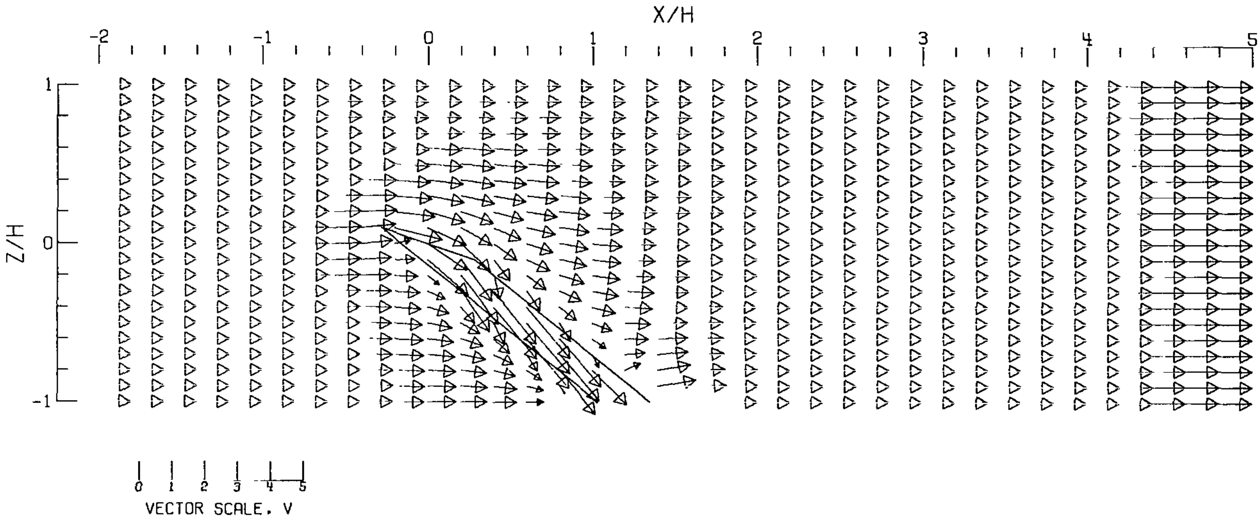

(D).- CLOSED-ON-BOTTOM-ONLY TUNNEL.

Figure 119.- Concluded.

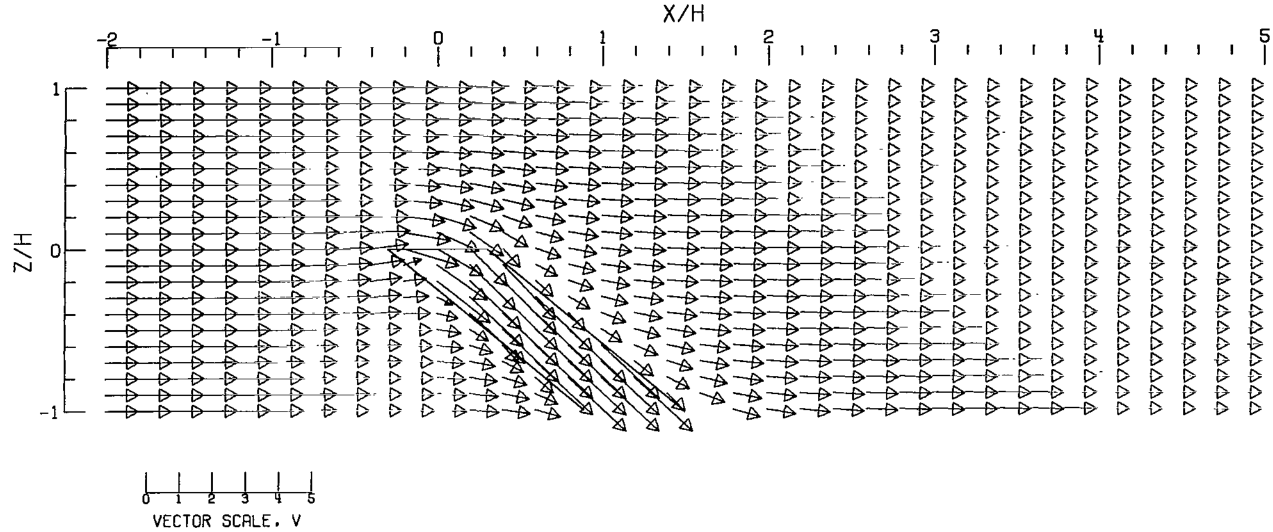

(A).- FREE AIR.

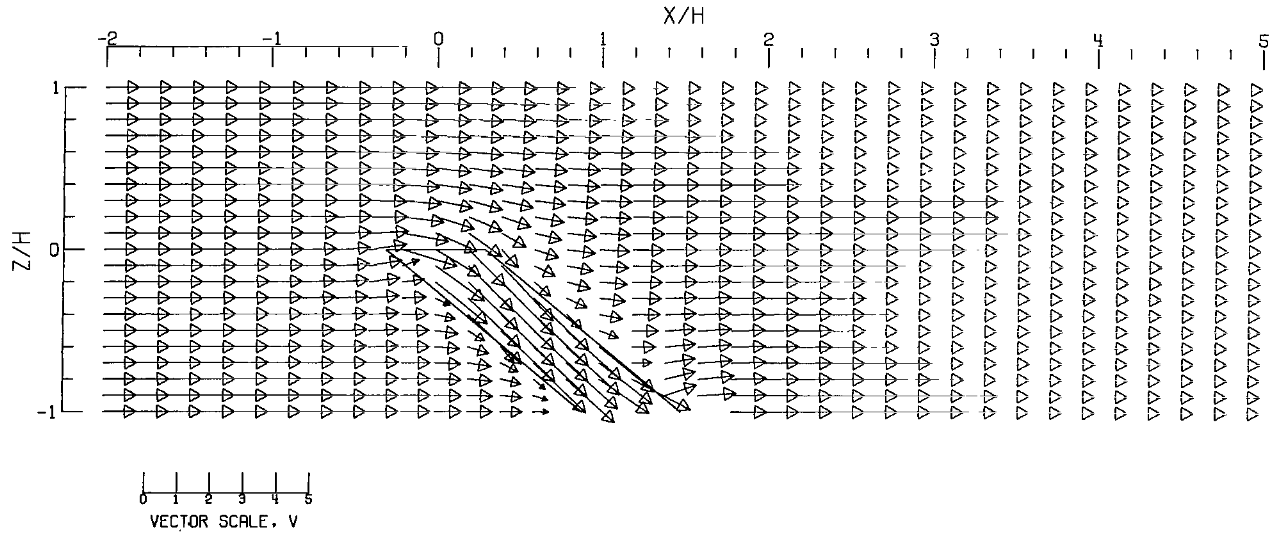

(B).- GROUND EFFECT.

Figure 120.- Flow vectors in the X-Z plane, calculated using doublet strings. The rotor and the edges of the wake are shown. ζ = 1.000; η = 1.0; γ = 0.5; σ = 0.600; α = 0.0°; χ = 50.0°; uniform loading.

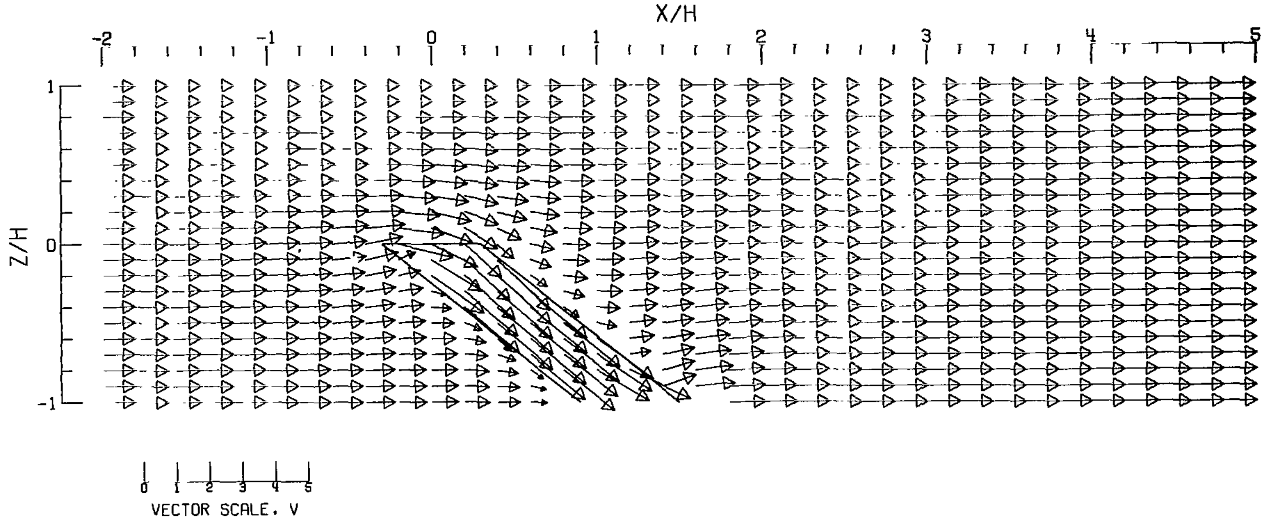

(C).- CLOSED TUNNEL.

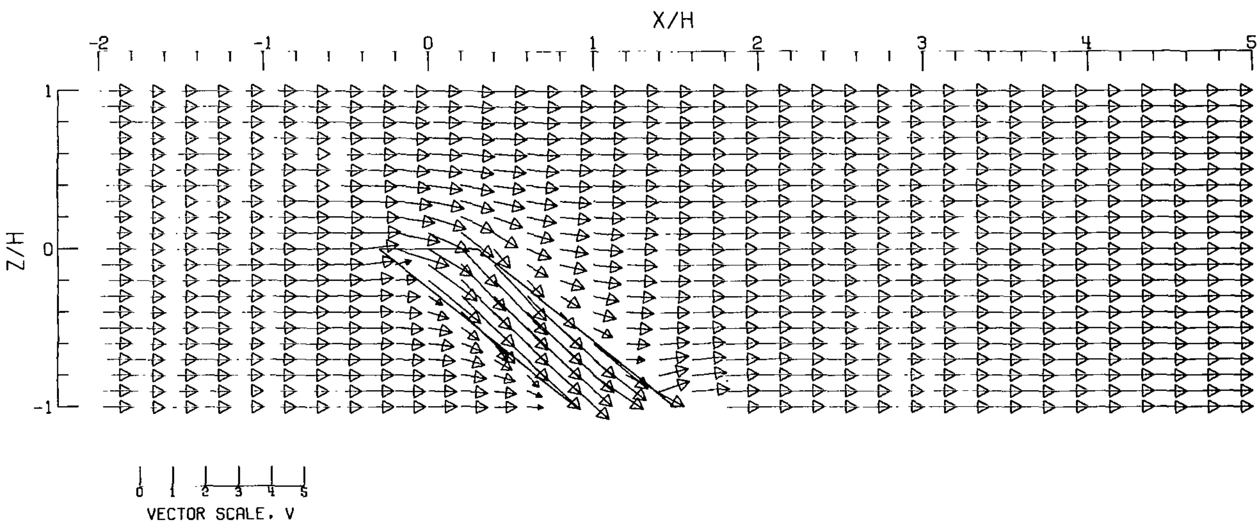

(D).- CLOSED-ON-BOTTOM-ONLY TUNNEL.

Figure 120.- Concluded.

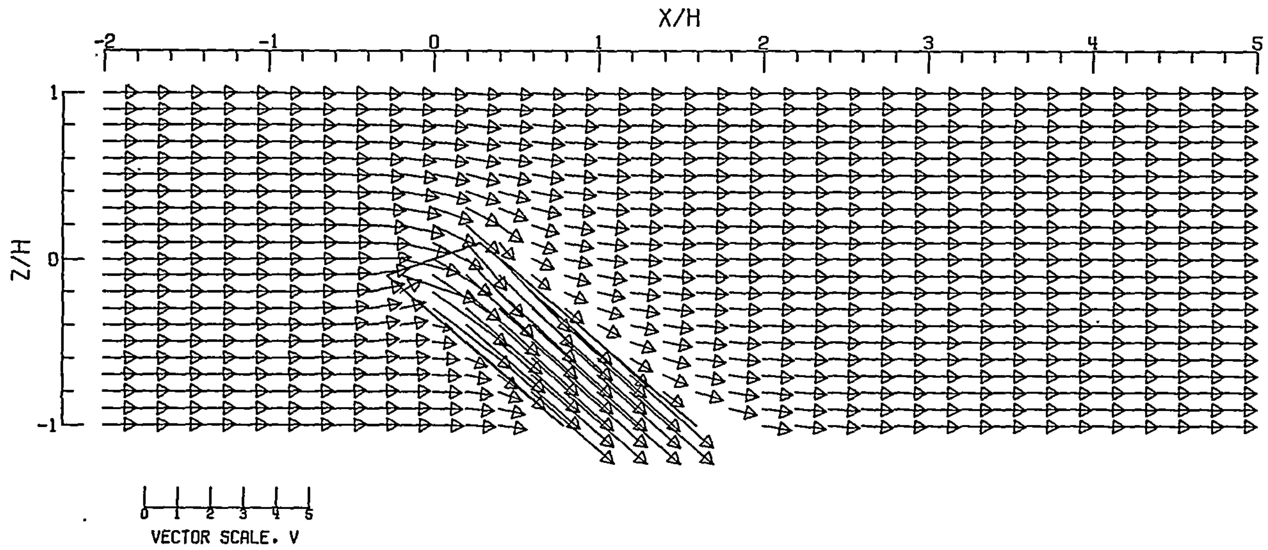

(A).- FREE AIR.

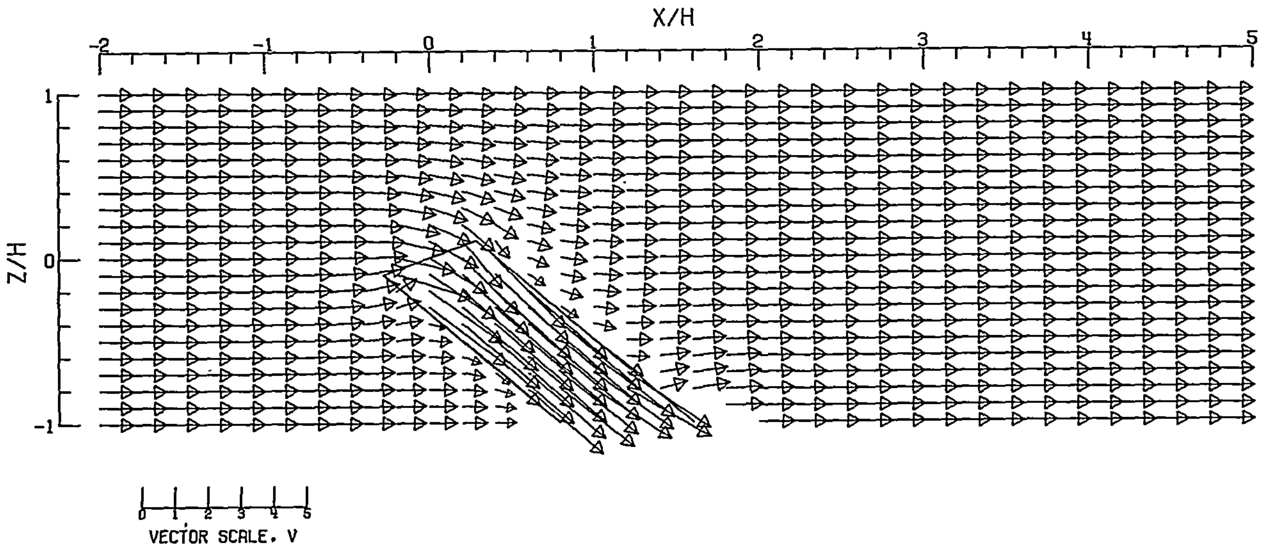

(B).- GROUND EFFECT.

Figure 121.- Flow vectors in the X-Z plane, calculated using doublet strings. The rotor and the edges of the wake are shown. $\zeta = 1.000$; $\eta = 1.0$; $\gamma = 0.5$; $\sigma = 0.600$; $\alpha = -20.0^{\circ}$; $\chi = 50.0^{\circ}$; uniform loading.

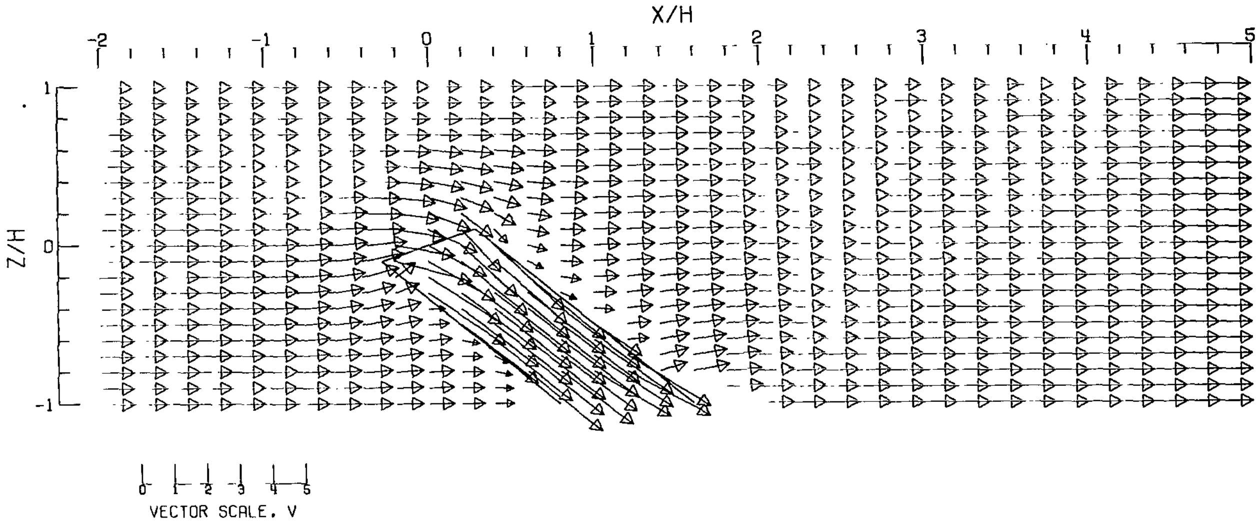

(C).- CLOSED TUNNEL.

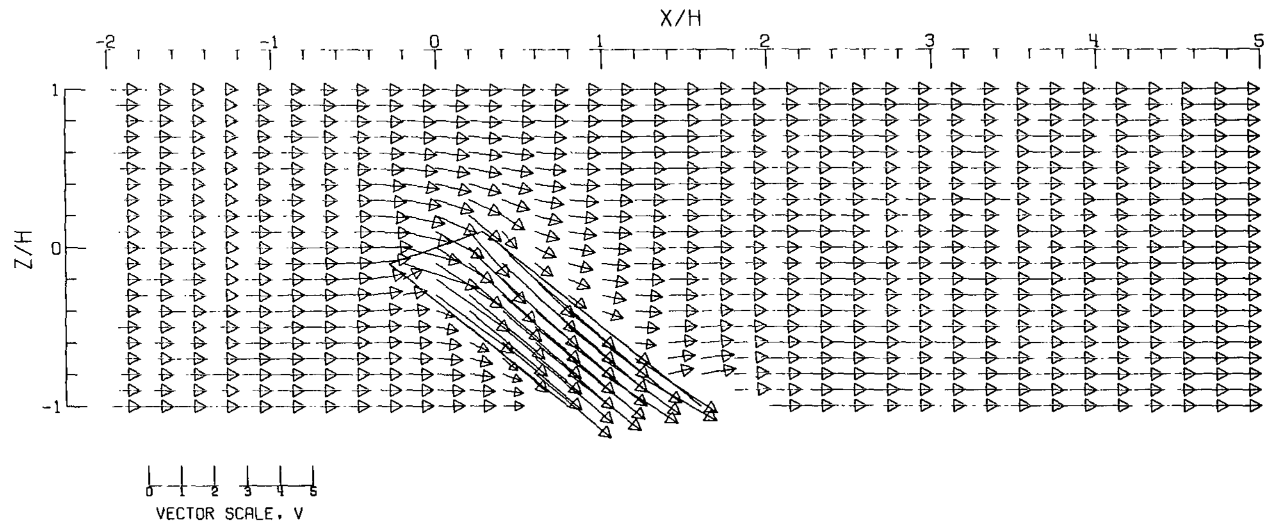

(D).- CLOSED-ON-BOTTOM-ONLY TUNNEL.

Figure 121.- Concluded.

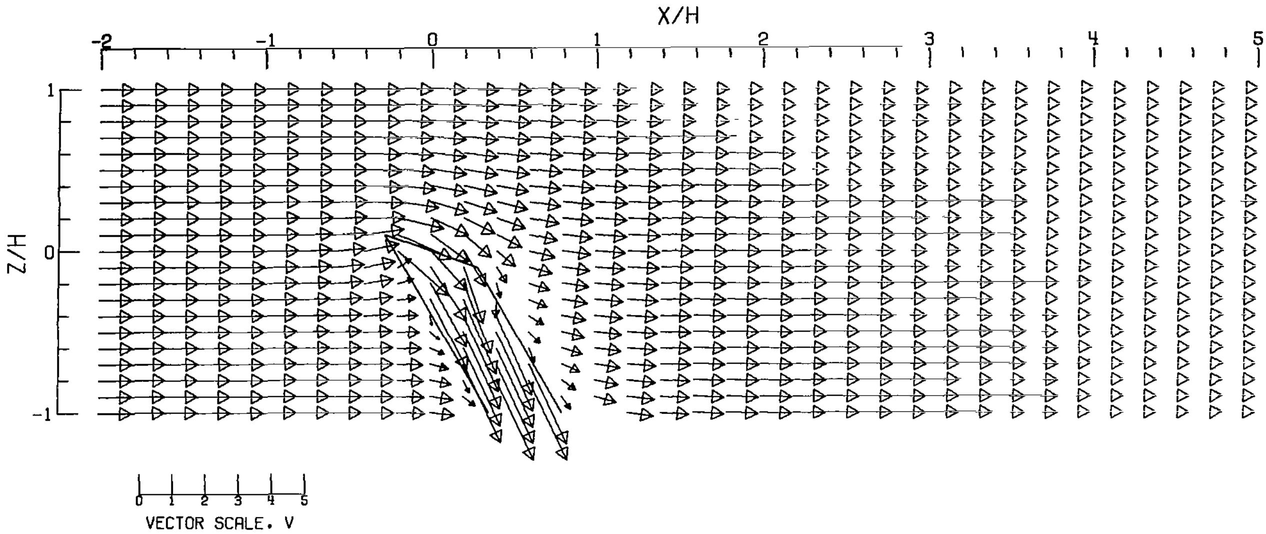

(A).- FREE AIR.

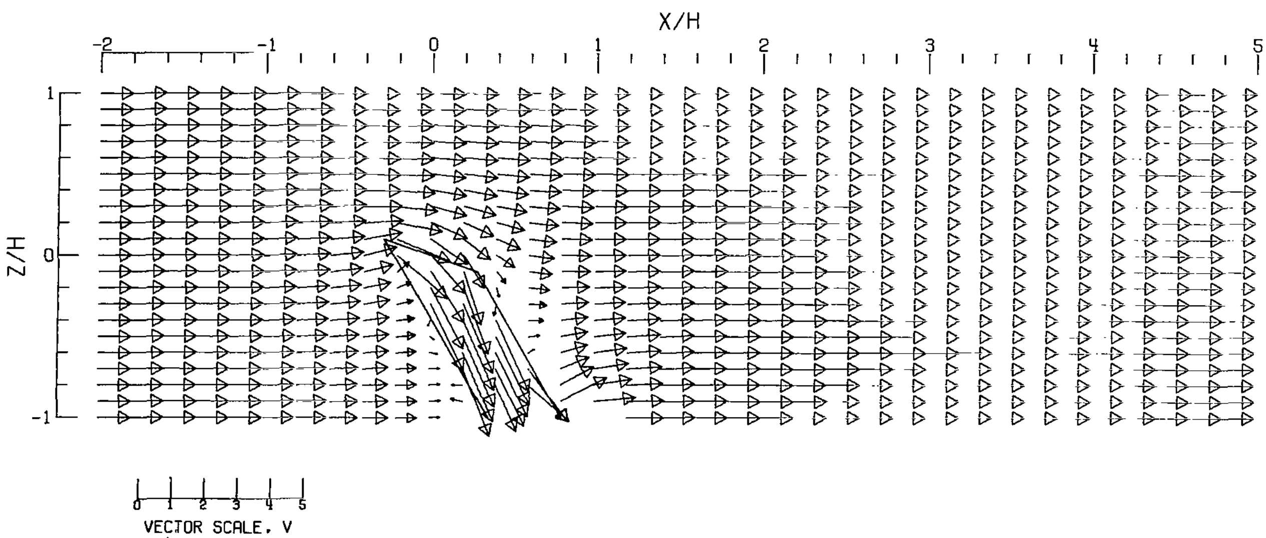

(B).- GROUND EFFECT.

Figure 122.- Flow vectors in the X-Z plane, calculated using doublet strings. The rotor and the edges of the wake are shown. ζ = 1.000; η = 1.0; γ = 0.5; σ = 0.600; α = 20.0°; χ = 30.0°; uniform loading.

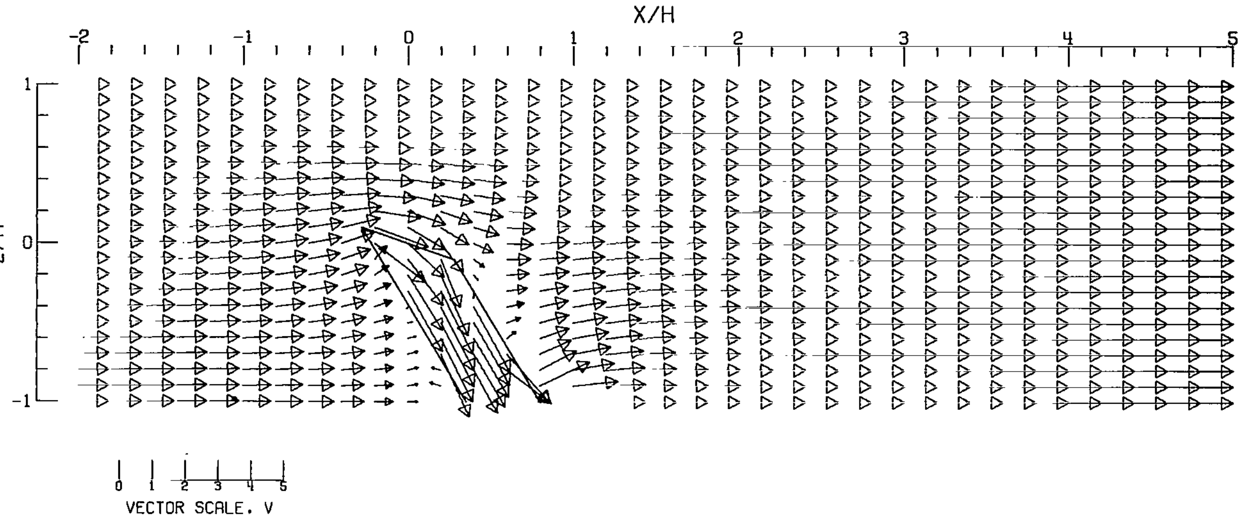

(C).- CLOSED TUNNEL.

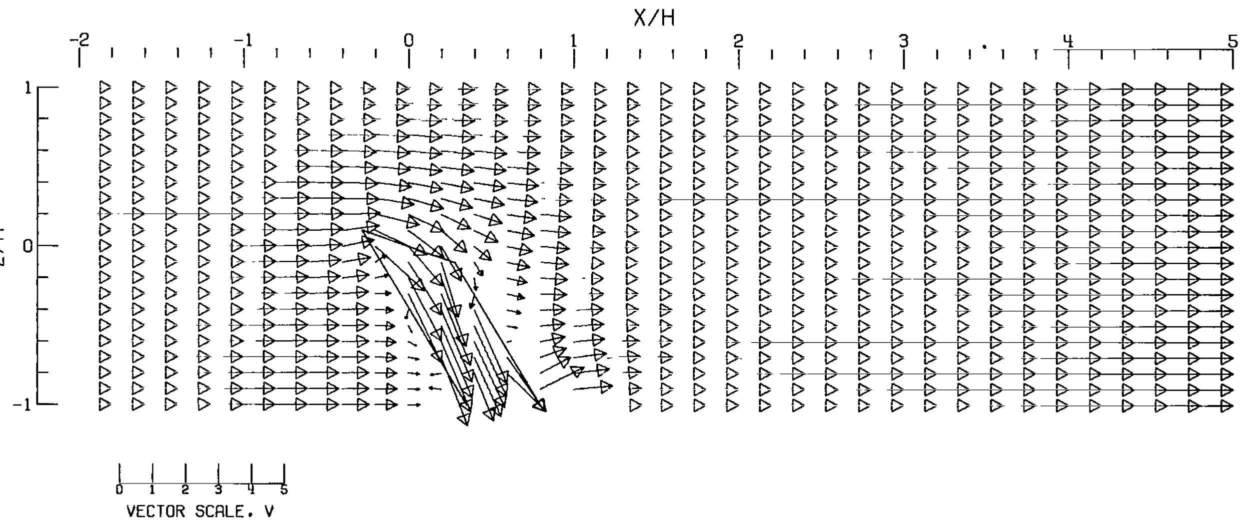

(D).- CLOSED-ON-BOTTOM-ONLY TUNNEL.

Figure 122.- Concluded.

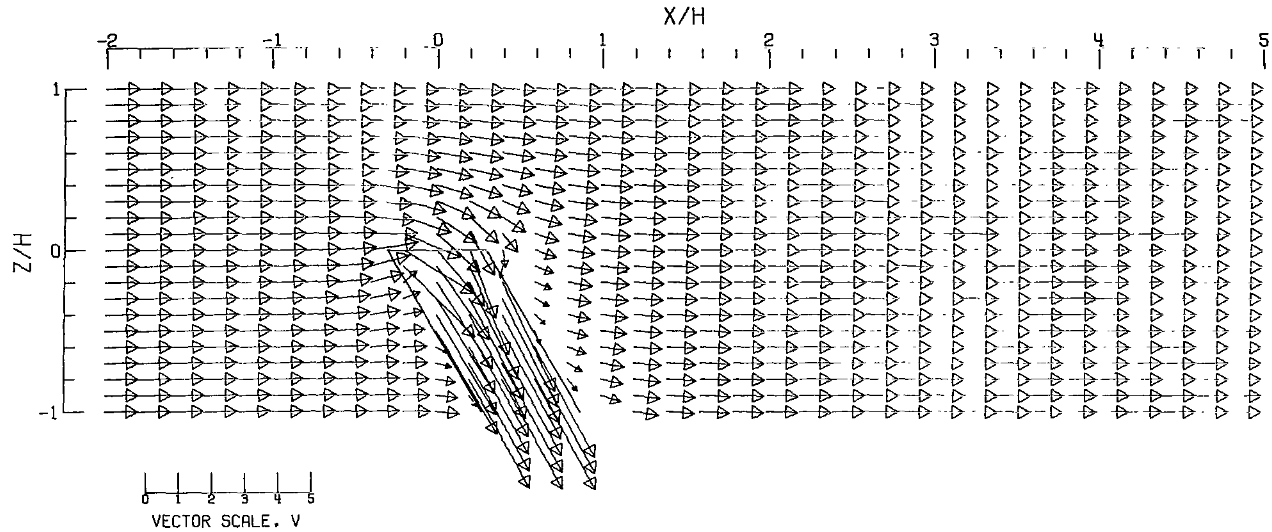

(A).- FREE AIR.

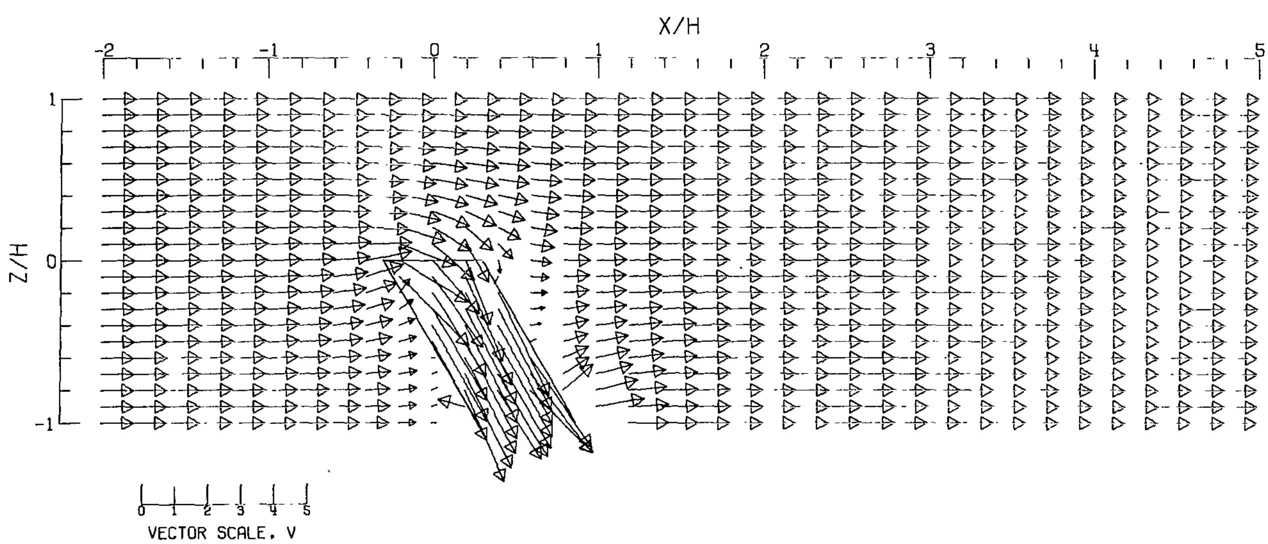

(B).- GROUND EFFECT.

Figure 123.- Flow vectors in the X-Z plane, calculated using doublet strings. The rotor and the edges of the wake are shown. $\zeta = 1.000$; $\eta = 1.0$; $\gamma = 0.5$; $\sigma = 0.600$; $\alpha = 0.0^{0}$; $\chi = 30.0^{0}$; uniform loading.

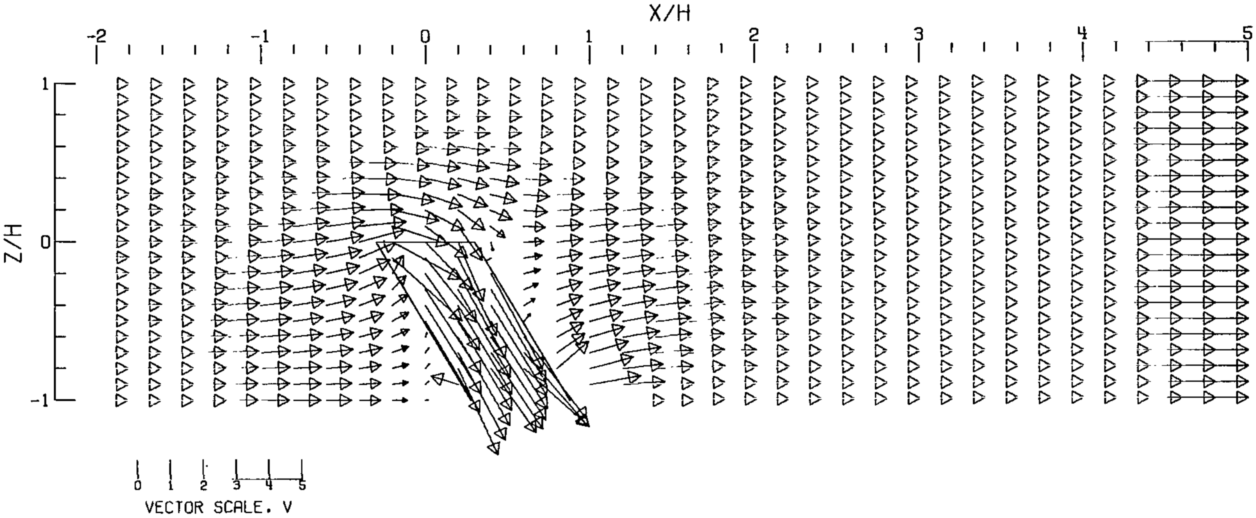

(C).- CLOSED TUNNEL.

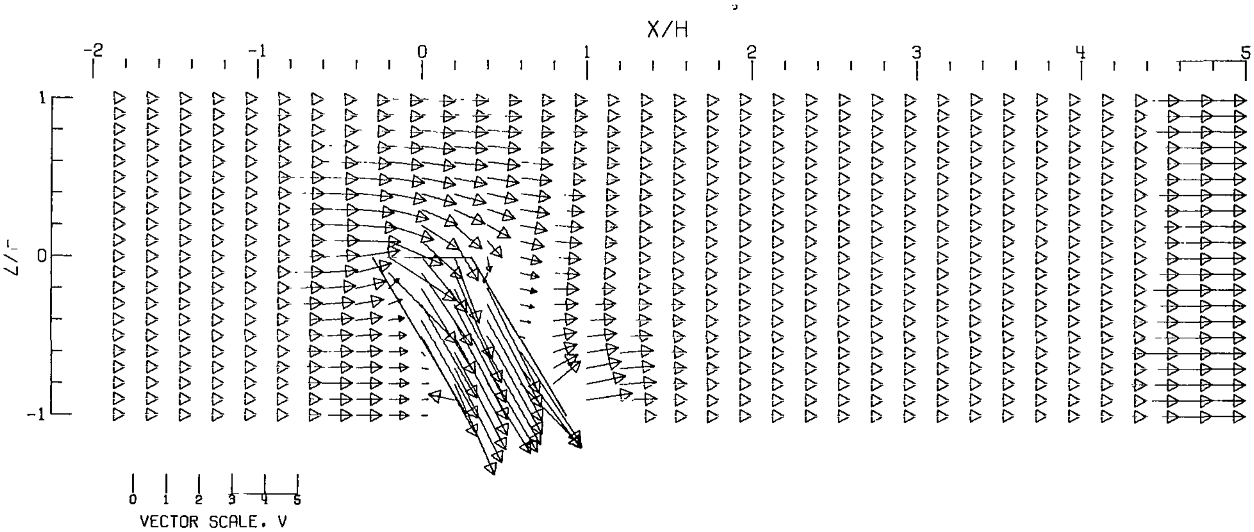

(D).- CLOSED-ON-BOTTOM-ONLY TUNNEL.

Figure 123.- Concluded.

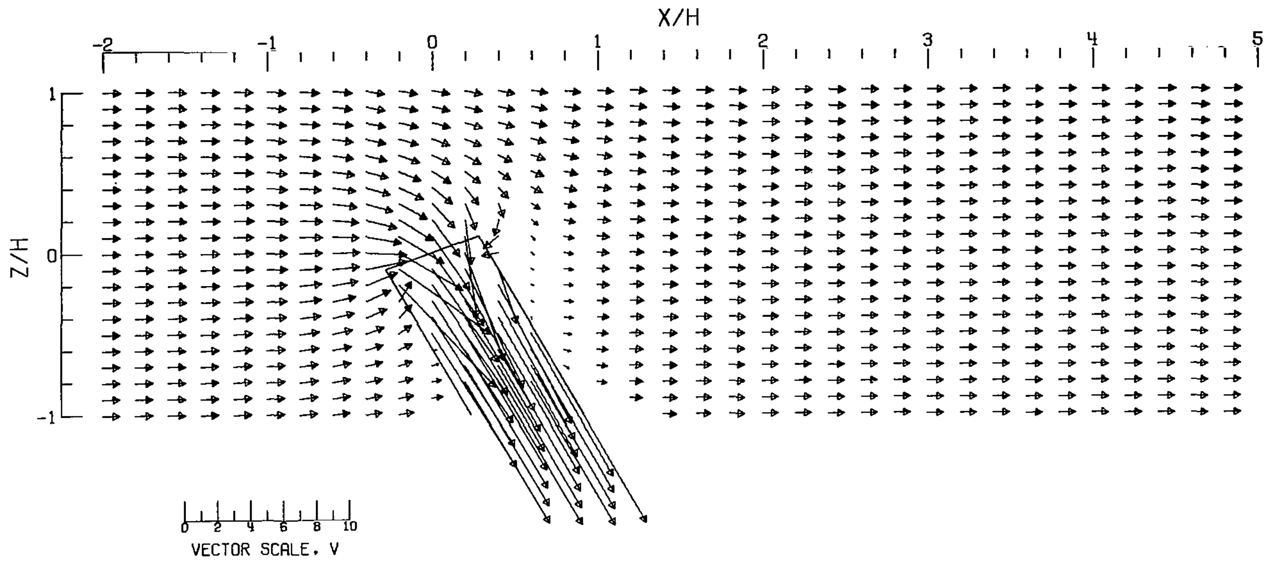

(A).- FREE AIR.

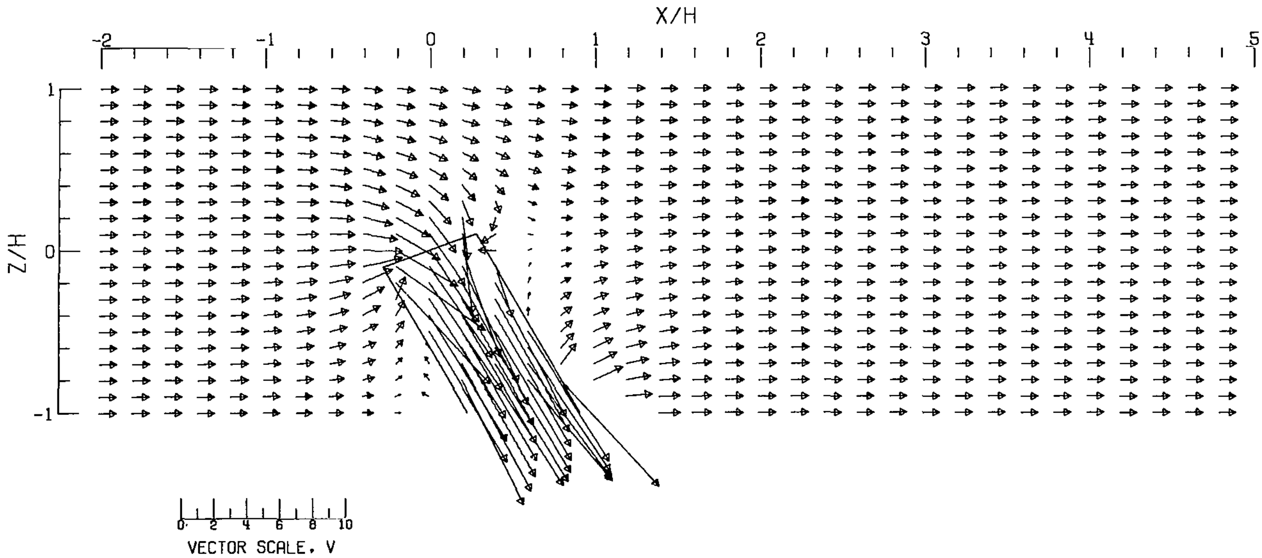

(B).- GROUND EFFECT.

Figure 124.- Flow vectors in the X-Z plane, calculated using doublet strings. The rotor and the edges of the wake are shown. ζ = 1.000; η = 1.0; γ = 0.5; σ = 0.600; α = -20.0°; χ = 30.0°; uniform loading.

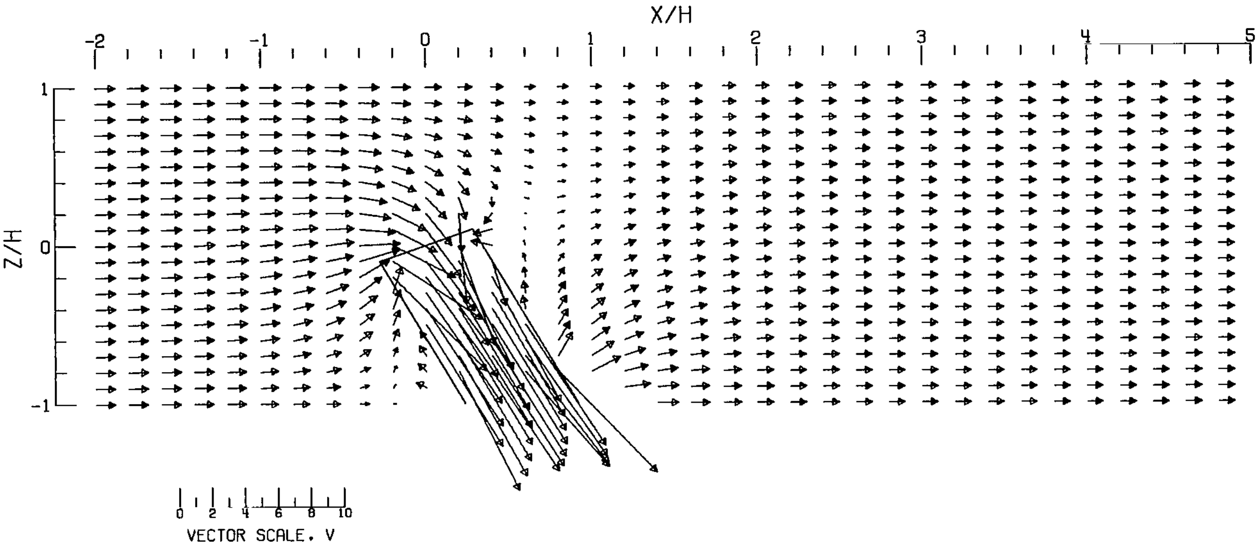

(C).- CLOSED TUNNEL.

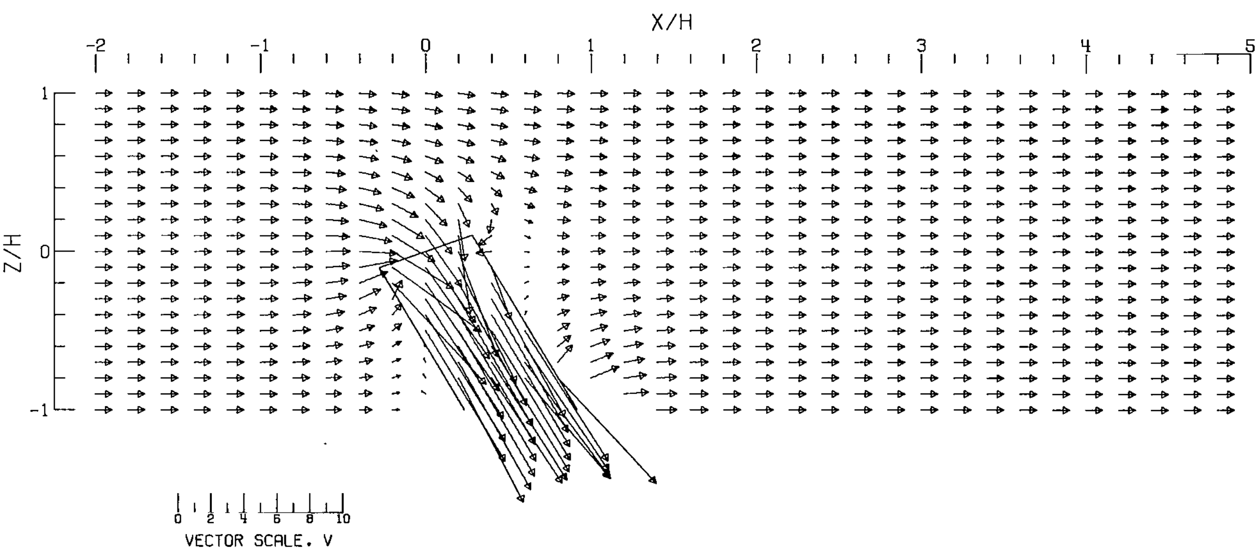

(D).- CLOSED-ON-BOTTOM-ONLY TUNNEL.

Figure 124.- Concluded.

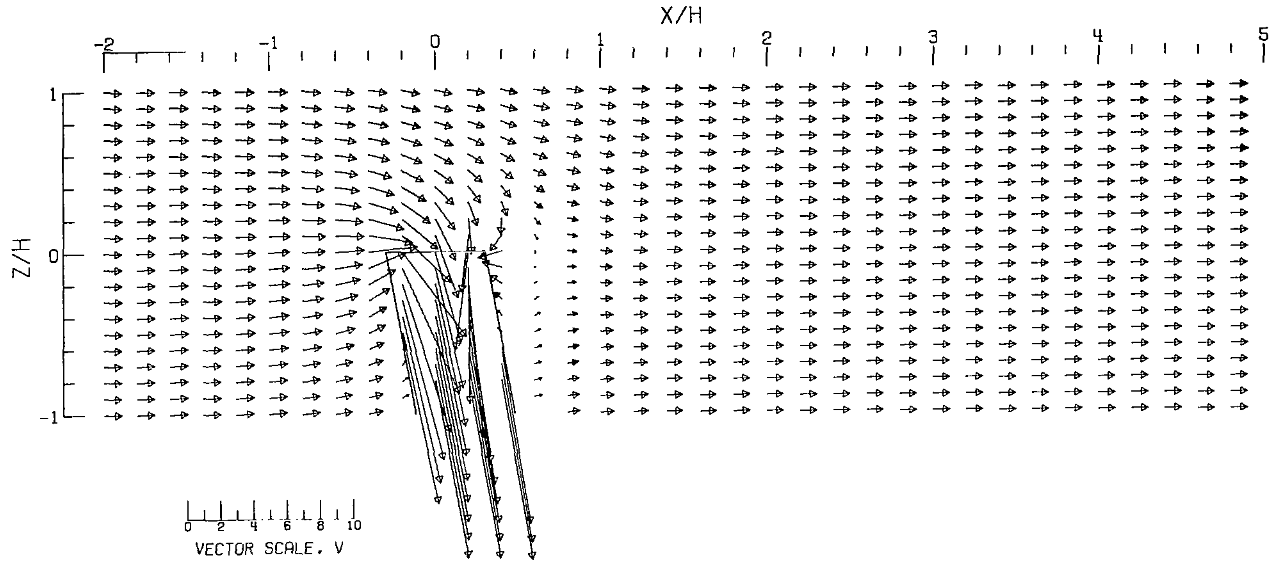

(A).- FREE AIR.

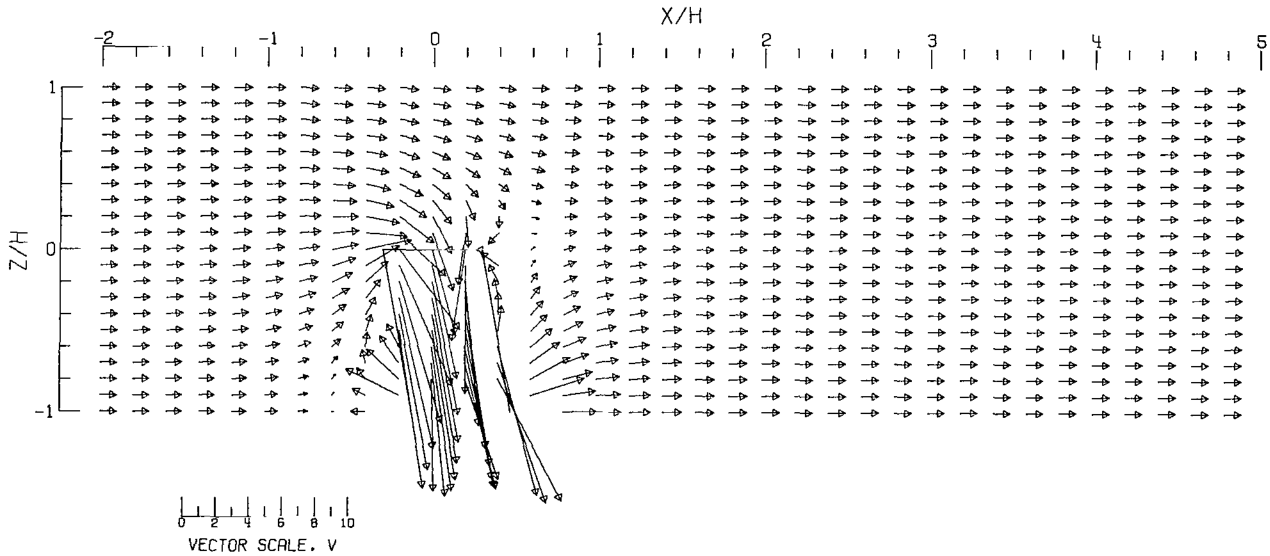

(B).- GROUND EFFECT.

Figure 125.- Flow vectors in the X-Z plane, calculated using doublet strings. The rotor and the edges of the wake are shown. ζ = 1.000; η = 1.0; γ = 0.5; σ = 0.600; α = 0.0°; χ = 10.0°; uniform loading.

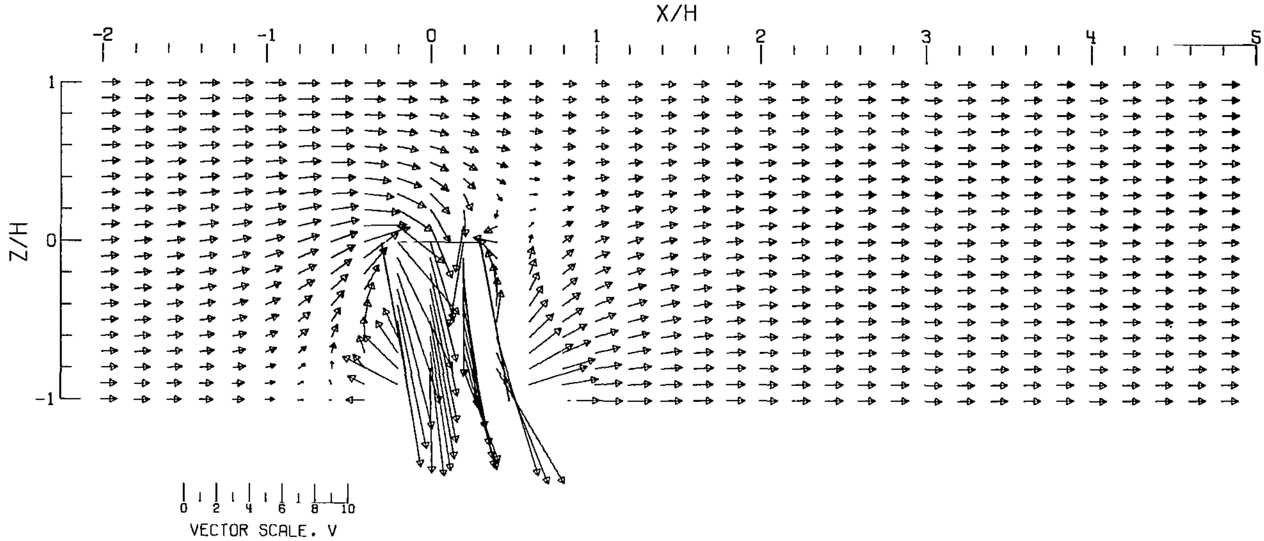

(C).- CLOSED TUNNEL.

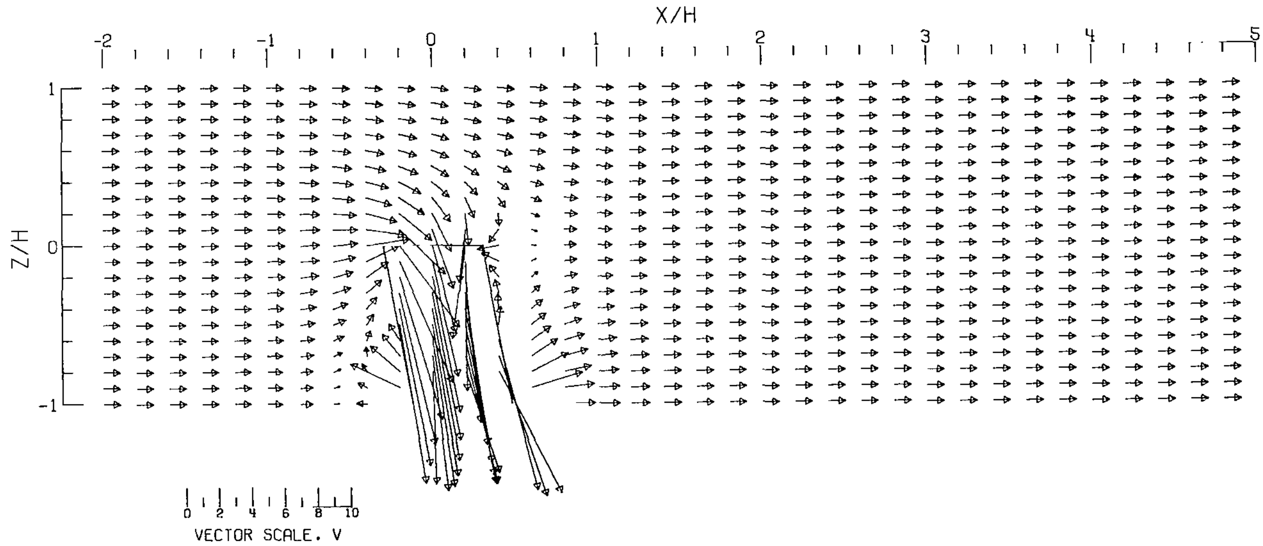

(D).- CLOSED-ON-BOTTOM-ONLY TUNNEL.

Figure 125.- Concluded.

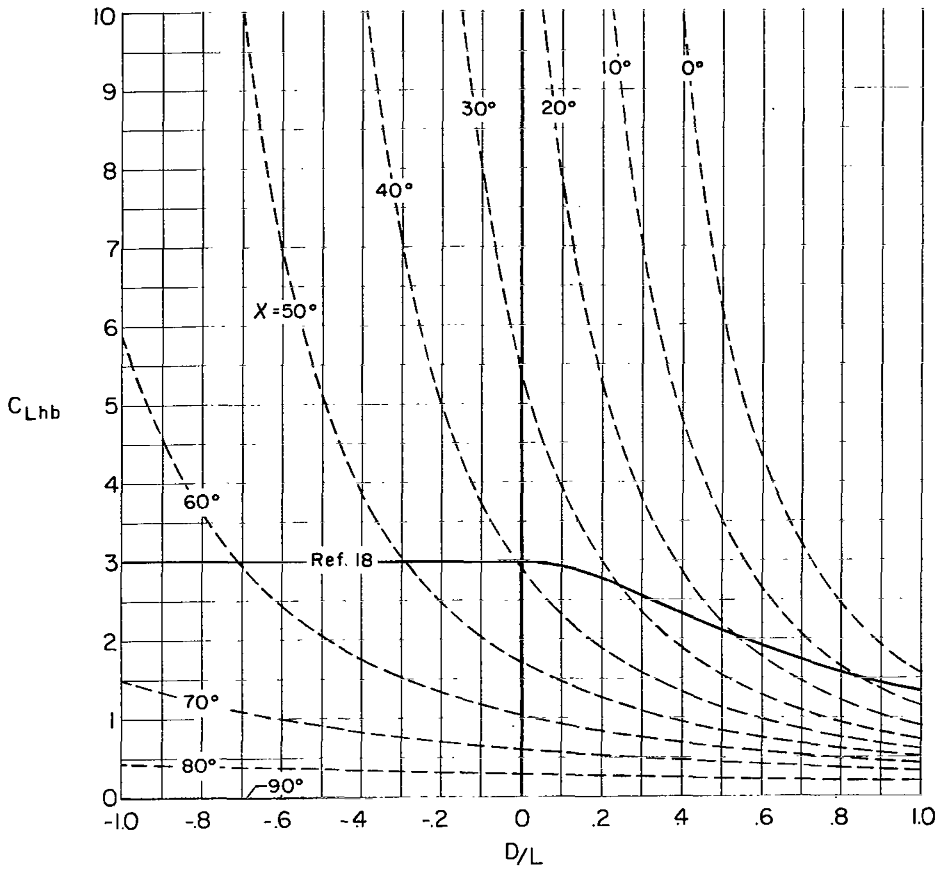

(a) b/h = 0.5.

Figure 126.- Lines of constant wake skew angle χ in terms of C_{Lhb} compared with the limiting values given for a closed wind tunnel by reference 18.

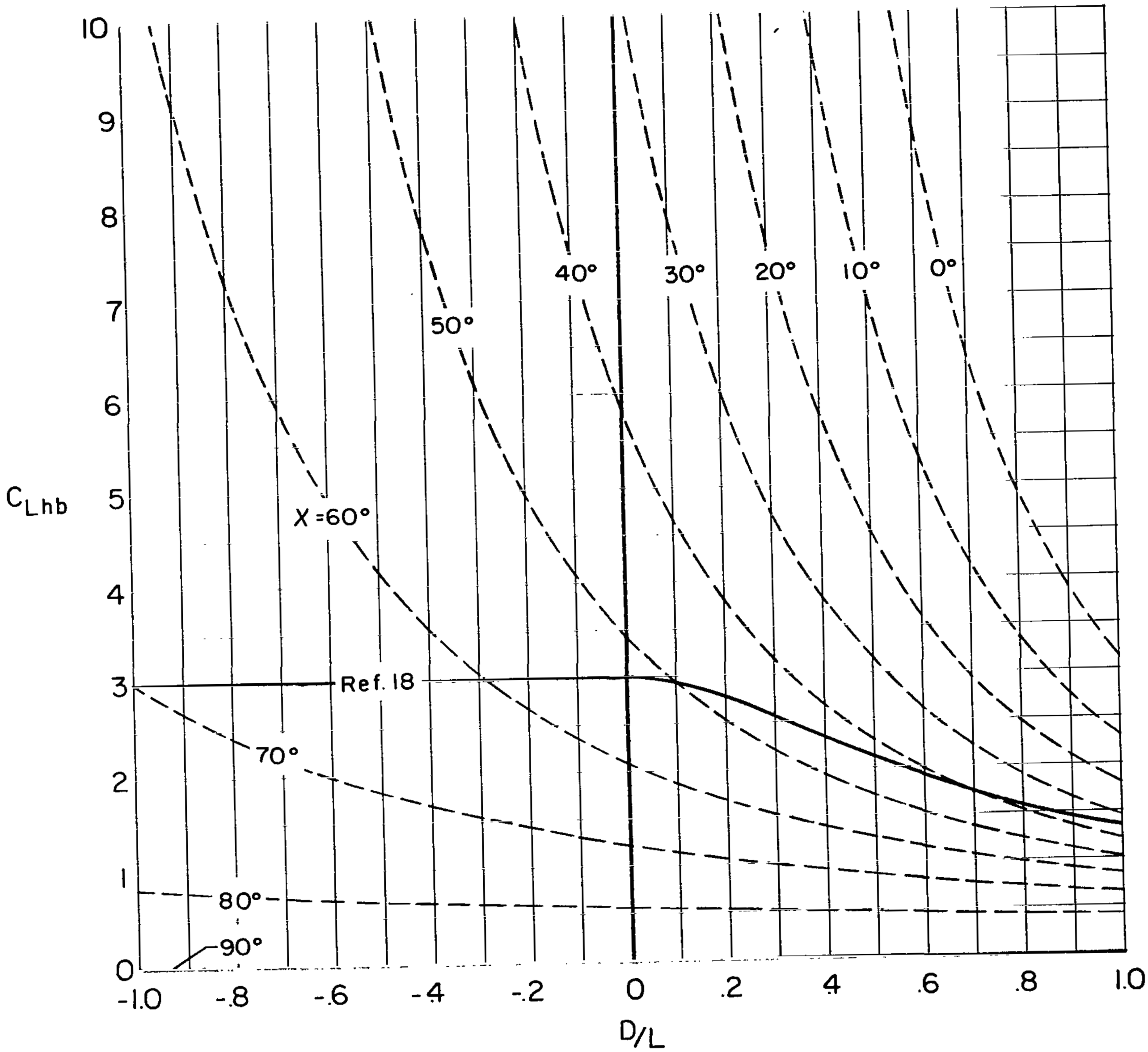

(b) b/h = 1.0.

Figure 126.- Continued.

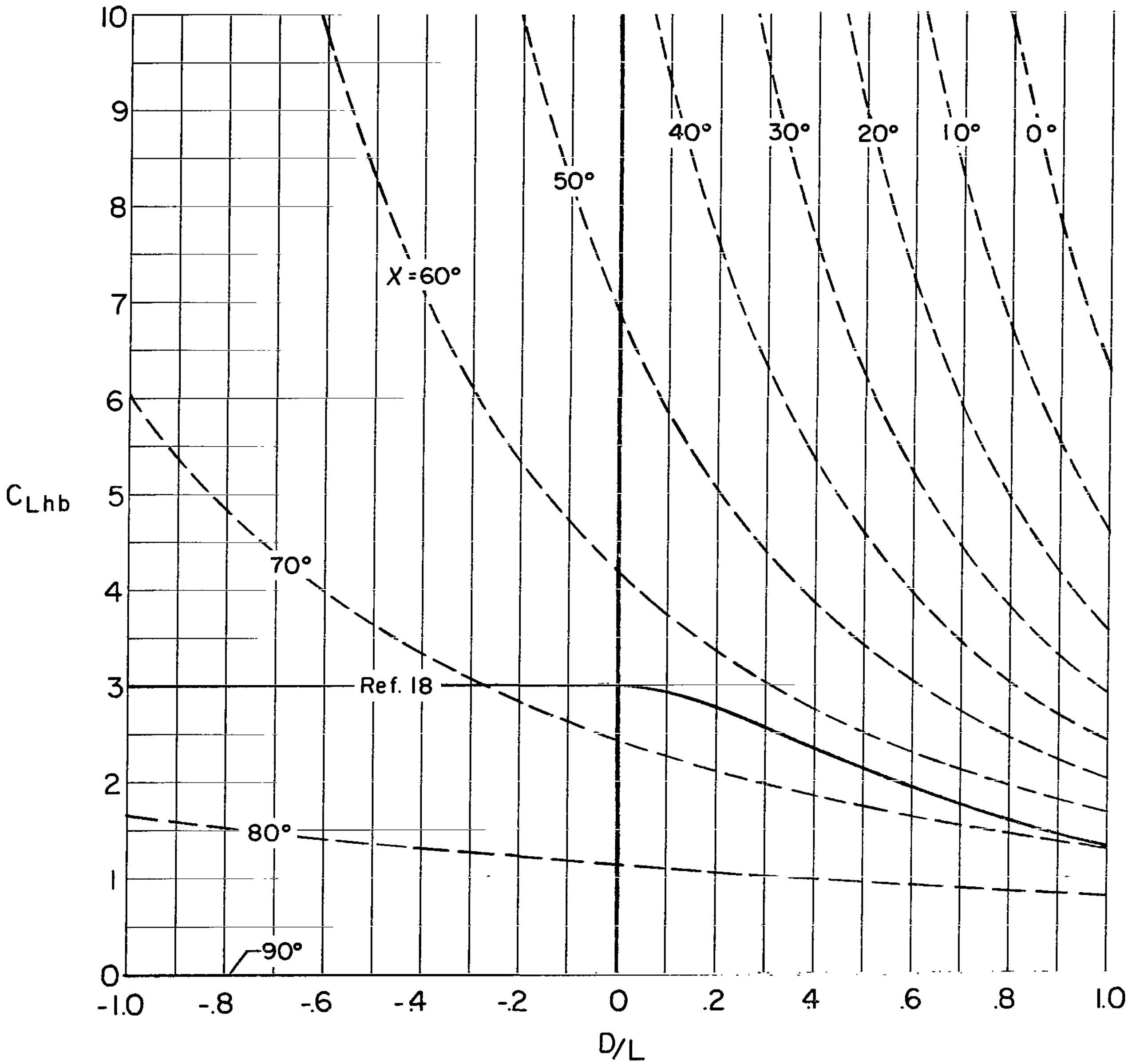

(c) b/h = 2.0.

Figure 126.- Concluded.

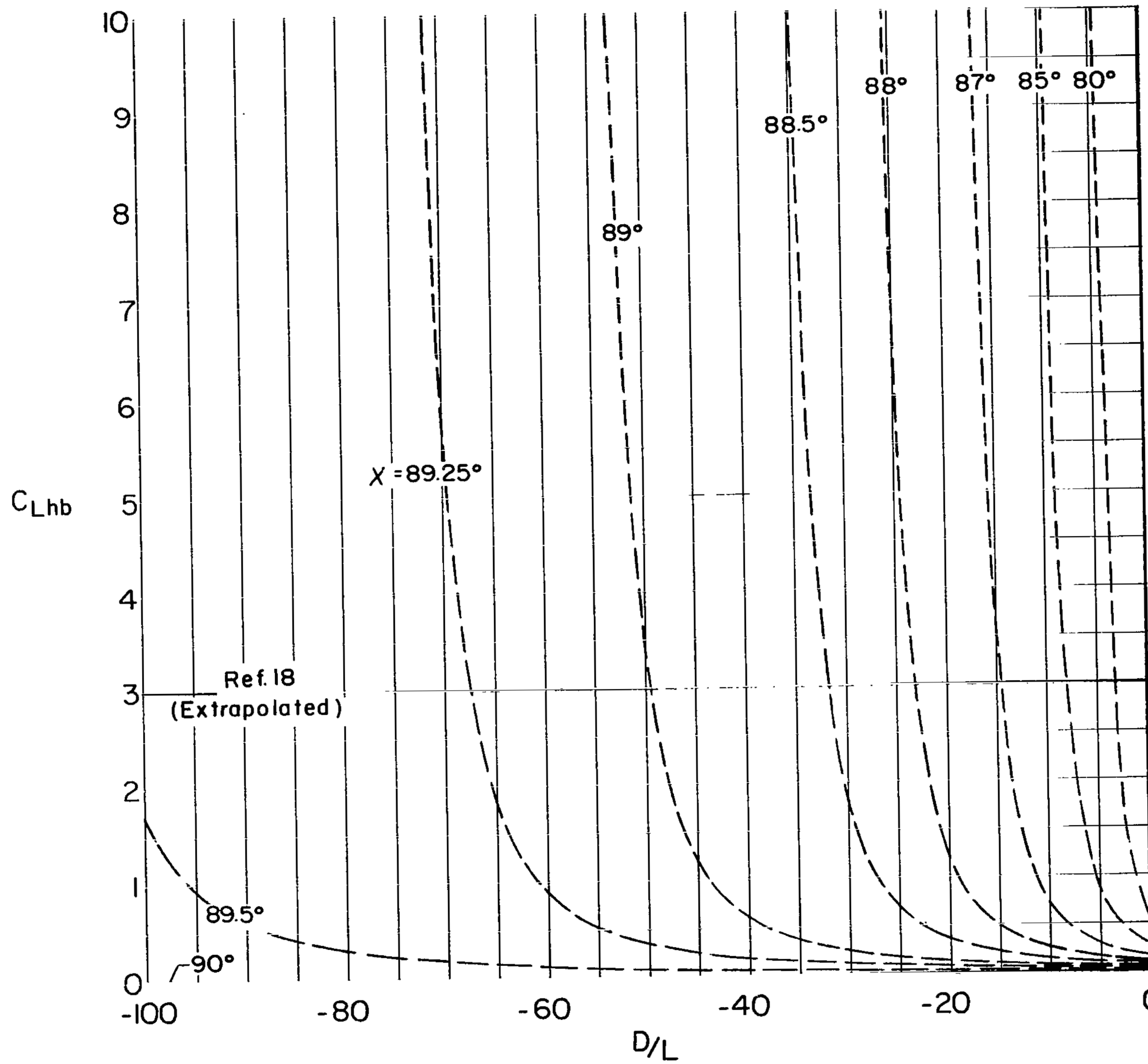

Figure 127.- Lines of constant wake skew angle χ in terms of C_{Lhb} compared with the limiting values for a closed tunnel extrapolated from reference 18.

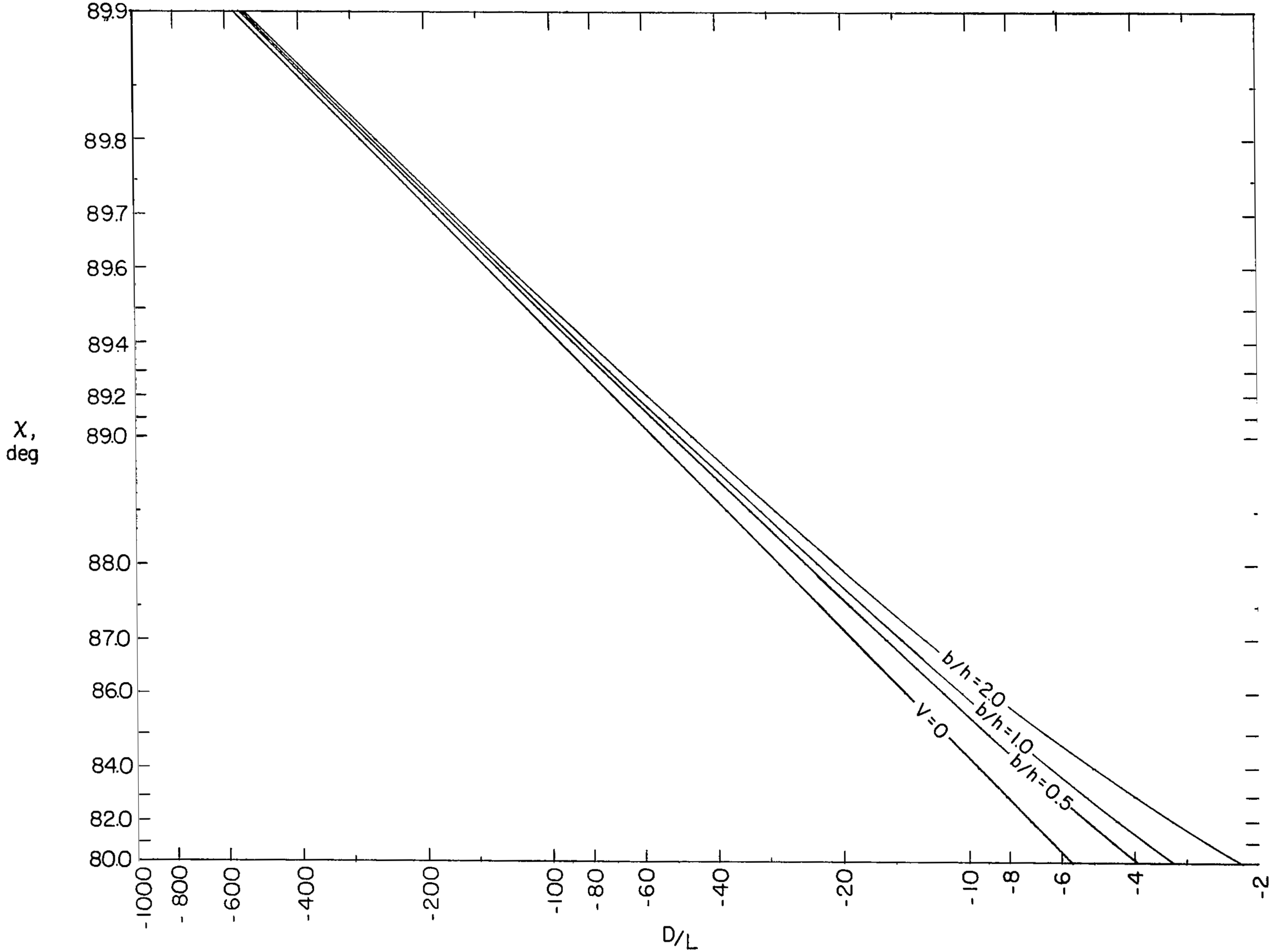

Figure 128.- Values of D/L which produce $C_{Lhb} = 3.0$ compared with the value of D/L which requires that V = 0.

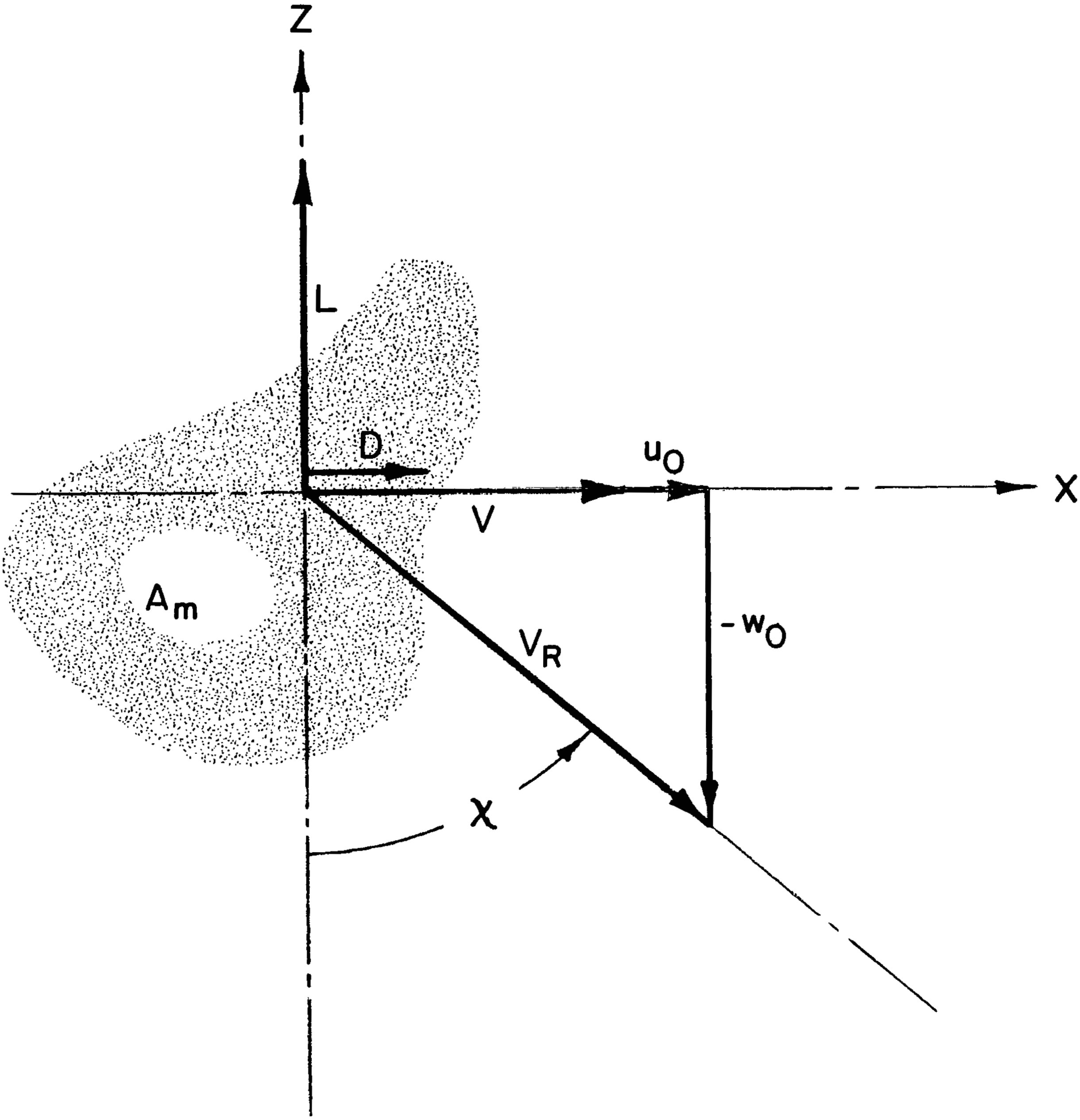

Figure 129.- Force and velocity vectors at aircraft.

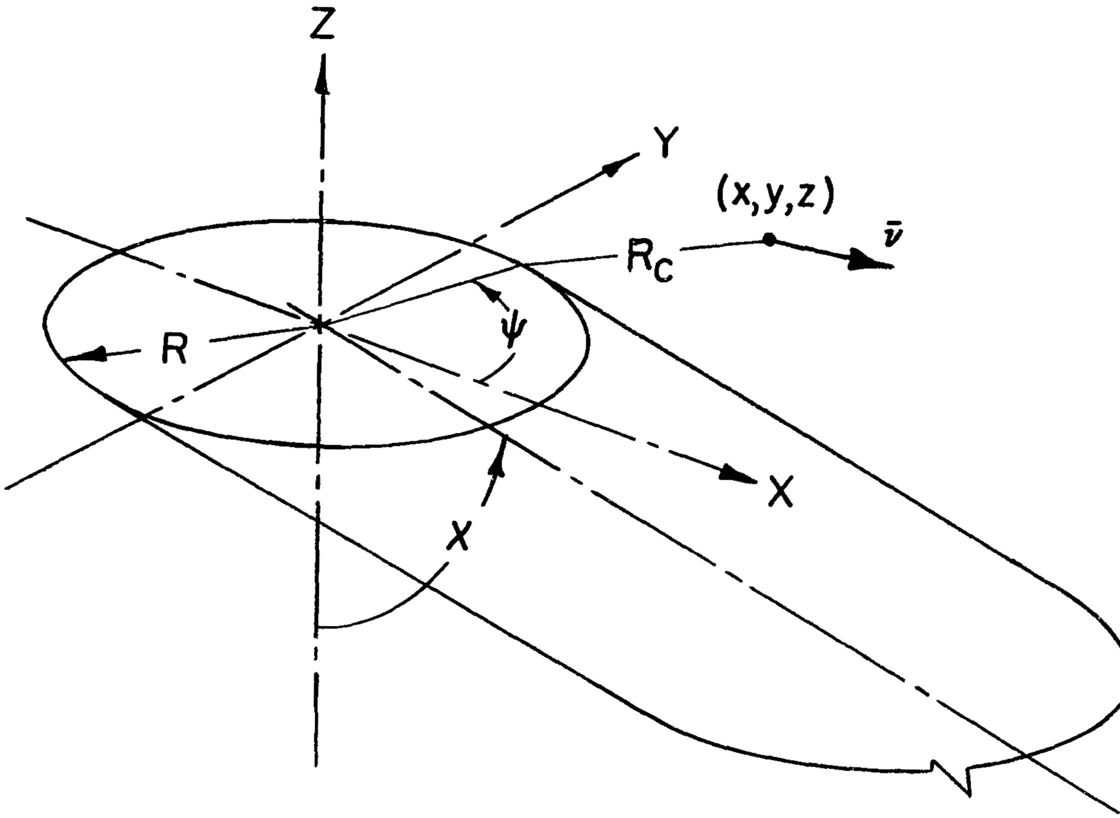

Figure 130.- Wake of a uniformly loaded rotor.

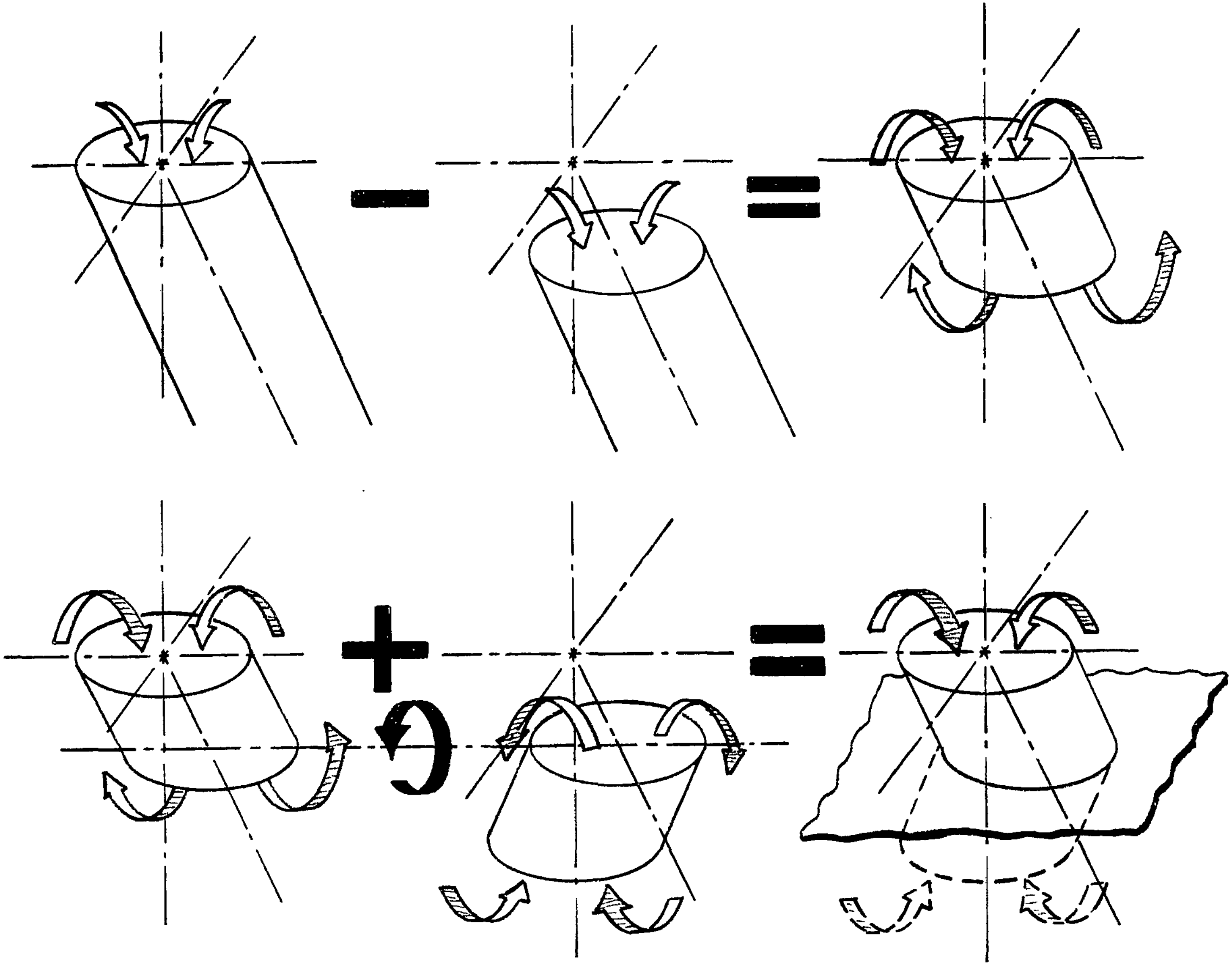

Figure 131.- Sketches illustrating use of superposition to obtain the field of a rotor in ground effect.

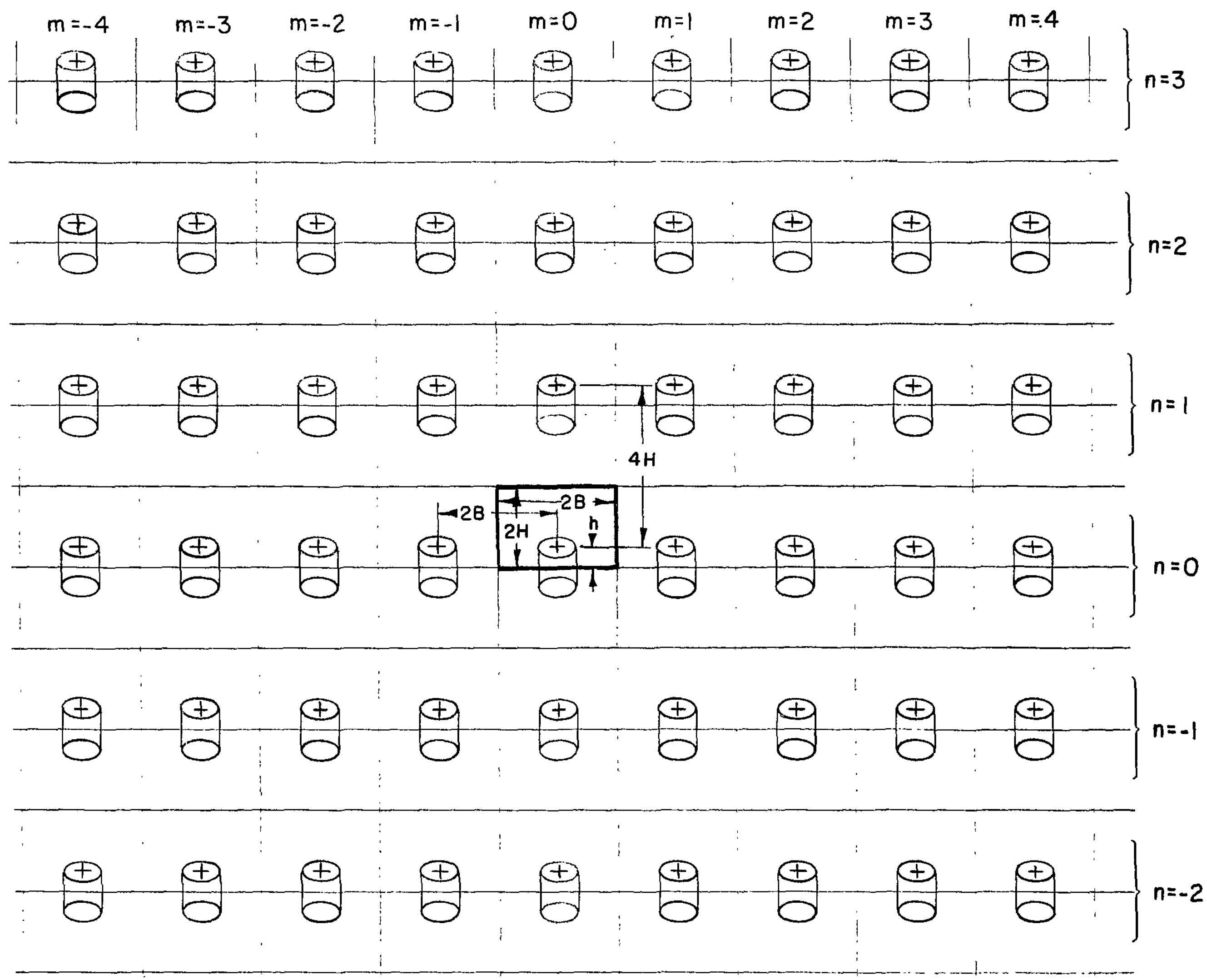

(a) Closed tunnel.

Figure 132.- Central portion of reflection pattern to obtain induced velocities in tunnel. Solid lines indicate closed boundaries; broken lines indicate open boundaries. Sense of vorticity is indicated by signs, + indicates sense same as basic tunnel model and - indicates sense opposite to basic tunnel model. Real boundaries are darkened.

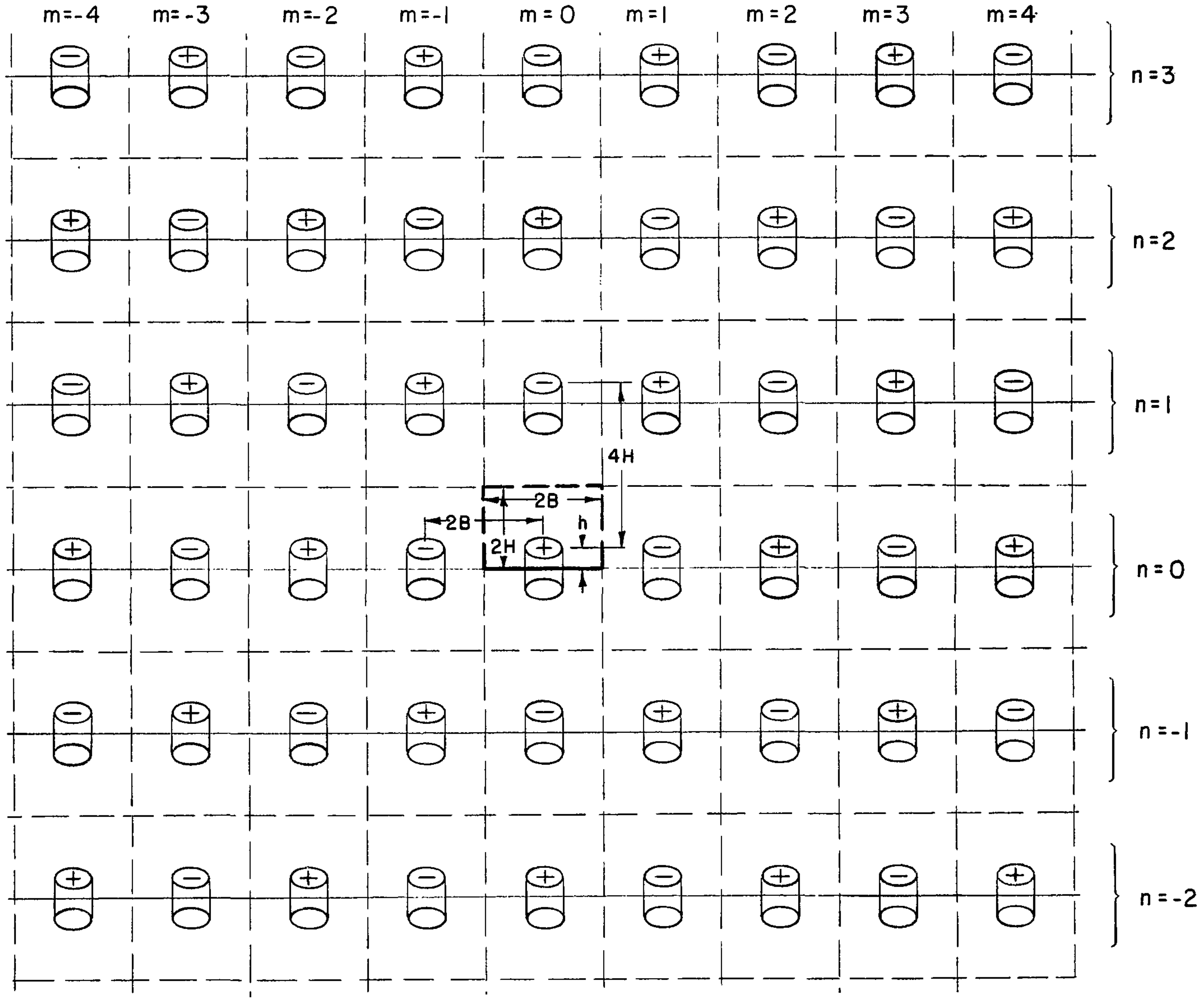

(b) Closed-on-bottom-only tunnel.

Figure 132.- Concluded.

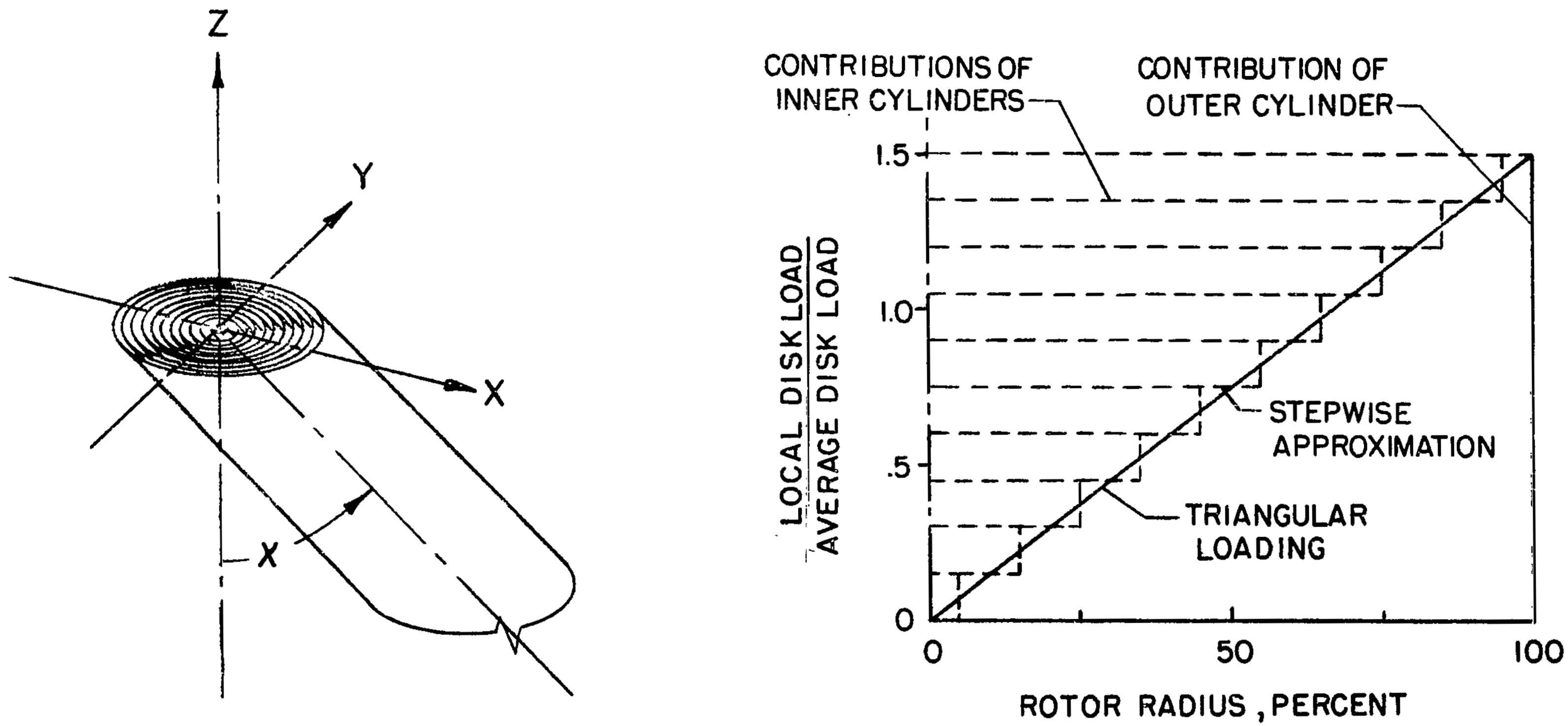

(a) Wake as a nest of vortex cylinders.

(b) Load distribution.

Figure 133.- Superposition technique used to obtain the induced field of a rotor having axisymmetric nonuniform disk-load distribution.

NASA-Langley, 1970 — 1 L-7042

NATIONAL AERONAUTICS AND SPACE ADMINISTRATION
WASHINGTON, D.C. 20546

OFFICIAL BUSINESS

FIRST CLASS MAIL

POSTAGE AND FEES
NATIONAL AERONAUTI
SPACE ADMINISTRAT

07U 001 26 51 3DS 70119 00903
AIR FORCE WEAPONS LABORATORY /WLOL/
KIRTLAND AFB, NEW MEXICO 87117

ATT E. LOU BOWMAN, CHIEF,TECH. LIBRARY

POSTMASTER: If Undeliverable (Sectio Postal Manual) Do Not

"The aeronautical and space activities of the United States shall be conducted so as to contribute . . . to the expansion of human knowledge of phenomena in the atmosphere and space. The Administration shall provide for the widest practicable and appropriate dissemination of information concerning its activities and the results thereof."

—NATIONAL AERONAUTICS AND SPACE ACT OF 1958

NASA SCIENTIFIC AND TECHNICAL PUBLICATIONS

TECHNICAL REPORTS: Scientific and technical information considered important, complete, and a lasting contribution to existing knowledge.

TECHNICAL NOTES: Information less broad in scope but nevertheless of importance as a contribution to existing knowledge.

TECHNICAL MEMORANDUMS: Information receiving limited distribution because of preliminary data, security classification, or other reasons.

CONTRACTOR REPORTS: Scientific and technical information generated under a NASA contract or grant and considered an important contribution to existing knowledge.

TECHNICAL TRANSLATIONS: Information published in a foreign language considered to merit NASA distribution in English.

SPECIAL PUBLICATIONS: Information derived from or of value to NASA activities. Publications include conference proceedings, monographs, data compilations, handbooks, sourcebooks, and special bibliographies.

TECHNOLOGY UTILIZATION PUBLICATIONS: Information on technology used by NASA that may be of particular interest in commercial and other non-aerospace applications. Publications include Tech Briefs, Technology Utilization Reports and Technology Surveys.

Details on the availability of these publications may be obtained from:

SCIENTIFIC AND TECHNICAL INFORMATION DIVISION

NATIONAL AERONAUTICS AND SPACE ADMINISTRATION

Washington, D.C. 20546